Development of Novel Treatment Strategies in Complement-mediated Thromboinflammatory and Autoimmune Diseases: Tethering of Host Immune Modulators by Modified Peptide Conjugates

Inauguraldissertation

zur

Erlangung der Würde eines Doktors der Philosophie

vorgelegt der

Philosophisch-Naturwissenschaftlichen Fakultät

der Universität Basel

von

Clément Martin Leopold Bechtler

2022

Originaldokument gespeichert auf dem Dokumentenserver der Universität Basel edoc.unibas.ch

Genehmigt von der Philosophisch-Naturwissenschaftlichen Fakultät

auf Antrag von

Prof. Dr. Daniel Ricklin
Prof. Dr. Dennis Gillingham
Prof. Dr. Tom Grossmann

Basel, den 14.12.2021

Prof. Dr. Marcel Mayor
(Dekan)

ABSTRACT

Host-defense pathways are essential to protect the organism against pathogens and maintain tissue homeostasis. The complement system is an integral part of innate immunity and recognizes a broad set of danger signals, upon which it initiates a swift and powerful effector response, including immune cell activation, enhanced phagocytosis and direct tissue damage. Furthermore, complement activation provides a platform for cross-talk to other host-defense pathways such as adaptive immunity and coagulation. While complement activation is beneficial under most circumstances, undesired activation on surfaces recognized as non-self (e.g. biomaterials and transplants) or in autoimmune diseases can have deleterious effects. The complement system is tightly controlled under physiologic conditions due to the broad and severe reactions it may entrain on host cells. One major regulator of complement activation is the plasma protein factor H (FH), which inhibits the central amplification loop where all three complement initiation pathways converge. The recruitment of FH to foreign surfaces is not only employed by pathogens as evasion strategy but is also considered an attractive therapeutic option. We could previously show that the 14 amino acid-long cyclic peptide 5C6 binds potently to FH and can, when conjugated to appropriate surface tethers, inhibit complement activation on biomedically relevant surfaces. Although initial proof-of-concept studies of 5C6 have been conducted previously, little was known about the interaction determinants within FH and 5C6 nor about the peptide's specificity, stability or activity in clinically relevant models. We addressed all these questions here and could demonstrate that 5C6 is highly selective for FH and binds murine and monkey FH in addition to the human regulator, thereby facilitating future translational studies. Additionally, we could demonstrate that 5C6's minimal binding region in FH consist of domains 10-14, suggesting a conformational binding epitope, and that 5C6 binding to FH is highly selective. By performing in-depth structure activity relationship studies on 5C6, we not only elucidated activity determinants but also identified a next-generation 5C6 analog with improved affinity, activity and stability.

In addition to evaluating 5C6 in models representing complement activation by nanoparticles and liposomal drug formulations, we also explored other peptide-based strategies to interfere in complement-related immune disorders. In the autoimmune disease IgA nephropathy (IgAN), for example, immune complexes can activate the complement system. Although the role of complement in IgAN has not been fully elucidated, the presence of the immune complexes is thought to drive the condition. The removal of autoantibodies causal to the immune complexes from circulation is therefore considered a promising therapeutic approach. One strategy to achieve this goal is to sequester the autoantibodies by immobilizing the respective epitope, an erroneously glycosylated polypeptide stretch in IgA1, to a polymer. We developed an improved synthesis protocol for producing the challenging glycopeptide epitope, a 20-mer peptide containing five glycosylated residues, at sufficient quantities to enable proof-of-concept studies. Our finding that the polymer-immobilized synthetic epitope is able to bind patient-derived autoantibodies serves as important validation of this approach and may pave the way for novel therapeutic strategies in IgAN.

Finally, based on the critical role of complement-coagulation cross-talk in many thromboinflammatory conditions, we investigated whether the coagulation cascade regulator FXIII-B, which is structurally similar to FH, also exerts complement-regulatory functions in analogy to FH. We could demonstrate that neither the ligand binding nor functional profile of FXIII-B corresponds to that of FH, thereby untangling a part of the complex interaction network between different host-defense pathways.

The described projects underline the potential impact that peptidic modalities may have in the treatment of complement-mediated diseases. Future optimization and translational efforts will reveal their full potential and, hopefully, bring these promising approaches closer to the bedside.

LIST OF ABBREVIATIONS

AMD	age-related macular degeneration
AMR	antibody-mediated rejection
ADP	adenosine diphosphate
ATP	adenosine triphosphate
C4BP	C4-binding protein
CARPA	complement activation-related pseudoallergy
CD	circular dichroism
CF	5(6)-carboxyflouorescein
COVID-19	coronavirus disease 2019
CRIg	complement receptor of the immunoglobulin family
CR1	complement receptor 1
CR2	complement receptor 2
DAF	decay-accelerating factor
DAMP	damage-associated molecular pattern
d	day
dmab	4-{N-[1-(4,4-dimethyl-2,6-dioxocyclohexylidene)-3-methyl-butyl]-amino}benzyl
ELISA	enzyme-linked immunosorbent assay
FB	factor B
FC	flow cytometry
FD	factor D
FH	factor H
FHL-1	factor H-like 1
HRP	horseradish peroxidase
Ig	immunoglobulin
IgAN	IgA nephropathy
IRI	ischemia-reperfusion injury
ITC	isothermal titration calorimetry
mAb	monoclonal antibody
MAP-1	mannose-binding lectin-associated protein 1
MCP	membrane cofactor protein
MD	molecular dynamics
mRNA	messenger ribonucleic acid
MST	microscale thermophoresis
NK cell	natural killer cell
NMR	nuclear magnetic resonance
PAMP	pathogen-associated molecular pattern
PEG	polyethylene glycol
PNH	paroxysmal nocturnal hemoglobinuria
PROTAC	proteolysis targeting chimera
PRR	pattern recognition receptor
RCM	ring-closing metathesis
RMSD	root mean square deviation
ROS	reactive oxygen species
SAR	structure-activity relationship
sMAP	small mannose-binding lectin-associated protein
SPPS	solid-phase peptide synthesis
SPR	surface plasmon resonance
Th cell	T-helper cell

TABLE OF CONTENTS

INTRODUCTION

THE COMPLEMENT SYSTEM

PHYSIOLOGY

The complement system comprises a cascade of more than 30 proteins, mostly circulating in plasma, which acts as a first-in-line defense mechanism towards pathogens, but is also central to general tissue homeostasis.[1,2] It is a long-known system, having been described initially by Eduard Buchner and Jules Bordet at the end of the 19th century and obtained its name by Paul Ehrlich, realizing that it is "complementing" the role of antibodies during an immune response.[2,3] In the past two decades, there has been a regained interest in the complement system due to its increasingly recognized role in a number of disease areas.[1,2,4–6] As the major part of humoral innate immunity, it recognizes specific molecular signatures, i.e. pathogen-associated molecular patterns (PAMPs) and damage-associated molecular patterns (DAMPs), through its pattern recognition receptors (PRRs) and initiates swiftly an immune response, both by relying on its own effector functions as well as via cross-talk with other branches of the immune system and coagulation.[5]

The whole complement cascade can be separated into three consequent phases of initiation, amplification and terminal effector generation. The initiation step can be further distinguished into three different initiation pathways, the classical (CP), lectin (LP) and alternative pathway (AP), with the CP obtaining its name by being the first one discovered.[5] Its PRR is the C1q protein, which mainly binds to antigen-bound IgG and IgM immunoglobulins, but also has the ability to bind directly to a number of structures such as lipopolysaccharides on gram-negative bacteria.[7] C1q is associated with a heterotetramer of two proteases in their inactive form, namely C1r and C1s, constituting the C1 complex $C1qr_2s_2$. Upon binding of C1q to a recognized PAMP or DAMP, C1r cleaves C1s leading to an active state.[8] Activated C1s can cleave the plasma protein C4 into the smaller C4a and the larger C4b (in the complement terminology, the a-fragment designates the smaller fragment, whereas the b-fragment is the larger one).[9] C4 has a reactive thioester, which upon cleavage to C4b becomes accessible and allows C4b to bind covalently to nucleophiles in close proximity, such as amines or hydroxyl groups on proteins. C4b can recruit C2 that is then cleaved by C1s to C2b and C2a, giving rise to the CP C3 convertase C4b2b as the final product of the CP initiation (**Figure 1**).[5]

In a similar fashion to the CP, the LP's PRRs (mannose-binding lectin (MBL), collectins and ficolins) recognize distinct glycosylation and acetylation patterns. This activates the MBL-associated serine proteases (MASPs), of which MASP-2 eventually cleaves C4 and C2, allowing the formation of C4b2b. The recognized patterns include fucose, mannose and *N*-acetylglucosamin which can be found on bacteria, viruses as well as ischemic and apoptotic cells (**Figure 1**).[10,11]

Finally, the AP is consistently active at a low level by slow hydrolysis ("tick-over") of the most abundant complement protein, C3, to form $C3(H_2O)$. This process is tightly controlled on host surfaces, but tilts towards activation on pathogen or other surfaces lacking complement regulators. $C3(H_2O)$ then binds factor B (FB), upon which FB can be cleaved by the protease factor D (FD) to form the initial AP C3 convertase $C3(H_2O)Bb$. The initiating C3 convertases of both the AP and CP/LP can cleave C3 into C3a and C3b, which, as C4b, can bind through its now revealed thioester to surrounding surfaces. C3b recruits FB, which again is cleaved by FD, forming the main AP C3 convertase, C3bBb. Importantly, as the product of C3 cleavage is part of a C3 convertase, C3b further fuels its own formation. Thus, this central step, in which all initiation pathways converge, is known as the amplification loop. Its central role for the entire cascade is illustrated by the observation that even when the initiation occurs by the CP, up to 80% of the total complement response is provided by the AP amplification loop.[12] Eventually, upon increasing density of deposited C3b, the C3 convertase gains the ability to cleave C5 into C5b and C5a and the pathway enters its terminal stage. C5b recruits C6, C7, C8 and several C9 proteins to assemble the pore-forming membrane attack complex (MAC), leading to lysis of the pathogen. The small cleavage products C3a and C5a are anaphylatoxins, strong pro-inflammatory polypeptides signaling through their respective C3a and C5a receptors (i.e. C3aR, and C5aR1 and C5aR2) on a number of immune cells, e.g. granulocytes, macrophages and natural killer (NK) cells, with effects such as initiation of cell migration (chemotaxis) and activation of these cells.[5,13] Additionally to the function

of C3b as a platform for C3 and C5 conversion, C3b has a number of other, important functions. Itself and its degradation product iC3b are opsonins, i.e. they tag particles such as bacteria for phagocytotic uptake, mediated by complement receptor of the immunoglobulin family (CRIg) on phagocytes. iC3b is particularly potent in that regard as it also strongly promotes phagocytosis through its interactions with complement receptors 3 and 4 (CR3 and CR4, respectively). C3b stimulates T helper (Th) 1 cells through its interaction with CD46, while iC3b (and further degradation products C3dg, C3d) bind to complement receptor 2 (CR2) on B-cells and facilitate their activation.[5,13–15] Degradation products of C3b (iC3b, C3dg, C3d) bind to complement receptor 2 (CR2) on B-cells and facilitate their activation.[15] Furthermore, iC3b binds as well to complement receptors 3 and 4 (CR4 and CR4, respectively) on phagocytotic cells, leading to strong stimulation of phagocytosis.[5] Thus, complement not only exerts immune reactions in its own right, but also interacts with cellular innate immunity and functions as a central initiator of and guide for adaptive immunity. Beyond that, complement also cross-talks with and activates coagulation, e.g. C5 cleavage products increase tissue factor and von Willebrand factor expression, but also vice-versa, thrombin and other proteases of the coagulation system can cleave C5 (**Figure 1**).[16,17]

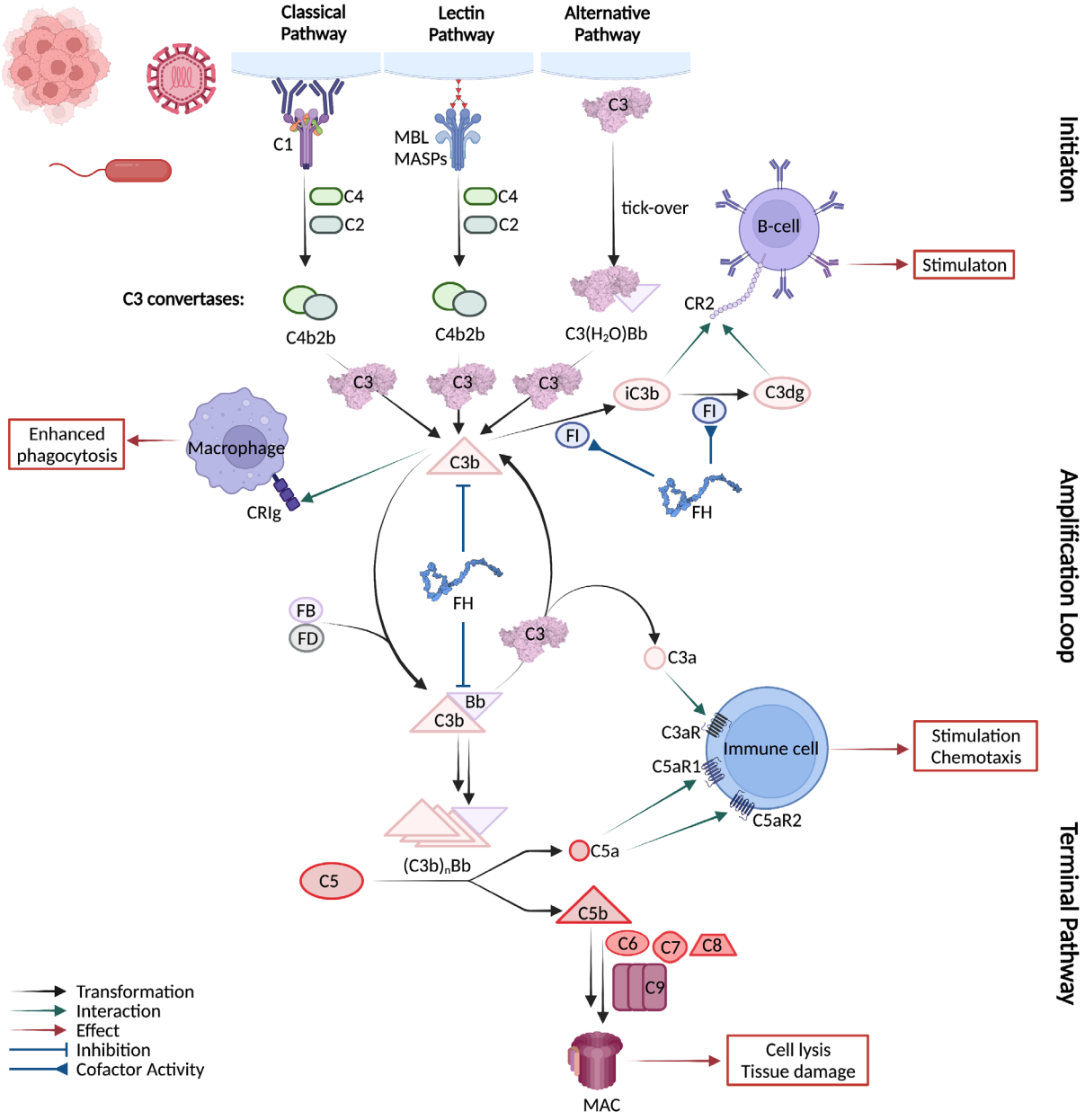

Figure 1: Schematic representation of the complement cascade and selected, pivotal interactions with other immune pathways. The cascade is initiated by the classical (CP), lectin (LP) or alternative pathway (AP) upon damage-associated molecular pattern (DAMP) or pathogen-associated molecular pattern (PAMP) recognition, or upon an imbalance between residual activation and inhibition. This leads to the formation of C3 convertases, cleaving C3 into C3b and C3a. C3b binds covalently to surfaces and is part of new C3 convertases which fuels a self-amplificatory loop. With increasing C3b concentrations, the convertase can cleave C5 into C5a and C5b, which functions as a basis for the lytic membrane-attack complex (MAC), while C3a and C5a are anaphylatoxins stimulating a variety of immune cells. Furthermore, C3b-tagging cells facilitates phagocytosis and degradation products of C3b (iC3b, C3dg) lower the threshold for B-cell activation. The plasma protein FH is a pivotal regulator of the complement system by inhibiting the central amplification loop. It inhibits C3 convertase formation and accelerates C3b degradation as a cofactor for the protease FI.

REGULATION

Due to its high reactivity, limited specificity, broad interaction profile and absence of a negative feedback loop, complement needs to be tightly controlled on several levels. One aspect of regulation is complement's intrinsic tendency to restrict activation to surfaces in close proximity due to the fast thioester hydrolysis of C3b or C4b, but additional regulation is necessary to protect host cells from deleterious effector functions.[6,18] Regulation of complement occurs at any stage throughout the cascade and can be further differentiated whether the inhibition is exerted by membrane or soluble proteins. For example, C1 inhibitor (C1-INH) is a serine protease inhibitor with broad specificity, inhibiting CP and LP proteases, but also coagulation factor XII, while small mannose-binding lectin-associated protein (sMAP) and mannose-binding lectin-associated protein 1 (MAP-1) exclusively inhibit LP initiation.[18,19] Looking at the other end of the cascade, the membrane protein CD59 and the plasma proteins vitronectin and clusterin are inhibitors of the MAC.[18]

Emphasizing the importance of the amplification loop for the whole system, most regulators, however, are targeted towards the C3 convertases. The inhibition is achieved by two distinct mechanisms: (1) by accelerating the natural decay of the convertase (be it C4b2b or C3bBb) and (2), by acting as co-factor for the protease factor I (FI), which degrades C3b into iC3b and further to C3dg. Both degradation products are unable to form convertases but play an important role in immune signaling. With regards to the decay acceleration, this is achieved both by preventing the formation of new convertases by binding to C3b or C4b as well as by disrupting already formed convertases.[18]

Among the membrane-bound regulators, complement receptor 1 (CR1) is the only one both displaying convertase decay acceleration and FI cofactor activity, while for the two other membrane-bound regulators, the names say it all: decay-accelerating factor (DAF) exclusively exerts its effect by decay acceleration and membrane cofactor protein (MCP) acts as FI cofactor.[10,18]

The soluble convertase inhibitors are C4b-binding protein (C4BP) and proteins belonging to the factor H (FH) family. C4BP binds to C4b but not C3b, and its action is therefore limited to the regulation of the CP and LP; it exerts both decay accelerating and cofactor activity. The proteins of the FH family, which include FH itself and its splice variant FH-like 1 (FHL-1), bind C3b and are hence soluble inhibitors of the AP, showing decay acceleration and cofactor functions. Furthermore, FH can be regarded as a pivotal regulator of the AP amplification loop, and therefore of the total complement response, as it is able to recognize self-surfaces and thereby acts as surface-directed inhibitor, facilitated by its high plasma concentration (2 µM).[20] It is composed of 20 globular complement control protein (CCP) domains, connected to each other by short flexible linkers as on a pearl string (**Figure 2A**). No high-resolution structure of full FH is available, but fragments could be crystallized alone or in complex. For example, the crystal structure of CCPs 1-4 in complex with C3b revealed the elongated form the FH domains adopt in this bound state (**Figure 2B**).[21] The binding to C3b is confined to CCPs 1-4 and 19-20, while CCPs 1-3 bind to FI and CCPs 7, 19 and 20 can recognize self-surface patterns such as heparin or sialic acid (**Figure 2C**).[20] Indeed, an engineered FH fragment, mini-FH, composed of CCPs 1-4 and 19-20 connected by a short glycine linker, has been shown to bind equipotently to C3b and was also able to reduce C3b formation to an increased extent compared to FH, demonstrating that the broad middle region of FH is not necessary for functional activity.[22] Due to the functional importance of the C- and N-terminal domains, these have received most interest in the complement field. Therefore, only a few low resolution structures, obtained by a combination of NMR and small angle X-ray scattering, exist

for the broad middle part of FH, e.g. CPs 11-12, or for the whole protein.[23,24] The splicing variant FHL-1 is composed of the first seven CCPs of FH and therefore also has regulatory activity, but differs from FH in ligand and tissue specificity and in plasma concentration (1 µM) (**Figure 2C**).[20,25–27] Additionally to FH and FHL-1, the homologous family of FH-related (FHR) proteins exist, which are considered to be negative regulators of FH. All five FHRs are formed of CCPs, allowing them to bind to self-surfaces and C3b, however, they all lack the regulatory domains allowing for C3 convertase inhibition (i.e. CCPs 1-4 of FH). They are therefore thought to act as competitors for FH regulation. For example, FHR-5 comprises CCPs 10-14 and 19-20 of FH, allowing it to bind C3b, but not to act as FI cofactor compared to FH (**Figure 2C**).[20] A showcase of the similarity between the complement and the coagulation cascade are the structures of FH and coagulation factor XIII, which exists as heterotetramer of A and B subunits in circulation. Its regulatory units, FXIIIB, are also composed of CCP domains, and upon dissociation of the factor XIIIA units, release the active protease FXIIIA (in its dimeric form, $FXIIIA_2$). Functionally, this is reminiscent of the C1 complex, where changes in conformation allow the pre-formed protease dimer to become functional. FXIII was reported to cleave C5, but there are conflicting reports if the more abundant FXIIIB subunit interacts with complement proteins, e.g. C3, C3b or C4b, and may even exert complement-regulatory functions.[28–31] Therefore, to decipher the intricacies of complement-coagulation crosstalk remains a very active field of research.

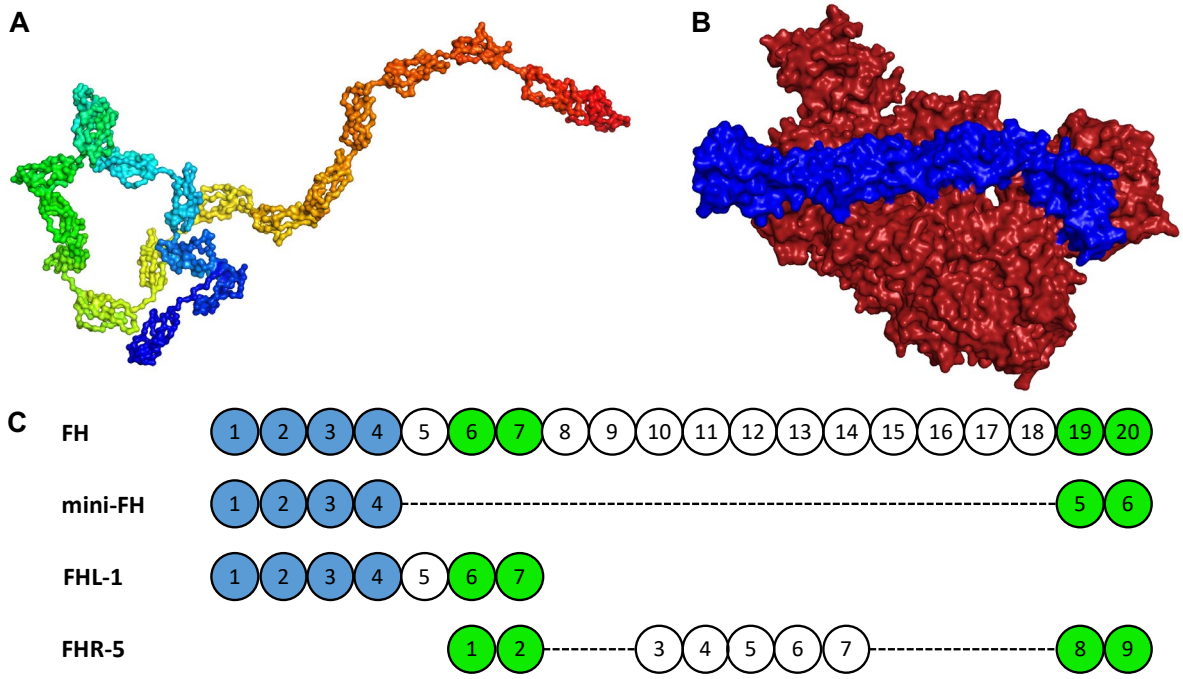

Figure 2: (**A**) Model of the solution structure of FH based on X-ray scattering data (PDB code: 3GAV), showing the 20 globular CCP domains aligned in a pearl string-like manner and connected by short linkers, color gradient from N-terminus (blue) to C-terminus (red). (**B**) Co-crystal structure of C3b (red) with FH's CCPs 1-4 (blue), showing a similarly extended arrangement as in the solution model with CCPs 2-4 and CCP 1 bend (PDB code: 2WII). (**C**) Domain architecture of FH, engineered mini-FH, splicing variant FHL-1 and homolog FHR-5. The regulatorily active domains are highlighted in blue, while the domains involved in self-recognition are highlighted in green.

PATHOPHYSIOLOGY

Complement's beneficiary yet also harmful contributions to a number of conditions, not necessarily as the only driving force but often as a critical contributor, have attracted increasing interest over the last years. Complement-mediated diseases can be generally attributed to one of three groups, i.e. excessive responses (hyperactivation), insufficiently regulated response or three, responses directed towards a target that should not trigger complement, i.e. a misguided response.[6] The most recent and prominent example for the devastating effects of complement hyperactivation are severe cases of coronavirus disease 2019 (COVID-19). The severity of the disease could be correlated to high

complement activation levels, suggesting that an overshooting reaction might contribute to the damage observed in organs such as the lungs and kidney, and would be particularly driven by the LP.[32–35] A typical disease with insufficient complement regulation is paroxysmal nocturnal hemoglobinuria (PNH). It is a somatic genetic disease in which hematopoietic progenitor cells, and consequently erythrocytes, lose the ability to synthesize the glycosyl phosphatidyl-inositol membrane anchor. As a consequence, erythrocytes are lacking DAF and CD59 and cannot sufficiently regulate complement activation anymore, leading to hemolysis, anemia and thrombotic complications.[36] Another disease with an unregulated complement response is IgA nephropathy (IgAN). IgAN patients are lacking full *O*-glycosylation in the hinge region of IgA1 immunoglobulins (the more common IgA class). This erroneous glycosylation pattern is then recognized by IgG and IgM, leading to characteristic immune complex deposits in the kidney and, consequently, impaired kidney function. The disease mechanism has not been fully understood to date, but antibody levels recognizing the erroneous IgA1s were demonstrated to correlate with the severity of the disease, as did complement products which were colocalized with the immune complex deposits. Interestingly, FHR-5 levels in the deposits correlated with disease severity, and inversely with FH levels, suggesting that an imbalance between FHR-5 and FH activity might distort complement regulation in IgAN. Beyond colocalization, *in vitro* data showed that MBL can recognize glycosylation patterns on IgA and consequently induce the LP. Furthermore, immune complexes may also activate the AP, providing possible links between the erroneous IgA1s and complement activation in IgAN.[37,38] For the third group of complement-mediated diseases, the misguided response can be directed towards altered self-tissues or to non-self surfaces of either biological or artificial origin. Ischemia-reperfusion injury (IRI) is a condition occurring when the blood flow is interrupted and then being restored again. It is observed upon stroke or cardiac arrest, but is also inevitable during transplantation. The underlying biology is complex, but it could be shown that both phases (i.e. ischemia and reperfusion) contribute to tissue damage. During the ischemic phase adenosine triphosphate (ATP) depletion leads to cell death, while upon restorage of blood flow, reactive oxygen species (ROS) are increasingly formed. Additional to this direct damage, immune pathways have been implicated in IRI, including the complement system. All pathways are involved, e.g. natural antibodies (antibodies present without prior immunization) have been shown to activate the CP, while an increase in fucose on cell membranes activated the LP and FB-knockout mice have been protected in a renal IRI model.[5,39,40] Complement is also heavily involved in antibody-mediated rejection (AMR) after transplantation, where donor-specific antibodies can activate complement and lead to tissue damage with C4d deposition, a degradation product of C4b, as maker for AMR in biopsies.[41] Similarly, due to complement's ability to react quickly and broadly to any non-self surfaces without complement regulators, it induces immune reactions to a number of artificial biomaterials, including liposomes, nanoparticles or hemodialysis filters.[42–44] These reactions typically include allergy-like symptoms such hypotension, dyspnea, chest tightness or fever and have therefore been referred to as 'complement activation-related pseudoallergies' (CARPAs), as they are occurring, in contrast to regular allergies, without the involvement of IgE.[45–48] Overall, CARPA is estimated to affect up to half a million patients in the US alone and has been described extensively for PEGylated liposomal drug formulations of the cytostatic doxorubicin (Doxil®, Caelyx®) and the antifungal amphotericin B (AmBisome®).[44,46,49–52] While the range of symptom severity is broad, including subclinical or very mild cases, CARPA can also have severe manifestations up to cardiogenic shock with a potentially deadly outcome. Additionally to the serious symptoms the patients are experiencing, the half-life and efficacy of the liposomes is reduced by CARPA.[53] The role of complement in these reactions has been well established, but exact contributions of different components are still under investigation. It could be shown that the size of the liposomes, lipid composition, charge and the drug itself (and here probably also the crystal type) play an important role, with higher net charge and larger liposome size being linked to more frequent CARPA.[46,47] Furthermore, the presence of PEG (polyethylene glycol) on the liposomes and anti-PEG antibodies in circulation have been shown to be particularly important, although antibody titers do not necessarily correlate with severity, probably due to different epitopes of the antibodies.[54,55] All complement pathways have been shown to

contribute, but when anti-PEG antibodies are involved, complement activation proceeds by CP and AP, or only AP, depending on the antibody types.[44,55]

COMPLEMENT-TARGETING THERAPEUTICS

Alongside the increased appreciation of complement's role in numerous disease areas, the interest to therapeutically target complement increased as well. Two events in particular fueled the activity in the complement drug discovery and development field: one was the publication of seminal studies in 2005 that a polymorphism in FH (Y402H) increases the risk for age-related macular degeneration (AMD) nearly three-fold and could explain more than 40% of all AMD cases.[56–58] In contrast to typical indications in the complement field (e.g. PNH or IgAN), which are rare diseases, AMD is a prevalent indication, affecting up to 3% of the population in the developed world.[59] It is a progressive, degenerative disease of the macula, the retinal region with the highest photosensor density, which is necessary for a focused sight. The progression of AMD eventually leads to blindness and is the leading cause of vision loss in the developed world.[60] The severity of the condition and the large number of affected patients has consequently attracted major interest from the pharmaceutical industry due to its commercial potential.[61] The second breakthrough was the development of the C5-targeting antibody eculizumab, culminating in its regulatory approval for PNH in 2007 as the first complement-specific drug on the market and important clinical validation of the approach.[62] Since then, indications for eculizumab have been extended and a successor with prolonged half-life (ravulizumab) has been approved.[61] Additionally, the complement drug discovery field in general has expanded regarding indications, targeted structures and drug modalities, now including small molecules, cyclic peptides, proteins (both antibodies and non-antibodies) and nucleic acids.[61,63,64] Since these defining moments, the AP proteases (i.e. FB, FD) and C3 received notable attention in drug discovery programs due to their central roles in various diseases. Blockade of the AP allows for substantial complement inhibition independently of the initiation pathway or in the occurrence of multiple pathway activation. While the anti-FD Fab fragment lampalizumab failed its clinical endpoints in phase III clinical trials for AMD, a phase II study for the antisense nucleotide IONIS-FB-L_{Rx} against the FB mRNA is currently in the recruitment phase, also for AMD.[65,66] Additionally, the small molecule FB inhibitor iptacopan (LNP023) is in clinical development in several indications, including IgAN.[61,67] The disappointing phase III trial results of lampalizumab have been suggested to be due to pharmacodynamic breakthrough, where small fractions of uninhibited FD might still lead to substantial activity due to its catalytic nature.[61] An alternative to inhibiting FB and FD without the risk of pharmacodynamic breakthrough is to block C3 directly and thereby prevent its cleavage. This was accomplished by the development of the compstatin family of peptidic C3 inhibitors, which prevent the binding of C3 to the convertase and broadly impair amplification and effector generation.[68] Pegcetacoplan, a pegylated derivative of compstatin, has been approved in May 2021 for PNH, while several compstatin analogs are being studied in other complement-mediated diseases.[68–70] Recognizing the central role of FH in AP inhibition, attempts to exploit its role for therapeutic applications are currently pursued. For example, it could be shown that supplemented FH can inhibit complement activation towards AmBisome® *in vitro*.[71] Furthermore, mini-FH and other engineered derivatives showed reduced C3 deposition *in vitro* and in FH-deficient mice, making this approach a promising approach under conditions with reduced FH concentration or function.[72,73]

Despite the successful preclinical application of systemic complement inhibition in altered self or non-self triggered complement responses, e.g. ischemia-reperfusion injury[74–79], clinical application has produced mixed results thus far[75,80–83] Eculizumab as anti-C5 therapy met its clinical endpoints for early AMR[84] but not in chronic AMR or IRI[41,85]. As an alternative to these approaches relying on systemic inhibition for biomaterial-induced complement activation, local inhibition is expected to be a superior approach due to reduced systemic side effects and stronger local efficacy, considering that complement is largely a surface-directed system. Interestingly, in contrast to the coagulation system, local inhibition of the complement system is scarcely employed as a therapeutic approach.[86–88] To achieve local AP inhibition, FH has been immobilized directly and successfully on polystyrene

surfaces.[89,90] However, applying this strategy in a clinical setting would require large quantities of FH (up to 4 pmol/cm^2, approx. 0.6 µg/cm^2)[12] and sufficient recombinant production is challenging, with similar limitations applying to the engineered FH analogs.[73] Similarly, a fusion protein between FH and CR2 (as a tether for surface-bound C3 degradation products) was shown to almost completely abolish AP activation in monkeys.[87] All these approaches validated functionally the importance of FH in complement-mediated conditions and its potential for therapeutic applications, despite the drawback protein-based drugs can hold, including intricate and costly production or potential immunogenicity.
Interestingly, similar strategies (i.e. FH-recruitment to a surface) for complement evasion can be found in nature. Many pathogens exploit FH-mediated complement protection by expressing FH-binding molecules on their surface, allowing them to recruit FH from the blood stream and, consequently, protect themselves from complement attack. More than 40 pathogens of different origin, including the bacterium *Neisseria meningitidis* and the protozoon *Trypanosoma brucei* (the cause of sleeping sickness), use this tactic, illustrating the broad relevance of this approach.[91–93] Inspired by natural complement evasion, we previously described the discovery of a 14 amino acid-long disulfide-bridged cyclic peptide (5C6) by phage display (**Figure 3**). It was able to potently bind FH with a dissociation constant (K_D) of approx. 100 nM and suppress C3b deposition. As 5C6's binding region could be determined to be located between CCPs 5-18 of FH, it is not interfering with FH's regulatory activity.[94] Furthermore, when immobilized using PEG-lipids as surface tethers, 5C6 could recruit FH to cell surfaces as well as inhibit complement activation from whole blood on model surfaces (**Figure 3C**).[95] This established 5C6 as yet another promising peptide-based therapeutic strategy in the complement field.

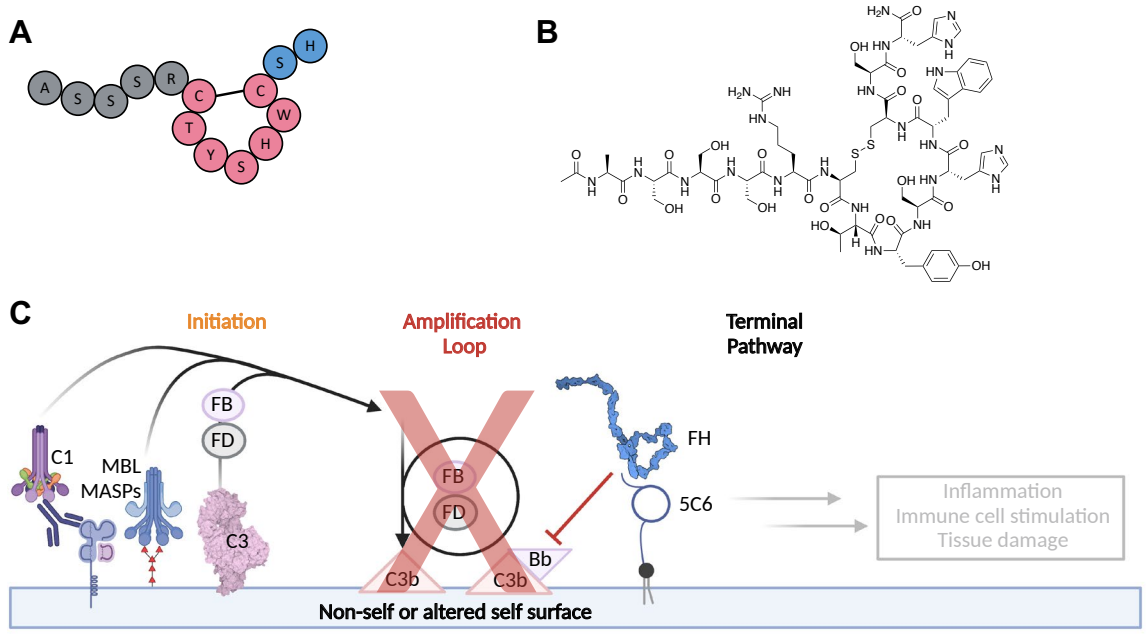

Figure 3: (**A**) Schematic and (**B**) chemical representation of the FH-binding peptide 5C6 with the exocyclic N-terminus colored in grey, the core cycle in purple and the exocyclic C-terminus in blue. (**C**) Therapeutic principle of 5C6. Independently of the initiation pathway, FH recruited by 5C6 to surfaces inhibits the central amplification loop and consequently downstream effect such as inflammation, immune cell stimulation or tissue damage.

PEPTIDES AS THERAPEUTICS

Beyond complement therapeutics, the application of peptides as a drug modality has also found increased application in various other indications. Traditionally, peptides have been mainly used for peptide hormone replacement therapies, such as insulin in diabetes, where the peptide as pharmaceutically active principle has been isolated from animal sources. Advances in recombinant biological production and synthesis has advanced the field further, leading to the development of very

small peptides with profound low-molecular-weight drug character, such as angiotensin-converting enzyme (ACE) inhibitors against hypertension. The number and complexity of developed peptides has been increasing since the 1990s with the regulatory approval of 52 peptide drugs in the period from 2000 to 2019 compared to just 5 between 1960 and 1979; peptides now cover a broad range of indications, including metabolic and endocrine indications, oncology and reproductive medicine.[96–98] Peptides, often defined as polymers of up to 50 amino acids, have long been considered not suitable as drugs due to their high molecular weight, polarity and proteolytic susceptibility. When compared to small molecules fulfilling Lipinski's rule of five or related physicochemical criteria, peptides typically lack oral bioavailability and feature low cell permeability.[96,99–102] However, based on developments in the broader drug discovery field as well as in peptide and organic chemistry, this perception has changed over the past decades.[99]

Research and development (R&D) productivity for drugs declined over the last decades, e.g. due to increasing challenges to continuously improve on the current standard of care. This made it necessary to address known biological targets by new means or new targets altogether.[103] For example, protein-protein interactions (PPIs) have been increasingly recognized to be pivotal in many biological processes. However, PPIs are typically mediated by shallow yet large interaction surfaces of up to 6000 $Å^2$, which are challenging to target with small molecules when compared to defined substrate pockets of enzymes as a classical target class for small molecules.[104] This required the development of new screening methods for small molecules using fragment-based methods, with limited successs,[104–106] but mainly sparked interest in new drug modalities beyond (or between) traditional small molecules and antibodies.[107] The term "new modalities" summarizes several different drug formats, but mostly designates modified peptides, proteolysis targeting chimeras (PROTACs) and nucleic acid-based approaches.[107] Additionally, in the field of autoimmune diseases, approaches are pursued where the epitope responsible for the autoimmune response is immobilized on a polymer and thus sequesters the disease-causing autoantibodies. The complexes are then degraded by phagocytes.[108] This approach can also be considered as a new modality with a similar aim as PROTACs, i.e. enabling the degradation of a disease-causing protein. Finally, new strategies also include mixed modalities, such as peptide-drug or peptide-lipid conjugates, in which two entities are combined with one being, for example, a targeting moiety for a specific tissue or cell-type, while the other moiety is the actual pharmacological effector molecule. Especially glycopeptides as a mixed modality have been considered as important research tools and potential therapeutic options due to the important role of protein glycosylation in autoimmune diseases such as IgAN or oncology, of which glycopeptides are obvious mimics.[107,109–111] All these new modalities specifically address the shortcomings of the traditional modalities, e.g. small interaction surface and promiscuity of small molecules or lack of cell penetration of antibodies, or circumvent related issues based on completely novel modes of action.

Within this group of new modalities, peptides and especially macrocyclic peptides, are ideally positioned to target PPIs, not tractable with small molecules or antibodies. Due to their larger size, peptides can disrupt PPIs or form *de novo* interactions with protein surfaces. They are also highly three dimensional due to the high ratio of sp^3-hybridized atoms, a property that was identified to be beneficial for successful development.[112] Furthermore, as poly-amino acids, peptides and proteins have an identical composition and peptides can adopt secondary or even tertiary structures, thus constituting the interaction interface of a PPI. However, linear peptides are usually highly flexible with only a limited number of conformations binding to the target, which leads to a strongly unfavorable binding entropy. Macrocyclic peptides, obtained by intramolecular reaction of linear peptide precursor and giving rise to a cyclic system with at least 12 atoms within the ring system[113], can be employed to address this problem. The macrocycle constrains the conformational freedom and therefore reduces the entropic penalty upon binding. Peptides can by cyclized either using functionalities on their side chains or on the N- or C-terminus, and have been used to stabilize specific secondary structures (i.e. stapled peptides) or to obtain completely novel and unique structures.[107,114–119]

Despite the advantages peptide drugs hold, some disadvantages also exist. Although smaller than antibodies (<5000 Da), peptides are usually not cell permeable. However, this can be achieved by conjugation to cell-penetrating peptide sequences or, in some cases, by passive mechanisms.[120,121] Cell-penetrating peptides have also been associated with cell toxicity (due to their membrane-disruptive potential based on high net positive charge), warranting some caution in their application.[107] Other approaches used to increase cell permeability (or affinity) include the use of D-amino acid and *N*-methylated residues, which are usually applied systemically by replacing residues one by one to determine the effect.[97]

This approach can also be used to tackle another major disadvantage of peptides, their proteolytic susceptibility. Cyclization, N-methylation and the use of D-amino acids provide large benefits as they strongly increase stability in circulation, typically increasing the half-life from the range of minutes to hours or even days.[119,122,123] Once degraded, peptides (linear or cyclic) show another strength: as their metabolic products are simple amino acids, peptide drugs have a very low toxicological risk, contributing to their consideration as very promising drug modality.[96,97]

All these approaches can be combined and pushed even further by replacing amides entirely or by merely using scaffolds projecting functional groups in an arrangement similar to a peptide, fading the difference between peptides, peptidomimetics and small molecules.[117,124] To classify this spectrum, a terminology based on the degree of modification compared to a native peptide has been established. Class A peptidomimetics are largely composed of α-amino acids with only minor modifications, while class B peptidomimetics contain more substantial changes to the peptide structure and can contain, for example, β-amino acids or non-amino acidic building blocks. Finally, class C and D peptidomimetics only exploit a peptide as template for a functional group arrangement or mode of action, respectively, and have a largely small molecular character.[124]

Overall, all these advances in the drug discovery of macrocyclic peptides would not have been possible without important progress in structural biology, synthetic chemistry and display technology. Structural biology elucidated more and more protein structures, allowing for a rational design of inhibitors in particular of protein mimetics, which mimic as well the tertiary structure of a protein.[103,125,126] Peptides can be obtained by chemical synthesis, allowing access to specifically tailored molecules in a more convenient way when compared to biotechnologically produced modalities. Solid-phase peptide synthesis (SPPS), described for the first time in 1963, enabled the rapid and parallel synthesis of peptides, including the compatibility with a large number of commercially available non-proteinogenic amino acid building blocks.[127,128] Additionally, ever-more selective reactions allow precise modifications on complex molecules containing a variety of functional groups, such as peptides, without the need for complex protecting group strategies. The ring-closing metathesis (RCM) reaction has proven particularly valuable due to its high specificity, usually high yields and applicability to numerous peptides, in particular for secondary structure stabilizations.[116,124,129] Among the many reactions used to form peptide macrocycles, photocatalytic and C-H activation reactions are increasingly used, giving access to novel chemical space and expanding cyclizations far beyond the amide and disulfide formations traditionally used.[119,130–132]

Finally, the advent of display technologies in which a "phenotypic" molecular structure is linked to a distinct genotypic, information-carrying group, such as RNA or DNA, enabled fast discovery of highly potent ligands due the huge numbers of compounds these libraries allow to screen (10^6 – 10^{14}, depending on the method and molecule size).[133–135] Genetically encoded evolutionary display technologies, i.e. phage display and mRNA display, are particularly useful to discover peptidic ligands. They not only allow to screen a library but also to select, i.e. enrich and develop towards, more potent ligands as the translational machinery can be used to directly translate the encoded sequence into the peptide sequence.[135] Importantly, cyclization methods compatible with these display technologies exist, which allow to select the already cyclized compound. This is particularly useful as it can be challenging to introduce a conformational constraint (such as a cyclization) during subsequent hit optimization without structural knowledge about the interaction.[119,135] Furthermore, substantial progress has been made in DNA-encoded libraries (DEL) to unravel reaction conditions compatible

with DNA for macrocyclizations, such as RCM under aqueous conditions. Peptidomimetic DELs with large side chain and backbone structures and functionality diversity have been reported, pushing forward the speed at which a highly varied chemical space can be accessed.[119,136] Pegcetacoplan, as a phage-display discovered cyclic peptide, demonstrates that hits obtained from display technology indeed enable the successful development of new drugs.[70]

In summary, cyclic peptides are ideally suited as next-generation therapeutics, especially for immunological conditions as many molecular interactions occur extracellularly. While having protein therapeutic-like affinity and selectivity, peptides are also synthetically accessible and tunable similar to small molecules. Cyclization strongly increases stability towards proteolytic degradation (one of the two major shortcomings of linear peptides) while progress is being made to increase the low membrane permeability of peptides (the other major shortcoming). Finally, by conjugation to targeting groups or other modifications, such as glycosylation, the selectivity can even be further increased.

AIMS

Modified peptides are a particularly promising drug modality to precisely target the intricate host-defense pathways. In this thesis, several aims based on this overarching principle were pursued. To start with, we wanted to give a short overview on how peptidic drug modalities can be developed to target host defense pathways as well as giving an overview on macrocyclization reactions for peptides (results chapter 1 and 2).[98,119] The main aim of the thesis, however, is focused on the characterization and optimization of 5C6 to enable its development as a possible therapeutic candidate for complement-mediated conditions such as CARPA. Although proof-of-concept studies on 5C6 had been performed[94,95], the knowledge about the structure-activity relationship (SAR) and the potential for further optimization for affinity and stability have remained limited. One aspect of the work was therefore to investigate in-depth individual residues for improvements in affinity, activity and stability, and to detect opportunities to replace the native disulfide bridge with other functional groups. This could give access to more reductively stable analogs while maintaining affinity; and ideally, to develop 5C6 towards a class A or B peptidomimetic. Furthermore, this would allow to introduce a cysteine for surface immobilization without the need for orthogonal protecting groups strategies. In addition to the SAR on the peptide sequence, there was only limited knowledge on spacing and surface tethering requirements for FH recruitment, on which we wanted to expand here. Also, selectivity, specificity, and activity are crucial for a good drug development candidate. Therefore, we aimed to determine the target selectivity in general but also explicitly for FHR-5, which is highly similar to the 5C6's binding region in FH. We also wanted to determine if 5C6 can bind FH of other species, necessary for preclinical development in vivo. Furthermore, we aimed at developing assays that would closely mimic clinical conditions such as CARPA and assess 5C6's activity in those assays to evaluate the translational value (results chapter 3 and 4).

Additionally, we expanded our approach to develop therapeutic strategies to target complement-mediated conditions for another condition with complement involvement, i.e. IgAN. We aimed at developing an approach using a polymer-immobilized glycopeptide to assess if sequestering of disease-causing autoantibodies of IgAN patients is achievable and to improve the synthesis of the challenging 20-mer glycopeptide (results chapter 5).

Finally, we wanted to further elucidate the crosstalk between the complement and coagulation cascade, highly relevant in thromboinflammatory conditions such as biomaterial-induced host defense reactions. Therefore, we performed binding and functional studies with FXIII to understand whether its structural similarity to FH translates into a similar repertoire of binding partners and activity (results chapter 6).

RESULTS

Review Article

CHAPTER 1: THERAPEUTIC PEPTIDES AS EMERGING OPTIONS TO RESTORE MISGUIDED HOST DEFENCE AND HOMEOSTASIS: FROM TEACHING TO CLINIC

Oliver Schwardt[1], Christina Lamers[1], Clément Bechtler[1], Daniel Ricklin[1]

[1] Molecular Pharmacy Group, Department of Pharmaceutical Sciences, University of Basel, Basel, Switzerland

Corresponding author:
Prof. Dr. D. Ricklin, E-mail: d.ricklin@unibas.ch
University of Basel, Department of Pharmaceutical Sciences, Klingelbergstrasse 50, CH-4056 Basel, Switzerland

Reference:
Schwardt, O.; Lamers, C.; Bechtler, C.; Ricklin, D. Therapeutic Peptides as Emerging Options to Restore Misguided Host Defence and Homeostasis: From Teaching to Concept to Clinic. *Chim. Int. J. Chem.* 2021, 75 (6), 495–499. https://doi.org/10.2533/CHIMIA.2021.495.

Contributions of Clément Bechtler:
- Manuscript preparation

doi:10.2533/chimia.2021.495 Chimia 75 (2021) 495–499 © O. Schwardt, C. Lamers, C. Bechtler, D. Ricklin

Therapeutic Peptides as Emerging Options to Restore Misguided Host Defence and Homeostasis: From Teaching to Concept to Clinic

Oliver Schwardt, Christina Lamers, Clément Bechtler, and Daniel Ricklin*

Abstract: Among the many molecular entities suitable for therapeutic use, peptides have emerged as a particularly attractive option for academic drug discovery and development. Their modular structure and extendibility, the availability of powerful and affordable screening platforms, and the relative ease-of-synthesis render therapeutic peptides highly approachable for teaching and research alike. With a strong focus on the therapeutic modulation of host defence pathways, including the complement and renin-angiotensin systems, the Molecular Pharmacy group at the University of Basel strongly relies on peptides to introduce students to practical aspects of modern drug design, to discover novel therapeutics for immune and inflammatory diseases, and to expand on options for the preclinical development of a promising drug class. Current projects reach from student-driven iterative design of peptidic angiotensin-converting enzyme inhibitors and the use of phage display technology to discover novel immune modulators to the development of protective peptide coatings for biomaterials and transplants and the structure-activity-relationship-guided optimization of therapeutic peptide drug candidates in late-stage clinical trials. Even at the current stage, peptides allow for a perfect circle between pharmaceutical research and education, and the recent spark of clinical applications for peptide-based drugs may only increase the value and relevance of this versatile drug class.

Keywords: ACE inhibitors · Complement · Host defence · Phage display · Peptide therapeutics

1. Coming Full Circle: Peptides as Central Element of Pharmaceutical Research and Education

Uniquely situated between low-molecular-weight (LMW) drugs and 'biologics' such as antibodies, therapeutic peptides represent a versatile class of pharmaceutical compounds consisting of amino acid chains (usually less than 40 residues).[1] Originally, therapeutic peptides have been gained solely from natural sources such as animal tissue as exemplified by the isolation and first clinical use of insulin in the 1920s in diabetic patients. Progress in sequence elucidation, chemical synthesis and biotechnology allowed for the rational design, *de novo* synthesis and large-scale production of peptidic drugs, leading to the approval of more than 100 therapeutic peptides spanning various clinical indications.[2] When compared to the development of LMW drugs, which often require synthesis routes tailored to a specific class, the modular structure and defined, automatable production (*i.e.* solid-phase peptide synthesis; SPPS) render peptides more easily available, particularly for academic institutions. In addition, *in vitro* selection methods, such as phage and mRNA display, enable the generation of large peptide libraries for screening purposes.[3] Since its first report,[4] phage display has evolved into an accelerator of hit generation for both antibody and peptide drugs.[5] The library is displayed on an outer membrane protein of the phage, such as pIII or pVIII, and can reach a diversity of $>10^9$ molecules. By linking the phenotype of a peptide library with its genotype, phage display facilitates deconvolution of identified hits. The advantage of phage display, *e.g.* compared to DNA-encoded libraries and mRNA display, is the use of bacteriophages as vector, which enables amplification of affinity-selected phages in *E. coli*. In recent years, the introduction of chemically-modified phage libraries that enable *in situ* macrocyclization to render peptides more stable and drug-like further increased its usability.[6] In mRNA display, a peptide library is covalently linked to its encoding mRNA during the translational process. The use of *in vitro* transcription and translation allows for easy incorporation of noncanonical amino acids and avoids transformation steps that can limit the diversity of phage libraries.[7]

Their high clinical relevance, accessibility and affordability greatly facilitates an integration of peptide drugs into the practical training of students while, at the same time, enabling academic drug discovery (Fig. 1). At the Department of Pharmaceutical Sciences of the University of Basel, therapeutic peptides have not only evolved to a recurrent theme in teaching and research but also provide valuable anchor points to Basel's vibrant academic and industrial environment.

2. Therapeutic Peptides in Teaching: The Lab Course 'Modern Drug Design'

Among the most valuable features of peptide drugs is that initial lead compounds can often be derived from natural sources (*e.g.* scissile loops as protease inhibitors) and further optimized or developed into LMW drugs. Inhibitors of the angiotensin-converting enzyme (ACE) are prominent examples, which we employ for educational purposes. The laboratory course 'Modern Drug Design' offers bachelor students in pharmaceutical sciences a hands-on experience in the rational design, synthesis, and biological evaluation of potential drug candidates (Fig. 2).[8] ACE, an endopeptidase, is a central component of the renin-angiotensin-

*Correspondence: Prof. Dr. D. Ricklin, E-mail: d.ricklin@unibas.ch
University of Basel, Department of Pharmaceutical Sciences, Klingelbergstrasse 50, CH-4056 Basel, Switzerland

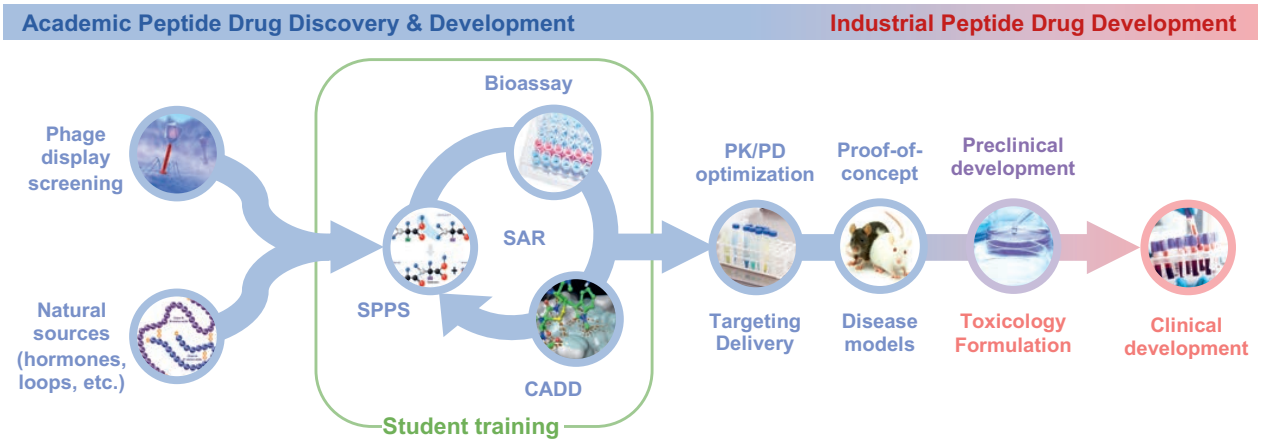

Fig. 1. Opportunities for integrating peptide therapeutics in academic research and education. Phage display libraries or natural proteins often serve as source or inspiration for peptide drug leads, which are then optimized through iterative cycles of solid-phase peptide synthesis (SPPS), evaluation in bioassays and computer-aided drug design (CADD) to obtain structure-activity relationships (SAR). Whereas initial development steps can often be conducted in academic labs, preclinical and clinical development is typically performed by industrial partners.

aldosterone system (RAAS), the body's most important blood pressure-regulating mechanism.[9] Within the RAAS cascade, ACE mediates the conversion of angiotensin I to the vasoconstrictor angiotensin II but also mediates the degradation of bradykinin. Consequently, inhibiting ACE impairs the formation of angiotensin II, thereby lowering blood pressure by reducing smooth vascular muscle contraction and peripheral resistance.[9] A nonapeptide inhibitor isolated from a snake venom, called teprotide, served as lead compound for ACE inhibitors but was not orally active.[10] However, systematic structure–activity relationship (SAR) analysis of peptidic ACE inhibitors and synthetic derivatives thereof led to the development of captopril, the first orally active ACE inhibitor approved for antihypertensive therapy.[11] Derivatives with improved efficacy and adverse effect profiles, such as enalapril, lisinopril, and ramipril, have subsequently been introduced to the market.[9b]

Developing next-generation ACE inhibitors is, of course, not the aim of the 'Modern Drug Design' course, but this drug class offers a highly illustrative example for iterative drug development. In the first part of the laboratory course, small peptidic ACE inhibitors (usually tripeptides with C-terminal proline) are identified by computer-aided drug design based on the experimental structure of the ACE-enalapril complex, and their potency is estimated *in silico*. Alongside good affinity and selectivity, ideal compounds should also show a balanced pharmacokinetic profile (PK; *e.g.* polar surface area, number of hydrogen-bond donors and acceptors). Thereafter, the most promising ACE inhibitor candidates are synthesized using SPPS. Starting from the preformed Fmoc-Pro-Trityl-solid support, tripeptides are obtained after two cycles of *N*-deprotection and coupling using natural and/or non-natural amino acid building blocks. The peptides are then cleaved from the solid phase and analyzed by HPLC and MS. Finally, the crude peptides are purified by preparative LC-MS. In the final stage of the lab training, the ACE inhibitory activity of the peptides is determined in a competitive fluorometric assay based on chromogenic substrate cleavage (*i.e.,* Abz-Gly-(*p*-NO_2-Phe)-Pro). The best inhibitors obtained in the practical course usually show IC_{50} values in the single-digit micromolar range, which is about 1000-fold weaker than the potency of commercial ACE inhibitors such as enalapril and captopril (Fig. 2).[12] The communication of the results to the next class of students allows for an iterative improvement of the design strategy.

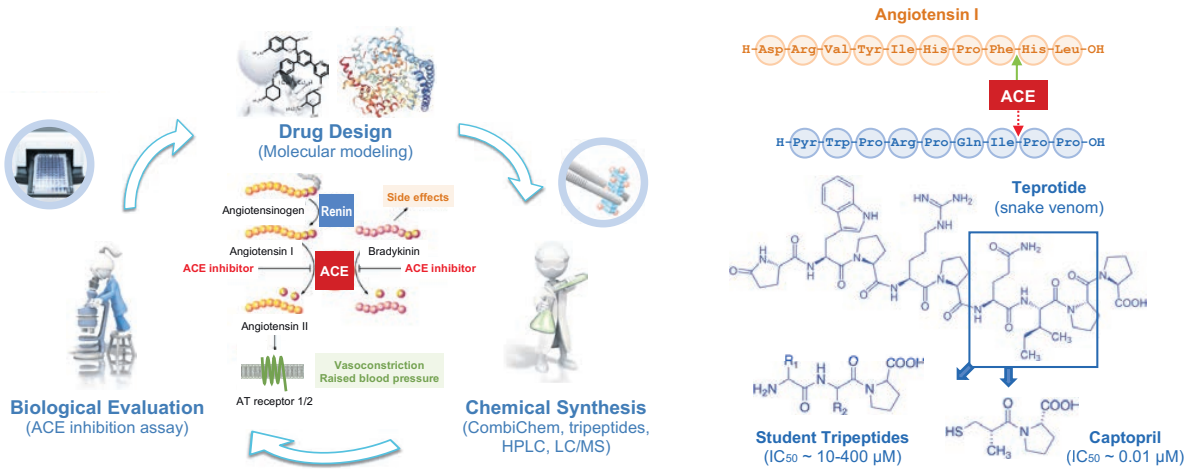

Fig. 2. Peptide-focused practical course 'Modern Drug Design' at the University of Basel. Based on the structure of enalapril-complexed angiotensin-converting enzyme (ACE), students use molecular modeling to design tripeptidic ACE inhibitors, synthesize them in the lab, evaluate their ACE-inhibitory potency and report results to subsequent student groups to enable iterative lead optimization.

3. Therapeutic Complement System Inhibition Using Peptide Drugs

In contrast to the educational project above, efficacy, selectivity and PK properties become highly relevant in drug discovery research. Compared to LMW drugs, peptide therapeutics typically feature low oral bioavailability and cell permeability but often show beneficial selectivity and safety profiles. In addition, their size facilitates a use as protein–protein interaction (PPI) inhibitors. These properties render peptide drugs ideally suited as therapeutic modulators of the plasma-based cascade systems that are central to host defence pathways, including the complement, coagulation and contact systems. While providing rapid protection against breached barriers and microbial invasion (*e.g.* after injury), the limited specificity of these defence pathways may turn them against the host and contribute to clinical complications in age-related, autoimmune or thromboinflammatory conditions.[13] During organ transplant rejection or COVID-19, for example, hyperacute activation of several pathways may induce tissue damage.[14] In such cases, rapid inhibition of the PPI-driven cascade systems becomes critical, whereas bioavailability and permeability are of low importance. With a focus on the complement system, our group investigates therapeutic strategies to curb erroneous host defence activity using peptides.

As integral part of humoral innate immunity, the complement system serves as fast-reacting pathogen and danger sensor that recognizes a broad spectrum of non-self (*e.g.* bacteria) and altered-self surfaces (*e.g.* apoptotic cells) and induces an appropriate immune response.[15] The detection of molecular patterns such as antibody complexes or microbial carbohydrate signatures triggers an activation cascade that involves some 50 proteins, including serine proteases, receptors and regulators, and generates potent effectors that lead to lytic or phagocytic cell removal and stimulate downstream immune responses (Fig. 3A). The spatio-temporarily controlled activation of three orthologous plasma proteins (*i.e.* C3, C4, C5) by protease complexes is central to this process. C3 convertases assembling on activating surfaces cleave C3 into the chemoattractant C3a and the opsonin C3b, which covalently binds to the surface through its thioester and tags the cell for immune processing. C3b can form new C3 convertases, which fuels an amplification loop and generates C5 convertases that activate C5 to produce the anaphylatoxin C5a and initiate the generation of lytic membrane-attack complexes (MAC). While host cells are typically protected from complement attack by regulators, any disruption of the delicate activation-regulation balance may cause clinical complications.[16] For example, a lack of regulators on erythrocytes leads to the rare yet severe haemolytic disease paroxysmal nocturnal haemoglobinuria (PNH). During organ transplantation, hypoxia leads to complement-mediated ischemia-reperfusion injury by exposing damage-associated patterns, whereas binding of antibodies to the foreign organ triggers a complement response that may lead to organ rejection.[16]

Despite the strong disease involvement of complement, the therapeutic arsenal is currently restricted to antibodies (*i.e.* eculizumab, ravulizumab) that act as PPI inhibitors of C5 activation, thereby preventing the generation of C5a and MAC.[17] While successfully used in PNH and other diseases, these antibodies are expensive and ill-suited for self-administration. Moreover, C5 may not be the ideal target for certain indications. Owing to the prevalence of PPI within the complement cascade, therapeutic peptides have emerged as intriguing options for complement inhibition. Indeed, macrocyclic peptides preventing the activation of C3 (*i.e.* pegcetacoplan, AMY-101), C5 (*i.e.* zilucoplan) or C5a receptor 1 (*i.e.* ALS205), or impairing initiation steps (*i.e.* RLS-0071) are in active clinical evaluation (Fig. 3A).[17a] Several administration options, including subcutaneous, intravitreal and even oral delivery are considered for complement-targeted peptides.

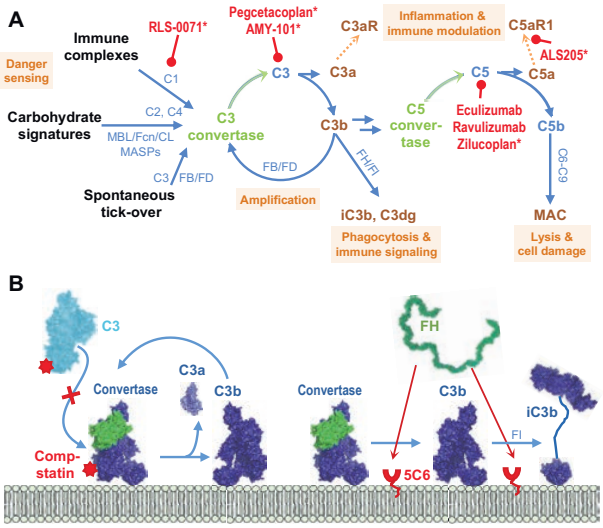

Fig. 3. A) Schematic overview of the complement system. Recognition of pathogen- or damage-associated signatures induces a cascade that generates inflammatory mediators and helps eliminating intruders. Yet, complement activation on host cells or biomedical surfaces contributes to various clinical conditions, thereby providing an attractive target for therapeutic interaction. Alongside two approved drugs (*i.e.* eculizumab, ravulizumab), several complement-targeted peptide therapeutics are currently in clinical evaluation (marked with an asterisk). B) In addition to blocking complement activation in circulation (*e.g.* by compstatin), biomedical surfaces may be protected using peptide coatings (*e.g.* 5C6) that attract host regulators such as factor H (FH).

Alongside their peptidic nature, these drug candidates all have in common that they block complement in circulation.[17a] At least in biomaterial- or transplant-associated reactions, preventing complement activation directly on the foreign surface may be more efficient. Moreover, this approach has the advantage to reduce complement activation *in situ* without concomitant systemic complement inhibition. Our group therefore develops peptide-based surface coatings to recruit circulating host regulators to biomedical surfaces and protect them from complement attack (Fig. 3B). Notably, a similar strategy is employed by various pathogens that express regulator-binding proteins as part of their immune evasion mechanism; as major complement regulator in solution and potent inhibitor of the central amplification loop, factor H (FH) is a particularly attractive target.[18] Following this nature-inspired approach, a 14-amino-acid long, cyclic peptide (termed 5C6; ASSSR[CTYSHWC]SH) was discovered by phage display screening. 5C6 showed nanomolar affinity for FH and was able to recruit FH to biomedical surfaces without affecting the regulator's functional activity.[19] The potential of 5C6 could be demonstrated in models where phospholipid-coupled 5C6 was inserted into cell membranes and impaired complement activation on erythrocytes and endothelial cells.[19,20] Currently, we are performing in-depth SAR studies to evaluate the importance of key residues, cyclization options and tethering strategies for the efficacy and stability of the peptide coating, with the aim to assess 5C6-derived options in preclinical models of complement-related diseases.

4. From Discovery to Clinic: The Compstatin Experience

The immense potential of peptide-focused academic drug discovery can be exemplified by the development of the compstatin family of C3 inhibitors (Fig. 4). The initial lead compound, compstatin, was identified at the University of Pennsylvania in 1996 using phage display technology.[21] While screening a li-

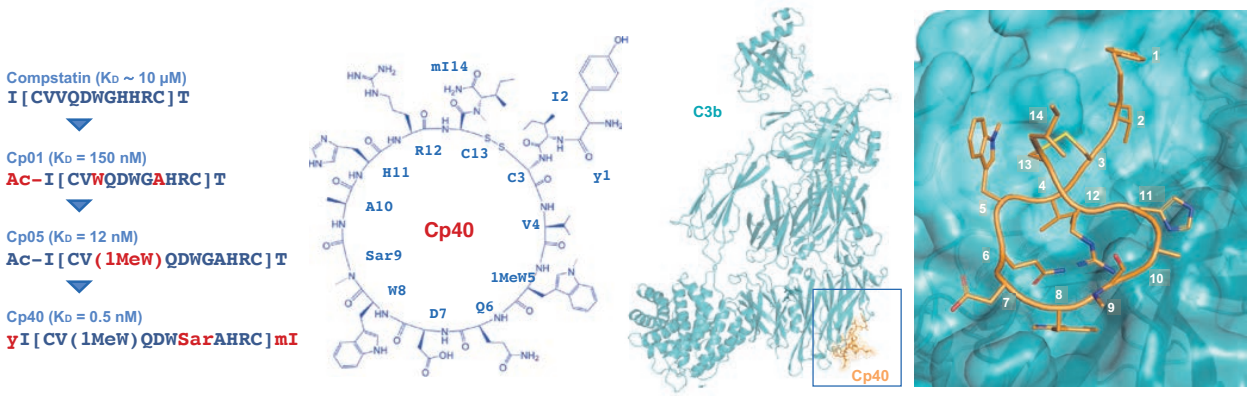

Fig. 4. Development of the compstatin family of peptidic C3 inhibitors. Starting from the initial lead, sequence optimization led to derivatives with largely improved affinity, resulting in the subnanomolar analog Cp40. Compstatin analogs tightly fit into a shallow binding site in the macroglobulin core of C3 and C3b, which mediates the interaction of C3 with the convertase.

brary of 27mer peptides against C3b, a 13 amino acid sequence containing one disulphide bridge was identified as potent binding motif. Initially guided by alanine scans and NMR structures, stepwise optimization through N-terminal acetylation and mutation of positions 4 and 9 resulted in the first nanomolar lead analogue Cp01.[22] Solving the crystal structure of target-bound Cp01 facilitated lead development and suggested that compstatin analogues act as PPI inhibitors that prevent the binding of C3 to the convertase, thereby impairing opsonization, amplification and effector generation.[23] The introduction of a non-proteinogenic amino acid (1-methyl-Trp) at position 4 produced analogue Cp05 with 12 nM affinity and good plasma stability,[24] while backbone *N*-methylation scans and N-terminal extension revealed next-generation compstatin derivatives (Cp10-Cp40) with enhanced target residence and PK profiles.[25] Thanks to strong academic collaboration, and despite a narrow species specificity for human/primate complement, compstatin derivatives were successfully evaluated in various preclinical models, which fuelled clinical development efforts.

Pegcetacoplan (Apellis), containing two Cp05 molecules bridged by a 40-kDa PEG moiety, has recently shown superiority to eculizumab in phase 3 clinical trials in PNH and is also developed for age-related macular degeneration and other indications.[26] Owing to its subnanomolar target affinity and beneficial PK properties, the Cp40-based candidate drug AMY-101 (Amyndas) can be administered in a non-PEGylated form and is currently being evaluated in phase 2 clinical trials for gingivitis and in COVID-19 patients.[27] Alongside its clinical success, compstatin provides an ideal model to explore optimization strategies for peptide therapeutics, including the introduction of albumin-binding tags, cystathionine bridges or charge/solubility modulators, among other examples.[28] Finally, recent SAR studies by our group on the interaction between Cp40 and C3b (Fig. 4) revealed surprising roles for structural water and intramolecular peptide interactions that may guide the future development of this promising drug class (Lamers *et al.,* under review).

5. Conclusion and Outlook

Peptide therapeutics have not only evolved into a rapidly emerging drug class with numerous clinical applications, particularly as PPI inhibitors to modulate erroneous host defence reactions, but also present an educational and experimental treasure chest for academic drug discovery and development. Recent advances in phage display, peptidomimetic design, targeting and peptide drug delivery paint a bright picture of the journey ahead.

Acknowledgements

The practical course 'Modern Drug Design' was introduced to the B.Sc. Pharmazeutische Wissenschaften of the University of Basel by Prof. em. Beat Ernst and Prof. Angelo Vedani†. In addition to the authors, Prof. Markus Lill, PD Dr. Martin Smieško, PD Dr. Said Rabbani, and several assistants of the Molecular Pharmacy and Computational Pharmacy groups at the Department of Pharmaceutical Sciences are involved in the current curricula. The compstatin and 5C6 technologies were discovered in the laboratory of Prof. John D. Lambris (University of Pennsylvania, Philadelphia, USA) and licenced to Apellis and Amyndas Pharmaceuticals. This work was supported by a grant from the Swiss National Science Foundation (31003A_176104 to DR).

Received: April 15, 2021

[1] J. L. Lau, M. K. Dunn, *Bioorg. Med. Chem.* **2018**, *26*, 2700, https://doi.org/10.1016/j.bmc.2017.06.052.
[2] M. Muttenthaler, G. F. King, D. J. Adams, P. F. Alewood, *Nat. Rev. Drug Discov.* **2021**, *20*, 309, https://doi.org/10.1038/s41573-020-00135-8.
[3] C. Sohrabi, A. Foster, A. Tavassoli, *Nat. Rev. Chem.* **2020**, *4*, 90, https://doi.org/10.1038/s41570-019-0159-2.
[4] G. P. Smith, *Science* **1985**, *228*, 1315, https://doi.org/10.1126/science.4001944.
[5] A. E. Nixon, D. J. Sexton, R. C. Ladner, *MAbs* **2014**, *6*, 73, https://doi.org/10.4161/mabs.27240.
[6] C. Heinis, T. Rutherford, S. Freund, G. Winter, *Nat. Chem. Biol.* **2009**, *5*, 502, https://doi.org/0.1038/nchembio.184.
[7] Y. Huang, M. M. Wiedmann, H. Suga, *Chem. Rev.* **2019**, *119*, 10360, https://doi.org/10.1021/acs.chemrev.8b00430.
[8] A. Vedani, O. Schwardt, S. Rabbani, B. Ernst, *Chimia* **2006**, *60*, 70, https://doi.org/10.2533/000942906777675137
[9] a) K. E. Bernstein, Z. Khan, J. F. Giani, D. Y. Cao, E. A. Bernstein, X. Z. Shen, *Nat. Rev. Nephrol.* **2018**, *14*, 325, https://doi.org/10.1038/nrneph.2018.15; b) K. E. Bernstein, F. S. Ong, W. L. Blackwell, K. H. Shah, J. F. Giani, R. A. Gonzalez-Villalobos, X. Z. Shen, S. Fuchs, R. M. Touyz, *Pharmacol. Rev.* **2013**, *65*, 1, https://doi.org/10.1124/pr.112.006809.
[10] E. G. Erdös, *Faseb J.* **2006**, *20*, 1034, https://doi.org/10.1096/fj.06-0602ufm.
[11] D. W. Cushman, M. A. Ondetti, *Nat. Med.* **1999**, *5*, 1110, https://doi.org/10.1038/13423.
[12] J. F. Waterfall, *Br. J. Clin. Pharmacol.* **1989**, *27 Suppl 2*, 139s, https://doi.org/10.1111/j.1365-2125.1989.tb03475.x.
[13] D. Ricklin, J. D. Lambris, *Immunol. Rev.* **2016**, *274*, 5, https://doi.org/10.1111/imr.12497.
[14] L. Lupu, A. Palmer, M. Huber-Lang, *Front. Immunol.* **2020**, *11*, 584514, https://doi.org/10.3389/fimmu.2020.584514.
[15] D. Ricklin, G. Hajishengallis, K. Yang, J. D. Lambris, *Nat. Immunol.* **2010**, *11*, 785, https://doi.org/10.1038/ni.1923.
[16] D. Ricklin, E. S. Reis, J. D. Lambris, *Nat. Rev. Nephrol.* **2016**, *12*, 383, https://doi.org/10.1038/nrneph.2016.70.
[17] a) D. C. Mastellos, D. Ricklin, J. D. Lambris, *Nat. Rev. Drug Discov.* **2019**, *18*, 707, https://doi.org/10.1038/s41573-019-0031-6; b) D. Ricklin, D.

C. Mastellos, E. S. Reis, J. D. Lambris, *Nat. Rev. Nephrol.* **2018**, *14*, 26, https://doi.org/10.1038/nrneph.2017.156.
[18] C. Q. Schmidt, J. D. Lambris, D. Ricklin, *Immunol. Rev.* **2016**, *274*, 152, https://doi.org/10.1111/imr.12475.
[19] Y. Q. Wu, H. Qu, G. Sfyroera, A. Tzekou, B. K. Kay, B. Nilsson, K. Nilsson Ekdahl, D. Ricklin, J. D. Lambris, *J. Immunol.* **2011**, *186*, 4269, https://doi.org/10.4049/jimmunol.1003802.
[20] P. H. Nilsson, K. N. Ekdahl, P. U. Magnusson, H. Qu, H. Iwata, D. Ricklin, J. Hong, J. D. Lambris, B. Nilsson, Y. Teramura, *Biomaterials* **2013**, *34*, 985, https://doi.org/10.1016/j.biomaterials.2012.10.040.
[21] A. Sahu, B. K. Kay, J. D. Lambris, *J. Immunol.* **1996**, *157*, 884.
[22] a) D. Morikis, N. Assa-Munt, A. Sahu, J. D. Lambris, *Protein Sci.* **1998**, *7*, 619, https://doi.org/10.1002/pro.5560070311; b) A. Sahu, A. M. Soulika, D. Morikis, L. Spruce, W. T. Moore, J. D. Lambris, *J. Immunol.* **2000**, *165*, 2491, https://doi.org/10.4049/jimmunol.165.5.2491; c) B. Mallik, M. Katragadda, L. A. Spruce, C. Carafides, C. G. Tsokos, D. Morikis, J. D. Lambris, *J. Med. Chem.* **2005**, *48*, 274, https://doi.org/10.1021/jm0495531.
[23] B. J. Janssen, E. F. Halff, J. D. Lambris, P. Gros, *J. Biol. Chem.* **2007**, *282*, 29241, https://doi.org/10.1074/jbc.M704587200.
[24] M. Katragadda, P. Magotti, G. Sfyroera, J. D. Lambris, *J. Med. Chem.* **2006**, *49*, 4616, https://doi.org/10.1021/jm0603419.
[25] a) H. Qu, P. Magotti, D. Ricklin, E. L. Wu, I. Kourtzelis, Y. Q. Wu, Y. N. Kaznessis, J. D. Lambris, *Mol. Immunol.* **2011**, *48*, 481, D https://doi.org/10.1016/j.molimm.2010.10.004; b) H. Qu, D. Ricklin, H. Bai, H. Chen, E. S. Reis, M. Maciejewski, A. Tzekou, R. A. DeAngelis, R. R. Resuello, F. Lupu, P. N. Barlow, J. D. Lambris, *Immunobiology* **2013**, *218*, 496, https://doi.org/10.1016/j.imbio.2012.06.003.
[26] P. Hillmen, J. Szer, I. Weitz, A. Röth, B. Höchsmann, J. Panse, K. Usuki, M. Griffin, J. J. Kiladjian, C. de Castro, H. Nishimori, L. Tan, M. Hamdani, P. Deschatelets, C. Francois, F. Grossi, T. Ajayi, A. Risitano, R. P. de la Tour, *N. Engl. J. Med.* **2021**, *384*, 1028, https://doi.org/10.1056/NEJMoa2029073.
[27] D. C. Mastellos, B. G. P. Pires da Silva, B. A. L. Fonseca, N. P. Fonseca, M. Auxiliadora-Martins, S. Mastaglio, A. Ruggeri, M. Sironi, P. Radermacher, A. Chrysanthopoulou, P. Skendros, K. Ritis, I. Manfra, S. Iacobelli, M. Huber-Lang, B. Nilsson, D. Yancopoulou, E. S. Connolly, C. Garlanda, F. Ciceri, A. M. Risitano, R. T. Calado, J. D. Lambris, *Clin. Immunol.* **2020**, *220*, 108598, https://doi.org/10.1016/j.clim.2020.108598.
[28] a) N. Berger, T. D. Alayi, R. R. G. Resuello, J. V. Tuplano, E. S. Reis, J. D. Lambris, *J. Med. Chem.* **2018**, *61*, 6153, https://doi.org/10.1021/acs.jmedchem.8b00560; b) Y. Huang, E. S. Reis, P. J. Knerr, W. A. van der Donk, D. Ricklin, J. D. Lambris, *ChemMedChem* **2014**, *9*, 2223, https://doi.org/10.1002/cmdc.201402212; c) P. J. Knerr, A. Tzekou, D. Ricklin, H. Qu, H. Chen, W. A. van der Donk, J. D. Lambris, *ACS Chem. Biol.* **2011**, *6*, 753, https://doi.org/10.1021/cb2000378.

License and Terms

This is an Open Access article under the terms of the Creative Commons Attribution License CC BY 4.0. The material may not be used for commercial purposes.

The license is subject to the CHIMIA terms and conditions: (*http://chimia.ch/component/sppagebuilder/?view=page&id=12*).

The definitive version of this article is the electronic one that can be found at https://doi.org/10.2533/chimia.2021.495

Review Article

CHAPTER 2: MACROCYCLIZATION STRATEGIES FOR CYCLIC PEPTIDES AND PEPTIDOMIMETICS

Clément Bechtler[1], Christina Lamers[1]

[1] Molecular Pharmacy Group, Department of Pharmaceutical Sciences, University of Basel, Basel, Switzerland

Corresponding author:
Dr. Christina Lamers
Department Pharmaceutical Sciences, University of Basel, Klingelbergstr. 50, 4056 Basel, Switzerland. E-mail: christina.lamers@unibas.ch

Reference:
Bechtler, C.; Lamers, C. Macrocyclization Strategies for Cyclic Peptides and Peptidomimetics. *RSC Medicinal Chemistry*. RSC 2021, pp 1325–1351. https://doi.org/10.1039/d1md00083g.

Contributions of Clément Bechtler:
- Conceptualization of manuscript
- Preparation of manuscript

RSC
Medicinal Chemistry

ROYAL SOCIETY OF CHEMISTRY

REVIEW

Check for updates

Cite this: *RSC Med. Chem.*, 2021, **12**, 1325

Macrocyclization strategies for cyclic peptides and peptidomimetics†

Clément Bechtler and Christina Lamers *

Received 10th March 2021,
Accepted 1st June 2021

DOI: 10.1039/d1md00083g

rsc.li/medchem

Peptides are a growing therapeutic class due to their unique spatial characteristics that can target traditionally "undruggable" protein–protein interactions and surfaces. Despite their advantages, peptides must overcome several key shortcomings to be considered as drug leads, including their high conformational flexibility and susceptibility to proteolytic cleavage. As a general approach for overcoming these challenges, macrocyclization of a linear peptide can usually improve these characteristics. Their synthetic accessibility makes peptide macrocycles very attractive, though traditional synthetic methods for macrocyclization can be challenging for peptides, especially for head-to-tail cyclization. This review provides an updated summary of the available macrocyclization chemistries, such as traditional lactam formation, azide–alkyne cycloadditions, ring-closing metathesis as well as unconventional cyclization reactions, and it is structured according to the obtained functional groups. Keeping peptide chemistry and screening in mind, the focus is given to reactions applicable in solution, on solid supports, and compatible with contemporary screening methods.

1. Introduction

Macrocyclic peptides are an interesting molecular format for drug discovery,[1] combining the advantages of small-molecule and biological therapeutics: synthetic accessibility, low immunogenicity and toxicity, high binding affinity and selectivity, and the ability to target protein surfaces traditionally considered "undruggable".[2–5] Furthermore, macrocyclization renders peptides more stable and can increase membrane permeability,[6] making it an important medicinal chemistry strategy in peptide drug development.[7] Advances in high-throughput *in vitro* screening techniques have accelerated the identification of biologically potent

Department Pharmaceutical Sciences, University of Basel, Klingelbergstr. 50, 4056 Basel, Switzerland. E-mail: christina.lamers@unibas.ch

† Electronic supplementary information (ESI) available. See DOI: 10.1039/d1md00083g

Clément Bechtler

Clément Bechtler graduated in 2015 from LMU Munich in Pharmacy. Afterwards, he moved to the University College London, working on small molecule inhibitors of the Nrf2-Keap1 interaction in the research group of Dr. Geoffrey Wells and obtaining an MPhil in Medicinal Chemistry. He started then his PhD in 2017 in Prof Daniel Ricklin's group at the University of Basel, where his work is focused on peptide macrocycles, aimed at reducing undesired complement system activity. His interests include the design and synthesis of peptide macrocycles as well as their biophysical and functional characterization.

Christina Lamers

Dr. Christina Lamers received her PhD from the Pharmaceutical Chemistry Department of the Goethe-University (Frankfurt/Main, Germany) in 2014. From 2015–2017 she was a post-doctoral fellow in the laboratory of Prof. Christian Heinis at EPFL (Lausanne, Switzerland), focusing on bicyclic peptides as therapeutics and their identification with phage display. During this postdoc she won a Marie-Curie individual fellowship. In November 2017 she joined the group of Prof. Daniel Ricklin as senior post-doctoral fellow at the Molecular Pharmacy Group, University of Basel (Switzerland), developing cyclic peptides as therapeutics to target the innate immune system.

This journal is © The Royal Society of Chemistry 2021

macrocyclic peptides,[3,8,9] and the field of macrocyclization is developing quickly to match.

The synthesis of cyclic peptides can be difficult to achieve by traditional methods, such as amide formation, because a defined pre-cyclization conformation must be formed, an entropically unfavorable process, before the desired intramolecular reaction can occur. This is especially true for head-to-tail cyclization, involving the cyclization of the C-terminus of the peptide with its N-terminus, because the preferred confirmation of amide bonds is all-*trans*, which leads to an extended peptide precursor.[10] The introduction of turn-inducing elements is a strategy to circumvent this.[11,12] Furthermore, most cyclizations need to be conducted in dilute solutions to favor the intramolecular reaction over intermolecular oligomerization.[12] A pseudo-dilution effect can also be achieved by anchoring the peptide to an insoluble polymer, though this requires three-dimensional orthogonality in the protecting group strategy and anchoring *via* a sidechain when a head-to-tail cyclization is the goal.

Besides head-to-tail, peptides can also be cyclized head-to-sidechain, sidechain-to-tail or sidechain-to-sidechain. In particular, sidechain-to-sidechain cyclization has been extensively used to stabilize secondary structures, such as α-helices and β-sheets, yielding so-called 'stapled petides',[13,14] or to generate protein epitopes[15,16] and antibody CDR mimetics.[17]

In recent years, great progress has been made in identifying new cyclization strategies for peptide macrocyclization, spanning a wide range of chemistries from cross-coupling and photochemical reactions[18] to enzymatic macrocyclization.[19] Chemoselective reactions,[20] reactions introducing orthogonality[21] and diversity, are pushing the chemical space of macrocyclic peptides to new, more drug-like modalities. The chemoselective approaches in particular, such as ligations,[22,23] will accelerate the increasing interest in peptide macrocycles since they allow peptide macrocyclization without the need for tedious protecting group strategies and are applicable to *in vitro* selection systems,[24] accelerating lead identification.

In this review, we compiled the most important and modern organic chemistry macrocyclization strategies, structured by the produced connectivity. With this, we provided a concise overview for how to choose the appropriate reaction for peptide macrocyclization based on desired functional group. Finally, we summarized the different approaches in ESI† Table S1 to give the reader a short guide for selecting suitable reactions based on their specific requirements. To underline the importance of peptide macrocyclization in medicinal chemistry we highlight some applied examples and their bioactivities in ESI† Table S2.

2. Amide bond formation

2.1 Traditional amide cyclization

Many naturally occurring pharmacologically active peptides are cyclized head-to-tail, rendering them more resistant to hydrolysis by exopeptidases due to the absence of an N- and C-terminus. To cyclize a linear peptide precursor by amide bond formation, traditionally the same coupling chemistry is used as in linear peptide bond formation.[8] However, conventional head-to-tail amide formation is non-trivial. Especially for head-to-tail cyclization of peptides shorter than seven residues, cyclodimerization and C-terminal epimerization can occur. In the retrosynthetic planning the ring disconnection must be chosen carefully, as for example, sterically hindered amino acids at the side of cyclization can reduce yields.[25] To improve yields and reduce side product formation, preorganization of the peptide backbone can create a high effective molarity of the reaction partner. This can be done through turn-inducing elements such as proline, D-amino acids, or *N*-methylation.[12] Conformational elements to pre-organize peptides for head-to-tail cyclization have been reviewed in detail.[12,26]

For amide formation, three main classes of peptide coupling reagents are used: carbodiimides, phosphonium reagents, and aminium–/uronium–iminium reagents.[27] The careful choice of coupling reagent and additives can reduce epimerization.[9,28] For example, PyBOP was used to complete the synthesis of cyclomarin C,[29] whereas for teixobactin, a mixture of HATU/Oxyma Pure/HOAt/DIEA was preferred.[30]

Amide bond formation is not chemoselective, and in-solution cyclization requires sidechain-protected peptides, often rendering them poorly soluble. By forming the amide on solid support, the pseudo-dilution effect helps to reduce intermolecular reactions. In principle, two strategies have been used to achieve a head-to-tail cyclization on solid support: anchoring the peptide to the resin *via* the sidechain of a trifunctional amino acid[31] or *via* the N-α atom of the C-terminus;[32] the C-terminal carboxylate can react after orthogonal deprotection to form the cyclized product. Notable applications of head-to-tail and sidechain-to-sidechain lactam formation aim at the stabilization of secondary structures.[33] For example, the design of a β-hairpin generated a protein–protein-interaction (PPI) inhibitor of the oncotarget p53-HDM2 that was smaller and had a higher activity compared to an α-helix (IC_{50} 0.53 μM *vs.* 1.1 μM, ESI† Table S2).[34]

2.2 Amide formation – sulfur mediated

In the last two decades, chemoselective reactions became the prevailing strategy for the synthesis of amide head-to-tail cyclized peptides.[22] A multitude of different synthesis strategies employ *S*-to-*N* transfer in so-called ligation reactions, which have been recently reviewed.[35,36]

Native chemical ligation (NCL) was introduced as a mild and site-selective amide-formation reaction for synthesizing proteins from peptide fragments,[37] and it was extended to the cyclization of peptides by Tam and coworkers.[38] Here, an N-terminal cysteine reacts with a C-terminal thioester in neutral, aqueous solution. The reversibility of the transthioesterification step ensures chemoselectivity, since

 This journal is © The Royal Society of Chemistry 2021

the irreversible *S*-to-*N* acyl transfer can only proceed at the N-terminal cysteine with its 1,2-aminothiol moiety (Scheme 1, a). This principle is exploited in the thia-zip peptide cyclization approach to access cyclotides.[39] The reversible transthioesterification starts at the most C-terminal cysteine sidechain due to proximity to the thioester and proceeds in a sequential manner until it reaches the N-terminal cysteine, where the irreversible *S*-to-*N* acyl transfer occurs to stop the process. This is followed by a subsequent oxidation to form the intramolecular disulfide bond, which was reported to proceed smoothly in most examples.[39]

The excellent chemoselectivity of NCL can be explained by the poor nucleophilicity of other sidechains at pH 7. Thiols, such as PhSH or BnSH are added as nucleophilic catalysts to enable intermolecular transthioesterification. Low levels of epimerization and no oligomerization have been observed even at high concentrations.

On-resin NCL was first introduced by Muir *et al.* for Boc-SPPS on a buffer-compatible aminomethylated PEGA resin functionalized with thiol groups.[40] Also, an Fmoc-SPPS-compatible NCL approach was reported, achieved by anchoring the sidechain of Asp to *p*-alkoxybenzyl ester as a linker for PEGA or CLEAR resin.[41] A more recent strategy facilitating on-resin NCL uses a methyldiaminobenzoyl (MeDbz) linker to the resin, which is stable under Fmoc-SPPS conditions. After the assembly of the linear peptide sequence, MeDbz is then activated with 4-nitrophenyl chloroformate. Following global deprotection, the resin is treated with tris(2-carboxyethyl)phosphine (TCEP) in aqueous buffer (pH 6.8) to yield the cyclic peptide (Scheme 1, b).[42]

Though NCL is a powerful method for chemoselective head-to-tail peptide cyclization, there are limitations, such as the need for a cysteine in the peptide sequence. However, most of those have been tackled by desulfurisation,[43] thiol-containing auxiliary groups, and cysteine surrogates, and the installation of the thioester has been accomplished *via* SPPS.[22]

A different chemoselective reaction uses the 1,2-aminothiol of an N-terminal cysteine that readily condenses with an aldehyde to form a thiazolidine ring. By incorporating the aldehyde as an oxidized C-terminal glycolaldehyde ester, a head-to-tail cyclized peptide can be obtained by a ring-contraction mechanism proceeding *via* a tricyclic intramolecular rearrangement (Scheme 2).[44]

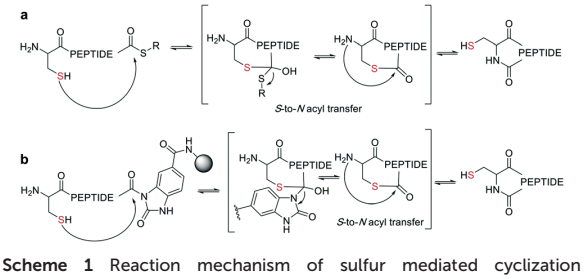

Scheme 1 Reaction mechanism of sulfur mediated cyclization strategies: a: native chemical ligation. b: On solid support.

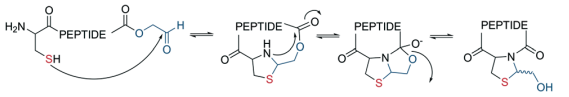

Scheme 2 Reaction mechanism of cyclization generating a thiazolidine.

As a contemporary approach, the head-to-tail ligation of a C-terminal carboxylic acid and a N-terminal thioamide can be promoted by AgI. Ag chemoselectively activates the N-terminal thioamide and brings it in proximity to the C-terminal carboxylate. An isoimide intermediate is formed after the extrusion of Ag_2S and undergoes acyl transfer, resulting in a traceless macrocyclization. The thioamide is introduced as the last step of SPPS by coupling benzotriazole-based thioacylating reagents. Subsequently, the linear peptide is released from the solid support, and cyclization occurs *via* Ag_2CO_3 in DCM/MeCN (Scheme 3).[45]

Other chemoselective ligation reactions have been reported where the cyclization occurs by the attack of a nucleophilic amine at the mildly activated C-terminus. Houghten *et al.* reported an aminolysis of a C-terminal thioester in the presence of imidazole in an aqueous solution. However, this reaction is not chemoselective over the ε-amino group of Lys and shows epimerization.[46] The use of other mildly activated esters (*e.g.*, selenoester,[47] 2-formylthiophenol,[48] selenobenzaldehyde[49]) can increase the reaction speed of the aminolysis, though their use has not yet been reported for peptide macrocyclizations (Scheme 4, a).[22] Similarly, a C-terminal 9-fluorenylmethyl (Fm)-thioester reacts with the N-terminus when activated *in situ* by Sanger's reagent (1-fluoro-2,4-dinitrobenzene). The linear precursor can be synthesized in solution using Boc-chemistry except for the last amino acid, whose Fmoc protection will be removed simultaneously with the cleavage of the Fm-protected thioester to facilitate the reaction with Sanger's reagent and subsequent aminolysis (Scheme 4, a).[50] By linking a linear peptide to a solid support using a diaminobenzyoyl (Dbz) linker, a macrocyclization by aminolysis can be achieved that is analogous to the NCL described above. The linear precursor is synthesized by Fmoc-SPPS, and the Dbz linker is subsequently activated by nitrite-mediated acyl benzotriazole formation to generate an activated C-terminus. This macrocyclization can be achieved under mild acidic conditions with the addition of HOAt and HOBt and in moderate to good yields (Scheme 4, b).[51] The advantage of these aminolysis strategies over NCL is their

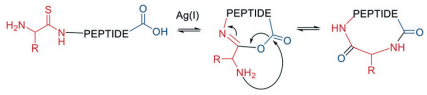

Scheme 3 Head-to-tail peptide cyclization, AgI mediated.

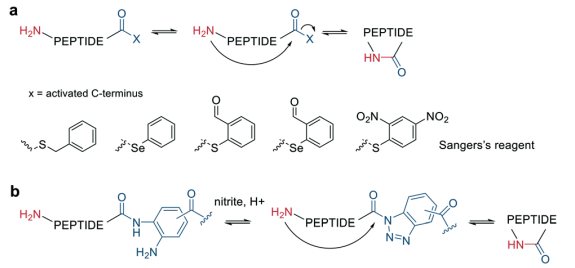

Scheme 4 Reaction mechanism of aminolysis mediated cyclization strategy. a: In solution approaches with activated esters, b: on solid support.

applicability to any peptide sequence without the need for a specific amino acid, such as cysteine.

Finally, a traceless Staudinger ligation can be used to head-to-tail cyclize a peptide in a chemoselective fashion. The C-terminal phosphino-thioester reacts with an N-terminal azide introduced by the noncanonical azidoglycine to yield a cyclic iminophosphorane, which collapses to an amide bond by eliminating the thiophosphorane (Scheme 5).[52]

2.3 Amide formation – mediated by other functional groups

Bode *et al.* reported a ligation reaction between a C-terminal ketoacid and the N-terminal hydroxylamine of proteins and peptides, termed the ketoacid-hydroxylamine (KAHA) ligation.[53,54] This ligation yields macrocyclic peptides from unprotected linear peptides under mild conditions and in polar protic and aprotic solvents.[55] *O*-Substituted and cyclic hydroxylamines have been investigated to prevent oxidation of the N-terminal hydroxylamine. For example, 5-oxaproline was especially suitable for peptide synthesis, as it generated a homoserine depsipeptide that rearranged to a homoserine peptide by an *O*-to-*N* acyl shift.[56] (Scheme 6, a and b). However, drawbacks of the KAHA ligation include a slow reaction, high epimerization rates, and the instability of hydroxylamines.

Ser/Thr ligation has been developed for the synthesis of proteins through the ligation of peptide fragments containing a serine or threonine.[57] The C-terminal ester is activated as a salicylaldehyde ester, which is generated by the on-resin phenolysis of an *N*-acyl-benzimidazolinone (Nbz) linker with salicylaldehyde dimethyl acetal in Na_2CO_3, DCM/THF. This produces macrocycles without C-terminal epimerization.[57] Ser/Thr ligation technology was extended to the backbone cyclization of tetrapeptides containing an N-terminal serine or threonine and C-terminal

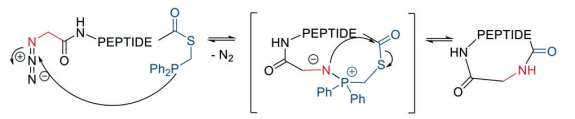

Scheme 5 Peptide macrocyclization by Staudinger reaction.

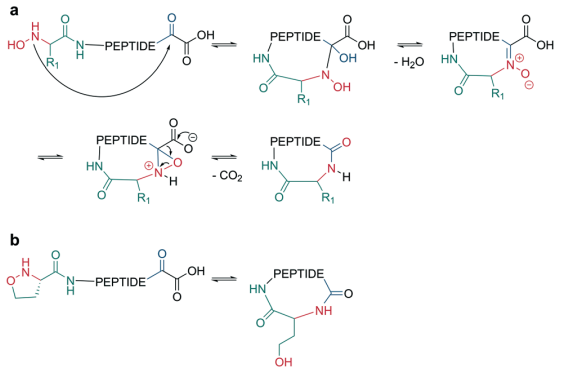

Scheme 6 Cyclization by KAHA ligation. a: KAHA I with free hydroxylamine, b: KAHA II with 5-oxaproline.

salicylaldehyde ester. The ligation of the unprotected peptide occurred in pyridine/acetic acid (1 : 2). After acidolysis with TFA/H_2O, the cyclic peptides were obtained with no epimerization (Scheme 7, a).[58]

Like the *S*-to-*N* migration used in NCL, macrocyclization of a depsipeptide can be achieved by an *O*-to-*N* migration. An *N*-Boc-protected serine is coupled to a solid support, and the alcohol group is reacted with the subsequent Fmoc-amino acid to create an *O*-acyl isopeptide bond. The remaining amino acids are coupled using standard Fmoc-SPPS to generate the depsipeptide. After cleavage from the resin, the depsipeptide is cyclized by amide bond formation of the N-terminus and C-terminal carboxylic acid. Following the removal of the *N*-Boc group of the serine residue, the final *O*-to-*N* acyl migration takes place under basic conditions (Scheme 7, b). This strategy still relies on a conventional head-to-tail cyclization, though the depsipeptide strategy does enable the synthesis of penta- or hexapeptides, which are usually hard to cyclize. However, for a constrained tetrapeptide, this strategy was not successful.[59]

The usage of auxiliary groups is another strategy for cyclizing difficult sequences. For example, 2-hydroxy-6-

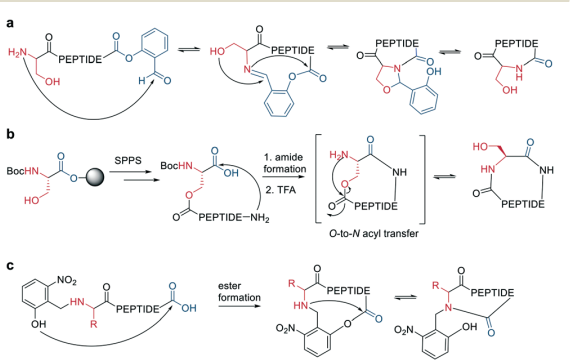

Scheme 7 Reaction mechanism of: a: Ser/Thr ligation in solution, b: on solid support, c: cyclization with the help of auxiliary groups.

This journal is © The Royal Society of Chemistry 2021

nitrobenzaldehyde can be reacted with the N-terminus of the peptide, and an ester is formed by the attack of the phenol on the C-terminus. The following *O*-to-*N* acyl migration generates the lactam, and the auxiliary group can be released by exploiting its photo lability (Scheme 7, c).[60]

Analogous to amide bond formations, isocyanates generated *in situ* react with hydrazides to yield semicarbazides (Scheme 8). The reaction has good yields (60–77%) for different scaffold sizes (*e.g.*, *i*, *i* + 4; *i*, *i* + 7) and is a more robust cyclization for smaller ring sizes.[61]

2.4 Macrocyclization chemistry employing imines and oximes

Inspired by natural products, Malins *et al.* developed new macrocyclization chemistry by forming an imine between an aldehyde and the N-terminal primary amine.[62] To install the aldehyde, they applied two different, previously reported solid-phase approaches, either (i) installing an aldehyde on an aspartate sidechain by reacting it with amino acetaldehyde dimethyl acetal as a masked aldehyde unit, or (ii) coupling an α-amino aldehyde on a tyrosine-glycine resin. In the latter strategy, the C-terminal aldehyde becomes accessible upon cleavage from the resin (Scheme 9, a).[62] Some of the tested peptide sequences readily cyclized in aqueous buffer after cleavage, while others remained linear, potentially due to the reversibility of imine formation. Therefore, different strategies to trap the imine have been reported, such as through the addition of nucleophiles like cyanide to trap the imine as α-aminonitriles. The resulting Strecker reaction proceeded in aqueous solution at room temperature in good yields while tolerating a broad range of sidechain functionalities, including Asp, Glu, Lys, His, Tyr, and Cys.[62]

Imines were also successfully and chemoselectively trapped as amines using $NaBH_3CN$ by reductive amination in aqueous NaOAc buffer (Scheme 9, b). Other intramolecular imine traps have been tested with aromatic rings, including indoles and imidazoles, which proceed *via* Pictet-Spengler macrocyclization (Scheme 9, c), and thio- or seleno-nucleophils, which trap the imine in a corresponding thia-/selenazolidine.[62] The reaction is also selective for the N-terminal primary amine over the ε-amino group of Lys, which is proposed to be due to the difference in pK_a.

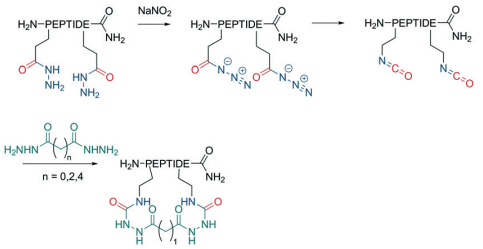

Scheme 8 Reaction of isocyanates with dicarboxylic acid hydrazides on an unprotected peptide.

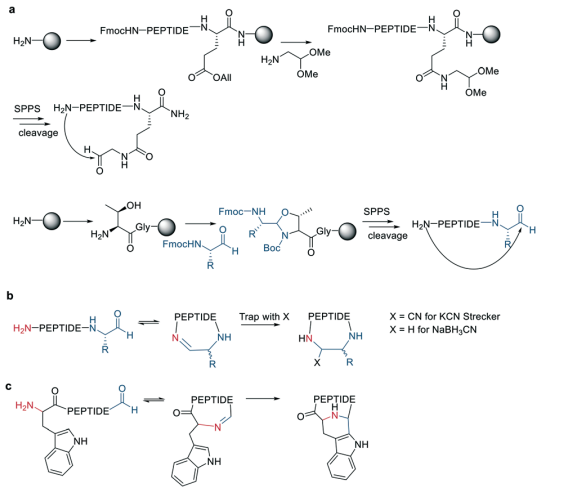

Scheme 9 Peptide cyclization *via* imine formation and subsequently trapping of the imine. a: On-resin strategies to generate the aldehyde. b: General reaction scheme of imine formation and trapping. c: Trapping *via* Pictet–Spengler.

Following imine formation, a nearby nitrogen can attack to generate a stable 4-imidazolidinone. Due to the high chemoselectivity for the intramolecular reaction, it can be carried out at high concentrations without an increase in oligomerization. Furthermore, the 4-imidazolidinone can act as a turn-inducing element, increasing intramolecular hydrogen bonds, conformational rigidity, and enzymatic stability. The reaction proceeds with high stereoselectivity, a high substrate scope, and fast kinetics in DMF/H_2O (Scheme 10, a).[63]

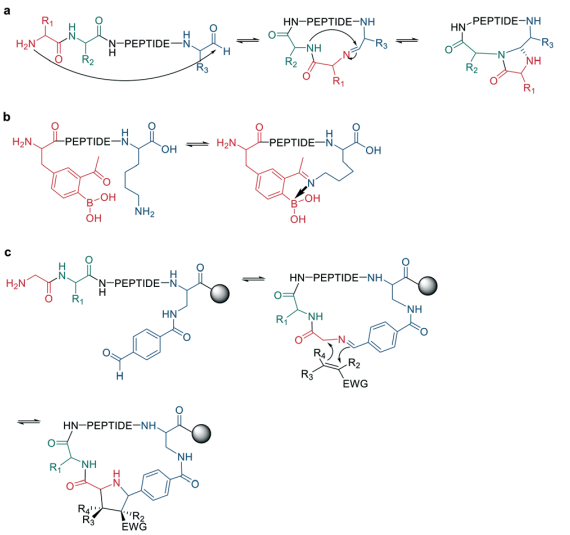

Scheme 10 Peptide cyclization by a: 4-imidazolidinone, b: iminoboronate formation or c: dipolar cycloaddition.

Another strategy to trap an imine is by a boronic acid, which can be introduced in the peptide to allow the cyclization to proceed rapidly and spontaneously under physiologic conditions. Interestingly, this cyclization can be rapidly reversed in response to acids, oxidation, and α-nucleophiles (hydrazine and amino alcohols). At neutral pH (6.8), the macrocycle is stable, while acidic conditions hydrolyze the iminoboronate (Scheme 10, b). When reduced ($NaCNBH_3$), the iminoboronate can be trapped irreversibly as aminoboronate in two diastereomers.[64]

A recent strategy traps the imine in a 1,3-dipolar cycloaddition, generating fused and spiro-ring systems that are frequently found in pharmacologically active natural products. The imine is generated on solid support by reacting 4-carboxybenzaldehyde with the primary amine of an N-terminal glycine (Scheme 10, c).[65]

Native peptides reacted with formaldehyde to form an imine with the ε-amino group of Lys, which can crosslink to nearby tyrosine or arginine residues. Tyrosine reacts in the *ortho* position *via* a C-nucleophilic attack of the iminium ion intermediate and a subsequent re-aromatization (Scheme 11).[66]

Schiff bases (imines, hydrazones, and oximes) are used in dynamic covalent chemistry approaches due to their hydrolytic reversibility, with oximes being generally the most stable. Side-chain cyclization *via* oxime formation is achieved using noncanonical amino acids containing a 1,2-aminoalcohol, which is oxidized by $NaIO_4$ to an aldehyde (Scheme 12). The aldehyde reacts with an noncanonical amino acid containing an aminooxy-sidechain to form an oxime in phosphate buffer (pH 7).[67] Oxime formation is thermodynamically favored but kinetically slow at neutral pH. It can be accelerated by acidic conditions or nucleophilic catalysts. Importantly, oxime formation generates two isomers (*E* and *Z* oximes). When using aminooxy noncanonical amino acids, ethanedithiol should be added as a nucleophilic scavenger during cleavage to prevent the peptide from reattaching to the resin. Furthermore, aminooxy amino acids have been reported to bind irreversibly to the stationary phase of some C_{18} columns.[67] Oxime formation has also been used to stabilize α-helical conformations (*i*, *i* + 4 spacing),[68] and oxime chemistry can be applied for stapling peptides using noncanonical amino acids with amino-alcohol or hydrazine sidechains. By adding commercially available di-

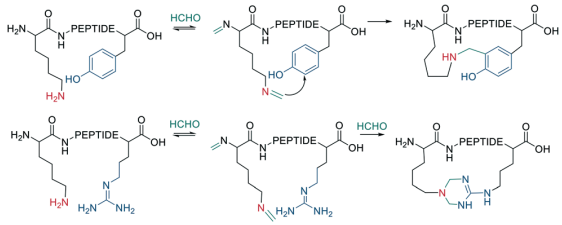

Scheme 11 Cooperative macrocyclization of iminium with nearby arginine or tyrosine sidechain.

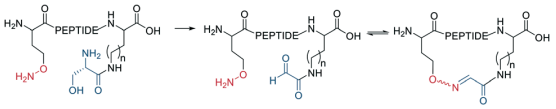

Scheme 12 Macrocyclization by oxime formation.

aldehyde scaffolds, the cyclization proceeds in phosphate buffer at pH 7.[69]

The noncanonical amino acid furanylalanine can be oxidized by *N*-bromosuccinimide (NBS) to form a ketoenal, which can react with nucleophilic sidechains (*e.g.*, Lys) to cyclize (Scheme 13). The reaction is irreversible after imine trapping by reduction with $NaCNBH_3$ and can be applied as a one-pot reaction, though cysteine and tyrosine were not tolerated.[70]

2.5 Amine-reactive stapling

A diverse set of amide-generating scaffolds for reactions with amines has been reported (Fig. 1). To cyclize peptides of an mRNA display library, a bifunctional NHS-scaffold (*e.g.*, disuccinimidyl glutarate) was used.[71] Di-NHS scaffolds (**1**–**8**) generate crosslinked peptides stabilizing α-helical structures with different residue spacings (*i*, *i* + 4 ≈ 5 Å, *i*, *i* + 7 ≈ 11 Å, and *i*, *i* + 11 ≈ 16 Å).[72] Using benzene-1,3,5-tricarboxylic acid (**9**) as an organic, planar, and tri-reactive scaffold, a bicyclic one-bead-two-compounds library was generated by amide formation to sidechain amino groups using PyBOP/HOBT/DIPEA. The library was applied to identify TNFα inhibitors with nanomolar affinities (450 nM), and the scaffold was essential to that affinity (linear sequence >10 μM, ESI† Table S2).[73] Bicyclic scaffolds can also be used to target intracellular targets (*e.g.*, tyrosine phosphatase 1B), by encompassing a cell-permeable sequence in one cycle of the bicyclic peptides.[74]

Nucleophilic aromatic substitution and palladium-catalyzed arylation chemistry for peptide stapling was first introduced to react with the highly nucleophilic thiolate of cysteines (see below and Fig. 2) and was subsequently adapted to react with amine sidechains. As electrophiles for the nucleophilic aromatic substitution, perfluoroaryl-, perfluorodiphenylsulfone-, and dichlorotriazine-derived scaffolds are used.[75] Installing an electron-withdrawing group at the *para* position of the electrophilic arene increases the

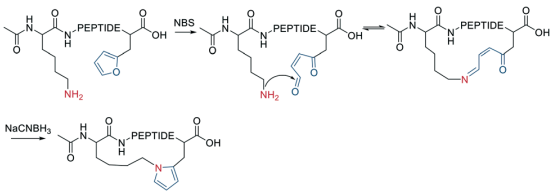

Scheme 13 Oxidation of furan ring and subsequent cyclization with amino sidechain of lysine.

This journal is © The Royal Society of Chemistry 2021

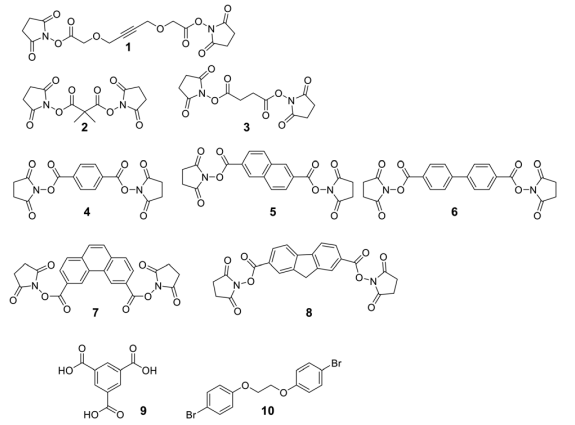

Fig. 1 Examples of scaffolds used for amino-to-amino sidechain stapling.

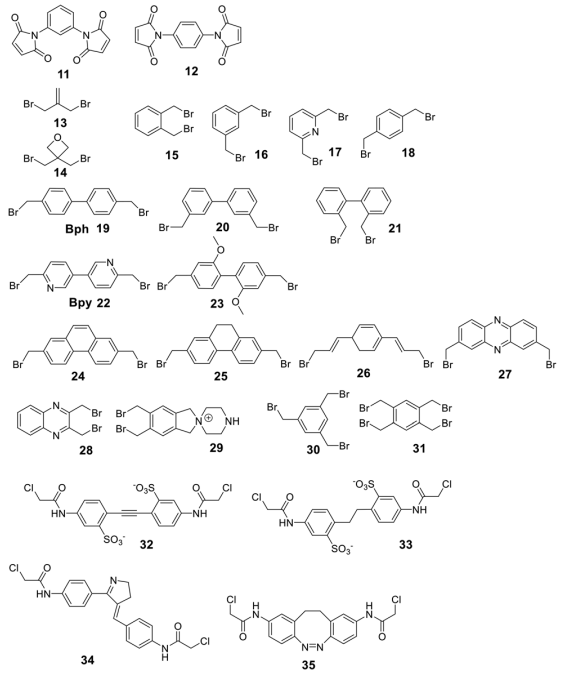

Fig. 2 Examples of scaffolds used for thiol-to-thiol sidechain stapling.

S_NAr efficiency. All reactions proceeded in DMF and tris-basic or DIPEA-basic conditions on unprotected peptides (except for Cys, which would react faster).[75] The lysine-aryl stapled peptides are stable under basic and oxidative conditions, in contrast to the Cys-aryl ones. On unprotected peptides, the palladium-catalyzed arylation of lysine is achieved in weak basic conditions and a preformed biarylphosphine-supported palladium(II)-aryl complex (*t*-BuBrettPhos).[76] Arg, Gln, Asn, the C-terminal amide, and the N-terminal primary amine are not compatible and lead to diarylation. The side reactions, however, can be suppressed when the Pd complex is the limiting reagent. Using 1,2-bis(4-bromophenoxy)ethane (**10**) as a scaffold, the p53 peptide was successfully stapled at *i*, *i* + 4 and *i*, *i* + 7.[76]

3. Disulfide cyclization

Cysteine is the preferred amino acid for chemical transformations of linear peptides due to the high nucleophilicity of the thiolate.[77] Disulfides are a common structural motif found in proteins and other natural compounds to stabilize tertiary structures and conformations. Therefore, the specific distances of disulfide bonds connected cysteines best suited for stabilizing α-helical (*i*, *i* + 7)[78] and β-sheet peptide conformations were identified early on.[79]

Disulfide formation proceeds readily between two proximal thiolates in an oxidative environment, such as air, I_2, DMSO, or H_2O_2. However, disulfides are inherently unstable in a reducing environment and towards nucleophiles, particularly other thiols (thiol exchange). To improve their stability, disulfide groups have been replaced with lactam, thioether, selenium, triazole or dicarba analogues, with most of these methods requiring significant modifications of the synthetic building blocks.

4. Thioacetal formation

The thioacetal as bridging motif has mostly attracted interest as a flexible, reduction-stable analogue for native disulfide bridges.[80–82] The *S*–*S* distance in a methylene thioacetal is approximately 2.95 Å compared to 2.05 Å in a disulfide, and it maintains a similar flexibility and positions for the attachment points (Scheme 14, right).[80] An early example of the formation of a methylene thioacetal was reported in 1999 by Ueki *et al.* when an enkephalin analogue with dimethylphosphinothioyl-protected cysteines was reacted with TBAF.[82] This strategy was also employed for the synthesis of other pharmacologically relevant peptides, such as vasopressin[83] and angiotensin II.[81] Although the affinity for the angiotensin II (AT_2) receptor decreased slightly, this nevertheless provided a 10-fold selectivity over the angiotensin I (AT_1) receptor (ESI† Table S2).[81]

The convenient formation of thioacetals in an aqueous environment and under mild conditions without the need for protecting groups was made possible by a procedure described by Kourra and Cramer,[80] which resembled harsher,

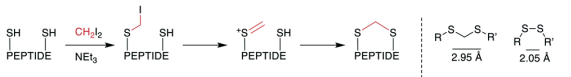

Scheme 14 Left: reaction scheme with intermediates for the formation of methylene thioacetals from disulfides. Right: structural similarities between disulfides and methylene thioacetals.

previously reported reaction conditions for the formation of methylene thioacetals and, more generally, dithioethers.[84] When thiols, or *in situ*-reduced disulfides, were reacted with diiodomethane and a base, they formed a methylene thioacetal with good yield. Mechanistically, one thiol replaces an iodide on CH_2I_2. Subsequently, the second iodide is eliminated, and the second thiol adds to the sulfonium ion (Scheme 14, left). The method proceeded with good yields for several peptide hormones and increased the reductive, serum, pH, and temperature stability while maintaining the affinity of oxytocin. Typically, the disulfide peptide is first reduced with TCEP, and the thioacetal is subsequently formed with 2.5–10 eq. of CH_2I_2 and 5–15 eq. of NEt_3 in H_2O/THF at room temperature over several hours. Encouraging results were obtained when this methodology was applied to insulin,[85] the 58-residue protein bovine pancreatic trypsin inhibitor,[86] adrenomedullin analogues,[87] peptide mimetics binding to the HIV *trans*-activation response RNA,[88] and in the chemical synthesis of the protein interleukin-2.[89]

5. Thioether formation

The nucleophilicity of a cysteine thiol can be further exploited in sidechain-to-sidechain stapling through thioether formation. This has been applied to induce α-helicity in peptides by employing bromo- or chloroacetate as a reactive moiety, which can be coupled to a sidechain (*e.g.*, ornithine,[90] *O*-[2-bromoethyl]-tyrosine[91]) or the N-terminus (applied using mRNA display).[92] Thioether formation occurs in aqueous buffers at pH 8 (Scheme 15, a).

Wang *et al.* applied the thiol–ene coupling to phage display screening by incorporating an electrophilic noncanonical amino acid (*N*ε-acryloyl-lysine) using amber suppression.[93] A thioether bond for cyclization can also be generated by a radical addition of the thiol group to an alkene (*e.g.*, allyloxycarbonyl protecting group[94]) in a thiol–ene reaction on solid support. The radical reaction can be initiated in the presence of ultra-violet light irradiation and a radical initiator (Scheme 15, b). Similarly, Tian *et al.* used a radical thiol–ene to react a cysteine thiolate with an alkene-containing noncanonical amino acid. The final cyclization of the peptide was achieved by conventional amide formation between the amine of the N-terminal Cys and the C-terminus (Scheme 15, c).[95]

Similarly, vinyl sulfonamides can react with cysteines as Michael acceptors for on-resin cyclization. The vinyl sulfonamide is introduced by an N-terminal coupling of the commercially available reagent 2-chloroethane sulfonyl chloride.[96] Thiol–yne coupling can also be employed for thioether-cyclization by reacting an alkyne-containing amino acid with cysteine under photo-induction, yielding mixtures of *E*- and *Z*-isomers (Scheme 15, d).[97] Thioethers are also formed by generating a dehydroalanine and subsequent Michael-addition with a thiolate.[98,99]

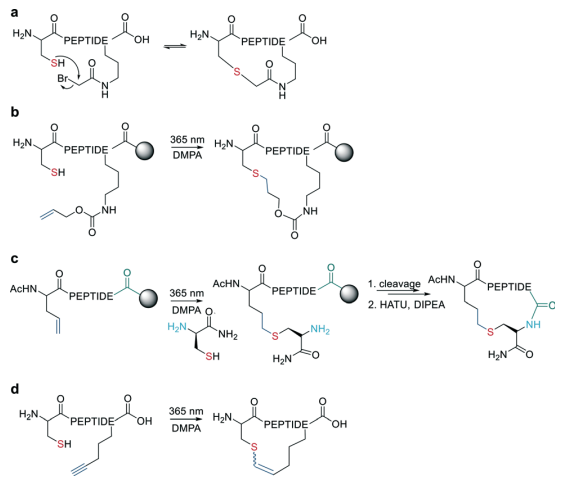

Scheme 15 Macrocyclization *via* thioether formation; DMPA = 2,2-dimethoxy-2-phenylaceto-phenone. a: Reaction of thiol with bromoacetate-moiety. b: Thiol–ene reaction in solution. c: Thiol–ene reaction on-resin. d: Thiol–yne reaction.

5.1 Scaffold thioether formation

Secondary structures can be stabilized by reacting two cysteines, which are usually first reduced with mild reagents such as TCEP, with organic scaffolds. In some examples, this stabilization has resulted in an increase in cell permeability.[100] Several electrophiles have been used for the cysteine scaffold cyclization reactions (Fig. 2). The first was reported by Kemp *et al.*, who showed that a β-sheet in a cyclic nonapeptide containing three cysteines could be stabilized using tribromomethylenebenzene (**30**).[101] The nucleophilic substitution of bromomethylenearyl compounds is fast and chemoselective for cysteine in aqueous, mildly basic solutions (*e.g.* MeCN/NH_4HCO_3, DMF/DIPEA at pH 7.8–8.5), with a high conversion at room temperature,[102] enabling the stapling of unprotected peptides.[16,17,101,102]

To achieve maximal stabilization of the secondary structure, Woolley *et al.* underlined the importance of a matching scaffold length and the distance distribution of attachment points, suggesting that enhanced rigidity improves the helicity.[103] The bromomethylenebenzene scaffolds (called CLIPS, **15**–**18**) have been used extensively to stabilize helicity by stapling cysteines at positions *i*, *i* + 4.[102] Additionally, bisarylmethylenebromide scaffolds (Bph **19**, Bpy **22**)[100] are suitable for a rigid *i*, *i* + 7 (9–13 Å) configuration, and water-soluble schaffold **29** (ref. 103) is used for *i*, *i* + 11 (14–20 Å) stapling. Aliphatic scaffolds, such as 3-bromo-2-(bromomethyl)prop-1-ene (**13**), have also been reacted with cysteine thiolate to fix secondary structures (*e.g. i*, *i* + 7 for a rigid, folded backbone). This introduction of the isobutylene scaffold also improved passive membrane permeability and plasma stability.[104] Similarly, the bisbromo-oxetane (**14**) was used to staple a secondary structure and improved important drug design parameters, such as solubility, basicity, lipophilicity, and metabolic stability.[105]

This journal is © The Royal Society of Chemistry 2021

Some scaffolds can also be used to add functionality to the peptide during the cyclization step. For example, dichloroacetone adds a ketone moiety to the macrocycle, which could serve as a handle for other modifications.[106] Another approach reacted tribromomethylenebenzene (**30**) monovalently with a wide variety of groups, including biotin, cholesterol, arachidonic acid and carboxyfluorescein, before cyclizing the unprotected peptide with the functionalized scaffold.[107] The same approach has been used for the bioconjugation of proteins and antibodies,[108] though a major drawback of bromomethylenearyl scaffolds is their limited solubility in aqueous solutions. Therefore, Smeenk *et al.* designed a bromomethylene scaffold (**29**) that combines improved solubility with the option for functionalization. Starting from a 1,2,4,5-tetrabromomethylenebenzene, derivatization with a 1,4-piperazine increases water solubility and offers a reactive amine to functionalize the scaffold.[109]

Cysteine-reactive scaffolds have also been used to introduce a photoswitch to cyclic peptides. Using an iodoacetamide-modified azobenzene scaffold (**36**), Woolley *et al.* reported a stapling method able to include α-helicity under photocontrol (Scheme 16).[110] Another chromophore for photoswitching, benzylidene-pyrroline (**34**), confers a 10 Å change in end-to-end distance upon isomerization. The conformation of the target peptide can be switched from the *Z*-isomer (400 nm) to *E*-isomer (446 nm) in aqueous, neutral solutions. The *Z*-isomer has a slow thermal relaxation, permitting separation of the isomers by HPLC. By crosslinking cysteine sidechains in an *i*, *i* + 11 spacing, the *E*-isomer can stabilize an α-helix, while the *Z*-isomer is too short.[111] Another example is the thiol-reactive chloroacetamido-substituted C2-bridged azobenzene (**35**) (407 nm, 518 nm), which caused model peptide FK-11 to undergo a helix-coil transition when cysteines at *i*, *i* + 11 were bridged.[112]

For linear peptides with more than two cysteines several scaffolds have been reported able to bridge multiple cysteines. For example, three cysteines can be bridged using 2,4,6-tris(bromomethylene)benzene (**30**), and four cysteines can be bridged using 1,2,4,5-tetrabromodurene (**31**).[102] However, organic scaffolds with three or four spatially isometric thiol-reactive groups yield a mixture of regioisomers. 2,3,5,6-tetrafluoro-1,4-dicyanobenzene (**43**, Fig. 3) was proposed to reduce regioisomers due to a drastically changed reactivity of the remaining C–F sites after the first substitution, resulting in a stepwise crosslinking process.[113] However, two regioisomers are still generated, except when bridging two cysteines and one penicillamine, where one specific bicyclic structure is yielded.[114]

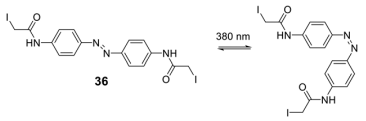

Scheme 16 Thiol-to-thiol scaffold to generate photoswitchable peptides.

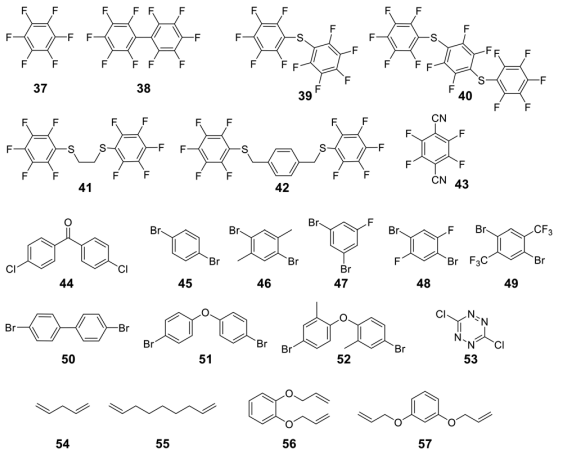

Fig. 3 Frequently used scaffold for thioether-based stapling by 1,4-disubstition with perfluoro-scaffolds (**37**–**42**), Pd-mediated coupling with aryl dihalids (**44**–**53**) and thiol–ene reaction (**54**–**57**).

Dichlorotetrazine was suggested as a reversible cyclization scaffold, which can be released by a photochemical trigger to generate thiocyanates and molecular nitrogen. The thiocyanates can be converted back to sulfhydryl groups (Cys) by reaction with cysteine. To tackle the low solubility of dichlorotetrazine in water, it was dissolved in chloroform and mixed vigorously with the peptide in phosphate buffer (pH 5).[115]

An emerging technique to promote cysteine stapling is the use of reactive aromatic linkers containing electron-withdrawing and activating moieties, such as perfluoroarenes (**39**–**44**,) that result exclusively in a 1,4-disubstitution.[116] Increased helicity, stability, and cellular permeability can be obtained by stapling with perfluoroaryl scaffolds, and multiple scaffolds for different cysteine distances have been reported.[117]

Furthermore, aryl dihalides (**45**–**53**) have been shown to react with cysteines of an unprotected peptide in the presence of palladium under mild aqueous conditions (pH 5.5–8.5, small amounts DMF, DMSO, or MeCN).[118] The careful choice of palladium ligand (RuPhos) led to a selective and fast C–S bond formation, though previous reports had shown that free thiols could inhibit palladium-catalyzed cross-coupling reactions[119] and that Pd(II) complexes could exhibit protease-like activity.[120] This approach is chemoselective over serine, in contrast to palladium-mediated allylation,[121] and the required bis-palladium crosslinking reagents can be generated in one-step from commercially available aryl dihalides.[122] The *S*-arylated peptide was shown to be stable towards acids, bases, and thiol nucleophiles.[118] However, cysteine-aryl homologues can be eliminated under basic conditions to form dehydroalanine or can be subject to oxidation.[75]

The thiol–ene reaction has also been applied for stapling and is especially suitable for certain bis-electrophilic linkers

that are not sufficiently activated for *S*-alkylation, *e.g.* alkyl halides (**54**–**57**).[77,123]

Allyl sulfones enable site-selective cysteine coupling by reacting as a Michael-acceptor. Interestingly, the allyl sulfones can be used as a handle to introduce up to 3 different functionalities simultaneously.[124] Another linker employing a Michael-addition reaction mechanism is 2,2-disubstituted cyclopentenedione, which also offers simultaneous derivatization and cyclization. The addition of a chaotropic agent increases the cyclization rate, though side reactions do occur, such as cysteine oxidation (SO_3H), disulfide formation, and epimerization.[125]

Thiol–maleimide adducts are widely used for bioconjugation and peptide stapling,[126,127] though the adducts decompose rapidly *via* hydrolysis and/or retro-Michael reactions. The addition of glutathione also reverses the stapling, which might find an application in targeted delivery.[127] In a Mitsunobu-alkylation, the dibromo-maleimide can be further modified to introduce an alkyne as click handle.[127] Zhang *et al.* have developed a maleimide derivative suitable as a scaffold for peptide stapling that is stable in aqueous solutions at pH 6–8.5 for multiple days.[128] Its reaction with thiols in neutral aqueous solution yields high conversion within minutes and is highly specific for cysteines. The bridged scaffold can further be reduced with $NaBH_4$ (Scheme 17) and can be synthesized with various functional groups (fluorescein, alkyne, biotin, and other).[128] The reaction of 1,2-aminothiol with the thio malononitrile TAMM (2-((alkylthio)(aryl)methylene)malononitrile), which can be introduced to a Cys sidechain as a chloroacetyl, forms a thiazolidine, inducing an elimination of dicyanomethanide to afford a 2-aryl-4,5-dihydrothiazole (ADT). This reaction proceeds under biocompatible conditions ($NaHCO_3$ or phosphate buffer, pH 7.4) (Scheme 18).[129]

4,5-Dibromo-1,2-dihydro-pyridazine-3,6-dione has been derivatized with TCEP to work as a reversible thiol-reactive

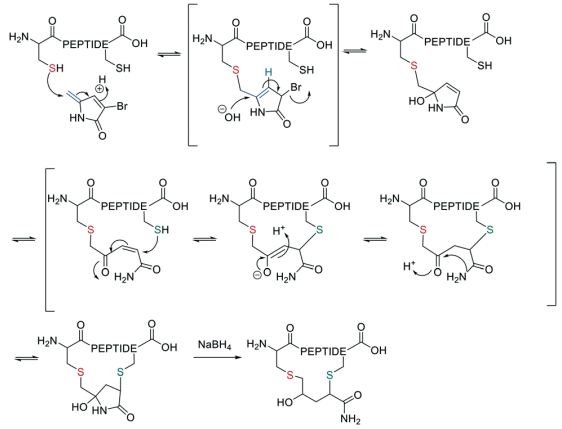

Scheme 17 Thiol-to-thiol scaffold using 3-bromo-methylene pyrrolone.

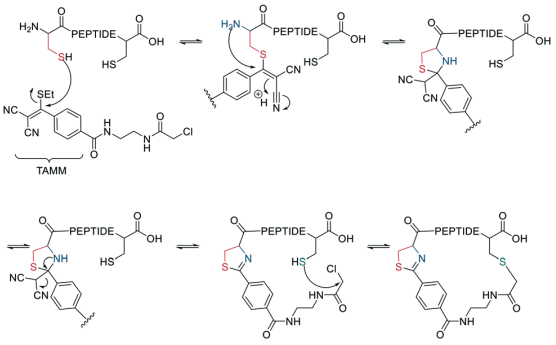

Scheme 18 Reaction mechanism of cyclization generating a dihydrothiazole by reaction with TAMM (2-((alkylthio)(aryl)methylene) malononitrile).

scaffold.[130] The reduction of disulfide bridges by the TCEP part could provide a high local concentration of the tethering group *in situ*.[131]

5.1.1. Scaffold thioether reactions on *in vitro* selection systems. To obtain bicyclic peptides on disulfide-free gIII phage, Heinis *et al.* applied the tribromomethylenebenzene (TBMB, **30**) scaffold to cyclize a peptide library containing three cysteines. The reaction proceeded with 10 μM TBMB in 20 mM NH_4HCO_3, 5 mM EDTA, pH 8 for 1 h.[132] The phages were still sufficiently infective, which enabled the phage display screening of bicyclic peptides. Further scaffolds suitable for building bicyclic peptides on phage by thioether formation have been reported.[133] To increase the diversity of phage displayed libraries, linear peptides containing four cysteines were cyclized on phage with a bi-reactive scaffold to generate three isomers with different conformations per linear peptide sequence. Twelve different scaffolds have been applied.[134] Similarly, mRNA-displayed peptides containing multiple noncanonical amino acids and two cysteines were also cyclized with dibromoxylene.[135] Further scaffolds applied on phages are decafluoro-diphenylsulfone (**41**, Fig. 3)[136] and 2,4-difluoro-6-hydroxy-1,3,5-benzenetricarbonitrile.[137] The latter scaffold is soluble in buffer (pH 7.4), in contrast to previously reported perfluoroaryl scaffolds, and is chemoselective for cysteine in neutral conditions. It reacts with primary amines under basic conditions (*e.g.*, pH 9.2).[137]

5.2 Scaffold-mediated cyclization of thiol and amine

Scaffolds with two electrophilic groups have been used to bridge a cysteine thiolate with the N-terminal amino group.[138,139] Kubota *et al.* introduced a stapling scaffold that can connect Cys and Lys sidechains on an unprotected peptide *via* Pd-mediated *S*-arylation and subsequent reaction of a tethered electrophile to the Lys sidechain.[140] Another chemoselective cyclization on unprotected peptides generates isoindole-bridged cyclic peptides *via* the reaction of a lysine or the N-terminus and cysteine thiolate with *ortho*-phthalaldehyde (OPA) in aqueous buffer (PBS pH 7.4).

This journal is © The Royal Society of Chemistry 2021

The reaction yields a rapid and clean transformation that tolerates diverse functionalities. The exact reaction mechanism could not be identified, since trapping the imine with $NaBH_4$ was unsuccessful. The isoindole moiety provides an option for further post-cyclization modifications.[141] This approach was reported simultaneously by Todorovic *et al.*, who called it fluorescent isoindole crosslinking (FlICK), highlighting the built-in fluorescence. To alter the spectral properties, five modified OPA have been used.[142]

Luo *et al.* developed dinitroimidazole as a bifunctional and highly soluble (10 mM) scaffold that can react selectively with Lys or Cys sidechains, depending on the reaction conditions.[143] In a wide pH range (pH 3.0–8.0), 1,4-dinitroimidazoles were cysteine-specific in aqueous solutions, while they modified Lys residues efficiently in organic solvents, such as dimethyl sulfoxide (DMSO) with weak bases through a ring-opening and ring-closing mechanism.[143]

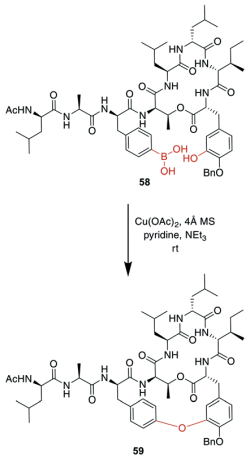

Scheme 19 Reaction scheme for a macrocyclization step in the total synthesis of seongsanamide B using the Evans–Chan–Lam reaction.

6. Ether formation

Ethers could be an interesting peptide bridging motif because they are flexible, have multiple conformations, and are more stable than disulfides or thioethers to reduction, oxidation, or nucleophiles,[144] yet there are limited examples of their use in peptide macrocyclization. Notably, biaryl ethers have played a role in the synthesis of many natural product peptides, in particular for antibiotic glycopeptides, such as vancomycin.[145–147]

Several methods can be used to obtain macrocyclic biaryl ether peptides, such as S_NAr reactions either in solution[145,148–151] or on-resin,[152,153] Ru-catalyzed reactions,[154] strained ring openings by phenols,[155] Ullman-type couplings,[156] and Evans–Chan–Lam reactions.[147,157] Similar to the formation of aryl ethers, Ru-catalyzed S_NAr reactions have also been employed in the syntheses of amines and thioethers.[158] Generally, all these methods require custom-made building blocks and protecting group strategies to obtain a selective reaction.

A recent example is the total synthesis of the bicyclic depsipeptide seongsanamide B, for which Shabani and Hutton used a late-stage Evans–Chan–Lam reaction to form the second macrocycle. The required phenyl boronic acid was introduced as pinacol ester that was stable through amide coupling conditions and TFA-mediated cleavage from the solid phase, and it was liberated prior to the Evans–Chan–Lam reaction. This in-solution reaction gave the desired product **59** with a 26% yield (Scheme 19).[147] Furthermore, the Tsuji–Trost reaction has been used on allylic esters and different native sidechains. In the absence of carboxylates, amines, histidines, or cysteines, the reaction is specific for tyrosine as a nucleophile. When amines or carboxylates are present, an excess of base is needed to form the more nucleophilic phenolate. Changing the catalyst from $Pd(PPh_3)_4$ to $[PdCl(C_3H_5)]_2$ and using xantphos as a ligand yields a histidine-coupled product when no additional base is added, providing chemoselectivity when reaction conditions are tightly controlled (Scheme 20).[159,160]

In a remarkable example of how modern synthetic methods enable formerly hard-to-imagine bond formations, Lee *et al.* applied Ni/photoredox catalysis to the macrocyclization of peptides. To form an ether bond between a C-terminal serine and a 2-bromobenzoyl moiety at the N-terminus, they combined a Ni^{II}-catalyst, 1,3-dicyano-2,4,5,6-tetrakis(diphenylamino)-benzene (4DAIPN), and irradiation with 450 nm light. However, if the C-terminus was an amide instead of an ester, it could react *via* the amide nitrogen instead of the serine sidechain (Scheme 21).[161]

To date, however, ether-containing cyclic peptides are predominantly accessed by other cyclization reactions, with the ether moiety introduced as part of a pre-formed building block.[144,162–165]

7. C–C single bond formation

7.1 Traditional cross couplings

Cross couplings, in which a new carbon–carbon bond is formed by transition metal catalysis, are one of the most important classes of reactions. In most of these reactions, a transition metal such as Pd inserts oxidatively into a carbon–(pseudo)halide bond, and subsequent transmetallation of an

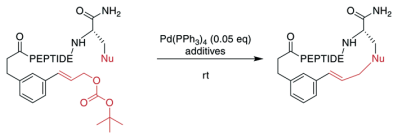

Scheme 20 Application of the Tsuji–Trost reaction to the macrocyclization of peptides. If the nucleophile is a Tyr, a macrocyclic ether is obtained. Nu = nucleophile (phenols, amines, carboxylates, imidazoles), PEPTIDE = 2 or 3 amino acids.

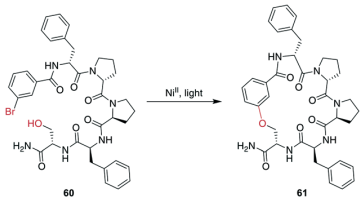

Scheme 21 Ni^{II}/photoredox-catalyzed ether formation between a bromo-benzoyl moiety and serine side chain.

organometallic compound leads to two organic fragments bound to the catalyst. Formation of the new carbon–carbon bond occurs by reductive elimination. The various cross couplings differ mainly in substrates and catalysts, but all require both reaction partners to be pre-functionalized, excepting the Sonogashira coupling and Heck reaction.[166,167]

Most of the typical C–C cross couplings, namely the Suzuki, Stille, Negishi, Tsuji–Trost, Heck, and Sonogashira couplings, have been used to generate peptide macrocycles, although less often than other metal-catalyzed reactions, such as the copper-catalyzed azide–alkyne cycloaddition (CuAAC) or ring-closing metathesis (RCM).[160] The use of the Suzuki coupling for amino acid modifications and peptides has been reviewed, including examples of macrocyclizations.[168,169] Overall, it has been used in solution[170] and on-resin to form five- and six-residue macrocycles.[171,172]

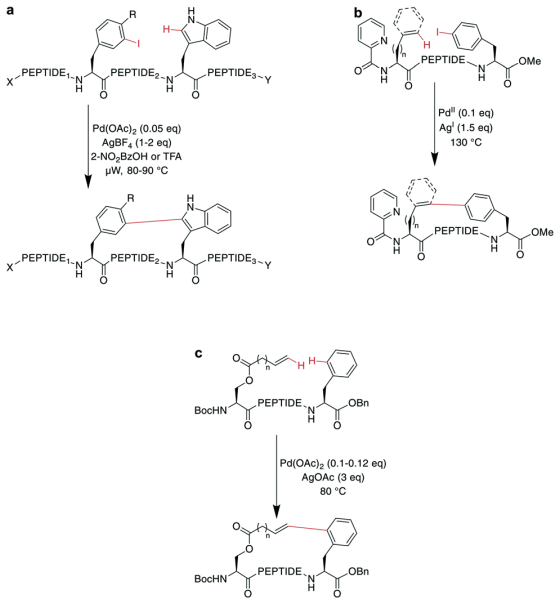

Scheme 22 a: Peptides macrocyclized through their Trp-C2 and a iodophenyl residue from Phe or Tyr; X = H, Ac; Y = OH, NH_2; R = H, OH; $PEPTIDE_1$ = 0–1 amino acids: $PEPTIDE_2$ = 0–3 amino acids; $PEPTIDE_3$ = 0–1 amino acids; b: a typical substrate for a macrocyclization between a sp^2-CH_2 group and a phenyl iodide; n = 1, 2; PEPTIDE = 2, 3, 4 or 6 amino acids; c: oxidative cross-coupling between an alkenyl ester and a phenyl group to obtain macrocyclic peptides; n = 0, 2; PEPTIDE = 1–4 amino acids.

7.2 CH-Activation

In contrast to traditional cross couplings, couplings mediated by CH activation do not require the introduction of an organometal in the substrate, which is an important advantage as these usually strongly basic groups are problematic for peptides.[160] In these reactions, one partner is a CH-group that typically reacts as a nucleophile with an organic halide, although more recent examples in which the CH group acts as an electrophile have also emerged. Typically, directing groups support the process by laying out the spatial arrangement and fine-tuning the electronic environment. The coupled CH-groups can be sp-, sp^2- or sp^3-hybridized centers, and for the latter group, β, γ, and δ modifications have been described.[173] Despite the versatility of CH-activation, the reaction is usually performed on protected peptides, which contrasts with other metal-catalyzed macrocyclizations, such as RCM and CuAAC.[174–177] CH activations on peptides, more generally as well as focused on macrocyclizations, have been reviewed recently.[160,173,178,179]

CH activation reactions can be used to selectively modify the C2 of the indole of Trp. These reactions have been used to successfully couple aryl halides to an assembled peptide using Pd-catalysis.[180] In a series of intramolecular cross couplings between Trp and *m*-iodotyrosine and *m*-iodophenylalanine, Mendive-Tapia *et al.* achieved up to 100% conversions of linear precursors by linking positions from *i*, *i* + 1 to *i*, *i* + 5, though overall isolated yields were low (Scheme 22a). The cyclized peptides were stable against proteolytic degradation,[181] and most amino acids, including His, Tyr, and Lys were tolerated, though Met was not compatible.[179,181] Recently, Han *et al.* showed that this type of reaction can also be used to cross couple phenyl iodides with sp^2-CH groups in the γ or δ position at the N-terminus when acylated with picolinic acid (Scheme 22b).[182] Removing the necessity to introduce an aryl halide, the Wang group coupled phenyl residues, including on the phenylalanine sidechain, to terminal alkenes under Pd-catalysis with added AgOAc (Scheme 22c).[174,183,184] Although most amino acids are tolerated in this reaction, sulfur-containing amino acids are not.[160]

Phthaloyl-protection of the N-terminus leads to modified acidity which was employed to specifically activate the β-hydrogens on aliphatic sidechains to couple to aromatic halides under Pd-catalysis for macrocyclization (Scheme 23a).[175,176] No epimerization occurs under the reaction conditions and cyclization between *i*, *i* + 4 and *i*, *i* + 3 residues was successful, but not for *i*, *i* + 2 residues. The reaction could be applied to the ring system A of the natural product celogentin C (Scheme 23b).[175,176] Conveniently, the procedure could also be performed on-resin with continued C-to-N elongation after the cyclization and phthaloyl group removal. The products showed massively increased tryptic stability,[176] and when applied to peptides with the integrin-binding motif

This journal is © The Royal Society of Chemistry 2021

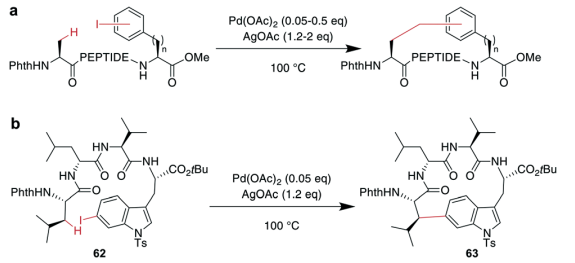

Scheme 23 a: General reaction scheme for the oxidative cross coupling between β-Hs and *meta*- or *para* phenyl iodides; PEPTIDE = 1 or 2 amino acids; *n* = 1, 3. b: The application of the method to the A ring of celogentin C.

RGD, binding to αvβ3 integrin-overexpressing cells was strongly increased (ESI† Table S2).[175]

More recently, transition metals other than Pd have been reported for CH activations. For example, Mn was shown to successfully alkylate the indole-C2 of *N*-pyridine Trp, where pyridine is essential as a directing group, providing an opportunity for selectivity when multiple Trp are present.[160] Combining this CH-activation with the introduction of a propargylic ester in the peptide yielded α,β-unsaturated esters, which are versatile handles that can be further derivatized using, for example, cyclo- or conjugate additions (Scheme 24).[185] Given the high temperatures generally employed for CH activations, this can also be achieved using Rh catalysis with acryl instead of propargylic esters with the addition of $AgSbF_6$ and $Cu(OAc)_2$ at 37 °C, an advantage for temperature-sensitive materials.[186]

7.3 Photocatalyzed reactions

Peptide macrocyclization can also be performed using unfunctionalized iridium (Ir)- or other transition-metal-catalyzed photoredox reactions, which have been recently reviewed.[18] Upon light irradiation, the Ir-catalyst promotes radical formation on the C-terminal carboxylate, leading to decarboxylation. The remaining carboradical undergoes a 1,4-addition with Michael acceptors, such as acrylates or malonates (Scheme 25). An impressive application of this methodology is the selective modification of the C-terminus of insulin, despite the presence of sidechain carboxylic acids

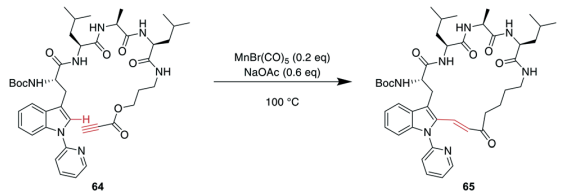

Scheme 24 Propargylic esters can be hydroarylated with *N*-(2-pyridyl)-derivatised Trp under MnI catalysis to yield macrocyclic 3-indolyl acrylates.

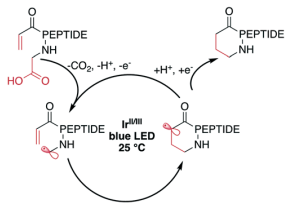

Scheme 25 Simplified reaction mechanism for the Ir-photocatalyzed macrocyclization of *N*-acroyl peptides.

and disulfides.[187] The reaction was successfully applied to form rings ranging from 11 to 47 atoms in size from protected peptides and tolerated all tested residues, including His, Met, Arg, and Tyr.[177] Similar efforts have been made using Ni-catalysts with phthalimide esters on the C-terminus.[160,188]

7.4 Glaser–Hay coupling

The Glaser reaction couples two alkynes to a dialkyne, creating a very rigid and extended bridging group (Scheme 26). This reaction occurs in the presence of O_2 under Cu-catalysis, involving Cu^I/Cu^{II} and possibly Cu^{III} oxidation states within the catalytic cycle.[189,190] Modifications including Ni^{2+} salts have also been described, and the addition of diol ligands seems to be beneficial for oxidation-sensitive molecules, such as peptides, as the diols remove Cu^{II} species by gel formation.[190,191] The reaction was employed successfully with *N*-, *O*-, and *C*-propargyl groups at *i*, *i* + 3 through *i*, *i* + 7 positions and could stabilize secondary structure motifs such as β-turns and α-helices.[192,193] The resulting bis-alkyne can be reduced by catalytic hydrogenation.[191]

8. C–C double bond formation: alkene metathesis

Alkene metathesis, the reaction between two alkenes to form two new alkenes, was propelled into popularity in the 1990s by the development of chemoselective and stable molybdenum (Mo)- and ruthenium (Ru)-based catalysts.[194–198] The reaction is most prominently applied to intramolecular reactions to generate cyclic systems, and labeled ring-closing metathesis (RCM) for this application. Its high tolerance for most functional groups as well as its usually high yields make it well suited for cyclizing relatively large, functionally diverse molecules. It has therefore been employed on a large number of complex structures, such as peptides and peptidomimetics. It

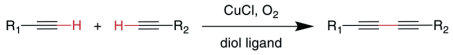

Scheme 26 General reaction scheme for the Glaser–Hay reaction applied to peptides.

can be performed in solution as well as on solid phase and has also been used in the synthesis of DNA-encoded libraries.[199,200]

Mechanistically, the catalyst-bound carbene or alkylidene first undergoes a [2 + 2]-cyclization with an alkene, leading to a metallacyclobutane intermediate. The subsequent ring opening can either revert unproductively to the starting materials or bind the catalyst to the substrate, which causes the release of another alkene (ethene for a terminal alkene substrate). This release is followed by a second [2 + 2] cycloaddition with the second alkene on the substrate, and finally, the formed metallacyclobutane opens to release the bridged product and the catalyst (Scheme 27). As all steps are in principle reversible, the reaction is under thermodynamic control such that the most stable product is the one predominantly formed, which is the *E*-alkene in an unstrained system. However, for macrocyclic peptides, mixtures of *E*/*Z*-alkenes are often obtained. By using two terminal alkenes the equilibrium is shifted towards the product side due to the released ethene gas, which is easily removed from the reaction mixture, leading to a high entropic contribution. However, in case of strained cyclic systems, RCM can still be challenging.[195]

The most common catalysts are Ru-based Grubbs **67–71** or, less frequently, Mo-based Schrock **66** catalysts. The Schrock catalysts are more reactive but less chemoselective and are water- and air-sensitive. Second (II) **68** and third (III) generation Grubbs **69** and Hoveyda–Grubbs **70–71** catalysts were developed to increase reactivity and thermostability (Fig. 4). For the Ru catalysts, unprotected amines are problematic though oxygen-bearing groups are tolerated, whereas the opposite is true for the Mo-catalysts.[195,197,201–203]

Typical rection conditions can vary substantially for different applications. Generally for peptide macrocyclizations, in-solution reactions tend to have lower concentrations (<10 mM), as high concentrations favor dimer over monomer formation, and catalyst loadings (<20 mol%). For on-resin reactions, MBHA or NovaPEG resins are considered superior to Wang and TentaGel, and the reaction is usually performed under microwave irradiation at elevated temperatures. A selection of reaction conditions can be found in the ESI† Tables S3 and S4, and publications containing comprehensive, general protocol descriptions are available.[204,205]

This reaction is among the most commonly applied to peptides for stabilizing secondary structures, in particular for

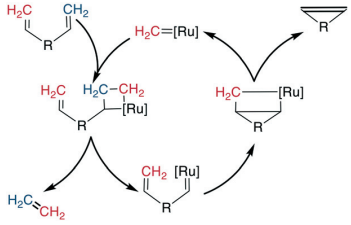

Scheme 27 Reaction scheme for the Ru-catalyzed RCM.

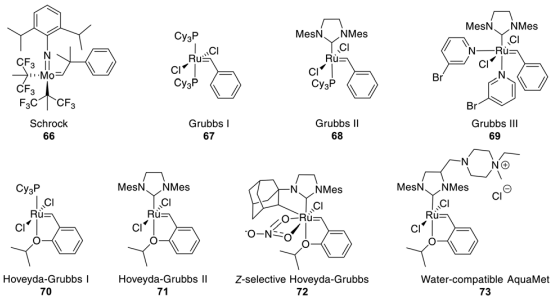

Fig. 4 Frequently employed catalysts for metathesis reactions (Cy = cyclohexyl, Mes = mesityl = 2,4,6 trimethylphenyl).

α-helices.[206–209] Furthermore, it has also been employed to stabilize or mimic other motifs, such as β-sheets,[210] β-turns,[211,212] polyproline II helices,[213] 3_{10} helices,[214,215] N-capping boxes,[216] and disulfide bridges.[217,218] The generated alkenes are generally more conformationally restricted than disulfides, but this is not always the case.[217] Usually, the stapled peptides display improved proteolytic stability and cell permeability,[208,219,220] with some exceptions.[221] The effect on affinity, either through a *de novo* staple or when using it as surrogate for another functional group, is highly dependent on the specific peptide-target interaction as well as the alkene stereoisomer (*E*/*Z*) and stereochemistry, typically requiring an empirical approach.[13,217,218,222,223]

A successful example of the application of RCM to a peptide was provided by Song *et al.* Here, the affinity of a peptide sequence based on the natural binding partner of initiation factor eIF4E could be increased six-fold (ESI† Table S2).[223] Furthermore, van Lierop *et al.* developed an insulin analogue in which the A6-A11 disulfide was replaced with an alkene. The *cis*-alkene analogue maintained affinity to the insulin receptors and showed improved efficacy in mice, whereas the *trans*-alkene had a 50-fold reduced binding affinity (ESI† Table S2).[224] The application of RCM to peptides has been reviewed previously,[209,219,225] including a perspective discussing all-hydrocarbon-stapled α-helical peptides in general.[208]

Alkenes for peptide stapling have been introduced as modified sidechains on carbon[13,204,226–230] as well as on the α-*N*,[231–234] side-chain aliphatic alcohols[206,229] and phenols,[235,236] C-terminal or side-chain acids,[46,237,238] N-terminal carbamates,[237] and cysteine thiol groups.[239] Often, when the alkene is introduced as a modified C-bound chain, α-methyl-α-alkenyl sidechains are used for additional helix stabilisation.[13]

Depending on the strategy, it can be advantageous to have access to *Z*- and *E*-isomers in one step. These can mostly be separated by HPLC,[218,240,241] though occasionally no separation is achieved.[242] Ru-Catalysts selectively forming *Z*-alkenes **72** have been developed (Fig. 4), including some for more challenging substrates, such as those containing steric hindrance or polar groups near the reaction center.[242,243]

This journal is © The Royal Society of Chemistry 2021

Available strategies for *Z*-selective RCM have been recently reviewed.[244] Substrates undergoing selective *E*-alkene formation have been reported, such as those containing α,α-disubstituted amino acids between the bridging amino acids.[214]

Demonstrating the impact of this reaction, chemists at Boehringer Ingelheim used RCM on a large industrial scale for the formation of a 15-membered macrocycle to produce an anti-hepatitis C peptidomimetic **76** (Scheme 28).[202,245,246] Notably, when switching from a Grubbs I **67** to a Hoveyda–Grubbs I **70** catalyst, the reaction rate decreased but exclusively yielded the desired product **75** without concomitant isomeric or epimerized compounds.[245] In contrast, switching to a Hoveyda-Grubbs II catalyst **71** drastically accelerated the reaction yet also increased the amount of dimers, emphasizing that the optimally balanced catalyst needs to be chosen carefully for specific reactivity requirements.[246]

To demonstrate the flexibility of RCM, Gleeson *et al.* exploited the fact that Brønsted acids can mask free amines by protonation. They applied RCM to otherwise unprotected oxytocin, octreotate, two α-conotoxins, and an insulin fragment. The choice of solvent here was crucial, as the conversion of oxytocin proceeded quantitatively in DMF and with 84% and 66% conversion in MeOH and EtOH, respectively, while no product formation was observed in DMSO, MeCN, or solvent mixtures containing water.[247] Cochrane *et al.* showed that the cyclization of unprotected peptides through allyl cysteinyl residues in solution with *t*BuOH/H_2O as the solvent could be achieved by adding 5000 eq. of $MgCl_2$,[239] which was thought to act as a mild Lewis acid to effectively block potential peptide coordination sites to the Ru catalyst.[200] Combining those previous findings, Masuda *et al.* were able to perform RCM on an unprotected model decapeptide in aqueous medium using the water-soluble Ru catalyst AquaMet **73**.[248,249] The use of

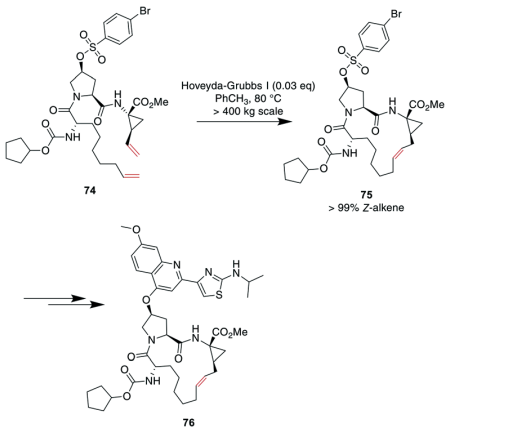

Scheme 28 Synthesis of peptidomimetic **76** on an industrial scale with RCM as a key transformation for closing the macrocycle.

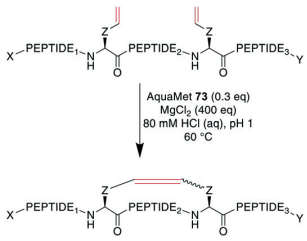

Scheme 29 Synthesis of unprotected alkene-bridged cyclic peptides under aqueous conditions with AquaMet **73** as Ru-catalyst. AA = amino acid, X = H, Ac; Y = OH, NH_2, Z = CH_2, $(CH_2)_3$, CH_2SCH_2, $PEPTIDE_1$ = 1 or 5 amino acids, $PEPTIDE_2$ = 2 or 5 amino acids, $PEPTIDE_3$ = 1 amino acid.

either acidic or neutral conditions in water or phosphate buffer containing $MgCl_2$ allowed the synthesis of an octreotide analogue from different alkenes in yields of 53–64%. Amine-containing buffers were not tolerated, and the addition of a chaotropic agent such as guanidinium·HCl improved the yields substantially in neutral conditions (Scheme 29). Importantly, changing the peptide sequence decreased yields under neutral conditions. Conversely, the acidic conditions proceeded consistently satisfyingly with yields from 48–81%, suggesting the broader scope of these conditions.[249]

Based on this work, Monty *et al.* embarked on the challenging task to optimize RCM for DNA-encoded libraries. Rationalizing that previously reported conditions[199] could be further improved by maintaining acidic conditions to mask coordinating groups in the substrate and that improved solvent composition was needed to prevent phase separation between *t*BuOH and high ionic strength water, NH_4Cl was added to the reaction conditions, and a mixture of H_2O : EtOH : MeOAc (5 : 4 : 1) was used as the solvent. Diverse sets of simple substrates were tested, and generally robust conversion could be observed, although certain functional groups were not or poorly tolerated, such as 1,1-substituted

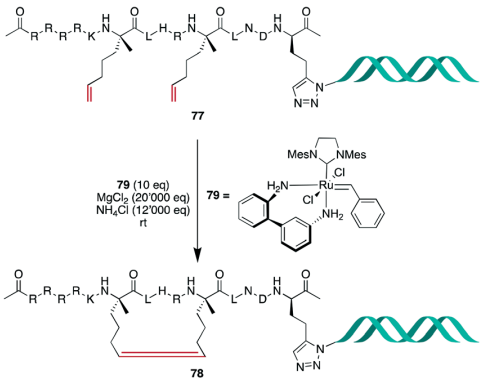

Scheme 30 Synthetic scheme for the synthesis of an alkene-bridged α-helical cyclic peptide with a DNA tag.

alkenes, pyridines, and sulfonamides. Finally, they could obtain an α-helical stapled peptide **78** with 52–65% conversion, depending on the linker length between the peptide and DNA tag (Scheme 30).[200]

9. C–C triple bond formation: ring-closing alkyne metathesis

The tungsten (W)- or Mo-catalyzed ring-closing alkyne metathesis (RCAM) produces a new alkyne in a similar fashion to alkene metathesis. An obvious difference to RCM is the resulting extended conformation and lack of isomers. The employed catalysts are high-valency W- and Mo-based complexes, particularly (tBuO)$_3$W≡CtBu **80** and (Ph$_3$SiO)Mo≡CPhOMe **81** (Scheme 31, right).

Mechanistically, an alkyne is first [2 + 2]-cycloadded to the catalyst-bound alkylidene to form a metallacyclobutadiene. The complex undergoes ring opening, binding the substrate to the catalyst. Upon cycloaddition of another alkyne and formation of a new metallacycle, the product is liberated after another ring opening (Scheme 31, left). Alkyne metathesis in general has already been comprehensively reviewed by Fürstner.[250]

Despite the similarities, the application of RCAM to peptides is less widespread than RCM.[251–255] An early application of RCAM to a peptide cyclization of the A, B, C and E rings of nisin was published in 2005 by Ghalit *et al.* The N- and C-terminal-protected tetra- to heptapeptides were cyclized in solution using (tBuO)$_3$W≡CtBu **80** as a catalyst with 18–82% yield, with smaller cycles producing better results.[253] In a further application, Cromm *et al.* synthesized bicyclic inhibitors against Rab8, a GTPase, using a combination of RCM and RCAM. The alkynes were successfully installed at position i, i + 3, i, i + 4, and i, i + 7 with (Ph$_3$SiO)Mo≡CPhOMe **81** as the catalyst, yielding compounds with improved affinities (ESI† Table S2). Nicely, the work also demonstrated that RCM and RCAM could be performed selectively with both alkynes and alkenes present and in both possible orders.[254]

The advantages of introducing alkynes include the possibility to further modify those, such as to *Z*-alkenes using Lindlar's catalyst,[256] to *E*-alkenes by hydrosliylation,[257] or to dibromoalkenes with CuBr$_2$.[254]

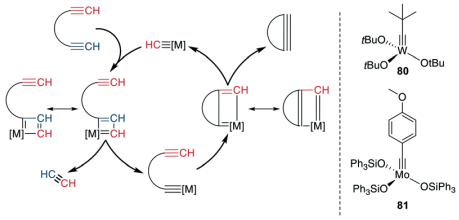

Scheme 31 Reaction mechanism for the RCAM (left) and commonly used catalysts (right), [M] = metal catalyst.

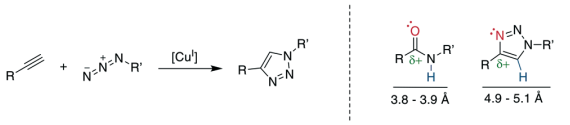

Scheme 32 Left: reaction scheme of the CuI-catalyzed azide–alkyne cycloaddition. Right: comparison of electronic and steric properties of the *Z*-amide and the 1,4-substituted 1,2,3-triazole. Red: H-bond acceptor position, blue: H-bond donor position.

10. Triazole formation

10.1 1,4-Disubstituted triazole formation: the copper-catalyzed azide–alkyne cycloaddition

The copper (Cu)-catalyzed azide–alkyne cycloaddition (CuAAC) is an advancement of the Huisgen 1,3-dipolar cycloaddition and is the exemplary "click reaction" as established by Kolb, Finn, and Sharpless in 2001.[258] Cu^I-Mediated catalysis provides the robust, selective, and water-compatible formation of 1,4-substituted 1,2,3-triazoles from a terminal alkyne and an azide (Scheme 32, left).[259,260] The 1,5-regioisomer is accessible through Ru-catalysis (*vide infra*), whereas traditional Huisgen cycloaddition conditions at high temperatures tend to give mixtures of isomers.[261] The resulting 1,2,3-triazole is metabolically stable and mimics a *Z*-amide in terms of position of H-bond acceptors and donors, though there are somewhat different distances for the substituents. Furthermore, the dipolarity of the triazole compares well to the amide's (Scheme 32, right).[262–264] The 1,2,3-triazole has been used to stabilize secondary structures or other motifs, including α-helices[265,266] 3$_{10}$-helices,[262,267] β-hairpins,[268] and disulfides.[21,269] The reaction has been used extensively for, among others, bioconjugation and materials science, with comprehensive reviews available.[12,263,264,270]

Despite its widespread usage, the detailed reaction mechanism has been challenging to establish. The current consensus[260] is that the catalytic cycle is initiated by the coordination of the Cu^I-species to the alkyne, followed by the tethering of the azide to the complex. The addition of the internal alkyne–carbon to the terminal azide–nitrogen forms a six-membered metallacycle. Reductive ring contraction and copper elimination releases the triazole (Scheme 33).

Many azides are commercially available, but can also be accessed by diazo transfer to primary amines, such as the ε-amino group of Lys.[271] Likewise, alkynes are commercially available or can be synthetically accessed by, for instance, the Corey–Fuchs reaction or Seyferth–Gilbert homologation.[264] When a short spacer on the C-terminus is desired for head-to-tail cyclization, it is possible to introduce a C-terminal propargylamine by using a silyl-based alkyne modifying (SAM)-resin.[272,273]

CuAAC does not require protecting groups and can be performed on-resin[267,271,274–278] as well as in solution,[262,265–269,279–295] which is more common and proceeds under mild conditions. Cu salts most frequently used are CuSO$_4$ with sodium ascorbate, or Cu^I salts such as CuI and

This journal is © The Royal Society of Chemistry 2021

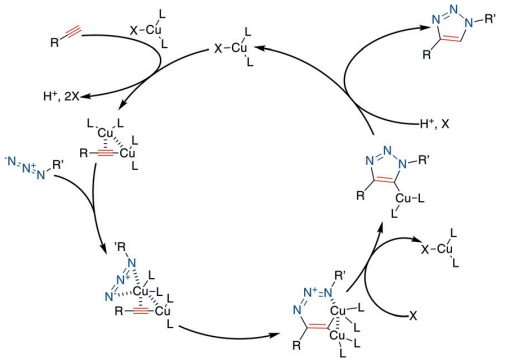

Scheme 33 Reaction mechanism of the CuAAC, X: mostly SO_4^{2-}, I^-, Br^-, Cl^-, PF_6^-, L = ligand such as THTPA, TBTA.

$Cu(MeCN)_4PF_6$. Where on-resin efforts fail, in solution approaches might still be successful, arguably due to the higher conformational flexibility of the starting material in solution.[282]

Cu species can oxidize His and Cys sidechains. In particular, Asp residues were shown to promote this by chelating Cu^{II} centers. The use of tris(triazolylmethyl)amine-based ligands, such as tris(3-hydroxypropyltriazolylmethyl) amine (THTPA) or tris[(1-benzyl-1*H*-1,2,3-triazol-4-yl)methyl] amine (TBTA), can substantially reduce this oxidative damage.[296] Furthermore, by stabilizing the Cu^I species, the ligands accelerate the reaction.[297,298] A selection of reported reaction conditions can be found in ESI† Tables S5 and S6.

Monitoring the reaction of an intramolecular CuAAC can be a challenge, as the starting material and product have the same molecular weight. To therefore indicate the reaction progress, one can use LCMS monitoring, the disappearance of the azide stretch at 2100 cm^{-1} in the IR,[287] or a modified Kaiser reaction.[299]

As for other macrocyclizations, dimerization (*i.e.* an inter- instead of intramolecular reaction) is a major issue for the CuAAC,[300] but can be reduced with higher Cu-concentrations[301] and tends to be less problematic for on-resin-CuAAC of peptide macrocycles with less than six amino acids.[300] Furthermore, for on-resin cyclization, this problem can frequently be addressed by changing the resin or solvent, particularly by using H-bond-disrupting solvents such as DMF or DMSO.[300,302,303] Jagasia *et al.* extensively discussed the different parameters that affect the preference for mono- *versus* dimeric macrocyclization.[302] Very recently, Kandler *et al.* performed an in-depth analysis of the parameters for on-resin CuAAC and found that when the macrocycle comprises six, seven, or eight amino acids, the monomeric form is predominantly obtained. DMF seemed to be the optimal solvent, and including 20% piperidine improved the monomer to dimer ratio.[303]

As an example of CuAAC in peptide therapeutics, Gori used it to replace one of the two disulfides in the α-conotoxin MrIA, yielding compounds as efficacious as the native disulfides in a rat model for neuropathic pain while strongly increasing the plasma stability.[21] By introducing two ω-azido amino acids within a peptide, the macrocyclization can also be done by two CuAACs employing a bis-alkynyl linker.[265,266,269,288–290,304] This has been used as a stapling approach at the *i*, *i* +7 position for an α-helix[265,266] and to successfully develop a peptidomimetic to allosterically target the kinase CK2, showing the potential of macrocyclic peptides even for a classical small-molecule target.[269] This scaffold approach to bridge a peptide by a bis-alkynyl linker was further advanced by Tran *et al.* who used triethynylbenzene as linker. In their explorative study on the C-terminal α-helix from the Gs protein, this allowed them to introduce further functionality at the remaining free alkyne, such as a dye or biotin, after having stapled the peptides either at positions *i*, *i* + 7 or *i*, *i* + 9 (Scheme 34).[286] Finally, the reaction was also used successfully in the synthesis of a DNA-encoded peptidomimetic library with 10^6 members to identify ligands against several targets with K_Ds in the μM range.[291] Showcasing the versatility of having a set of chemoselective reactions, several efforts have successfully obtained multicyclic peptides by combining different cyclisation strategies, such as CuAAC, enzymatically-mediated lactamization, oxime ligations, or thioether formation on scaffolds, yielding structurally unique moieties.[305–307]

10.2 1,5-Disubstituted 1,2,3-triazole formation: ruthenium-catalyzed azide–alkyne cycloaddition

A 1,5-disubstiuted 1,2,3-triazole is similar to an *E*-amide bond in terms of H-bond acceptor and donor positions and can function as a bioisostere for it. Additionally, as the C_α–C_α distance in a 1,5-substituted triazole formed between β-azidohomoalanine and propargyl glycine is similar to the C_α–C_α distance in a cysteine disulfide (4.1–4.2 Å *versus* 3.9–4.0 Å), it has also attracted substantial interest as a disulfide mimetic (Scheme 35, right).[308–310]

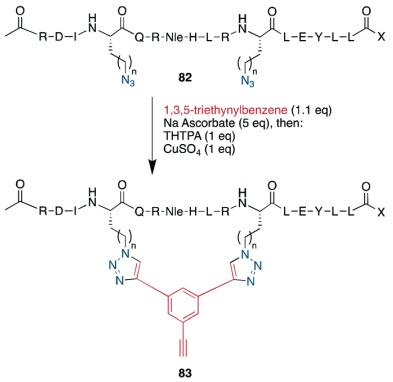

Scheme 34 Performing CuAAC on helical peptides like **82** with triethynylbenzene allowed Tran *et al.* to additionally to stapling them to introduce further functionality on the cyclisation products such as **83**, *n* = 1–3.

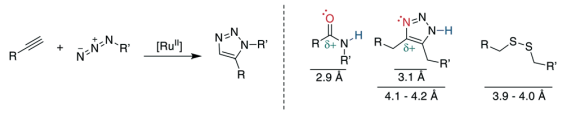

Scheme 35 Left: reaction scheme for the Ru^{II}-catalysed RuAAC, right: comparison of electronic and steric properties of the 1,4-substitued 1,2,3-triazole and the *E*-amide as well as a disulfide bond. Red: H-bond acceptor position, blue: H-bond donor position.

Similarly to the 1,4-disubstituted triazoles, their 1,5-disubstituted counterparts can be obtained regioselectively by a transition-metal catalyzed cycloaddition, although by Ru- instead of Cu-catalysis (RuAAC) (Scheme 35, left).[311] In contrast to the CuAAC, internal alkynes can also undergo RuAAC, allowing the introduction of additional substituents.[311,312] Here, the regioisomer obtained depends on the steric and electronic properties of the alkyne substituents.[312] Common catalysts include [Cp*RuCl], $Cp^*RuCl(PPh_3)_2$, **84** and Cp*RuCl(COD) **85** (Scheme 36, right), the latter reported to work particularly well for secondary azides[313] and reacts at room temperature.[314] With Ru-catalysis, carboxylic acids and sidechains need to be protected,[308,310,315] though the reaction can still be used in solution[310,316–318] as well as on solid support,[287,304,308,309,319] usually with 15–50 mol% catalyst loading at elevated temperatures and in DMF. An overview of reaction conditions can be found in ESI† Tables S7 and S8.

Mechanistically, the catalytic cycle begins with the displacement of Ru-ligands and coordination of the azide and alkyne. Oxidative coupling forms a metallacycle *via* a new bond between the less sterically hindered, more electronegative carbon of the alkyne and the terminal nitrogen of the azide. After reductive elimination, this produces the 1,5-disubsituted 1,2,3-triazole for terminal alkynes (Scheme 36, left).[314] Under high temperatures reminiscent of classical Huisgen conditions, the 1,4-substitution regioisomer can also be obtained.[316] Shortly after its discovery, this reaction was already applied as a turn inducer in a peptoid[320] and as a replacement of an *E*-amide in RNase A.[313] It was later used as a disulfide substitute in the sunflower trypsin inhibitor 1 (SFTI-1).[321]

Multiple examples underline the higher bioisostery for disulfides of 1,5-sbstituted triazoles over 1,4-substituted triazoles. For example, the affinity was retained after the replacement of a disulfide in urotensin-II analogues by a 1,5-triazole, whereas the affinity was reduced or completely lost for 1,4-triazoles, which could be linked to structural reasons.[287] Similar observations were made for SFTI-1 (ESI† Table S2).[308,310] Further examples demonstrate the impressive potential of 1,5-disubstutited triazoles as disulfide isosteres by improving pharmacokinetic or creating changes in the pharmacodynamic profile.[304,309,319]

10.3 1,5-Disubstituted 1,2,3-triazole formation: alternative approaches

As an alternative approach to the metal-catalyzed formation of 1,5-disubstituted triazoles, the Rademann group published an elegant method to introduce a 1,5-disubstituted 1,2,3-triazole on-resin. A resin-bound phophsphoranylidene acetate reacts with the carboxyl group of an Fmoc-amino acid, which can subsequently be elongated using standard SPPS. Treatment with acid liberates an α-carbonyl phosphorous ylide that, upon treatment with an azide, directly yields a 1,5-disubstituted triazole without metal-catalysis (Scheme 37).[322] This was subsequently transferred to the on-resin cyclization of peptides. For dipeptide synthesis, only dimeric products were obtained, while tri- and tetrapeptides yielded mixtures of dimeric and monomeric products. A penta- and an octapeptide were obtained exclusively as monomeric products, making the method more attractive for larger macrocyles.[323]

11. Macrocyclization *via* multicomponent reactions

In recent years, the interest in multicomponent reactions for peptide macrocyclization is increasing and has been recently reviewed in detail.[324] The Ugi reaction, which is a 4-component reaction combining isocyanide, amino, carboxylic acid, and aldehyde functionalities, yields *N*-methylated amides. The advantage of this reaction for peptide cyclization is the possibility of increasing molecular diversity during the ring closing step through the use of non-amino-acid building blocks. It was first applied in the context of peptide synthesis to obtain linear peptide esters[325] and peptidomimetics,[326] while cyclic peptides were generated though several subsequent Ugi reactions.[327] The Ugi reaction has been used in the synthesis of head-to-tail cyclic peptides from linear peptides (amine and carboxylic acid) and conventional

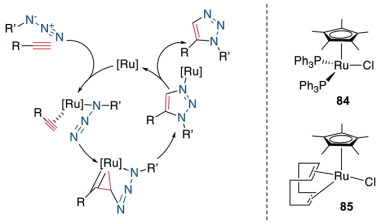

Scheme 36 Left: mechanism of the RuAAC, right: structures of commonly used catalysts for RuAAC. [Ru] = ruthenium catalyst.

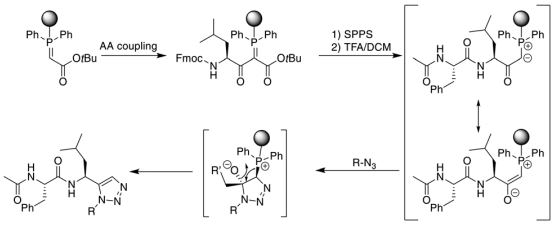

Scheme 37 Synthetic scheme for the metal-free synthesis of 1,5-substituted triazole peptides. AA = amino acid.

This journal is © The Royal Society of Chemistry 2021

aldehydes. Due to the lack of diastereoselectivity[328] and cyclodimerization, which can form the dominant product, low yields are achieved. The low selectivity can be explained by a kinetically competitive intermolecular process due to the slow transannular attack of the amine onto the mixed anhydride, which Hili *et al.* solved using *tert*-butyl-isocyanide and an aziridine aldehyde to obtain a cyclic piperazinone in high yields as a single diastereoisomer.[329] With an amino aldehyde, the attack of the exocyclic nucleophilic aziridine is fast. A non-nucleophilic solvent, such as trifluoroethanol, prevents the premature solvolysis of the mixed anhydride (Scheme 38, a).[329] For later bioconjugation, the activated aziridine ring within the cyclic peptide can be used *via* nucleophilic ring opening (Scheme 38, b).

Ugi-mediated head-to-tail cyclization was adapted to on-resin macrocyclization using side-chain attachment of the C-terminal amino acid and an orthogonal protecting group strategy (allyl ester) to selectively deprotect the C-terminal COOH on resin followed by Fmoc removal and reaction with an aziridine aldehyde dimer and *tert*-butyl isocyanide in equal parts DCM/TFE (Scheme 38, b).[330]

The Ugi reaction is also suitable for sidechain-to-sidechain and sidechain-to-tail/head cyclization, which was shown to be faster and more efficient than head-to-tail cyclization, probably due to the higher flexibility of the sidechains. By carefully choosing the isocyanide component, the diversity of the peptide scaffold can be increased *via* *N*-substitution of the newly formed amide.[331] This approach was applied to stabilize secondary structures and simultaneously functionalize the sidechain-tethering lactam. To achieve this on-resin, a peptide was built using three dimensional orthogonal protecting groups for asparagine and lysine (alloc, allyl). Condensation of paraformaldehyde with pyrrolidine generated a pyrrolidinium ion, which is crucial for complete conversion to the imine by aminocatalysis mediated transamination, since on-resin imine formation is difficult to achieve with paraformaldehyde.[332] Careful washing removes any remaining base before isonitrile is added to finally cyclize the peptide.[333]

As for many cyclization chemistries, the scaffold strategy has also been applied for Ugi multi component reactions (MCR), where linear peptides containing two acidic amino

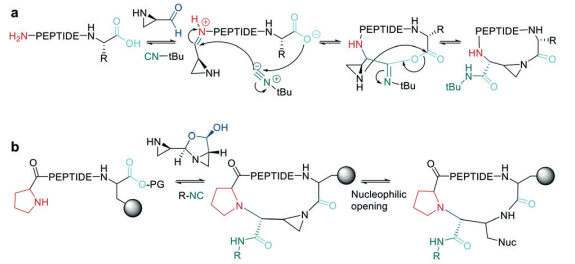

Scheme 38 Mechanism of Ugi reaction using aziridine aldehyde a: in solution and b: on resin.

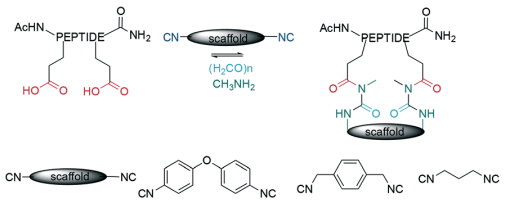

Scheme 39 Synthetic scheme for the four component Ugi reaction.

acids are coupled with diisocyanide scaffolds to generate sidechain-to-sidechain cyclized peptides (Scheme 39). Cyclization here is achieved in a pseudo-dilution protocol by slowly adding the peptide diacid and the diisocyanide to a mixture containing the preformed imine. However, this is slow, with reaction times of 96 h.[334] A recent report highlighted the diversity achieved by distinct combinations of amino and isocyanide components, identifying stapled peptides that inhibited p53/MDM2/X.[335]

Macrocyclization *via* Ugi MCR can be combined with subsequent disulfide formation to generate bicyclic peptides.[336] A similar approach called the sulfur-switch Ugi reaction was proposed to synthesize disulfide-linked cyclic peptides *de novo* from four components, followed by oxidative cyclization of the two cysteines with I_2 to form disulfides (Scheme 40, a). The double mercapto input that is possible on each Ugi component yields six topologically possible combinations.[337] To generate macrocyclic peptides in solution and on resin, the carboxylic acid in the classic four-component Ugi is replaced by an electron-poor phenol (such as 3-nitrotyrosine) in the Ugi-smiles reaction to yield tertiary nitroanilines (Scheme 40, b).[338]

The Petasis reaction, also known as the borono-Mannich reaction,[339] was reported for late-stage diversification (on-resin) and stapling (in solution, Scheme 40, c) of peptides. This three-component condensation of an aldehyde/ketone, an amine (*e.g.*, Lys sidechain), and an aryl/vinyl boronic

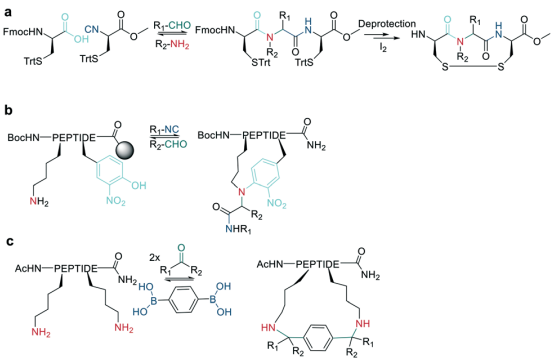

Scheme 40 a: Sulfur-Ugi-switch reaction of an *in situ* assembled peptide with successive disulfide formation. b: Ugi-smiles reaction with nitro-tyrosine as acidic component. c: Petasis reaction for peptide scaffolding.

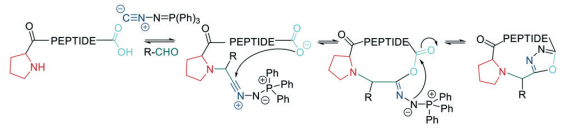

Scheme 41 Multicomponent reaction for peptide macrocyclization employing an aldehyde and (*N*-isocyanimino)triphenylphosphorane to form a 1,3,4-oxadiazole.

ester/boronic acid depends on imine formation *via* transamination, as described for the on-resin Ugi reaction above, and the addition of boronic acid. The outcome and conversion rate of the Petasis reaction depends on the reactivity of the boronic acid, leading to singly and doubly modified products. To achieve stapling in solution, pseudo-dilution conditions were used by the slow addition of boronic acid and peptide to a solution of oxo-component.[340]

A head-to-tail peptidomimetic can be generated in one step *via* the multicomponent reaction of an aldehyde, linear peptide, and (*N*-isocyanimino)triphenylphosphorane.[6] The resulting backbone contains a 1,3,4-oxadiazole, which was shown to stabilize a unique intramolecular hydrogen-bond network and enable a high passive membrane permeability in contrast to the analogous homodetic macrocycles. Oxadiazoles have also been a focus of medicinal chemistry for being a proteolytically stable isostere of amides. The aldehyde component serves as a linker between the N-terminus, and oxadiazole and can mimic amino acid sidechains based on aldehyde substituents; for example, phenylacetaldehyde mimics phenylalanine and isovaleraldehyde mimics leucine. However, the reaction produces both diastereomers. For efficient cyclization, this macrocyclization approach uses a zwitterionic control element, which prevents oligomerization even for more constrained 4-*mer* sequences and at high concentrations (5–100 mM peptide). It was proposed that the positively charged triphenylphosphonium ion augments interaction between the chain termini, leading to a more efficient macrocyclization (Scheme 41).

Conclusions

The favorable properties of peptidic macrocycles and peptidomimetics as potential drug leads have led to the rapid evolution of peptide chemistry beyond traditional amide formation. This is especially true for chemistries that expand the chemical space, such as derivatizing natural linear peptides with organic scaffolds, as these are expected to further improve the drug-like properties of peptides and peptidomimetics and extend the chemical space towards new therapeutic chimeric modalities. With more and more mild, specific, and mutually orthogonal cyclization methods at hand, the possibility for synthesizing highly conformationally constrained, more chemically diverse peptides and peptidomimetics in a controlled manner is continuously increasing. Given that modifying the peptide structure post-discovery can reduce the binding affinity compared to the initial hit, the increasing number of reactions compatible with *in vitro* selection systems and encoded combinatorial libraries will accelerate drug discovery efforts of those new macrocyclic peptidomimetic modalities, opening a great future for peptide-derived drug discovery.

Author contributions

CB and CL have both conceptualized and written the manuscript.

Conflicts of interest

There are no conflicts to declare.

Acknowledgements

We thank Prof. Daniel Ricklin for his support and guidance and Dr. Kaycie Butler (Butler SciComm) for language editing. Funding from the SNF (No. 31003A_176104) for CB and from University Basel Fund for Excellent Junior Researcher for CL is gratefully acknowledged.

References

1 A. Zorzi, K. Deyle and C. Heinis, *Curr. Opin. Chem. Biol.*, 2017, **38**, 24–29.
2 T. Passioura, *Biochemistry*, 2020, **59**, 139–145.
3 A. A. Vinogradov, Y. Yin and H. Suga, *J. Am. Chem. Soc.*, 2019, **141**, 4167–4181.
4 P. G. Dougherty, Z. Qian and D. Pei, *Biochem. J.*, 2017, **474**, 1109–1125.
5 N. S. Robertson and D. R. Spring, *Molecules*, 2018, **23**, 959.
6 J. R. Frost, C. C. G. Scully and A. K. Yudin, *Nat. Chem.*, 2016, **8**, 1105–1111.
7 M. Muttenthaler, G. F. King, D. J. Adams and P. F. Alewood, *Nat. Rev. Drug Discovery*, 2021, **20**, 309–325.
8 A. Bhat, L. R. Roberts and J. J. Dwyer, *Eur. J. Med. Chem.*, 2015, **94**, 471–479.
9 X. Jing and K. Jin, *Med. Res. Rev.*, 2020, **40**, 753–810.
10 V. Martí-Centelles, M. D. Pandey, M. I. Burguete and S. V. Luis, *Chem. Rev.*, 2015, **115**, 8769–8834.
11 J. M. Humphrey and A. R. Chamberlin, *Chem. Rev.*, 1997, **97**, 2243–2266.
12 C. J. White and A. K. Yudin, *Nat. Chem.*, 2011, **3**, 509–524.
13 C. E. Schafmeister, J. Po and G. L. Verdine, *J. Am. Chem. Soc.*, 2000, **122**, 5891–5892.
14 T. A. Hill, N. E. Shepherd, F. Diness and D. P. Fairlie, *Angew. Chem., Int. Ed.*, 2014, **53**, 13020–13041.
15 A. Luther, K. Moehle, E. Chevalier, G. Dale and D. Obrecht, *Curr. Opin. Chem. Biol.*, 2017, **38**, 45–51.
16 P. Timmerman, W. C. Puijk and R. H. Meloen, *J. Mol. Recognit.*, 2007, **20**, 283–299.
17 P. Timmerman, R. Barderas, J. Desmet, D. Altschuh, S. Schochat, M. J. Hollestelle, J. W. M. Höppener, A. Monasterio, J. I. Casal and R. H. Meloen, *J. Biol. Chem.*, 2009, **284**, 34126–34134.

 This journal is © The Royal Society of Chemistry 2021

18 L. Raynal, N. C. Rose, J. R. Donald and C. D. Spicer, *Chem. – Eur. J.*, 2021, **27**, 69–88.
19 M. Schmidt, A. Toplak, P. J. L. M. Quaedflieg, J. H. van Maarseveen and T. Nuijens, *Drug Discovery Today: Technol.*, 2017, **26**, 11–16.
20 R. Wills, V. Adebomi and M. Raj, *ChemBioChem*, 2020, **21**, 52–62.
21 A. Gori, C. I. A. Wang, P. J. Harvey, K. J. Rosengren, R. F. Bhola, M. L. Gelmi, R. Longhi, M. J. Christie, R. J. Lewis, P. F. Alewood and A. Brust, *Angew. Chem., Int. Ed.*, 2015, **54**, 1361–1364.
22 H. Y. Chow, Y. Zhang, E. Matheson and X. Li, *Chem. Rev.*, 2019, **119**, 9971–10001.
23 V. Agouridas, O. El Mahdi, V. Diemer, M. Cargoët, J. C. M. Monbaliu and O. Melnyk, *Chem. Rev.*, 2019, **119**, 7328–7443.
24 C. Sohrabi, A. Foster and A. Tavassoli, *Nat. Rev. Chem.*, 2020, **4**, 90–101.
25 J. M. Humphrey and A. R. Chamberlin, *Chem. Rev.*, 1997, **97**, 2243–2266.
26 J. Blankenstein and J. Zhu, *Eur. J. Org. Chem.*, 2005, 1949–1964.
27 J. W. Taylor, *Biopolymers*, 2002, **66**, 49–75.
28 A. El-Faham and F. Albericio, *Chem. Rev.*, 2011, **111**, 6557–6602.
29 S. J. Wen and Z. J. Yao, *Org. Lett.*, 2004, **6**, 2721–2724.
30 K. Jin, I. H. Sam, K. H. L. Po, D. Lin, E. H. G. Zadeh, S. Chen, Y. Yuan and X. Li, *Nat. Commun.*, 2016, 12364, DOI: 10.1038/ncomms12394.
31 P. Rovero, L. Quartara and G. Fabbri, *Tetrahedron Lett.*, 1991, **32**, 2639–2642.
32 G. T. Bourne, W. D. F. Meutermans, P. F. Alewood, R. P. McGeary, M. Scanlon, A. A. Watson and M. L. Smythe, *J. Org. Chem.*, 1999, **64**, 3095–3101.
33 N. E. Shepherd, H. N. Hoang, G. Abbenante and D. P. Fairlie, *J. Am. Chem. Soc.*, 2005, **127**, 2974–2983.
34 R. Fasan, R. L. A. Dias, K. Moehle, O. Zerbe, J. W. Vrijbloed, D. Obrecht and J. A. Robinson, *Angew. Chem., Int. Ed.*, 2004, **43**, 2109–2112.
35 H. Y. Chow, Y. Zhang, E. Matheson and X. Li, *Chem. Rev.*, 2019, **119**, 9971–10001.
36 K. Shinbara, W. Liu, R. H. P. van Neer, T. Katoh, H. Suga, R. Herman, P. Van Neer, T. Katoh, R. H. P. van Neer, T. Katoh and H. Suga, *Front. Chem.*, 2020, **8**, 1–19.
37 P. E. Dawson, T. W. Muir, I. Clark-Lewis and S. B. H. Kent, *Science*, 1994, **266**, 776–779.
38 L. Zhang and J. P. Tam, *J. Am. Chem. Soc.*, 1997, **119**, 2363–2370.
39 J. P. Tam, Y. A. Lu and Q. Yu, *J. Am. Chem. Soc.*, 1999, **121**, 4316–4324.
40 J. A. Camarero, G. J. Cotton, A. Adeva and T. W. Muir, *J. Pept. Res.*, 1998, **51**, 303–316.
41 J. Tulla-Puche and G. Barany, *J. Org. Chem.*, 2004, **69**, 4101–4107.
42 B. H. Gless and C. A. Olsen, *J. Org. Chem.*, 2018, **83**, 10525–10534.
43 L. Z. Yan and P. E. Dawson, *J. Am. Chem. Soc.*, 2001, **123**, 526–533.
44 P. Botti, T. D. Pallin and J. P. Tam, *J. Am. Chem. Soc.*, 1996, **118**, 10018–10024.
45 V. J. Thombare and C. A. Hutton, *Angew. Chem., Int. Ed.*, 2019, **58**, 5052–5056.
46 Y. Li, A. Yongye, M. Giulianotti, K. Martinez-Mayorga, Y. Yu and R. A. Houghten, *J. Comb. Chem.*, 2009, **11**(6), 1066–1072.
47 J.-J. Du, L.-M. Xin, Z. Lei, S.-Y. Zou, W.-B. Xu, C.-W. Wang, L. Zhang, X.-F. Gao and J. Guo, *Chin. Chem. Lett.*, 2018, **29**, 1127–1130.
48 C. L. Tung, C. T. T. Wong and X. Li, *Org. Biomol. Chem.*, 2015, **13**, 6922–6926.
49 M. Raj, H. Wu, S. L. Blosser, M. A. Vittoria and P. S. Arora, *J. Am. Chem. Soc.*, 2015, **137**, 6932–6940.
50 K. Sasaki and D. Crich, *Org. Lett.*, 2010, **12**, 3254–3257.
51 T. Ohara, M. Kaneda, T. Saito, N. Fujii, H. Ohno and S. Oishi, *Bioorg. Med. Chem. Lett.*, 2018, **28**, 1283–1286.
52 R. Kleineweischede and C. P. R. Hackenberger, *Angew. Chem., Int. Ed.*, 2008, **47**, 5984–5988.
53 J. W. Bode, R. M. Fox and K. D. Baucom, *Angew. Chem., Int. Ed.*, 2006, **45**, 1248–1252.
54 T. Fukuzumi, L. Ju and J. W. Bode, *Org. Biomol. Chem.*, 2012, **10**, 5837–5844.
55 Y. L. Huang, R. Frey, M. E. Juarez-Garcia and J. W. Bode, *Heterocycles*, 2012, **84**, 1179–1191.
56 V. R. Pattabiraman, A. O. Ogunkoya and J. W. Bode, *Angew. Chem., Int. Ed.*, 2012, **51**, 5114–5118.
57 Y. Zhang, C. Xu, H. Y. Lam, C. L. Lee and X. Li, *Proc. Natl. Acad. Sci. U. S. A.*, 2013, **110**, 6657–6662.
58 C. T. T. Wong, H. Y. Lam, T. Song, G. Chen and X. Li, *Angew. Chem., Int. Ed.*, 2013, **52**, 10212–10215.
59 J. Lécaillon, P. Gilles, G. Subra, J. Martinez and M. Amblard, *Tetrahedron Lett.*, 2008, **49**, 4674–4676.
60 W. D. F. Meutermans, S. W. Golding, G. T. Bourne, L. P. Miranda, M. J. Dooley, P. F. Alewood and M. L. Smythe, *J. Am. Chem. Soc.*, 1991, **121**, 9790–9796.
61 A. A. Vinogradov, Z. N. Choo, K. A. Totaro and B. L. Pentelute, *Org. Lett.*, 2016, **18**, 1226–1229.
62 L. R. Malins, J. N. Degruyter, K. J. Robbins, P. M. Scola, M. D. Eastgate, M. R. Ghadiri and P. S. Baran, *J. Am. Chem. Soc.*, 2017, **139**, 5233–5241.
63 V. Adebomi, R. D. Cohen, R. Wills, H. A. H. Chavers, G. E. Martin and M. Raj, *Angew. Chem.*, 2019, **131**, 19249–19256.
64 A. Bandyopadhyay and J. Gao, *J. Am. Chem. Soc.*, 2016, **138**, 2098–2101.
65 S. M. Guéret, S. Thavam, R. J. Carbajo, M. Potowski, N. Larsson, G. Dahl, A. Dellsén, T. N. Grossmann, A. T. Plowright, E. Valeur, M. Lemurell and H. Waldmann, *J. Am. Chem. Soc.*, 2020, **142**, 4904–4915.
66 B. Li, H. Tang, A. Turlik, Z. Wan, X.-S. Xue, L. Li, X. Yang, J. Li, G. He, K. N. Houk and G. Chen, *Angew. Chem.*, 2020, 2–9.
67 C. M. Haney, M. T. Loch and W. S. Horne, *Chem. Commun.*, 2011, **47**, 10915–10917.

This journal is © The Royal Society of Chemistry 2021

68 C. M. Haney and W. S. Horne, *Chem. – Eur. J.*, 2013, **19**, 11342–11351.
69 C. M. Haney and W. S. Horne, *J. Pept. Sci.*, 2014, **20**, 108–114.
70 K. W. Decoene, W. Vannecke, T. Passioura, H. Suga and A. Madder, *Biomedicines*, 2018, **6**, 1–12.
71 S. W. Millward, T. T. Takahashi and R. W. Roberts, *J. Am. Chem. Soc.*, 2005, **127**, 14142–14143.
72 K. Fujimoto, M. Kajino and M. Inouye, *Chem. – Eur. J.*, 2008, **14**, 857–863.
73 W. Lian, P. Upadhyaya, C. A. Rhodes, Y. Liu and D. Pei, *J. Am. Chem. Soc.*, 2013, **135**, 11990–11995.
74 W. Lian, B. Jiang, Z. Qian and D. Pei, *J. Am. Chem. Soc.*, 2014, **136**, 9830–9833.
75 G. Lautrette, F. Touti, H. G. Lee, P. Dai and B. L. Pentelute, *J. Am. Chem. Soc.*, 2016, **138**, 8340–8343.
76 H. G. Lee, G. Lautrette, B. L. Pentelute and S. L. Buchwald, *Angew. Chem.*, 2017, **129**, 3225–3229.
77 D. P. Fairlie and A. D. de Araujo, *Biopolymers*, 2016, **106**, 843–852.
78 D. Y. Jackson, D. S. King, J. Chmielewski, S. Singh and P. G. Schultz, *J. Am. Chem. Soc.*, 1991, **113**, 9392–9394.
79 A. M. Almeida, R. Li and S. H. Gellman, *J. Am. Chem. Soc.*, 2012, **134**, 75–78.
80 C. M. B. K. Kourra and N. Cramer, *Chem. Sci.*, 2016, **7**, 7007–7012.
81 S. Lindman, G. Lindeberg, P. A. Frändberg, F. Nyberg, A. Karlén and A. Hallberg, *Bioorg. Med. Chem.*, 2003, **11**, 2947–2954.
82 M. Ueki, T. Ikeo, K. Hokari, K. Nakamura, A. Saeki and H. Komatsu, *Bull. Chem. Soc. Jpn.*, 1999, **72**, 829–838.
83 M. Uekia, T. Ikeoa, M. Iwadateb, T. Asakurab, M. P. Williamsonc and J. Slaninová, *Bioorg. Med. Chem. Lett.*, 1999, **9**, 1767–1772.
84 H. I. Mosberg, J. R. Omnaas and A. Goldstein, *Mol. Pharmacol.*, 1987, **31**, 599–602.
85 N. Zheng, P. Karra, M. A. Vandenberg, J. H. Kim, M. J. Webber, W. L. Holland and D. H.-C. Chou, *J. Med. Chem.*, 2019, **62**, 11437–11443.
86 R. Mousa, S. Lansky, G. Shoham and N. Metanis, *Chem. Sci.*, 2018, **9**, 4814–4820.
87 J. P. Fischer, R. Schönauer, S. Els-Heindl, D. Bierer, J. Koebberling, B. Riedl and A. G. Beck-Sickinger, *J. Pept. Sci.*, 2019, **25**, 1–13.
88 S. S. Chavali, S. M. Mali, J. L. Jenkins, R. Fasan and J. E. Wedekind, *J. Biol. Chem.*, 2020, **295**, 16470–16486.
89 C. E. Murar, M. Ninomiya, S. Shimura, U. Karakus, O. Boyman and J. W. Bode, *Angew. Chem.*, 2020, **132**, 8503–8507.
90 F. M. Brunel and P. E. Dawson, *Chem. Commun.*, 2005, 2552–2554.
91 N. Bionda, A. L. Cryan and R. Fasan, *ACS Chem. Biol.*, 2014, **9**, 2008–2013.
92 Y. Goto, A. Ohta, Y. Sako, Y. Yamagishi, H. Murakami and H. Suga, *ACS Chem. Biol.*, 2008, **3**, 120–129.
93 X. S. Wang, P. H. C. Chen, J. T. Hampton, J. M. Tharp, C. A. Reed, S. K. Das, D. S. Wang, H. S. Hayatshahi, Y. Shen, J. Liu and W. R. Liu, *Angew. Chem., Int. Ed.*, 2019, **58**, 15904–15909.
94 A. A. Aimetti, R. K. Shoemaker, C. C. Lin and K. S. Anseth, *Chem. Commun.*, 2010, **46**, 4061–4063.
95 Y. Tian, D. Yang, X. Ye and Z. Li, *Chem. Rec.*, 2017, **17**, 874–885.
96 B. P. Sutherland, B. M. El-Zaatari, N. I. Halaszynski, J. M. French, S. Bai and C. J. Kloxin, *Bioconjugate Chem.*, 2018, **29**, 3987–3992.
97 Y. Tian, J. Li, H. Zhao, X. Zeng, D. Wang, Q. Liu, X. Niu, X. Huang, N. Xu and Z. Li, *Chem. Sci.*, 2016, **7**, 3325–3330.
98 J. M. Chalker, S. B. Gunnoo, O. Boutureira, S. C. Gerstberger, M. Fernández-González, G. J. L. Bernardes, L. Griffin, H. Hailu, C. J. Schofield and B. G. Davis, *Chem. Sci.*, 2011, **2**, 1666–1676.
99 J. M. Chalker, L. Lercher, N. R. Rose, C. J. Schofield and B. G. Davis, *Angew. Chem., Int. Ed.*, 2012, **51**, 1835–1839.
100 A. Muppidi, Z. Wang, X. Li, J. Chen and Q. Lin, *Chem. Commun.*, 2011, **47**, 9396–9398.
101 D. S. Kemp and P. McNamara, *Tetrahedron Lett.*, 1981, **22**, 4571–4574.
102 P. Timmerman, J. Beld, W. C. Puijk and R. H. Meloen, *ChemBioChem*, 2005, **6**, 821–824.
103 F. Zhang, O. Sadovski, S. J. Xin and G. A. Woolley, *J. Am. Chem. Soc.*, 2007, **129**, 14154–14155.
104 S. Sun, I. Compañón, N. Martínez-Sáez, J. D. Seixas, O. Boutureira, F. Corzana and G. J. L. Bernardes, *ChemBioChem*, 2018, **19**, 48–52.
105 N. Martínez-Sáez, S. Sun, D. Oldrini, P. Sormanni, O. Boutureira, F. Carboni, I. Compañón, M. J. Deery, M. Vendruscolo, F. Corzana, R. Adamo and G. J. L. Bernardes, *Angew. Chem., Int. Ed.*, 2017, **56**, 14963–14967.
106 N. Assem, D. J. Ferreira, D. W. Wolan and P. E. Dawson, *Angew. Chem., Int. Ed.*, 2015, **54**, 8665–8668.
107 G. K. Dewkar, P. B. Carneiro and M. C. T. Hartman, *Org. Lett.*, 2009, **11**, 4708–4711.
108 I. Ramos-Tomillero, G. Perez-Chacon, B. Somovilla-Crespo, F. Sanchez-Madrid, J. M. Domínguez, C. Cuevas, J. M. Zapata, H. Rodríguez and F. Albericio, *Bioconjugate Chem.*, 2018, **29**, 1199–1208.
109 L. E. J. Smeenk, N. Dailly, H. Hiemstra, J. H. Van Maarseveen and P. Timmerman, *Org. Lett.*, 2012, **14**, 1194–1197.
110 G. A. Woolley, *Acc. Chem. Res.*, 2005, **38**, 486–493.
111 M. Blanco-Lomas, S. Samanta, P. J. Campos, G. A. Woolley and D. Sampedro, *J. Am. Chem. Soc.*, 2012, **134**, 6960–6963.
112 S. Samanta, C. Qin, A. J. Lough and G. A. Woolley, *Angew. Chem.*, 2012, **124**, 6558–6561.
113 W. Liu, Y. Zheng, X. Kong, C. Heinis, Y. Zhao and C. Wu, *Angew. Chem., Int. Ed.*, 2017, **56**, 4458–4463.
114 J. Wang, M. Zha, Q. Fei, W. Liu, Y. Zhao and C. Wu, *Chem. – Eur. J.*, 2017, **23**, 15150–15155.
115 S. P. Brown and A. B. Smith, *J. Am. Chem. Soc.*, 2015, **137**, 4034–4037.
116 A. M. Spokoyny, Y. Zou, J. J. Ling, H. Yu, Y. Lin and B. L. Pentelute, *J. Am. Chem. Soc.*, 2013, **135**, 5946–5949.

This journal is © The Royal Society of Chemistry 2021

117 Y. Zou, A. M. Spokoyny, C. Zhang, M. D. Simon, H. Yu, Y. S. Lin and B. L. Pentelute, *Org. Biomol. Chem.*, 2014, **12**, 566–573.

118 E. V. Vinogradova, C. Zhang, A. M. Spokoyny, B. L. Pentelute and S. L. Buchwald, *Nature*, 2015, **526**, 687–691.

119 D. T. Bong and M. R. Ghadiri, *Org. Lett.*, 2001, **3**, 2509–2511.

120 E. N. Korneeva, M. V. Ovchinnikov and N. M. Kostić, *Inorg. Chim. Acta*, 1996, **243**, 9–13.

121 S. D. Tilley and M. B. Francis, *J. Am. Chem. Soc.*, 2006, **128**, 1080–1081.

122 A. J. Rojas, C. Zhang, E. V. Vinogradova, N. H. Buchwald, J. Reilly, B. L. Pentelute and S. L. Buchwald, *Chem. Sci.*, 2017, **8**, 4257–4263.

123 Y. Wang and D. H. C. Chou, *Angew. Chem., Int. Ed.*, 2015, **54**, 10931–10934.

124 T. Wang, A. Riegger, M. Lamla, S. Wiese, P. Oeckl, M. Otto, Y. Wu, S. Fischer, H. Barth, S. L. Kuan and T. Weil, *Chem. Sci.*, 2016, **7**, 3234–3239.

125 O. Brun, L. J. Archibald, J. Agramunt, E. Pedroso and A. Grandas, *Org. Lett.*, 2017, **19**, 992–995.

126 M. E. B. Smith, F. F. Schumacher, C. P. Ryan, L. M. Tedaldi, D. Papaioannou, G. Waksman, S. Caddick and J. R. Baker, *J. Am. Chem. Soc.*, 2010, **132**, 1960–1965.

127 C. M. Grison, G. M. Burslem, J. A. Miles, L. K. A. Pilsl, D. J. Yeo, Z. Imani, S. L. Warriner, M. E. Webb and A. J. Wilson, *Chem. Sci.*, 2017, **8**, 5166–5171.

128 Y. Zhang, C. Zang, G. An, M. Shang, Z. Cui, G. Chen, Z. Xi and C. Zhou, *Nat. Commun.*, 2020, **11**, 1–10.

129 X. Zheng, Z. Li, W. Gao, X. Meng, X. Li, L. Y. P. Luk, Y. Zhao, Y. H. Tsai and C. Wu, *J. Am. Chem. Soc.*, 2020, **142**, 5097–5103.

130 V. Chudasama, M. E. B. Smith, F. F. Schumacher, D. Papaioannou, G. Waksman, J. R. Baker and S. Caddick, *Chem. Commun.*, 2011, **47**, 8781–8783.

131 M. T. W. Lee, A. Maruani, J. R. Baker, S. Caddick and V. Chudasama, *Chem. Sci.*, 2016, **7**, 799–802.

132 C. Heinis, T. Rutherford, S. Freund and G. Winter, *Nat. Chem. Biol.*, 2009, **5**, 502–507.

133 S. Chen, D. Bertoldo, A. Angelini, F. Pojer and C. Heinis, *Angew. Chem., Int. Ed.*, 2014, **53**, 1602–1606.

134 S. S. Kale, C. Villequey, X. D. Kong, A. Zorzi, K. Deyle and C. Heinis, *Nat. Chem.*, 2018, **10**, 715–723.

135 Y. V. Guillen Schlippe, M. C. T. Hartman, K. Josephson and J. W. Szostak, *J. Am. Chem. Soc.*, 2012, **134**, 10469–10477.

136 S. Kalhor-Monfared, M. R. Jafari, J. T. Patterson, P. I. Kitov, J. J. Dwyer, J. M. Nuss and R. Derda, *Chem. Sci.*, 2016, **7**, 3785–3790.

137 X. Zheng, W. Liu, Z. Liu, Y. Zhao and C. Wu, *Bioconjugate Chem.*, 2020, **31**, 2085–2091.

138 J. R. Frost, J. Z. Essman, C. Huang, N. A. Pierson, N. Pissarnitski and T. Meng, *Pept. Sci.*, 2020, **112**, e24160.

139 S. S. Kale, M. Bergeron-Brlek, Y. Wu, M. G. Kumar, M. V. Pham, J. Bortoli, J. Vesin, X. D. Kong, J. F. Machado, K. Deyle, P. Gonschorek, G. Turcatti, L. Cendron, A. Angelini and C. Heinis, *Sci. Adv.*, 2019, **5**, 1–10.

140 K. Kubota, P. Dai, B. L. Pentelute and S. L. Buchwald, *J. Am. Chem. Soc.*, 2018, **140**, 3128–3133.

141 Y. Zhang, Q. Zhang, C. T. T. Wong and X. Li, *J. Am. Chem. Soc.*, 2019, **141**, 12274–12279.

142 M. Todorovic, K. D. Schwab, J. Zeisler, C. Zhang, F. Bénard and D. M. Perrin, *Angew. Chem., Int. Ed.*, 2019, **58**, 14120–14124.

143 Q. Luo, Y. Tao, W. Sheng, J. Lu and H. Wang, *Nat. Commun.*, 2019, **10**, 1–9.

144 R. Zhao, P. Shi, J. Chen, S. Sun, J. Chen, J. Cui, F. Wu, G. Fang, C. Tian, J. Shi, D. Bierer, L. Liu and Y.-M. Li, *Chem. Sci.*, 2020, **11**, 7927–7932.

145 K. C. Nicolaou, N. F. Jain, S. Natarajan, R. Hughes, M. E. Solomon, H. Li, J. M. Ramanjulu, M. Takayanagi, A. E. Koumbis and T. Bando, *Angew. Chem., Int. Ed.*, 1998, **37**, 2714–2716.

146 S. C. Stolze and M. Kaiser, *Synthesis*, 2012, **44**, 1755–1777.

147 S. Shabani and C. A. Hutton, *Org. Lett.*, 2020, **22**, 4557–4561.

148 P. Cristau, J.-P. Vors and J. Zhu, *Org. Lett.*, 2001, **3**, 4079–4082.

149 M. Bois-Choussy, P. Cristau and J. Zhu, *Angew. Chem., Int. Ed.*, 2003, **42**, 4238–4241.

150 A. T. Londregan, K. A. Farley, C. Limberakis, P. B. Mullins and D. W. Piotrowski, *Org. Lett.*, 2012, **14**, 2890–2893.

151 J. Zhu, *Chimia*, 2013, **67**, 916–920.

152 K. Burgess, D. Lim, M. Bois-Choussy and J. Zhu, *Tetrahedron Lett.*, 1997, **38**, 3345–3348.

153 C. Fotsch, G. Kumaravel, S. K. Sharma, A. D. Wu, J. S. Gounarides, N. R. Nirmala and R. C. Petter, *Tetrahedron Lett.*, 1999, **9**, 2125–2130.

154 A. J. Pearson, G. Bignan, P. Zhang and M. Chelliah, *J. Org. Chem.*, 1996, **3263**, 3940–3941.

155 S. J. Lee, M. M. Joullié, J. Lee and M. M. Joullí, *Chem. Sci.*, 2018, **9**, 2432–2436.

156 Q. Cai, B. Zou and D. Ma, *Angew. Chem., Int. Ed.*, 2006, **45**, 1276–1279.

157 C. P. Decicco, Y. Song and D. A. Evans, *Org. Lett.*, 2001, **3**, 1029–1032.

158 C. W. West and D. H. Rich, *Org. Lett.*, 1999, **1**, 1819–1822.

159 K. V. Lawson, T. E. Rose and P. G. Harran, *Proc. Natl. Acad. Sci. U. S. A.*, 2013, **110**, E3753–E3760.

160 D. G. Rivera, G. M. Ojeda-Carralero, L. Reguera and E. V. Van Der Eycken, *Chem. Soc. Rev.*, 2020, **49**, 2039–2059.

161 H. Lee, N. C. Boyer, Q. Deng, H.-Y. Kim, T. K. Sawyer and N. Sciammetta, *Chem. Sci.*, 2019, **10**, 5073–5078.

162 Y. A. Kim, H. N. Shin, M. S. Park, S. H. Cho and S. Y. Han, *Tetrahedron Lett.*, 2003, **44**, 2557–2560.

163 Q. Cai, G. He and D. Ma, *J. Org. Chem.*, 2006, **71**, 5268–5273.

164 M. Toumi, F. Couty and G. Evano, *J. Org. Chem.*, 2008, **73**, 1270–1281.

165 G. Cao, K. Yang, Y. Li, L. Huang and D. Teng, *Molecules*, 2016, **21**, 212.

166 J. Choi and G. C. Fu, *Science*, 2017, **356**, eaaf7230.

167 C. C. C. J. Seechurn, M. O. Kitching, T. J. Colacot and V. Snieckus, *Angew. Chem., Int. Ed.*, 2012, **51**, 5062–5085.

This journal is © The Royal Society of Chemistry 2021

168 T. Willemse, W. Schepens, H. W. T. Van Vlijmen, B. U. W. Maes and S. Ballet, *Catalysts*, 2017, **7**, 74.
169 H. Gruß and N. Sewald, *Chem. – Eur. J.*, 2020, **26**, 5328–5340.
170 M. Pérez-González and R. F. W. Jackson, *Chem. Commun.*, 2000, 2423–2424.
171 A. Afonso, L. Feliu and M. Planas, *Tetrahedron*, 2011, **67**, 2238–2245.
172 I. Ng-Choi, À. Oliveras, L. Feliu and M. Planas, *Beilstein J. Org. Chem.*, 2019, **15**, 761–768.
173 B.-B. Zhan, M.-X. Jiang and B.-F. Shi, *Chem. Commun.*, 2020, **56**, 13950.
174 Z. Bai, C. Cai, Z. Yu and H. Wang, *Angew. Chem., Int. Ed.*, 2018, **57**, 13912–13916.
175 J. Tang, Y. He, H. Chen, W. Sheng and H. Wang, *Chem. Sci.*, 2017, **8**, 4565–4570.
176 A. F. M. Noisier, J. García, I. A. Ionuț and F. Albericio, *Angew. Chem., Int. Ed.*, 2017, **56**, 314–318.
177 S. J. McCarver, J. X. Qiao, J. Carpenter, R. M. Borzilleri, M. A. Poss, M. D. Eastgate, M. M. Miller and D. W. C. MacMillan, *Angew. Chem.*, 2017, **129**, 746–750.
178 A. F. M. Noisier and M. A. Brimble, *Chem. Rev.*, 2014, **114**, 8775–8806.
179 W. Wang, M. M. Lorion, J. Shah, A. R. Kapdi and L. Ackermann, *Angew. Chem., Int. Ed.*, 2018, **57**, 14700–14717.
180 J. Ruiz-Rodríguez, F. Albericio and R. Lavilla, *Chem. – Eur. J.*, 2010, **16**, 1124–1127.
181 L. Mendive-Tapia, S. Preciado, J. García, R. Ramón, N. Kielland, F. Albericio and R. Lavilla, *Nat. Commun.*, 2015, **6**, 7160.
182 B. Han, B. Li, L. Qi, P. Yang, G. He and G. Chen, *Org. Lett.*, 2020, **22**, 6879–6883.
183 J. Tang, H. Chen, Y. He, W. Sheng, Q. Bai and H. Wang, *Nat. Commun.*, 2018, **9**, 3383.
184 J. Tan, J. Wu, S. Liu, H. Yao and H. Wang, *Sci. Adv.*, 2019, **5**, eaaw0323.
185 N. Kaplaneris, F. Kaltenhäuser, G. Sirvinskaite, S. Fan, T. De Oliveira, L.-C. Conradi and L. Ackermann, *Sci. Adv.*, 2021, **7**, eabe6202.
186 J. Liu, X. Liu, F. Zhang, J. Qu, H. Sun and Q. Zhu, *Chem. – Eur. J.*, 2020, **26**, 16122–16128.
187 S. Bloom, C. Liu, D. K. Kölmel, J. X. Qiao, Y. Zhang, M. A. Poss, W. R. Ewing and D. W. C. MacMillan, *Nat. Chem.*, 2018, **10**, 205.
188 T. Qin, L. R. Malins, J. T. Edwards, R. R. Merchant, A. J. E. Novak, J. Z. Zhong, R. B. Mills, M. Yan, C. Yuan, M. D. Eastgate and P. S. Baran, *Angew. Chem., Int. Ed.*, 2017, **56**, 260–265.
189 M. H. Vilhelmsen, J. Jensen, C. G. Tortzen and M. B. Nielsen, *Eur. J. Org. Chem.*, 2013, **3**, 701–711.
190 A. P. Silvestri, P. A. Cistrone and P. E. Dawson, *Angew. Chem., Int. Ed.*, 2017, **56**, 10438–10442.
191 S. Verlinden, N. Geudens, J. C. Martins, D. Tourwé, S. Ballet and G. Verniest, *Org. Biomol. Chem.*, 2015, **13**, 9398–9404.
192 N. Auberger, M. Di Pisa, M. Larregola, G. Chassaing, E. Peroni, S. Lavielle, A. M. Papini, O. Lequin and J. M. Mallet, *Bioorg. Med. Chem.*, 2014, **22**, 6924–6932.
193 P. A. Cistrone, A. P. Silvestri, J. C. J. Hintzen and P. E. Dawson, *ChemBioChem*, 2018, **19**, 1031–1035.
194 R. H. Grubbs and S. Chang, *Tetrahedron*, 1998, **54**, 4413–4450.
195 A. Fürstner, *Angew. Chem., Int. Ed.*, 2000, **39**, 3012–3043.
196 R. H. Grubbs, *Tetrahedron*, 2004, **60**, 7117–7140.
197 A. Gradillas and J. Pérez-Castells, *Angew. Chem., Int. Ed.*, 2006, **45**, 6086–6101.
198 A. H. Hoveyda and A. R. Zhugralin, *Nature*, 2007, **450**, 243–251.
199 X. Lu, L. Fan, C. B. Phelps, C. P. Davie and C. P. Donahue, *Bioconjugate Chem.*, 2017, **28**, 1625–1629.
200 O. B. C. Monty, P. Nyshadham, K. M. Bohren, M. Palaniappan, M. M. Matzuk, D. W. Young and N. Simmons, *ACS Comb. Sci.*, 2020, **22**, 80–88.
201 T. M. Trnka and R. H. Grubbs, *Acc. Chem. Res.*, 2001, **34**, 18–29.
202 A. H. Hoveyda and A. R. Zhugralin, *Nature*, 2007, **450**, 243–251.
203 E. C. Gleeson, W. R. Jackson and A. J. Robinson, *Tetrahedron Lett.*, 2016, **57**, 4325–4333.
204 Y.-W. Kim, T. N. Grossmann and G. L. Verdine, *Nat. Protoc.*, 2011, **6**, 761–771.
205 F. Bernal and S. G. Katz, *Methods Mol. Biol.*, 2014, **1176**, 107–114.
206 H. E. Blackwell and R. H. Grubbs, *Angew. Chem., Int. Ed.*, 1998, **37**, 3281–3284.
207 Y. S. Chang, B. Graves, V. Guerlavais, C. Tovar, K. Packman, K. H. To, K. A. Olson, K. Kesavan, P. Gangurde, A. Mukherjee, T. Baker, K. Darlak, C. Elkin, Z. Filipovic, F. Z. Qureshi, H. Cai, P. Berry, E. Feyfant, X. E. Shi, J. Horstick, D. A. Annis, A. M. Manning, N. Fotouhi, H. Nash, L. T. Vassilev and T. K. Sawyer, *Proc. Natl. Acad. Sci. U. S. A.*, 2013, **110**, E3445–E3454.
208 L. D. Walensky and G. H. Bird, *J. Med. Chem.*, 2014, **57**, 6275–6288.
209 Y. H. Lau, P. De Andrade, Y. Wu and D. R. Spring, *Chem. Soc. Rev.*, 2015, **44**, 91–102.
210 T. D. Clark, M. Reza Ghadiri and D. E. Angew Chem, *Angew. Chem.*, 1995, **117**, 201–203.
211 J. Pernerstorfer, *Chem. Commun.*, 1997, 1949–1950.
212 B. E. Fink, P. R. Kym and J. A. Katzenellenbogen, *J. Am. Chem. Soc.*, 1998, **120**, 4334–4344.
213 F. Liu, A. Giubellino, P. C. Simister, W. Qian, M. C. Giano, S. M. Feller, D. P. Bottaro and T. R. Burke, *Biopolymers*, 2011, **96**, 780–788.
214 A. K. Boal, I. Guryanov, A. Moretto, M. Crisma, E. L. Lanni, C. Toniolo, R. H. Grubbs and D. J. O'Leary, *J. Am. Chem. Soc.*, 2007, **129**, 6986–6987.
215 Ø. Jacobsen, J. Klaveness, O. Petter Ottersen, M. R. Amiry-Moghaddam and P. Rongved, *Org. Biomol. Chem.*, 2009, **7**, 1599–1611.
216 T. K. Pham and Y. W. Kim, *Bioorg. Chem.*, 2020, **101**, 104024.

This journal is © The Royal Society of Chemistry 2021

217 P. Martín-Gago, R. Ramón, E. Aragón, J. Fernández-Carneado, P. Martin-Malpartida, X. Verdaguer, P. López-Ruiz, B. Colás, M. A. Cortes, B. Ponsati, M. J. Macias and A. Riera, *Bioorg. Med. Chem. Lett.*, 2014, **24**, 103–107.

218 B. Van Lierop, S. Chee Ong, A. Belgi, C. Delaine, S. Andrikopoulos, N. L. Haworth, J. G. Menting, M. C. Lawrence, A. J. Robinson and B. E. Forbes, *Sci. Rep.*, 2017, **7**, 17239.

219 Ø. Jacobsen, J. Klaveness and P. Rongved, *Molecules*, 2010, **15**, 6638–6677.

220 G. H. Bird, N. Madani, A. F. Perry, A. M. Princiotto, J. G. Supko, X. He, E. Gavathiotis, J. G. Sodroski, L. D. Walensky and S. H. Snyder, *Proc. Natl. Acad. Sci. U. S. A.*, 2010, **107**, 14093–14098.

221 M. A. Hossain, L. M. Haugaard-Kedström, K. J. Rosengren, R. A. D. Bathgate and J. D. Wade, *Org. Biomol. Chem.*, 2015, **13**, 10895–10903.

222 Z. Amso, R. Kowalczyk, Y.-E. Park, M. Watson, J.-M. Lin, D. S. Musson, J. Cornish and M. A. Brimble, *Org. Biomol. Chem.*, 2016, **14**, 6231–6243.

223 J. M. Song, E. E. Gallagher, A. Menon, L. D. Mishra and A. L. Garner, *Org. Biomol. Chem.*, 2019, **17**, 6414–6419.

224 B. Van Lierop, S. Chee Ong, A. Belgi, C. Delaine, S. Andrikopoulos, N. L. Haworth, J. G. Menting, M. C. Lawrence, A. J. Robinson and B. E. Forbes, *Sci. Rep.*, 2017, **7**, 1–13.

225 P. M. Cromm, J. Spiegel and T. N. Grossmann, *ACS Chem. Biol.*, 2015, **10**, 1362–1375.

226 S. J. Miller, H. E. Blackwell and R. H. Grubbs, *J. Am. Chem. Soc.*, 1996, **118**, 9606–9614.

227 R. J. Platt, T. S. Han, B. R. Green, M. D. Smith, J. Skalicky, P. Gruszczyński, H. S. White, B. Olivera, G. Bulaj and J. Gajewiak, *J. Biol. Chem.*, 2012, **287**, 20727–20736.

228 Y.-W. Kim, P. S. Kutchukian and G. L. Verdine, *Org. Lett.*, 2010, **12**, 3046–3049.

229 M. N. Islam, M. S. Islam, M. A. Hoque, T. Kato, N. Nishino, A. Ito and M. Yoshida, *Bioorg. Med. Chem.*, 2014, **22**, 3862–3870.

230 A. M. Heapy, G. M. Williams, J. D. Fraser and M. A. Brimble, *Org. Lett.*, 2012, **14**, 878–881.

231 J. F. Reichwein, B. Wels, J. A. W. Kruijtzer, C. Versluis and R. M. J. Liskamp, *Angew. Chem., Int. Ed.*, 1999, **38**, 3684–3687.

232 J. F. Reichwein, C. Versluis and R. M. J. Liskamp, *J. Org. Chem.*, 2000, **65**, 6187–6195.

233 J. Lawrence, M. Jourdan, Y. Vallée and V. Blandin, *Org. Biomol. Chem.*, 2008, **6**, 4575–4581.

234 F. Liu, A. G. Stephen, A. A. Waheed, E. O. Freed, R. J. Fisher and T. R. Burke, *Bioorg. Med. Chem. Lett.*, 2010, **20**, 318–321.

235 W. J. Fang, T. F. Murray and J. V. Aldrich, *Bioorg. Med. Chem.*, 2018, **26**, 1157–1161.

236 S. A. Gisemba and J. V. Aldrich, *J. Org. Chem.*, 2020, **85**, 1407–1415.

237 U. Kazmaier, C. Hebach, A. Watzke, S. Maier, H. Mues and V. Huch, *Org. Biomol. Chem.*, 2005, **3**, 136–145.

238 I. W. Hamley, G. Cheng, V. Castelletto, S. Handschin and R. Mezzenga, *Chem. Commun.*, 2012, **48**, 3757–3759.

239 S. A. Cochrane, Z. Huang and J. C. Vederas, *Org. Biomol. Chem.*, 2013, **11**, 630–639.

240 J. L. Stymiest, B. F. Mitchell, S. Wong and J. C. Vederas, *Org. Lett.*, 2003, **5**, 47–49.

241 F. J. Dekker, N. J. De Mol, M. J. E. Fischer, J. Kemmink and R. M. J. Liskamp, *Org. Biomol. Chem.*, 2003, **1**, 3297–3303.

242 S. L. Mangold, D. J. Oleary and R. H. Grubbs, *J. Am. Chem. Soc.*, 2014, **136**, 12469–12478.

243 C. Xu, X. Shen and A. H. Hoveyda, *J. Am. Chem. Soc.*, 2017, **139**, 10919–10928.

244 K. M. Dawood and K. Nomura, *Adv. Synth. Catal.*, 2021, **363**, 1970–1997.

245 M. Poirier, N. Aubry, C. Boucher, J.-M. Ferland, S. Laplante and Y. S. Tsantrizos, *J. Org. Chem.*, 2005, **70**, 10765–10773.

246 N. K. Yee, V. Farina, I. N. Houpis, N. Haddad, R. P. Frutos, F. Gallou, X.-J. Wang, X. Wei, R. D. Simpson, X. Feng, V. Fuchs, Y. Xu, J. Tan, L. Zhang, J. Xu, L. L. Smith-Keenan, J. Vitous, M. D. Ridges, E. M. Spinelli, M. Johnson, K. Donsbach, T. Nicola, M. Brenner, E. Winter, P. Kreye and W. Samstag, *J. Org. Chem.*, 2006, **71**, 7133–7145.

247 E. C. Gleeson, W. R. Jackson and A. J. Robinson, *Chem. Commun.*, 2017, **53**, 9769–9772.

248 K. Skowerski, G. Szczepaniak, C. Wierzbicka, Ł. Gu$ajski, M. $ Bieniek and K. Grela, *Catal. Sci. Technol.*, 2012, **2**, 2424–2427.

249 S. Masuda, S. Tsuda and T. Yoshiya, *Org. Biomol. Chem.*, 2018, **16**, 9364–9367.

250 A. Fürstner, *Angew. Chem., Int. Ed.*, 2013, **52**, 2794–2819.

251 B. Aguilera, L. B. Wolf, P. Nieczypor, F. P. J. T. Rutjes, H. S. Overkleeft, J. C. M. van Hest, H. E. Schoemaker, B. Wang, J. C. Mol, A. Fürstner, M. Overhand, G. A. van der Marel and J. H. van Boom, *J. Org. Chem.*, 2001, **66**, 3584–3589.

252 M. Ijsselstijn, B. Aguilera, G. A. Van Der Marel, J. H. Van Boom, F. L. Van Delft, H. E. Schoemaker, H. S. Overkleeft, F. P. J. T. Rutjes and M. Overhand, *Tetrahedron Lett.*, 2004, **45**, 4379–4382.

253 N. Ghalit, A. J. Poot, A. Fürstner, D. T. S. Rijkers and R. M. J. Liskamp, *Org. Lett.*, 2005, **7**, 2961–2964.

254 P. M. Cromm, S. Schaubach, J. Spiegel, A. Fürstner, T. N. Grossmann and H. Waldmann, *Nat. Commun.*, 2016, **7**, 11300.

255 P. M. Cromm, K. Wallraven, A. Glas, D. Bier, A. Fürstner, C. Ottmann and T. N. Grossmann, *ChemBioChem*, 2016, **17**, 1915–1919.

256 K. R. Campos, D. Cai, M. Journet, J. J. Kowal, R. D. Larsen and P. J. Reider, *J. Org. Chem.*, 2001, **66**, 3634–3635.

257 A. Fürstner and K. Radkowski, *Chem. Commun.*, 2002, 2182–2183.

258 H. C. Kolb, M. G. Finn and K. B. Sharpless, *Angew. Chem., Int. Ed.*, 2001, **40**, 2004–2021.

259 C. W. Tornøe, C. Christensen and M. Meldal, *J. Org. Chem.*, 2002, **67**, 3057–3064.

260 V. V. Rostovtsev, L. G. Green, V. V. Fokin and K. B. Sharpless, *Angew. Chem.*, 2002, **114**, 2708–2711.

This journal is © The Royal Society of Chemistry 2021

261 W. S. Horne, C. A. Olsen, J. M. Beierle, A. Montero and M. R. Ghadiri, *Angew. Chem., Int. Ed.*, 2009, **48**, 4718–4724.
262 Ø. Jacobsen, H. Maekawa, N.-H. Ge, C. H. G€ Orbitz, P. P. Rongved, O. P. Ottersen, M. Amiry-Moghaddam and J. Klaveness, *J. Org. Chem.*, 2011, **76**, 1228–1238.
263 V. Castro, H. Rodríguez and F. Albericio, *ACS Comb. Sci.*, 2016, **18**, 1–14.
264 L. Recnik, W. Kandioller and T. L. Mindt, *Molecules*, 2020, **25**, 3576.
265 Y. H. Lau, P. De Andrade, S.-T. Quah, M. Rossmann, L. Laraia, N. Sköld, S. Sköld, T. J. Sum, P. J. E. Rowling, T. L. Joseph, C. Verma, M. Hyvönen, H. Hyvönen, L. S. Itzhaki, A. R. Venkitaraman, C. J. Brown, D. P. Lane and D. R. Spring, *Chem. Sci.*, 2014, **5**, 1804–1809.
266 L. Zhang, T. Navaratna, J. Liao and G. M. Thurber, *Bioconjugate Chem.*, 2015, **26**, 329–337.
267 L. Frankiewicz, C. Betti, K. Guillemyn, D. Tourwé, Y. Jacquot and S. Ballet, *J. Pept. Sci.*, 2013, **19**, 423–432.
268 G. Chouhan and K. James, *Org. Lett.*, 2013, **15**, 1206–1209.
269 J. Iegre, P. Brear, D. J. Baker, Y. S. Tan, E. L. Atkinson, H. F. Sore, D. H. O' Donovan, C. S. Verma, M. Hyvönen, H. Hyvönen and D. R. Spring, *Chem. Sci.*, 2019, **10**, 5056–5063.
270 M. Meldal and C. W. Tornøe, *Chem. Rev.*, 2008, **108**, 2952–3015.
271 C. Ngambenjawong, J. M. B. Pineda and S. H. Pun, *Bioconjugate Chem.*, 2016, **27**, 2854–2862.
272 M. Strack, É. Billard, D. Chatenet and W. D. Lubell, *Bioorg. Med. Chem. Lett.*, 2017, **27**, 3412–3416.
273 M. Strack, S. Langklotz, J. E. Bandow, N. Metzler-Nolte and H. B. Albada, *J. Org. Chem.*, 2012, **77**, 9954–9958.
274 M. Roice, I. Johannsen and M. Meldal, *QSAR Comb. Sci.*, 2004, **23**, 662–673.
275 V. Goncalves, B. Gautier, A. Regazzetti, P. Coric, S. Bouaziz, C. Garbay, M. Vidal and N. Inguimbert, *Bioorg. Med. Chem. Lett.*, 2007, **17**, 5590–5594.
276 S. Ingale and P. E. Dawson, *Org. Lett.*, 2011, **13**, 2822–2825.
277 B. B. Metaferia, M. Rittler, J. S. Gheeya, A. Lee, H. Hempel, A. Plaza, W. G. Stetler-Stevenson, C. A. Bewley and J. Khan, *Bioorg. Med. Chem. Lett.*, 2010, **20**, 7337–7340.
278 R. A. Turner, A. G. Oliver and R. S. Lokey, *Org. Lett.*, 2007, **9**, 5011–5014.
279 C. Testa, D. D'addona, M. Scrima, A. M. Tedeschi, A. M. D'ursi, C. Bernhard, F. Denat, C. Bello, P. Rovero, M. Chorev and A. M. Papini, *Pept. Sci.*, 2018, **110**, e24071.
280 C. Testa, M. Scrima, M. Grimaldi, A. M. D'Ursi, M. L. Dirain, N. Lubin-Germain, A. Singh, C. Haskell-Luevano, M. Chorev, P. Rovero and A. M. Papini, *J. Med. Chem.*, 2014, **57**, 9424–9434.
281 V. D. Bock, R. Perciaccante, T. P. Jansen, H. Hiemstra and J. H. Van Maarseveen, *Org. Lett.*, 2006, **8**, 919–922.
282 S. Cantel, A. Le, C. Isaad, M. Scrima, J. J. Levy, R. D. Dimarchi, P. Rovero, J. A. Halperin, A. Maria D'ursi, A. M. Papini and M. Chorev, *J. Org. Chem.*, 2008, **73**, 5663–5674.
283 J. H. Park and M. L. Waters, *Org. Biomol. Chem.*, 2013, **11**, 69–77.
284 Y. Liu, L. Zhang, J. Wan, Y. Li, Y. Xu and Y. Pan, *Tetrahedron*, 2008, **64**, 10728–10734.
285 J. H. Van Maarseveen, W. S. Horne and M. R. Ghadiri, *Org. Lett.*, 2005, **7**, 4503–4506.
286 P. T. Tran, C. Ø. Larsen, T. Røndbjerg, M. De Foresta, M. B. A. Kunze, A. Marek, J. H. Løper, L.-E. Boyhus, A. Knuhtsen, K. Lindorff-Larsen and D. S. Pedersen, *Chem. – Eur. J.*, 2017, **23**, 3490–3495.
287 S. Pacifico, A. Kerckhoffs, A. J. Fallow, R. E. Foreman, R. Guerrini, J. Mcdonald, D. G. Lambert and A. G. Jamieson, *Org. Biomol. Chem.*, 2017, **15**, 4704–4710.
288 M. M. Wiedmann, Y. S. Tan, Y. Wu, S. Aibara, W. Xu, H. F. Sore, C. S. Verma, L. Itzhaki, M. Stewart, J. D. Brenton and D. R. Spring, *Angew. Chem., Int. Ed.*, 2017, **56**, 524–529.
289 J. Iegre, N. S. Ahmed, J. S. Gaynord, Y. Wu, K. M. Herlihy, Y. S. Tan, M. E. Lopes-Pires, R. Jha, Y. H. Lau, H. F. Sore, C. Verma, D. H. O' Donovan, N. Pugh and D. R. Spring, *Chem. Sci.*, 2018, **9**, 4638–4643.
290 W. Xu, Y. H. Lau, G. Fischer, Y. S. Tan, A. Chattopadhyay, M. De La Roche, M. Hyvö, C. Verma, D. R. Spring and L. S. Itzhaki, *J. Am. Chem. Soc.*, 2017, **139**, 2245–2256.
291 Y. Onda, G. Bassi, A. Elsayed, F. Ulrich, S. Oehler, L. Plais, J. Scheuermann and D. Neri, *Chem. – Eur. J.*, 2021, 7160–7167.
292 M. Horn, F. Reichart, S. Natividad-Tietz, D. Diaz and I. Neundorf, *Chem. Commun.*, 2016, **52**, 2261–2264.
293 P. M. Weerawarna, Y. Kim, A. C. G. Kankanamalage, V. C. Damalanka, G. H. Lushington, K. R. Alliston, N. Mehzabeen, K. P. Battaile, S. Lovell, K.-O. Chang and W. C. Groutas, *Eur. J. Med. Chem.*, 2016, **119**, 300–318.
294 A. L. C. Isaad, A. M. Papini, M. Chorev and P. Rovero, *J. Pept. Sci.*, 2009, **15**, 451–454.
295 V. Celentano, D. Diana, C. Di Salvo, L. De Rosa, A. Romanelli, R. Fattorusso and L. D. D'Andrea, *Chem. – Eur. J.*, 2016, **22**, 5534–5537.
296 S. Li, H. Cai, J. He, H. Chen, S. Lam, T. Cai, Z. Zhu, S. J. Bark and C. Cai, *Bioconjugate Chem.*, 2016, **27**, 2315–2322.
297 T. R. Chan, R. Hilgraf, K. B. Sharpless and V. V. Fokin, *Org. Lett.*, 2004, **6**, 2853–2855.
298 Z. Zhu, H. Chen, S. Li, X. Yang, E. Bittner and C. Cai, *Catal. Sci. Technol.*, 2017, **7**, 2474–2485.
299 S. Punna and M. G. Finn, *Synlett*, 2004, **2004**, 99–100.
300 D. S. Pedersen and A. Abell, *Eur. J. Org. Chem.*, 2011, 2399–2411.
301 Y. L. Angell and K. Burgess, *Chem. Soc. Rev.*, 2007, **36**, 1674–1689.
302 R. Jagasia, J. M. Holub, M. Bollinger, K. Kirshenbaum and M. G. Finn, *J. Org. Chem.*, 2009, **74**, 2964–2974.
303 R. Kandler, S. Das and A. Nag, *RSC Adv.*, 2021, **11**, 4842–4852.
304 S. R. Tala, A. Singh, C. J. Lensing, S. M. Schnell, K. T. Freeman, J. R. Rocca and C. Haskell-Luevano, *ACS Chem. Neurosci.*, 2017, **9**, 1001–1013.
305 G. J. J. Richelle, S. Ori, H. Hiemstra, J. H. van Maarseveen and P. Timmerman, *Angew. Chem., Int. Ed.*, 2018, **57**, 501–505.

This journal is © The Royal Society of Chemistry 2021

306 G. J. J. Richelle, M. Schmidt, H. Ippel, T. M. Hackeng, J. H. van Maarseveen, T. Nuijens and P. Timmerman, *ChemBioChem*, 2018, **19**, 1934–1938.
307 D. E. Streefkerk, M. Schmidt, J. H. Ippel, T. M. Hackeng, T. Nuijens, P. Timmerman and J. H. Van Maarseveen, *Org. Lett.*, 2019, **21**, 2095–2100.
308 M. Empting, O. Avrutina, R. Meusinger, S. Fabritz, M. Reinwarth, M. Biesalski, S. Voigt, G. Buntkowsky and H. Kolmar, *Angew. Chem., Int. Ed.*, 2011, **50**, 5207–5211.
309 A. Knuhtsen, C. Whitmore, F. S. Mcwhinnie, L. Mcdougall, R. Whiting, B. O. Smith, C. M. Timperley, A. C. Green, K. I. Kinnear and A. G. Jamieson, *Chem. Sci.*, 2019, **10**, 1671–1676.
310 A. M. White, S. J. de Veer, G. Wu, P. J. Harvey, K. Yap, G. J. King, J. E. Swedberg, C. K. Wang, R. H. P. Law, T. Durek and D. J. Craik, *Angew. Chem., Int. Ed.*, 2020, **59**, 11273–11277.
311 L. Zhang, X. Chen, P. Xue, H. H. Y. Sun, I. D. Williams, K. B. Sharpless, V. V. Fokin and G. Jia, *J. Am. Chem. Soc.*, 2005, **127**, 15998–15999.
312 M. M. Majireck and S. M. Weinreb, *J. Org. Chem.*, 2006, **71**, 8680–8683.
313 A. Tam, U. Arnold, M. B. Soellner and R. T. Raines, *J. Am. Chem. Soc.*, 2007, **129**, 12670–12671.
314 B. C. Boren, S. Narayan, L. K. Rasmussen, L. Zhang, H. Zhao, Z. Lin, G. Jia and V. V. Fokin, *J. Am. Chem. Soc.*, 2008, **130**, 8923–8930.
315 O. Kracker, J. Góra, J. Krzciuk-Gula, A. Marion, B. Neumann, H. G. Stammler, A. Nieß, I. Antes, R. Latajka and N. Sewald, *Chem. – Eur. J.*, 2018, **24**, 953–961.
316 M. R. Krause, R. Goddard and S. Kubik, *J. Org. Chem.*, 2011, **76**, 7084–7095.
317 J. Zhang, J. Kemmink, D. T. S. Rijkers and R. M. J. Liskamp, *Org. Lett.*, 2011, **13**, 3438–3441.
318 J. Zhang, J. Kemmink, D. T. S. Rijkers and R. M. J. Liskamp, *Chem. Commun.*, 2013, **49**, 4498–4500.
319 S. Tomassi, A. M. Trotta, C. Ieranò, F. Merlino, A. Messere, G. Rea, F. Santoro, D. Brancaccio, A. Carotenuto, V. M. D'Amore, F. S. Di Leva, E. Novellino, S. Cosconati, L. Marinelli, S. Scala and S. Di Maro, *Chem. – Eur. J.*, 2020, **26**, 10113–10125.
320 J. K. Pokorski, L. M. M. Jenkins, H. Feng, S. R. Durell, Y. Bai and D. H. Appella, *Org. Lett.*, 2007, **9**, 2381–2382.
321 M. Tischler, D. Nasu, M. Empting, S. Schmelz, D. W. Heinz, P. Rottmann, H. Kolmar, G. Buntkowsky, D. Tietze and O. Avrutina, *Angew. Chem., Int. Ed.*, 2012, **51**, 3708–3712.
322 Ahsanullah, P. Schmieder, R. Kühne and J. Rademann, *Angew. Chem., Int. Ed.*, 2009, **48**, 5042–5045.
323 Ahsanullah and J. Rademann, *Angew. Chem., Int. Ed.*, 2010, **49**, 5378–5382.
324 L. Reguera and D. G. Rivera, *Chem. Rev.*, 2019, **119**, 9836–9860.
325 A. Demharter, W. Hörl, E. Herdtweck and I. Ugi, *Angew. Chem., Int. Ed. Engl.*, 1996, **35**, 173–175.
326 C. Hebach and U. Kazmaier, *Chem. Commun.*, 2003, 596–597.
327 O. E. Vercillo, C. K. Z. Andrade and L. A. Wessjohann, *Org. Lett.*, 2008, **10**, 205–208.
328 A. Dömling and I. Ugi, *Angew. Chem., Int. Ed.*, 2000, **39**, 3168–3210.
329 R. Hili, V. Rai and A. K. Yudin, *J. Am. Chem. Soc.*, 2010, **132**, 2889–2891.
330 A. P. Treder, J. L. Hickey, M. C. J. Tremblay, S. Zaretsky, C. C. G. Scully, J. Mancuso, A. Doucet, A. K. Yudin and E. Marsault, *Chem. – Eur. J.*, 2015, **21**, 9249–9255.
331 A. V. Vasco, C. S. Pérez, F. E. Morales, H. E. Garay, D. Vasilev, J. A. Gavín, L. A. Wessjohann and D. G. Rivera, *J. Org. Chem.*, 2015, **80**, 6697–6707.
332 F. E. Morales, H. E. Garay, D. F. Muñoz, Y. E. Augusto, A. J. Otero-González, O. Reyes Acosta and D. G. Rivera, *Org. Lett.*, 2015, **17**, 2728–2731.
333 A. V. Vasco, Y. Méndez, A. Porzel, J. Balbach, L. A. Wessjohann and D. G. Rivera, *Bioconjugate Chem.*, 2019, **30**, 253–259.
334 M. G. Ricardo, F. E. Morales, H. Garay, O. Reyes, D. Vasilev, L. A. Wessjohann and D. G. Rivera, *Org. Biomol. Chem.*, 2015, **13**, 438–446.
335 M. G. Ricardo, A. M. Ali, J. Plewka, E. Surmiak, B. Labuzek, C. G. Neochoritis, J. Atmaj, L. Skalniak, R. Zhang, T. A. Holak, M. Groves, D. G. Rivera and A. Dömling, *Angew. Chem., Int. Ed.*, 2020, **59**, 5235–5241.
336 B. K. W. Chung, J. L. Hickey, C. C. G. Scully, S. Zaretsky and A. K. Yudin, *MedChemComm*, 2013, **4**, 1124–1128.
337 T. M. Vishwanatha, E. Bergamaschi and A. Dömling, *Org. Lett.*, 2017, **19**, 3195–3198.
338 M. C. Morejón, A. Laub, B. Westermann, D. G. Rivera and L. A. Wessjohann, *Org. Lett.*, 2016, **18**, 4096–4099.
339 N. A. Petasis, I. A. Zavialov and L. Angeles, *J. Am. Chem. Soc.*, 1997, **7863**, 445–446.
340 M. G. Ricardo, J. F. Marrrero, O. Valdés, D. G. Rivera and L. A. Wessjohann, *Chem. – Eur. J.*, 2019, **25**, 769–774.

This journal is © The Royal Society of Chemistry 2021

Electronic Supplementary Material (ESI) for RSC Medicinal Chemistry.
This journal is © The Royal Society of Chemistry 2021

Macrocyclization strategies for cyclic peptides and peptidomimetics

Clément Bechtler[a] and Christina Lamers[a]*

Department Pharmaceutical Sciences, University of Basel, Klingelbergstr. 50, 4056 Basel, Switzerland.

Supplementary Table S1: Commonly used macrocyclization reactions for peptides. The required reaction partners are listed as well as if they have been reported to work succesfully on-resin, in solution, in a chemoselective way or on unprotected petides, a green tick signfiying it has been reported, a red cross that it has not been reported.

Bond or functional group formed	Required functional groups: Reaction partner I (N-terminus)	Reaction partner II (C-terminus)	Reaction	On-resin	In solution	Chemoselective	Unprotected	Comments
Amide	H_2N-	-COOH	Amide coupling	✓	✓	?	✓	
	HNCys-	-COSR	NCL	✓	✓	✓	✓	
	HNAla-	-COSR	NCL + desulfurisation	✓	✓	✓	✓	
	H_2N-	-COSR	aminolysis	?	✓	✓	Lys	Other lysine needs to be protected
	H_2N-	-COO-Sanger	aminolysis	?	✓	✓	Lys	Other lysine needs to be protected
	H_2N-	-COO-Dbz	aminolysis	✓	✓	✓	?	
	N_3CH_2NH-	$-COSCH_2PPh_2$	Staudinger	?	✓	✓	?	
	2-amino thioamide-	-COOH	Ag-promoted lactamisation	✓	✓	✓	✓	
	HNCys-	-glycolaldehyde	Thiazolidine formation	?	✓	✓	?	Or sidechain aldehyde
	RONH-	-Ketoacide	KAHA	?	✓	✓	?	Mild conditions
	5-oxaproline-	-Ketoacide	KAHA II	?	✓	✓	?	Introduces homoserine, epimerization
	HNSer/Thr-	-COO-salicylaldehyde	Ser/Thr ligation	✓	✓		?	
	H_2N-	-COOH	Lactam formation, subsequent O-to-N transfer		✓		?	Depsipeptide mediated
	2-OH-6-NO_2-benzyl-NH-	-COOH	Lacton formation and O-to-N migration		✓			
	H_2N--COOH	*tert*-butyl-isocyanide and aziridine aldehyde	MCR, disrupted Ugi	✓	✓	?	?	
N-substituted amide	COOH, $-NH_2$, -CHO, -NC	-	MCR, Ugi		✓	?	?	
Amine	H_2N-nitrotyrosine	-CHO, -NC	MCR, Ugi-Smiles	✓	✓	?	?	
	$-NH_2$ (Lys)	Diborono-benzene scaffold	Petasis reachtion stapling	✓	✓	?	?	
Imine to amine	H_2N-	-CHO	Trapping imine: CN^- Strecker Reduction with BH_3CN		✓	✓		
	H_2NTrp/His-	-CHO	Trapping imine Pictet-Spengler		✓	✓		
	H_2N-	-CHO	Intramolecular 4-imidazolidinone formation		✓	✓		CyClick
	NH_2-Gly-	Carboxybenzaldehyde on sidechain	Trapping imine with dipolarophiles	✓		✓		
	NH_2 (Lys)	HCHO	Trapping with Trp or Arg		✓	✓		
Imine	H_2N-	-CHO	Trapping imine as iminoboronate		✓	✓		Introduction of non-natural amino acid; reversible upon stimuli (pH, oxidation, small molecules)
Imine to pyrrole	NH_2 (Lys)	Furan to diketoene	Ketoenal formation		✓	✓		
Oxime	hydroxylamine	aldehyde	oxime		✓	✓		E- and Z-isomer
-S-S-	Thiol	Thiol	oxidation	✓	✓	✓		
$-S-CH_2-S-$	Thiol	Thiol	Methylene thioacetal formation	?	✓	✓	✓	
-S-	Thiol	Bromo/chloroacetate	Attached to Lys-sidechain or N-terminal amino group	✓	✓	✓	✓	Primary amines have to be protected; can be applied on in vitro techniques
	Thiol	alkene	Thiol-ene	✓	✓	✓	✓	Alkene as acryloyl, compatible on phage

	Thiol	alkene	Radical thiol-ene	✓	✓	✓		Alkene as allyloxy PG or non-natural AA
	Thiol	alkyne	Radical thiol-yne		✓	✓		Generates E- and Z- isomer
	Thiol	DHA	Michael-addition	✓	✓	✓		
	Thiol	scaffolds		✓	✓	✓		
C-O	Alcohol	Aryl boronic acid	Evans-Chan-Lam coupling	?	✓	✓	?	Also for aryl amines or aryl thioethers
	Alcohol	Carbonate	Tsuji-Trost reaction	?	✓	✓	✓	
	Alcohol	Aryl bromide	Metal-photoredox-catalsed reactions	?	✓	✓	?	
C-C	Organometal, alkene	Halide	Traditional cross coupling	✓	✓	✓	?	Suzuki couplings on unprotected peptides reported, but usually protected
	Alkene, allyl, aryl	Aryl, aryl halide	CH activation – cross coupling	?	✓	✓	?	
	Acrylate	C-terminal carboxylic acid	Ir-photocatlysed reaction	?	✓	✓	✓	
	Alkyne	Alkyne	Glaser-Hay coupling	✓	✓	✓	?	
C=C	Alkene	Alkene	RCM	✓	✓	✓	✓	Also suitable for DNA-enocded libraries
C≡C	Alkyne	Alkyne	RCAM	✓	✓	✓	?	
1,4-Disubstiuted triazole	Alkyne	Azide	CuAAC	✓	✓	✓	✓	
1,5-Disubstiuted triazole	Alkyne	Azide	RuAAC	✓	✓	✓	?	
1,5-Disubstiuted triazole	Alkyne	Azide	Metal-free Dipolar cycloaddition	✓	?	✓	?	

Supplementary Table S2: Selection of examples in which peptide macorcyclizations were used to improve biological properties of peptides. AT_2 = Angiotensin II receptor type 2, AT_1 = Angiotensin II receptor type 1, OXTR = oxytocin receptor, IR = insulin receptor, pAkt = phosphorylated Akt, eIF4E = eukaryotic translation initiation factor 4E, UTR = urotensin II receptor.

Functional group or bond formed	Reaction	Aim	Change of	Target	Result	Comment	Reference
Lactam	Lactam coupling head-to-tail	β-hairpin as smaller α-helix mimetic	Secondary structure (α-helix)	p53-HDM2	IC_{50} 0.53 µM (8 AA β-hairpin) vs 1.1 µM (15 AA α-helix)		[1]
	Lactam sidechain-to-sidechain	Smallest α-helix (pentapeptide)			Induction of α-helix in water		[2]
	NCL	Improve proteolytic stability	Free N- and C-terminus	α-conotoxin MII derivatives on nicotinic acetylcholine receptor	Improved proteolytic stability (20%)	Preserve full activity (1.3 µM)	[3]
	Aldehyde + N-term. Cys	Synthesis natural compound		Lugdunin	S. aureus MIC 1.5 µg/mL		[4]
	Serine ligation	Synthesis natural compound		Daptomycin	First total synthesis		[5]
	Scaffold	PPI	Linear peptide	TNFα:TNFα receptor	3.1 µM (ELISA) K_D 0.45 µM	scaffold essential for affinity (KD >10 µM)	[6]
Oxime		Affinity and proteolytic stability	Linear peptide	p53 HDM2/X	IC_{50} HDM2 110 nM; HDMX 340 nM (linear: 1.5 µM; 7.5 µM)	10- to 15- fold higher stability, 40% higher helicity	[7]
Disulfide	Oxidation of Cysteines		Linear vs lactam vs disulfide cyclized	ERα	K_i 0.17 µM vs 0.22 µM vs 0.025 µM	Stabilized helicity	[8]
Thioacetal	TBAF-mediated thioacetalization	Selectivity	Linear peptide	AT_2	selectivity over AT_1 increased from 0.5-fold to 10-fold	Change of affinity strongly dependent on linker length;	[9]
	CH_2I_2-mediated thioacetalization		Disulfide	OXTR	6-fold decrease in affinity	only weak decrease in affinity, serum stability increased 2.5-fold	[10]
	CH_2I_2-mediated thioacetalization	Affinity and serum stability	Disulfide	IR	2-fold decrease in pAkt signalling, but strongly increased serum stability		[11]
Thioether	Scaffold	Activity, helicity	Linear vs stapled peptide	Mdm2/Mdmx	Mdm2: IC_{50} 57 nM vs 5.4 nM Mdmx: IC_{50} 1800 nM vs 14 nM	Increased cell permeability of stapled peptides	[12]
	Photo controllable scaffold	Activity, helicity	Linear vs trans vs cis	Bcl-xl	K_D 134 nM vs 825 nM vs 42 nM	Opportunity to activate apoptotic process under light control	[13]
C-C single bond	$C(sp^3)$–H activation-mediated macrocyclization	Binding, stability	Linear peptide	Integrins	>100-fold increased proteolytic stability	When applied to RGD-containing peptides: binding to αvβ3 integrin-overexpressing cells strongly increased	[14])
Alkene	RCM	Affinity	Linear peptide	eIF4E	6-fold increase in affinity	Affinity dependent on ring size	[15]
	RCM	Activity, stability	Linear peptide	Bcl-xl	K_D 154 nM vs 69 nM; stability 60 fold improved	intramolecular H-bond mimetic	[16]
	RCM	Affinity, helicity	Linear peptide	p53 MDM2/X	K_i (MDM2) 14 nM vs 1 nM, K_i (MDX) 47 nM vs 7 nM		[17]

		Insulin Activity	Disulfide	IR	Cis-Isomer showed increased efficacy in mice compared to native insulin	Binding of trans-isomer to IR (A and B) 50-fold reduced	[18]
Alkyne	RCAM	Affinity	Linear peptide	Rab8a	>10-fold increase in affinity	Affinity strongly dependent on linker lenght	[19]
1,4-substituted 1,2,3-triazole	CuAAC	Affinity, helicity	Linear peptide	BCL9 β-catenin	K_i 0.6 μM vs 0.13 μM; Helicity 44% vs 90%	improved stability	[20]
	CuAAC	Activity	Disulfide		Equipotent as the disulfide in rat model for neuropathic pain	Drastically increased plasma stability	[21]
1,5-substituted 1,2,3-triazole	RuAAC	Affinity	Disulfide	UTR	Maintained affinity	1,4-substituted triazole analogues lost affinity	[22]
	RuAAC	Inhibitory activity, hepatic stability	Disulfide	Set of proteases	Reduced inhibition 5-100-fold compared to disulfide; hepatic stability of triazoles increased >2 - >6-fold		[23]

Supplementary Table S3: Example reaction conditions used for in solution RCM for peptides. stochi. = stochiometric, TCE = 1,1,2-trichloroethane, TFE = 1,1,1-trifluoroethanol, rt = room temperature

Substrate conc.	**Catalyst**	**Catalyst loading**	**Solvent**	**T (°C)**	**other conditions**	**t**	**Yields**	**workup**	**Comment**	**Ref.**
5 mM	Grubbs I	20%	$CHCl_3$	25 °C		3 -4 h	85-90%			[24]
5 mM	Hoveyda-Grubbs I	2.50%	DCM	40 °C		20 h	85%			[25]
10 mM	Hoveyda-Grubbs I	5%	DCM	40 °C (reflux)		24 h	87%			[26]
2.5 mM	Grubbs II	stochi.	TCE/DMF				67%			[27]
7 mM	Grubbs I	20%	DCM	rt	dry, degassed	48 h	40%			[28]
0.6 mM	Grubbs II	10%	DCM	reflux	dry	24 h	9% (overall: SPPS, cleavage, macrolactamizstion, RCM)	Removed solvent	Gave specifically cis alkene	[29]
4 mM	Grubbs II	15-20%	DCM	rt		6-7.5 h	42-52%		Catalyst added in two portions, second portion after 2- 3 h	[30]
10 mM	Hoveyda-Grubbs II	20%	TFE/DCM (4:1)	**rt**		48 h	20-30%	Removed solvent, purified by HPLC		[31]

Supplementary Table S4: Example reaction conditions used for on resin RCM for peptides. † = nominal concentration (resin loading/solvent volume), DCE = 1,2-dichloroethane, TCE = 1,1,2-trichloroethane, rt = room temperature, µW = microwave, * = not specified which generation.

Substrate conc.†	Catalyst	Catalyst loading	Additives (eq)	Solvent	T (°C)	Other conditions	t	Yields	Workup	Comment	Ref.
	Grubbs II	15%		DCM	100 °C		75 min				[32]
82 mM	Hoveyda-Grubbs II	20%		DCM	100 °C	µW (300 W)	1 h	29%		Was essential to change from chlorotritiyl to HMBA resin	[33]
	Hoveyda-Grubbs II	15%		DCM/DMF	100 °C	µW (120 W)	2 h	7 - 16%			[34]
5.5 mM	Grubbs II	18%	2,6-Dichlorotoluene (3.6 eq)	TCE	reflux	N_2	16 h	45		Mixture of E/Z (9%/37%)	[35]
33.3 mM	Hoveyda-Grubbs*	200 g/mol (x2)		TCE	50 °C		overnight				[36]
13 mM	Grubbs I	40%		DCM	rt	Ar	48 h				[37]
24 mM	Grubbs II	20%	LiCl (0.8 eq.)	DCM/DMF (95/5)	100 °C	µW (100 W)	2 h	95%		RCM was unsuccesful on full length peptide, needed to be done on truncated version which was afterwards elongated, 3:1 E:Z	[38]
33.3 mM	Grubbs II	10%	LiCl (4 eq.)	DCM:DMF (4:1)	40 °C, reflux	dry, degassed	48 h	22% (overall: SPPS, RCM, cleavage)	Washed with DMSO for 12 h after RCM, filtration, washed with DCM, MeOH		[29]
	Hoveyda-Grubbs II			DCE	50 °C		8 h		Washed with DMF, DCM		[17]
	Grubbs II	20%	LiCl	DCM	100 °C	µW (60 W)	1 h				[39]
24 mM	Grubbs II	20%	LiCl (0.8)	DCM:DMF (19:1 or 20:1)	100 °C	µW (80 - 100 W)	1 - 2 h	100%			[40]
	Hoveyda-Grubbs II	30%		DCM:DMF (4:1)	100 °C	µW (100 W)	2 h	26% (crude)			[41]
	Hoveyda-Grubbs II	20-35%		TFE:DCM (4:1)	rt		48 h	20-30% (overall, convsersion > 90%)	Wash with DMSO:DMF (1:1) overnight	Reaction on Novapeg resin required only 20% catalyst, on Wang resin 35%	[31]

Supplementary Table S5: Example reaction conditions used for solution CuAAC for peptides. TFE = 1,1,1-trifluoroethanol, TBTA = tris[(1-benzyl-1*H*-1,2,3-triazol-4-yl)methyl]amine, THTPA = tris(3-hydroxypropyltriazolylmethyl)amine, rt = room temperature.

Substrate conc.	Cu salt (eq)	Ascorbate (eq)	Additives (eq)	Solvent	T	Other conditions	time	Yield	Workup	Comment	Ref.
1 mM	$CuSO_4$ x 5 H_2O (3)	6		NH_4CO_3 buffer (0.1 M)	rt	Ar	30 min		pH 2 (TFA), SPE (C18)		42
1.2 M (!)	CuBr (1)	-	DBU (3)	DCM	rt	dry, N_2	12 h		Washed with 3 M HCl, extracted with DCM		43
0.775 mM	$CuSO_4$ x 5 H_2O (14)	Large excess		H_2O:*t*BuOH (2:1)	rt		Overnight		Concentrated, lyophilise, C18 HPLC		44
0.5 mM	$CuSO_4$ x 5 H_2O (14)	13		H_2O:*t*BuOH (2:1)	rt		1 h		HPLC (C12)		45
0.954 mM	$CuSO_4$ x 5 H_2O (8.4)	8.45		H_2O:*t*BuOH (2:1)	rt		overnight		Concentrated, lyophilise, C18 HPLC (SPE)		46
1 mM	CuBr (0.2)	-	DBU (3)	$PhCH_3$	110 °C		16 h	70%		CuI gave substantial iodoatriazole adducts	47
0.15 mM	CuI.$P(OEt)_3$ (0.31)	-	DIPEA (3)	DCM	rt	Protected from light	42 h	83%			48
0.3 mM	$CuSO_4$ x 5 H_2O (4.4)	4.4	-	H_2O:*t*BuOH (2:1)	rt		Overnight				49
1 mM	$Cu(MeCN)_4][PF_6]$ (1.8)	2.1	Tris-tri(methylazolyl)-amine (2.7)	10 mM Na-Phosphate, pH 8	rt	Protected from light	Overnight				50
10 mM	$Cu(MeCN)_4][PF_6]$ (0.05)	-	TBTA (0.05)	DCM	55 °C		12 h	39-79%			51
0.8 mM	$CuSO_4$ x 5 H_2O (4)	6	-	H_2O:*t*BuOH (1:1)	rt		Overnight				36
10 mg/mL	CuBr (0.01)	-	DBU (0.03)	DCM	rt		6 h				52
1 mM	CuI (2)	-	DIPEA (2), 2,6-lutidine (2)	MeCN	rt	Ar, degassed	12 h				53
0.5 mM	$CuSO_4$ (1)	5	THTPA (1)	H_2O:*t*BuOH (1:1) or H_2O:TFE (1:1)	rt		< 1 h	13-51%			54
1 mg/mL	$CuSO_4$ (1)	1	DIPEA (8)	H_2O	rt	Degassed	12 h				22
0.1 mM	$Cu(MeCN)_4][PF_6]$ (0.95)	-		THF:MeOH (1:1)	40 °C	Degassed	20 h	64-83%			55
0.5 mM	$CuSO_4$ (2)	10	THTPA (2)	DMF/H_2O (2:1)	rt		5 min				56,57
0.8 mg/mL	$CuSO_4$ x 5 H_2O (1)	3	THTPA (1)	H_2O:*t*BuOH (1:1)	rt	N_2, degassed		52-92%	Diluted with H_2O, lyophilised, HPLC		58
1.5 mM	$CuSO_4$ (10)	10	TBTA (10)	H_2O:*t*BuOH (1:1)	rt		12 h		HPLC		59
0.91 mg/mL	$CuSO_4$ x 5 H_2O (1)	3	THTPA (1)	H_2O:*t*BuOH (1:1)	rt	N_2	16 h				60
1 mg/mL	$CuSO_4$ x 5 H_2O (1)	3	THTPA (1)	H_2O:*t*BuOH (1:1)	rt	N_2	16 h				61
	$CuSO_4$ x 5 H_2O (1)	3	THTPA (1)	H_2O:*t*BuOH (1:1)	rt	N_2	15 min - 2 h				62

	$CuSO_4$ x 5 H_2O (1)	3	THTPA (1)	H_2O:*t*BuOH (1:1)	rt	N_2, degassed	16 h				[63]
0.01 mM	$CuSO_4$ (4)	4	-	buffer pH 8 (250 mM Na borate, 1M NaCl)	60 °C		30 min				[64]
1 mM	CuBr (0.8)	-	-	$PhCH_3$	Reflux	Ar	Overnight	43%	Celite filtration, DCM wash of filter, flash column chromatography		[65].
1.1 mM	CuI.$P(OEt)_3$ (1.5)	-	-	DCM	rt	Protected from light	5 days	75%	Solvent removal, flash chromatography		[66]
1 mM	$Cu(MeCN)_4][PF_6]$ (1.5)	-		$PhCH_3$/MeOH (4:1)	rt	N_2	24 h	0-46%	Solvent removal, flash chromatography	Yield depended on chain length of employed azide	[67]
0.35 mM	$CuSO_4$ (2)	10	THTPA (10)	H_2O	37 °C	N_2	3 h	45-55%	Monitored by HPLC, purification by HPLC		[23]
1 mg/mL	$CuSO_4$ x 5 H_2O (1)	1	DIPEA (8)	H_2O	rt	Ar, degassed	Overnight	7.5-12.8% (overall)	Lyophilisation, HPLC prufication by HPLC		[68]
	$CuSO_4$ x 5 H_2O (2)	3	THTPA (1) for some	H_2O:*t*BuOH (1:1)	rt	N_2 ,degassed	overnight		SPE, HPLC purification	.	[69]
2 mM	$CuSO_4$ x 10 H_2O (2.5)	10		H_2O:*t*BuOH (1:1.5)			overnight		Removal tBuOH, filtration, HPLC purifcation		[70].
1 mM	CuBr (0.2)	-	DBU (3)	$PhCH_3$	reflux	Ar, degassed	16 h	36-56%	Celite filtration, DCM wash of filter, flash column chromatography	Head-to-tail, tetrapeptide	[71]
0.2 mM	CuI (2)	-	TBTA (2), DIPEA (2), 2,6-lutidine (2)	MeCN	rt	Ar, degassed	48 h		Removed solvent, HPLC purification	Head-to-tail, tetrapeptide	[72]
1 mM	CuI (0.33)	-	DIPEA (3), 2,6-lutidine (2)	MeCN:THF (4:1)	rt	Degassed	14 h	57-92%	Filtration, removal of solvent, HPLC purification	Head-to-tail, pentapeptide	[73]
	CuBr (1)	1	DIPEA (10), 2,6-lutidine (10)	DMF:H_2O	rt		18 h		Washed with DMF, DCM		[74]

Supplementary Table S6: Example reaction conditions used for on-resin CuAAC for peptides. TBTA = tris[(1-benzyl-1*H*-1,2,3-triazol-4-yl)methyl]amine, † = nominal concentration (resin loading/solvent volume), rt = room temperature.

Substrate conc.†	Cu salt (eq)	Ascorbate (eq	Additives (eq)	Solvent	T	Other conditions	Time	Yield	Workup	Ref.
15 µL/mg resin	CuI (2)	-	DIPEA (50 eq)	THF			16 h	76%		[75]
625 mL/mmol	CuI (0.5)	1	2,6-Lutidine (2 eq)	NMP/H_2O (4:1)			48 - 96 h	8.4%		[76]
20 mg/mL	CuBr (1)	1	2,6-Lutidine (10 eq), DIPEA (10 eq)	DMSO	rt	Degassed	16 h			[77]
	CuBr	yes	2,6-Lutidine, DIPEA	DMF/MeCN	rt		8 h	22% (overall)		[78]
	CuBr (1)	3	2,6-Lutidine (10 eq), DIPEA (10 eq)	DMF/MeCN (10/3)	rt	Degassed	6 h	20%-75%		[79]
	CuI (2)	2	DIPEA (3)	DMF	rt		Overnight			[36]
	$[Cu(CH_3CN)_4]$ $[PF_6]$ (1)	-	TBTA (1), DIPEA (2)	DMF			24 h			[80]
	CuI (1.5)	7 (as ascorbic acid)	Piperidine (20 vol%)	DMF	rt	Light protected	15 h		Wash with 5% sodium diethyldithiocarbaamte, 5% DIEPA in DMF, MeOH, DMF, NMP	[81]

Supplementary Table S7: Example reaction conditions used for in solution RuAAC for peptides. cod = 1,5-cycloocatadien, rt = room temperature.

Substrate conc.	Catalyst	Catalyst loading	Solvent	T	Other conditions	Time	Yield	Workup	Comment	Ref.
1.9 mM	$[Cp^*RuCl]_4$	3.75%	DMF	115 °C	µW (200 W)	30 min	10%	Removal of DMF in vacuo, extraction DCM/water, silica column chromatography followed by RP-8	Desired product only minor, major product correct m/z, but no symmetry in NMR --> probably 1,4-analogue	[82]
5 mM	$[Cp^*RuCl]_4$	30%	THF/MeOH	50 °C	-	24 h	40%			[83]
5 mM	$[Cp^*RuCl]_4$	15%	THF/MeOH (95:5)	50 °C	N_2	24 h	14-68%	Removal of solvent, flash chromatography		[84]
3.1 mM	Cp*RuCl(cod)	50%	DMF	80 °C	dry	18 h	3.4-7.0% (overall: SPPS, RuAAC, deprotection)	Addition of DCM, washed organic phase with H_2O+0.05% TFA, removal of solvent, redissolved in H_2O/MeCN (1:1)+0.05% TFA, lyophilised	Sidechain protected peptide	[85]

Supplementary Table S8: Example reaction conditions used for on-resin solution RuAAC for peptides. † = nominal concentration (resin loading/solvent volume), cod = 1,5-cycloocatadien

Substrate conc.†	Catalyst	Catalyst loading	Solvent	T	Other conditions	Time	Yield	Workup	Ref.
200 mM	Cp*RuCl(cod)	3.75%	DMF	60 °C	Dry, degassed, Ar	6 h		Wash with DMF, MeOH, DCM	[22]
< 12.5 mM	Cp*RuCl(cod)	30%	DMF	60 °C	µW (30 W)	5 h	2.1% (overall)	Wash with MeOH, 0.5% dietyhldithiocarbamate in DMF, DMF, DCM	[68]
25 mM	Cp*RuCl(cod)	15%	DMF	70 °C	Dry, degassed	1 h	8-21%	Monitored by IR, continued with Fmoc-deprotection	[86]
	Cp*RuCl(cod)	50%	DMF	60 °C	µW (30 W), N_2	3 h		Wash with MeOH, 2% dietyhldithiocarbamate in DMF, DMF	[69]
75 mM	Cp*RuCl(PPh_3)$_2$		DMF	65 °C	µW, degassed, Ar	2.5 h		Wash with DMF, Et_2O	[70]

1 R. Fasan, R. L. A. Dias, K. Moehle, O. Zerbe, J. W. Vrijbloed, D. Obrecht and J. A. Robinson, *Angew. Chemie - Int. Ed.*, 2004, **43**, 2109–2112.
2 N. E. Shepherd, H. N. Hoang, G. Abbenante and D. P. Fairlie, *J. Am. Chem. Soc.*, 2005, **127**, 2974–2983.
3 R. J. Clark, H. Fischer, L. Dempster, N. L. Daly, K. J. Rosengren, S. T. Nevin, F. A. Meunier, D. J. Adams and D. J. Craik, *Proc. Natl. Acad. Sci. U. S. A.*, 2005, **102**, 13767–13772.
4 A. Zipperer, M. C. Konnerth, C. Laux, A. Berscheid, D. Janek, C. Weidenmaier, M. Burian, N. A. Schilling, C. Slavetinsky, M. Marschal, M. Willmann, H. Kalbacher, B. Schittek, H. Brötz-Oesterhelt, S. Grond, A. Peschel and B. Krismer, *Nature*, 2016, **535**, 511–516.
5 H. Y. Lam, Y. Zhang, H. Liu, J. Xu, C. T. T. Wong, C. Xu and X. Li, *J. Am. Chem. Soc.*, 2013, **135**, 6272–6279.
6 W. Lian, P. Upadhyaya, C. A. Rhodes, Y. Liu and D. Pei, *J. Am. Chem. Soc.*, 2013, **135**, 11990–11995.
7 J. M. Smith, J. R. Frost and R. Fasan, *Chem. Commun.*, 2014, **50**, 5027–5030.
8 A. M. Leduc, J. O. Trent, J. L. Wittliff, K. S. Bramlett, S. L. Briggs, N. Y. Chirgadze, Y. Wang, T. P. Burris and A. F. Spatola, *Proc. Natl. Acad. Sci. U. S. A.*, 2003, **100**, 11273–11278.
9 S. Lindman, G. Lindeberg, P. A. Frändberg, F. Nyberg, A. Karlén and A. Hallberg, *Bioorganic Med. Chem.*, 2003, **11**, 2947–2954.
10 C. M. B. K. Kourra and N. Cramer, *Chem Sci*, 2016, **7**, 7007–7012.
11 N. Zheng, P. Karra, M. A. Vandenberg, J. H. Kim, M. J. Webber, W. L. Holland and D. H.-C. Chou, *J. Med. Chem.*, 2019, **62**, 11437–11443.
12 A. Muppidi, Z. Wang, X. Li, J. Chen and Q. Lin, *Chem. Commun.*, 2011, **47**, 9396–9398.
13 S. Kneissl, E. J. Loveridge, C. Williams, M. P. Crump and R. K. Allemann, *Chembiochem*, 2008, **9**, 3046–3054.
14 J. Tang, Y. He, H. Chen, W. Sheng and H. Wang, *Chem. Sci.*, 2017, **8**, 4565–4570.
15 J. M. Song, E. E. Gallagher, A. Menon, L. D. Mishra and A. L. Garner, *Org. Biomol. Chem.*, 2019, **17**, 6414–6419.
16 D. Wang, W. Liao and P. S. Arora, *Angew. Chemie - Int. Ed.*, 2005, **44**, 6525–6529.
17 Y. S. Chang, B. Graves, V. Guerlavais, C. Tovar, K. Packman, K. H. To, K. A. Olson, K. Kesavan, P. Gangurde, A. Mukherjee, T. Baker, K. Darlak, C. Elkin, Z. Filipovic, F. Z. Qureshi, H. Cai, P. Berry, E. Feyfant, X. E. Shi, J. Horstick, D. A. Annis, A. M. Manning, N. Fotouhi, H. Nash, L. T. Vassilev and T. K. Sawyer, *Proc. Natl. Acad. Sci. U. S. A.*, 2013, **110**, E3445–E3454.
18 B. Van Lierop, S. Chee Ong, A. Belgi, C. Delaine, S. Andrikopoulos, N. L. Haworth, J. G. Menting, M. C. Lawrence, A. J. Robinson and B. E. Forbes, *Sci. Rep.*, 2017, **7**, 1–13.
19 P. M. Cromm, S. Schaubach, J. Spiegel, A. Fürstner, T. N. Grossmann and H. Waldmann, *Nat. Commun.*, 2016, **7**, 11300.
20 S. A. Kawamoto, A. Coleska, X. Ran, H. Yi, C. Y. Yang and S. Wang, *J. Med. Chem.*, 2012, **55**, 1137–1146.
21 A. Gori, C. I. A. Wang, P. J. Harvey, K. J. Rosengren, R. F. Bhola, M. L. Gelmi, R. Longhi, M. J. Christie, R. J. Lewis, P. F. Alewood and A. Brust, *Angew. Chemie - Int. Ed.*, 2015, **54**, 1361–1364.
22 S. Pacifico, A. Kerckhoffs, A. J. Fallow, R. E. Foreman, R. Guerrini, J. Mcdonald, D. G. Lambert and A. G. Jamieson, *Org. Biomol. Chem*, 2017, **15**, 4704–4710.
23 A. M. White, S. J. de Veer, G. Wu, P. J. Harvey, K. Yap, G. J. King, J. E. Swedberg, C. K. Wang, R. H. P. Law, T. Durek and D. J. Craik, *Angew. Chemie - Int. Ed.*, 2020, **59**, 11273–11277.
24 H. E. Blackwell and R. H. Grubbs, *Angew. Chemie Int. Ed.*, 1998, **37**, 3281–3284.
25 M. Poirier, N. Aubry, C. Boucher, J.-M. Ferland, S. Laplante and Y. S. Tsantrizos, *J. Org. Chem.*, 2005, **70**, 10765–10773.
26 N. K. Yee, V. Farina, I. N. Houpis, N. Haddad, R. P. Frutos, F. Gallou, X.-J. Wang, X. Wei, R. D. Simpson, X. Feng, V. Fuchs, Y. Xu, J. Tan, L. Zhang, J. Xu, L. L. Smith-Keenan, J. Vitous, M. D.

61 Y. H. Lau, P. De Andrade, S.-T. Quah, M. Rossmann, L. Laraia, N. Sköld, S. Sköld, T. J. Sum, P. J. E. Rowling, T. L. Joseph, C. Verma, M. Hyvönen, H. Hyvönen, L. S. Itzhaki, A. R. Venkitaraman, C. J. Brown, D. P. Lane and D. R. Spring, *Chem. Sci.*, 2014, **5**, 1804–1809.

62 J. Iegre, N. S. Ahmed, J. S. Gaynord, Y. Wu, K. M. Herlihy, Y. S. Tan, M. E. Lopes-Pires, R. Jha, Y. H. Lau, H. F. Sore, C. Verma, D. H. O' Donovan, N. Pugh and D. R. Spring, *Chem. Sci.*, 2018, **9**, 4638–4643.

63 W. Xu, Y. H. Lau, G. Fischer, Y. S. Tan, A. Chattopadhyay, M. De La Roche, M. Hyvö, C. Verma, D. R. Spring and L. S. Itzhaki, *J. Am. Chem. Soc.*, 2017, **139**, 2245–2256.

64 Y. Onda, G. Bassi, A. Elsayed, F. Ulrich, S. Oehler, L. Plais, J. Scheuermann and D. Neri, *Chem. – A Eur. J.*, , DOI:10.1002/chem.202005423.

65 Q. Luo, Y. Tao, W. Sheng, J. Lu and H. Wang, *Nat. Commun.*, 2019, **10**, 1–9.

66 F. Tahoori, S. Balalaie, R. Sheikhnejad, M. Sadjadi and P. Boloori, *Amino Acids*, 2014, **46**, 1033–1046.

67 J. Zhang, J. Kemmink, D. T. S. Rijkers and R. M. J. Liskamp, *Org. Lett.*, 2011, **13**, 3438–3441.

68 M. Empting, O. Avrutina, R. Meusinger, S. Fabritz, M. Reinwarth, M. Biesalski, S. Voigt, G. Buntkowsky and H. Kolmar, *Angew. Chemie - Int. Ed.*, 2011, **50**, 5207–5211.

69 S. R. Tala, A. Singh, C. J. Lensing, S. M. Schnell, K. T. Freeman, J. R. Rocca and C. Haskell-Luevano, *ACS Chem. Neurosci.*, 2017, **9**, 1001–1013.

70 S. Tomassi, A. M. Trotta, C. Ieranò, F. Merlino, A. Messere, G. Rea, F. Santoro, D. Brancaccio, A. Carotenuto, V. M. D'Amore, F. S. Di Leva, E. Novellino, S. Cosconati, L. Marinelli, S. Scala and S. Di Maro, *Chem. - A Eur. J.*, 2020, **26**, 10113–10125.

71 V. D. Bock, D. Speijer, H. Hiemstra and J. H. Van Maarseveen, *Org. Biomol. Chem.*, 2007, **5**, 971–975.

72 W. S. Horne, C. A. Olsen, J. M. Beierle, A. Montero and M. R. Ghadiri, *Angew. Chemie - Int. Ed.*, 2009, **48**, 4718–4724.

73 T. S. Hu, R. Tannert, H. D. Arndt and H. Waldmann, *Chem. Commun.*, 2007, 3942–3944.

74 C. Testa, D. D'addona, M. Scrima, A. M. Tedeschi, A. M. D'ursi, C. Bernhard, F. Denat, C. Bello, P. Rovero, M. Chorev and A. M. Papini, *Pept. Sci.*, , DOI:10.1002/pep2.24071.

75 M. Roice, I. Johannsen and M. Meldal, *QSAR Comb. Sci.*, 2004, **23**, 662–673.

76 V. Goncalves, B. Gautier, A. Regazzetti, P. Coric, S. Bouaziz, C. Garbay, M. Vidal and N. Inguimbert, *Bioorg. Med. Chem. Lett.*, 2007, **17**, 5590–5594.

77 S. Ingale and P. E. Dawson, *Org. Lett.*, 2011, **13**, 2822–2825.

78 B. B. Metaferia, M. Rittler, J. S. Gheeya, A. Lee, H. Hempel, A. Plaza, W. G. Stetler-Stevenson, C. A. Bewley and J. Khan, *Bioorganic Med. Chem. Lett.*, 2010, **20**, 7337–7340.

79 R. A. Turner, A. G. Oliver and R. S. Lokey, *Org. Lett.*, 2007, **9**, 5011–5014.

80 C. Ngambenjawong, J. M. B. Pineda and S. H. Pun, *Bioconjug. Chem.*, 2016, **27**, 2854–2862.

81 R. Kandler, S. Das and A. Nag, *RSC Adv.*, 2021, **11**, 4842–4852.

82 M. R. Krause, R. Goddard and S. Kubik, *J. Org. Chem.*, 2011, **76**, 7084–7095.

83 Y. Zhang, C. Xu, H. Y. Lam, C. L. Lee and X. Li, *Proc. Natl. Acad. Sci. U. S. A.*, 2013, **110**, 6657–6662.

84 W. Wu, Z. Zhang and L. S. Liebeskind, *J. Am. Chem. Soc.*, 2011, **133**, 14256–14259.

85 C. J. White and A. K. Yudin, *Nat. Chem.*, 2011, **3**, 509–524.

86 A. Knuhtsen, C. Whitmore, F. S. Mcwhinnie, L. Mcdougall, R. Whiting, B. O. Smith, C. M. Timperley, A. C. Green, K. I. Kinnear and A. G. Jamieson, *Chem. Sci.*, 2019, **10**, 1671–1676.

Original Article

CHAPTER 3: COMPLEMENT INHIBITION BY FACTOR-H RECRUITMENT: ACTIVITY, TARGET INTERACTION AND SELECTIVITY PROFILE OF THE 5C6 PEPTIDE

Clément Bechtler[1,a], Sophia Koutsogiannaki[2,a], Ekaterina Umnyakova[1], Amal Hamid[1], Avneesh Gautam[2], Yiannis Sarigiannis[2,4], Richard B. Pouw[1], Christina Lamers[1], Christoph Q. Schmidt[3], John D. Lambris[2,b], Daniel Ricklin[1,b]

[1] Molecular Pharmacy Group, Department of Pharmaceutical Sciences, University of Basel, Basel, Switzerland
[2] Department of Pathology & Laboratory Medicine, Perelman School of Medicine, University of Pennsylvania, Philadelphia, USA
[3] Institute of Pharmacology of Natural Products & Clinical Pharmacology, Ulm University, Ulm, Germany
[4] Current Address: Department of Life & Health Sciences, University of Nicosia, Nicosia, Cyprus

[a] equal contributions
[b] shared supervision

Corresponding author:
Prof. Dr. D. Ricklin
University of Basel, Department of Pharmaceutical Sciences, Klingelbergstrasse 50, CH-4056 Basel, Switzerland. E-mail: d.ricklin@unibas.ch

Under review in the Journal of Controlled Release (ISSN: 0168-3659)

Contributions of Clément Bechtler:

- Design, synthesis and evaluation of 5C6 analogs
- Development and performance of biophysical (SPR, MST, ITC, BLI) and flow cytometry assays
- Manuscript preparation

Complement Inhibition by Factor H Recruitment: Activity, Target Interaction and Selectivity Profile of the 5C6 Peptide

Clément Bechtler[1,a], Sophia Koutsogiannaki[2,a], Ekaterina Umnyakova[1], Amal Hamid[1], Avneesh Gautam[2], Yiannis Sarigiannis[2,4], Richard B. Pouw[1], Christina Lamers[1], Christoph Q. Schmidt[3], John D. Lambris[2,b], Daniel Ricklin[1,b]

[1] Molecular Pharmacy Group, Department of Pharmaceutical Sciences, University of Basel, Basel, Switzerland
[2] Department of Pathology & Laboratory Medicine, Perelman School of Medicine, University of Pennsylvania, Philadelphia, USA
[3] Institute of Pharmacology of Natural Products & Clinical Pharmacology, Ulm University, Ulm, Germany
[4] Current Address: Department of Life & Health Sciences, University of Nicosia, Nicosia, Cyprus

[a] equal contributions
[b] shared supervision

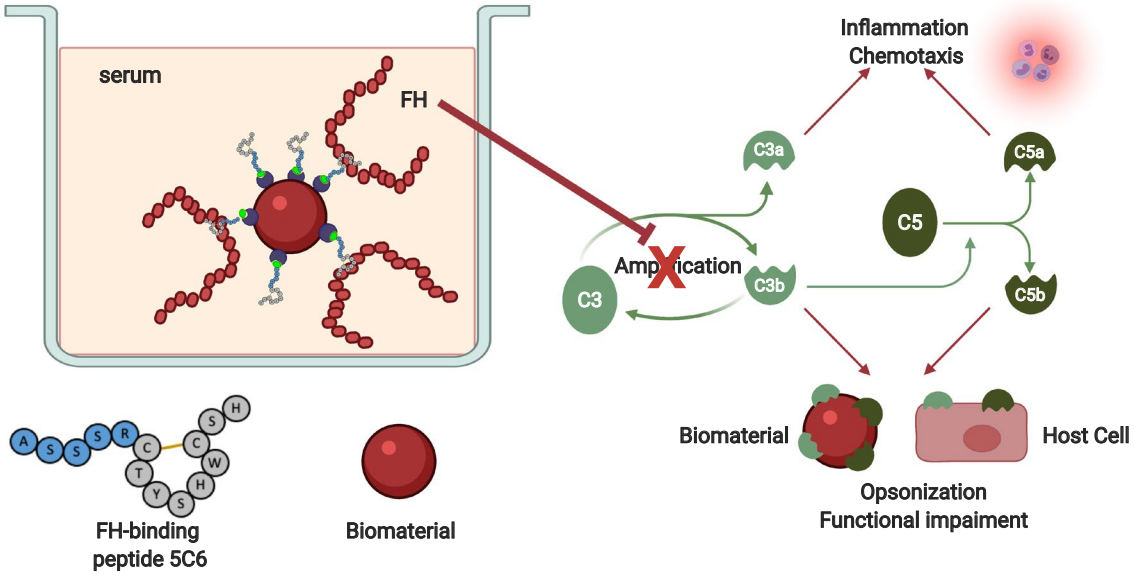

Keywords: complement, factor H recruitment, factor H binding peptide, biomaterial protection

HIGHLIGHTS

- Coatings with the cyclic peptide 5C6, which recruits complement regulator factor H (FH), impair complement activation on biomaterial particles.
- The main contact interfaces that define the recruiting activity could be localized on the cyclic core and C-terminus of 5C6 and CCP domains 10-14 of FH.
- Tethering strategies profoundly influence FH-recruiting activities with N-terminal coating being the preferred option.
- 5C6 exerts strong target selectivity for FH with no observable binding to the partially homologous deregulator FHR-5.
- 5C6 not only binds human FH but also the murine regulator, thereby enabling translational studies.

ABSTRACT

The use of biomaterials in modern medicine has led to reduced morbidity and mortality in a variety of interventions such as transplantation or hemodialysis. However, immune-mediated reactions still present a serious complication of these interventions. One of the drivers of these reactions is the complement system, the main part of the humoral innate immunity, which acts as a first-in-line defense system in its own right but also coordinates other immune pathways. A central regulator of the complement system is the abundant plasma protein factor H (FH), which impairs the amplification of complement responses. Previously, we could show that it is possible to recruit FH to biomedical surfaces using the phage display-derived cyclic peptide 5C6 and, consequently, reduce deposition of C3b, an activation product of the complement system. However, the optimal orientation of 5C6 on surfaces, structural determinants within the peptide for the binding or a precise binding region on FH were unknown. Here, we show that the cyclic core and the C-terminal region of 5C6 are essential for its interaction with FH and that immobilization through its N-terminus strongly increases FH recruitment and reduces C3b deposition in a nanoparticle-like assay. Furthermore, we could demonstrate that 5C6 selectively binds to FH but not to related proteins. The observation that 5C6 also binds murine FH raises the potential for translational evaluation in animal models. This work presents an important step forward for developing 5C6 as a probe or therapeutic molecule for reducing complement activation on biomaterials.

INTRODUCTION

Biomedical materials in the broadest sense, including transplants, implants, nanoparticles or dialysis membranes, contributed substantially to advance medicine and improve prognoses for patients over a range of conditions.[1] However, despite important innovations, immune reactions to non-self surfaces remain a substantial impediment for further progress.[2] For example, up to 30% of patients waiting for a kidney allograft transplant have anti-HLA antibodies, potentially leading to acute or long-term rejection of the transplant[3] and up to 50% of patients obtaining a kidney allograft show subclinical rejection[4]. Moreover, ischemia-reperfusion injury (IRI) and delayed graft function (DGF) are frequent, immune-mediated complications that affect the transplantation outcome.[5] Furthermore, adverse host defense reactions to biomaterials are also observed in patients receiving hemodialysis, increasing the risk of thrombosis and cardiovascular events and, consequently, morbidity and mortality.[2,6] Also, accelerated clearance of nanoparticles and pseudo-allergic reactions to liposomes have been reported.[7,8]

One pivotal driver of these reactions is the complement system, which acts as a rapid sensor of non-self surfaces and induces a series of effector functions to eliminate microbial intruders or apoptotic cells.[9] However, complement may also be triggered by foreign biomedical surfaces and may, directly and through cross-talks with other host defense pathways, lead to detrimental clinical consequences such as thromboinflammation, anaphylactoid reactions or reduced efficacy and rejection of the biomaterial.[10]

The initiation of the complement cascade can occur by different pathways, which are all relevant in biomaterial-mediated complement activation (**Fig. 1A-B**). Whereas antibody complexes, induced either by adhesion to materials or recognition of donor antigens, may trigger the classical pathway (CP), certain carbohydrate or acetylation signatures may induce the lectin pathway (LP). Both routes lead to the formation of a C3 convertase complex (i.e., C4b2b). In addition, adhesion of the abundant plasma protein C3 to surfaces induces a conformational activation that enables the formation of an initiating C3 convertase of the alternative pathway (AP). All three pathways converge to the same AP-mediated amplification loop by activating C3 into C3b, which binds covalently to surfaces and tags them for immune cell recognition and phagocytosis (i.e., opsonization). As C3b is itself able to form a C3 convertase (i.e., C3bBb) upon interaction with factor B (FB) and factor D (FD), opsonization is rapidly amplified in absence of regulators.[10] In many cases, this amplification process has been shown to be the driver of the overall complement response, independently of the initiation pathway.[11] Accumulating C3b deposition enables the generation of convertases that activate complement

component C5 to form membrane attack complexes (MAC), which may lyse or damage cells. Finally, the activation of C3 and C5 produces the anaphylatoxins C3a and C5a, respectively, which exert direct effector functions (e.g., recruitment and priming of immune cells) and enable crosstalk within host defense reactions. For example, C5a-mediated increase of tissue factor (TF) expression may have a potential impact on thrombosis risk in hemodialysis patients.[6]

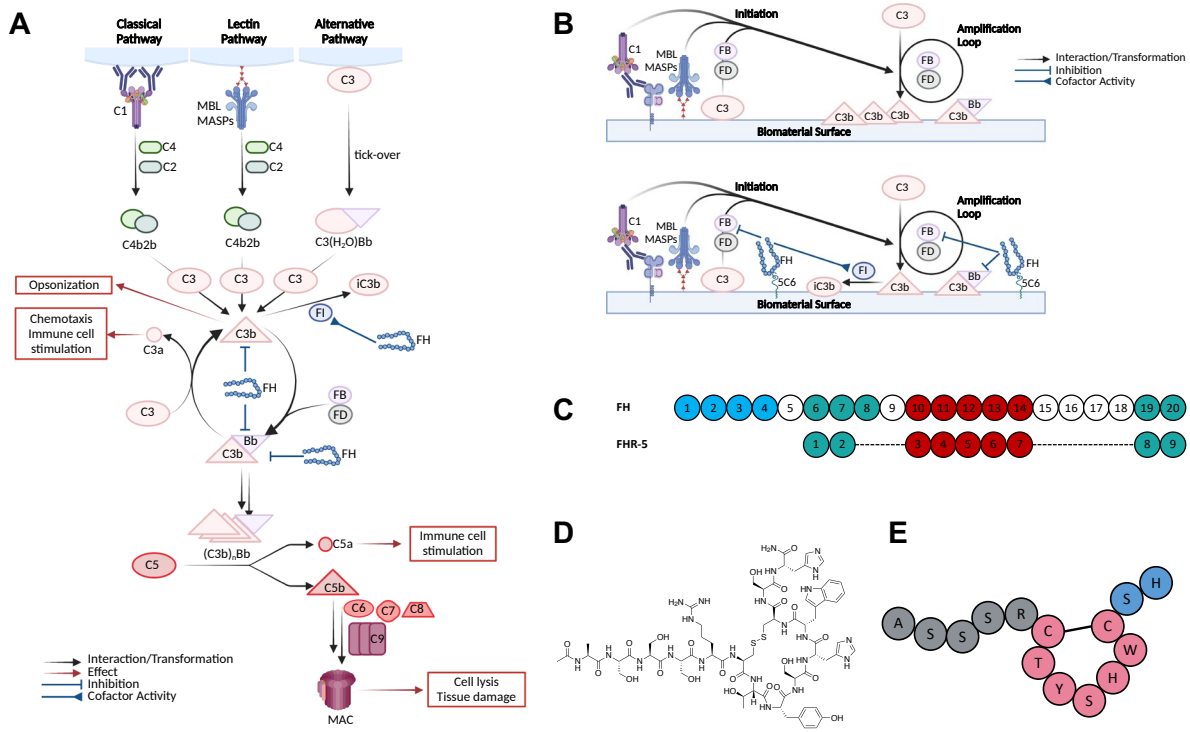

Figure 1: **Complement activation on biomedical surfaces and therapeutic protection via 5C6-mediated recruitment of FH.** (**A**) Overview of the complement cascade, which can be initiated through the classical, lectin or alternative pathway. They all lead to the formation of C3 convertases (C4b2b or C3(H_2O)Bb), which cleave C3 into C3a and C3b. C3b itself forms a C3 convertase (C3bBb) and fuels a self-amplification loop. Increasing C3b deposition enables the formation of C5 convertases, which cleave C5 into the strong anaphylatoxin C5a and C5b that is part of the membrane attack complex (MAC). Factor H (FH) regulates this system at the crucial point of the self-amplification loop by accelerating the degradation of C3bBb, competing with FB for C3b binding and acting as cofactor for Factor I (FI) in the cleavage of C3b into iC3b. (**B**) On biomaterials, complement can be activated by different means and contribute to a variety of clinical complications (top). Coating by FH-recruiting peptides such as 5C6 may prevent material-induced complement activation and effector generation (bottom). (**C**) Domain architecture of FH and FH-related protein 5 (FHR-5), which does not contain regulatory domains (blue) but has sequence homology to the core (red) and recognition regions (green) of FH. (**D-E**) Structure of FH-binding peptide 5C6 in chemical (**D**) and schematic (**E**) representation**.** The three main regions of 5C6, namely the N-terminal, cyclic core and C-terminal regions are colored in grey, purple and blue, respectively.

Due to the strong reactivity of the complement system, its activation is tightly controlled on host cells and in circulation by a panel of membrane-bound and soluble regulators of complement activation.[10] Among those, the plasma protein factor H (FH) is unique by controlling solution phase AP activation but also protecting host cells by recognizing self-associated patterns (e.g., glycosaminoglycans, sialic acids). FH regulates complement activation by competing with FB for C3b binding, accelerating the decay of existing convertases, and enabling the factor I (FI)-mediated degradation of C3b to iC3b (**Fig. 1B**). The abundant regulator (plasma concentration ≈ 2 µM) thereby interferes in the central amplification loop, independently of the initial activation pathway.[12] Another unique feature of FH is its elongated structure consisting of 20 consecutive complement control protein (CCP) domains, with FH however being folded back over itself giving it compact center (**Fig. 1C**).[13–15] Whereas the regulatory activity is largely confined to the four N-terminal CCP domains, CCP6-8 and CCP19-20 are primarily involved in surface binding through recognition of polyanionic residues (e.g., GAGs, sialic acids). Both CCP1-4 and CCP19-20 contain C3b-binding sites.[16]

The important role of FH in complement regulation is also reflected by the observation that many pathogenic microorganisms exploit the regulator as part of their complement evasion strategies upon infecting a host. For example, bacteria (*e.g., Streptococcus pneumoniae, Neisseria meningitidis)*, fungi (*e.g., Candida albicans*) and protozoa (e.g., *Trypanosoma brucei)* all recruit FH to their surfaces and consequently protect themselves from complement attack.[17,18]

Taking inspiration from this natural process to employing it to protect biomaterials, we previously described a disulfide-bridged cyclic peptide (termed 5C6; **Fig. 1D-E**), which showed nanomolar binding affinity to FH.[19] We could demonstrate that 5C6 binds to the non-regulatory core region of FH, containing CCP domains 5-18[20], and that 5C6 binding to FH did not impair FH function. On the contrary, 5C6 could reduce complement activation in the presence of FH, measured as reduced C3b deposition on inducing surfaces. Furthermore, 5C6 was able to recruit FH to biomedically relevant cell and material surfaces when combined with appropriate tethering motifs.[19,21] Thus far, however, neither determinants of target binding and surface tethering nor the selectivity and species specificity profiles of 5C6 have been explored in detail.

Herein, we present further insights into the nature of the 5C6-FH interaction. We investigated the importance of the different regions and residues of 5C6 for the interaction, and could further narrow down the FH domains necessary for 5C6 binding. We compared different tethering strategies and revealed that coating via the N-terminus results in higher recruiting capacities when compared to the previously used C-terminal tethering. Furthermore, we could show that 5C6 exclusively binds FH, and in particular does not bind to FH-related protein 5 (FHR-5), which shares substantial sequence identity with the core region of FH but lacks C3b regulating activity (**Fig. 1C**).[12,22] Finally, we investigated if 5C6 was able to bind FH from different species and detected recruitment of murine FH.

RESULTS

5C6 binds to a conformational site formed by CCP domains 10-14 of FH. Previously, we could demonstrate that 5C6 (Ac-ASSSR[CTYSHWC]SH-$CONH_2$; **Fig. 1D-E**) is interacting with CCP domains 5-18 of FH, and that FH's functional activity is maintained when bound to 5C6.[19,21] To further elucidate which FH domains are involved in the 5C6 interaction, we performed direct binding assays using a panel of recombinant FH fragments, in which terminal domains were gradually deleted from FH8-15 (**Fig. 2A**). All fragments were expressed in mammalian cell culture with suitable yield and purity (with the exception of FH12-15) (**Fig. 2B**). Surface plasmon resonance (SPR) was employed for the initial fragment screening, by immobilizing biotinylated 5C6 on a streptavidin sensor chip and injecting different FH fragments (**Fig. 2C**, Suppl. Fig. S1). Alongside the parental FH8-15, only fragments FH9-15, FH10-15, FH8-14 and FH10-14 showed substantial binding to the 5C6 surface. Further clipping of domains from the N-terminus (FH11-15, FH12-15) or C-terminus (FH10-13) led to a loss of recognition (**Fig. 2C**). The fragment screening study thereby suggest that CCP domains 10-14 of FH comprise the minimum binding region for 5C6 on FH.

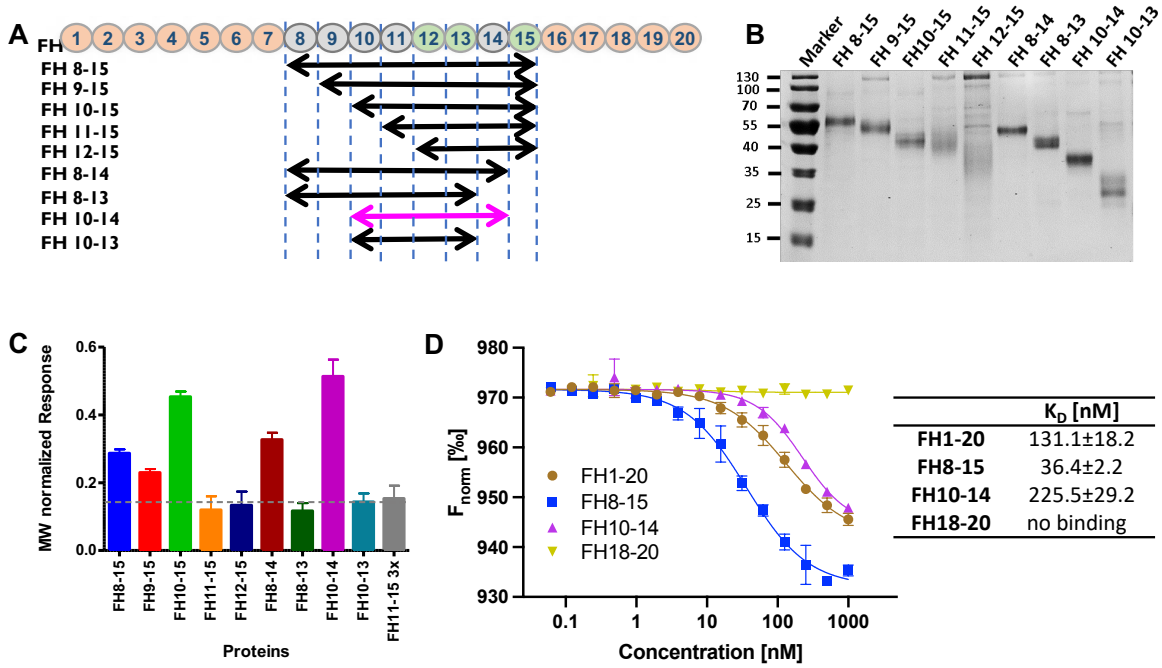

	K_D [nM]
FH1-20	131.1±18.2
FH8-15	36.4±2.2
FH10-14	225.5±29.2
FH18-20	no binding

Figure 2: **Identification of the minimum 5C6-binding region on FH.** (**A**) Library of recombinant domain truncation fragments of FH8-15. (**B**) Characterization of FH fragment library by SDS-PAGE. (**C**) SPR-based screening of FH fragment on 5C6-coated sensor chip. (**D**) MST binding curves and respective K_Ds of CF-labelled 5C6 to full-length FH, FH8-15, FH10-14 and FH18-20. All samples were measured in triplicates and the error bar indicates the standard deviation.

To validate FH10-14 as the relevant FH fragment for 5C6 binding and characterize the 5C6-FH interaction in solution, microscale thermophoresis (MST) with 5(6)-carboxyfluorescein (CF)-labeled 5C6 was employed. As expected, no binding to FH18-20 was observed, whereas 5C6 bound to full-length FH, FH8-15 and FH10-14 in a concentration-dependent manner with K_D values in the nanomolar range (**Fig. 2D, Table 1**). Differences in affinity existing between the different fragments might relate to differences in binding site accessibility or fixation of conformations in the presence (or absence) of other domains.

The central cycle and C-terminus of 5C6 primarily define the target interaction. In order to investigate the structure-activity relationship (SAR) of 5C6, we developed binding assays to assess affinity and kinetic parameters of the parent peptide and its derivatives. For this, recombinant FH8-15 was immobilized on a sensor chip and a concentration series of 5C6 was injected. As expected, 5C6 showed a dose-dependent and saturable binding to FH8-15 with a K_D of approximately 100 nM (**Fig. 3A**). MST was used as complementary method for validating the SPR results. MST has the advantage of not requiring protein immobilization, thus observing binding in solution, yet at the disadvantage of requiring one binding partner being fluorescently labelled. When 5C6 was the labelled binding partner, a dose-dependent change in signal (i. e. normalized fluorescence) was observed; in contrast, this was not the case when FH was labelled (Suppl. Fig. S2). This format selectivity may be caused by a masking of the binding site by the amine-reactive label or because the preferred labelling region is too distant from the binding area. For screening purposes, we therefore used the MST assay in a competitive format, in which CF-labeled 5C6 is displaced from FH8-15 by increasing concentrations of 5C6 derivatives. Indeed, the labelled analogue could be displaced in a dose-dependent manner by unlabeled 5C6 with an IC_{50} of 143±15 nM (**Fig. 3B**), which is well in line with the SPR results.

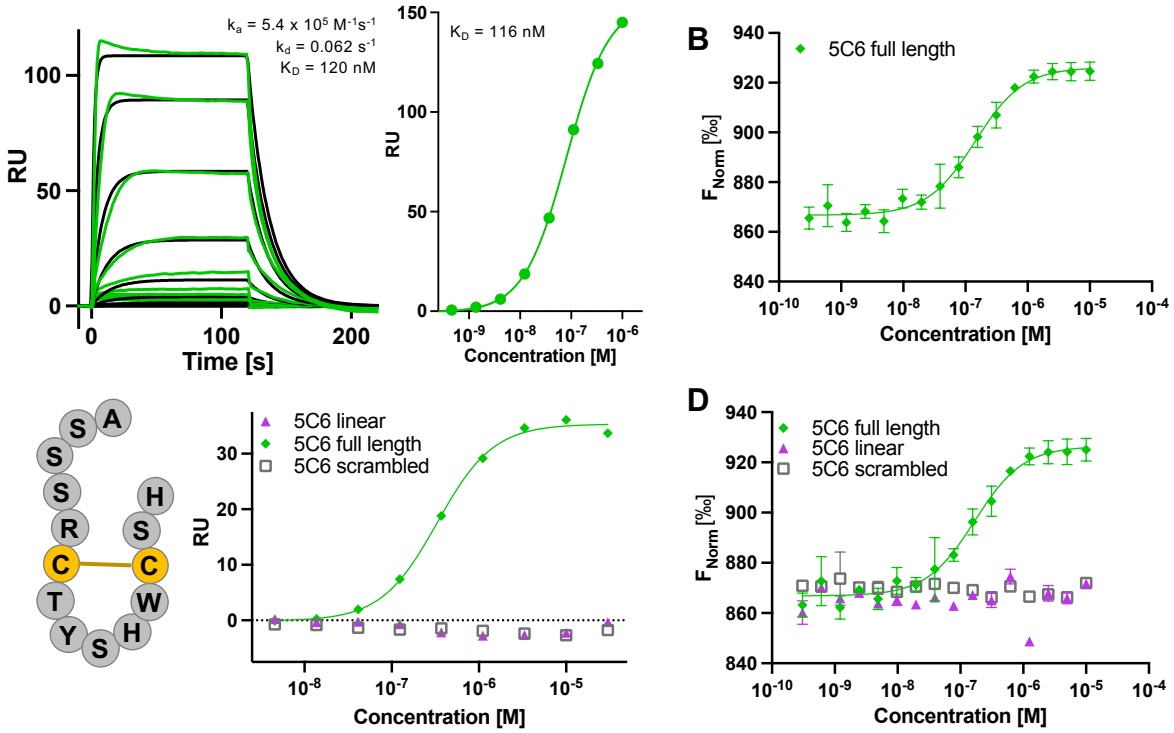

Figure 3: (**A**) SPR sensorgram with the experimental values in green and the kinetic fit in black (left) and concentration-response plot of 5C6 (right). (**B**) MST concentration-response plot of 5C6. (**C**) Schematic representation of 5C6 with the disulfide-forming cysteines highlighted (left) and representative SPR concentration-response plot of 5C6 analogues (right). (**D**) Representative MST concentration-response plot of 5C6 analogues. Error bars indicate standard deviation from duplicate samples.

During phage-display library screening, 5C6 was identified as a cyclic peptide. Cyclization often confers an advantage regarding the biological activity of peptidic ligands by reducing conformational flexibility.[23] We therefore assessed the impact of the cyclic structure of 5C6 by replacing both Cys with Ser residues to ensure that no spontaneous formation of a covalent cycle occurs (i.e., linear 5C6). In addition, we also tested a 5C6 derivative, in which the order of the amino acid residues had been changed (scrambled 5C6; Ac-SSHAS[CRWSSYC]HT-$CONH_2$) to exclude that binding events are mediated by non-specific physicochemical properties rather than the specific sequence. As expected, sequence scrambling completely abrogated the binding to FH both in the SPR (**Fig. 3C**) and MST (**Fig. 3D**) assays. Importantly, the affinity of 5C6 dropped to the level of the scrambled peptide upon linearization (**Fig. 3C-D, Table 2**), thereby confirming the importance of the cyclic nature of 5C6. Subsequent SAR studies were therefore performed using disulfide-bridged, cyclic 5C6.

Table 2: Affinities of 5C6 derivatives in direct (SPR) and competitive (MST) binding assays. *n*= 2, error is SEM.

	SPR K_D [nM]	MST IC_{50} [nM]
5C6	81±3	311±51
5C6 scrambled	no binding	no binding
5C6 linear	no binding	no binding
5C6 N-truncated	140±5	493±207
5C6 ΔH14	no binding	no binding
5C6 ΔS13 ΔH14	no binding	no binding

The contribution of individual residues in a peptide ligand to target binding can best be assessed by an alanine scan. With the exception of the native Ala1 and the essential Cys6 and Cys12, residues were changed individually to Ala and FH-binding affinities were determined by SPR (**Fig. 4A**). To be able to confirm these results with an ELISA, all tested analogues had an additional C-terminal Lys, carrying a

biotin group on the ε-amino group. Broadly, the residues could be grouped into three categories according to their impact on affinity. Firstly, substituting either of the five N-terminal residues or Ser13 did only lead to small or even beneficial affinity changes, thereby indicating a minor contribution to FH recognition. Secondly, markedly weaker affinities (up to seven-fold increase in K_D) were observed when replacing Thr7 and His10, suggesting active participation in target binding. Finally, a critical role in the interaction was shown for residues Tyr8, Ser9, Trp11 and His14, the substitution of which resulted in a profound or complete loss of affinity (**Fig. 4A**). The SPR-derived ranking of the 5C6 analogs was largely confirmed by ELISA (Suppl. Fig. S3). The alanine scan thereby identifies residues in the cyclic center and the C-terminus as most essential contributors to FH recognition, whereas the linear N-terminus appears to play a minor role.

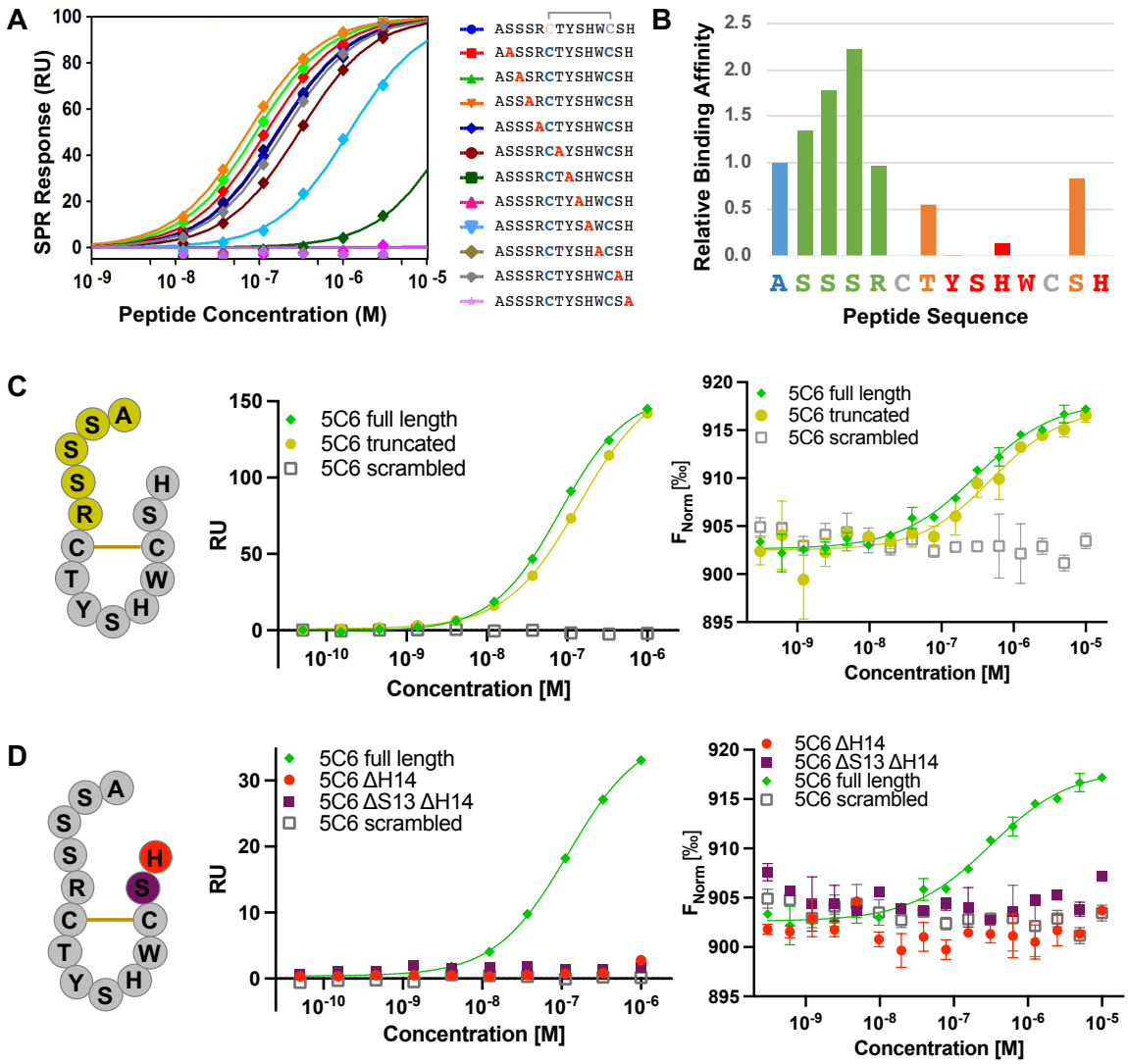

Figure 4: (**A**) Concentration-response plots for the alanine scan analogs of 5C6. (**B**) Relative binding affinities of alanine scan analogs of 5C6, determined by SPR. (**C**) Schematic representation of 5C6 with the exocyclic N-terminus highlighted and representative SPR and MST concentration-response plots (from left to right). (**D**) Schematic representation of 5C6 with the exocyclic C-terminus highlighted and representative SPR and MST concentration-response plots (from left to right). RU: response units, F_{Norm}: normalized fluorescence

The observation that individual substitutions of all five N-terminal residues bears no negative consequences for FH binding raised the question whether the entire N-terminal exocyclic part of 5C6 may be removed, resulting in a peptide of largely reduced size (i.e., from fourteen to nine residues). Indeed, the affinity of this truncated 5C6 (tr5C6) is only slightly affected and only reduced by a factor of 1.5 (**Fig. 4B**, **Table 2**). As nevertheless a difference could be observed, we tested full length and

truncated 5C6 with ITC (isothermal calorimetry) to better understand the nature of the difference. As expected, removing the rather flexible N-terminus of 5C6 largely reduced the entropic penalty of binding to FH by 20 kJ/mol. However, the enthalpic contribution to the binding decreased by a similar amount, suggesting that the global N-terminus contributes specifically to the interaction (Suppl. Fig. S4).

To evaluate the importance of the C-terminal exocyclic part, we synthesized two derivatives by removing either the full C-terminus (ΔS13 ΔH14) or exclusively His14 (ΔH14). In line with the alanine scan, complete deletion of the C-terminus as well as the exclusive removal of His14 completely abolished affinity, indicating a crucial role of the C-terminal residues for the FH-5C6 interaction (**Fig. 4C**, **Table 2**). Of note, the differential importance of the exocyclic portions is also reflected by the impact of chemical modifications on the termini. Using truncated 5C6 as a template, we synthesized analogues with either a free amine or *N*-acetyl group on the N-terminus (while maintaining the C-terminal amide) and a derivative with a C-terminal carboxylic acid instead of an amide (while maintaining the N-terminal acetamide group). Testing the derivatives by SPR and MST showed that the absence or presence of an acetyl group on the N-terminus did not have a large impact on the binding affinity, although having the free amine seemed to be slightly preferred. In contrast, changing the amide to an acid on the C-terminus led to a significant reduction in affinity indicating an influence of the charge at the C-terminus (Suppl. Fig. S5). These combined studies confirm that the intact cyclic core and exocyclic C-terminus of 5C6 are required for FH binding, whereas the N-terminus has a minor impact on target recognition and may be removed or substituted by tethers or other labels.

Tethering via the N-terminus improves the FH-recruiting capacity of 5C6. In our previous proof-of-concept studies, we showed that 5C6 immobilized through its C-terminus can efficiently recruit FH and protect model surfaces from complement attack[21]. C-terminal tethering was an obvious choice as it reflects the way the peptide is attached to the phage during phage display screening. However, our SAR results suggest that the accessibility of the C-terminus of 5C6 for target binding is critical whereas the N-terminus may be more amenable to modifications. In order to understand whether further improvements in FH recruitment can be achieved via alternative attachment points, we synthesized 5C6 analogs with an ε-amino biotinylated Lys (K(biot)) on either their N- or C-termini (**Fig. 5A**). Initial studies showed that immobilization through the C-terminus requires spacing between the surface tether and the peptide, with a PEG6 spacer conferring good capturing activity (Suppl. Fig. S6). A PEG6 spacer was therefore included in all C-terminally tethered analogs. In the case of N-terminal immobilization, the natural exocyclic part (i.e., ASSSR) may serve as suitable spacer, yet we also investigated whether the addition of, or replacement by a PEG6 spacer may provide activity benefits. The analogues were first evaluated for direct interaction with FH using biolayer interferometry (BLI), in which each peptide was coated on a streptavidin sensor tip and incubated with purified FH. BLI demonstrated a clear preference for FH recruitment of the N-terminally tethered peptides compared to the C-terminal ones with the latter one only showing marginally higher binding than the scrambled control peptides. In contrast, all N-terminally coated peptides featured strong binding to FH, with both full-length analogs showing similar responses. Interestingly, the addition of a PEG6 spacer did not improve FH recruitment whereas the replacement of the exocyclic peptide stretch by the similarly sized PEG6 even led to a notable decrease in binding activity (**Fig. 5B**). This suggests that the N-terminus itself already provides sufficient spacing between the surface tether and the rest of the peptide. The signal could be amplified using a polyclonal anti-FH antibody, allowing a further improved differentiation of binding affinity between the different peptides (Suppl. Fig. S7).

A

Peptide	Sequence	Tether	Spacer	Sequence
n-5C6	Full	N-term	No	Ac-K(biot)------ASSSR[CTYSHWC]SH----------CONH$_2$
ns-5C6	Full	N-term	Yes	Ac-K(biot)-PEG6-ASSSR[CTYSHWC]SH----------CONH$_2$
ns-tr5C6	Truncated	N-term	Yes	Ac-K(biot)-PEG6------[CTYSHWC]SH----------CONH$_2$
5C6-cs	Full	C-term	Yes	Ac----------ASSSR[CTYSHWC]SH-PEG6-K(biot)-CONH$_2$
tr5C6-cs	Truncated	C-term	Yes	Ac----------[CTYSHWC]SH-PEG6-K(biot)-CONH$_2$
ns-scr5C6	Scrambled	N-term	Yes	Ac-K(biot)-PEG6-SSHAS[CRWSSYC]HT----------CONH$_2$
scr5C6-cs	Scrambled	C-term	Yes	Ac----------SSHAS[CRWSSYC]HT-PEG6-K(biot)-CONH$_2$
scrlin5C6-cs	Scr/linear	C-term	Yes	Ac----------YSSSW-AHASTRA-SH-PEG6-K(biot)-CONH$_2$

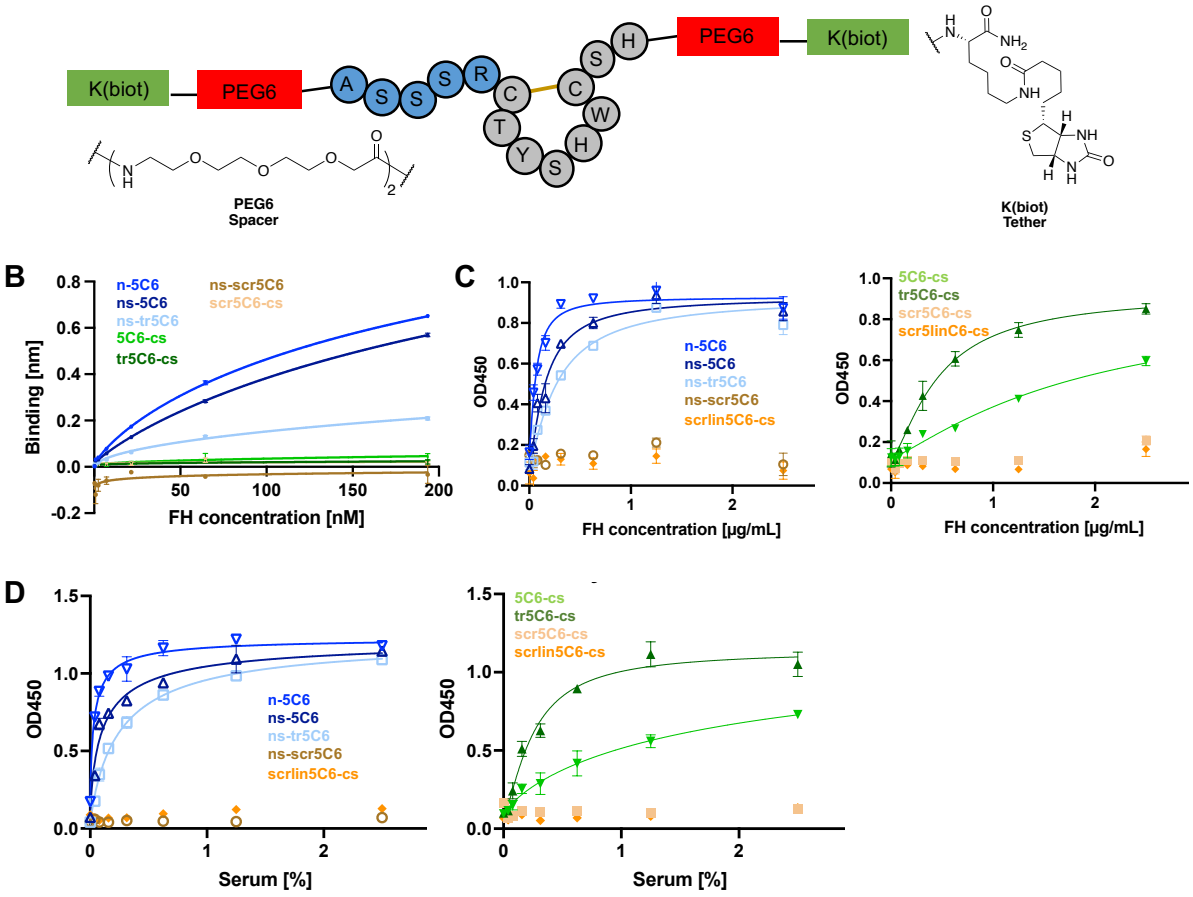

Figure 5: (**A**): Structures of the PEG6 spacer with six PEG units and K(biot) as a model surface tether and the different attachment positions of the spacer and K(biot) onto 5C6. (**B**) BLI concentration-response plots of N- or C-terminally biotinylated 5C6 derivatives. (**C**) ELISA concentration-response plots of N-terminally (left) or C-terminally (right) biotinylated 5C6 derivatives using purified FH as FH-source. (**D**) ELISA concentration-response plots of N-terminally (left) or C-terminally (right) biotinylated 5C6 derivatives using normal human serum as FH-source. Samples were prepared and measured in duplicates, error bars indicate standard deviation and indicated OD450 values corresponds to sample values with blank subtraction.

The FH-recruitment capacity of the peptide series was further evaluated by ELISA, in which peptides were tethered to streptavidin-coated plates and the binding of FH was detected by a polyclonal anti-FH antibody and a secondary horseradish peroxidase (HRP)-conjugated antibody. The ELISA with purified FH showed that C-terminally biotinylated peptides are indeed able to recruit FH, as reported in our previous studies[19], although at a substantially lower capacity when compared to the N-terminally tethered counterparts (**Fig. 5C**). As observed with BLI, when immobilization is done via the N-terminus, no additional spacing is required as directly coated full-length 5C6 recruits FH with the highest activity. Interestingly, for C-terminally tethered peptides the truncated 5C6 recruits FH more efficiently than full-length 5C6 (**Fig. 5C**), likely due to a better accessibility of the truncated peptide when immobilized through its C-terminus. When serum dilutions with up to 2.5% (v/v) normal human serum (NHS) were used as FH source, the same results could be observed, showing that the more complex matrix of NHS is not impeding the preferential binding of FH to 5C6 (**Fig. 5D**).

Improved 5C6 coating efficiently recruits FH to nanoparticle-like surfaces and impairs opsonization.
Potential clinical application of 5C6 include the protective coating of liposomes, nanoparticles or other globular biomaterial particles. To assess the recruiting and complement-regulatory properties of 5C6-derived coating under *ex vivo* conditions, we employed a magnetic streptavidin bead assay, which has recently been established.[24,25] These beads represent a relevant biomaterial surrogate that is comparable to smaller, medically used magnetic nanoparticles.[26] The flow cytometry-based setup mimics the envisioned use of 5C6, i.e*.,* surface-coating of the peptide and recruiting FH from solution, and can be used to simultaneously assess FH recruitment and complement activation by measuring C3b deposition. Whereas polyclonal anti-FH antibodies generated notable background binding, the use of a monoclonal antibody recognizing the CCP16/17 of FH (clone aFH.16, kindly provided by Sanquin Research)[27,28] enabled a clean detection (Suppl. Fig. S8).
In line with previous experiments, purified FH could be recruited to the beads by N-terminally tethered 5C6 derivatives with full-length 5C6 showing stronger FH recruitment when compared to the truncated derivative (**Fig. 6A**). Importantly, the signal was FH-dependent and no FH binding was observed for scrambled 5C6 or non-coated beads, demonstrating specific and 5C6-mediated binding. Encouraged by the selectivity profile, we subsequently assessed the activities of the peptide panel using 10% (v/v) NHS as FH source. In agreement with the BLI and ELISA results, we observed strong recruitment of FH with the N-terminally tethered peptides, most prominently for full-length 5C6 without additional PEG spacer (**Fig. 6B,** left). The PEG6-spaced, truncated 5C6 still showed notable FH binding in NHS when compared to control conditions, yet at substantially lower capacity than when using purified FH. For the C-terminally coated peptides, no relevant FH recruitment could be detected, which is in line with the BLI results but in contrast to the ELISA results. To exclude any interference of FH recruitment by C3b deposition on the beads, we repeated the assay in serum containing EDTA, which broadly prevents complement activation. Importantly, the recruitment profile remained largely unchanged under these conditions, thereby confirming 5C6 as the relevant FH-recruiting entity (**Fig. 6B**, right).
Having confirmed active FH recruitment to the beads, we explored whether this mechanism would impair complement activation and whether differences in FH binding among the peptide panel would translate to C3b deposition levels. This readout was chosen as C3b is the main effector of the amplification loop and since its covalent deposition enables a direct measurement on the beads. In comparison to the FH signals, the detection of C3b deposition revealed an opposite trend as peptide coating showing the strongest capacity for FH resulted in lowest C3b densities (**Fig. 6B-C**). Again, N-terminally tethered peptides were most effective, in particular full-length 5C6 without additional PEG spacer (**Fig. 6C**, left). Interestingly, and despite no notable FH binding being observed, C-terminally tethered peptides still showed a reduction in C3b deposition when compared to scrambled controls, indicating that even small amounts of captured FH may lead to a substantial reduction in opsonization. As expected, the addition of EDTA to normal human serum completely abrogated complement activation and, consequently, C3b deposition (**Fig. 6C**, right). These assays demonstrate that the active recruitment of FH to biomaterial surfaces by 5C6 may impair opsonization and that the coating efficacy is directly affected by a proper orientation and spacing of 5C6 on the surface.

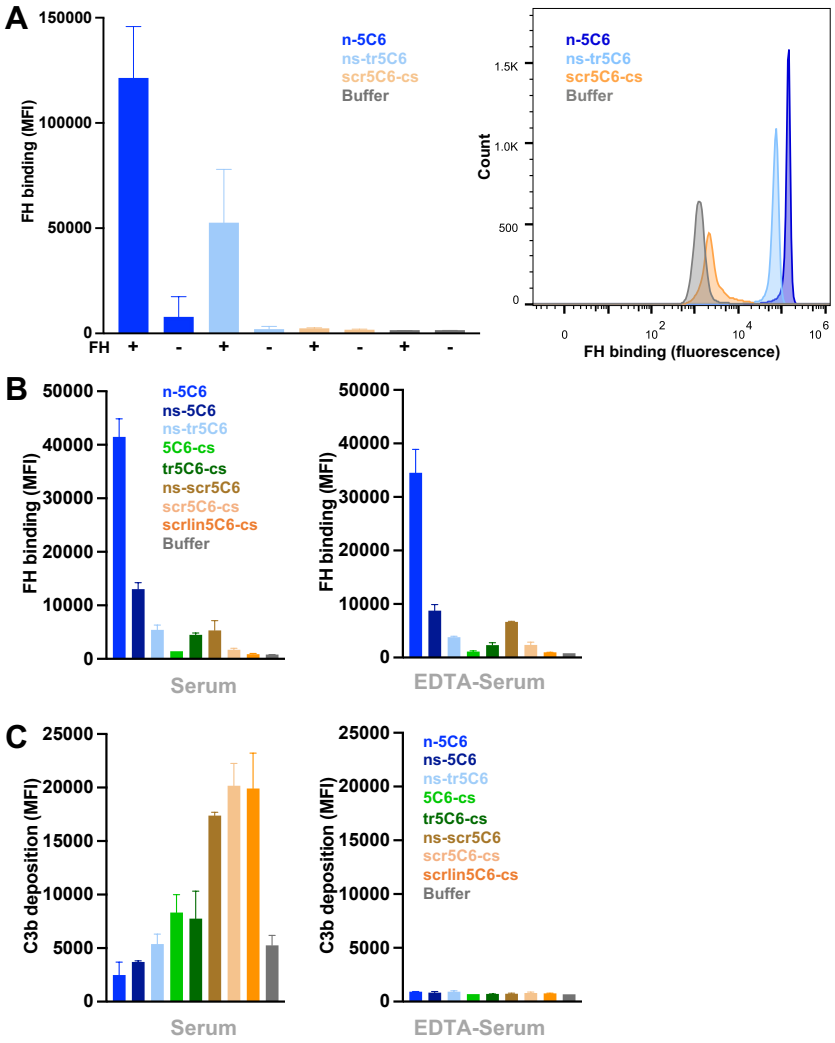

Figure 6: (**A**): Median-fluorescence intensity (MFI) of beads loaded with N-terminally biotinylated 5C6 derivatives, scrambled 5C6 or unloaded beads (left) and the representative histograms of the samples in the presence of FH (right). (**B**): MFI of FH binding from 10% (v/v) NHS (left) or 10% (v/v) NHS inhibited with 10 mM EDTA (left) of magnetic streptavidin beads loaded with biotinylated 5C6 derivatives, scrambled 5C6 derivatives or unloaded beads. (**C**): Median-fluorescence intensity of C3b deposition from 10% (v/v) NHS (left) or 10% (v/v) NHS inhibited with 10 mM EDTA (right) of magnetic streptavidin beads loaded with biotinylated 5C6 derivatives, scrambled 5C6 derivatives or unloaded beads. Bars indicate mean of independent duplicates; error bars indicate standard deviation, n = 2.

5C6 shows strong target selectivity for FH. A narrow target selectivity profile is considered critical for both the activity and safety of 5C6 coating, as a recruitment of plasma proteins that reduce or even counteract the regulatory effect of FH needs to be avoided. This is particularly important for FH-related proteins, homologues of FH that share surface recognition but not regulatory properties with FH and have been shown to act as competitors of FH on certain surfaces.[29] Within the FHR family, FHR-5 may impose the highest risk of crossreactivity for 5C6 as its CCP domains 3-7 show considerable sequence identity (i.e., 60% identity, 72% similarity)[30,31] to CCP10-14 of FH, which comprise the 5C6 binding region (**Fig. 1C**).[22] However, a few regions in CCP3 and CCP6 of FHR5 differ significantly, notably regarding the presence of charged residues, from the corresponding CCP10 and CCP13 domains in FH (Suppl. Fig. S9A).[31]

To address question of target selectivity, we performed a set of pulldown experiments, in which 5C6-coated streptavidin beads were incubated with serum overnight at 4 °C and bound components were eluted with 10% SDS. Eluates were run on SDS-PAGE gels under non-reducing conditions and visualized by silver staining, or alternatively transferred onto nitrocellulose membranes for Western blotting. The gel showed that FH can be successfully pulled down by full-length 5C6 when surface-tethered

through its N-terminus (**Fig. 7A**, left, lanes 10-12) and seems to be particularly efficient if no additional PEG spacer is added (**Fig. 7A**, left, lanes 10, 11). While higher molecular structures also appear in the gel, these are present in all serum- and bead-containing samples, which renders a 5C6-mediated effect unlikely. Interestingly, neither the N-terminally tethered tr5C6 (**Fig. 7A**, left, lane 9) nor the C-terminally tethered peptides appeared to have pulled down FH efficiently under these conditions (**Fig. 7A**, left, lanes 7, 8). Of note, no protein corresponding to the size of FHR-5 (i.e., 65 kDa) was detected in any sample.

To confirm the selectivity for FH over FHR-5 and increase the sensitivity of the assay, the eluates were evaluated by Western blot using a polyclonal antibody capable of recognizing both FH and FHR-5. Interestingly, weak but notable FH signals could be detected for those peptides that were negative in silver staining, confirming the BLI and ELISA binding assay results (**Fig. 7A**, right, lanes 7-9). As expected, the successful pulldown was dependent on the presence of the correct sequence and biotin but independent of the biotin position (**Fig. 7A-B**, lanes 3 -6). Importantly, FHR-5 signals could be detected in the control lane (purified FHR-5) but in none of the samples, thereby supporting the target selectivity of 5C6.

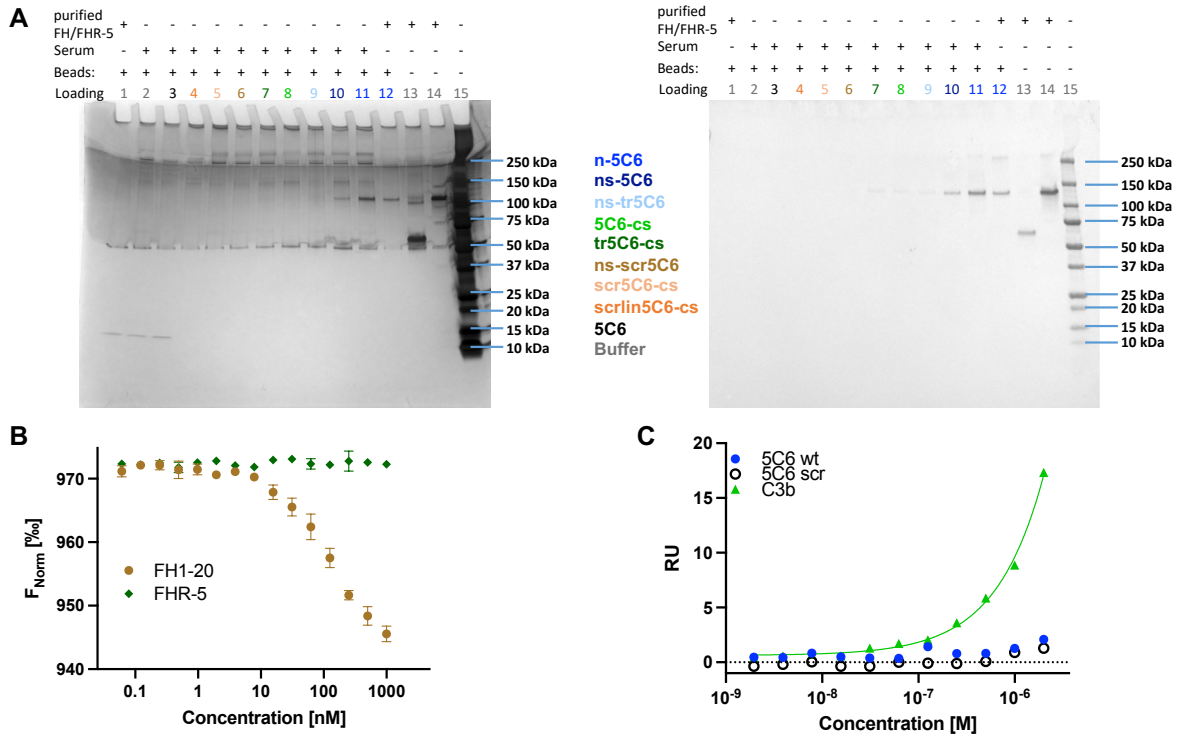

Figure 7: (**A**): SDS-PAGE gel with silver staining (left) and Western blot (right) of pulldown experiment with 5C6 and serum. Lanes from left to right: 1: beads + purified FH, 2: beads + 20% serum, 3: beads + unbiotinylated 5C6 + 20% serum, 4: beads + scrlin5C6-cs + 20% serum, 5: beads + scr5C6-cs + 20% serum, 6: beads + ns-scr5C6 + 20% serum, 7: beads + tr5C6-cs + 20% serum, 8: beads + 5C6-cs + 20% serum, 9: beads + ns-tr5C6 + 20% serum, 10: beads + ns-5C6 + 20% serum, 11: beads n-5C6 + 20% serum, 12: beads + n-5C6 + FH, 13: FHR-5 reference, 14: FH reference, 15: ladder. (**B**): MST concentration-response plot of FH1-20 (brown) and FHR-5 (green). Samples were prepared and measured as triplicates, error bars indicate standard deviation. (**C**): Representative SPR concentration-response plot of 5C6 wt, 5C6 scr and C3b to FHR-5 immobilized on a biosensor surface

Since the pull-down assay may be affected by lower plasma concentration or weaker binding profiles of FHR-5, we also employed the MST-based direct binding and SPR assays to verify the absence of interaction between 5C6 and FHR-5. In contrast to FH, which showed a dose-dependent signal in MST, FHR-5 did not show any binding activity for concentrations up to 1 µM (**Fig. 7B**) nor did immobilized FHR-5 bind 5C6, despite binding its natural ligands C3b and C-reactive protein[12] (**Fig. 7C**, Suppl. Fig. S9B). Additionally, when we used FHR-5 in our FH ELISA, no dose-dependent binding could be detected for any of the tested peptides, despite some background signals, whereas C-reactive protein (CRP) did

bind as expected and previously reported (Suppl. Fig. S9C).[32] Hence, all evidence suggests that no relevant binding between 5C6 and FHR-5 is occurring.

5C6 recruits FH from human, monkey and mouse serum. For proof-of-concept studies and preclinical development, the applicability of a lead compound in animal models of disease is critical. To assess the species specificity of 5C6, the established capturing ELISA was performed with plasma or serum from mice, rats, pigs and monkeys as relevant species. Based on their cross-reactivities, different detection antibodies had to be used, which limits the qualitative and quantitative evaluation across species. Importantly, concentration-dependent FH binding could also be observed for murine serum; although the overall detection signal appears to be affected by some non-specific binding, there was a marked difference between recruitment by active 5C6 and the scrambled control (**Fig. 8A**). Despite confirmed cross-reactivity of the detection antibody for mouse and rat FH, no notable recruitment of FH from rat serum could be detected under these conditions (Suppl. Fig. S10A). Similarly, no dose-dependent signal could be observed for purified rat FH in our direct MST binding assay (Suppl. Fig. S10B). Considering the high sequence identity between murine and rat FH (Suppl. Fig. 10C), this species specificity for FH recruitment by 5C6 was unexpected, yet might be caused by changes to key interacting residues or in conformational differences within the domains. Similar to rat serum, no recruitment of FH from porcine serum could be detected (Supp. Fig. 9D). Due to the limited availability of antibodies with confirmed reactivity to pig FH, a detection issue cannot be fully excluded even if the used antibody was able to detect a band corresponding to the size of FH when porcine serum was evaluated by Western blot (Supp. Fig. 9C). Finally, FH could be recruited from the serum of cynomolgus monkeys, although to a lower extent as for human or murine serum (**Fig. 8B**). Our study suggests that 5C6 exerts some species specificity but could be used in mouse models of disease and in preclinical non-human primate studies.

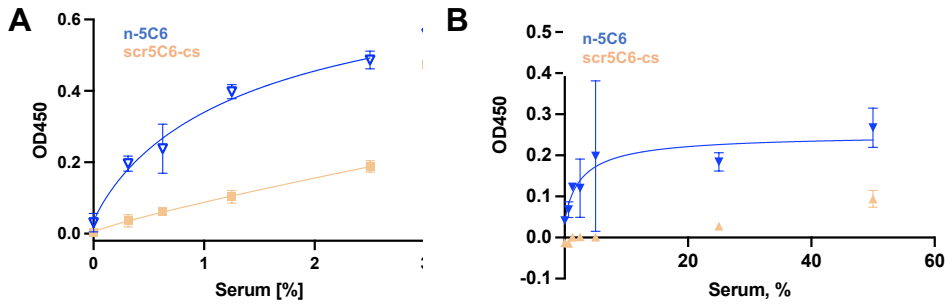

Figure 8: (**A**) Concentration-response plots of dilutions of murine serum to immobilized 5C6 derivatives, measured by ELISA. (**B**) Concentration-response plots of dilutions of cynomolgus serum to immobilized 5C6 derivatives, measured by ELISA.

DISCUSSION

In this study, we were able to provide structural and functional insight into the mechanism of FH-recruiting by the cyclic peptide 5C6, which was previously shown to provide protection from complement attack when coated to cell or material surfaces.[19,21] While the non-regulatory core of FH was previously identified as binding area for 5C6, we could now define the minimum binding region to CCP domains 10-14, which suggest a conformational rather than single-domain site. We further determined that only the cyclic but not the linear peptide can confer recruiting activity and that both the cyclic core and the exocyclic C-terminus essentially contribute to the interaction with FH. While not essential, the exocyclic N-terminus of 5C6 may serve as spacer for coating strategies, especially since our studies revealed a strong benefit of N- over C-terminal tethering. These findings, alongside newly established binding and functional assays used in this study, are expected to guide the rational optimization of 5C6 and facilitate the development of much-needed therapeutic options to impair biosurface-induced clinical complications.

Immune system-mediated adverse events, including inflammation, thrombosis and/or pseudoallergic reactions, continue to present major obstacles both in the clinical applications of biomaterials and in

transplantation medicine. In addition, the attack by host defense systems may lead to functional impairment or even rejection of the foreign bodies. Several strategies are being used or developed to reduce such complications, including broadly immunosuppressive and/or anti-inflammatory therapies with profound systemic impact. Preventing initiating host defense reactions directly on the biomedical surface may provide an elegant and less intrusive alternative, which mimics an evolutionary validated strategy employed by host and microbial cells alike. The recruitment of complement regulators is intriguing due to the early and upstream involvement of complement in the sensing of foreign surfaces. Among those, FH provides a particularly attractive target as it inhibits the amplification loop, which acts independently of the initiating pathway and often drives the overall complement response, including the generation of inflammatory or cell-damaging effectors. Promising clinical evaluation results of drug candidates inhibiting FB or FD, or C3 in the case of the compstatin family, serve as important validation of therapeutic complement inhibition at the AP/C3 level.[33,34]Compstatin analogs such as Cp40 (AMY-101, Amyndas)[35] have been successfully evaluated in preclinical models of hemodialysis or transplantation[36,37], among other indications, and one family member (pegcetacoplan; Empaveli, Apellis) has recently been approved for paroxysmal nocturnal hemoglobinuria (PNH).[38] Whereas soluble complement inhibitors provide a broadly applicable strategy for various indications, a more targeted, surface-directed approach could be applied to exogenous complement activators such as extracorporeal circuits and dialysis filters, nanoparticles and liposomal drug formulations, or transplants and implants by applying regulator-recruiting coating before exposing them to blood or interstitial fluids.

The therapeutic value of engaging the potent complement-regulatory capacity of FH in biomaterial settings has long been recognized. Direct immobilization of FH on polystyrene surfaces has been successfully established[39,40], but a clinical application of this strategy may prove challenging due to the large required quantities (up to 4 pmol/cm^2, approx. 0.6 µg/cm^2)[11] and the demanding recombinant production of FH[41]. Although smaller FH fragments (e.g., miniFH) have been used successfully *in vitro* as well *in vivo* in circulation[41,42], no coating studies have been reported. These approaches validate functionally the importance of FH in complement-mediated conditions, despite the drawback protein-based drugs hold (high cost of goods, potential immunogenicity). Employing 5C6 as a synthetic-chemically accessible peptide renders access to the required amounts of coating entities much more suitable and facilitates the conjugation with suitable tethering moieties.

Synthetic polymers, and in particular PEG, are often used alone or as elongated spacers, to reduce immune reactions towards protein drugs, drug carriers and biomaterials[2,43]. However, PEG coatings have also been identified as the source of complications since the binding of natural anti-PEG antibodies may trigger complement activation and induce pseudoallergic reactions[8,40,44]. It has been described that such antibodies typically recognize epitopes of 6-7 ethylene glycol units and therefore, immunogenicity problems might even arise from small PEG linkers.[45] By transitioning to N-terminal tethering and using the natural exocyclic N-terminus as spacer, we eliminate the reliance on PEG spacing between 5C6 and the biosurface to circumvent potential immunogenicity issues related to PEG. The C-terminal immobilization used in previous studies reflected the peptide presentation during phage display screening and required additional spacing to enable FH binding. The critical role of the exocyclic C-terminal residues revealed by the alanine scan suggested that a freely accessible C-terminus may be beneficial for the recruitment of FH, which was confirmed in binding and functional studies. The preference for N-terminal tethering may also facilitate the production of derivatives with distinct tethers either during SPPS or by amine-reactive conjugation. This could include unspecific (phospho-)lipid anchors or specificity-mediating tethers such as antibody fragments, as has been used in the retinal delivery of a FH-construct in a murine age-related macular degeneration model[46], or saccharides targeting the endothelium as has been used in soluble complement receptor 1 (sCR1)[41].

Rational optimization of 5C6 for enhanced target binding would benefit from structural information. Unfortunately, structural models for the previously identified binding area of FH CCP8-15 are scarce due to the expected flexibility of the segment and its minor functional importance. Small-angle X-ray studies of full-length FH indeed suggest structural variability in this core region of FH.[47] We therefore

aimed at identifying a single- or dual-domain segment amenable for structural analysis, yet our studies revealed that the minimum interacting region of FH comprise a five-domain stretch encompassing CCPs 10-14. This finding suggests that the FH core needs to assume an ordered, folded-back conformation to form the 5C6 binding site, which is in agreement with current hypotheses about the structure of FH and visible in some of the solution models.[14,16,47]

Our observation that 5C6 shows strong selectivity for FH over FHR-5 that features a region with homology to FH10-14 is of great functional importance, to exclude the possibility that concurring recruitment of a deregulator may impair the coating activity. But it may also provide evidence that CCP10 of FH plays an important role in 5C6 binding due to the presence of a strongly dissimilar patch in residues 567-582 of CCP10 when compared to the corresponding region in FHR-5. Intriguingly, this area is also among the few with relatively large differences between murine and rat FH, which showed unexpected differences in species specificity. Further structural and interaction studies will be needed to deepen our understating of the structural determinants of this interaction.

Important for future translational efforts, we could show that 5C6 is able to bind FH from different species, in particular from mouse and non-human primate origin, which will facilitate the evaluation of 5C6 in animal model systems, including established models of biomaterial-induced complement activation and AMR.[48–51] Again, further studies will be required to delineate the exact species specificity profile of 5C6 since the detection of FH recruitment in ELISA-type assays not only relies on the affinity of 5C6 for FH but also on the quality, affinity and selectivity of the detection antibodies. Even for some of model animals relevant for transplantation and biomaterial studies, such as pigs, the availability of well-characterized and validated detection systems remains scarce. Yet our findings that N-terminal tethering provides strongly enhanced and highly selective recruiting activity towards FH from human but also murine serum paves the avenue towards *in vivo* models for further preclinical evaluation of 5C6 in relevant indication areas.

CONCLUSIONS

The great promise of using 5C6 as a FH-recruiting coating to curb complement attack was previously shown in proof-of-concept studies, following the sequence and orientation as provided by the initial phage library screening.[19,21] Herein, we provided important new insights on the target interaction of 5C6, including the binding area on FH and the peptide's structural prerequisites for FH recruitment, massively improved tethering options, target selectivity and species specificity. We could show that both the cyclic moiety and the exocyclic C-terminus are critical for target interaction, whereas the N-terminus does not seem to engage substantially with FH but instead can be utilized as spacer for surface tethering. In fact, N-terminal immobilization appears to be beneficial for affinity and recruiting activity even in absence of additional PEG spacers. Finally, we could show that 5C6 is able to bind FH from different species, notably murine FH, facilitating the investigation of 5C6 in translational animal model systems, and that 5C6 selectively binds FH. This renders 5C6 a promising preclinical candidate for the development of protective coatings to reduce or even prevent complement-mediated adverse reactions to biomedical cell and material surfaces.

MATERIALS AND METHODS

General materials. Chemical reagents and solvents were obtained from Sigma-Aldrich (St. Louis, USA), Bachem (Bubendorf, Switzerland) ChemImpex (Wood Dale, USA), Carbolution (St. Ingbert, Germany), CEM (Matthews, USA) or VWR (Radnor, USA), if not mentioned otherwise, and used without further purification. Buffer and Tween-20 stock solutions were obtained from Xantec (Düsseldorf, Germany). Bovine Serum Albumin (BSA) and 3,3',5,5'-tetramethylbenzidin (TMB) were from Sigma-Aldrich (St. Louis, USA). FHL-1 was provided by Christoph Q. Schmid (University of Ulm, Germany), FHR-5 was obtained from R&D Systems (Minneapolis, USA) and C-reactive protein (CRP) was from BioVison (Milpitas, USA). If not mentioned otherwise, other full length complement proteins as well as mouse and rat sera were obtained from Complement Technology (Tyler, USA). Pig serum was from Innovative Research (Novi, USA), while cynomologus monkey (*Macaca facicularis)* serum was from Biocultures

(Mtius) Ltd, Senneville, Mauritius. Normal human serum was pooled from five unrelated, anonymized healthy donors, obtained with informed consent according to the local ethics committee and following the guidelines of the Declaration of Helsinki (Blutspendezentrum Basel, Switzerland).

Peptide synthesis. Linear peptides were synthesized on a Liberty Blue Automated Peptide Synthesizer (CEM, Matthews, USA) using a microwave-assisted solid-phase peptide synthesis (SPPS) Fmoc/*t*-Bu strategy on an MBHA-Rink Amide resin with diisopropyl carbodiimide (DIC) (6 eq.) and Oxyma (6 eq.) as couplings agents and 6 eq. of Fmoc-protected amino acids in DMF. For C-terminal acids, Cl-MPA ProTide resin was used and loading achieved with 1.0 M DIPEA and 0.125 M KI. For Arg residues, double coupling was used and for Fmoc-PEG3-OH (purePEG, San Diego, USA) 5 eq. were employed. Biotin was introduced as Fmoc-Lys(biot)-OH (purePEG, San Diego, USA), which was dissolved in DMF/NMP (1/1) and double coupled with 3 eq. per coupling. Fmoc deprotection was achieved with 10% piperazine in NMP/EtOH (9/1), N-terminal acetylation with 10% Ac_2O in DMF. 5(6)-Carboyfluorescein (CF) was coupled on resin with 3 eq. using HOBt (3 eq.) and DIC (3 eq.) as coupling reagents in DMF for 60 min at room temperature (rt). After SPPS, the peptides were washed with DMF and DCM (three times each), cleaved off the resin and side-chain protecting groups removed simultaneously with 92.5% trifluoroacetic acid (TFA)/2.5% H_2O/2.5% triisopropylsilane/2.5% ethane dithiol for 3 h at rt, precipitated with to -20 °C chilled Et_2O, span down (6500 rpm, 5 min, 4 °C), the supernatant discarded and the procedure repeated twice.

The crude linear peptides were dissolved in H_2O (1.6 mM), the pH adjusted to 8 – 9 with 5% NH_4OH and 3 eq. of H_2O_2 (1 eq. for biotinylated peptides) added and vigorously stirred for up to 1 h at rt. The reaction was quenched by adjusting the pH to 2 with TFA and the solution was lyophilized.

Peptides were purified on an Agilent 1260 Infinity II LCMS (Agilent, Santa Clara, USA) with a reverse phase C18-column (5.0 µM, 19 mm x 250 mm; Waters, Milford, USA) and a linear gradient from 95% A (H_2O + 0.1% TFA)/5% B (MeCN + 0.1% TFA) to usually 50% A/50% B over usually 22.5 min.

Peptide identity was confirmed by ESI-MS on a MicromassZQ (Waters, Milford, USA). Purity was determined by UV absorption at 214 nm on an Agilent 1100 HPLC (Agilent, Santa Clara, USA), using a reverse phase C18-column (Atlantis T3, 3 µM, 2.1 x 100 mm; Waters, Milford, USA) or phenylhexyl column (XSelect CSH, 3.5 µM, 4.6 mm x 100 mm, Waters, Milford, USA). Peptides were eluted with a gradient from 95% A (H_2O + 0.1% TFA)/5% B (MeCN + 0.1% TFA) to 5% A/95% B, usually over 15 min. Peptides were purified to at least 95% purity, based on UV absoprtion at 214 nm.

Protein expression and expression. Domain deletion constructs of FH were cloned in pSECTAG2 vector and expressed with the mammalian expression system. Those constructs were transfected into HEK 293T cells by using Lipofectamine 2000 (ThermoFisher Scientific, MA, USA) with the manufacturer's instructions. Transfected cells were allowed to express protein for 3 days by incubating at 5% CO_2 in 37 °C, thereafter culture supernatants were harvested, and cell debris was removed by centrifugation at 2000 rpm for 10 min. Clarified supernatants were stored at 4°C until further used. Multiple rounds of expressed proteins were pooled and loaded on His-Trap column (1 ml, GE healthcare) for the purification. After loading of proteins, columns were washed with 10 column volumes (CV) of PBS and proteins were eluted with 5 CV of elution buffer (PBS with 500 mM imidazole). Eluted proteins were buffer exchange to PBS and analysed by SDS-PAGE. FH8-15 was expressed in *Pichia pastoris* as previously described.[15,52]

SPR experiments. Two approaches were followed. First, biotinylated 5C6 (Ac-5C6-$(PEG3)_2$-K(biot)-$CONH_2$) was immobilized on a streptavidin biosensor chip (SA, Cytiva, Marlborough, USA) on a Biacore 3000. The binding experiments were performed by injecting 100 nM of a FH fragment in 10 mM HBS containing 0.005% Tween-20 and 1 mM $MgCl_2$ (HBST-Mg) or PBS as running buffer at a flow rate of 20 µL/min for 2 min and the fragments were allowed to dissociate for 3 min.

Second, different FH fragments were immobilized on a CM5 chip (Cytiva, Marlborough, USA) at a flow rate of 5 µL/min. The surface was activated by injecting 0.4 M N-(3-Dimethylaminopropyl)-N′-ethylcarbodiimide hydrochloride (EDC) and 0.1 M *N*-hydroxy succinimide (1/1) (1:1) for 7 - 10 min, then the proteins injected at 10 – 20 µg/mL in 10 mM NaOAc buffer (pH 4.5) for 6 min or until sufficient immobilization was achieved. Finally, the surfaces were deactivated with ethanolamine (1.0 M, pH 8.5)

for 7 - 10 min. The reference flow cell was treated the same way, except for the FH8-15 injection; 5C6 was injected at 30 µL/min.
For the alanine scan series experiments, FH8-15 was immobilized as described above with HBS containing 0.005% Tween20 and 3 mM EDTA. 5C6 derivatives with individual amino acids replaced by Ala, with the exception of Ala1, Cys6 and Cys13, and containing a C-terminal Lys(biotin) were ordered from GL Biochem (Shanghai, China). The purity and identity of all peptides were validated in-house using LC-MS as described above.
For the other experiments, FH8-15 was immobilized on a CMD500M biosensor (Xantec, Düsseldorf, Germany) on a Biacore T200 (Cytiva, Marlborough, USA) at a flow rate of 10 µL/min using amine reactivity as described above. 5C6 derivatives were injected as dilution series and association and dissociation were measured each for up to 180 s, depending on the kinetic profile. The running buffer was PBS containing 0.005% Tween-20 and the flow rate 30 µL/min. The surface was regenerated between injections with 1 M NaCl (30 s contact time, 10 s stabilization period).
For the experiments with immobilized FHR-5, FHR-5 was immobilized in the same manner as FH8-15. The flow rate for the experiments was 10 µL/min and running buffer used was PBS with 0.005% Tween-20 and 50 µM EDTA, except for the binding assay with CRP, where HBS with 0.005% Tween-20 and 2 mM $CaCl_2$ was used.
Direct MST assay. Interactions between 5C6 and FH, FH fragments and FHR-5 were examined with a microscale thermophoresis (MST) assay on a Monolith (Nanotemper, Munich, Germany). 50 nM CF-5C6 (CF-ASSSR[CTYSHWC]SH-$CONH_2$) were incubated with dilution series of FH, FH fragments or FHR-5 in PBS containing 0.05% Tween-20. The interaction was measured at 25 °C with the blue laser, MST power set to medium and LED power to 20%, the hot phase was set to 0.5 – 1.5 s.
Competitive MST assay. Interactions were examined on a Monolith (Nanotemper, Munich, Germany). 80 nM CF-5C6 and 40 nM FH were incubated with dilution series of unlabeled 5C6 analogues in PBS containing 0.05% Tween-20. The interaction was measured at 25 °C with the blue laser, MST power set to high and LED power to low, the hot phase was set to 4 – 5 s.
ITC experiments. FH8-15 was dialyzed overnight at 4 °C against PBS with a Pur-A-Lyzer Midi 3500 Dialysis Kit (Sigma-Aldrich, (St. Louis, USA). Experiments were performed on a MicroCal ITC200 (Malvern Panalytical, Malvern, United Kingdom) with a total number of 20 injections. The cell temperature was set to 25 °C, the reference power to 6 µcal/s and the initial delay to 180 s. The 5C6 concentration in the syringe was 200 µM and the FH8-15 concentration 20 µM. In the first injection, 0.5 µL were injected over 0.8 s, whereas for the remaining 19 injections, 2.0 µL over 4.0 s were injected. The spacing between injections were 150 s and the filter set to 2. The data was analyzed with AFFINImeter (Santiago de Compostela, Spain) using the “simple model”.
Competitive ELISA. 96-well plates were incubated overnight at 4 °C with 10 µg/mL streptavidin (New England Biolabs, Ipswich, USA) in PBS and washed twice with PBS. Then, the plate was saturated for 1.5 h with PBS containing 2% (w/v) BSA, washed twice with PBS containing 0.05% (v/v) Tween-20 (PBST) and the parent biotinylated peptide was immobilized at 10 µg/mL in PBS for 1 h at rt. After washing two times with PBST, serial dilutions (1:1 starting at 50 uM) of each peptide from the Alanine-scan library (GL Biochem), pre-incubated with 25 nM FH (A137c, Complement Tech) for 15 min at RT, were added to the plate to compete with the immobilized parent peptide for binding to FH. The plates were incubated for 1 h at rt, followed by two washes with PBST. Subsequently, 100 µL of a polyclonal rabbit anti-human FH antibody (1:1000) in PBS containing 1% BSA (PBSB) were added to the plate for 1 h at rt. The plate was washed three times with PBST, incubated for 1 h at rt with a horseradish peroxidase (HRP)-coupled polyclonal goat anti-rabbit IgG antibody (1:1000) (#172-1019, Biorad) in PBSB and washed three times with PBST. The detection reaction was initiated by adding 2,2'-azino-bis(3-ethylbenzothiazoline-6-sulfonic acid) (ABTS) substrate solution (Roche, Basel, Switzerland) and the absorption measured at 405 nm.
Bead pulldown experiments. Magnetic streptavidin beads (Dynabeads M-270, Thermo Fisher Scientific, Waltham, USA) were washed twice with PBS. To 8 µL of the beads solution, 500 µL peptide solution in PBS with 0.1% BSA (PBSB) were added (final peptide concentration: 5 µM) and incubated

at rt for 30 min under shaking. The samples were washed once with PBS containing 0.1% Tween-20 (PBST) and twice with PBS. Then, 20% (v/v) normal human serum or 39 nM FH in PBSB were added and incubated overnight at 4 °C under shaking. After washing once with 1 M NaCl in 20 mM phosphate buffer (pH 7.3), three times with PBST containing 0.1% BSA (PBSBT) and two times with PBS, the samples were eluted with 100 µL loading buffer (22 mM Tris, 6.7% glycerol, 1.3% SDS, bromophenol blue, pH 6.8) and heated to 70 °C for 10 min. Mini-protean TGX SDS PAGE gels 4-20% (BioRad, Hercules, USA) were loaded with samples, 600 ng FH or FHR-5, or ladder and run for 30 min at 200 V and washed twice with H_2O. For staining, the gel was incubated with 2.5% (w/v) $AgNO_3$ according to the manufacturer's instructions (Cytiva, Marlborough, USA). For the Western blot, the gel was transferred onto a nitrocellulose membrane (1 h, 18 V) and blocked overnight at 4 °C with 1% (v/v) Western Blocking Reagent (Roche, Basel, Switzerland) in PBS, then washed three times for 10 min with PBST. The membrane was incubated for 60 min with a polyclonal goat anti-human FH antibody (0.04%) (Complement Technology, Tyler, USA), washed three times for 10 min with PBST followed by incubation for 20 min with an HRP-conjugated rabbit anti-goat IgG antibody (0.04%) (Thermo Fisher Scientific, Waltham, USA). Afterwards, the membrane was washed three times with PBST and twice with PBS for 10 min each. 25 mL of Pierce 1-Step Ultra TMB Blotting Solution (Thermo Fisher Scientific, Waltham, USA) were added and incubated for 5 min. The reaction was stopped by adding an equal amount of H_2O, and the membrane was washed twice with H_2O. Images of gels and blots were obtained using a GelDoc XR+ (BioRad, Hercules, USA).

Biolayer interferometry. Measurements were performed on an Octet K2 (Sartorius, Göttingen, Germany), with shaking set to 1000 rpm for all steps and the assay performed in a polypropylene, flat-bottom, black 96-well plate (Greiner, Kremsmünster, Austria). Biotinylated peptides were diluted in PBS containing 0.005% Tween-20 and 50 µM EDTA (PBSTE) and immobilized on streptavidin biosensors (Sartorius, Göttingen, Germany) at 10 µg/mL for 180 s. Association with FH dilutions in PBSTE was observed for 180 s and signal amplification with a polyclonal goat-anti human FH IgG (0.1%) (Quidel, San Diego, USA) in PBSTE observed for 600 s. Regeneration of the surface was achieved with 0.3 M HCl for 30 s.

Non-competitive ELISA. All sample and reagent dilutions were made in PBS containing 3% (w/v) BSA (PBSB). Maxisorp 96-well plates (Thermo Fisher Scientific, Waltham, USA) were incubated overnight at 4 °C with 10 µg/mL streptavidin (Sigma-Aldrich, St. Louis, USA) in 50 mM bicarbonate buffer (pH 9.9). The plates were washed twice with PBS, saturated with PBSB for 2 h, then washed twice with PBSB containing 0.05% (v/v) Tween-20 (PBSBT). Biotinylated peptides or controls at 10 µg/mL in PBSB were added, allowed to bind for 1 h at rt and then washed three times with PBS containing 0.05% (v/v) Tween-20 (PBST). FH, FHR-5 or serum dilutions were added and incubated for 1 h at rt. The plates were washed three times with PBST, the primary anti-FH antibodies (0.1%, v/v) added, incubated for 1 h and washed four times with PBST. Secondary horseradish peroxidase (HRP)-coupled antibodies (0.1%, v/v) were added, incubated for 1 h and washed three times with PBST, then twice with PBS. The detection reaction was initiated by adding 1 mg/mL TMB with 0.003% ppm H_2O_2 (m/V) in 110 mM NaOAc (pH 5.5)/DMSO (99/1) (final composition) and allowed to proceed for 5 min. The reaction was stopped by adding 2 M H_2SO_4 and the absorption at 450 nm was measured on a Synergy HT plate reader (Biotek, Winooski, USA). The primary antibody used for binding human FH was a polyclonal goat IgG (Complement Technology, Tyler, USA), for murine and rat FH monoclonal murine IgG_1 1A2 (Hycult, Uden, Netherlands) was used, whereas for pig FH, the same polyclonal goat anti-FH was used as for human FH as well as another polyclonal goat-anti human FH IgG (Quidel, San Diego, USA) and the monoclonal murine IgG L20/30 (Hycult, Uden, Netherlands). For detecting FH from monkey serum, murine anti-human FH IgG_1 aFH.16 (Sanquin Research, Amsterdam, Netherlands) was used. Secondary, HRP-coupled antibodies used were rabbit anti-goat IgG (Thermo Fisher Scientific, Waltham, USA) or goat anti-mouse IgG (Biolegend, San Diego, USA).

Nanoparticle-like assay. Magnetic streptavidin beads (Dynabeads M-270, Thermo Fisher Scientific, Waltham, USA) were washed twice with PBS containing 2% (w/v) BSA and 0.005% (v/v) Tween-20 (PBSBT). In a twin.tect PCR plate (Eppendorf, Hamburg, Germany), 0.2 µL of bead solution were

incubated with 800 nM peptide (100 equivalents) solution in PBSBT or just PBSBT for 30 min at rt. The beads were washed four times with PBSBT and incubated with 200 nM FH, 10% (v/v) normal human serum or 10% normal human serum with 20 mM EDTA, all diluted in PBS, for 60 min at 37 °C while shaking (1050 rpm). The beads were washed four times with PBSBT and incubated with 1 µg/mL of either murine anti-human FH IgG_1 aFH.16 (Sanquin Research, Amsterdam, Netherlands), labelled with CF647 (Sigma-Aldrich, St. Louis, USA) according to the manufacturer's instructions, or APC-labelled murine anti-human C3b IgG_1 3E7 (Biolegend, San Diego, USA) for 30 min at rt while shaking (1050 rpm). The beads were washed four times with PBSBT, resuspended in 100 µL PBSBT, transferred into a 96-well plate (Agilent, Santa Clara, USA) and measured on a CytoFLEX B4-R3-V0 (Beckman Coulter, Indianapolis, USA). Signals were gated on the beads based on forward scatter-height (FCS-H) and sideward scatter-heigh (SSC-H).

Numerical and statistical analyses. Concentration-response fits (including K_D and IC_{50} values) were obtained with non-linear regression analysis using the agonist vs response, variable slope, four parameters-model in GraphPad Prism, version 9.2.0 for MacOS (GraphPad Software, San Diego, California USA, www.graphpad.com). Kinetic SPR fits were performed with Scrubber, version 2.0c for Windows (BioLogic Software, Campbell, Australia).

ACKNOWLEDGMENTS

We express our sincere gratitude to Dr. Ilse Jongerius (Sanquin Research, The Netherlands) for providing us with the mouse anti-human FH antibody aFH.16. This study was supported by grants from the Swiss National Science Foundation (No 31003A_176104), National Institute of Health (P01-AI068730), European Union (FP7-HEALTH-2013-INNOVATION-1) and DFG (3018/2-2 to CQS).

AUTHOR CONTRIBUTIONS

CB designed, synthesized and characterized 5C6 analogs, with assistance from AH. AG and CQS designed and produced recombinant FH fragments. YS synthesized PEGylated 5C6 analogs. CB, SK, EU, AH and RP designed and/or performed direct binding and functional studies. DR, CL and JDL conceived and supervised studies. CB and DR wrote the initial draft of the manuscript with all authors being involved in the writing, editing and discussion of the paper.

CONFLICT OF INTEREST

DR, JDL, CQS and RBP are co-inventors of patents describing complement inhibitors and their therapeutic use. JDL is the inventor of the 5C6 and compstatin technologies and the founder of Amyndas Pharmaceuticals, which has licensed both technologies. The other authors do not report conflicts of interest in the context of this study.

REFERENCES

(1) Othman, Z.; Cillero Pastor, B.; van Rijt, S.; Habibovic, P. Understanding Interactions between Biomaterials and Biological Systems Using Proteomics. *Biomaterials*. Elsevier Ltd June 1, 2018, pp 191–204. https://doi.org/10.1016/j.biomaterials.2018.03.020.

(2) Ekdahl, K. N.; Huang, S.; Nilsson, B.; Teramura, Y. Complement Inhibition in Biomaterial- and Biosurface-Induced Thromboinflammation. *Semin. Immunol.* **2016**, *28* (3), 268–277. https://doi.org/10.1016/j.smim.2016.04.006.

(3) Tatapudi, V. S.; Montgomery, R. A. Therapeutic Modulation of the Complement System in Kidney Transplantation: Clinical Indications and Emerging Drug Leads. *Frontiers in Immunology*. Frontiers Media S.A. October 1, 2019, p 2306. https://doi.org/10.3389/fimmu.2019.02306.

(4) Loupy, A.; Vernerey, D.; Tinel, C.; Aubert, O.; Van Huyen, J. P. D.; Rabant, M.; Verine, J.; Nochy, D.; Empana, J. P.; Martinez, F.; et al. Subclinical Rejection Phenotypes at 1 Year Post-Transplant and Outcome of Kidney Allografts. *J. Am. Soc. Nephrol.* **2015**, *26* (7), 1721–1731. https://doi.org/10.1681/ASN.2014040399.

(5) Berger, M.; Lefaucheur, C.; Jordan, S. C. Update on C1 Esterase Inhibitor in Human Solid

Organ Transplantation. *Transplantation* **2019**, *103* (9), 1763–1775. https://doi.org/10.1097/TP.0000000000002717.
(6) Kourtzelis, I.; Markiewski, M. M.; Doumas, M.; Rafail, S.; Kambas, K.; Mitroulis, I.; Panagoutsos, S.; Passadakis, P.; Vargemezis, V.; Magotti, P.; et al. Complement Anaphylatoxin C5a Contributes to Hemodialysis-Associated Thrombosis. *Blood* **2010**, *116* (4), 631–639. https://doi.org/10.1182/blood-2010-01-264051.
(7) Vu, V. P.; Gifford, G. B.; Chen, F.; Benasutti, H.; Wang, G.; Groman, E. V.; Scheinman, R.; Saba, L.; Moghimi, S. M.; Simberg, D. Immunoglobulin Deposition on Biomolecule Corona Determines Complement Opsonization Efficiency of Preclinical and Clinical Nanoparticles. *Nat. Nanotechnol.* **2019**, *14* (3), 260–268. https://doi.org/10.1038/s41565-018-0344-3.
(8) Gabizon, A.; Szebeni, J. Complement Activation: A Potential Threat on the Safety of Poly(Ethylene Glycol)-Coated Nanomedicines. *ACS Nano*. American Chemical Society July 28, 2020, pp 7682–7688. https://doi.org/10.1021/acsnano.0c03648.
(9) Nilsson, B.; Korsgren, O.; Lambris, J. D.; Ekdahl, K. N. Can Cells and Biomaterials in Therapeutic Medicine Be Shielded from Innate Immune Recognition? *Trends in Immunology*. Elsevier Current Trends January 1, 2010, pp 32–38. https://doi.org/10.1016/j.it.2009.09.005.
(10) Ricklin, D.; Reis, E. S.; Lambris, J. D. Complement in Disease: A Defence System Turning Offensive. *Nat Rev Nephrol* **2016**, *12* (7), 383–401. https://doi.org/10.1038/nrneph.2016.70.
(11) Engberg, A. E.; Sandholm, K.; Bexborn, F.; Persson, J.; Nilsson, B.; Lindahl, G.; Ekdahl, K. N. Inhibition of Complement Activation on a Model Biomaterial Surface by Streptococcal M Protein-Derived Peptides. *Biomaterials* **2009**, *30* (13), 2653–2659. https://doi.org/10.1016/j.biomaterials.2009.01.001.
(12) Sánchez-Corral, P.; Pouw, R. B.; López-Trascasa, M.; Józsi, M. Self-Damage Caused by Dysregulation of the Complement Alternative Pathway: Relevance of the Factor H Protein Family. *Front. Immunol.* **2018**, *9* (1607). https://doi.org/10.3389/fimmu.2018.01607.
(13) Aslam, M.; Perkins, S. J. Folded-Back Solution Structure of Monomeric Factor H of Human Complement by Synchrotron X-Ray and Neutron Scattering, Analytical Ultracentrifugation and Constrained Molecular Modelling. *J. Mol. Biol.* **2001**, *309* (5), 1117–1138. https://doi.org/10.1006/jmbi.2001.4720.
(14) Schmidt, C. Q.; Herbert, A. P.; Mertens, H. D. T.; Guariento, M.; Soares, D. C.; Uhrin, D.; Rowe, A. J.; Svergun, D. I.; Barlow, P. N. The Central Portion of Factor H (Modules 10-15) Is Compact and Contains a Structurally Deviant CCP Module. *J. Mol. Biol.* **2010**, *395* (1), 105–122. https://doi.org/10.1016/j.jmb.2009.10.010.
(15) Makou, E.; Mertens, H. D. T.; MacIejewski, M.; Soares, D. C.; Matis, I.; Schmidt, C. Q.; Herbert, A. P.; Svergun, D. I.; Barlow, P. N. Solution Structure of CCP Modules 10–12 Illuminates Functional Architecture of the Complement Regulator, Factor H. *J. Mol. Biol.* **2012**, *424* (5), 295–312. https://doi.org/10.1016/J.JMB.2012.09.013.
(16) Schmidt, C. Q.; Lambris, J. D.; Ricklin, D. Protection of Host Cells by Complement Regulators. *Immunol. Rev.* **2016**, *274* (1), 152–171. https://doi.org/10.1111/imr.12475.
(17) Lambris, J. D.; Ricklin, D.; Geisbrecht, B. V. Complement Evasion by Human Pathogens. *Nat. Rev. Microbiol.* **2008**, *6*, 132. https://doi.org/10.1038/nrmicro1824https://www.nature.com/articles/nrmicro1824#supplementary-information.
(18) Macleod, O. J. S.; Bart, J. M.; MacGregor, P.; Peacock, L.; Savill, N. J.; Hester, S.; Ravel, S.; Sunter, J. D.; Trevor, C.; Rust, S.; et al. A Receptor for the Complement Regulator Factor H Increases Transmission of Trypanosomes to Tsetse Flies. *Nat. Commun.* **2020**, *11* (1), 1–12. https://doi.org/10.1038/s41467-020-15125-y.
(19) Wu, Y.-Q. Q.; Qu, H.; Sfyroera, G.; Tzekou, A.; Kay, B. K.; Nilsson, B.; Nilsson Ekdahl, K.; Ricklin, D.; Lambris, J. D. Protection of Nonself Surfaces from Complement Attack by Factor H-Binding Peptides: Implications for Therapeutic Medicine. *J. Immunol.* **2011**, *186* (7), 4269–4277. https://doi.org/10.4049/jimmunol.1003802.

(20) Schmidt, C. Q.; Herbert, A. P.; Kavanagh, D.; Gandy, C.; Fenton, C. J.; Blaum, B. S.; Lyon, M.; Uhrín, D.; Barlow, P. N. A New Map of Glycosaminoglycan and C3b Binding Sites on Factor H. *J. Immunol.* **2008**, *181* (4), 2610–2619. https://doi.org/10.4049/jimmunol.181.4.2610.

(21) Nilsson, P. H.; Ekdahl, K. N.; Magnusson, P. U.; Qu, H.; Iwata, H.; Ricklin, D.; Hong, J.; Lambris, J. D.; Nilsson, B.; Teramura, Y. Autoregulation of Thromboinflammation on Biomaterial Surfaces by a Multicomponent Therapeutic Coating. *Biomaterials* **2013**, *34* (4), 985–994. https://doi.org/10.1016/j.biomaterials.2012.10.040.

(22) Skerka, C.; Chen, Q.; Fremeaux-Bacchi, V.; Roumenina, L. T. Complement Factor H Related Proteins (CFHRs). *Molecular Immunology*. Pergamon December 5, 2013, pp 170–180. https://doi.org/10.1016/j.molimm.2013.06.001.

(23) Bechtler, C.; Lamers, C. Macrocyclization Strategies for Cyclic Peptides and Peptidomimetics. *RSC Med. Chem.* **2021**. https://doi.org/10.1039/D1MD00083G.

(24) Zwarthoff, S. A.; Berends, E. T. M.; Mol, S.; Ruyken, M.; Aerts, P. C.; Józsi, M.; de Haas, C. J. C.; Rooijakkers, S. H. M.; Gorham, R. D. Functional Characterization of Alternative and Classical Pathway C3/C5 Convertase Activity and Inhibition Using Purified Models. *Front. Immunol.* **2018**, *9* (JUL), 1691. https://doi.org/10.3389/fimmu.2018.01691.

(25) Zwarthoff, S. A.; Widmer, K.; Kuipers, A.; Strasser, J.; Ruyken, M.; Aerts, P. C.; de Haas, C. J. C.; Ugurlar, D.; den Boer, M. A.; Vidarsson, G.; et al. C1q Binding to Surface-Bound IgG Is Stabilized by C1r2s2 Proteases. *Proc. Natl. Acad. Sci. U. S. A.* **2021**, *118* (26). https://doi.org/10.1073/pnas.2102787118.

(26) Colombo, M.; Carregal-Romero, S.; Casula, M. F.; Gutiérrez, L.; Morales, M. P.; Böhm, I. B.; Heverhagen, J. T.; Prosperi, D.; Parak, W. J. Biological Applications of Magnetic Nanoparticles. *Chem. Soc. Rev.* **2012**, *41* (11), 4306–4334. https://doi.org/10.1039/c2cs15337h.

(27) Pouw, R. B.; Brouwer, M. C.; Geissler, J.; van Herpen, L. V.; Zeerleder, S. S.; Wuillemin, W. A.; Wouters, D.; Kuijpers, T. W. Complement Factor H-Related Protein 3 Serum Levels Are Low Compared to Factor H and Mainly Determined by Gene Copy Number Variation in CFHR3. *PLoS One* **2016**, *11* (3), e0152164. https://doi.org/10.1371/journal.pone.0152164.

(28) Pouw, R. B.; Brouwer, M. C.; de Gast, M.; van Beek, A. E.; van den Heuvel, L. P.; Schmidt, C. Q.; van der Ende, A.; Sánchez-Corral, P.; Kuijpers, T. W.; Wouters, D. Potentiation of Complement Regulator Factor H Protects Human Endothelial Cells from Complement Attack in AHUS Sera. *Blood Adv.* **2019**, *3* (4), 621–632. https://doi.org/10.1182/bloodadvances.2018025692.

(29) Pouw, R. B.; Vredevoogd, D. W.; Kuijpers, T. W.; Wouters, D. Of Mice and Men: The Factor H Protein Family and Complement Regulation. *Mol. Immunol.* **2015**, *67* (1), 12–20. https://doi.org/https://doi.org/10.1016/j.molimm.2015.03.011.

(30) Madeira, F.; Park, Y. mi; Lee, J.; Buso, N.; Gur, T.; Madhusoodanan, N.; Basutkar, P.; Tivey, A. R. N.; Potter, S. C.; Finn, R. D.; et al. The EMBL-EBI Search and Sequence Analysis Tools APIs in 2019. *Nucleic Acids Res.* **2019**, *47* (W1), W636–W641. https://doi.org/10.1093/NAR/GKZ268.

(31) Bateman, A.; Martin, M. J.; Orchard, S.; Magrane, M.; Agivetova, R.; Ahmad, S.; Alpi, E.; Bowler-Barnett, E. H.; Britto, R.; Bursteinas, B.; et al. UniProt: The Universal Protein Knowledgebase in 2021. *Nucleic Acids Res.* **2021**, *49* (D1), D480–D489. https://doi.org/10.1093/nar/gkaa1100.

(32) McRae, J. L.; Duthy, T. G.; Griggs, K. M.; Ormsby, R. J.; Cowan, P. J.; Cromer, B. A.; McKinstry, W. J.; Parker, M. W.; Murphy, B. F.; Gordon, D. L. Human Factor H-Related Protein 5 Has Cofactor Activity, Inhibits C3 Convertase Activity, Binds Heparin and C-Reactive Protein, and Associates with Lipoprotein. *J. Immunol.* **2005**, *174* (10), 6250–6256. https://doi.org/10.4049/jimmunol.174.10.6250.

(33) Mastellos, D. C.; Ricklin, D.; Lambris, J. D. Clinical Promise of Next-Generation Complement Therapeutics. *Nat. Rev. Drug Discov.* **2019**. https://doi.org/10.1038/s41573-019-0031-6.

(34) Pouw, R. B.; Ricklin, D. Tipping the Balance: Intricate Roles of the Complement System in Disease and Therapy. *Semin. Immunopathol.* **2021**, 1–15. https://doi.org/10.1007/s00281-

021-00892-7.
(35) Qu, H.; Ricklin, D.; Bai, H.; Chen, H.; Reis, E. S.; Maciejewski, M.; Tzekou, A.; DeAngelis, R. A.; Resuello, R. R. G.; Lupu, F.; et al. New Analogs of the Clinical Complement Inhibitor Compstatin with Subnanomolar Affinity and Enhanced Pharmacokinetic Properties. *Immunobiology* **2013**, *218* (4), 496–505. https://doi.org/10.1016/j.imbio.2012.06.003.
(36) Reis, E. S.; DeAngelis, R. A.; Chen, H.; Resuello, R. R. G.; Ricklin, D.; Lambris, J. D. Therapeutic C3 Inhibitor Cp40 Abrogates Complement Activation Induced by Modern Hemodialysis Filters. *Immunobiology* **2015**, *220* (4), 476–482. https://doi.org/10.1016/j.imbio.2014.10.026.
(37) Abicht, J.-M.; Kourtzelis, I.; Reichart, B.; Koutsogiannaki, S.; Primikyri, A.; Lambris, J. D.; Chavakis, T.; Holdt, L.; Kind, A.; Guethoff, S.; et al. Complement C3 Inhibitor Cp40 Attenuates Xenoreactions in Pig Hearts Perfused with Human Blood. *Xenotransplantation* **2017**, *24* (1), e12262. https://doi.org/10.1111/xen.12262.
(38) Mastellos, D. C.; Ricklin, D.; Sfyroera, G.; Sahu, A. From Discovery to Approval: A Brief History of the Compstatin Family of Complement C3 Inhibitors. *Clin. Immunol.* **2021**, 108785. https://doi.org/10.1016/j.clim.2021.108785.
(39) Andersson, J.; Larsson, R.; Richter, R.; Ekdahl, K. N.; Nilsson, B. Binding of a Model Regulator of Complement Activation (RCA) to a Biomaterial Surface: Surface-Bound Factor H Inhibits Complement Activation. *Biomaterials* **2001**, *22* (17), 2435–2443. https://doi.org/10.1016/S0142-9612(00)00431-2.
(40) Andersson, J.; Bexborn, F.; Klinth, J.; Nilsson, B.; Ekdahl, K. N. Surface-Attached PEO in the Form of Activated Pluronic with Immobilized Factor H Reduces Both Coagulation and Complement Activation in a Whole-Blood Model. *J. Biomed. Mater. Res. Part A* **2006**, *76A* (1), 25–34. https://doi.org/10.1002/jbm.a.30377.
(41) de Boer, E. C. W.; van Mourik, A. G.; Jongerius, I. Therapeutic Lessons to Be Learned From the Role of Complement Regulators as Double-Edged Sword in Health and Disease. *Front. Immunol.* **2020**, *11* (December), 1–21. https://doi.org/10.3389/fimmu.2020.578069.
(42) Schmidt, C. Q.; Bai, H.; Lin, Z.; Risitano, A. M.; Barlow, P. N.; Ricklin, D.; Lambris, J. D. Rational Engineering of a Minimized Immune Inhibitor with Unique Triple-Targeting Properties. *J. Immunol.* **2013**, *190* (11), 5712–5721. https://doi.org/10.4049/jimmunol.1203548.
(43) Veronese, F. M.; Pasut, G. PEGylation, Successful Approach to Drug Delivery. *Drug Discovery Today*. Elsevier Current Trends November 1, 2005, pp 1451–1458. https://doi.org/10.1016/S1359-6446(05)03575-0.
(44) Hamad, I.; Hunter, A. C.; Szebeni, J.; Moghimi, S. M. Poly(Ethylene Glycol)s Generate Complement Activation Products in Human Serum through Increased Alternative Pathway Turnover and a MASP-2-Dependent Process. *Mol. Immunol.* **2008**, *46* (2), 225–232. https://doi.org/10.1016/j.molimm.2008.08.276.
(45) Zhang, P.; Sun, F.; Liu, S.; Jiang, S. Anti-PEG Antibodies in the Clinic: Current Issues and beyond PEGylation. *J. Control. Release* **2016**, *244*, 184–193. https://doi.org/10.1016/j.jconrel.2016.06.040.
(46) Annamalai, B.; Parsons, N.; Nicholson, C.; Joseph, K.; Coughlin, B.; Yang, X.; Jones, B. W.; Tomlinson, S.; Rohrer, B. Natural Immunoglobulin M-Based Delivery of a Complement Alternative Pathway Inhibitor in Mouse Models of Retinal Degeneration. *Exp. Eye Res.* **2021**, *207*, 108583. https://doi.org/10.1016/j.exer.2021.108583.
(47) Okemefuna, A. I.; Nan, R.; Gor, J.; Perkins, S. J. Electrostatic Interactions Contribute to the Folded-Back Conformation of Wild Type Human Factor H. *J. Mol. Biol.* **2009**, *391* (1), 98–118. https://doi.org/https://doi.org/10.1016/j.jmb.2009.06.010.
(48) Wang, H.; Arp, J.; Liu, W.; Faas, S. J.; Jiang, J.; Gies, D. R.; Ramcharran, S.; Garcia, B.; Zhong, R.; Rother, R. P. Inhibition of Terminal Complement Components in Presensitized Transplant Recipients Prevents Antibody-Mediated Rejection Leading to Long-Term Graft Survival and Accommodation. *J. Immunol.* **2007**, *179* (7), 4451–4463. https://doi.org/10.4049/jimmunol.179.7.4451.

(49) Wasowska, B. A.; Lee, C. Y.; Halushka, M. K.; Baldwin, W. M. New Concepts of Complement in Allorecognition and Graft Rejection. *Cell. Immunol.* **2007**, *248* (1), 18–30. https://doi.org/10.1016/J.CELLIMM.2007.04.009.
(50) III, W. M. B.; Valujskikh, A.; Fairchild, R. L. Antibody-Mediated Rejection: Emergence of Animal Models to Answer Clinical Questions. *Am. J. Transplant.* **2010**, *10* (5), 1135–1142. https://doi.org/10.1111/J.1600-6143.2010.03065.X.
(51) Frazão, L. P.; Castro, J. V. de; Neves, N. M. In Vivo Evaluation of the Biocompatibility of Biomaterial Device. *Adv. Exp. Med. Biol.* **2020**, *1250*, 109–124. https://doi.org/10.1007/978-981-15-3262-7_8.
(52) Schmidt, C. Q.; Slingsby, F. C.; Richards, A.; Barlow, P. N. Production of Biologically Active Complement Factor H in Therapeutically Useful Quantities. *Protein Expr. Purif.* **2011**, *76* (2), 254–263. https://doi.org/10.1016/j.pep.2010.12.002.

SUPPLEMENTARY INFORMTATION

SUPPLEMENTARY FIGURES

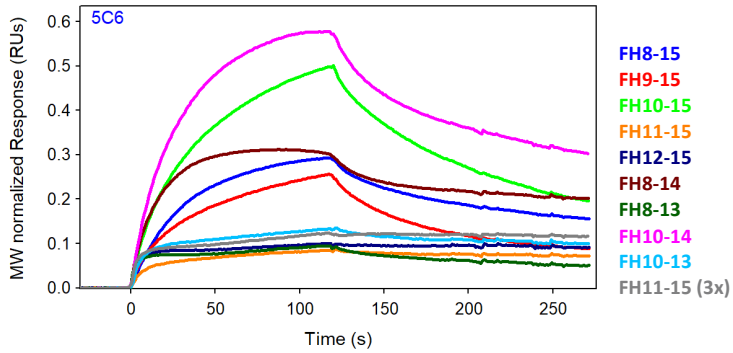

Figure S1: SPR sensorgrams of recombinant FH fragments at 100 nM with immobilized 5C6, representative of three experiments.

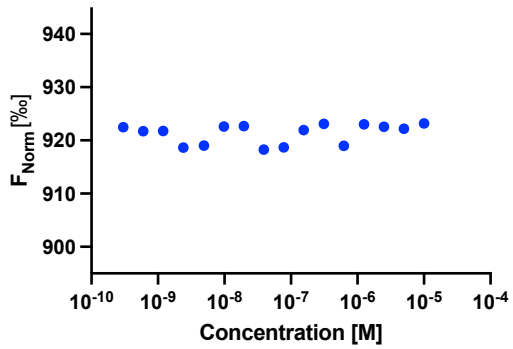

Figure S2: Representative MST concentration-response plot of 5C6 and FH8-15 labelled with the amine-reactive Nanotemper Technologies Monolith NT Protein Labeling Kit Red-NHS (Nanotemper, Munich, Germany) according to the manufacturer's instructions. The assay was performed at 136 nM labelled FH8-15 concentration, the red laser, an MST power of 40% and LED power of 15%.

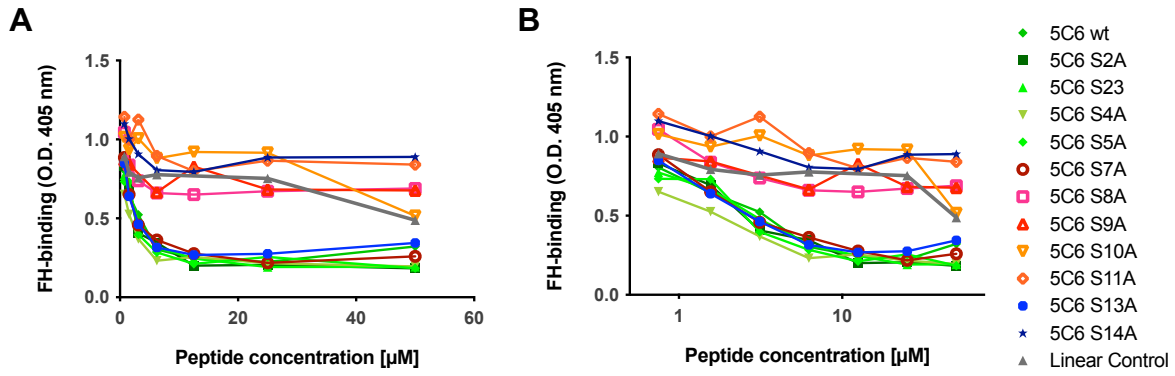

Figure S3: Concentration-response plots for the alanine scan analogs of 5C6 with linear (**A**) and log10 (**B**) scales, determined by competitive ELISA.

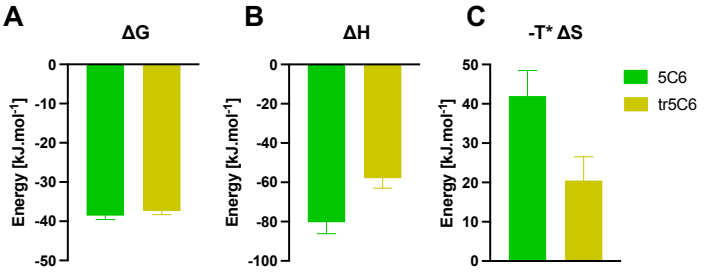

D

	5C6	tr5C6
K_D [nM]	182±51	292±76
ΔG [kJ/mol]	-38.6±1.0	-37.4±0.9
ΔH [kJ/mol]	-80.6±5.5	-57.9±5.1
-T *ΔS [kJ/mol]	42.0±6.5	20.5±6.1

Figure S4: (**A**) Free energy, (**B**) enthalpic and (**C**) entropic profile of the interaction of 5C6 and tr5C6 with FH8-15, measured by ITC. (**D**) Summary of the affinity and thermodynamic parameters of the interactions. *n* = 2, error is SD, except for the K_D, where it is SEM.

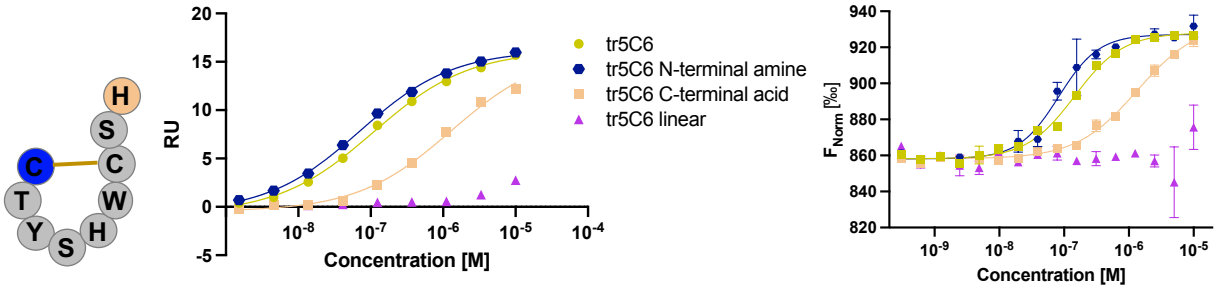

Figure S5: Schematic representation of 5C6 with the modified residues highlighted and representative SPR and MST concentration-response plots (from left to right).

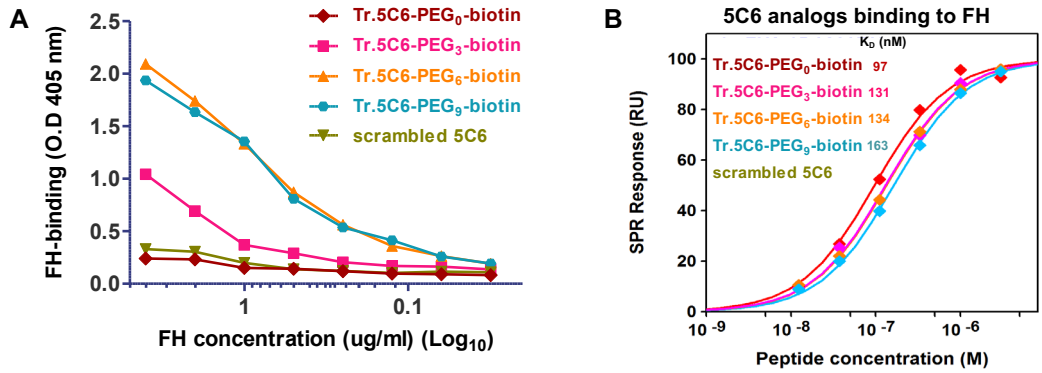

Figure S6: Binding of 5C6 analogs modified with PEG of different lengths to FH, measured by ELISA (**A**) and SPR (**B**).

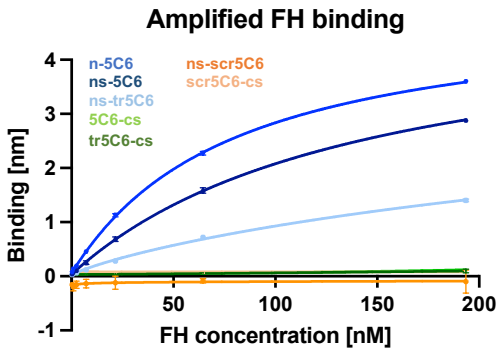

Figure S7: BLI concentration-response plots of 5C6 derivatives immobilised through K(biot) on streptavidin biosensors with signal amplification using an anti-FH antibody.

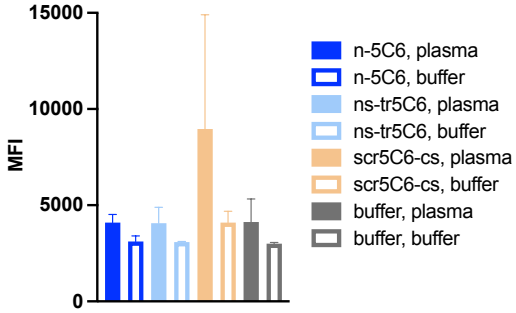

Figure S8: Median fluorescence intensity (MFI) of beads loaded with biotinylated 5C6 derivatives and incubated with citrated plasma. Detection of FH was performed with a primary polyclonal goat anti-human FH antibody and secondary, FITC-labelled polyclonal rabbit anti-goat IgG.

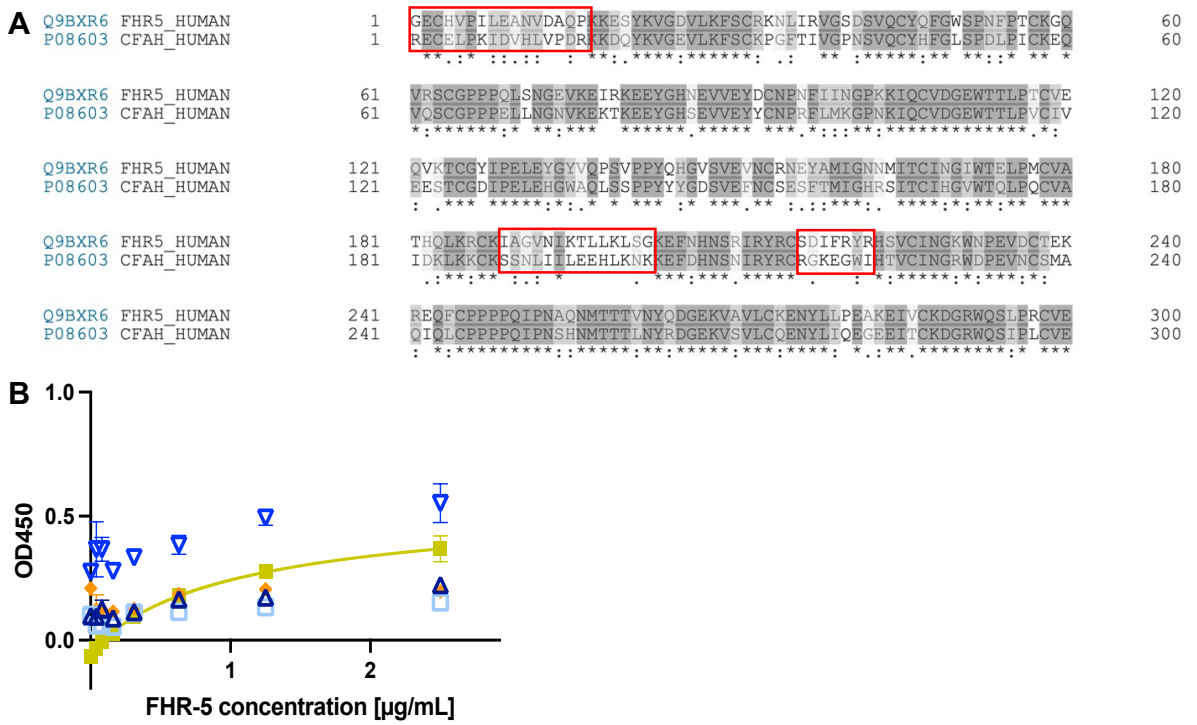

Figure S9: Sequence alignment of residues 567-866 of FH and 145-444 of FHR-5. Dark grey background indicates an identical residue, medium grey a similar residue (> 0.5 in the Gonnet PAM 250 matrix), light grey a weakly similar residue (<= 0.5 in the Gonnet PAM 250 matrix) and no background shading a dissimilar residue. Alignment and depiction obtained from uniprot.[31]

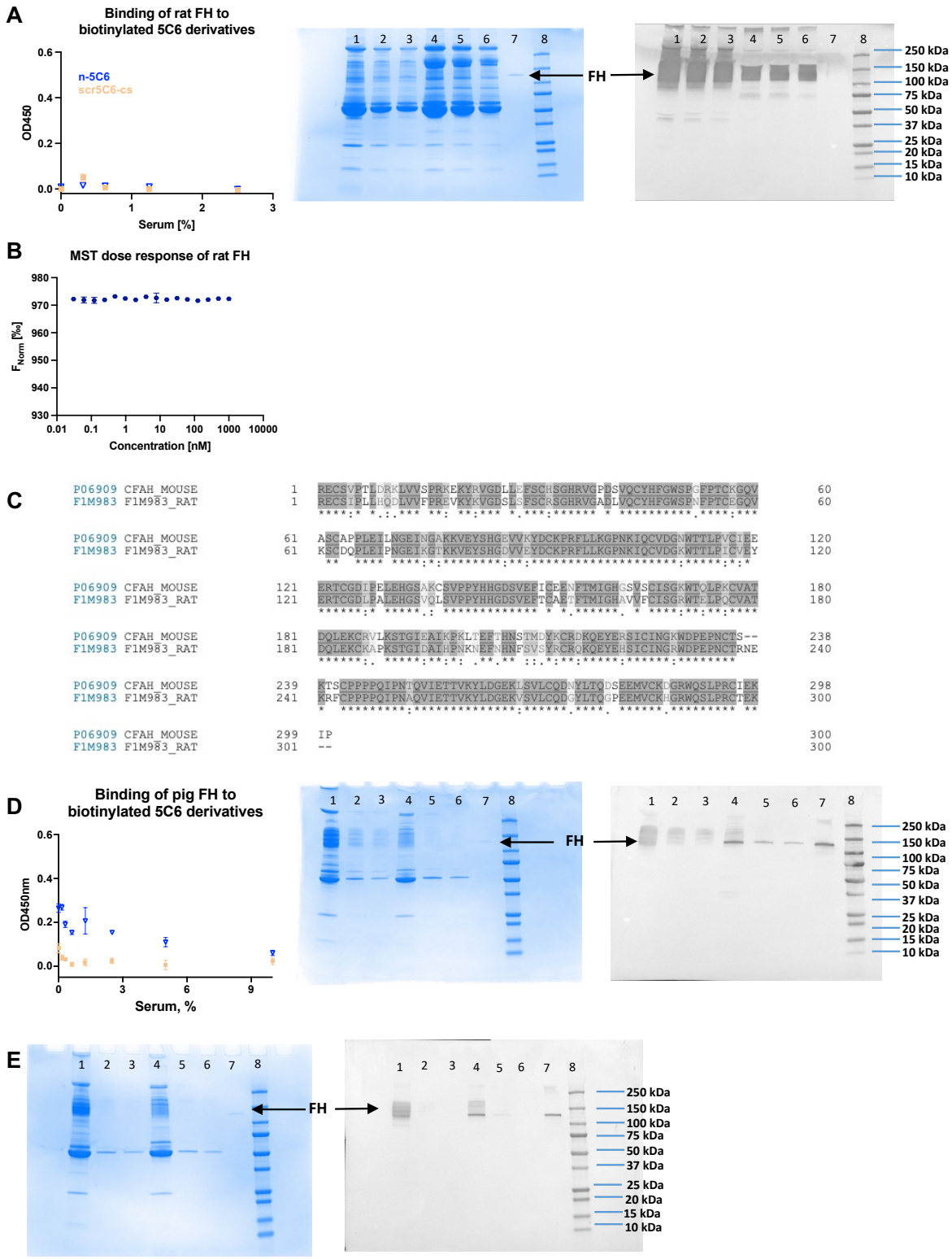

Figure S10: (**A**): Concentration-response plot of rat serum dilutions to biotinylated immobilized 5C6 derivatives, measured by ELISA (left), SDS-PAGE gel with Coomassie blue staining (middle) and Western Blot (right) of FH from murine (lanes 1-3) and rat serum dilutions 1:10, 1:20, 1:40 (lanes 4-6). Detection of FH was achieved with a monoclonal and cross-reactive anti-murine FH IgG L20/30 (Hycult, Uden, Netherlands). Lane 7: human FH reference, lane 8: ladder. (**B**) MST concentration-response plot of plasma-purified rat FH to carboxyfluorescein-labelled 5C6. (**C**): Sequence overlay of residues 567-866 of murine and rat FH, corresponding to human FH's CCPs 10-14. Dark grey backgrounds indicate an identical residue, medium grey a similar residue (> 0.5 in the Gonnet PAM 250 matrix), light grey a weakly similar residues (<= 0.5 in the Gonnet PAM 250 matrix) and no background shading a dissimilar residue. (**D**): Dose response-plot of pig serum dilutions to biotinylated immobilized 5C6

derivatives, measured by sandwich ELISA (left), SDS-PAGE gel with Coomassie blue staining (middle) and Western Blot (right of FH from pig (lanes 1-3) and human serum dilutions 1:50, 1:500, 1:1000 (lanes 4-6). Lane 7: human FH reference, lane 8: ladder. Detection of FH was achieved with a polyclonal goat IgG (Complement Technology, Tyler, USA). (**E**): SDS-PAGE gel with Coomassie blue staining (left) and Western Blot (right) of monkey (lanes 1-3) and human serum dilutions 1:50, 1:500, 1:1000 (lanes 4-6). Detection of FH was achieved with the murine anti-human FH IgG_1 aFH.16).

SUPPLEMENTARY METHODS: PEPTIDE CHARACTERIZATION

5C6 full length (5C6). Ac-ASSSR[CTYSHWC]SH-$CONH_2$, $C_{68}H_{95}N_{23}O_{22}S_2$, M_W = 1650.77 g/mol, M_{exact} = 1649.65 Da. ESI-MS: calculated: 825.84 $[M+2H]^{2+}$, 550.89 $[M+3H]^{3+}$, found: 825.89 $[M+2H]^{2+}$, 550.94 $[M+3H]^{3+}$; HPLC: t_R = 6.637 min.

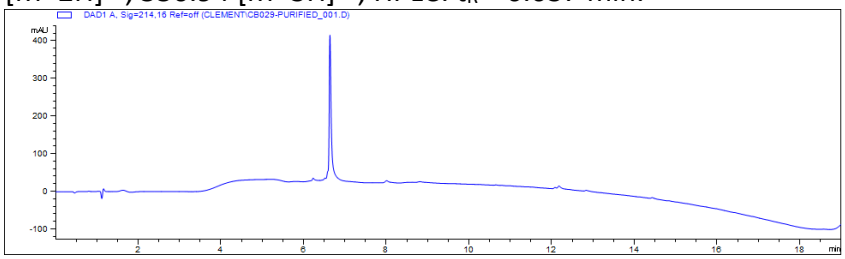

5C6 truncated (tr5C6). Ac-[CTYSHWC]SH-$CONH_2$, $C_{50}H_{63}N_{15}O_{14}S_2$, M_W = 1162.27 g/mol, M_{exact} = 1161.41 Da. ESI-MS: calculated: 1162.42 $[M+H]^{+}$, 581.72 $[M+2H]^{2+}$, found: 1162.19 $[M+H]^{+}$, 581.61 $[M+2H]^{2+}$; HPLC: t_R = 7.059 min.

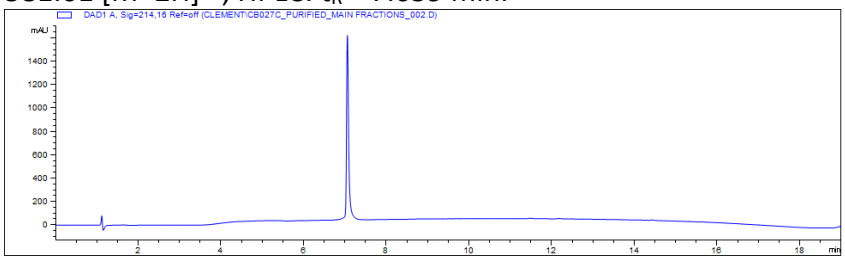

5C6 scrambled. Ac-SSHAS[CRWSSYC]HT-$CONH_2$, $C_{68}H_{95}N_{23}O_{22}S_2$, M_W = 1650.77 g/mol, M_{exact} = 1649.65 Da. ESI-MS: calculated: 1650.66 $[M+H]^{+}$, 825.84 $[M+2H]^{2+}$, 550.89 $[M+3H]^{3+}$, found: 1651.91 $[M+H]^{+}$, 825.89 $[M+2H]^{2+}$, 550.94 $[M+3H]^{3+}$; HPLC: t_R = 13.738 min.

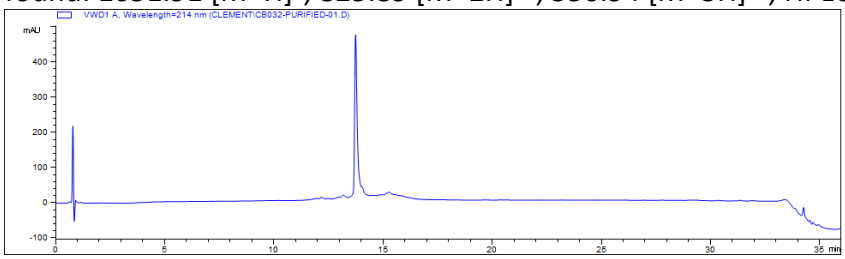

5C6 linear. Ac-ASSSRSTYSHWSSH-$CONH_2$, $C_{68}H_{97}N_{23}O_{24}$, M_W = 1620.66 g/mol, M_{exact} = 1619.71 Da. ESI-MS: calculated: 810.87 $[M+2H]^{2+}$, 540.91 $[M+3H]^{3+}$, found: 811.33 $[M+2H]^{2+}$, 540.94 $[M+3H]^{3+}$; HPLC: t_R = 6.581 min.

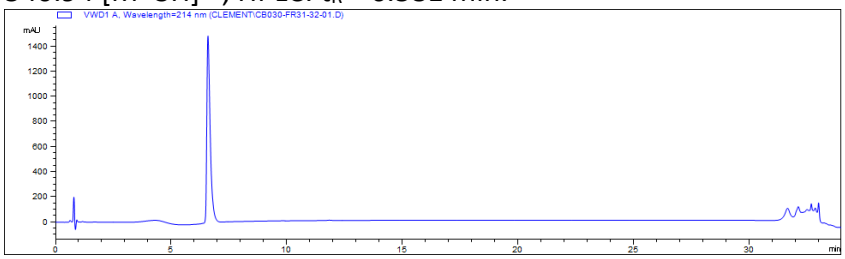

5C6 truncated linear (tr5C6 linear). Ac-STYSHWSSH-$CONH_2$, $C_{50}H_{65}N_{15}O_{16}$, M_W = 1132.16 g/mol, M_{exact} = 1131.47 Da. ESI-MS: calculated: 1132.48 $[M+H]^{+}$, 566.75 $[M+2H]^{2+}$, found: 1132.41 $[M+H]^{+}$, 566.72 $[M+2H]^{2+}$; HPLC: t_R = 7.470 min.

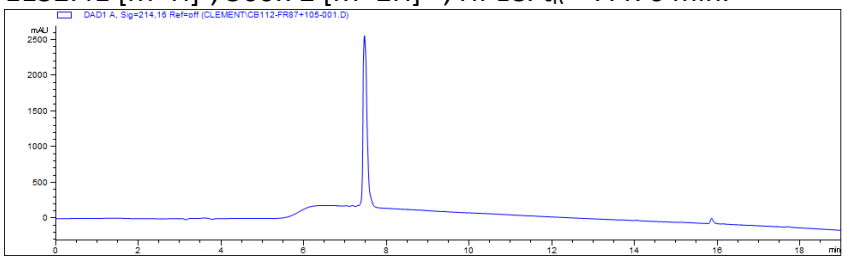

5C6 ΔH14. Ac-ASSSR[CTYSHWC]S-$CONH_2$, $C_{62}H_{88}N_{20}O_{21}S_2$, M_W = 1513.63 g/mol, M_{exact} = 1512.59 Da. ESI-MS: calculated: 1513.60 $[M+H]^{+}$, 757.31 $[M+2H]^{2+}$, found: 1513.32 $[M+H]^{+}$, 757.20 $[M+2H]^{2+}$; HPLC: t_R = 6.693 min.

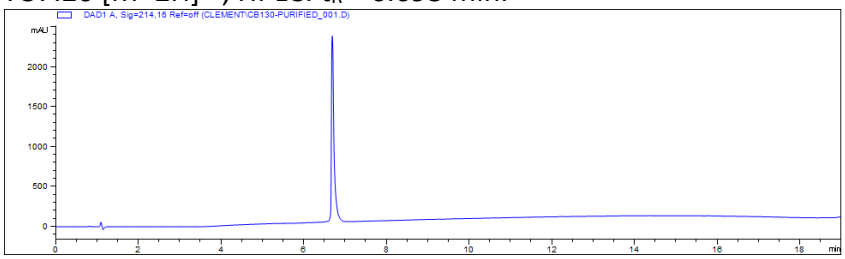

5C6 ΔS13 ΔH14. Ac-ASSSR[CTYSHWC]-$CONH_2$, $C_{59}H_{83}N_{19}O_{19}S_2$, M_W = 1426.56 g/mol, M_{exact} = 1425.55 Da. ESI-MS: calculated: 1426.56 $[M+H]^{+}$, 713.79 $[M+2H]^{2+}$, found: 1426.58 $[M+H]^{+}$, 713.82 $[M+2H]^{2+}$; HPLC: t_R = 7.032 min.

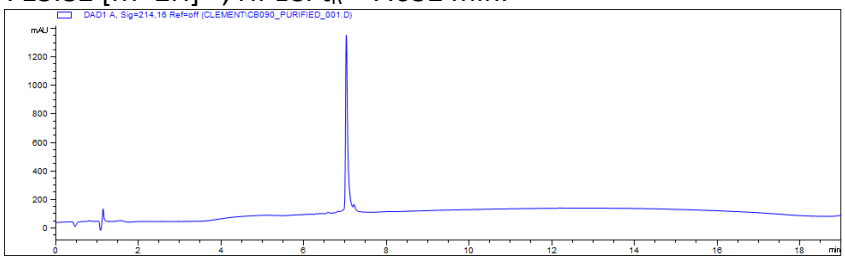

5C6 truncated N-terminal amine (tr5C6 N-terminal amine). H_2N-[CTYSHWC]SH-$CONH_2$, $C_{48}H_{61}N_{15}O_{13}S_2$, M_W = 1120.23 g/mol, M_{exact} = 1119.40 Da. ESI-MS: calculated: 1120.41 $[M+H]^+$, 560.71 $[M+2H]^{2+}$, found: 1120.10 $[M+H]^+$, 560.67 $[M+2H]^{2+}$; HPLC: t_R = 6.551 min.

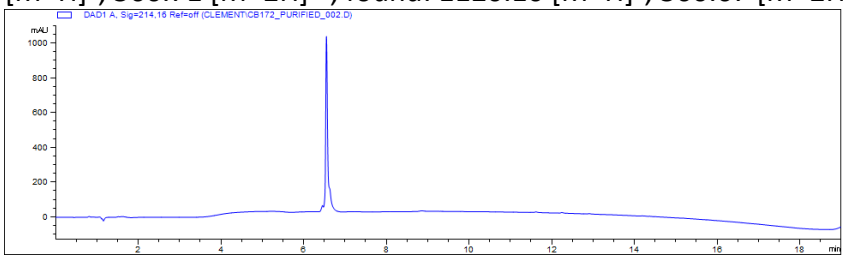

5C6 truncated C-terminal acid (tr5C6 C-terminal acid). Ac-[CTYSHWC]SH-CO_2H, $C_{50}H_{62}N_{14}O_{15}S_2$, M_W = 1163.25 g/mol, M_{exact} = 1162.40 Da. ESI-MS: calculated: 1163.41 $[M+H]^+$, 582.21 $[M+2H]^{2+}$, found: 1163.21 $[M+H]^+$, 582.09 $[M+2H]^{2+}$; HPLC: t_R = 7.129 min.

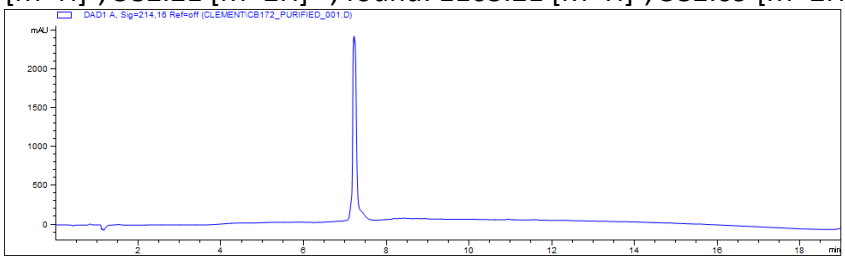

5C6 N-terminal carboxyfluorescein (CF-5C6). CF-ASSSR[CTYSHWC]SH-$CONH_2$, $C_{87}H_{103}N_{23}O_{27}S_2$, M_W = 1967.04 g/mol, M_{exact} = 1965.68 Da. ESI-MS: calculated: 983.81 $[M+2H]^{2+}$, 656.21 $[M+3H]^{3+}$, found: 983.85 $[M+2H]^{2+}$, 656.22 $[M+3H]^{3+}$; HPLC: t_R = 7.857 min.

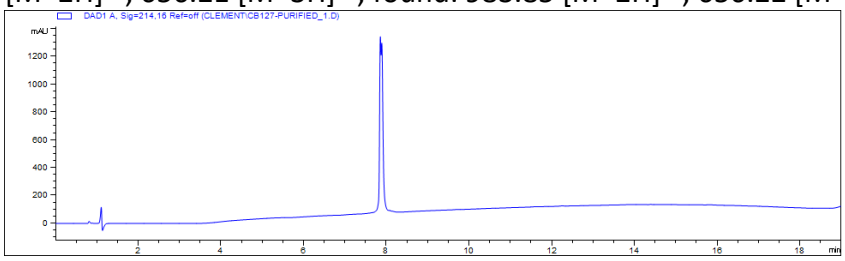

5C6 biotinylated N-term, full length, no spacer. Ac-K(biot)ASSSR[CTYSHWC]SH-$CONH_2$, $C_{84}H_{121}N_{27}O_{25}S_3$, M_W = 2005.24 g/mol, M_{exact} = 2003.82 Da. ESI-MS: calculated: 1002.92 $[M+2H]^{2+}$, 668.95 $[M+3H]^{3+}$, found: 1003.29 $[M+2H]^{2+}$, 668.87 $[M+3H]^{3+}$; HPLC: t_R = 7.019 min.

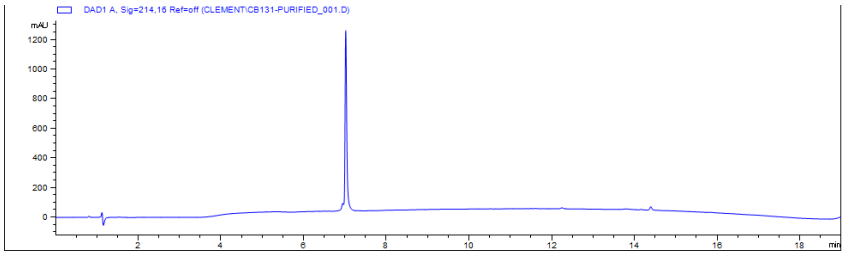

5C6 biotinylated N-term, full length, with spacer. Ac-K(biot)$(PEG3)_2$ASSSR[CTYSHWC]SH-$CONH_2$, $C_{100}H_{151}N_{29}O_{33}S_3$, M_W = 2383.66 g/mol, M_{exact} = 2382.02 Da. ESI-MS: calculated: 1192.02 $[M+2H]^{2+}$, 795.02 $[M+3H]^{3+}$, found: 1192.31 $[M+2H]^{2+}$, 795.30 $[M+3H]^{3+}$; HPLC: t_R = 7.188 min.

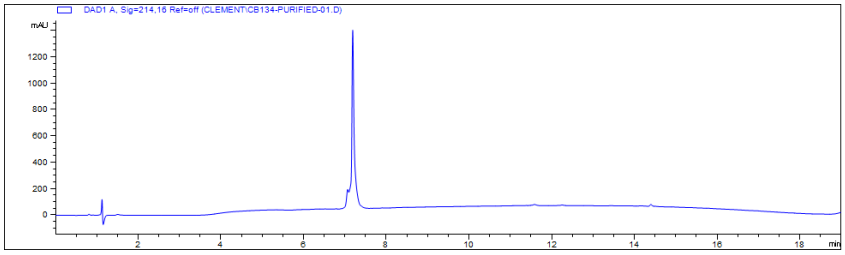

5C6 biotinylated N-term, truncated, with spacer. Ac-K(biot)$(PEG3)_2$[CTYSHWC]SH-$CONH_2$, $C_{82}H_{119}N_{21}O_{25}S_3$, M_W = 1895.16 g/mol, M_{exact} = 1893.78 Da. ESI-MS: calculated: 1894.79 $[M+H]^+$, 947.90 $[M+2H]^{2+}$, found: 1895.29 $[M+H]^+$, 947.88 $[M+2H]^{2+}$; HPLC: t_R = 7.732 min.

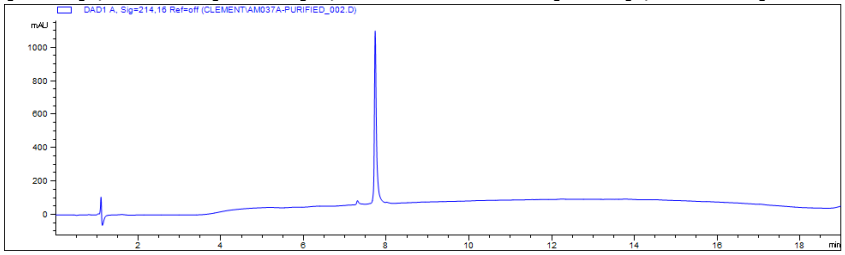

5C6 biotinylated C-term, full length, with spacer. Ac-ASSSR[CTYSHWC]SH-$(PEG3)_2$K(biot)-$CONH_2$, $C_{100}H_{151}N_{29}O_{33}S_3$, M_W = 2383.66 g/mol, M_{exact} = 2382.02 Da. ESI-MS: calculated: 1192.02 $[M+2H]^{2+}$, 795.02 $[M+3H]^{3+}$, found: 1192.44 $[M+2H]^{2+}$, 795.14 $[M+3H]^{3+}$; HPLC: t_R = 7.203 min.

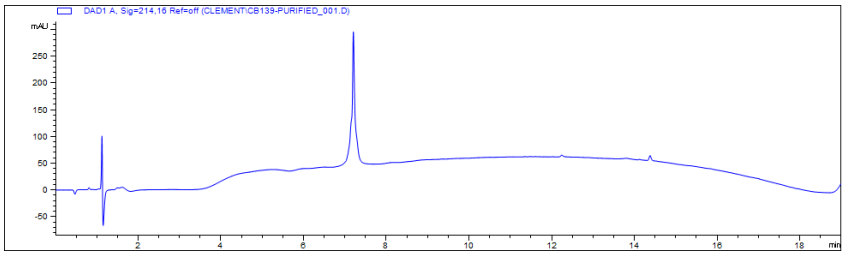

5C6 biotinylated C-term, truncated, with spacer. Ac-[CTYSHWC]SH$(PEG3)_2$K(biot)-$CONH_2$, $C_{82}H_{119}N_{21}O_{25}S_3$, M_W = 1895.16 g/mol, M_{exact} = 1893.78 Da. ESI-MS: calculated: 1894.79 $[M+H]^+$, 947.88 $[M+2H]^{2+}$, found: 1895.36 $[M+H]^+$, 947.88 $[M+2H]^{2+}$; HPLC: t_R = 7.750 min.

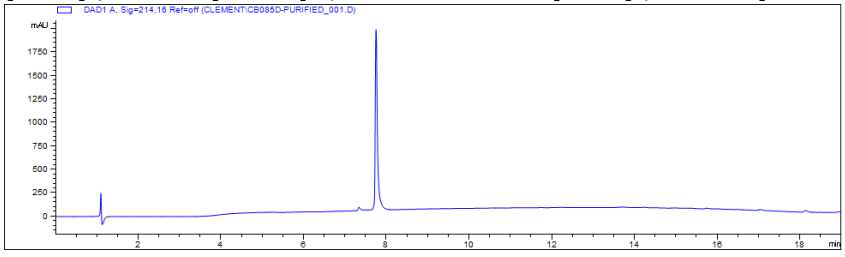

5C6 biotinylated N-term, scrambled, with spacer. Ac-K(biot)$(PEG3)_2$SSHAS[CRWSSYC]HT-$CONH_2$, $C_{100}H_{151}N_{29}O_{33}S_3$, M_W = 2383.66 g/mol, M_{exact} = 2382.02 Da. ESI-MS: calculated: 1192.02 $[M+2H]^{2+}$, 795.02 $[M+3H]^{3+}$, found: 1192.61 $[M+2H]^{2+}$, 795.38 $[M+3H]^{3+}$; HPLC: t_R = 7.220 min.

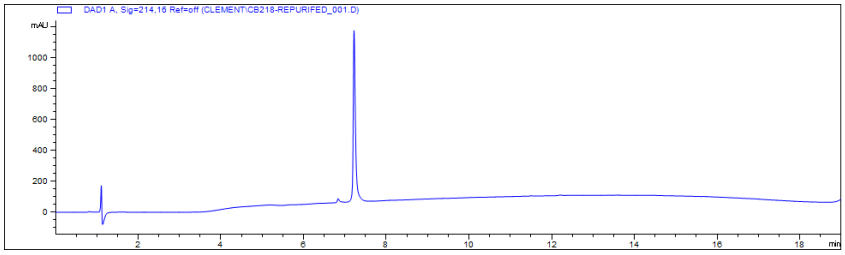

5C6 biotinylated C-term, scrambled, with spacer. Ac-SSHAS[CRWSSYC]HT$(PEG3)_2$K(biot)-$CONH_2$, $C_{100}H_{151}N_{29}O_{33}S_3$, M_W = 2383.66 g/mol, M_{exact} = 2382.02 Da. ESI-MS: calculated: 2383.03 $[M+H]^+$, 1192.02 $[M+2H]^{2+}$, 795.02 $[M+3H]^{3+}$, found: 2383.63 $[M+H]^+$, 1192.38 $[M+2H]^{2+}$, 795.15 $[M+3H]^{3+}$; HPLC: t_R = 7.422 min.

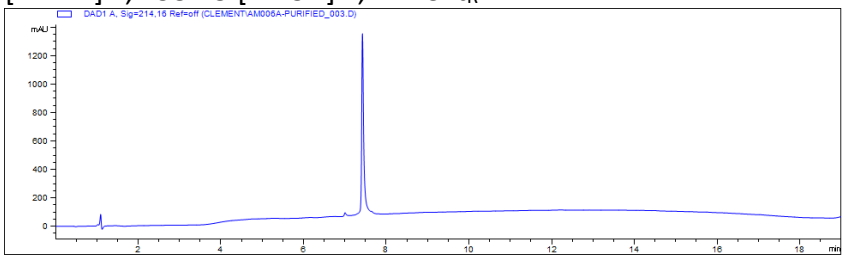

5C6 biotinylated C-term, scrambled+linear, with spacer.
Ac-YSSSWAHASTRASH$(PEG3)_2$K(biot)-$CONH_2$, $C_{100}H_{153}N_{29}O_{33}S$, M_W = 2321.55 g/mol, M_{exact} = 2320.09 Da. ESI-MS: calculated: 2321.10 $[M+H]^+$, 1161.06 $[M+2H]^{2+}$, 774.37 $[M+3H]^{3+}$, found: 2322.00 $[M+H]^+$, 1161.49 $[M+2H]^{2+}$, 774.49 $[M+3H]^{3+}$; HPLC: t_R = 7.309 min.

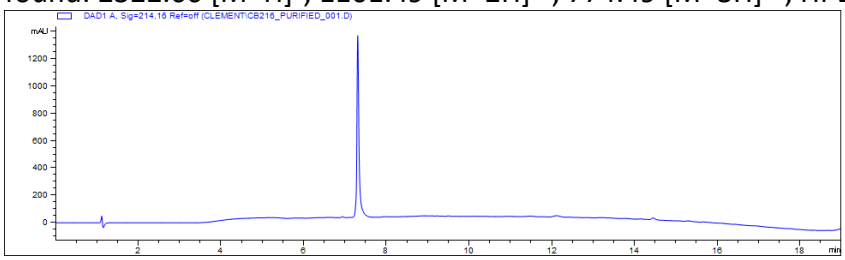

Original Article

CHAPTER 4: SYNTHETIC, FUNCTIONAL AND STRUCTURAL STUDIES ON THE FH BINDING PEPTIDE 5C6: DEVELOPMENT OF IMPROVED COMPLEMENT-INHIBITING CONJUGATES TO PREVENT BIOMATERIAL-INDUCED COMPLICATIONS

Clément Bechtler[1], Ekaterina Umnyakova[1], Lukas Kaufmann[1], Martin Smieško[2], Thomas Müntener[3], Sophia Koutsogiannaki[4], Yiannis Sarigiannis[4], Christina Lamers[1], Richard B. Pouw[1], Oliver Schwardt[1], Sebastian Hiller[3], John D. Lambris[4], Daniel Ricklin[1]

[1] Molecular Pharmacy Group, Department of Pharmaceutical Sciences, University of Basel, Basel, Switzerland
[2] Computational Pharmacy Group, Department of Pharmaceutical Sciences, University of Basel, Basel, Switzerland
[3] Structural Biology and Biophysics Focus Area, Biozentrum, University of Basel, Basel, Switzerland
[4] Department of Pathology & Laboratory Medicine, Perelman School of Medicine, University of Pennsylvania, Philadelphia, USA

Under review in the *Journal of Controlled Release* (ISSN: 0168-3659)

Contributions of Clément Bechtler:

- Design, synthesis and evaluation of 5C6 analogs
- Development, performance and analysis of biophysical assays (SPR, MST, ITC, BLI, CD)
- Support in NMR structure elucidation (signal assignment)
- Manuscript preparation

Synthetic, Functional and Structural Studies on the FH-Binding Peptide 5C6: Development of Improved Complement-Inhibiting Conjugates to Prevent Biomaterial-Induced Complications

Clément Bechtler[1], Ekaterina Umnyakova[1], Lukas Kaufmann[1], Martin Smieško[2], Thomas Müntener[3], Sophia Koutsogiannaki[4], Yiannis Sarigiannis[4], Christina Lamers[1], Richard B. Pouw[1], Oliver Schwardt[1], Sebastian Hiller[3], John D. Lambris[4], Daniel Ricklin[1]

[1] Molecular Pharmacy Group, Department of Pharmaceutical Sciences, University of Basel, Basel, Switzerland
[2] Computational Pharmacy Group, Department of Pharmaceutical Sciences, University of Basel, Basel, Switzerland
[3] Structural Biology and Biophysics Focus Area, Biozentrum, University of Basel, Basel, Switzerland
[4] Department of Pathology & Laboratory Medicine, Perelman School of Medicine, University of Pennsylvania, Philadelphia, USA

ABSTRACT

Liposomal drug formulations have enabled the use of efficacious yet toxic drugs by providing beneficial delivery and targeting profiles. Despite the undoubted advantage of such drug carriers, they themselves can be at the origin of immune-mediated toxicity, potentially with severe clinical consequences. One pivotal contributor to carrier-induced adverse reactions is the complement system, an innate immune pathway that triggers fast effector responses upon recognizing non-self surfaces. While host cells are protected from complement attack by specialized regulators, including the plasma protein factor H (FH) that inhibits complement's central amplification loop, artificial surfaces such as liposomes lack this protection. We could previously show that artificial and cellular surfaces coated with the cyclic peptide 5C6 actively recruit FH from plasma to impair complement activation in situ, and could describe the key activity determinants of 5C6. Here we provide in-depth structure activity relationship studies that resulted in the design, synthesis and evaluation of next-generation 5C6 analogs with improved target affinity, functional activity and stability. Additionally, we solved the solution structure of the core region of 5C6, shedding additional light on the structural features relevant to the interaction with FH to guide rational optimization endeavors in the future.

INTRODUCTION

As central part of humoral innate immunity, the complement system acts as fast-sensing and fast-reacting first line of defense against microbial intruders. It consists of more than 50 proteins, including circulating enzymes and effector proteins as well as membrane-bound receptors and regulators. Upon recognition of pathogen- or damage-associated surface patterns, such as immune complexes or carbohydrate signatures by proteins of the classical and lectin pathways, respectively, an enzyme cascade is initiated that leads to the surface deposition of opsonins C4b and C3b. Surface-bound C3b engages the serine protease factor B (FB) and factor D (FD) to form C3 convertase complexes (C3bBb) that cleave the plasma protein C3 into C3b. Via this positive feedback mechanism, referred to as alternative pathway (AP), the complement response can be quickly amplified. The accumulation of opsonins not only mediates binding to immune cell receptors but also enables the formation of C5 convertases that produce the potent anaphylatoxin C5a and initiate the formation of lytic membrane attack complexes (MAC). Together, these effector cascade proceeds quickly to form active effectors that mediate chemotaxis, immune cell activation and phagocytosis but also induce direct cell damage (**Figure 1A**).[1,2]

Due to its fast reactivity and strong immunological effects, complement needs to be tightly regulated on host cell surfaces and in solution to avoid potentially devastating effects of misguided activation. Complement regulation therefore occurs on different levels ranging from initiation (e.g., by C1 inhibitor) to MAC formation (by CD59).[1,3] The AP as driving mechanism of complement amplification is controlled by several circulating and membrane-bound regulators. Among those, the abundant (≈ 2 µM) plasma protein factor H (FH) is the main AP regulator in solution but it also recognizes self-surface patterns, e.g. polyanionic groups such as sialic acids, and consequently act as a surface-directed regulator. Structurally, FH is composed of 20 globular complement control protein (CCP) domains which are sequentially connected by short, flexible linkers. By inhibiting the central amplification loop, FH can act independently of the initiation pathway. It acts via three mechanisms, i.e. by competing with FB to prevent formation of the AP C3 convertase, by accelerating the decay of existing convertases, and by acting as co-factor for factor I (FI), which degrades C3b to fragments that are no longer capable of forming C3 or C5 convertases (**Figure 1A**). While CCPs 1-4 bind C3b and mediate regulation, CCPs 6-7 and 19-20 are involved in self- and/or opsonin-recognition.[4]

The central role of FH in controlling complement is underlined by the fact that many pathogens, e.g. *Neisseria meningitidis* and *Trypanosoma brucei,* recruit FH to their surface and by this, protect themselves from complement attack.[5,6] Inspired by these natural complement escape mechanisms, we have previously described a disulfide-bridged cyclic, 14 amino acid long peptide, termed 5C6 **1**, which is able to bind FH with high affinity (K_D ≈ 100 nM) and, when combined with appropriate surface tethers, is able to recruit FH to biomedical surfaces (**Figure 1B, C**).[7,8] Importantly, we showed that 5C6's minimal binding region is within CCPs 10-14 of FH; consequently, 5C6 can recruit FH without impeding its functional activity. Indeed, 5C6 was able to reduce complement activation on various model surfaces representing biomaterial or xenotransplantation applications (**Figure 1D**).[7–9] We also determined important structural features, such as the cyclic nature and H14 within 5C6, and established that N-terminal immobilization leads to superior FH recruitment which correlated with stronger complement inhibition on biomaterial particles, in line with the findings that the exocyclic N-terminus contributes only to a minor extent to binding and a truncated derivative (tr5C6 **2**) largely maintains binding affinity to FH (**Figure 1C, D**).[9]

FH-recruiting coatings may prove valuable in various indications, in which non-self cells are recognized and attacked by complement (e.g., solid organ transplants, especially when damaged by ischemia-reperfusion injury)[10,11] or when artificial surfaces are exposed to blood (e.g., hemodialysis filters)[12]. Another condition that has gained increasing attention are adverse reactions to nanomedicines and liposomal drug formulations, where complement activation may induce inflammatory responses or complement activation-related pseudoallergies (CARPAs); in the USA alone, up to 500'000 patients may be affected annually by such complications.[13–15] The severity of the condition can vary widely, from subclinical with mild hypotension to cardiogenic shock with lethal outcome. CARPA has been

prominently described and investigated for PEGylated liposomal drug formulations of the cytostatic doxorubicin (Doxil®/Caelyx®) and the antifungal amphotericin B (AmBisome®).[16–18] Beside adverse drug effects, complement attack also leads to reduced efficacy of the products, thereby preventing patient access to primordial treatment. Although the precise mechanism of CARPA remains to be elucidated, several factors affecting its occurrence and severity have been described, including the nature of the encapsulated drug, the composition, charge, and size of the liposome and, in the case of pegylated liposomes, the presence of anti-PEG antibodies.[13,16,18–24] While such antibodies appear to play an important role, their titer does not necessarily correlate with the severity of CARPA.[25] Based on this heterogeneity of triggers, the contributions of individual complement initiation pathways has been shown to vary; yet even in cases of antibody-mediated activation, the AP appears to be a critical contributor or even driver of the response.[26,27] Inhibition of the amplification loop therefore presents a promising strategy to curb complement-mediated hypersensitivity reactions. Indeed, the validity of this hypothesis was recently confirmed *in vitro*, where AmBisome®-induced complement activation in serum could be reduced by addition of FH.[28] Rather than applying exogenous FH, which as a biologic will likely feature high production cost and requires parenteral administration, the addition of coatings based on FH-recruiting peptides during or after production of liposomal drugs may offer a broadly applicable and cost-effective alternative. The recruiting activity, tethering and stability of the peptides are critical factors to achieve this goal.

Herein, we performed in-depth structure-activity relationship (SAR) studies of 5C6, including peptidomimetic replacements for the disulfide bridge, and achieved an 8-fold increase in FH affinity with an improved activity and stability profile. We also present the solution structure of tr5C6 **2**, facilitating future optimization efforts.

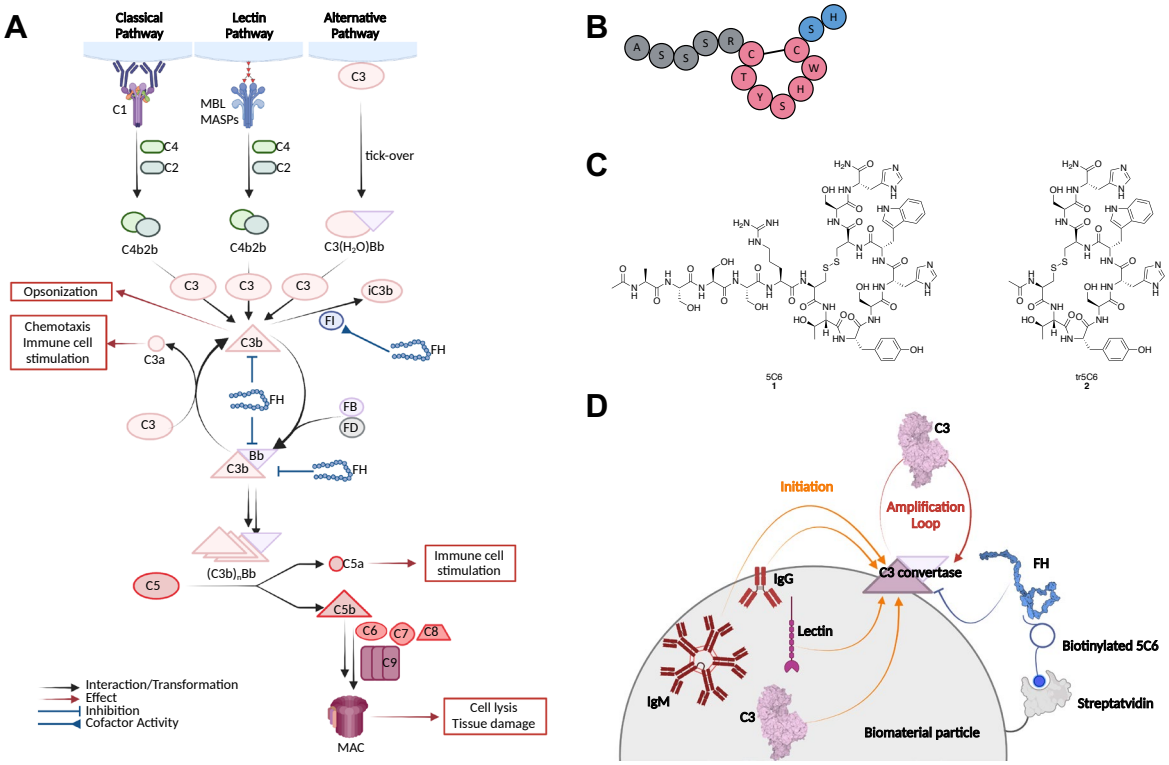

Figure 1: (**A**) Schematic representation of the complement cascade with the three initiation pathways (classical, lectin and alternative pathways), central amplification loop and terminal pathway. Upon activation, C3 convertases (C4b2b or C3(H_2O)Bb) are formed, leading to deposition of C3b which increases further C3 cleavage in a self-amplificatory response. With further increased C3b density on the surfaces, the convertases start cleaving C5 as well leading to finally form the membrane attack complex (MAC), a pore-forming protein complex, in the terminal pathway. The plasma protein FH regulates the amplification loop by reducing convertase formation and accelerating its decay and degradation. (**B**) Schematic representation of the FH-binding peptide 5C6 **1** with the exocyclic N-terminus in grey, the core cycle in purple and the exocyclic C-terminus in blue. Truncated 5C6 (tr5C6) **2**, which shows a comparable binding affinity to FH, shares the same

cyclic core, but lacks the exocyclic N-terminal region. (**C**) Chemical structures of 5C6 **1** (left) and tr5C6 **2** (right), respectively. (**D**) Simplified view of complement activation on biomaterial particles and inhibition of it by 5C6 conjugates. All initiation pathways have been shown to be involved in the activation of complement on biomaterials such as nanoparticles, leading to the formation of C3 convertases which fuels itself further in the amplification loop. This can be reduced by linking 5C6 **1** to a certain tether recognizing a surface (e.g. biotin-streptavidin), and consequent FH recruitment from the solution phase to the surface.

RESULTS AND DISCUSSION

In a recent study, we were able to elucidate the structural features of 5C6 **1** that define its interaction with FH, including the presence of an intact cycle or the accessibility of the C-terminus.[9] Based on this insight, we now performed detailed SAR studies. We investigated systematically each position from R5 to H14, which we had previously determined to play a role in FH binding by an alanine scan, as well as a further expansion on the C-terminus.[9] Furthermore, we investigated the ring size, alternatives to the native disulfide bridge and the influence of *N*-methylation on the core tr5C6 **2**. To provide a quantitative assessment of the applied changes, binding affinities for immobilized recombinant FH8-15 were determined using surface plasmon resonance (SPR) as described previously and normalized on the molecular weight.[9] Absolute K_D values were affected by immobilization density, leading to variation between experimental series but high reproducibility within each series. Activities are therefore reported as relative K_D based on 5C6 **1** or its truncated derivative (tr5C6) **2**, which were included in every SPR run. Sequence-scrambled (scr5C6) or linearized 5C6 (lin5C6), in which the Cys residues had been replaced by Ser, were used as negative controls.

***N*-methylation of 5C6 does not improve FH binding.** As backbone *N*-methylation is an established method to modulate pharmacodynamic and pharmacokinetic properties of peptides[29], we synthesized backbone *N*-methylated tr5C6 peptides containing an *N*-methyl group on every residue except the cysteines. The binding affinities of the analogues partially reflected the findings of our previously reported alanine scan[9] as methylation of S9 and W11 fully abolished binding to FH8-15. Interestingly however, methylation of H10 led to a complete activity loss, whereas the H10A substitution only reduced affinity 7-fold. Similarly, the S13A substitution had a minor, but methylation of S13 a severe impact on affinity; this may suggest that S13 methylation may affect the presentation of the adjacent H14, which was demonstrated to be critical for the interaction.[9] In contrast, although methylation of H14 reduced affinity 200-fold, it was not completely abolished as was the case for the H14A substitution. Overall, no *N*-methylation showed a beneficial effect and all methylations, with the exception of T7, profoundly reduced target binding (**Figure 2A**, **Table 1**). Competitive ELISA experiments, in which the analogues in solution competed with immobilized 5C6 for FH binding, confirmed these observations (**Figure 2B**).

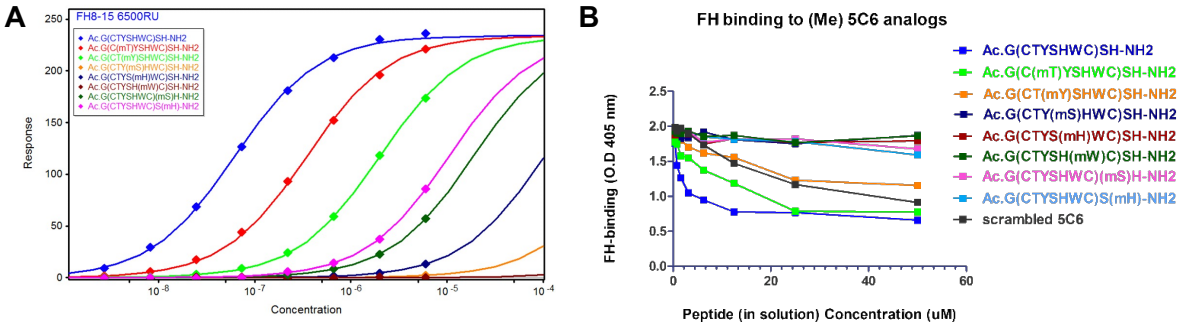

Figure 2 (**A**) Dose-response plots for the *N*-methylation scan analogs of 5C6 measured by SPR. (**B**) Dose-response plots for the *N*-methylation scan analogs of 5C6 measured by a competitive ELISA with the *N*-methylated peptides in solution.

Table 1: Relative binding affinities of the *N*-methylation scan analogs based on truncated 5C6 (tr5C6) **2** as determined by SPR.

Peptide[1]	Sequence	rel. K_D±SEM
tr5C6+5G wild type	Ac–G[CTYSHWC]SH–$CONH_2$	1.00±0.00
tr5C6+5G T7(mT)	Ac–G[C(**mT**)YSHWC]SH–$CONH_2$	5.94±0.31
tr5C6+5G Y8(mY)	Ac–G[CT(**mY**)SHWC]SH–$CONH_2$	31.4±0.9
tr5C6+5G S9(mS)	Ac–G[CTY(**mS**)HWC]SH–$CONH_2$	no binding
tr5C6+5G H10(mH)	Ac–G[CTYS(**mH**)WC]SH–$CONH_2$	no binding
tr5C6+5G W11(mW)	Ac–G[CTYSH(**mW**)C]SH–$CONH_2$	no binding
tr5C6+5G S13(mS)	Ac–G[CTYSHWC](**mS**)H–$CONH_2$	321±19
tr5C6+5G H14(mH)	Ac–G[CTYSHWC]S(**mH**)–$CONH_2$	177±8
5C6 scr	Ac–YSSSWAHASTRASH(K(PEG4–biotin)–$CONH_2$	no binding

[1] An N-terminal glycine residue was added to the N-methylation series for technical reasons; it does not notably affect the binding properties of tr5C6.

Side chain substitutions affect the interaction with FH. Our previously conducted alanine scan of 5C6 revealed that in particular residues Y8, S9 H10, W11 and H14 are crucial for binding to FH, while residues R5, T7 and S13 only contribute in a limited way. We therefore focused our SAR studies on replacing key residues with similar substituents and assessing broader side chain variations on positions with less-pronounced effect on affinity to explore whether additional contacts may be forged. The following sections show the findings obtained for each of the varied positions, from R5 to H14.

R5W substitution improves affinity. Although we had previously shown that removing the entire exocyclic N-terminal segment only slightly reduces the affinity to FH, we interpreted this difference as an indication that the N-terminus is still involved to a certain degree in the interaction with FH. Given that the cyclic core and the C-terminus are central for binding to FH, we hypothesized that the additional interaction might be mediated by R5, the residues closest to the macrocycle, and replaced the Arg by a set of different amino acids covering diverse functionality (Trp, Glu, Ser, Lys, Leu). Also, since the exocyclic N-terminus may serve as a spacer for surface tethering, the presence of Arg at this position may negatively affect the stability of coated peptide. We therefore investigated the substitution of R5 in the context of full-length 5C6. Interestingly, all substitutions led to two- to five-fold decease in affinity (including the assumed similar R5K), except for the R5W substitution which increased affinity slightly (**Figure 3A**, **Table 2**). A comparable improvement was observed when the R5W analog was tested in a competitive microscale thermophoresis (MST) assay[9], in which unlabeled analogs are competing with N-terminally carboxyfluorescein (CF)-labeled 5C6 for FH binding in solution (**Figure 3B**). To explore the basis of this improvement, we compared the thermodynamic profiles of the R5W analogue and the parental compound using isothermal titration calorimetry (ITC). Both peptides showed similar thermodynamic profiles and comparable affinities (**Supplementary Figure S1**), suggesting that the type of contacts the Trp establishes are similar to the ones establishes by Arg. This, and the finding that the R5K analog was less affine, might suggest that Arg and Trp π-stack with a FH residue, which Lys cannot.[30]

Table 2: Relative binding affinities of the broad R5 analogs of 5C6, determined by SPR, prepared and measured in duplicates.

Peptide	Sequence	rel. K_D±SEM
5C6 wt	Ac–ASSS**R**[CTYSHWC]SH–$CONH_2$	1.00±0.00
5C6 R5W	Ac–ASSS**W**[CTYSHWC]SH–$CONH_2$	0.78±0.19
5C6 R5E	Ac–ASSS**E**[CTYSHWC]SH–$CONH_2$	2.24±0.14
5C6 R5L	Ac–ASSS**L**[CTYSHWC]SH–$CONH_2$	3.44±0.99
5C6 R5S	Ac–ASSS**S**[CTYSHWC]SH–$CONH_2$	3.76±1.25
5C6 R5K	Ac–ASSS**K**[CTYSHWC]SH–$CONH_2$	5.43±0.09
5C6 ΔS13 ΔH14	Ac–ASSSR[CTYSHWC] –$CONH_2$	no binding

Based on these findings, we extended the R5 series with analogs featuring aromatic proteinogenic amino acids (i.e. Phe, His, Tyr) or the non-proteinogenic amino acids 3-(2-thienyl)-L-alanine (thi) **3**, 3-

(3-Pyridyl)-L-alanine (pyr) **4**, 1-methyl-L-tryptophan (MeW) **5** and 3-(2-naphthyl)-L-alanine (Nal) **6** to cover aromatic side chains with different sizes and functionalities (**Figure 3C**). Most analogues showed similar affinities to 5C6 **1** and 5C6 R5W (**Figure 3D**, **Table 3**). In contrast, the R5(MeW) analog had a 7-fold reduced affinity (**Figure 3D**, **Table 3**) at a largely maintained kinetic off-rate (k_d) when compared to R5W, suggesting that the indole scaffold mediates slower dissociation of 5C6 from FH, but methylation of the indole hampers formation of the 5C6-FH complex. Indeed, the improved k_d is also mainly responsible for the improved affinity of R5W over 5C6 **1** while the on-rate (k_a) remained largely unchanged (**Figure 3E**, **Table 4**).

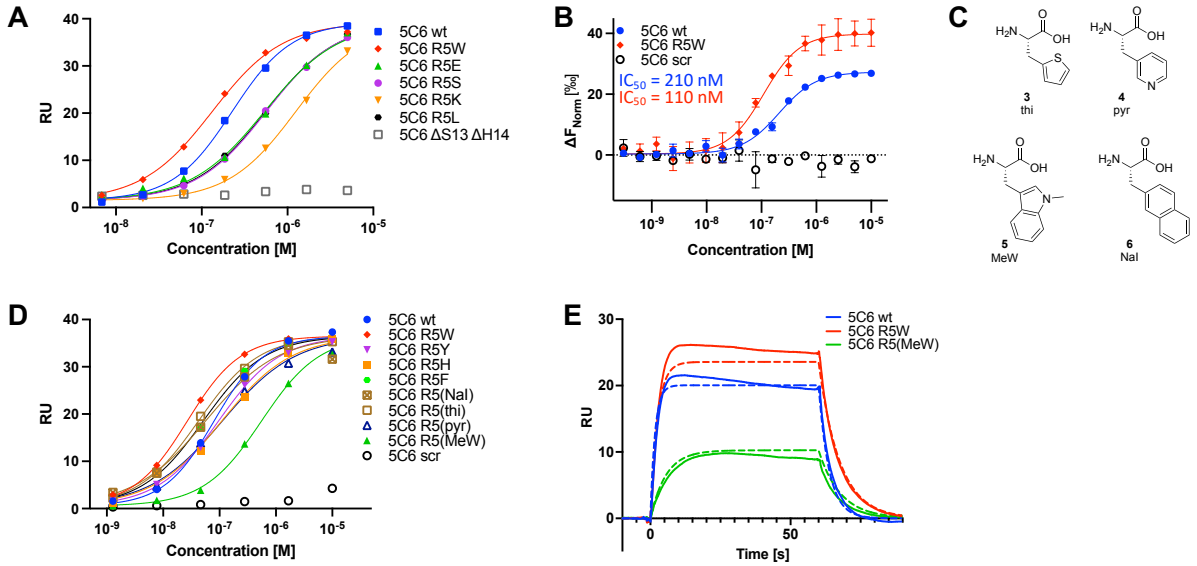

Figure 3: (**A**) Dose-response plots for R5 analogs of 5C6 measured by SPR. (**B**) Competitive MST dose-response plots for 5C6 wt **1**, 5C6 R5W and 5C6 scr. (**C**) Structures of non-canonical amino acids 3-(2-thienyl)-L-alanine (thi) **3**, 3-(3-Pyridyl)-L-alanine (pyr) **4**, 1-methyl-L-tryptophan (MeW) **5** and 3-(2-naphthyl)-L-alanine (Nal) **6** used for the aromatic R5 peptide series. (**D**) Dose-response plots for aromatic R5 analogs of 5C6 measured by SPR (**E**) SPR sensorgram of 5C6 wt **1** (blue), 5C6 R5W (red) and 5C6 R5(MeW) (green) at 370 nM with the slower dissociation rates of the indole-containing analogs and the slower association rate of the R5(MeW) analog clearly to see. Full lines are the experimental, dashed lines are the fitted values.

Table 3: Relative binding affinities of the aromatic R5 analogs of 5C6, determined by SPR, *n* = 2.

Peptide	Sequence	rel. K_D±SEM
5C6 wt **1**	Ac–ASSS **R** [CTYSHWC]SH–$CONH_2$	1.00±0.00
5C6 R5W	Ac–ASSS **W** [CTYSHWC]SH–$CONH_2$	0.21±0.12
5C6 R5Y	Ac–ASSS **Y** [CTYSHWC]SH–$CONH_2$	1.07±0.14
5C6 R5H	Ac–ASSS **H** [CTYSHWC]SH–$CONH_2$	1.51±0.12
5C6 R5F	Ac–ASSS **F** [CTYSHWC]SH–$CONH_2$	0.52±0.13
5C6 R5(thi)	Ac–ASSS(**thi**)[CTYSHWC]SH–$CONH_2$	0.34±0.19
5C6 R5(pyr)	Ac–ASSS(**pyr**)[CTYSHWC]SH–$CONH_2$	1.05±0.35
5C6 R5(MeW)	Ac–ASSS(**MeW**)[CTYSHWC]SH–$CONH_2$	7.45±0.48
5C6 R5(Nal)	Ac–ASSS(**Nal**)[CTYSHWC]SH–$CONH_2$	0.53±0.18
5C6 scr	Ac–SSHA S [CRWSSYC]HT–$CONH_2$	no binding

Table 4: Kinetic constants of 5C6 wt **1** and R5W as well as R5(MeW) analogs. Determined by SPR, *n* = 2.

Peptide	Sequence	k_a [$M^{-1}.s^{-1}$]	k_d [s^{-1}]
5C6 wt	Ac–ASSS **R** [CTYSHWC]SH–$CONH_2$	$(8.60±1.24)·10^5$	0.228±0.055
5C6 R5W	Ac–ASSS **W** [CTYSHWC]SH–$CONH_2$	$(7.31±0.09)·10^5$	0.125±0.013
5C6 R5(MeW)	Ac–ASSS(**MeW**)[CTYSHWC]SH–$CONH_2$	$(1.11±0.44)·10^5$	0.126±0.003

Although not essential, the exocyclic N-terminus bears potential for optimization. While none of the exocyclic residues of the N-terminus of 5C6 were identified as essential by the alanine scan, the replacement of Ser 2, 3 or 4 by Ala had a minor but notable beneficial effect. We therefore synthesized an analogue which combines the favorable R5W substitution with serine-to-alanine mutations for all

three positions (i.e. 5C6 S234A R5W). This S234A seemed to slightly improve affinity (**Figure 4A**, **Table 5**), although not driven by a further decreased kinetic dissociation rate, but a faster association (**Figure 4B**). Even though we could show that the 5 position appears to be involved in the binding to FH, this had not been established for positions 1-4. Therefore, we also completely removed these four residues, either while retaining the wild type Arg at position 5 or by also including the R5W substitution (i.e. 5C6 Δ1-4 and 5C6 Δ1-4 R5W, respectively). 5C6 Δ1-4 showed a two-fold improved affinity, while the additional R5W change further improved affinity, even stronger than for 5C6 **1**. However, even at very low concentrations, 5C6 Δ1-4 R5W showed some response, which is why some minor, unspecific contribution to the observed binding cannot be fully excluded. To validate these findings, we tested the same series as well in our competitive MST assay[9], with the same trends observable. In particular, the removal of residues 1-4 and the R5W substitution were additive, also leading to a seven-fold improved IC_{50} (**Figure 4C**, **Table 5**). In summary, removal, of residues 1-4 and changes to R5 are beneficial for FH binding, suggesting that although the N-terminus is not crucial for the interaction, it might still hold potential for further improvement of binding.

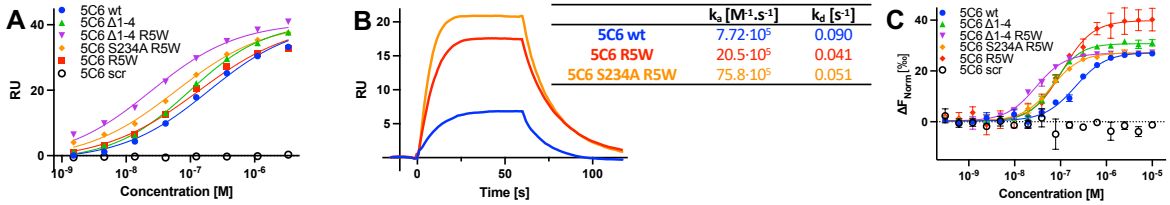

Figure 4: (**A**) Representative SPR dose-response plots for the 5C6 analogs with a globally modified N-terminus. (**B**) SPR sensorgrams at 39 nM concentration for 5C6 wt **1**, 5C6 R5W and 5C6 S234A R5W. (**C**) Competitive MST dose-response plots for the 5C6 analogs with a globally modified N-terminus.

Table 5: Relative KDs and absolute IC_{50}s of the N-terminally globally modified analogs of 5C6, determined by SPR and MST, respectively, *n* = 2.

Peptide	Sequence	rel. K_D±SEM (SPR)	IC_{50} ±SEM [nM] (MST)
5C6 wt	Ac–**ASSSR**[CTYSHWC]SH–$CONH_2$	1.00±0.00	210±25
5C6 Δ1-4	Ac–**R**[CTYSHWC]SH–$CONH_2$	0.49±0.02	74±6
5C6 Δ1-4 R5W	Ac–**W**[CTYSHWC]SH–$CONH_2$	0.14±0.01	29±3
5C6 S234A R5W	Ac–**AAAAW**[CTYSHWC]SH–$CONH_2$	0.42±0.11	64±7
5C6 R5W	Ac–**ASSSW**[CTYSHWC]SH–$CONH_2$	0.68±0.03	110±8
5C6 scr	Ac–SSHAS[CRWSSYC]HT–$CONH_2$	no binding	no binding

T7 tolerates substitution. Our previous work on 5C6 had shown that the side chain of T7 is not strongly involved in the binding to FH.[9] To therefore cover a large chemical space, we replaced T7 with all proteinogenic amino acids (but Cys), focusing our efforts on tr5C6 **2** for ease of synthesis. As expected, the position proved rather tolerant towards change, in particular towards residues with a hydrogen bond acceptor (HBA) in the same position as Thr (i.e. T7N, T7S, T7D), an aromatic group (i.e. T7Y, T7F, T7H, T7W) or a basic group (i.e. T7R, T7K), which all showed at least 50% of the response of tr5C6 **2** at 100 nM peptide concentration in our SPR binding assay (**Figure 5A**). As there is a more than 2-fold difference in response between tr5C6 and T7V, but also between T7N and T7Q, this suggests that the OH group of Thr is indeed contributing to binding, albeit to a modest extent, by providing a HBA or hydrogen-bond donor (HBD) at a suitable position. Based on these findings, we investigated more closely the T7N, T7S, T7D, T7Y and T7F analogues. The positively charged analogs T7K and T7R did show SPR responses without complete saturation, potentially due to electrostatic interference with biosensor surface, and were therefore omitted from the analysis. As already indicated by the single concentration screening, the tested analogs showed comparable affinities with less than twofold changes over tr5C6 **2**, but none of the substitutions showed superior affinity. (**Figure 5B, Table 6**).

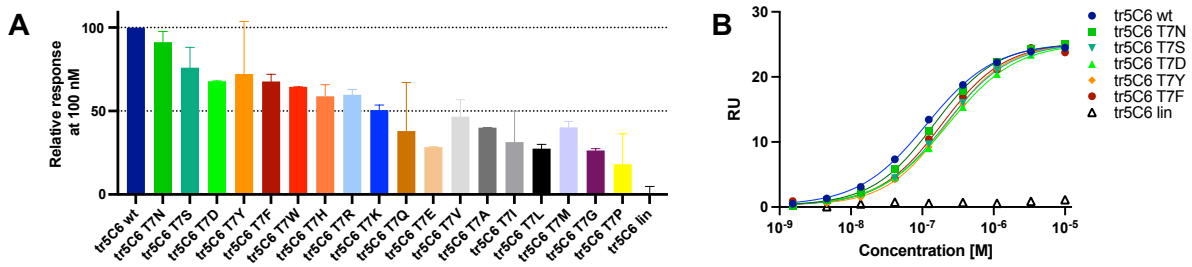

Figure 5: (**A**) Relative SPR responses at 100 nM of T7 substitution analogs of tr5C6 **2**, normalized on the response of tr5C6 wt **2**, which was set to 100; *n* = 2. (**B**) Representative SPR dose-response plots for the subset of T7 analogs with the highest relative response at 100 nM.

Table 6: Relative binding affinities of the most promising T7 analogs of 5C6, determined by SPR, *n* = 3.

Peptide	Sequence	rel. K_D±SEM
tr5C6 wt	Ac–[C**T**YSHWC]SH–$CONH_2$	1.00±0.00
tr5C6 T7N	Ac–[C**N**YSHWC]SH–$CONH_2$	1.30±0.47
tr5C6 T7S	Ac–[C**S**YSHWC]SH–$CONH_2$	1.28±0.28
tr5C6 T7D	Ac–[C**D**YSHWC]SH–$CONH_2$	1.94±0.65
tr5C6 T7Y	Ac–[C**Y**YSHWC]SH–$CONH_2$	2.01±0.67
tr5C6 T7F	Ac–[C**F**YSHWC]SH–$CONH_2$	1.18±0.25
tr5C6 lin	Ac– STYSHWS SH–$CONH_2$	no binding

Changes to Y8 have a strong impact on affinity. The complete affinity loss of the Y8A mutant in our previous Ala scan indicated a key role for this residue in FH binding.[9] To confirm its importance and explore how functional group properties (and size) would affect affinity, we investigated a limited series of distinct Y8 analogues (Y8L, Y8S, Y8E, Y8K). Since the *N*-methylation scan indicated a negative impact of conformational constraints at this position, we also synthesized and tested the Y8G analog to have a peptide with increased flexibility. All analogs showed a major affinity drop with the least yet still profound impact observed for Y8G. With the importance of Tyr at this position confirmed, we added the D-Tyr analog (Y8y) to the series to evaluate the effect of side chain orientation. This change also led to substantial affinity drop, underlining that both the functionality and orientation of the side chain at this position are essential (**Figure 6**, **Table 7**).

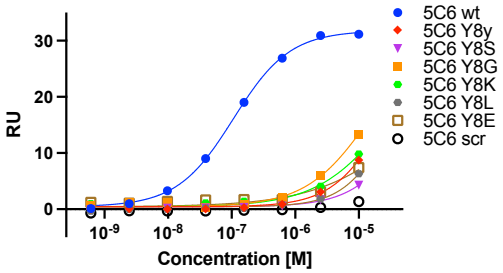

Figure 6: Representative dose-response plots for the Y8 analog series of 5C6 measured by SPR.

Table 7: Relative binding affinities of the aromatic Y8 analogs of 5C6, determined by SPR, *n* = 2.

Peptide	Sequence	rel. K_D±SEM
5C6 wt	Ac–ASSSR[CT**Y**SHWC]SH–$CONH_2$	1.00±0.00
5C6 Y8y	Ac–ASSSR[CT**y**SHWC]SH–$CONH_2$	172±86
5C6 Y8L	Ac–ASSSR[CT**L**SHWC]SH–$CONH_2$	219±109
5C6 Y8S	Ac–ASSSR[CT**S**SHWC]SH–$CONH_2$	345±192
5C6 Y8G	Ac–ASSSR[CT**G**SHWC]SH–$CONH_2$	70±40
5C6 Y8K	Ac–ASSSR[CT**K**SHWC]SH–$CONH_2$	3243±3099
5C6 Y8E	Ac–ASSSR[CT**E**SHWC]SH–$CONH_2$	497±277
5C6 scr	Ac–ASSSR[CTYSHWC]SH–$CONH_2$	no binding

The proper positioning of a hydrogen bond acceptor at position 9 is critical. To assess the contribution of S9, we initially introduced broad changes, i.e. replacing Ser **7** with (S)-2-aminobutyric acid (abu **8**), ornithine (orn **9**), Asp (**10**) and Phe (**11**) (**Figure 7A**, top row). None of the derivatives showed notable affinity for FH8-15 (**Figure 7B**, **Table 8**). The abolished affinity in S9(abu) suggested an essential role of the hydroxyl group of S9. Based on these results, we designed and synthesized a second, narrower S9 series, which would allow us to differentiate between the necessity of having only a HBD or a combined HBD/HBA function at this position. For this purpose, we substituted Ser with (S)-2,3-diaminopropionic acid (dapa **11**), which should be fully protonated at pH 7.4 and therefore act as HBD. Additionally, we wanted to study small structural changes by using building blocks with increased conformational constraint (Thr **12**) or a spacing (homoserine, hS **13**) of the hydroxyl group. Finally, we tested amides (Asn **14**, Gln **15**) as side chains with both HBA and HBD functionality, although spatially separated when compared to a hydroxyl group (**Figure 7A**, bottom row). Underlining the importance of S9's hydroxyl group, only the two analogs having HBD functions at the same position as S9 (i.e. S9T and S9(dapa)) showed residual affinity although with a more than 20-fold decrease. The observed drop for S9(dapa) suggests that for S9, both HBD and HBA are necessary for potent binding, although other effects such as charge repulsion or an increased dehydration penalty of S9(dapa) might also contribute to the observed effect. Additionally, the massive reduction in affinity of the S9T substitution hints at the need to maintain accessibility to a tight binding pocket for S9 or the need for a specific spatial arrangement for optimal interaction with both aspects possibly being impeded by the additional methyl group of Thr.

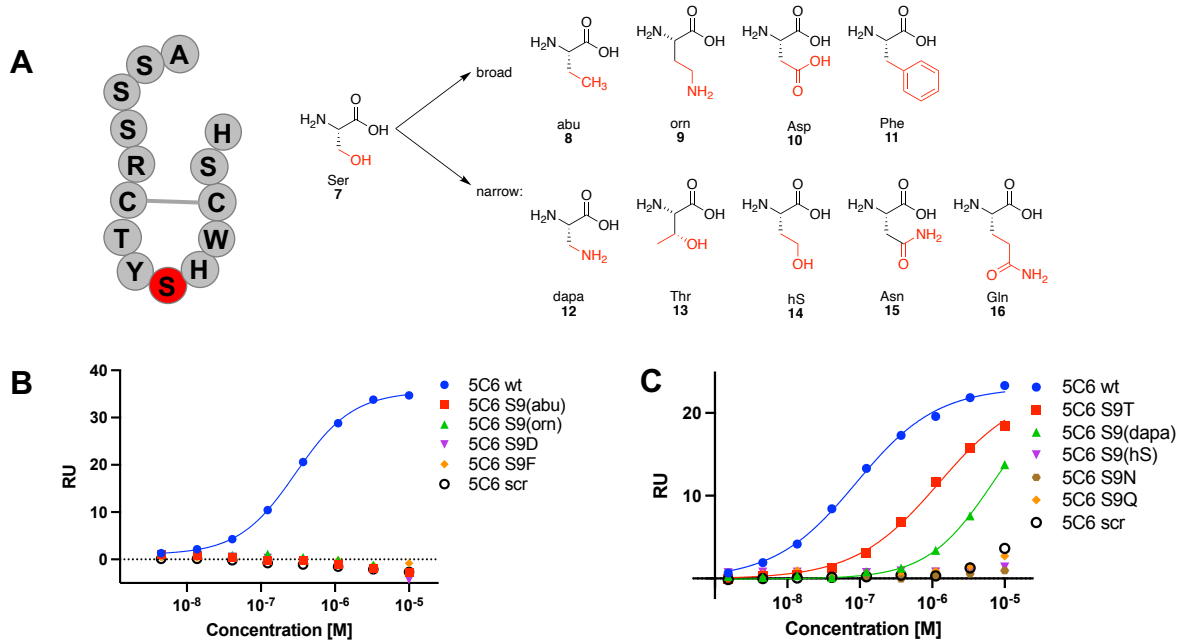

Figure 7: (**A**) Position for S9 within 5C6 and its substitution in the broad (top) and narrow (bottom) analog series. (**B**) Representative dose-response plots for the broad S9 analog series of 5C6 measured by SPR. (**C**) Representative dose-response plots for the narrow S9 analog series of 5C6 measured by SPR.

Table 8: Relative binding affinities of the narrow S9 analogs of 5C6, determined by SPR, *n* =2.

Peptide	Sequence	rel. K_D±SEM
5C6 wt	Ac–ASSSR[CTY **S** HWC]SH–$CONH_2$	1.00±0.00
5C6 S9T	Ac–ASSSR[CTY **T** HWC]SH–$CONH_2$	26.7±12.8
5C6 S9(dapa)	Ac–ASSSR[CTY(**dapa**)HWC]SH–$CONH_2$	127.9±51.1
5C6 S9(hS)	Ac–ASSSR[CTY(**hS**)HWC]SH–$CONH_2$	no binding
5C6 S9N	Ac–ASSSR[CTY **N** HWC]SH–$CONH_2$	no binding
5C6 S9Q	Ac–ASSSR[CTY **Q** HWC]SH–$CONH_2$	no binding
5C6 scr	Ac–SSHAS[CRW S SYC]HT–$CONH_2$	no binding

H10 can be replaced by 3-methyl histidine. When compared to most of the other residues in the cyclic core of 5C6 **1**, the substitution of H10 with Ala in our previous alanine scan only led to a moderate decrease of affinity.[9] We therefore initially investigated analogs covering a variety of functional groups, namely H10T, H10L, H10(orn), H10F and H10E which occupy a similar space as His. All analogs drastically lost affinity (≈100-fold), with H10E even being completely inactive (**Figure 8A, Table 9**). Based on these results, we synthesized a second library of tr5C6 **2** analogs with substitutions closer to the native His **17**, including H10F **11** (as comparison with previous series), 2-furfuryl alanine (fur, **18**) as another small but less polar and neutral, aromatic heterocycle, and with methylated imidazoles, i.e. 1-metyhl histidine (1-MeH, **19**) or 3-methyl histidine (3-MeH, **20**) (**Figure 8B**). Having either imidazole nitrogen methylated prevents tautomerization and the respective position from participating in hydrogen bonding. Interestingly, the fur **18** and 1-MeH **19** analogs lost affinity to a comparable extent as did H10F, whereas the 3-MeH **20** analog maintained affinity, although with a faster kinetic profile (**Figure 8C, Tables 10-11**). In combination, this suggests that the 1-position of the imidazole plays an important role for the interaction, and that negatively charged residues within the binding region of FH might be in proximity, leading to abolishment of the affinity in the H10E analog.

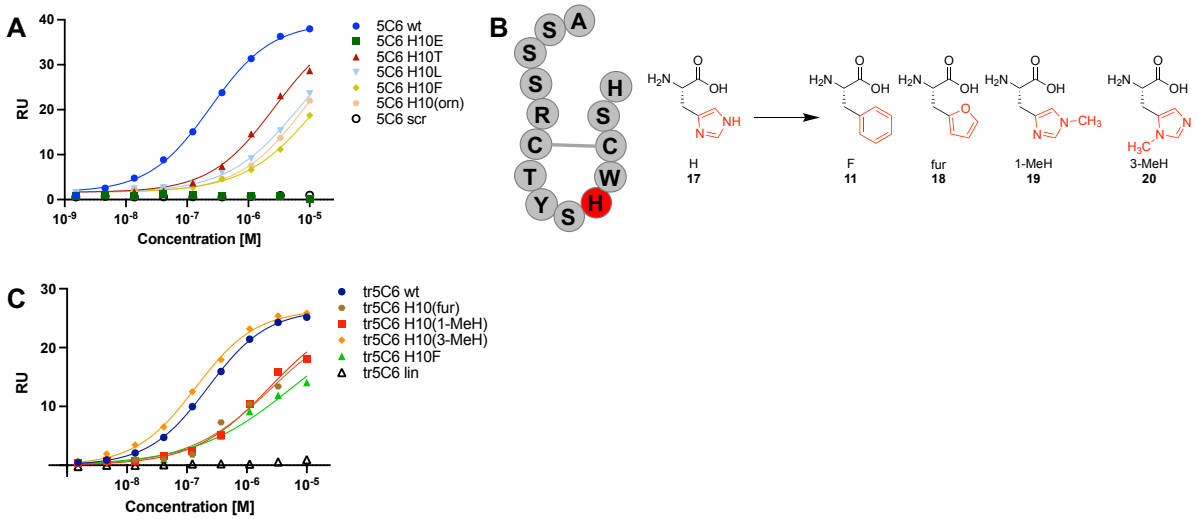

Figure 8: (**A**) Representative dose-response plot for the broad H10 analog series of 5C6 measured by SPR. (**B**) His analogs used in the narrow H10 substitution library. (**C**) Representative dose-response plot for the narrow H10 analog series of 5C6 measured by SPR.

Table 9: Relative binding affinities of the aromatic R5 analogs of 5C6, determined by SPR, *n* =2.

Peptide	Sequence	rel. K_D±SEM
5C6 wt	Ac–ASSSR[CTYS **H** WC]SH–$CONH_2$	1.00±0.00
5C6 H10E	Ac–ASSSR[CTYS **E** WC]SH–$CONH_2$	no binding
5C6 H10T	Ac–ASSSR[CTYS **T** WC]SH–$CONH_2$	8.44±2.67
5C6 H10L	Ac–ASSSR[CTYS **L** WC]SH–$CONH_2$	22.4±5.9
5C6 H10F	Ac–ASSSR[CTYS **F** WC]SH–$CONH_2$	36.7±19.8
5C6 H10(orn)	Ac–ASSSR[CTYS(**orn**)WC]SH–$CONH_2$	31.2±3.7
5C6 scr	Ac–SSHAS[CRWS S YC]HT–$CONH_2$	no binding

Table 10: Relative binding affinities of the subset of the narrow H10 analogs with, determined by SPR, *n* = 2.

Peptide	Sequence	rel. K_D±SEM
tr5C6 wt	Ac–[CTYS **H** WC]SH–$CONH_2$	1.00±0.00
tr5C6 H10F	Ac–[CTYS **F** WC]SH–$CONH_2$	75.4±50.0
tr5C6 H10(fur)	Ac–[CTYS (**fur**) WC]SH–$CONH_2$	26.6±14.7
tr5C6 H10(1-MeH)	Ac–[CTYS(**1-MeH**)WC]SH–$CONH_2$	18.1±7.42
tr5C6 H10(3-MeH)	Ac–[CTYS(**3-MeH**)WC]SH–$CONH_2$	1.00±0.37
tr5C6 lin	Ac– STYSHWS SH–$CONH_2$	no binding

Table 11: Kinetic constants of the narrow H10 library, determined by SPR, *n* = 2.

Peptide	Sequence	k_a±SEM [1/M.s]	k_d±SEM [1/s]
tr5C6 wt	Ac–[CTYS **H** WC]SH–CONH$_2$	(8.9±2.8)·10^5	0.106±0.001
tr5C6 H10F	Ac–[CTYS **F** WC]SH–CONH$_2$	(9.0±7.2)·10^5	0.667±0.109
tr5C6 H10(fur)	Ac–[CTYS **(fur)** WC]SH–CONH$_2$	(2.0±0.5)·10^5	0.554±0.027
tr5C6 H10(1-MeH)	Ac–[CTYS(**1-MeH**)WC]SH–CONH$_2$	(3.8±0.0)·10^5	0.670±0.059
tr5C6 H10(3-MeH)	Ac–[CTYS(**3-MeH**)WC]SH–CONH$_2$	(12.0±0.3)·10^5	0.141±0.006
tr5C6 lin	Ac– STYS H WS SH–CONH$_2$	no binding	no binding

Large aromatic groups are necessary at the W11 position. As W11 was identified as key residue during the previous Ala scan[9] we directly started to screen the W11 position with closely related side chains of Trp, i.e. MeW, NaI, Phe, Tyr and His, to cover both larger and smaller aromatic groups with or without additional functionalities such as phenols or basic groups. Additionally, given the promising R5W substitution, we explored whether a W11R substitution would also be tolerated. While W11R and derivatives with monocyclic aromatic side chains (W11F, W11Y, W11H) completely lost FH-binding affinity, analogs with bicyclic side chains (R11(MeW), R11(NaI)) showed residual binding (**Figure 9**) with the loss being more pronounced for the naphthalene analog than for W11(MeW) (**Table 12**). This suggests that larger aromatic groups are necessary, but that space is limited. The drop in affinity upon methylation suggests a role in binding of the indole *N*-H. It could be involved in a hydrogen bond (although not an essential one given the moderate drop in affinity), or the drop could also be due to steric reasons.

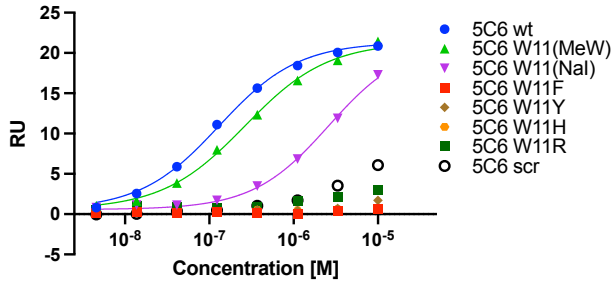

Figure 9: Representative SPR dose-response plots for the W11 substitution series of 5C6 measured by SPR.

Table 12: Relative binding affinities of the W11 substitution series of 5C6, determined by SPR, prepared and measured in duplicates.

Peptide	Sequence	rel. K_D±SEM
5C6 wt	Ac–ASSSR[CTYSH **W** C]SH–CONH$_2$	1.00±0.00
5C6 W11(MeW)	Ac–ASSSR[CTYSH(**MeW**)C]SH–CONH$_2$	4.5±2.5
5C6 W11(NaI)	Ac–ASSSR[CTYSH(**NaI**)C]SH–CONH$_2$	41.6±21.8
5C6 W11F	Ac–ASSSR[CTYSH **F** C]SH–CONH$_2$	no binding
5C6 W11Y	Ac–ASSSR[CTYSH **Y** C]SH–CONH$_2$	no binding
5C6 W11H	Ac–ASSSR[CTYSH **H** C]SH–CONH$_2$	no binding
5C6 W11R	Ac–ASSSR[CTYSH **R** C]SH–CONH$_2$	no binding
5C6 scr	Ac–SSHAS[CRWSS Y C]HT–CONH$_2$	no binding

Substituting S13 with Thr improves affinity. Similar to the T7 position, we had previously found that replacement of Ser13 by Ala has only weak effects on affinity.[9] We investigated a library containing tr5C6 **2** analogs where S13 had been replaced with all proteinogenic amino acids (but Cys). When screened at a single concentration, a broad activity profile was observed with some analogs showing maintained or improved affinity while other substitutions led to moderate or profound drops. S13P abolished affinity, in line with the *N*-methylation scan that pointed to the importance of a proper conformational arrangement of the adjacent C-terminal H14 for potent binding to FH. S13D and S13E also showed much weaker binding, supporting our previously reported finding that having a carboxylic acid instead of an amide at the C-terminus impedes binding, i.e. that negative charges at the C-terminus are unfavorable. In contrast, S13T, S13Q, S13K, S13R and S13L showed higher responses than the parent peptide (**Figure10A**). Interestingly, S13V did not show an increased response despite being sterically similar to S13T and functionally similar to S13L. The most promising substitutions (S13T,

S13Q, S13K, S13R and S13L) were subjected to full kinetic analysis. While all analogs showed slightly improved affinities with variations in the kinetic profiles, the affinity gain was most notable for S13T and S13K (**Figure 10B**, **Table 13**), with the former showing improvements in both k_a and k_d whereas a more profoundly enhanced k_{on} was compensated by faster off-rates in S13K. Conversely, S13L showed a favorable k_d at less notably enhanced k_a (**Table 14**). In summary, this position tolerates a number of residues with a certain preference for small to medium-sized residues, possibly with a polar or positively charged group. The strong drop in affinity for S13P confirms the sensitivity of this position towards conformational restrictions already observed in the *N*-methylation scan. Change to negatively charged residues reduces the affinity too.

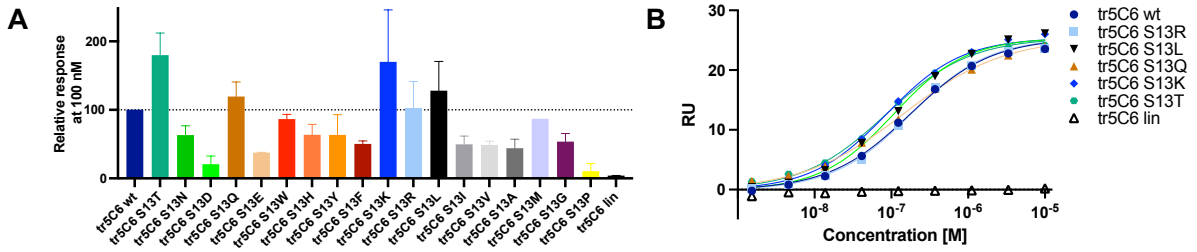

Figure 10: (**A**) Relative SPR responses at 100 nM of S13 substitution analogs of tr5C6 **2**, normalized on the response of tr5C6 wt **2**, which was set to 100; *n* = 2. (**B**) Complete SPR dose-response plots for the subset of S13 analogs with the highest relative response at 100 nM.

Table 13: Relative binding affinities of the subset of S13 analogs with the highest relative response at 100 nM, determined by SPR, *n* = 2.

Peptide	Sequence	rel. K_D±SEM
tr5C6 wt	Ac–[CTYSHWC]**S**H–$CONH_2$	1.00±0.00
tr5C6 S13T	Ac–[CTYSHWC]**T**H–$CONH_2$	0.40±0.09
tr5C6 S13L	Ac–[CTYSHWC]**L**H–$CONH_2$	0.52±0.09
tr5C6 S13Q	Ac–[CTYSHWC]**Q**H–$CONH_2$	0.70±0.12
tr5C6 S13K	Ac–[CTYSHWC]**K**H–$CONH_2$	0.39±0.11
tr5C6 S13R	Ac–[CTYSHWC]**R**H–$CONH_2$	0.74±0.11
tr5C6 lin	Ac– STYSHWS SH–$CONH_2$	no binding

Table 14: Kinetic constants of the subset of S13 analogs with the highest relative response at 100 nM, determined by SPR, *n* = 2.

Peptide	Sequence	k_a±SEM [$M^{-1}.s^{-1}$]	k_d±SEM [s^{-1}]
tr5C6 wt	Ac–[CTYSHWC]**S**H–$CONH_2$	$(6.5±2.2)\cdot10^5$	0.137±0.008
tr5C6 S13T	Ac–[CTYSHWC]**T**H–$CONH_2$	$(14.7±1.4)\cdot10^5$	0.124±0.007
tr5C6 S13L	Ac–[CTYSHWC]**L**H–$CONH_2$	$(10.5±1.7)\cdot10^5$	0.119±0.008
tr5C6 S13Q	Ac–[CTYSHWC]**Q**H–$CONH_2$	$(15.0±2.4)\cdot10^5$	0.222±0.005
tr5C6 S13K	Ac–[CTYSHWC]**K**H–$CONH_2$	$(20.6±5.3)\cdot10^5$	0.167±0.008
tr5C6 S13R	Ac–[CTYSHWC]**R**H–$CONH_2$	$(9.8±0.3)\cdot10^5$	0.158±0.008
tr5C6 lin	Ac– STYSHWS SH–$CONH_2$	no binding	no binding

An unmodified imidazole in the side chain is important at position H14. The H14 position has been proven to be important in the alanine scan.[9] This also includes the correct positioning as a frame shift by removal of the adjacent amino acid (ΔS13; **Supplementary Figure S2B**) or N-methylation (see above) have a strong negative impact. We therefore focused on the role of the imidazole ring and included substitutions in the library to determine the relevance of aromaticity or positive charge (i.e. H14F, H14(orn), H14(dapa)) and analogs with more subtle changes (H14(3-MeH), H14(1-MeH), H14(pyr), H14h). We also included a 1,2,3-triazole analog **21** (H14(triA)), which maintains both nitrogen positions within the aromatic ring system, but is not basic or acidic to a relevant extent anymore at pH 7.4. 5C6 H14(triA) **21** was accessible by Cu-catalyzed azide-alkyne cycloaddition (CuAAC) between the cyclic peptide **22** having a (*S*)-propargyl glycine (prG) residue **23** at position 14 and trimethyl silyl azide (TMS-N_3) (**Scheme 1**), based on previously described conditions.[31]

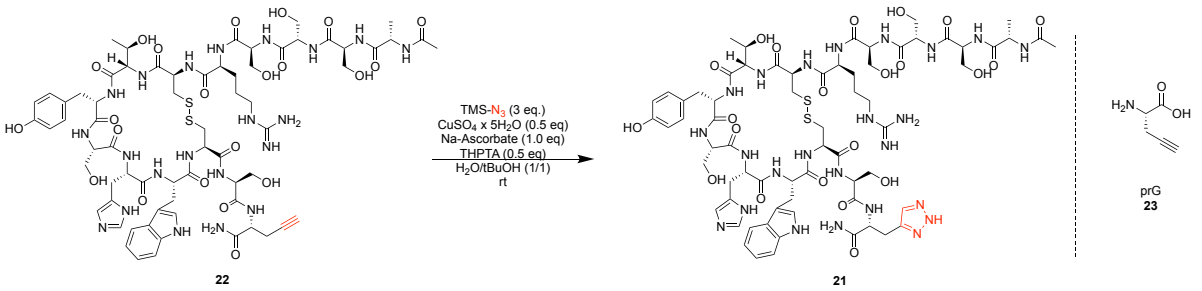

Scheme 1: Synthetic scheme for the CuAAC of 5C6 analogue **22** to obtain 5C6 H14(triA) **21** (left) and the structure of the prG **23** building block (right).

All analogs let to a dramatic loss in affinity, except for H14h. This exception suggests some flexibility in the spatial arrangement which might be due to its terminal position and contrasts other positions, e.g. Y8, where the change to a D-amino acid abolished affinity. All other analogs in the H14 series, including the closely related H14(1-MeH), H14(3-MeH) and H14(triA) **21**, had an at least 100-fold reduced affinity. H14(orn) and H14F derivatives maintained residual affinity (**Figure 11**, **Table 15**), which indicates a role both of aromaticity and basicity in the interaction of 5C6's H14 with FH. Additionally, as H14(1-MeH), H14(3-MeH), and H14(triA) showed detrimental loss of affinity, the role of the nitrogen atoms within the imidazole is crucial for interaction, although steric clashes due to a tight binding pocket at the H14 position might as well lead to a loss of affinity for the methylated analogs.

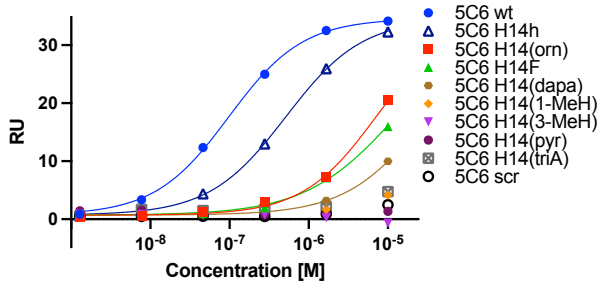

Figure 11: Representative SPR dose-response plots for the H14 analog series of 5C6, measured by SPR.

Table 15: Relative binding affinities of the subset of H14 analogs series, determined by SPR, *n* = 2.

Peptide	Sequence	rel. K_D±SEM
5C6 wt	Ac–ASSSR[CTYSHWC]S **H** –$CONH_2$	1.00±0.00
5C6 H14(orn)	Ac–ASSSR[CTYSHWC]S **(orn)** –$CONH_2$	96±23
5C6 H14(dapa)	Ac–ASSSR[CTYSHWC]S**(dapa)** –$CONH_2$	260±56
5C6 H14F	Ac–ASSSR[CTYSHWC]S **F** –$CONH_2$	106±24
5C6 H14h	Ac–ASSSR[CTYSHWC]S **h** –$CONH_2$	4.25±1.01
5C6 H14(1-MeH)	Ac–ASSSR[CTYSHWC]S**(1-MeH)**–$CONH_2$	no binding
5C6 H14(3-MeH)	Ac–ASSSR[CTYSHWC]S**(3-MeH)**–$CONH_2$	no binding
5C6 H14(triA)	Ac–ASSSR[CTYSHWC]S **(triA)**–$CONH_2$	no binding
5C6 H14(pyr)	Ac–ASSSR[CTYSHWC]S **(pyr)** –$CONH_2$	no binding
5C6 scr	Ac–SSHAS[CRWSSYC]H T –$CONH_2$	no binding

C-terminal elongation of 5C6 can modulate affinity. When considering the critical role of position 14 of 5C6 for the interaction with FH, we hypothesized that the exocyclic C-terminal tail of the peptide is in close proximity to the protein and that C-terminal elongation could provide additional contacts. We therefore synthesized a small library with additional residues at the C-terminus (+15V, +15S, +15K, +15D, +15F, +15(pyr)). All analogs showed affinities comparable to 5C6 **1** except for the +15D elongation, which resulted in a 20-fold affinity drop. While the affinity was maintained or even slightly improved for both the +15S and +15F derivatives (**Figure 12, Table 16**), the +15F analog showed a more pronounced shift in the kinetic profile (slower k_{on} and k_{off}) (**Table 17**).

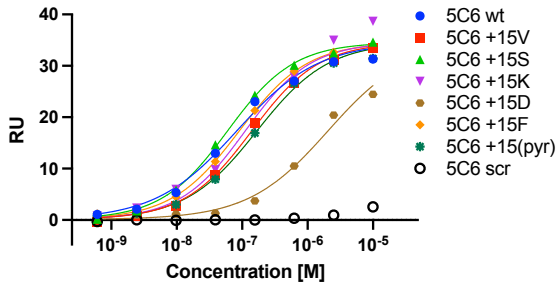

Figure 12: Representative SPR dose-response plots for the +15 series of 5C6, measured by SPR.

Table 16: Relative binding affinities for the 5C6+15 series, determined by SPR, *n* = 2.

Peptide	Sequence			rel. K_D±SEM
5C6 wt	Ac–ASSSR[CTYSHWC]SH		–$CONH_2$	1.00±0.00
5C6 +15V	Ac–ASSSR[CTYSHWC]SH	**V**	–$CONH_2$	1.39±0.31
5C6 +15S	Ac–ASSSR[CTYSHWC]SH	**S**	–$CONH_2$	0.75±0.03
5C6 +15S	Ac–ASSSR[CTYSHWC]SH	**K**	–$CONH_2$	1.19±0.16
5C6 +15D	Ac–ASSSR[CTYSHWC]SH	**D**	–$CONH_2$	21.48±3.30
5C6 +15F	Ac–ASSSR[CTYSHWC]SH	**F**	–$CONH_2$	0.93±0.16
5C6 +15(pyr)	Ac–ASSSR[CTYSHWC]SH	(**pyr**)	–$CONH_2$	1.69±0.34
5C6 scr	Ac–SSHAS[CRWSSYC]HT		–$CONH_2$	no binding

Table 17: Kinetic constants of the 5C6+15 series, determined by SPR, *n* = 2.

Peptide	Sequence			k_a±SEM [$M^{-1}.s^{-1}$]	k_d±SEM [s^{-1}]
5C6 wt	Ac–ASSSR[CTYSHWC]SH		–$CONH_2$	$(9.6±2.2)·10^5$	0.086±0.002
5C6 +15V	Ac–ASSSR[CTYSHWC]SH	**V**	–$CONH_2$	$(5.8±0.0)·10^5$	0.079±0.003
5C6 +15S	Ac–ASSSR[CTYSHWC]SH	**S**	–$CONH_2$	$(10.7±2.5)·10^5$	0.077±0.004
5C6 +15K	Ac–ASSSR[CTYSHWC]SH	**K**	–$CONH_2$	$(6.5±0.6)·10^5$	0.077±0.001
5C6 +15D	Ac–ASSSR[CTYSHWC]SH	**D**	–$CONH_2$	$(1.8±0.2)·10^5$	0.344±0.012
5C6 +15F	Ac–ASSSR[CTYSHWC]SH	**F**	–$CONH_2$	$(5.8±0.2)·10^5$	0.055±0.002
5C6 +15(pyr)	Ac–ASSSR[CTYSHWC]SH	(**pyr**)	–$CONH_2$	$(7.2±0.5)·10^5$	0.114±0.003
5C6 scr	Ac–SSHAS[CRWSSYC]HT		–$CONH_2$	no binding	no binding

Larger or smaller macrocycle sizes are not well tolerated. Having investigated all positions within 5C6 that were known to be relevant for the interaction, we next turned our attention to the size of the macrocycle. As the removal of individual amino acids from the core leads to a complete loss of activity, as shown for T7 that does not strongly engage with the target (**Supplementary Figure S2A**), we focused on subtle changes in the disulfide bridge. We addressed this by substituting C6 and/or C12 by L-homocysteine (hC) **24** or (*S*)-2-amino-5-thio-pentanoic acid (tpa) **25** (**Figure 13A**), therefore incrementally increasing the overall ring size by one to four methylene units. For ease-of-synthesis, we focused our efforts on tr5C6 **2**.

Even the addition of a single methylene unit (tr5C6 C6(hC)) led to a considerable loss of affinity (≈10-fold), which became more pronounced with further increases of the ring size. However, FH binding was not completely abrogated and even the largest analog (tr5C6 C6(tpa) C12(tpa)) showed residual responses above the level of the linear control peptide (**Figure 13B, Table 18**). Although enlarged ring sizes may negatively affect the bioactive conformation of 5C6, they still maintain a superior conformational pre-organization compared to the linear peptide.

Similarly, we substituted C6 with 2-thiogylcolic acid **26** (tga, **Figure 13A**) to obtain a disulfide-bridged macrocycle with one methylene unit less. The resulting analog showed a profound affinity drop. Since introducing tga **26** not only removed a methylene unit in the macrocycle but also the N-terminal acetyl group, we also included a derivative in which C6 is substituted with 3-mercaptopropionic acid **27** (mpa, **Figure 13A**). This leads to analog **28,** which has the same macrocycle size as tr5C6 **2** but lacks the *N*-acetyl moiety (**Figure 14A**). As the C6(mpa) analog even showed slightly improved binding, the affinity loss seen for the tga analog can clearly be attributed to the reduced size of the macrocycle and is not due to the removal of *N*-acetyl group (**Figure 13C, Table 18**).

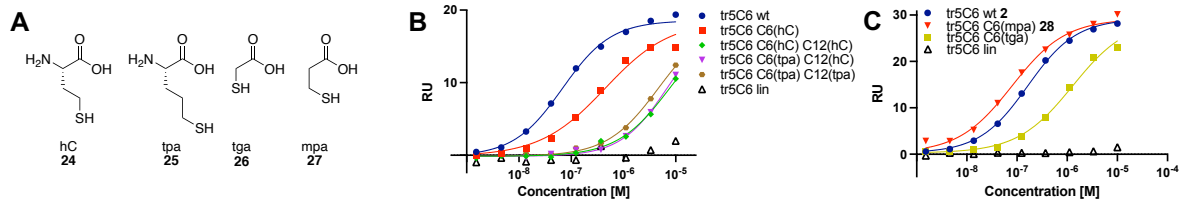

Figure 13: (**A**) Structures of Cys analogs homocysteine (hC, **24**), (*S*)-2-amino-5-thio-pentanoic acid (tpa, **25**), 2-thioglycolic acid (tga, **26**) and 3-mercaptopropionic acid (mpa, **27**) which have been used to subsitute Cys and obtain disulfide macrocycles of different size than tr5C6 **2**. (**B**) Representative dose-response plots for the larger macrocycle analogs of tr5C6 **2**, measured by SPR. (**C**) Representative dose-response plots for the smaller macrocycle analogs C6(tga) of tr5C6 **2**, measured by SPR.

Table 18: Relative binding affinities of the larger macrocycle analogs of tr5C6, determined by SPR, *n* = 2. hC: L-homocysteine, tpa: (*S*)-2-amino-5-thio-pentanoic acid, tga: 2-thioglycolic acid, mpa: 3-mercaptopropionic acid.

Peptide	Sequence	rel. K_D±SEM
tr5C6 wt	Ac–[**C** TYSHW **C**]SH–$CONH_2$	1.00±0.00
tr5C6 C6(hC)	Ac–[(**hC**)TYSHW **C**]SH–$CONH_2$	11.8±5.2
tr5C6 C6(hC) C12(hC)	Ac–[(**hC**)TYSHW(**hC**)]SH–$CONH_2$	123.7±11.7
tr5C6 C6(tpa) C12(hC)	Ac–[(**tpa**)TYSHW(**hC**)]SH–$CONH_2$	111.8±12.0
tr5C6 C6(tpa) C12(tpa)	Ac–[(**tpa**)TYSHW(**tpa**)]SH–$CONH_2$	156.3±88.2
tr5C6 C6(tga)	[(**tga**)TYSHW **C**]SH–$CONH_2$	44.5±34.1
tr5C6 C6(mpa)	[(**mpa**)TYSHW **C**]SH–$CONH_2$	0.5±0.0
tr5C6 lin	Ac–[**S** TYSHW **S**]SH–$CONH_2$	no binding

Substituting the disulfide with flexible bioisosteres reduces affinity. We subsequently investigated whether the disulfide could be replaced by other bridging groups while keeping the overall ring size similar. Bioisosteric disulfide replacements can prove challenging[32] and the impact on the target binding profile is difficult to predict. Nevertheless, using alternative bridges may in some cases favorably affect affinity and typically improves the *in vivo* stability by avoiding the reductive susceptibility of disulfides[33]. As surface tethers are often conjugated to peptides via thiol-reactive chemistry (e.g. maleimide), the replacement of the disulfide would facilitate the introduction of N- or C-terminal cysteines for such purposes.

We initially focused on a diselenide, which is considered the closest disulfide bioisostere due to similar bond lengths and electronegativity and has been used to improve stability while maintaining structural integrity and biological activity.[34,35] Selenocysteine (Sec) (**29**, **Figure 14B**) was introduced as 4-methoxybenzyl (mob)-protected Fmoc-amino acid during standard SPPS. The simultaneous cleavage from the solid phase, deprotection and cyclization was achieved by treating the peptide on solid phase with triethylsilane (TES) and thioanisole in trifluoroacetic acid (TFA) at 40 °C as described by Jenny *et al*.[36] In our case, the diselenide analog **30** (**Figure 14A**) showed a more than 20-fold reduced affinity compared to tr5C6 **2** (**Figure 15A**, **Table 19**).

Second, we investigated the use of thioethers as reductively stable disulfide analogs using a method for protein thioglycosylation described by Bernardes *et al.*,[37] in which an existing disulfide is converted to the thioether by reacting with hexamethylphosphorous triamide (HMPT). The proposed reaction proceeds via a dehydroalanine intermediate, formed by the elimination of a thiophosphonium salt, to which another thiolate subsequently adds in a 1,4-manner. Hence, this reaction likely results in a loss of stereochemical information on the αC which, alongside changes in ring size and functional group, may affect the biological activity. The reaction proceeded smoothly when employed on tr5C6 **2** and tr5C6 C6(tga) yielding the respective thioether analogues **31** and **32** (**Figure 14A**). Attempts to obtain larger thioethers by replacing a cysteine with homocysteine yielded only traces of product. Similar to the smaller disulfide macrocycle, the thioether analog of tr5C6 (i.e. **31**) showed a 10-fold affinity loss, with the smaller tr5C6 C6(tga) analog (i.e. **32**) showing further reduction in affinity (**Figure 15B, Table 19**).

Another attractive alternative to disulfides is presented by methylene thioacetals, which may produce macrocycles with the same size by simply shifting the order of atoms in the bridge (requiring non-commercial building blocks for preserving an exit vector at the N-terminus) or with a slight ring size increase by one methylene unit when starting from tr5C6 **2**. The synthesis of the thioacetal analogues **33** and **34** of tr5C6 **2** and tr5C6 C6(tga), respectively, was achieved by using the methylene insertion procedure with CH_2I_2 reported by Kourra and Cramer (**Figure 14B**).[38] Additionally, we included analog **28** where C6 was substituted with 3-mercaptopropionic acid **27** in order to distinguish changes in affinity from the absence of the N-terminal *N*-acetyl group from those in the bridging moiety in **34**. While peptide **33** lost affinity compared to the parental disulfide analog **2**, the change was minor (3-fold) when compared to the 11-fold reduction for tr5C6 C6(hC), which contains the same atoms in the macrocycle yet in different order. Peptide **34** (tr5C6 C6(tga) cyc+CH_2) showed even an improved affinity, although this appeared to be largely driven by the removal of the N-acetyl group (**Figure 15C, Table 19**). Overall, this suggests that the disulfide could be replaced by other groups as long as a similar ring size and geometry is maintained.

Rigidization of the bridge leads to affinity losses. Next, we turned our attention to lactam analogues of tr5C6 **2**. A replacement of the disulfide by a lactam would, in contrast to the previous changes, not only affect the ring size but also increase rigidity. Due to 5C6's sensitivity to ring size and geometry, this substitution was expected to have a profound impact on affinity, by either strongly favoring or disfavoring bioactive conformations. To approximately maintain the overall size, the lactamization was achieved by replacing C12 with Asp and C6 with β-alanine (ba, **35, Figure 14B**). Additionally, to directly compare an analog with even further rigidization, we synthesized the respective analogue with *N*-methyl β-alanine (mba, **36, Figure 14B**) at position 6. To facilitate monitoring and optimization, we used a solution phase approach, hypothesizing that the terminal amines will preferably react with the activated acid over other side chain nucleophiles under mild basic conditions (**Scheme 2A**). Using this strategy, the desired products **37** and **38** could be obtained for both amides as determined by MS and a negative Kaiser test (**Figure 14B**). However, FH binding was abrogated in both cases, suggesting that the rigid conformation induced by lactams is unfavorable for target binding (**Figure 15D, Table 19**).

Another functional group that has been used successfully as disulfide replacement is 1,5-disubstituted 1,2,3-triazole, due to the similar distance between the Cβ-atoms in both bridge types.[32] The triazole analogue **39** was obtained by on-resin ruthenium-catalyzed azide-alkyne cycloaddition (RuAAC), using Cp*RuCl(COD) as catalyst under microwave conditions as reported previously and using (*S*)-3-azidoalanine (aza, **40**) and prG **23** as building blocks (**Figure 14**, **Scheme 2B**).[39] Additionally, we also synthesized the respective 1,4-disubstituted triazole **41** on-resin, based on previously published CuAAC conditions[40] to include another readily accessible modification by using 2-azido acetic acid (aaa, **42**) as building block to maintain the number of atoms in the bridge (**Figure 14, Scheme 2C**). In line with a closer mimicry of the disulfide by the 1,5-stubstitutied triazole, peptidomimetic **39** maintained some affinity to FH (although 200-fold reduced) whereas the 1,4-triazole **41** completely lost affinity, likely by introducing an unfavorable arrangement of the macrocycle (**Figure 15E, Table 19**).

Hydrocarbon, in particular alkene, linkers have been used extensively in peptidic macrocycles, driven by the orthogonality of the ring-closing metathesis (RCM) reaction with other reactions used in peptide chemistry and its typically high yields. Commercially available building blocks allow for the convenient introduction of the required substrates and on-resin RMC facilitates easy removal of catalyst and reagent. We chose to either replace both cysteines with (*S*)-allyl glycine (alG) **43**, which maintains the total number of atoms in the macrocycle, or to combine C12aIG with a C6 substitution for 5-hexenoic acid (ha) **44,** i.e. to introduce one additional methylene group (**Figure 15B**). In both cases, the linear peptides were assembled by SPPS followed by on-resin RCM with a second generation Grubbs catalyst. After cleavage from the solid phase, for both alkene-bridged peptides **45** and **46**, two isomers were obtained, expected to be the respective E- and Z-isomers (**Figure 14A, Scheme 2D**). Additional to the alkene bridged peptides, we also synthesized the saturated analogue of **47** by

substituting C12 with (S)-2-amino suberic acid (asu) **48** and a macrolactamization on the α-amino group of T7 (**Figure 14**, **Scheme 2E**). The alkene analog **45** with the same number of atoms in the macrocycle as in tr5C6 **2** showed a distinct affinity for FH8-15 depending on the isomer. The isomer with longer retention time in RP-HPLC (isomer 2) showed good binding to FH, although its unexpectedly higher saturation levels (R_{max}) than tr5C6 **2** might lead to an overestimation of its affinity. This effect does not seem to be artificial, as it was observed for different batches of **45** for a number of FH-coated sensor chips. If the experimental values are allowed to reach different maximal values in the dose-response fit (i.e., if **45** isomer 2's dose-response fit is not forced to reach a lower maximum than it would if fit without constrain), the modest loss of a factor of 3 drops to a more substantial factor 10 (**Figure 15F**, **Table 19**, **Supplementary Figure S3**, **Supplementary Table S1**). Independently of R_{max} and the dose response fit differences, isomer 2 of peptide **45** showed a 2.5-fold improved kinetic dissociation rate yet at a strongly reduced kinetic association rate (**Figure 15G**). In the case of isomer 1 of **45**, both the kinetic association and dissociation rates were negatively affected, leading to generally unfavorable binding profile (**Figure 15G**). This might hint at that **45** isomer 2 allows for an overall confirmation more similar to the disulfide and presents itself therefore as an attractive alternative to the disulfide. However, as both isomers showed a reduced affinity, we did not further pursue studies to assign the structures of the isomers. Looking at the other analogs within the series, the saturated analog **47** further lost affinity, whereas the larger, unsaturated **46** (again isolated as two isomers) almost completely lost its affinity to FH, independently of the isomeric form (**Figure 15F**, **Table 19**).

In summary, all the peptidomimetic analogs of tr5C6 **2** had a reduced affinity compared to the disulfide albeit to different degrees, with the thioacetal **33** and alkene **45** presenting the most attractive alternatives to the disulfide. The sensitivity of changing the disulfide to even closely related groups in terms of polarity, geometry or size emphasizes the importance of the overall macrocycle arrangement in achieving a bioactive conformation with proper display of the side chains for potent interaction.

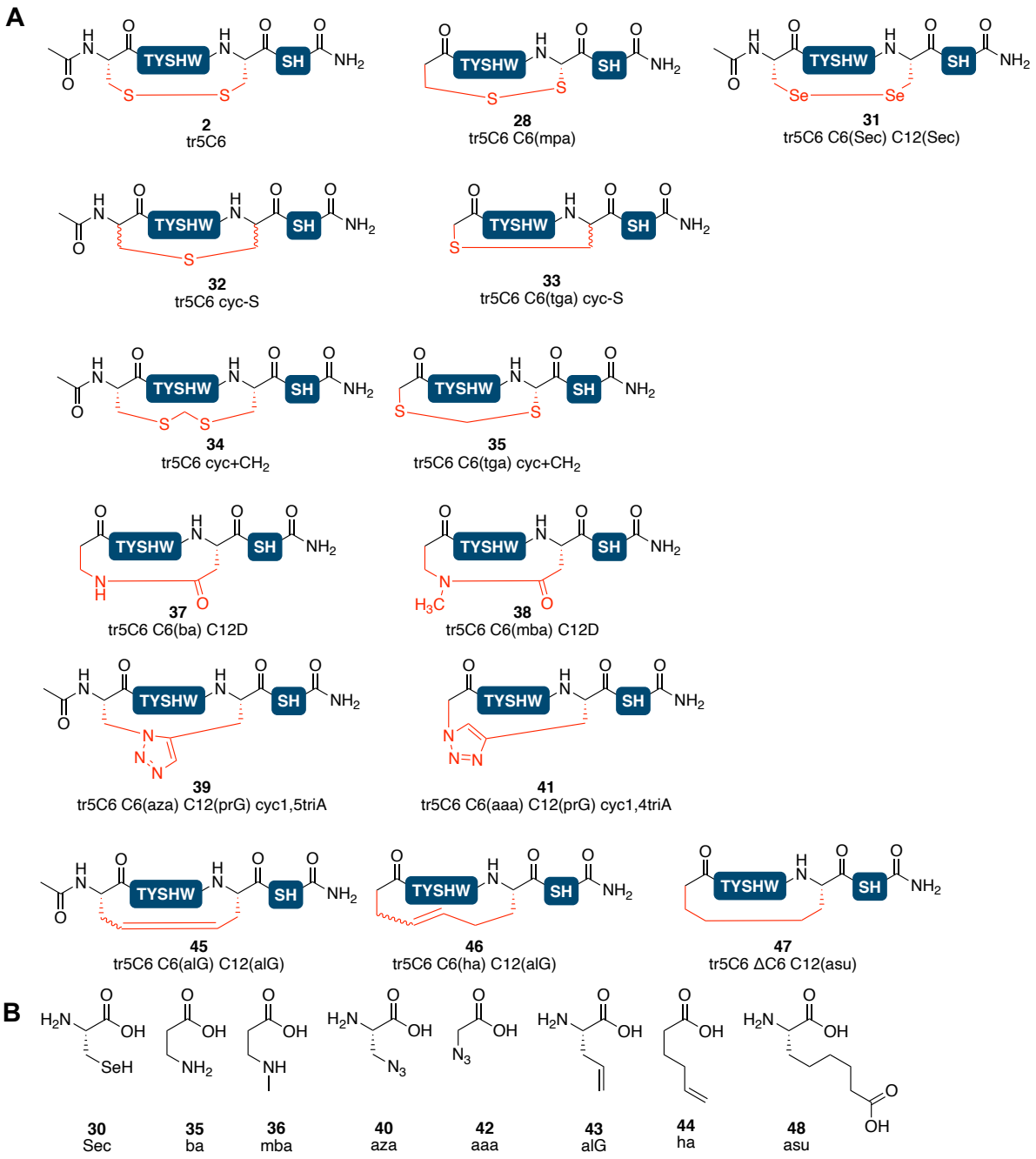

Figure 14: (**A**) Overview of the peptidomimetic macrocycle analogues of tr5C6 **2**. (**B**) Building blocks used in the synthesis of the peptidomimetic macrocycle analogues of tr5C6 **2**.

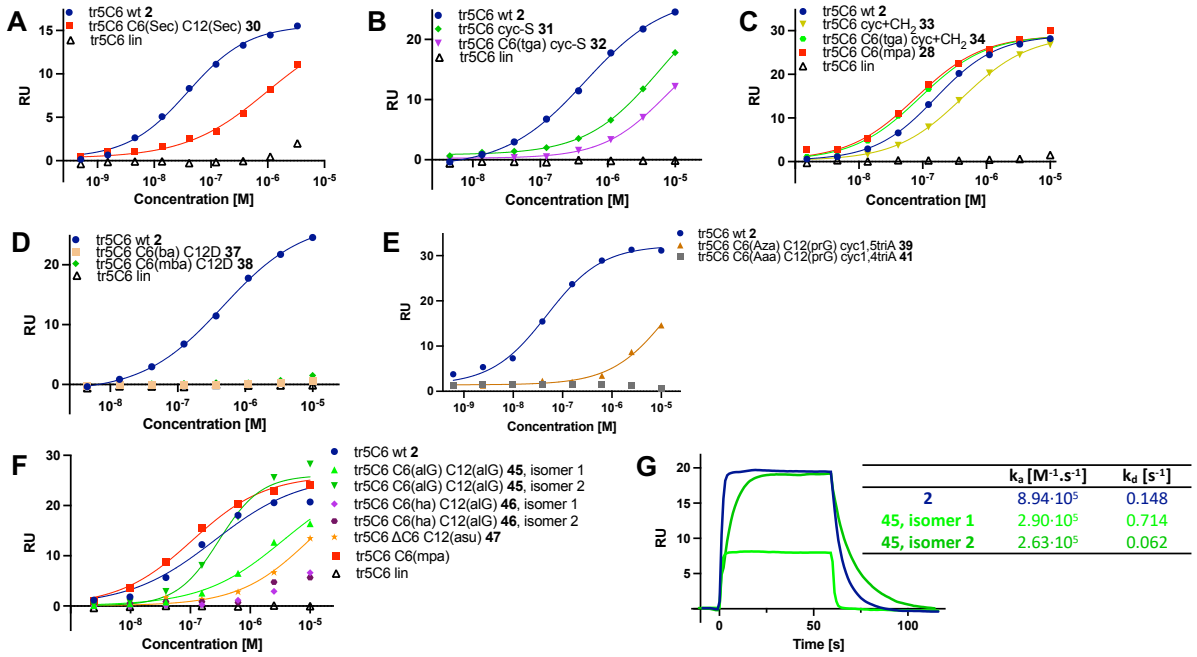

Figure 15: Representative SPR dose-response plots (molecular weight-normalized signals) of the peptidomimetic disulfide analogs of tr5C6 **2,** i.e. selenocystine **31** (**A**), thioethers **31** and **32** (**B**), thioacetals **33** and **34** (**C**), lactams **37** and **38** (**D**), triazoles **39** and **40** (**E**) and hydrocarbons **45** – **47** (**F**). (**G**) SPR sensorgrams at 625 nM concentration of both isomers of alkene peptidomimetics **45** and tr5C6 wt **2**.

Table 19: Relative binding affinities of the peptidomimetic macrocycle analogs of tr5C6, determined by SPR, prepared and measured in duplicates. sec: L-selenocysteine, C-S: desulfurized cysteine, tga: thioglycolic acid, C-S: desulfurized cysteine, C+CH_2: cysteine with additional methylene group, ba: β-alanine, mba: *N*-methyl β-alanine, aza: (S)-3-azidoalanine, prG: a (*S*)-propargyl glycine, aaa: 2-azido acetic acid, alG: (S)-allyl glycine, ha: 5-hexenoic acid, asu: (S)-2-amino suberic acid.

Peptide	Structure	Sequence	rel. K_D±SEM
tr5C6 wt	**2**	Ac–[**C** TYSHW **C**]SH–$CONH_2$	1.00±0.00
tr5C6 C6(Sec) C12(Sec)	**30**	Ac–[(**Sec**)TYSHW (**Sec**)]SH–$CONH_2$	23.2±1.5
tr5C6 cyc-S	**31**	Ac–[**C** TYSHW (**C-S**)]SH–$CONH_2$	10.2±2.1
tr5C6 C6(tga) cyc-S	**32**	[(**tga**)TYSHW (**C-S**)]SH–$CONH_2$	14.9±0.3
tr5C6 cyc+CH_2	**33**	Ac–[**C** TYSHW(**C+CH₂**)]SH–$CONH_2$	3.4±0.7
tr5C6 C6(tga) cyc+CH_2	**34**	[(**tga**)TYSHW(**C+CH₂**)]SH–$CONH_2$	0.4±0.2
tr5C6 C6(mpa)	**28**	[(**mpa**)TYSHW **C**]SH–$CONH_2$	0.5±0.0
tr5C6 C6(ba) C12D	**37**	[(**ba**) TYSHW **D**]SH–$CONH_2$	no binding
tr5C6 C6(mba) C12D	**38**	[(**mba**)TYSHW **D**]SH–$CONH_2$	no binding
tr5C6 C6(aza) C12(prG) cyc1,5triA	**39**	Ac–[(**aza**)TYSHW (**prG**)]SH–$CONH_2$	284±12
tr5C6 C6(aaa) C12(prG) cyc1,4triA	**41**	[(**aaa**)TYSHW (**prG**)]SH–$CONH_2$	no binding
tr5C6 C6(alG) C12(alG), isomer 1	**45**	Ac–[(**alG**)TYSHW (**alG**)]SH–$CONH_2$	20.9±6.9
tr5C6 C6(alG) C12(alG), isomer 2	**45**	Ac–[(**alG**)TYSHW (**alG**)]SH–$CONH_2$	3.1±1.9
tr5C6 C6(ha) C12(alG), isomer 1	**46**	[(**ha**) TYSHW (**alG**)]SH–$CONH_2$	no binding
tr5C6 C6(ha) C12(alG), isomer 2	**46**	[(**ha**) TYSHW (**alG**)]SH–$CONH_2$	no binding
tr5C6 ΔC6 C12(asu)	**47**	[TYSHW (**asu**)]SH–$CONH_2$	46.2±8.1
tr5C6 lin		Ac–[**S** TYSHW **S**]SH–$CONH_2$	no binding

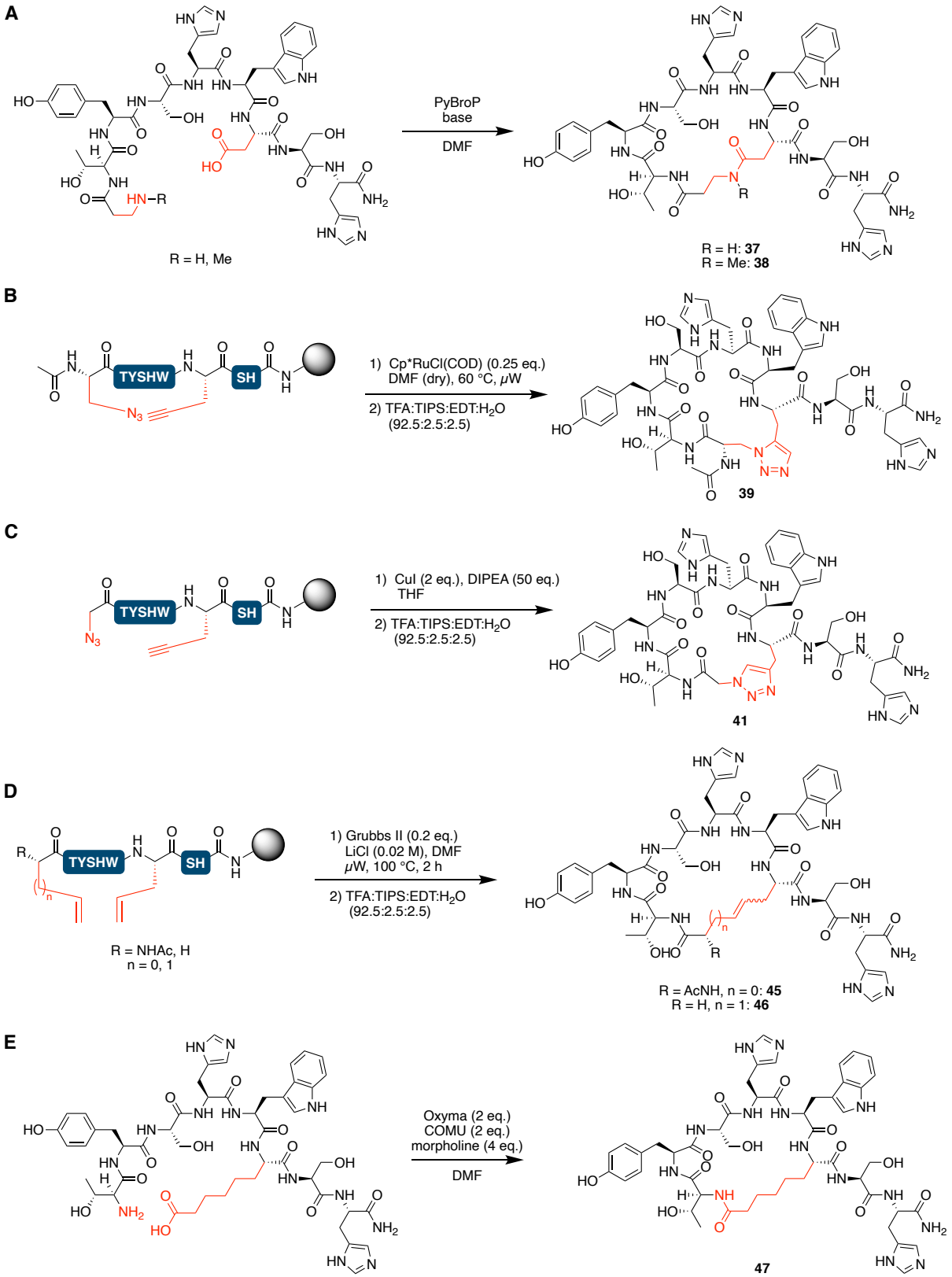

Scheme 2: (**A**) Synthetic schemes for the access to lactam analogues **37** (R = H) and **38** (R = Me) (**A**), 1,5-disubstituted 1,2,3-triazole analog **39** (**B**), 1,4-disubstituted 1,2,3-triazole analog **41** (**C**), alkene analogs **45**, **46** (**D**) and alkane analog **47** (**E**) of tr5C6 **2**.

Combination of individual optimizations has an additive effect. Our SAR study revealed that while changes to size, geometry and residue profile of the macrocyclic core are generally not well tolerated, individual adjustments to the exocyclic N-terminus (i.e. truncation, R5W) and C-terminus (i.e., S13T, elongation) led to notable improvements. Based on these and previous findings[9], we combined the R5W and S13T substitutions while also introducing either the +15S or +15F modification, i.e. peptides **49** (Ac-ASSSW[CTYSHWC]THS) and **50** (Ac-ASSSW[CTYSHWC]THF-$CONH_2$), respectively (**Figure 16A**). Interestingly, **49** showed only a 2-fold increase in affinity whereas the binding of **50** was improved 8-fold (K_D = 8 nM), suggesting that Phe is preferred over Ser at the C-terminus (**Figure 16B**, **Table 20**, **Supplementary Figure S4A**). When we additionally removed the four N-terminal amino acid of **50** (i.e. **51**; **Figure 16A**), the affinity further improved two-fold to 4 nM, with an 18-fold affinity improvement over full-length 5C6 **1** (**Figure 16B**, **Table 22**, **Supplementary Figure S4B**). While the affinity enhancement for both **50** and **51** is mediated by improved association and dissociation rates, the kinetic profile of **50** is even more shifted towards slower dissociation kinetics, rendering it particularly interesting for further development (**Figure 16C**). When we tested **50** and **51** with MST, the same trends could be observed as with SPR although to a lesser extent (4- and 5-fold improved IC_{50}, respectively), which may be related to the difference between direct and competitive binding assay formats (**Figure 16D**, **Table 22**). Interestingly, 5C6 Δ1-4 R5W was the most potent peptide in MST with an IC_{50} of 29 nM and exceeded **51**'s IC_{50} of 42 nM (**Figure 16D**, **Table 22**), whereas the opposite was true in the SPR assay (Rel. K_D of 0.14 and 0.06, respectively). This could be caused by different conformations between full-length FH in solution (MST) and immobilized FH8-15 (SPR). The SPR format may allow for improved exploitation of the additional contacts by the S13T and +15F changes, which would be in line with the results of **50** that showed a stronger increase in affinity in SPR compared to MST (8-fold compared to 4-fold relative to wt 5C6 **1**; **Tables 20**, **22**).
Importantly, both assays confirm that a combination of R5W, S13T and +15F position show additive beneficial effects that result in the most active 5C6 derivative described to date. While further affinity gains may be achieved by removing or replacing residues 1-4, this may be less relevant when considering the intended use of the exocyclic N-terminus as spacer during surface coating.

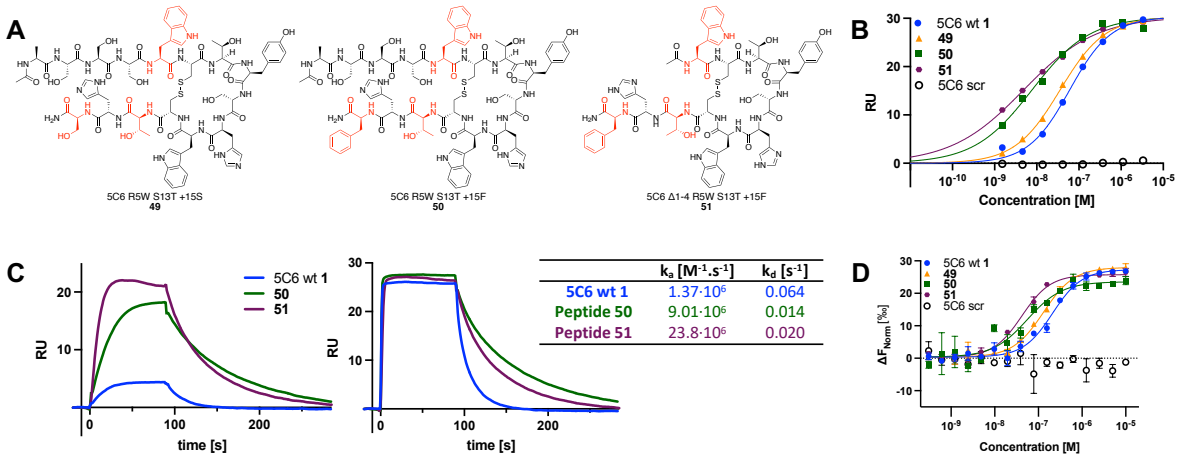

Figure 16: (**A**) Structures of the peptides **49**, **50** and **51**, carrying combination of changes. (**B**) Representative SPR dose-response plots for the globally modified 5C6 analogs. (**C**) SPR sensorgrams at 7.7 nM (left) and 1670 nM (right) concentration for 5C6 wt **1** and analogs **50** and **51**, showing the fastest association rate for **51** and the slowest dissociation rate for **50**, respectively. (**D**) Competitive MST dose-response plots for the globally modified 5C6 analogs.

Table 20: Absolute and relative K_Ds of the globally modified analogs of 5C6 with a full N-terminus, determined by SPR, *n* = 2.

Peptide	Sequence	K_D±SEM [nM]	rel. K_D±SEM
5C6 wt	Ac–ASSS**R**[CTYSHWC]**S**H –$CONH_2$	67.8±7.6	1.00±0.00
49	Ac–ASSS**W**[CTYSHWC]**T**H**S**–$CONH_2$	31.9±3.8	0.48±0.11
50	Ac–ASSS**W**[CTYSHWC]**T**H**F**–$CONH_2$	8.4±0.7	0.12±0.00
5C6 scr	Ac–SSHAS[CRWSSYC]HT –$CONH_2$	no binding	no binding

Table 21: Absolute and relative K_Ds of the globally modified analogs of 5C6 with a truncated N-terminus, determined by SPR, *n* = 2.

Peptide	Sequence			K_D±SEM [nM]	rel. K_D±SEM
5C6 wt	Ac–**ASSSR**[CTYSHW	**C**	]**S**H –$CONH_2$	64.7±4.5	1.00±0.00
51	Ac– **W**[CTYSHW	**C**	]**THF**–$CONH_2$	3.6±1.3	0.06±0.02
5C6 scr	Ac–SSHAS[CRWSSY	C	]HT –$CONH_2$	no binding	no binding

Table 22: Absolute IC_{50}s of the globally modified analogs of 5C6, determined by MST, *n* = 2.

Peptide	Sequence			IC_{50}±SEM [nM]
5C6 wt	Ac–**ASSSR**[CTYSHW	**C**	]**S**H –$CONH_2$	210±25
49	Ac–**ASSSW**[CTYSHW	**C**	]**THS**–$CONH_2$	131±15
50	Ac–**ASSSW**[CTYSHW	**C**	]**THF**–$CONH_2$	56±8
51	Ac– **W**[CTYSHW	**C**	]**THF**–$CONH_2$	42±6
5C6 scr	Ac–SSHAS[CRWSSY	C	]HT –$CONH_2$	no binding

FH-recruiting activity of lead compound 50. Considering the beneficial target affinity of the lead compound **50**, we evaluated whether this would translate into enhanced FH recruitment to surfaces and complement inhibitory activity. For this purpose, we synthesized an analog of **50** with an N-terminal ε-*N* biotinylated Lys (K(biot)) (i.e. **52**; **Figure 17A**), based on our recent insight into the ideal positioning and spacing for 5C6-based coatings in our nanoparticle-like magnetic beads assay.[9] While the biotinylation resulted in a two-fold affinity drop in SPR compared to **50**, the resulting **52** still showed 3-fold better affinity over 5C6 **1** (**Supplementary Figure S5A, Supplementary Table S2**).
To simultaneously assess FH recruitment and complement inhibition, measured as a reduction of C3b deposition, the biotinylated peptides were incubated with streptavidin beads, followed by incubation with normal human serum or EDTA serum, in which complement activation is impaired. FH recruitment and C3b deposition were assessed by flow cytometry (FC) using corresponding detection antibodies. Under the assay conditions, **52** showed a notable but not significant tendency to recruit more FH from serum to the beads, which could be caused by saturation effects in the end-point assay (**Figure 17B**). Importantly, C3b deposition was significantly reduced when compared to 5C6 wt **1** carrying as well an N-terminal K(biot), demonstrating that the enhanced affinity translates into an increased activity (**Figure 17C**). As shown previously, only C3b deposition but not FH-recruitment was dependent on complement activity (**Supplementary Figure S5B**, **C**).

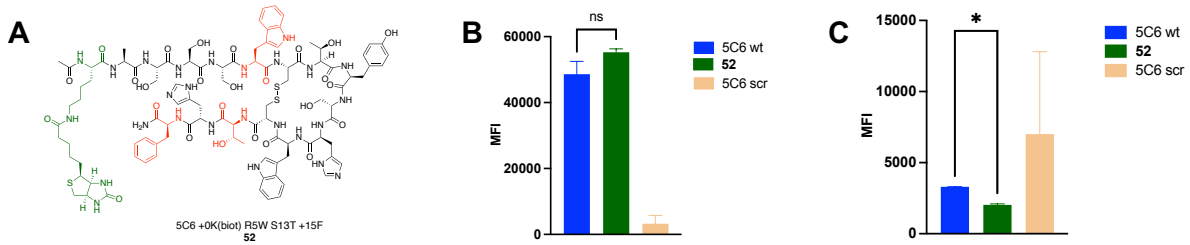

Figure 17: (**A**) Structure of peptide **52**, the N-terminally biotinylated analog of peptide **50**. (**B**) Median-fluorescence intensity (MFI) of FH binding of beads loaded with N-terminally biotinylated 5C6 derivatives and incubated with normal human serum. (**C**) MFI of C3b deposition of beads loaded with N-terminally biotinylated 5C6 derivatives and incubated with normal human serum. Bars indicate mean of independent duplicates; error bars indicate standard deviation, ns: non-significant ($p > 0.05$), *: significant ($p < 0.05$).

Synthesis and evaluation of lipid-coupled 5C6 derivatives. In parallel to our SAR efforts, we also aimed at evaluating the activity of 5C6 in clinically relevant models such as CARPA models and assess the suitability of different lipids as surface tether for cells (e.g. erythrocytes) or liposomes (e.g. Caelyx®). We used two functional assays for the assessment, i.e. a well-established alternative pathway hemolytic assay[41] and a liposomal lysis assay using the commercial doxorubicin formulation Cealyx®[27]. We synthesized a set of 5C6-lipid conjugates, however, none showed complement-inhibitory activity which we could attribute to an insufficient FH-recruitment activity, possibly due to the more complex surface compared to magnetic beads (**Supplementary Scheme S1**, **Supplementary Figures S6**, **S7**).

Peptide 50 is more stable than the parental 5C6. Given the susceptibility of Arg-containing peptide bonds to proteolytic cleavage, we hypothesized that the R5W substitution present in peptide **50** might increase stability over 5C6 wt **1**. Such resistance for proteases that cleave C-terminally of Arg (e.g. trypsin) would be particularly important for the intended use of the exocyclic N-terminus as spacer during surface tethering. To assess the proteolytic stability of peptide **50**, we incubated both 5C6 **1** and **50** with trypsin and determined peptide fragmentation by LCMS over time. As expected, 5C6 **1** was already completely degraded after 1 h; in contrast, 80% of the initial peptide amount could be still detected after 4 h in the case of **50** (**Figure 18A**).
Additionally, we investigated the *in vitro* stability of **50** in normal human serum. Again, the peptide showed a favorable stability profile with 63% of the peptide being detectable after 24 h (**Figure 18B, Supplementary Figure S8**). C-terminal degradation was identified as the major metabolic route, with the main product being the ΔF15 derivative; with increasing time, metabolites with fully cleaved C-terminus accumulated. As we envisage N-terminal immobilization of the peptide on biomaterials in future applications, this suggests that it could be securely immobilized over extended periods and, as the presence of F15 is not a prerequisite for binding, that the peptide might also maintain activity for extended periods with the main degradation product is peptide **50** ΔF15. Therefore, 15F might not only increase the affinity, but also function as sacrificial shield for the proteolytic degradation of H14. In contrast, for 5C6 wt **1**, only 33% of intact peptide were detected after 24 h in plasma (**Figure 18C**). Again, C-terminal proteolytic degradation appears to be the main degradation pathway for 5C6 but due to the different conditions and the use of unnormalized ion count, additional studies will be required to confirm these results.
Finally, we also investigated the stability of 5C6 **1** towards a number of harsh short-term conditions and milder storage conditions. Whereas 5C6 was stable in 0.1 M HCl, it was almost completely degraded after 2 h in 0.1 M NaOH. Additionally, 5C6 was stable in PBS at 37 °C over 24 h and towards 20 eq. glutathione (**Figure 18D**). In the storage stability assays, 5C6 in H_2O was completely stable over 3 weeks in the full temperature range from -80°C to rt. In contrast, 5C6 dissolved in PBS pH 7.4 was only stable in frozen form but not at 4 °C or rt (**Figure 18E, F**). This could possibly be due to different charge states under these conditions, with the calculated isoelectric point[42] of 5C6 wt **1** of 8.1 being relatively close to the PBS's pH 7.4, whereas the aqueous solution of 5C6 had a pH of 6.0. This is also in line with the results of the stability in acid or base, with the much higher stability under acidic conditions. These observations provide important initial indications for future pharmaceutical development of 5C6, although future studies need to confirm that **50** behaves accordingly.

The endocyclic residues of tr5C6 assume a rigid conformation in solution. As we had previously[9] and here shown, the cyclic nature and macrocyclic conformation of 5C6 plays a critical role for its interaction with FH. To further improve our understanding of the nature of the structural determinants, we determined the NMR solution structure of tr5C6 **2**. Overall, tr5C6 **2** showed a relatively compact form with the Y8 and W11 side chains pointing towards the center of the macrocycle (**Figure 19A**). When assessing the 10 conformers with the lowest energy, residues Y8, S9, H10 and W11 assumed fixed positions (**Figure 19B**, green), whereas the disulfide bridge and T7 showed moderate (**Figure 19B,** yellow) and the exocyclic C-terminus highly flexibility (**Figure 19B,** orange). This is well in line with the affinity data, where minor changes to the position of the S9 hydroxyl group or the Y8y substitution were detrimental to binding, whereas the H14h substitution only had a minor effect. This suggests that changes to Y8 or S9 may disrupt primordial contacts to FH, whereas the flexibility of H14 renders it more tolerant towards stereochemical modifications. When mapping the most important residues within tr5C6 **2**, Y8, S9 and W11 point towards one direction (front top in **Figure 20C**), while H14 points away from the other residues, possibly suggesting that Y8, S9, and W11 are oriented to one domain of FH, while H14 stabilizes the interaction by binding to another domain. Of note, it is well possible that the conformation of H14 in the complex-bound state might differ substantially from the preferred conformational state in solution when considering its flexibility.

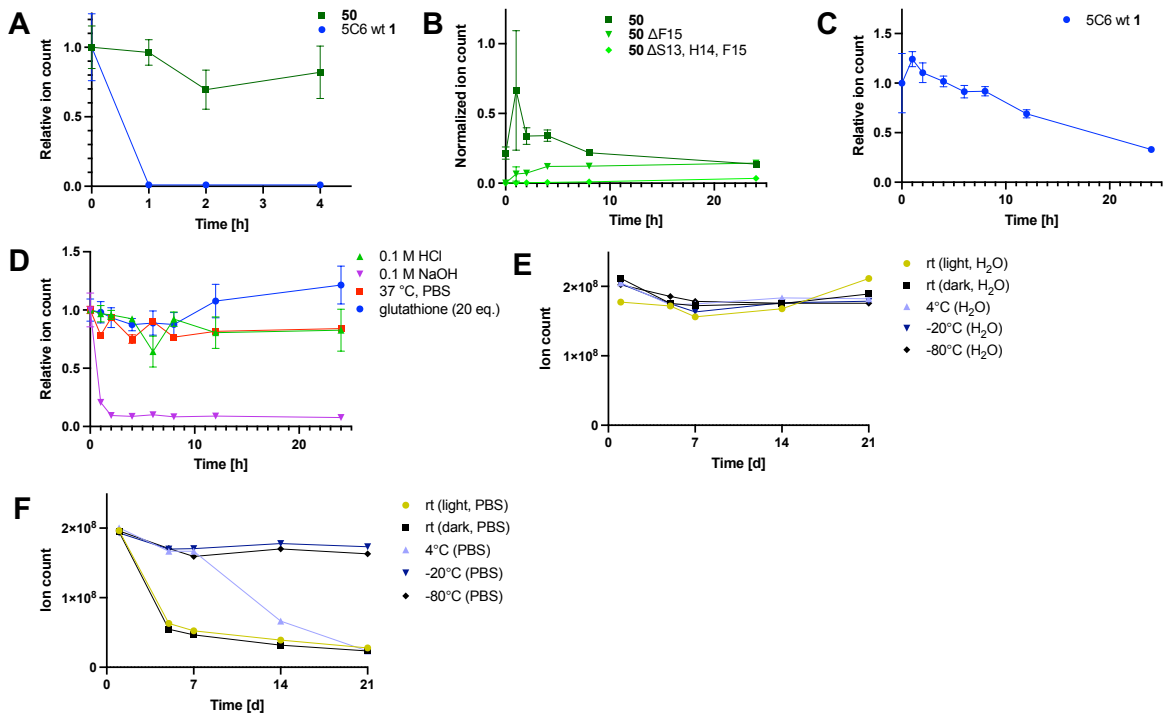

Figure 18: (**A**) Stability of peptide **50** and 5C6 wt **1** towards trypsin (trypsin:peptide: 1:25 (m:m)) by LCMS. (**B**) Stability of peptide **50**, including the formation of the two main degradation products peptide **50** ΔF15 and peptide **50** ΔS13, H14, F15 in normal human serum. (**C**) Stability of 5C6 wt in human plasma by LCMS. (**D**) Stability of 5C6 wt in 0.1 M HCl (green), 0.1 M NaOH (purple), PBS at 37 °C (red) and 20 eq. glutathione (blue) by LCMS. (**E**) and (**F**): Stability of 5C6 in H_2O (**E**) or PBS (**F**) over a period of 3 weeks at different temperature and with or without light exposure in the case of the storage at room temperature, by LCMS. Relative ion count is the ion count divided by the average ion count at t = 0 h, normalized ion count is the ion count divided by the ion count of the internal standard in the respective sample.

To further understand the difference in activity we observed between the cyclic and linear 5C6, we subjected tr5C6 **2** and tr5C6 lin to circular dichroism spectroscopy (CD) analysis. Generally, both peptides showed a similar profile with global minima near 200 nm, typically seen for unordered peptide stretches (**Figure 19D**).[43] Consequently, the overall composition of secondary motifs for the linear and cyclic tr5C6 is comparable (**Table 23**). The most abundant components are unordered and strand structural motifs, which are considered the most frequent motifs, at least for short linear peptides, alongside polyproline II helices.[44] Unsurprisingly, both peptides have low α-helical properties, as the *i*, *i*+6 connectivity in the macrocycle is unfavorable compared to the preferred *i*, *i*+4 connectivity for two *S*-amino acids being bridged.[45] Finally, the difference in minima amplitude could be due to the difference in sequence which can strongly influence absorbance in the low wavelength region of CD spectra.[46] Nevertheless, the overall similar composition of secondary structure between linear and cyclic peptide was somewhat surprising due to the strong importance of the presence, size and conformation of the macrocycle and contrasts the effects of cyclization observed with other peptides of similar size, despite their natural propensity to form α-helices.[47,48] Investigating where this similarity might stem from, we subjected both structures to molecular dynamics (MD) simulations, using the NMR structure as initial conformation. While the conformation strongly differed for the backbone and αCs within the cyclic core (further side chains and exocyclic C-terminus were not considered due to their high flexibility) between linear and cyclic 5C6 (RMSD = 3.7 Å), the linear analog maintained a relatively compact form which was quite stable over the time course, in particular due to a π-stacking interaction between W11 and H14 not present in the cyclic derivatives (**Figure 19E**, **Supplementary Figure S9**). This compact arrangement could also explain the observed similarities in the CD spectrum. Additionally, we also subjected the peptidomimetic thioacetal **33**, 1,5-disubstituted triazole **39**, and E- and Z-isomers of alkene **45** analogs to MD analysis to see how differently they behave compared to the native disulfide. They all behaved similarly, with the most abundant cluster for each having RMSDs between 1.8 Å and 2.3 Å, similar to the structure of tr5C6 **2** itself, where the most abundant cluster

had an RMSD of 2.1 Å compared to the NMR structure (**Supplementary Table S3**). For all structures, the crucial stretch from Y8 to W11 largely maintained its position, only with the orientation of the W11 side chain tilted, however, this was also the case of the most abundant MD cluster of **2** and therefore does not explain the differences observed in affinity between the different peptidomimetics (**Figure 19F**). However, this confirms the sensitivity of 5C6 towards subtle changes in affinity with these first structural insights facilitating the rational development of 5C6 derivatives with improved target binding properties in the future.

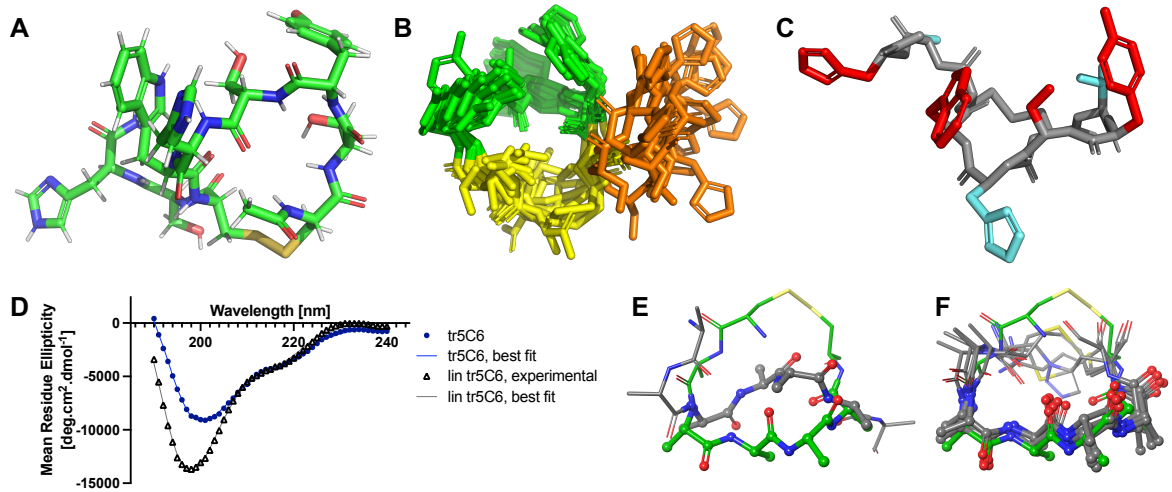

Figure 19: (**A**) NMR solution structure of tr5C6 **2** as weighted average of the 10 lowest energy conformers, with distance restraints based on the 2D [^{1}H, ^{1}H] ROESY signals. (**B**) Ensemble of the 10 lowest energy conformers of tr5C6 **2** with residues having very fixed orientations (i.e. Y8, S9, H10, W11) in green, moderately fixed orientations (i.e. C6, T7, C12) in yellow and no fixed orientations (i.e. 13, H14) in orange. (**C**) Average solution structure of tr5C6 **2** with the crucial side chains highlighted in red, other side chains in cyan and the backbone and disulfide in grey. Y8, S9 and W11 point in one direction, whereas H14 points away from those. (**D**) CD spectra of tr5C6 **2** and tr5C6 lin with experimental values as symbols and fit as line. (**E-F**) Overlay of the cyclic core of the NMR solution tr5C6 **2** (green) and the most MD abundant conformer cluster of the respective region of tr5C6 lin (grey, **E**) or the peptidomimetic analogs **33**, **39** and E- and Z-alkenes of **45** (grey, **F**). The residues Y8-W11 showing a fixed position in the NMR structure are in bold balls and sticks, the other residues in thin sticks.

Table 23: Secondary structure components, based on CD data analyzed with dichroweb[49]. Ideal describes secondary structural motifs with ideal angles, in contrast to the non-ideal ones. Ratios given as % of the total structure. * = fit as -1%, set to 0 here.

Peptide	Helix (ideal)	Helix (non-ideal)	Strand (ideal)	Strand (non-ideal)	Turns	Unordered
tr5C6 **2**	1	7	21	13	23	34
tr5C6 lin	0*	6	22	13	23	36

CONCLUSIONS

Although nanomedicines such as liposomes allow patients to receive drugs with higher efficacy and reduced toxicity, immune-mediated reactions to these particulate drug carriers still present an unmet challenge. Among those, CARPA imposes a well-known clinical problem with potentially lethal outcome, but the detailed molecular intricacies remain elusive. The pivotal role of the complement system with contributions from all pathways has been described, with FH having been successfully used in vitro to reduce complement activation by pegylated liposomes.[28] Furthermore, FH, its smaller, recombinant derivative mini-FH, and fusion proteins of domains from FH and complement receptor 2 have all been used successfully to protect erythrocytes from lysis, both in vitro and in vivo.[3,50,51] While these efforts validate the use of FH to reduce complement-mediated damage as a promising therapeutic approach, they share the drawback of using protein entities that rely on time- and cost-intensive production processes and bear potential immunogenicity risks. The use of modalities with lower molecular weight, including peptides, would largely circumvent these challenges. We could previously show that the cyclic peptide 5C6 can be used to recruit FH from solution to a number on surfaces and, consequently, inhibit complement activation thereon.[7–9] This strategy might therefore

present a promising opportunity to inhibit liposome-mediated CARPA without the disadvantages of protein-based approaches.

Here, we presented a thorough and comprehensive SAR study on 5C6, to our knowledge the only known low- to medium weight, synthetic ligand for FH, which enabled us to identify a next generation lead compound with improved target affinity (K_D = 8 nM), activity and proteolytic stability. Structural studies showed that Y8, S9 and W11 within the macrocycle have a highly restricted conformational freedom, explaining their stark sensitivity towards minor changes as well as the high sensitivity of affinity towards macrocycle size and geometry. Although no peptidomimetic bioisostere was able to reproduce the affinity contribution of the native disulfide, the thioacetal and alkene bridges might provide suitable alternatives in further studies. While removal of the four most N-terminal residues appears to be beneficial for affinity, a certain minimum spacing between 5C6 and the surface tether is required. In direct binding studies and on material surfaces, our previous studies suggested that the five N-terminal amino acids are sufficient as spacer. However, the functional studies conducted here suggest that this tethering strategy is not sufficient on more granular and decorated membrane-featuring surfaces such as cells or pegylated liposomes. Appropriate tether and spacer combination may therefore be needed and optimized individually for each target surface. Due to its higher affinity and activity, analog **52** might overcome some of those shortcomings. Although we could previously demonstrate the inhibitory effect of lipid-5C6 conjugates on hemolysis[8], a large PEG linker was employed in these studies, which may explain the observed differences. Further studies are required to decipher and optimize the requirements of spacing and tether for different surfaces. Since 5C6 was recently shown to bind murine FH[9], future studies may likely be conducted under in vivo conditions and elucidate the full translational potential of 5C6 to contributing to improved treatment options for CARPA and other biomaterial and transplant-related complications.

MATERIALS AND METHODS

General materials. Chemical reagents and solvents were obtained from Sigma-Aldrich (St. Louis, USA), ChemImpex (Wood Dale, USA), Carbolution (St. Ingbert, Germany), CEM (Matthews, USA) or VWR (Radnor, USA), if not mentioned otherwise, and used without further purification. DSPE-NHS was from Avanti Polar Lipids (Alabaster, USA), Fmoc-K(CF)-OH was from Anaspec (Fremont, USA). Buffer and Tween-20 stock solutions were obtained from Xantec (Düsseldorf, Germany). Bovine Serum Albumin (BSA) and 3,3',5,5'-tetramethylbenzidin (TMB) were from Sigma-Aldrich (St. Louis, USA). If not mentioned otherwise, full length complement proteins as well as mouse and rat sera were obtained from Complement Technology (Tyler, USA). FHR-5 was obtained from R&D Systems (Minneapolis, USA). Normal human serum was pooled from five unrelated, anonymized healthy donors, obtained with informed consent according to the local ethics committee and following the guidelines of the Declaration of Helsinki (Blutspendezentrum Basel, Switzerland).

Peptide synthesis. All peptides were synthesized with the general method, if not mentioned otherwise, and as previously described (Bechtler et al Journal 2021). In brief, linear peptides were synthesized on a Liberty Blue Automated Peptide Synthesizer (CEM, Matthews, USA) using a microwave-assisted solid-phase peptide synthesis (SPPS) Fmoc/*t*-Bu strategy on an MBHA-Rink Amide resin with diisopropyl carbodiimide (DIC) (6 eq.) and Oxyma (6 eq.) as couplings agents and 6 eq. of Fmoc-protected amino acids in DMF. For C-terminal acids, Cl-MPA ProTide resin was used and loading achieved with 1.0 M DIPEA and 0.125 M KI. For Arg, double coupling was used and for Fmoc-PEG3-OH (purePEG, San Diego, USA) 5 eq. were employed. Biotin was introduced as Fmoc-Lys(biot)-OH (purePEG, San Diego, USA), which was dissolved in DMF/NMP (1/1) and double coupled with 3 eq. per coupling. Fmoc deprotection was achieved with 10% piperazine in NMP/EtOH (9/1), N-terminal acetylation with 10% Ac_2O in DMF. 5(6)-Carboyfluorescein (CF) was coupled on resin with 3 eq. using HOBt (3 eq.) and DIC (3 eq.) as coupling reagents in DMF for 60 min at room temperature (rt). After SPPS, the peptides were washed with DMF and DCM (three times each). In the cases in which the peptides were not further manipulated on the solid-phase, they were cleaved off the resin and side-chain deprotected with 92.5% trifluoroacetic acid (TFA)/2.5% H_2O/2.5% triisopropylsilane/2.5%

ethane dithiol for 3 h at rt, precipitated with -20 °C-cold Et_2O, span down (6500 rpm, 5 min, 4 °C), the supernatant discarded and the procedure repeated twice. The T7 series was ordered from Agentide (Morristown, USA), whereas the S13 peptide series was ordered from GL Biochem (Shanghai, China).

Disulfide formation with H_2O_2. If not mentioned otherwise, the crude linear peptides were dissolved to 1.6 mM (based on the mass of the crude product) in H_2O or mixtures of H_2O/MeOH in case of low solubilities, the pH adjusted to 8 – 9 with 5% NH_4OH (aq.) and 3 eq. of H_2O_2 (1 eq. for biotinylated peptides) added and vigorously stirred for up to 1 h at rt. The reaction was quenched by adjusting the pH to 2 with TFA and the solution was lyophilized.

Disulfide formation with DMSO. Alternatively, the crude peptide was dissolved in H_2O/MeOH/DMSO (9/9/4) to 1 mM (based on the mass of the crude product) the pH basified by a few drops 5% NH_4OH (aq.) and the reaction mixture stirred at room temperature for up to 32 h while monitoring by MS. Upon completion of the reaction, MeOH was removed under reduced pressure and the remaining aqueous solution lyophilized.

Thioacetal formation. The method was used as established by Kourra and Cramer (Kourra, Crama, Chem. Sci. 2016). In brief, the peptides were dissolved in H_2O/THF (ratios between 5/1 to 1.3/1, depending on the solubility) and CH_2I_2 (6 eq.) and NEt_3 (9 eq.) added. The reaction was stirred at room temperature for up to 27 h until completion and monitored by MS. THF was removed under reduced pressure and the remaining aqueous solution lyophilized.

Other reactions. Other, specific reaction conditions are described for the individual peptides in the supplementary information.

Peptide purification. Peptides were purified on an Agilent 1260 Infinity II LCMS (Agilent, Santa Clara, USA) with a reverse phase C18-column (5.0 µM, 19 mm x 250 mm; Waters, Milford, USA) and a linear gradient from 95% A (H_2O + 0.1% TFA)/5% B (MeCN + 0.1% TFA) to usually 50% A/50% B over usually 22.5 min.

Peptide characterization. Peptide identity was confirmed by ESI-MS on a micromassZQ (Waters, Milford, USA). Purity was determined by UV absorption at 214 nm on an Agilent 1100 HPLC (Agilent, Santa Clara, USA), using a reverse phase C18-column (Atlantis T3, 3 µM, 2.1 x 100 mm; Agilent, Santa Clara, USA), phenylhexyl column (XSelect CSH, 3.5 µM, 4.6 mm x 100 mm, Waters, Milford, USA) or, in the case of DSPE-5C6, a C8 column (Agilent Zorbax 300SB-C8, 5 µM, 300 Å pore size, 9.4 mm x 250 mm, Agilent, Santa Clara, USA). Peptides were eluted with a gradient from 95% A (H_2O + 0.1% TFA)/5% B (MeCN + 0.1% TFA) to 5% A/95% B, usually over 15 min. Peptides were purified to at least 95%, if not mentioned otherwise. The identity and purity of the purchased T7 and S13 peptide series was confirmed on an Agilent 1100/1200 series LCMS with a 6410 Triple Quad MS/MS (Agilent, Santa Clara, USA) using a reverse phase C18-column (Luna C182), 5 µM, 2.1 x 150 mm; Phenomenex, Torrence, USA). Peptides were eluted with a gradient from 95% A (H_2O + 0.1% formic acid)/5% B (MeCN + 0.1% formic acid) to 5% A/95% B over 6 min.

Competitive ELISA. 96-well plates were incubated overnight at 4 °C with 10 µg/mL streptavidin (New England Biolabs, Ipswich, USA) in PBS and washed twice with PBS. Then, the plate was saturated for 1.5 h with PBS containing 2% (w/v) BSA, washed twice with PBS containing 0.05% (v/v) Tween-20 (PBST) and the parent biotinylated peptide was immobilized at 10 µg/mL in PBS for 1 h at rt. After washing two times with PBST, serial dilutions (1:1 starting at 50 µM) of each peptide from the *N*-methylation scan library (GL Biochem), pre-incubated with 25 nM FH (A137c, Complement Tech) for 15 min at rt, were added to the plate to compete with the immobilized parent peptide for binding to FH. The plates were incubated for 1 h at rt, followed by two washes with PBST. Subsequently, 100 µL of a polyclonal rabbit anti-human FH antibody (1:1000) in PBS containing 1% BSA (PBSB) were added to the plate for 1 h at rt. The plate was washed three times with PBST, incubated for 1 h at rt with a horseradish peroxidase (HRP)-coupled polyclonal goat anti-rabbit IgG antibody (1:1000) (#172-1019, Biorad) in PBSB and washed three times with PBST. The detection reaction was initiated by adding 2,2'-azino-bis(3-ethylbenzothiazoline-6-sulfonic acid) (ABTS) substrate solution (Roche, Basel, Switzerland) and the absorption measured at 405 nm.

Direct SPR assay. FH8-15 was immobilized on a CMD500M biosensor (Xantec, Düsseldorf, Germany) on a Biacore T200 (Cytiva, Marlborough, USA) with a flow rate of 10 µL/min. Activation was achieved by injecting 0.4 M EDC and 0.1 M *N*-hydroxy succinimide (1/1) for 7 min. Then, the FH8-15 solution, typically at 10-20 µg/mL, was injected until sufficient immobilization was obtained. The surface was inactivated with ethanolamine (1.0 M, pH 8.5) for 7 min. The reference flow cell was treated the same way, except for the FH8-15 injection. 5C6 derivatives were injected as dilution series and association and dissociation were measured each for 60 s, the running buffer was PBS containing 0.005% Tween-20, usually with 50 µM EDTA, and the flow rate 30 µL/min. The surface was regenerated between injections with 1 M NaCl (50 s contact time, 10 s stabilization period). All experiments were performed at 25 °C. As the exact K_D values determined by SPR showed some variance, due to differences in FH density on the biosensor upon immobilization, we present the data here as relative K_D, with $rel.K_D = \frac{K_D(analog)}{K_D(reference)}$, with the reference being either the wild type (wt) full length **1** or wild type truncated 5C6 **2** (tr5C6, i.e. without the exocyclic five N-terminal amino acids; **Figure 1B-C**). Typically, the affinities measured for full length 5C6 **1** were between 60 and 250 nM, whereas they were 150 and 450 nM for tr5C6 **2**.

Competitive MST assay. Interactions were examined on a Monolith (Nanotemper, Munich, Germany). 80 nM CF-5C6 and 40 nM FH were incubated with dilution series of unlabeled 5C6 analogues in PBS containing 0.05% Tween-20. The interaction was measured at 25 °C with the blue laser, MST power set to high and LED power to low, the hot phase was set to 4 – 5 s.

ITC assay. FH8-15 was dialyzed overnight at 4 °C against PBS with a Pur-A-Lyzer Midi 3500 Dialysis Kit (Sigma-Aldrich, (St. Louis, USA). Experiments were performed on a MicroCal ITC200 (Malvern Panalytical, Malvern, United Kingdom) with a total number of 20 injections. The cell temperature was set to 25 °C, the reference power to 6 µcal/s and the initial delay to 180 s. The 5C6 concentration in the syringe was 200 µM and the FH8-15 concentration 20 µM. In the first injection, 0.5 µL were injected over 0.8 s, whereas for the remaining 19 injections, 2.0 µL over 4.0 s were injected. The spacing between injections were 150 s and the filter set to 2. The data was analyzed with AFFINImeter (Santiago de Compostela, Spain) using the "simple model".

FC assay with magnetic streptavidin beads. As previously described (Bechtler et al. 2021), magnetic streptavidin beads (Dynabeads M-270, Thermo Fisher Scientific, Waltham, USA) were washed twice with PBS containing 2% (w/v) BSA and 0.005% (v/v) Tween-20 (PBSBT). In a twin.tect PCR plate (Eppendorf, Hamburg, Germany), 0.2 µL of bead solution were incubated with 800 nM peptide (100 equivalents) solution in PBSBT or PBSBT alone for 30 min at rt. The beads were washed four times with PBSBT and incubated with 200 nM FH, 10% (v/v) normal human serum or 10% normal human serum with 20 mM EDTA, all diluted in PBS, for 60 min at 37 °C while shaking (1050 rpm). The beads were washed four times with PBSBT and incubated with 1 µg/mL of either murine anti-human FH IgG_1 aFH.16 (Sanquin Research, Amsterdam, Netherlands), labelled with CF647 (Sigma-Aldrich, St. Louis, USA) according to the manufacturer's instructions, or APC-labelled murine anti-human C3b IgG_1 3E7 (Biolegend, San Diego, USA) for 30 min at rt while shaking (1050 rpm). The beads were washed four times with PBSBT, resuspended in 100 µL PBSBT, transferred into a 96-well plate (Agilent, Santa Clara, USA) and measured on a CytoFLEX B4-R3-V0 (Beckman Coulter, Indianapolis, USA). Signals were gated on the beads based on forward scatter-height (FCS-H) and sideward scatter-heigh (SSC-H).

Hemolytic assay. Rabbit erythrocytes (ACILA, Weiterstadt, Germany) were incubated with dilution series of lipid 5C6 conjugates, known complement inhibitors, buffer, H_2O or DMSO in Hepes-buffered saline with 0.3% BSA (HBSB) containing 5 mM $MgCl_2$ and 5 mM EGTA (HBSB-MgEGTA) at 37 °C for 60 min, followed by centrifugation at 1000 rcf and 4 °C for 5 min. The supernatant was discarded and the pellet resuspended in HBSB-MgEGTA and normal human serum to achieve a final concentration of 7% (v/v) serum. The samples were incubated at 37 °C for 30 min, after which 150 µL of HBSB containing 20 mM EDTA (HBSBE) were added to 50 µL sample, and the sample centrifuged as described above. 50 µL of the supernatant was transferred into a new plate and the absorbance measured at 405 nm on Synergy HT plate reader (Biotek, Winooski, USA).

Flow cytometry assays with erythrocytes. Rabbit erythrocytes (ACILA, Weiterstadt, Germany) (final dilution: 1:2000) were incubated with dilution series or a single concentration of lipid-5C6 conjugates, 5C6, buffer or DMSO for 60 min at 37 °C, followed by centrifugation at 1000 rcf at 4 °C for 5 min, and resuspended in 100 µL HBSB-MgEGTA. In the case of assessing the insertion of myr-5C6 +15K(CF) into the erythrocytes, the samples were directly measured with FC. For assessing FH recruitment, the samples were incubated with 0.2 µM FH in HBSBE or HBSBE alone at 37 °C for 60 min. The samples were centrifuged at 1000 rcf at 4 °C for 5 min, the supernatant discarded, the pellets resuspended in 100 µL HBSBE containing 1 µg/mL murine anti-human FH IgG_1 aFH.16 (Sanquin Research, Amsterdam, Netherlands), labelled with CF647 (Sigma-Aldrich, St. Louis, USA) according to the manufacturer's instructions and incubated at 37 °C for 60 min. After centrifugation at 1000 rcf at 4 °C for 5 min, the pellets were resuspended in 100 µL HBSBE and measured on a CytoFLEX B4-R3-V0 (Beckman Coulter, Indianapolis, USA). Signals were gated on the beads based on forward scatter-height (FCS-H) and sideward scatter-heigh (SSC-H).

Liposomal doxorubicin release assays. 1% (v/v) of the pegylated liposomal formulation of doxorubicin Caelyx (Janssen Pharmaceutical, Beerse, Belgium) was incubated with appropriate concentrations of lipid-5C6 conjugates, known complement inhibitors or under control conditions in HBS containing 0.3% BSA, 0.15 mM CaI_2 and 0.5 mM $MgCl_2$ (HBSB-CM) for 2 h at room temperature in a final volume of 50 µL. After the 2 h, 50 µL (final concentration: 50 % (v/v)) of normal human serum or inactivated normal human serum (by heating for 1 h at 56 °C), containing the monoclonal murine anti-PEG IgM antibody ANPEG-1 (ANP Technologies, Newark, USA) were added, with a final concentration of ANPEG-1 of 50 µg/mL. After incubation at 37 °C for 30 min, fluorescence was measured at 485/590 nm on a Synergy HT plate reader (Biotek, Winooski, USA).

Stability assay. Samples were measured on a 6410 Triple Quad (Agilent, Santa Clara, USA) using a C18 reverse phase column (Phenomenex Luna, 5 µM, C18(2), 100 Å pore size, 30 mm x 250 mm) and H_2O with 0.1% formic acid as eluent A and MeCN with 0.1% formic acid as eluent B. Peptides were eluted with a gradient of 5%B to 80% over 7.5 min. Trypsin (Promega, Madison, USA) was used according to the manufacturer's instruction, i.e. is in a ratio 1:25 to peptide (m:m) in 100 mM $NH_4(HCO_3)$ with 1 mM $CaCl_2$, pH 8. 25 µL aliquots of the respective samples were quenched with 25 µL 5% TFA. Plasma was reconstituted from lyophilized human plasma (Sigma-Aldrich, St. Louis, USA). The stability assays with trypsin, serum or plasma were performed at 37 °C, the other assays were performed at room temperature, unless specified otherwise. In the case of serum and plasma stability, 10 µL were taken from each sample at the respective time points, precipitated with 90 µL of to 4 °C chilled MeOH, centrifuged at 1913 rcf for 30 min at 4 °C and 50 µL transferred into a new polypropylene plate, V-shape 96-well plate (Agilent, Santa Clara, USA). The samples in 0.1 M HCl and 0.1 M NaOH were quenched with the same volumes of 0.1 M NaOH and 0.1 M HCl, respectively. For each peptide or degradation product, the strongest ionic species was used for quantitation. For the serum stability, piroxicam was used as internal standard and the ion count responses normalized on the piroxicam ion count in the respective sample.

NMR. All NMR spectra were recorded at 25°C on a Bruker Avance-900 spectrometer equipped with a cryogenic triple-resonance probe. The 2D [1H,1H]-ROESY experiment was recorded in a total experiment time of 10 h. The ^1H carrier was centered on the water resonance, the interscan delay was set to 1 s and the ROESY spin lock duration was set to 200 ms. In the direct dimension, 16k complex points were recorded in an acquisition time of 648 ms. In the indirect dimension, 1000 complex points were measured with a maximal evolution time of 65 ms. NMR data was processed using NMRPipe[52] and analyzed with Sparky[53]. Structure calculations were performed in Xplor-NIH version 3.0.3 using standard protocols.[54] A set of 81 NOEs and 8 $^3J_{HN\text{-}H\alpha}$ coupling constants were used as experimental restraints and the ten lowest energy conformations were selected.

CD. The experiments were performed on a Chirascan spectrophotometer (Applied Photophysics, Leatherhead, UK) at 25 °C in 10 mM sodium phosphate buffer (pH 7.4). Samples were measured with a time constant of 5 s, a 1 nm bandwidth and background subtraction against buffer. The mean residue ellipticity was normalized on the concentration (measured at 205 nm) and the resulting normalized

mean residue ellipticity analyzed with the dichroweb tool[49] with CDSSTR as analysis program and set 4 as reference set.

MD. Starting geometry of the 5C6 peptide was taken from NMR experiment (averaged structure). The mutation on the disulfide bridge of analoga was introduced using 3D Builder panel in Maestro in situ, i.e. only local minimization of replaced atoms was performed in order not to affect the overall ring conformation. This way all simulations started from the same ring geometry. All MD simulations in this study were performed using the Desmond (v2019-1) simulation engine.[55] The orthorhombic periodic boundary systems with a buffer of 10 Å to the next protein atom were solvated with TIP3P solvent molecules. After the default equilibration protocol of Desmond, all simulations were conducted in an NPT ensemble at a temperature of 300 K maintained by the Nosé−Hoover thermostat and atmospheric pressure regulated by the Martyna−Tobias−Klein barostat. We selected the OPLS_2005 force field and a time step of 2 fs for the RESPA integrator. Long-range interactions were treated with the u-series algorithm[56] and bonds to hydrogen atoms were restrained using the M-SHAKE algorithm. Short-range interactions were cut off at 9 Å. Each system was simulated for 96 ns with atomic coordinates recorded at an interval of 96 ps. The first half of the simulation time, i.e. 48 ns were considered a pre-equilibration period in order for the conformational effects to balance. The second part of the simulation (48 – 96 ns) was used for analysis: 100 frames were clustered using the trj_cluster.py script (highest occupied cluster) that is part of Maestro. In the clustering routine, we limited the number of output clusters to 5 and information on the cluster population and the total number of clusters are given in Supplementary Table S3. Clustering RMSD calculations were performed using the backbone atoms of residues 6 to 12 (Cys-Cys) of the peptide, including the βC atoms. The structures from the most representative clusters were aligned with the one constructed based on NMR restraints.

Numerical and statistical analyses. GraphPad Prism, version 9.2.0 for MacOS (GraphPad Software, San Diego, California USA, www.graphpad.com) was used for dose-response fits (including K_D and IC_{50} values) with non-linear regression analysis using the agonist vs response, variable slope, four parameters-model as well as for determining statistical significance with a paired t-test and assuming Gaussian distribution. Kinetic SPR fits were performed with Scrubber, version 2.0c for Windows (BioLogic Software, Campbell, Australia).

ACKNOWLEDGEMENTS

We would like to thank Dr. Ilse Jongerius, Sanquin Research for providing us with the mouse anti-human FH antibody aFH.16 and Dr. Timothy Sharpe, Biophiysics Core Facility, Biozentrum, University of Basel for support in the ITC and CD experiments. This study was supported by grants from the Swiss National Science Foundation (No 31003A_176104).

AUTHOR CONTRIBUTIONS

CB designed, synthesized and characterized 5C6 analogs, with assistance from LK and support from CL and OS. CB designed and/or performed biophysical binding assays and circular dichroism experiments, and assays with erythrocytes with supervision from RP. EU and CB designed and/or performed liposomal and bead assays. TM and CB performed/and or analyzed nuclear magnetic resonance experiments. MS performed and analyzed molecular dynamic simulations with assistance from CB. SK performed and analyzed enzyme-linked immunosorbent assays. DR conceived and supervised studies. CB wrote the initial draft of the manuscript with all authors being involved in the writing, editing and discussion of the paper.

CONFLICT OF INTEREST

DR, JDL and RBP are co-inventors of patents describing complement inhibitors and their therapeutic use. JDL is inventor of the 5C6 technology and founder of Amyndas Pharmaceuticals, which has licensed the technology. The other authors do not report conflicts of interest in the context of this study.

REFERENCES

(1) Ricklin, D.; Hajishengallis, G.; Yang, K.; Lambris, J. D. Complement: A Key System for Immune Surveillance and Homeostasis. *Nat. Immunol.* **2010**, *11* (9), 785–797. https://doi.org/10.1038/ni.1923.

(2) Ricklin, D.; Reis, E. S.; Lambris, J. D. Complement in Disease: A Defence System Turning Offensive. *Nat Rev Nephrol* **2016**, *12* (7), 383–401. https://doi.org/10.1038/nrneph.2016.70.

(3) de Boer, E. C. W.; van Mourik, A. G.; Jongerius, I. Therapeutic Lessons to Be Learned From the Role of Complement Regulators as Double-Edged Sword in Health and Disease. *Front. Immunol.* **2020**, *11* (December), 1–21. https://doi.org/10.3389/fimmu.2020.578069.

(4) Sánchez-Corral, P.; Pouw, R. B.; López-Trascasa, M.; Józsi, M. Self-Damage Caused by Dysregulation of the Complement Alternative Pathway: Relevance of the Factor H Protein Family. *Front. Immunol.* **2018**, *9* (1607). https://doi.org/10.3389/fimmu.2018.01607.

(5) Lambris, J. D.; Ricklin, D.; Geisbrecht, B. V. Complement Evasion by Human Pathogens. *Nat. Rev. Microbiol.* **2008**, *6*, 132. https://doi.org/10.1038/nrmicro1824https://www.nature.com/articles/nrmicro1824#supplementary-information.

(6) Macleod, O. J. S.; Bart, J. M.; MacGregor, P.; Peacock, L.; Savill, N. J.; Hester, S.; Ravel, S.; Sunter, J. D.; Trevor, C.; Rust, S.; Vaughan, T. J.; Minter, R.; Mohammed, S.; Gibson, W.; Taylor, M. C.; Higgins, M. K.; Carrington, M. A Receptor for the Complement Regulator Factor H Increases Transmission of Trypanosomes to Tsetse Flies. *Nat. Commun.* **2020**, *11* (1), 1–12. https://doi.org/10.1038/s41467-020-15125-y.

(7) Wu, Y.-Q. Q.; Qu, H.; Sfyroera, G.; Tzekou, A.; Kay, B. K.; Nilsson, B.; Nilsson Ekdahl, K.; Ricklin, D.; Lambris, J. D. Protection of Nonself Surfaces from Complement Attack by Factor H-Binding Peptides: Implications for Therapeutic Medicine. *J. Immunol.* **2011**, *186* (7), 4269–4277. https://doi.org/10.4049/jimmunol.1003802.

(8) Nilsson, P. H.; Ekdahl, K. N.; Magnusson, P. U.; Qu, H.; Iwata, H.; Ricklin, D.; Hong, J.; Lambris, J. D.; Nilsson, B.; Teramura, Y. Autoregulation of Thromboinflammation on Biomaterial Surfaces by a Multicomponent Therapeutic Coating. *Biomaterials* **2013**, *34* (4), 985–994. https://doi.org/10.1016/j.biomaterials.2012.10.040.

(9) Bechtler, C.; Koutsogiannaki, S.; Umnyakova, E.; Hamid, A.; Gautam, A.; Pouw, R. B.; Lamers, C.; Schmidt, C. Q.; Lambris, J. D.; Ricklin, D. Complement Inhibition by Factor H Recruitment : Activity , Target Interaction and Selectivity Profile of the 5C6 Peptide; *under review*

(10) Stites, E.; Le Quintrec, M.; Thurman, J. M. The Complement System and Antibody-Mediated Transplant Rejection. *J. Immunol.* **2015**, *195* (12), 5525–5531. https://doi.org/10.4049/jimmunol.1501686.

(11) Nauser, C. L.; Farrar, C. A.; Sacks, S. H. Complement Recognition Pathways in Renal Transplantation. *J. Am. Soc. Nephrol.* **2017**, *28* (9), 2571–2578. https://doi.org/10.1681/asn.2017010079.

(12) Ekdahl, K. N.; Huang, S.; Nilsson, B.; Teramura, Y. Complement Inhibition in Biomaterial- and Biosurface-Induced Thromboinflammation. *Semin. Immunol.* **2016**, *28* (3), 268–277. https://doi.org/10.1016/j.smim.2016.04.006.

(13) Szebeni, J. Complement Activation-Related Pseudoallergy: A Stress Reaction in Blood Triggered by Nanomedicines and Biologicals. *Molecular Immunology*. Elsevier Ltd October 1, 2014, pp 163–173. https://doi.org/10.1016/j.molimm.2014.06.038.

(14) Vu, V. P.; Gifford, G. B.; Chen, F.; Benasutti, H.; Wang, G.; Groman, E. V.; Scheinman, R.; Saba, L.; Moghimi, S. M.; Simberg, D. Immunoglobulin Deposition on Biomolecule Corona Determines Complement Opsonization Efficiency of Preclinical and Clinical Nanoparticles. *Nat. Nanotechnol.* **2019**, *14* (3), 260–268. https://doi.org/10.1038/s41565-018-0344-3.

(15) Fülöp, T.; Mészáros, T.; Kozma, G.; Szebeni, J.; Józsi, M. Infusion Reactions Associated with the Medical Application of Monoclonal Antibodies: The Role of Complement Activation and Possibility of Inhibition by Factor H. *Antibodies* **2018**, *7* (1), 14.

https://doi.org/10.3390/antib7010014.
(16) Szebeni, J.; Bedőcs, P.; Rozsnyay, Z.; Weiszhár, Z.; Urbanics, R.; Rosivall, L.; Cohen, R.; Garbuzenko, O.; Báthori, G.; Tóth, M.; Bünger, R.; Barenholz, Y. Liposome-Induced Complement Activation and Related Cardiopulmonary Distress in Pigs: Factors Promoting Reactogenicity of Doxil and AmBisome. *Nanomedicine Nanotechnology, Biol. Med.* **2012**, *8* (2), 176–184. https://doi.org/10.1016/J.NANO.2011.06.003.
(17) Stone, N. R. H.; Bicanic, T.; Salim, R.; Hope, W. Liposomal Amphotericin B (AmBisome®): A Review of the Pharmacokinetics, Pharmacodynamics, Clinical Experience and Future Directions. *Drugs* **2016**, *76* (4), 485–500. https://doi.org/10.1007/s40265-016-0538-7.
(18) Gabizon, A.; Szebeni, J. Complement Activation: A Potential Threat on the Safety of Poly(Ethylene Glycol)-Coated Nanomedicines. *ACS Nano*. American Chemical Society July 28, 2020, pp 7682–7688. https://doi.org/10.1021/acsnano.0c03648.
(19) Szebeni, J.; Baranyi, L.; Savay, S.; Bodo, M.; Morse, D. S.; Basta, M.; Stahl, G. L.; Bünger, R.; Alving, C. R. Liposome-Induced Pulmonary Hypertension: Properties and Mechanism of a Complement-Mediated Pseudoallergic Reaction. *Am. J. Physiol. Hear. Circ. Physiol.* **2000**, *279*, H1319–H1328. https://doi.org/10.1152/AJPHEART.2000.279.3.H1319.
(20) Hamad, I.; Hunter, A. C.; Szebeni, J.; Moghimi, S. M. Poly(Ethylene Glycol)s Generate Complement Activation Products in Human Serum through Increased Alternative Pathway Turnover and a MASP-2-Dependent Process. *Mol. Immunol.* **2008**, *46* (2), 225–232. https://doi.org/10.1016/j.molimm.2008.08.276.
(21) Sou, K.; Tsuchida, E. Electrostatic Interactions and Complement Activation on the Surface of Phospholipid Vesicle Containing Acidic Lipids: Effect of the Structure of Acidic Groups. *Biochim. Biophys. Acta - Biomembr.* **2008**, *1778* (4), 1035–1041. https://doi.org/10.1016/j.bbamem.2008.01.006.
(22) Moghimi, S. M.; Hamad, I. Liposome-Mediated Triggering of Complement Cascade. *J. Liposome Res.* **2008**, *18* (3), 195–209. https://doi.org/10.1080/08982100802309552.
(23) Szebeni, J.; Muggia, F.; Gabizon, A.; Barenholz, Y. Activation of Complement by Therapeutic Liposomes and Other Lipid Excipient-Based Therapeutic Products: Prediction and Prevention. *Advanced Drug Delivery Reviews*. Elsevier September 16, 2011, pp 1020–1030. https://doi.org/10.1016/j.addr.2011.06.017.
(24) Wibroe, P. P.; Ahmadvand, D.; Oghabian, M. A.; Yaghmur, A.; Moghimi, S. M. An Integrated Assessment of Morphology, Size, and Complement Activation of the PEGylated Liposomal Doxorubicin Products Doxil®, Caelyx®, DOXOrubicin, and SinaDoxosome. *J. Control. Release* **2016**, *221*, 1–8. https://doi.org/10.1016/j.jconrel.2015.11.021.
(25) Neun, B. W.; Barenholz, Y.; Szebeni, J.; Dobrovolskaia, M. A. Understanding the Role of Anti-PEG Antibodies in the Complement Activation by Doxil in Vitro. *Molecules* **2018**, *23* (7), 1700. https://doi.org/10.3390/molecules23071700.
(26) Moghimi, S. M.; Simberg, D.; Papini, E.; Farhangrazi, Z. S. Complement Activation by Drug Carriers and Particulate Pharmaceuticals: Principles, Challenges and Opportunities. *Adv. Drug Deliv. Rev.* **2020**, *157*, 83–95. https://doi.org/10.1016/j.addr.2020.04.012.
(27) Chen, E.; Chen, B. M.; Su, Y. C.; Chang, Y. C.; Cheng, T. L.; Barenholz, Y.; Roffler, S. R. Premature Drug Release from Polyethylene Glycol (PEG)-Coated Liposomal Doxorubicin via Formation of the Membrane Attack Complex. *ACS Nano* **2020**, *14* (7), 7808–7822. https://doi.org/10.1021/acsnano.9b07218.
(28) Mészáros, T.; Csincsi, Á. I.; Uzonyi, B.; Hebecker, M.; Fülöp, T. G.; Erdei, A.; Szebeni, J.; Józsi, M. Factor H Inhibits Complement Activation Induced by Liposomal and Micellar Drugs and the Therapeutic Antibody Rituximab in Vitro. *Nanomedicine Nanotechnology, Biol. Med.* **2016**, *12* (4), 1023–1031. https://doi.org/10.1016/j.nano.2015.11.019.
(29) Chatterjee, J.; Gilon, C.; Hoffman, A.; Kessler, H. N-Methylation of Peptides: A New Perspective in Medicinal Chemistry. *Acc. Chem. Res.* **2008**, *41* (10), 1331–1342. https://doi.org/10.1021/ar8000603.

(30) Vernon, R. M. C.; Chong, P. A.; Tsang, B.; Kim, T. H.; Bah, A.; Farber, P.; Lin, H.; Forman-Kay, J. D. Pi-Pi Contacts Are an Overlooked Protein Feature Relevant to Phase Separation. *Elife* **2018**, *7*. https://doi.org/10.7554/eLife.31486.

(31) Lopes, A. B.; Wagner, P.; De Souza, R. O. M. A.; Germain, N. L.; Uziel, J.; Bourguignon, J. J.; Schmitt, M.; Miranda, L. S. M. Functionalization of 2H-1,2,3-Triazole C-Nucleoside Template via N2 Selective Arylation. *J. Org. Chem.* **2016**, *81* (11), 4540–4549. https://doi.org/10.1021/acs.joc.6b00323.

(32) Bechtler, C.; Lamers, C. Macrocyclization Strategies for Cyclic Peptides and Peptidomimetics. *RSC Med. Chem.* **2021**, *12* (8), 1325–1351. https://doi.org/10.1039/d1md00083g.

(33) Gori, A.; Gagni, P.; Rinaldi, S. Disulfide Bond Mimetics: Strategies and Challenges. *Chem. – A Eur. J.* **2017**, *23* (60), 14987–14995. https://doi.org/10.1002/chem.201703199.

(34) Muttenthaler, M.; Alewood, P. F. Selenopeptide Chemistry. *J. Pept. Sci.* **2008**, *14* (12), 1223–1239. https://doi.org/10.1002/psc.1075.

(35) Medini, K.; Harris, P. W. R.; Menorca, A.; Hards, K.; Cook, G. M.; Brimble, M. A. Synthesis and Activity of a Diselenide Bond Mimetic of the Antimicrobial Protein Caenopore-5. *Chem. Sci.* **2016**, *7* (3), 2005–2010. https://doi.org/10.1039/c5sc04187b.

(36) Jenny, K. A.; Ste.Marie, E. J.; Mose, G.; Ruggles, E. L.; Hondal, R. J. Facile Removal of 4-Methoxybenzyl Protecting Group from Selenocysteine. *J. Pept. Sci.* **2019**, *25* (10), e3209. https://doi.org/10.1002/psc.3209.

(37) Bernardes, G. J. L.; Grayson, E. J.; Thompson, S.; Chalker, J. M.; Errey, J. C.; El Oualid, F.; Claridge, T. D. W.; Davis, B. G. From Disulfide- to Thioether-Linked Glycoproteins. *Angew. Chemie Int. Ed.* **2008**, *47* (12), 2244–2247. https://doi.org/10.1002/anie.200704381.

(38) Kourra, C. M. B. K.; Cramer, N. Converting Disulfide Bridges in Native Peptides to Stable Methylene Thioacetals. *Chem. Sci.* **2016**, *7* (12), 7007–7012. https://doi.org/10.1039/C6SC02285E.

(39) Empting, M.; Avrutina, O.; Meusinger, R.; Fabritz, S.; Reinwarth, M.; Biesalski, M.; Voigt, S.; Buntkowsky, G.; Kolmar, H. "Triazole Bridge": Disulfide-Bond Replacement by Ruthenium-Catalyzed Formation of 1,5-Disubstituted 1,2,3-Triazoles. *Angew. Chemie - Int. Ed.* **2011**, *50* (22), 5207–5211. https://doi.org/10.1002/anie.201008142.

(40) Roice, M.; Johannsen, I.; Meldal, M. High Capacity Poly(Ethylene Glycol) Based Amino Polymers for Peptide and Organic Synthesis. *QSAR Comb. Sci.* **2004**, *23* (8), 662–673. https://doi.org/doi:10.1002/qsar.200420021.

(41) Servais, G.; Walmagh, J.; Duchateau, J. Simple Quantitative Haemolytic Microassay for Determination of Complement Alternative Pathway Activation (AP50). *J. Immunol. Methods* **1991**, *140* (1), 93–100. https://doi.org/10.1016/0022-1759(91)90130-8.

(42) Gasteiger, E.; Hoogland, C.; Gattiker, A.; Duvaud, S.; Wilkins, M. R.; Appel, R. D.; Bairoch, A. Protein Analysis Tools on the ExPASy Server. In *The Proteomics Protocols Handbook*; Walker, J. M., Ed.; 2005; pp 571–605.

(43) Kelly, S. M.; Jess, T. J.; Price, N. C. How to Study Proteins by Circular Dichroism. *Biochim. Biophys. Acta - Proteins Proteomics* **2005**, *1751* (2), 119–139. https://doi.org/10.1016/j.bbapap.2005.06.005.

(44) Eker, F.; Griebenow, K.; Schweitzer-Stenner, R. Stable Conformations of Tripeptides in Aqueous Solution Studied by UV Circular Dichroism Spectroscopy. *J. Am. Chem. Soc.* **2003**, *125* (27), 8178–8185. https://doi.org/10.1021/ja034625j.

(45) Kim, Y.-W.; Grossmann, T. N.; Verdine, G. L. Synthesis of All-Hydrocarbon Stapled α-Helical Peptides by Ring-Closing Olefin Metathesis. *Nat. Protoc.* **2011**, *6* (6), 761–771. https://doi.org/10.1038/nprot.2011.324.

(46) Gokce, I.; Woody, R. W.; Anderluh, G.; Lakey, J. H. Single Peptide Bonds Exhibit Poly(Pro)II ("random Coil") Circular Dichroism Spectra. *J. Am. Chem. Soc.* **2005**, *127* (27), 9700–9701. https://doi.org/10.1021/ja052632x.

(47) Chang, Y. S.; Graves, B.; Guerlavais, V.; Tovar, C.; Packman, K.; To, K. H.; Olson, K. A.; Kesavan,

K.; Gangurde, P.; Mukherjee, A.; Baker, T.; Darlak, K.; Elkin, C.; Filipovic, Z.; Qureshi, F. Z.; Cai, H.; Berry, P.; Feyfant, E.; Shi, X. E.; Horstick, J.; Annis, D. A.; Manning, A. M.; Fotouhi, N.; Nash, H.; Vassilev, L. T.; Sawyer, T. K. Stapled α-Helical Peptide Drug Development: A Potent Dual Inhibitor of MDM2 and MDMX for P53-Dependent Cancer Therapy. *Proc. Natl. Acad. Sci. U. S. A.* **2013**, *110* (36), E3445–E3454. https://doi.org/10.1073/pnas.1303002110.

(48) Jeganathan, S.; Wendt, M.; Kiehstaller, S.; Brancaccio, D.; Kuepper, A.; Pospiech, N.; Carotenuto, A.; Novellino, E.; Hennig, S.; Grossmann, T. N. Constrained Peptides with Fine-Tuned Flexibility Inhibit NF-Y Transcription Factor Assembly. *Angew. Chemie* **2019**, *131* (48), 17512–17519. https://doi.org/10.1002/ANGE.201907901.

(49) Miles, A. J.; Ramalli, S. G.; Wallace, B. A. DichroWeb, a Website for Calculating Protein Secondary Structure from Circular Dichroism Spectroscopic Data. *Protein Sci.* **2021**, 1–10. https://doi.org/10.1002/pro.4153.

(50) Schmidt, C. Q.; Bai, H.; Lin, Z.; Risitano, A. M.; Barlow, P. N.; Ricklin, D.; Lambris, J. D. Rational Engineering of a Minimized Immune Inhibitor with Unique Triple-Targeting Properties. *J. Immunol.* **2013**, *190* (11), 5712–5721. https://doi.org/10.4049/jimmunol.1203548.

(51) Fridkis-Hareli, M.; Storek, M.; Mazsaroff, I.; Risitano, A. M.; Lundberg, A. S.; Horvath, C. J.; Holers, M. V. Design and Development of TT30, a Novel C3d-Targeted C3/C5 Convertase Inhibitor for Treatment of Human Complement Alternative Pathway-Mediated Diseases. *Blood* **2011**, *118* (17), 4705–4713. https://doi.org/10.1182/blood-2011-06-359646.

(52) Delaglio, F.; Grzesiek, S.; Vuister, G. W.; Zhu, G.; Pfeifer, J.; Bax, A. NMRPipe: A Multidimensional Spectral Processing System Based on UNIX Pipes. *J. Biomol. NMR* **1995**, *6* (3), 277–293. https://doi.org/10.1007/BF00197809.

(53) Lee, W.; Tonelli, M.; Markley, J. L. NMRFAM-SPARKY: Enhanced Software for Biomolecular NMR Spectroscopy. *Bioinformatics* **2015**, *31* (8), 1325–1327. https://doi.org/10.1093/bioinformatics/btu830.

(54) Schwieters, C. D.; Kuszewski, J. J.; Marius Clore, G. Using Xplor–NIH for NMR Molecular Structure Determination. *Prog. Nucl. Magn. Reson. Spectrosc.* **2006**, *48* (1), 47–62. https://doi.org/10.1016/J.PNMRS.2005.10.001.

(55) Bowers, K. J.; Chow, D. E.; Xu, H.; Dror, R. O.; Eastwood, M. P.; Gregersen, B. A.; Klepeis, J. L.; Kolossvary, I.; Moraes, M. A.; Sacerdoti, F. D.; Salmon, J. K.; Shan, Y.; Shaw, D. E. Scalable Algorithms for Molecular Dynamics Simulations on Commodity Clusters. **2007**, 43–43. https://doi.org/10.1109/SC.2006.54.

(56) Shaw, D. E.; Grossman, J. P.; Bank, J. A.; Batson, B.; Butts, J. A.; Chao, J. C.; Deneroff, M. M.; Dror, R. O.; Even, A.; Fenton, C. H.; Forte, A.; Gagliardo, J.; Gill, G.; Greskamp, B.; Ho, C. R.; Ierardi, D. J.; Iserovich, L.; Kuskin, J. S.; Larson, R. H.; Layman, T.; Lee, L. S.; Lerer, A. K.; Li, C.; Killebrew, D.; Mackenzie, K. M.; Mok, S. Y. H.; Moraes, M. A.; Mueller, R.; Nociolo, L. J.; Peticolas, J. L.; Quan, T.; Ramot, D.; Salmon, J. K.; Scarpazza, D. P.; Ben Schafer, U.; Siddique, N.; Snyder, C. W.; Spengler, J.; Tang, P. T. P.; Theobald, M.; Toma, H.; Towles, B.; Vitale, B.; Wang, S. C.; Young, C. Anton 2: Raising the Bar for Performance and Programmability in a Special-Purpose Molecular Dynamics Supercomputer. *Int. Conf. High Perform. Comput. Networking, Storage Anal. SC* **2014**, *2015-January* (January), 41–53. https://doi.org/10.1109/SC.2014.9.

SUPPLEMENTARY INFORMATION

SUPPLEMENTARY FIGURES AND TABLES

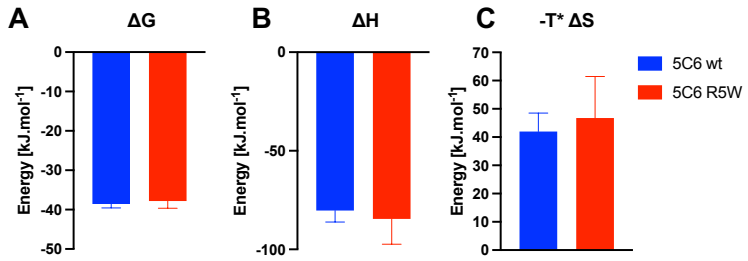

D

	5C6 wt	5C6 R5W
K_D [nM]	182±51	270±185
ΔG [kJ/mol]	-38.6±1.0	-37.8±0.9
ΔH [kJ/mol]	-80.6±5.5	-84.6±12.8
-T *ΔS [kJ/mol]	42.0±6.5	46.8±14.7

Figure S1: (**A**) Free energy, (**B**) enthalpic and (**C**) entropic profile of the interaction of 5C6 wt and 5C6 R5W with FH8-15, measured by ITC. (**D**) Summary of the affinity and thermodynamic parameters of the interactions. *n* = 2, error is SD, except for the K_D, where it is SEM.

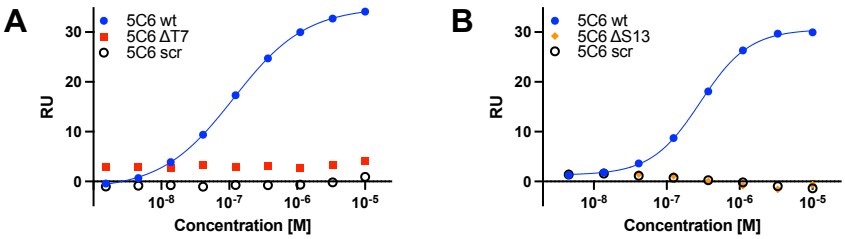

Figure S2: Representative SPR dose-response plots of 5C6 ΔT7 (**A**) and 5C6 ΔS13 (**B**) alongside wild type and scrambled 5C6

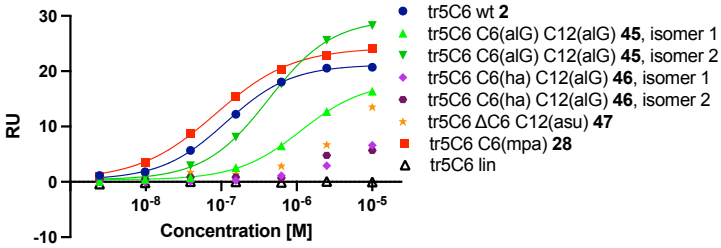

Figure S3: Representative SPR dose-response plots of the hydrocarbon-bridged peptidomimetic analogs of tr5C6 wt **2**, without shared maximum value for the dose-response plot.

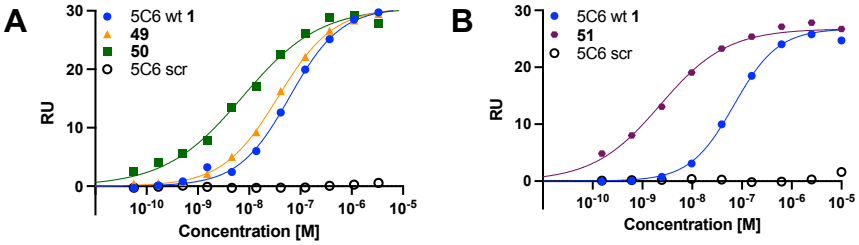

Figure S4: Representative SPR dose-response plots for the globally modified 5C6 analogs with a full (**A**) or with a truncated N-terminus (**B**).

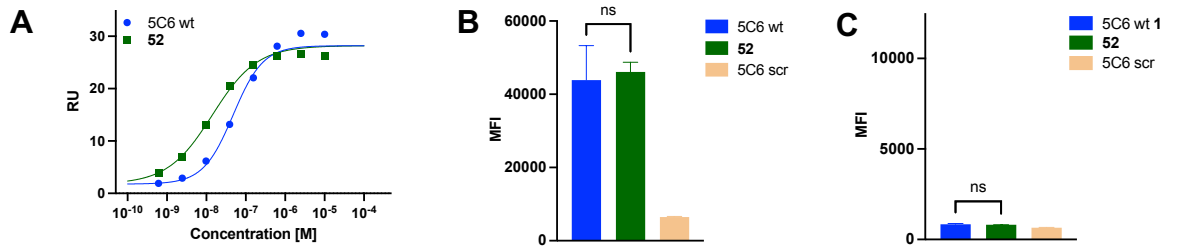

Figure S5: (**A**) Representative SPR dose-response plots for the N-terminally biotinylated peptide **50**. (**B**) Median-fluorescence intensity (MFI) of FH binding of beads loaded with N-terminally biotinylated 5C6 derivatives and incubated with human serum inhibited with 10 mM EDTA. (**C**) MFI of C3b deposition of beads loaded with N-terminally biotinylated 5C6 derivatives and incubated with human serum inhibited with 10 mM EDTA. Bars indicate mean of independent duplicates; error bars indicate standard deviation, ns: non-significant ($p > 0.05$).

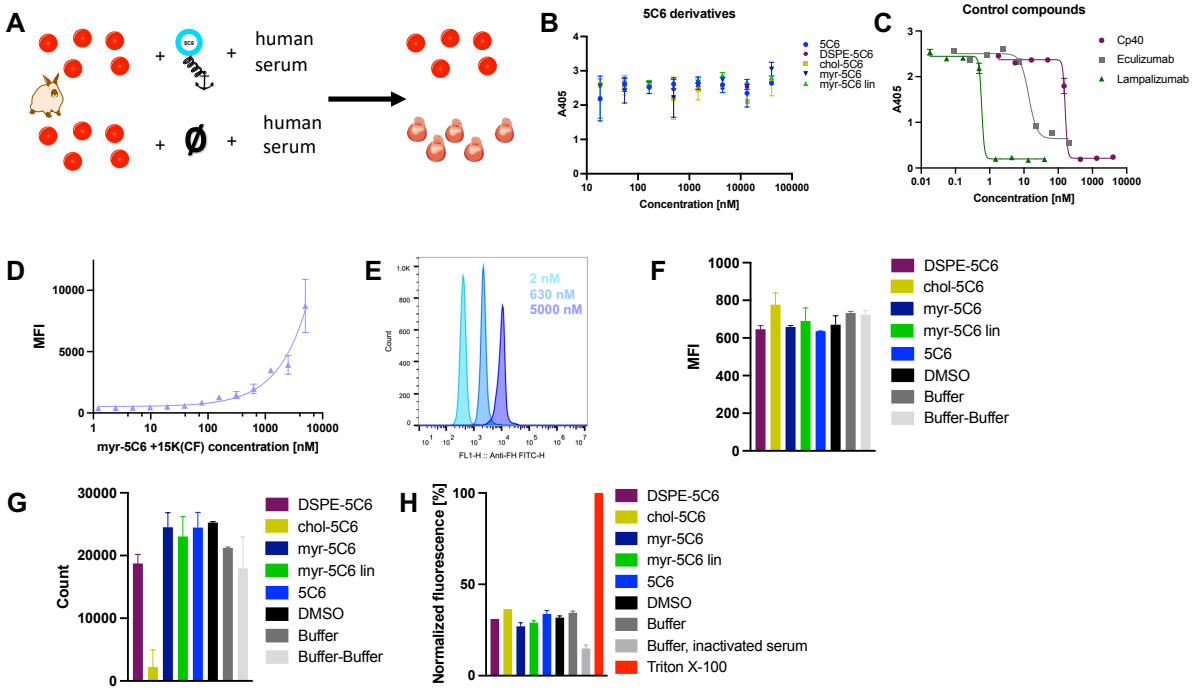

Figure S6: (**A**) Schematic set-up of the hemolytic assay. (**B**) Measured absorbance in the hemolytic assay for rabbit erythrocytes incubated with the lipid-5C6 conjugates. (**C**) Measured absorbance in the hemolytic assay for rabbit erythrocytes incubated with known complement inhibitors. (**D**) Dose-dependent increase of fluorescence, measured as MFI, for rabbit erythrocytes incubated with increasing concentrations of myr-5C6 +15K(CF). (**E**) MFI histograms for selected concentrations of myr-5C6 +15K(CF) incubated with rabbit erythrocytes. (**F**) and (**G**): MFI and counts, respectively of rabbit erythrocytes incubated sequentially with lipid-5C6 conjugates, FH and labelled anti-FH. DMSO and Buffer describe incubation conditions where instead with peptides, the erythrocytes were incubated with DMSO or buffer instead, in the Buffer-Buffer conditions, the FH incubation step was additionally replaced with a buffer incubation. (**H**) Fluorescence of doxorubicin released from Caelyx® liposomes after incubation with different lipid-5C6 conjugates or under control conditions, followed by incubation with murine anti-PEG IgMs and human serum. Fluorescence is normalized on fluorescence after complete liposome lysis with the detergent triton X-100.

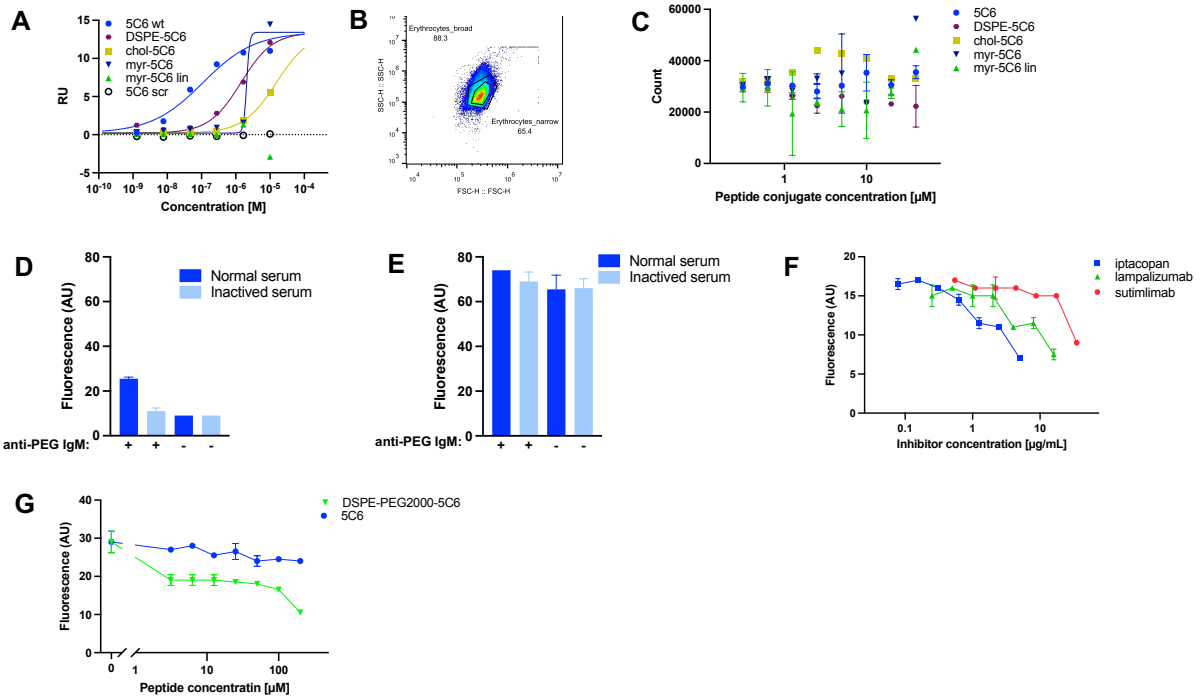

Figure S7: (**A**) Representative SPR dose-response plots for the lipid-5C6 conjugates (**B**) Dot-plot of forward scatter (FSC) and sideward scatter (SSC) showing the gating strategy used in the FC assays with rabbit erythrocytes. The "Erythrocytes_narrow" gate was used for all calculations in all assays. (**C**) Count of rabbit erythrocytes after incubation with different concentrations of lipid-5C6 conjugates. (**D**) Florescence of Caelyx® liposomes incubated with normal or inactivated human serum in the absence or presence of murine anti-PEG IgMs. Bars indicate mean of independent duplicates; error bars indicate standard deviation. (**E**) Florescence of Caelyx liposomes incubated with 1% triton X-100 as well as normal or inactivated human serum in the absence or presence of murine anti-PEG IgMs. (**F**) The complement inhibitors iptacopan, lampalizumab and sutimlimab inhibited the release of doxorubicin from Caelyx in a dose-dependent manner, measured as doxorubicin fluorescence. (**G**) Fluorescence of doxorubicin released from Caelyx liposomes after incubation with unconjugated 5C6 or with crude DSPE-PEG2000-5C6, followed by incubation with murine anti-PEG IgMs and normal human serum.

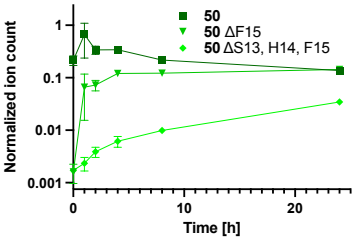

Figure S8: Stability of peptide **50** and the formation of the two main degradation products peptide **50** ΔF15 and peptide **50** ΔS13, H14, F15 in normal human serum, log10 count for the normalized ion count, which is the sample ion count divided by the ion count of the internal standard in the respective sample.

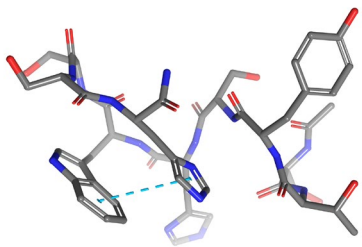

Figure S9: Structure of the most abundant cluster of tr5C6 lin, with the π-stacking interaction between W11 and H14 indicated with a cyan line. Although the peptide is not cyclized, it does not preferentially adapt a fully extended conformation.

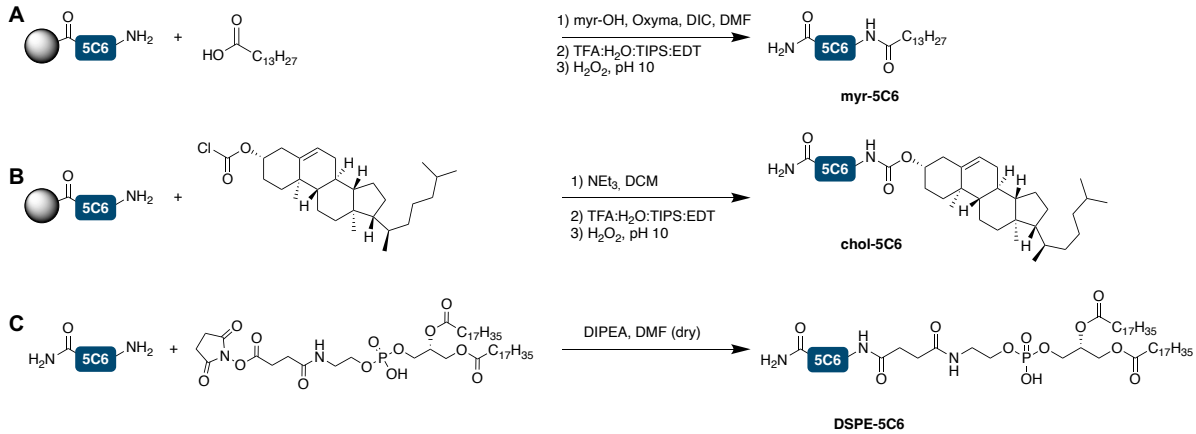

Scheme S1: Synthetic schemes for the lipid coupled 5C6 conjugates, i.e. myr-5C6 (**A**), chol-5C6 (**B**) and DSPE-5C6 (**C**).

Table S1: Relative SPR binding affinities of the hydrocarbon peptidomimetic macrocycle analogs of tr5C6 wt **2**, fitted without shared maximum value in the dose-response plot.

Peptide	Structure	Sequence	rel. K_D±SEM
tr5C6 wt	**2**	Ac–[**C** TYSHW **C**]SH–$CONH_2$	1.00±0.00
tr5C6 C6(alG) C12(alG), isomer 1	**45**	Ac–[**(alG)**TYSHW **(alG)**]SH–$CONH_2$	13.1±3.2
tr5C6 C6(alG) C12(alG), isomer 2	**45**	Ac–[**(alG)**TYSHW **(alG)**]SH–$CONH_2$	10.1±6.3
tr5C6 C6(ha) C12(alG), isomer 1	**46**	[**(ha)** TYSHW **(alG)**]SH–$CONH_2$	no binding
tr5C6 C6(ha) C12(alG), isomer 2	**46**	[**(ha)** TYSHW **(alG)**]SH–$CONH_2$	no binding
tr5C6 ΔC6 C12(asu)	**47**	[TYSHW **(asu)**]SH–$CONH_2$	no binding

Table S2: Relative SPR binding affinities of CB228 and the lipid conjugates of 5C6, *n* = 2.

Peptide	Sequence	rel. K_D±SEM
5C6 wt	Ac– ASSS**R**[**C**TYSHW**C**]**S**H –$CONH_2$	1.00±0.00
peptide **52**	Ac–**K(biot)**ASSS**W**[**C**TYSHW**C**]**T**H**F**–$CONH_2$	0.31±0.01
DSPE-5C6	Ac–**DSPE**– ASSS**R**[**C**TYSHW**C**]**S**H –$CONH_2$	14.4±1.5
chol-5C6	Ac–**chol**– ASSS**R**[**C**TYSHW**C**]**S**H –$CONH_2$	128±11
myr-5C6	Ac–**myr**– ASSS**R**[**C**TYSHW**C**]**S**H –$CONH_2$	113±94
myr-5C6 lin	Ac–**myr**– ASSS**R** **S**TYSHW**S** **S**H –$CONH_2$	no binding

Table S3: RMSD of most abundant cluster for tr5C6 **2**, tr5C6 lin, thioacetal **33**, 1,5-triazole **39** and E- as well as Z-isomers of alkene **45** and the number of frames (out of 100) for each of the most abundant clusters. C+CH_2: cysteine with additional methylene group, aza: (S)-3-azidoalanine, prG: a (*S*)-propargyl glycine, RMSD: root mean square deviation

Peptide	Structure	Sequence	RMSD [Å]	number of structures/ cluster
tr5C6 wt	**2**	Ac–[**C** TYSHW **C**]SH–$CONH_2$	2.1	18
tr5C6 cyc+CH_2	**33**	Ac–[**C** TYSHW(**C+CH₂**)]SH–$CONH_2$	2.1	14
tr5C6 C6(aza) C12(prG) cyc1,5triA	**39**	Ac–[**(aza)**TYSHW **(prG)**]SH–$CONH_2$	2.0	32
tr5C6 C6(alG) C12(alG), E-isomer	**45**	Ac–[**(alG)**TYSHW **(alG)**]SH–$CONH_2$	2.3	23
tr5C6 C6(alG) C12(alG), Z-isomer	**45**	Ac–[**(alG)**TYSHW **(alG)**]SH–$CONH_2$	1.8	21
tr5C6 lin		Ac–[**S** TYSHW **S**]SH–$CONH_2$	3.7	15

SUPPLEMENTARY METHODS: PEPTIDE SYNTHESIS AND CHARACTERIZATION

If not specified otherwise, the peptides were synthesized according to the general SPPS, cleavage and cyclization with H_2O_2 conditions outlined in the methods section. If not mentioned otherwise, peptides were > 95% pure, based on the UV trace at λ = 214 nm on RP-HPLC.

5C6 wild type (1, 5C6 wt). Ac-ASSSR[CTYSHWC]SH-$CONH_2$, $C_{68}H_{95}N_{23}O_{22}S_2$, M_W = 1650.77 g/mol, M_{exact} = 1649.65 Da. ESI-MS: calculated: 825.84 $[M+2H]^{2+}$, 550.89 $[M+3H]^{3+}$, found: 825.89 $[M+2H]^{2+}$, 550.94 $[M+3H]^{3+}$; HPLC: t_R = 6.637 min.

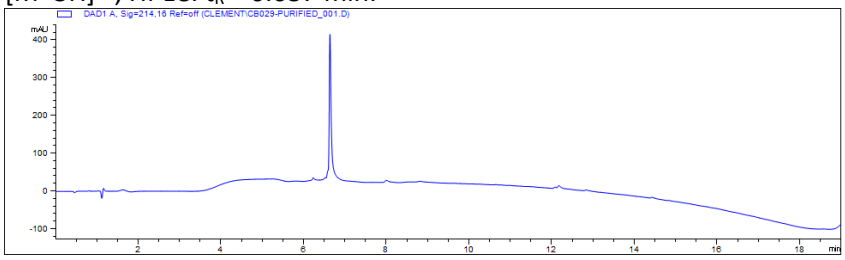

5C6 truncated (2, tr5C6). Ac-[CTYSHWC]SH-$CONH_2$, $C_{50}H_{63}N_{15}O_{14}S_2$, M_W = 1162.27 g/mol, M_{exact} = 1161.41 Da. ESI-MS: calculated: 1162.42 $[M+H]^+$, 581.72 $[M+2H]^{2+}$, found: 1162.19 $[M+H]^+$, 581.61 $[M+2H]^{2+}$; HPLC: t_R = 7.059 min.

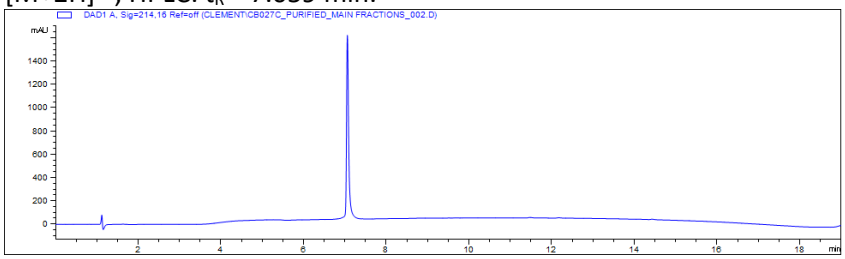

5C6 scrambled. Ac-SSHAS[CRWSSYC]HT-$CONH_2$, $C_{68}H_{95}N_{23}O_{22}S_2$, M_W = 1650.77 g/mol, M_{exact} = 1649.65 Da. ESI-MS: calculated: 1650.66 $[M+H]^+$, 825.84 $[M+2H]^{2+}$, 550.89 $[M+3H]^{3+}$, found: 1651.91 $[M+H]^+$, 825.89 $[M+2H]^{2+}$, 550.94 $[M+3H]^{3+}$; HPLC: t_R = 13.738 min.

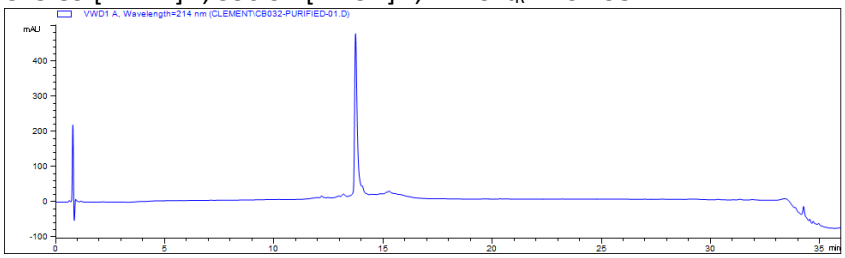

5C6 linear. Ac-ASSSRSTYSHWSSH-$CONH_2$, $C_{68}H_{97}N_{23}O_{24}$, M_W = 1620.66 g/mol, M_{exact} = 1619.71 Da. ESI-MS: calculated: 810.87 $[M+2H]^{2+}$, 540.91 $[M+3H]^{3+}$, found: 811.33 $[M+2H]^{2+}$, 540.94 $[M+3H]^{3+}$; HPLC: t_R = 6.581 min.

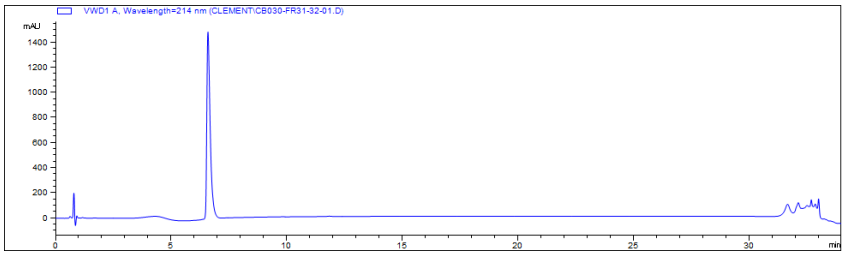

5C6 truncated linear (tr5C6 linear). Ac-STYSHWSSH-$CONH_2$, $C_{50}H_{65}N_{15}O_{16}$, M_W = 1132.16 g/mol, M_{exact} = 1131.47 Da. ESI-MS: calculated: 1132.48 $[M+H]^+$, 566.75 $[M+2H]^{2+}$, found: 1132.41 $[M+H]^+$, 566.72 $[M+2H]^{2+}$; HPLC: t_R = 7.470 min.

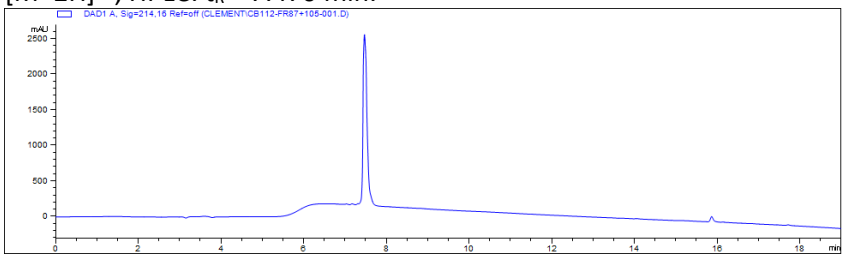

5C6 ΔS13 ΔH14. Ac-ASSSR[CTYSHWC]-$CONH_2$, $C_{59}H_{83}N_{19}O_{19}S_2$, M_W = 1426.56 g/mol, M_{exact} = 1425.55 Da. ESI-MS: calculated: 1426.56 $[M+H]^+$, 713.79 $[M+2H]^{2+}$, found: 1426.58 $[M+H]^+$, 713.82 $[M+2H]^{2+}$; HPLC: t_R = 7.032 min.

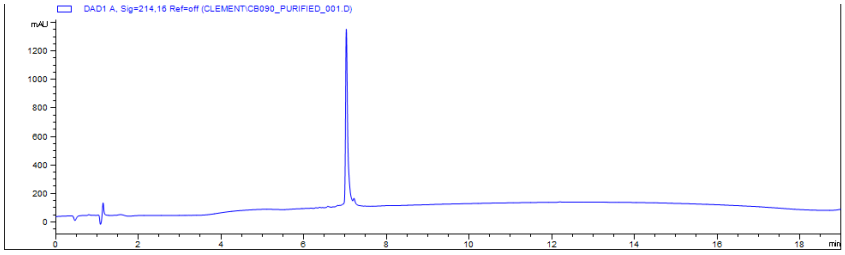

5C6 R5W. Ac-ASSSW[CTYSHWC]SH-$CONH_2$, $C_{73}H9_3N_{21}O_{22}S_2$, M_W = 1680.79 g/mol, M_{exact} = 1679.62 Da. ESI-MS: calculated: 1426.56 $[M+H]^+$, 713.79 $[M+2H]^{2+}$, found: 1426.58 $[M+H]^+$, 713.82 $[M+2H]^{2+}$; HPLC: t_R = 9.604 min.

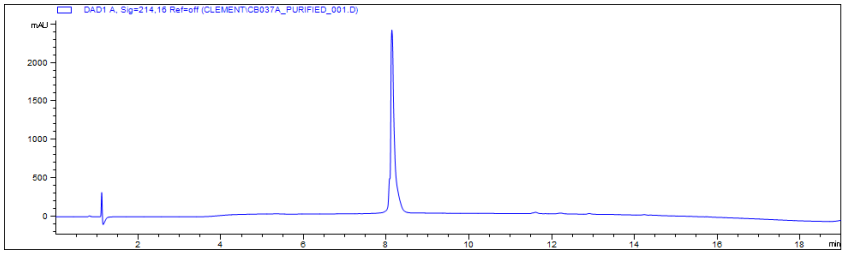

5C6 R5S. Ac-ASSSS[CTYSHWC]SH-$CONH_2$, $C_{65}H_{88}N_{20}O_{23}S_2$, M_W = 1581.66 g/mol, M_{exact} = 1580.58 Da. ESI-MS: calculated: 1581.59 $[M+H]^+$, 791.30 $[M+2H]^{2+}$, found: 1581.43 $[M+H]^+$, 791.27 $[M+2H]^{2+}$; HPLC: t_R = 6.778 min.

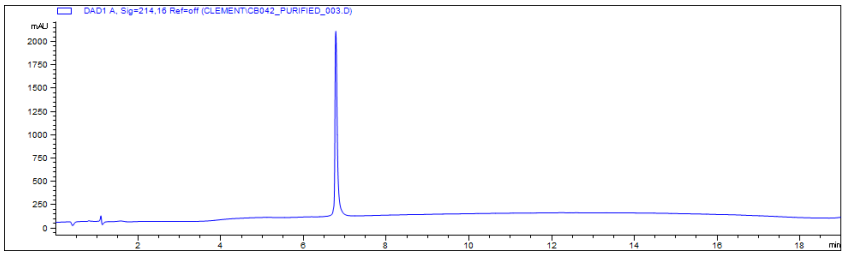

5C6 R5E. Ac-ASSSE[CTYSHWC]SH-$CONH_2$, $C_{67}H_{90}N_{20}O_{24}S_2$, M_W = 1623.69 g/mol, M_{exact} = 1622.59 Da. ESI-MS: calculated: 1623.60 $[M+H]^+$, 812.31 $[M+2H]^{2+}$, found: 1623.57 $[M+H]^+$, 812.34 $[M+2H]^{2+}$; HPLC: t_R = 6.909 min.

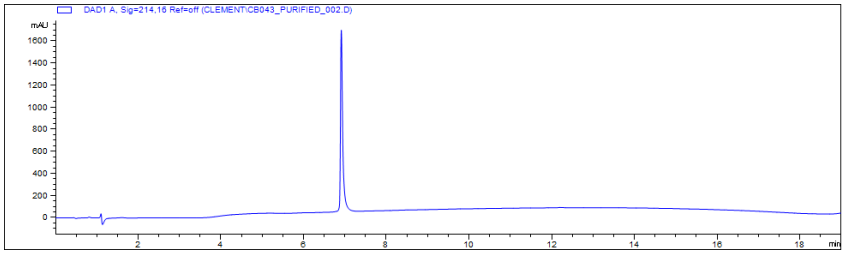

5C6 R5K. Ac-ASSSK[CTYSHWC]SH-$CONH_2$, $C_{68}H_{95}N_{21}O_{22}S_2$, M_W = 1622.75 g/mol, M_{exact} = 1621.64 Da. ESI-MS: calculated: 1622.65 $[M+H]^+$, 811.83 $[M+2H]^{2+}$, found: 1622.34 $[M+H]^+$, 811.88 $[M+2H]^{2+}$; HPLC: t_R = 6.622 min.

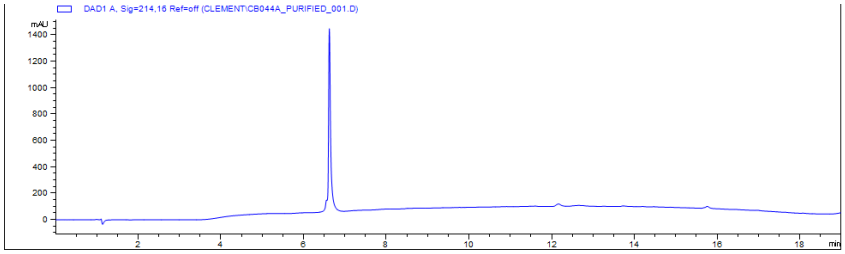

5C6 R5L. Ac-ASSSL[CTYSHWC]SH-$CONH_2$, $C_{68}H_{94}N_{20}O_{22}S_2$, M_W = 1607.74 g/mol, M_{exact} = 1606.63 Da. ESI-MS: calculated: 1607.64 $[M+H]^+$, 804.33 $[M+2H]^{2+}$, found: 1607.46 $[M+H]^+$, 804.33 $[M+2H]^{2+}$. HPLC: t_R = 7.905 min.

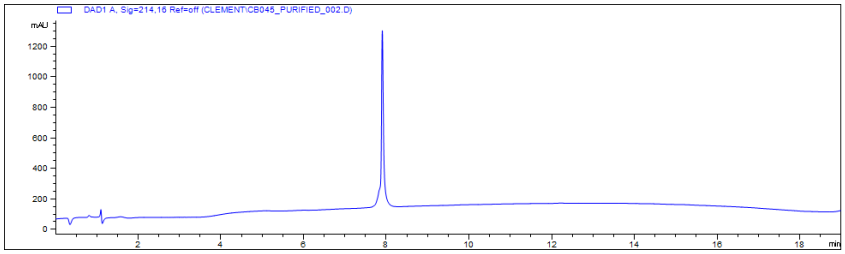

5C6 R5Y. Ac-ASSSY[CTYSHWC]SH-$CONH_2$, $C_{71}H_{92}N_{20}O_{23}S_2$, M_W = 1657.75 g/mol, M_{exact} = 1656.61 Da. ESI-MS: calculated: 1657.62 $[M+H]^+$, 829.32 $[M+2H]^{2+}$, found: 1658.30 $[M+H]^+$, 829.29 $[M+2H]^{2+}$; HPLC: t_R = 7.441 min.

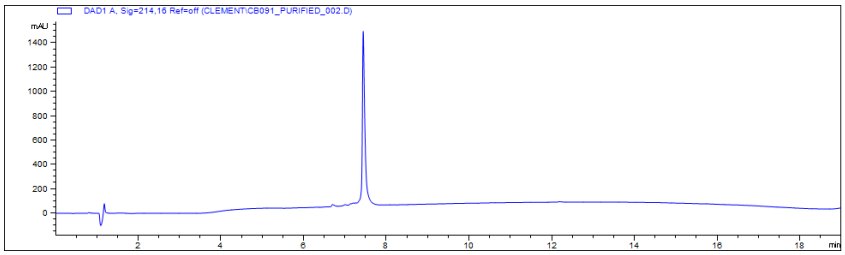

5C6 R5H. Ac-ASSSH[CTYSHWC]SH-$CONH_2$, $C_{68}H_{90}N_{22}O_{22}S_2$, M_W = 1631.72 g/mol, M_{exact} = 1630.60 Da. ESI-MS: calculated: 1631.61 $[M+H]^+$, 816.31 $[M+2H]^{2+}$, found: 1632.40 $[M+H]^+$, 816.37 $[M+2H]^{2+}$; HPLC: t_R = 6.672 min.

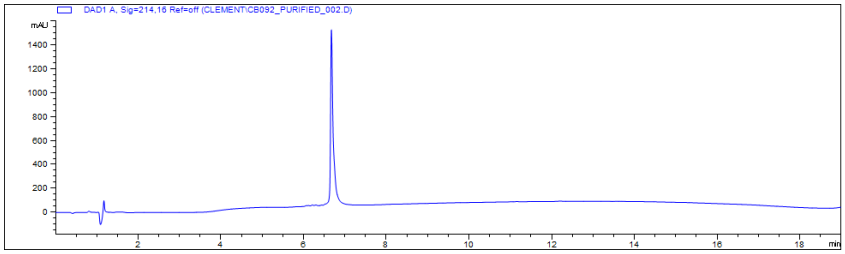

5C6 R5F. Ac-ASSSF[CTYSHWC]SH-$CONH_2$, $C_{71}H_{92}N_{20}O_{22}S_2$, M_W = 1641.76 g/mol, M_{exact} = 1640.61 Da. ESI-MS: calculated: 1641.62 $[M+H]^+$, 821.32 $[M+2H]^{2+}$, found: 1641.51 $[M+H]^+$, 821.33 $[M+2H]^{2+}$; HPLC: t_R = 8.082 min.

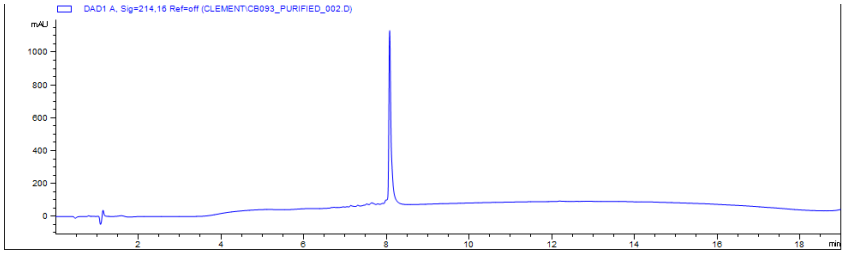

5C6 R5(NaI). Ac-ASSS(NaI)[CTYSHWC]SH-$CONH_2$, $C_{75}H_{94}N_{20}O_{22}S_2$, M_W = 1690.82 g/mol, M_{exact} = 1690.63 Da. ESI-MS: calculated: 846.33 $[M+2H]^{2+}$, 868.31 $[M+2Na]^{2+}$, found: 846.29 $[M+2H]^{2+}$, 869.13 $[M+2Na]^{2+}$; HPLC: t_R = 8.852 min.

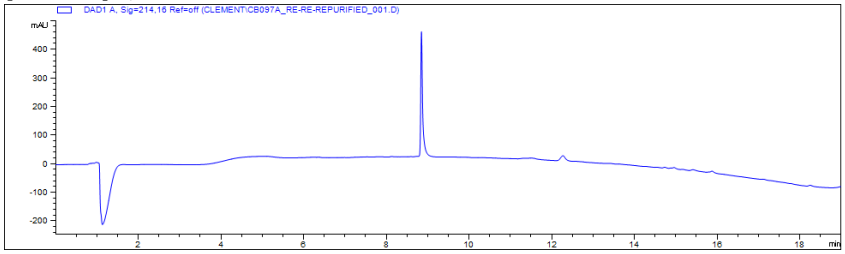

5C6 R5(thi). Ac-ASSS(thi)[CTYSHWC]SH-$CONH_2$, $C_{69}H_{90}N_{20}O_{22}S_3$, M_W = 1647.78 g/mol, M_{exact} = 1646.57 Da. ESI-MS: calculated: 1647.58 $[M+H]^+$, 824.30 $[M+2H]^{2+}$, found: 1647.49 $[M+H]^+$, 824.25 $[M+2H]^{2+}$; HPLC: t_R = 7.869 min.

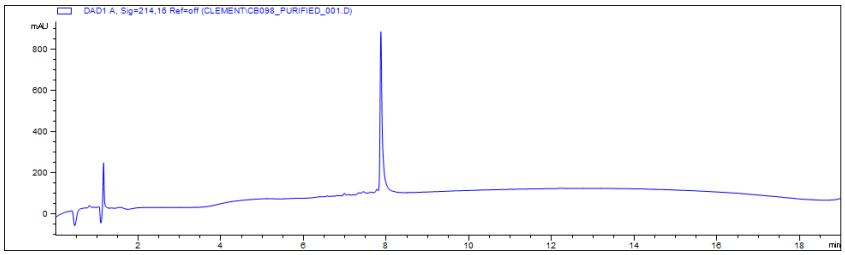

5C6 R5(pyr). Ac-ASSS(pyr)[CTYSHWC]SH-$CONH_2$, $C_{70}H_{91}N_{21}O_{22}S_2$, M_W = 1642.74 g/mol, M_{exact} = 1641.61 Da. ESI-MS: calculated: 1642.62 $[M+H]^+$, 821.82 $[M+2H]^{2+}$, found: 1642.40 $[M+H]^+$, 821.94 $[M+2H]^{2+}$; HPLC: t_R = 6.700 min.

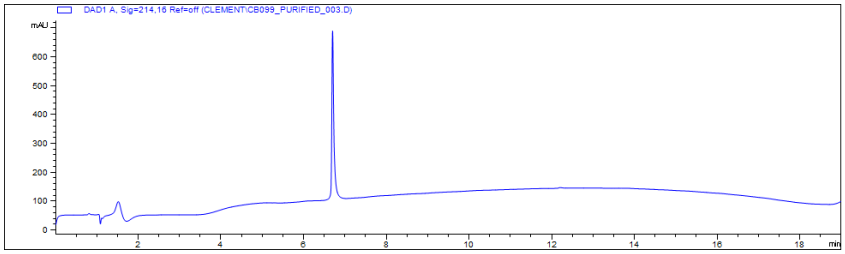

5C6 R5(MeW). Ac-ASSS(MeW)[CTYSHWC]SH-$CONH_2$, $C_{74}H_{95}N_{21}O_{22}S_2$, M_W = 1694.82 g/mol, M_{exact} = 1693.64 Da. ESI-MS: calculated: 847.83 $[M+2H]^{2+}$, 858.82 $[M+H+Na]^{2+}$, found: 858.87 $[M+2H]^{2+}$, 713.82 $[M+H+Na]^{2+}$; HPLC: t_R = 8.643 min.

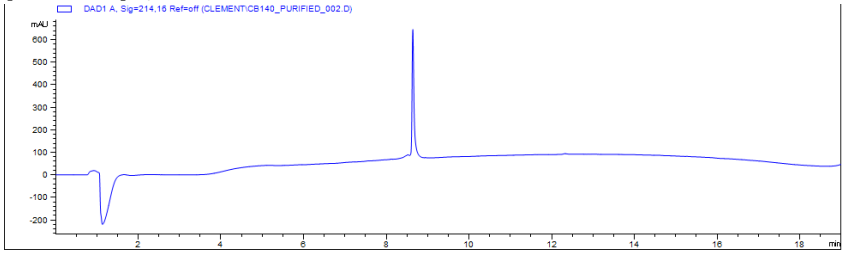

5C6 Δ1-4. Ac-R[CTYSHWC]SH-$CONH_2$, $C_{56}H_{75}N_{19}O_{15}S_2$, M_W = 1318.45 g/mol, M_{exact} = 1317.51 Da. ESI-MS: calculated: 1318.52 $[M+H]^+$, 659.77 $[M+2H]^{2+}$, found: 1318.50 $[M+H]^+$, 660.10 $[M+2H]^{2+}$; HPLC: t_R = 6.819 min.

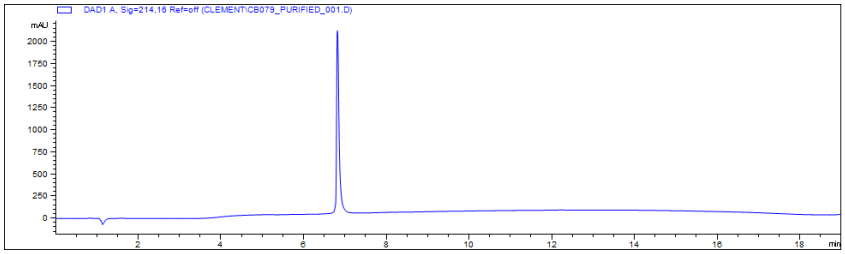

5C6 Δ1-4 R5W. Ac-W[CTYSHWC]SH-$CONH_2$, $C_{61}H_{73}N_{17}O_{15}S_2$, M_W = 1348.48 g/mol, M_{exact} = 1347.49 Da. ESI-MS: calculated: 1348.50 $[M+H]^+$, found: 1348.33 $[M+H]^+$; HPLC: t_R = 8.373 min.

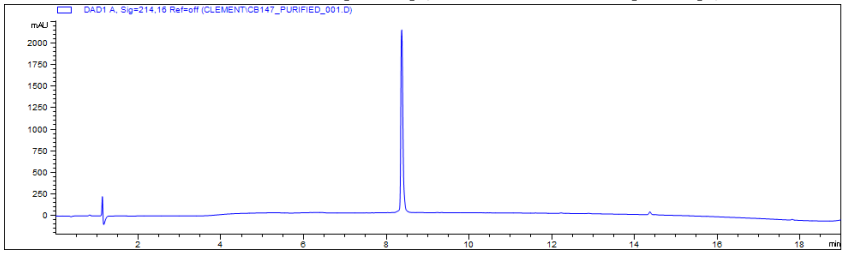

5C6 S234A R5W. Ac-AAAAW[CTYSHWC]SH-CONH$_2$, $C_{73}H_{93}N_{21}O_{19}S_2$, M_W = 1632.80 g/mol, M_{exact} = 1631.64 Da. ESI-MS: calculated: 1632.65 $[M+H]^+$, 816.83 $[M+2H]^{2+}$, found: 1632.47 $[M+H]^+$, 816.84 $[M+2H]^{2+}$; HPLC: t_R = 9.049 min.

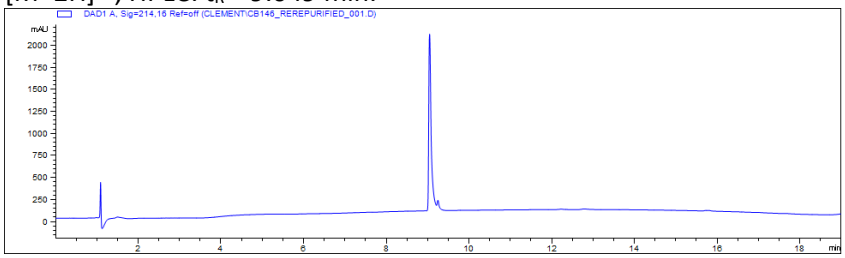

5C6 Y8L. Ac-ASSSL[CTGSHWC]SH-CONH$_2$, $C_{65}H_{97}N_{23}O_{21}S_2$, M_W = 1599.67 g/mol, M_{exact} = 1599.67 Da. ESI-MS: calculated: 1600.68 $[M+H]^+$, 800.85 $[M+2H]^{2+}$, found: 1600.39 $[M+H]^+$, 800.79 $[M+2H]^{2+}$; HPLC: t_R = 7.110 min.

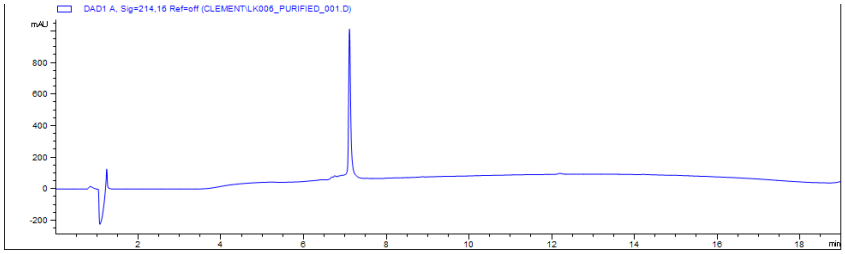

5C6 Y8S. Ac-ASSSR[CTSSHWC]SH-CONH$_2$, $C_{62}H_{91}N_{23}O_{22}S_2$, M_W = 1574.67 g/mol, M_{exact} = 1573.62 Da. ESI-MS: calculated: 1574.63 $[M+H]^+$, 787.82 $[M+2H]^{2+}$, found: 1574.15 $[M+H]^+$, 787.74 $[M+2H]^{2+}$; HPLC: t_R = 5.999 min.

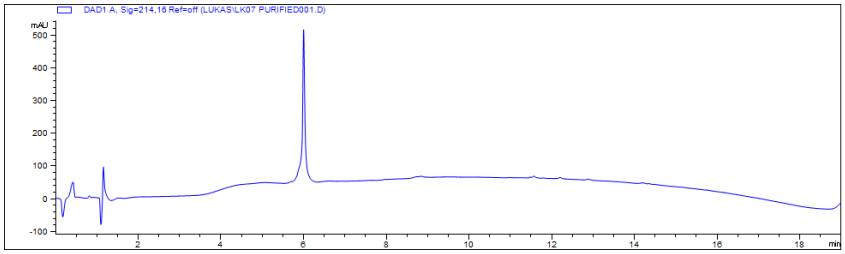

5C6 Y8G. Ac-ASSSR[CTGSHWC]SH-CONH$_2$, $C_{61}H_{89}N_{23}O_{21}S_2$, M_W = 1544.64 g/mol, M_{exact} = 1543.60 Da. ESI-MS: calculated: 1544.61 $[M+H]^+$, 772.81 $[M+2H]^{2+}$, found: 1544.11 $[M+H]^+$, 772.64 $[M+2H]^{2+}$; HPLC: t_R = 5.962 min.

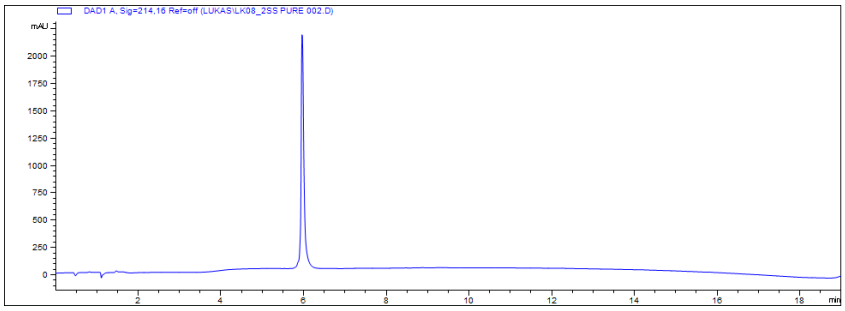

5C6 Y8K. Ac-ASSSK[CTGSHWC]SH-$CONH_2$, $C_{65}H_{98}N_{24}O_{21}S_2$, M_W = 1615.77 g/mol, M_{exact} = 1614.77 Da. ESI-MS: calculated: 1615.69 $[M+H]^+$, 808.35 $[M+2H]^{2+}$, found: 1616.16 $[M+H]^+$, 808.14 $[M+2H]^{2+}$; HPLC: t_R = 5.987 min.

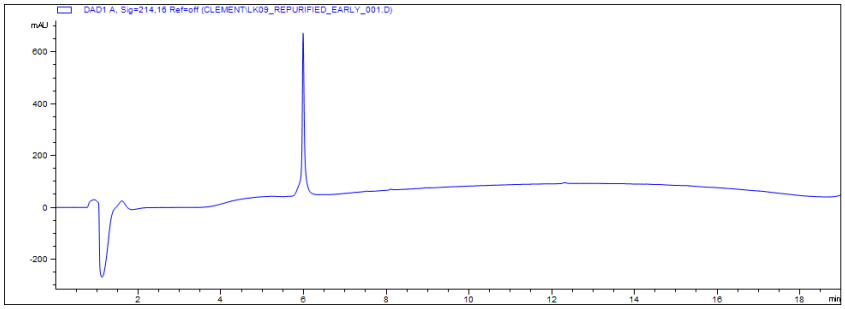

5C6 Y8E. Ac-ASSSR[CTSSHWC]SH-$CONH_2$, $C_{64}H_{93}N_{23}O_{23}S_2$, M_W = 1616.71 g/mol, M_{exact} = 1615.63 Da. ESI-MS: calculated: 1616.64 $[M+H]^+$, 808.83 $[M+2H]^{2+}$, found: 1616.43 $[M+H]^+$, 808.75 $[M+2H]^{2+}$; HPLC: t_R = 6.232 min.

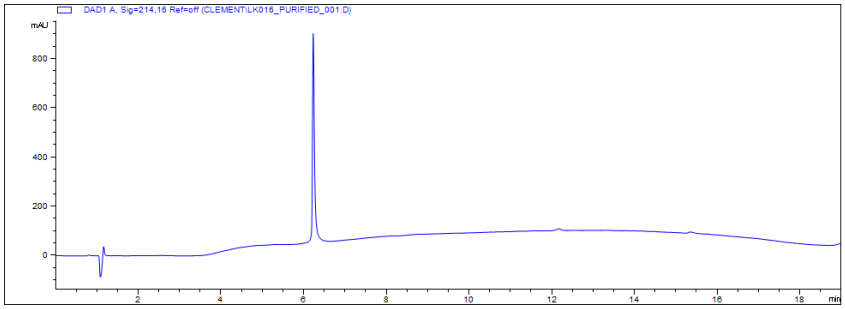

5C6 Y8y Ac-ASSSR[CTySHWC]SH-$CONH_2$, $C_{68}H_{95}N_{23}O_{22}S_2$, M_W = 1650.77 g/mol, M_{exact} = 1649.65 Da. ESI-MS: calculated: 825.84 $[M+2H]^{2+}$, 550.89 $[M+3H]^{3+}$, found: 825.75 $[M+2H]^{2+}$, 551.08 $[M+3H]^{3+}$; HPLC: t_R = 6.4947 min.

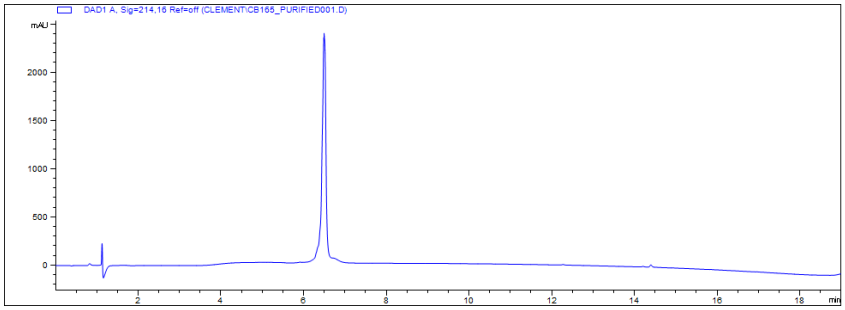

5C6 S9F. Ac-ASSSR[CTYFHWC]SH-$CONH_2$, $C_{74}H_{99}N_{23}O_{21}S_2$, M_W = 1710.87 g/mol, M_{exact} = 1709.68 Da. ESI-MS: calculated: 1711.88 $[M+H]^+$, 856.45 $[M+2H]^{2+}$, found: 1711.32 $[M+H]^+$, 855.81 $[M+2H]^{2+}$; HPLC: t_R = 6.714 min.

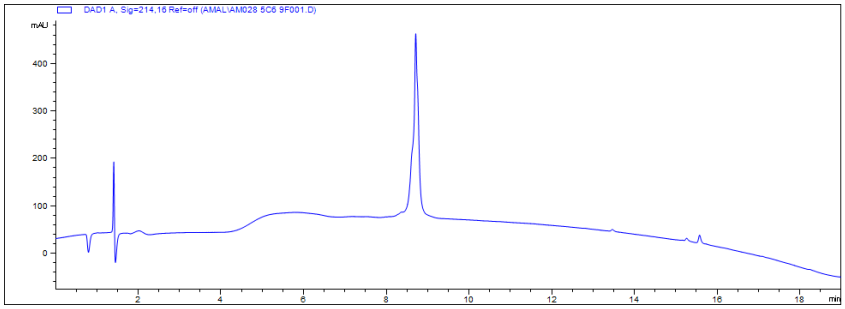

5C6 S9D. Ac-ASSSR[CTYDHWC]SH-$CONH_2$, $C_{69}H_{95}N_{23}O_{23}S_2$, M_W = 1678.78 g/mol, M_{exact} = 1677.64 Da. ESI-MS: calculated: 1678.65 $[M+H]^+$, 839.83 $[M+2H]^{2+}$, found: 1678.35 $[M+H]^+$, 839.89 $[M+2H]^{2+}$; HPLC: t_R = 6.688 min.

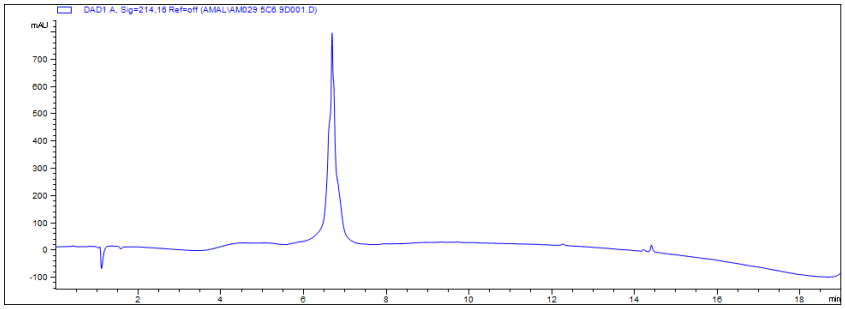

5C6 S9(abu). Ac-ASSSR[CTY(abu)HWC]SH-$CONH_2$, $C_{69}H_{97}N_{23}O_{21}S_2$, M_W = 1648.80 g/mol, M_{exact} = 1647.67 Da. ESI-MS: calculated: 1648.68 $[M+H]^+$, 824.85 $[M+2H]^{2+}$, found: 1648.51 $[M+H]^+$, 824.87 $[M+2H]^{2+}$; HPLC: t_R = 7.205 min.

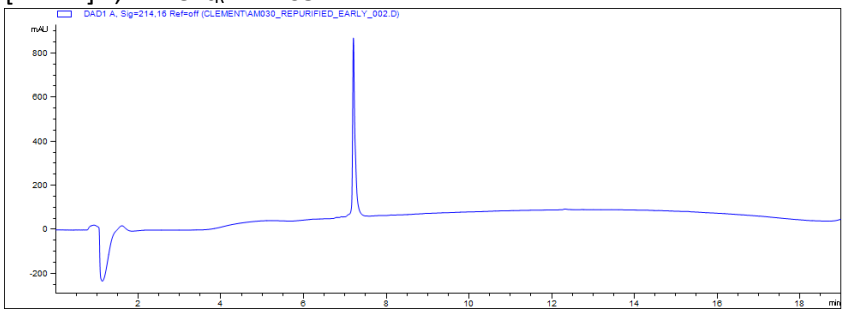

5C6 S9(orn). Ac-ASSSR[CTY(orn)HWC]SH-$CONH_2$, $C_{70}H_{100}N_{24}O_{21}S_2$, M_W = 1677.84 g/mol, M_{exact} = 1676.69 Da. ESI-MS: calculated: 1676.69 $[M+H]^+$, 839.36 $[M+2H]^{2+}$, found: 1677.40 $[M+H]^+$, 839.28 $[M+2H]^{2+}$; HPLC: t_R = 6.409 min.

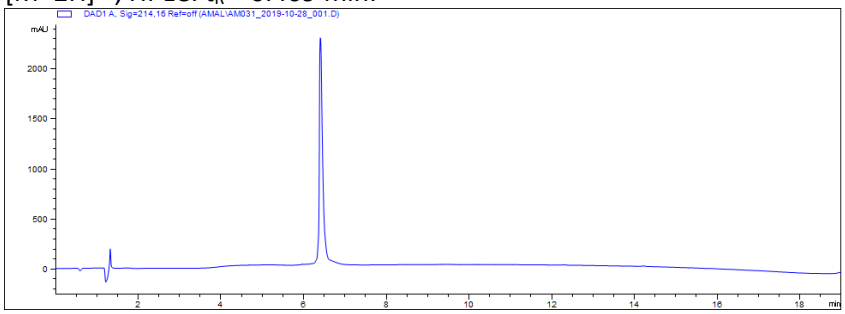

5C6 S9N. Ac-ASSSR[CTYNHWC]SH-$CONH_2$, $C_{69}H_{96}N_{24}O_{22}S_2$, M_W = 1677.79 g/mol, M_{exact} = 1677.66 Da. ESI-MS: calculated: 1676.67 $[M+H]^+$, 839.34 $[M+2H]^{2+}$, found: 1677.67 $[M+H]^+$, 839.21 $[M+2H]^{2+}$; HPLC: t_R = 6.832 min.

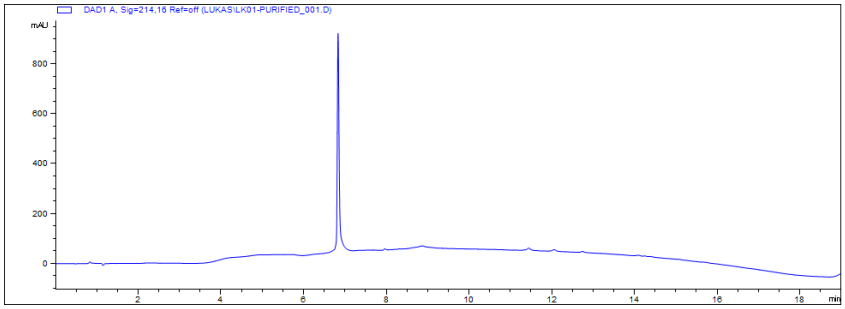

5C6 S9T. Ac-ASSSR[CTYTHWC]SH-$CONH_2$, $C_{69}H_{97}N_{23}O_{22}S_2$, M_W = 1664.79 g/mol, M_{exact} = 1663.66 Da. ESI-MS: calculated: 1664.67 $[M+H]^+$, 832.84 $[M+2H]^{2+}$, found: 1665.17 $[M+H]^+$, 832.75 $[M+2H]^{2+}$; HPLC: t_R = 6.923 min.

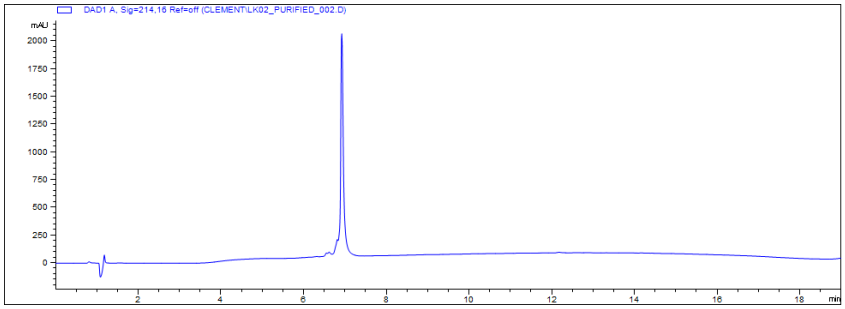

5C6 S9(dapa). Ac-ASSSR[CTY(dapa)HWC]SH-$CONH_2$, $C_{68}H_{96}N_{24}O_{21}S_2$, M_W = 1649.78 g/mol, M_{exact} = 1648.66 Da. ESI-MS: calculated: 1649.67 $[M+H]^+$, 825.34 $[M+2H]^{2+}$, found: 16450.01 $[M+H]^+$, 825.21 $[M+2H]^{2+}$; HPLC: t_R = 6.234 min.

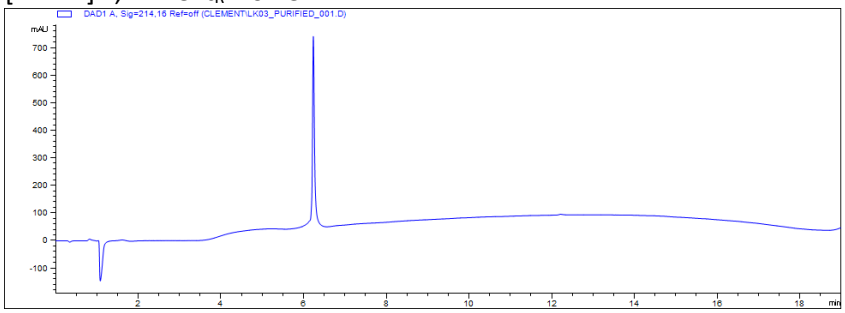

5C6 S9Q. Ac-ASSSR[CTYQHWC]SH-$CONH_2$, $C_{70}H_{98}N_{24}O_{22}S_2$, M_W = 1697.82 g/mol, M_{exact} = 1690.67 Da. ESI-MS: calculated: 1691.68 $[M+H]^+$, 846.35 $[M+2H]^{2+}$, found: 1691.20 $[M+H]^+$, 846.08 $[M+2H]^{2+}$; HPLC: t_R = 6.584 min.

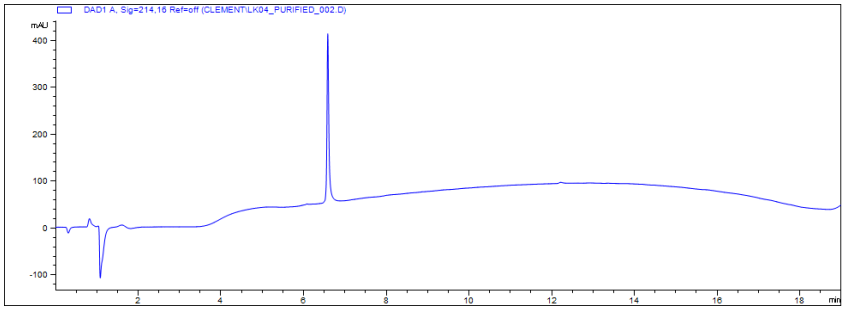

5C6 S9(hS). Ac-ASSSR[CTY(hS)HWC]SH-$CONH_2$, $C_{69}H_{97}N_{23}O_{22}S_2$, M_W = 1666.81 g/mol, M_{exact} = 1663.66 Da. ESI-MS: calculated: 1664.67 $[M+H]^+$, 832.84 $[M+2H]^{2+}$, found: 1664.24 $[M+H]^+$, 832.82 $[M+2H]^{2+}$; HPLC: t_R = 6.650 min.

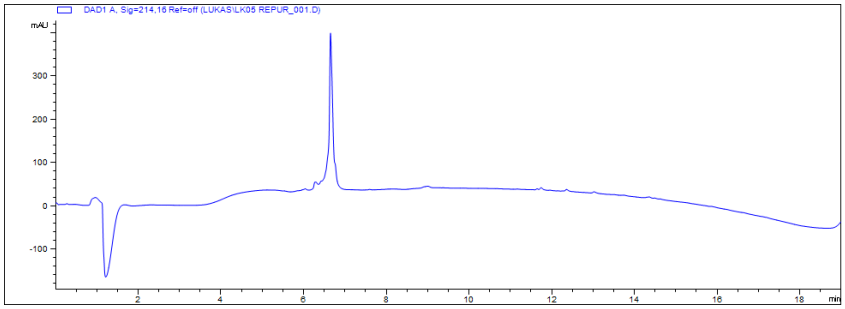

5C6 H10T. Ac-ASSSR[CTYSTWC]SH-$CONH_2$, $C_{66}H_{95}N_{21}O_{23}S_2$, M_W = 1614.73 g/mol, M_{exact} = 1613.64 Da. ESI-MS: calculated: 1614.65 $[M+H]^+$, 807.83 $[M+2H]^{2+}$, found: 1614.46 $[M+H]^+$, 807.80 $[M+2H]^{2+}$; HPLC: t_R = 6.971 min.

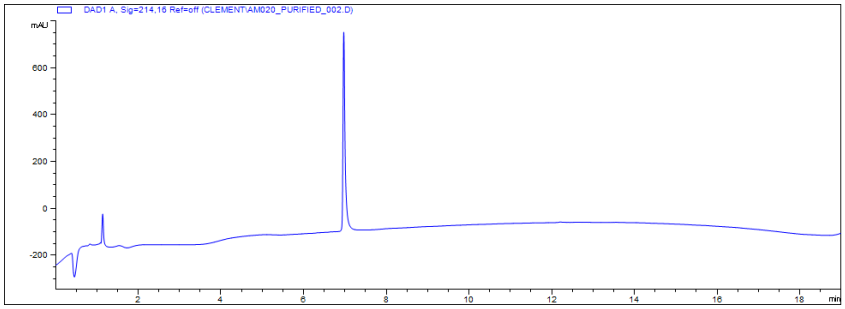

5C6 H10L. Ac-ASSSR[CTYSLWC]SH-$CONH_2$, $C_{68}H_{99}N_{21}O_{22}S_2$, M_W = 1626.79 g/mol, M_{exact} = 1625.67 Da. ESI-MS: calculated: 1626.68 $[M+H]^+$, 813.85 $[M+2H]^{2+}$, found: 1627.44 $[M+H]^+$, 813.92 $[M+2H]^{2+}$; HPLC: t_R = 8.138 min.

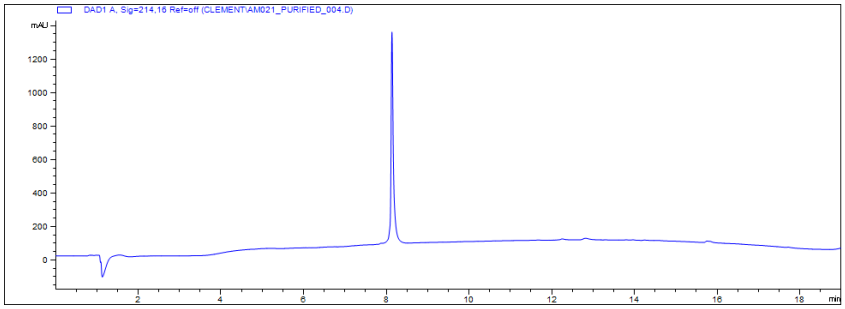

5C6 H10(orn). Ac-ASSSR[CTYS(orn)WC]SH-$CONH_2$, $C_{67}H_{98}N_{22}O_{22}S_2$, M_W = 1627.77 g/mol, M_{exact} = 1626.67 Da. ESI-MS: calculated: 1627.68 $[M+H]^+$, 814.35 $[M+2H]^{2+}$, found: 1627.55 $[M+H]^+$, 814.35 $[M+2H]^{2+}$; HPLC: t_R = 6.558 min.

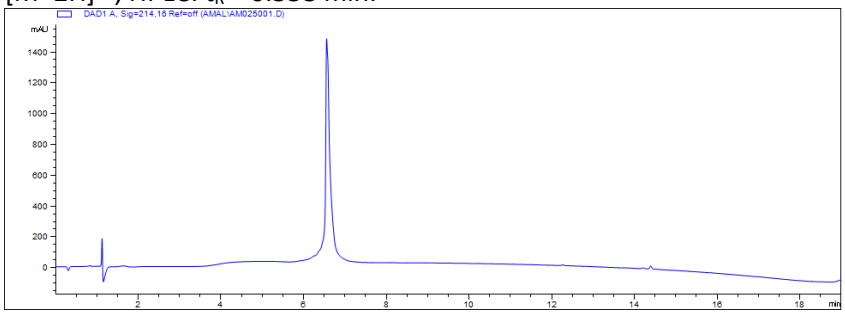

5C6 H10F. Ac-ASSSR[CTYSFWC]SH-$CONH_2$, $C_{71}H_{97}N_{21}O_{22}S_2$, M_W = 1660.80 g/mol, M_{exact} = 1659.66 Da. ESI-MS: calculated: 1660.67 $[M+H]^+$, 830.84 $[M+2H]^{2+}$, found: 1661.36 $[M+H]^+$, 830.78 $[M+2H]^{2+}$; HPLC: t_R = 7.986 min.

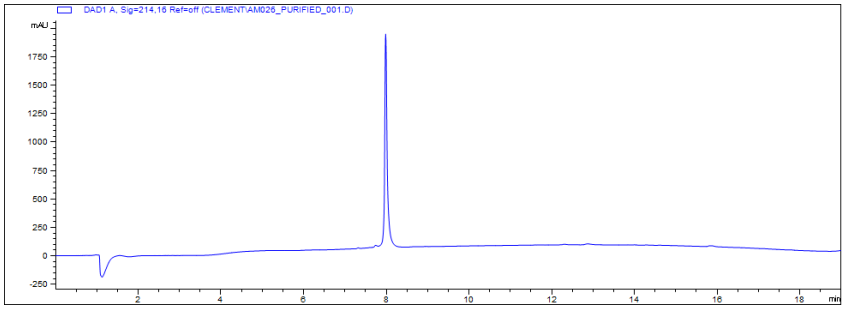

5C6 H10E. Ac-ASSSR[CTYSEWC]SH-$CONH_2$, $C_{67}H_{95}N_{21}O_{24}S_2$, M_W = 1642.74 g/mol, M_{exact} = 1641.63 Da. ESI-MS: calculated: 1642.64 $[M+H]^+$, 821.83 $[M+2H]^{2+}$, found: 1642.40 $[M+H]^+$, 821.74 $[M+2H]^{2+}$; HPLC: t_R = 7.0346 min.

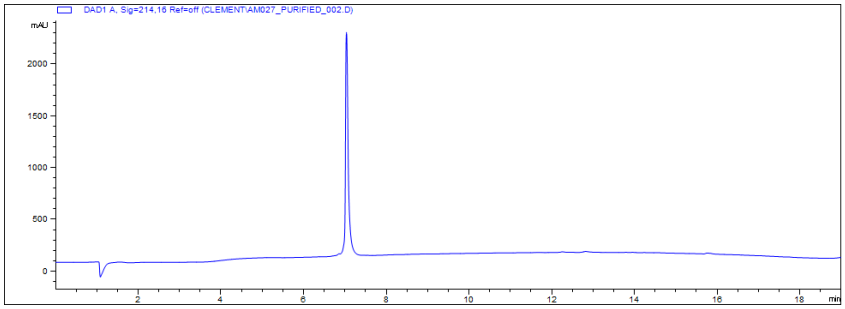

tr5C6 H10F. Ac-[CTYSFWC]SH-$CONH_2$, $C_{53}H_{65}N_{13}O_{14}S_2$, M_W = 1172.30 g/mol, M_{exact} = 1171.42 Da. ESI-MS: calculated: 1172.43 $[M+H]^+$, found: 1172.25 $[M+H]^+$; HPLC: t_R = 6.759 min.

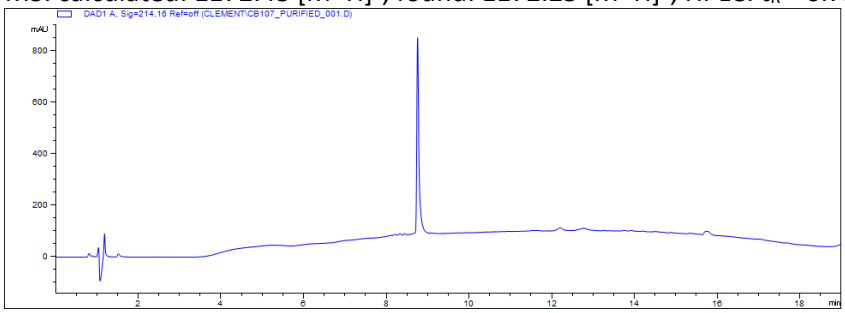

tr5C6 H10(1-MeH). Ac-[CTYS(1-MeH)WC]SH-$CONH_2$, $C_{51}H_{65}N_{15}O_{14}S_2$, M_W = 1176.29 g/mol, M_{exact} = 1175.43 Da. ESI-MS: calculated: 1175.33 $[M+H]^+$, 588.73 $[M+2H]^{2+}$, found: 1176.33 $[M+H]^+$, 588.87 $[M+2H]^{2+}$; HPLC: t_R = 7.286 min.

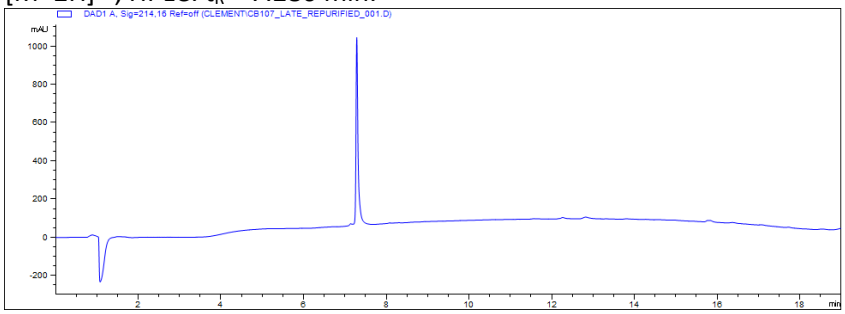

tr5C6 H10(3-MeH). Ac-[CTYS(1-MeH)WC]SH-$CONH_2$, $C_{51}H_{65}N_{15}O_{14}S_2$, M_W = 1176.29 g/mol, M_{exact} = 1175.43 Da. ESI-MS: calculated: 1175.33 $[M+H]^+$, 588.73 $[M+2H]^{2+}$, found: 1176.33 $[M+H]^+$, 588.75 $[M+2H]^{2+}$; HPLC: t_R = 7.221 min.

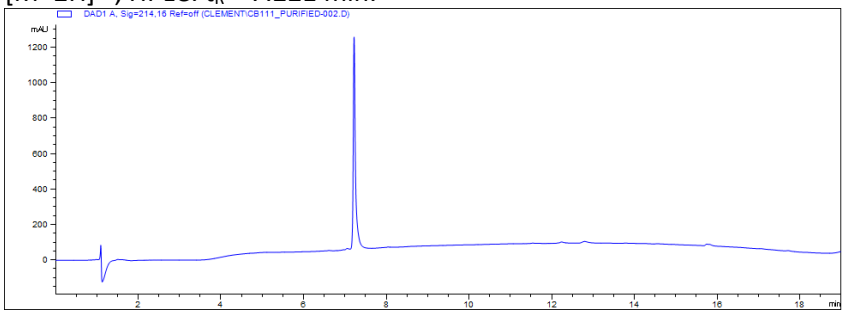

tr5C6 H10(fur). Ac-[CTYS(fur)WC]SH-$CONH_2$, $C_{51}H_{63}N_{13}O_{15}S_2$, M_W = 1162.26 g/mol, M_{exact} = 1161.40 Da. ESI-MS: calculated: 1162.41 $[M+H]^+$, 1184.39 $[M+Na]^+$, found: 1162.26 $[M+H]^+$, 1184.22 $[M+Na]^+$; HPLC: t_R = 8.444 min.

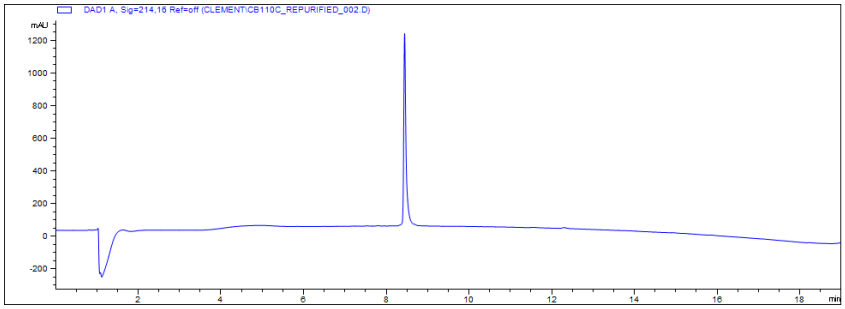

5C6 W11F. Ac-ASSSR[CTYSHFC]SH-$CONH_2$, $C_{66}H_{94}N_{22}O_{22}S_2$, M_W = 1611.73 g/mol, M_{exact} = 1610.64 Da. ESI-MS: calculated: 1611.65 $[M+H]^+$, 806.33 $[M+2H]^{2+}$, found: 1611.14 $[M+H]^+$, 806.45 $[M+2H]^{2+}$; HPLC: t_R = 6.535 min.

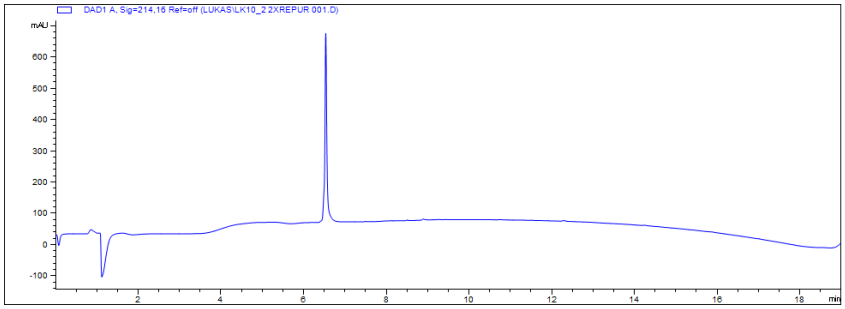

5C6 W11H. Ac-ASSSR[CTYSHHC]SH-$CONH_2$, $C_{63}H_{92}N_{24}O_{22}S_2$, M_W = 1601.70 g/mol, M_{exact} = 1600.63 Da. ESI-MS: calculated: 1601.64 $[M+H]^+$, 801.33 $[M+2H]^{2+}$, found: 1601.41 $[M+H]^+$, 801.83 $[M+2H]^{2+}$; HPLC: t_R = 5.409 min.

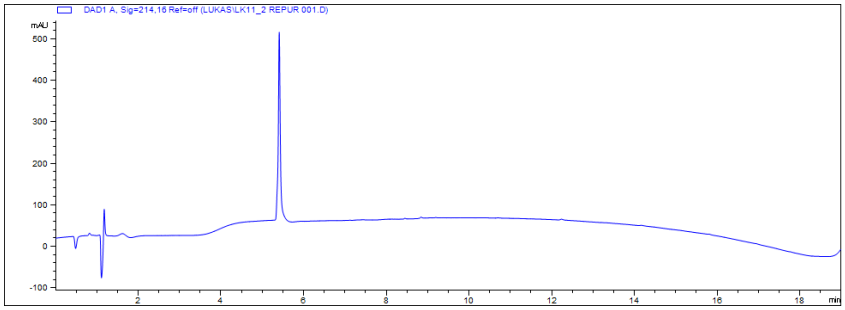

5C6 W11Y. Ac-ASSSR[CTYSHYC]SH-$CONH_2$, $C_{66}H_{94}N_{22}O_{23}S_2$, M_W = 1627.73 g/mol, M_{exact} = 1626.63 Da. ESI-MS: calculated: 1627.64 $[M+H]^+$, 814.33 $[M+2H]^{2+}$, found: 1627.28 $[M+H]^+$, 814.31 $[M+2H]^{2+}$; HPLC: t_R = 5.998 min.

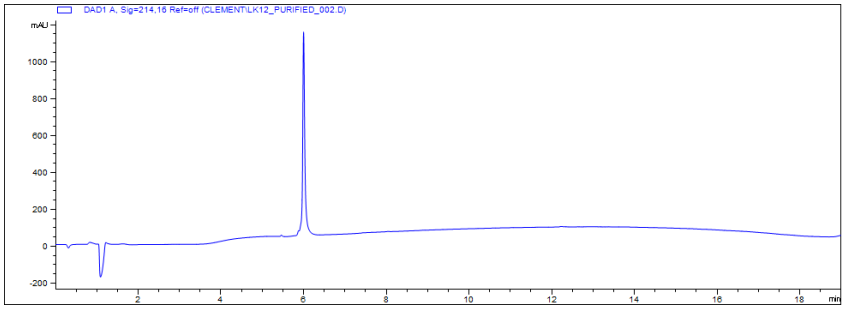

5C6 W11R. Ac-ASSSR[CTYSHRC]SH-$CONH_2$, $C_{63}H_{97}N_{25}O_{22}S_2$, M_W = 1620.74 g/mol, M_{exact} = 1619.67 Da. ESI-MS: calculated: 1620.75 $[M+H]^+$, 810.88 $[M+2H]^{2+}$, found: 1620.17 $[M+H]^+$, 810.72 $[M+2H]^{2+}$; HPLC: t_R = 5.450 min.

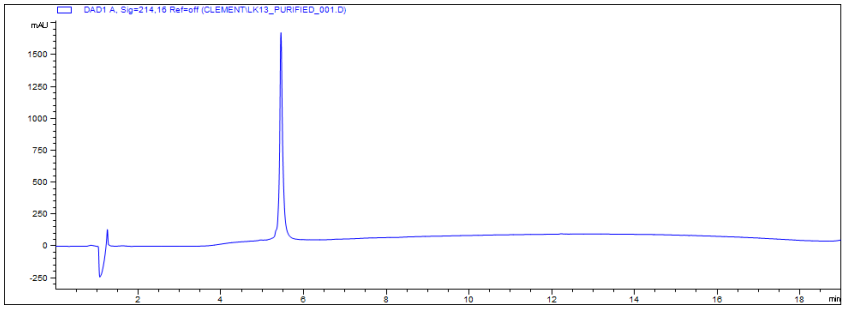

5C6 W11(MeW). Ac-ASSSR[CTYSH(MeW)C]SH-$CONH_2$, $C_{69}H_{97}N_{23}O_{22}S_2$, M_W = 1664,79 g/mol, M_{exact} = 1663.66 Da. ESI-MS: calculated: 1664.67 $[M+H]^+$, 832.84 $[M+2H]^{2+}$, found: 1664.32 $[M+H]^+$, 832.94 $[M+2H]^{2+}$; HPLC: t_R = 7.117 min.

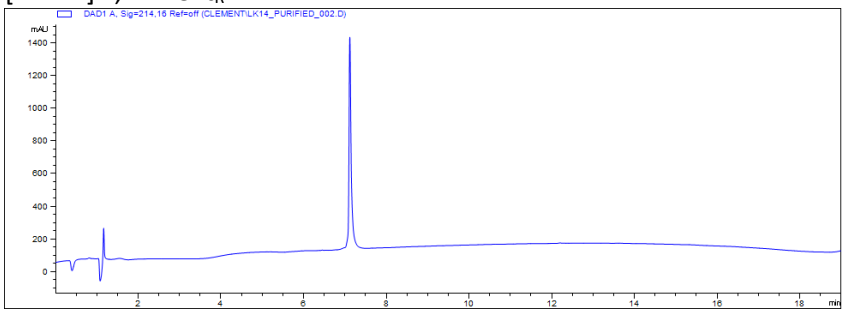

5C6 W11(NaI). Ac-ASSSR[CTYSH(NaI)C]SH-$CONH_2$, $C_{70}H_{96}N_{22}O_{22}S_2$, M_W = 1661.79 g/mol, M_{exact} = 1660.65 Da. ESI-MS: calculated: 1661.66 $[M+H]^+$, 831.34 $[M+2H]^{2+}$, found: 1661.30 $[M+H]^+$, 831.43 $[M+2H]^{2+}$; HPLC: t_R = 7.366 min.

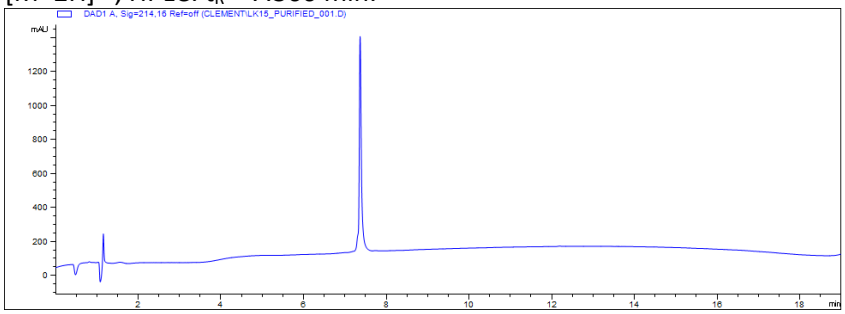

5C6 H14(orn). Ac-ASSSR[CTYSHWC]S(orn)-$CONH_2$, $C_{65}H_{94}N_{22}O_{22}S_2$, M_W = 1627.77 g/mol, M_{exact} = 1626.67 Da. ESI-MS: calculated: 1627.68 $[M+H]^+$, 814.35 $[M+2H]^{2+}$, found: 1628.60 $[M+H]^+$, 814.39 $[M+2H]^{2+}$; HPLC: t_R = 6.639 min.

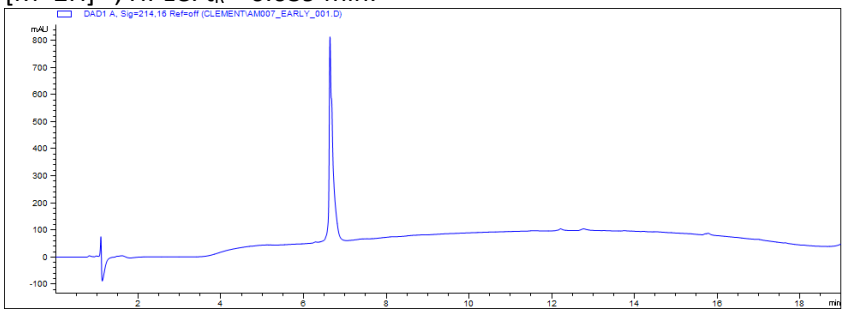

5C6 H14(dapa). Ac-ASSSR[CTYSHWC]S(dapa)-$CONH_2$, $C_{65}H_{94}N_{22}O_{22}S_2$, M_W = 1599.72 g/mol, M_{exact} = 1598.64 Da. ESI-MS: calculated: 1599.65 $[M+H]^+$, 800.33 $[M+2H]^{2+}$, found: 1599.30 $[M+H]^+$, 800.25 $[M+2H]^{2+}$; HPLC: t_R = 7.366 min.

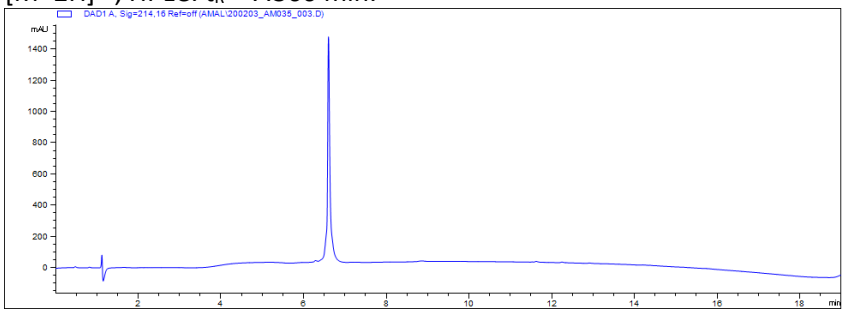

5C6 H14F. Ac-ASSSR[CTYSHWC]SF-$CONH_2$, $C_{71}H_{97}N_{21}O_{22}S_2$, M_W = 1660.80 g/mol, M_{exact} = 159.66 Da. ESI-MS: calculated: 1661.66 $[M+H]^+$, 830.84 $[M+2H]^{2+}$, found: 1661.43 $[M+H]^+$, 830.85 $[M+2H]^{2+}$; HPLC: t_R = 7.921 min.

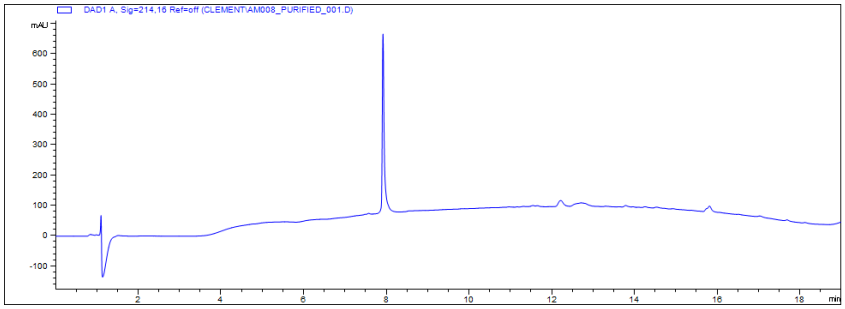

5C6 H14(pyr). Ac-ASSSR[CTYSHWC]S(pyr)-$CONH_2$, $C_{70}H_{96}N_{22}O_{22}S_2$, M_W = 1661.79 g/mol, M_{exact} = 1660.65 Da. ESI-MS: calculated: 1661.66 $[M+H]^+$, 831.34 $[M+2H]^{2+}$, found: 1662.24 $[M+H]^+$, 831.26 $[M+2H]^{2+}$; HPLC: t_R = 7.578 min.

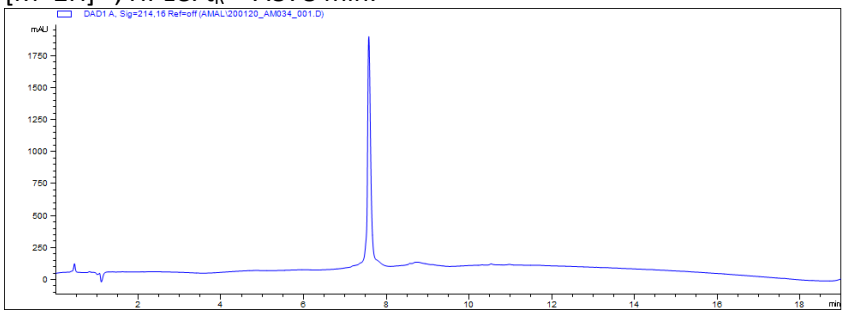

5C6 H14(triA) (21). Ac-ASSSR[CTYSHWC]S(triA)-$CONH_2$, $C_{67}H_{94}N_{24}O_{22}S_2$, M_W = 1651.76 g/mol, M_{exact} = 1650.24 Da. Ac-ASSSR[CTYSHWC]S(prG)-$CONH_2$ (prG = (*S*)-propargyl glycine)) was synthesized using the standards SPPS and cleavage conditions, followed by disulfide formation with H_2O_2. The resulting crude product (20.0 mg, $1.24 \cdot 10^{-5}$ mol) was dissolved to 1.0 mM in H_2O/*t*BuOH (1/1) and $CuSO_4 \cdot H_2O$ ($0.62 \cdot 10^{-5}$ mol, 0.5 eq.), Tris(3-hydroxypropyltriazolylmethyl)amine (THTPA, $0.62 \cdot 10^{-5}$ mol, 0.5 eq) and sodium ascorbate ($1.24 \cdot 10^{-5}$ mol, 1 eq.) added as aqueous solutions. Finally, TMS-N_3 was added ($3.73 \cdot 10^{-5}$ mol, 1.7 µL, 3.0 eq.) upon which the solution turned yellow and then quickly bright green. The reaction mixture was stirred at rt while monitoring by MS. After 7 h, the reaction mixture was diluted with H_2O and lyophilized, and yielded 5.46 mg ($0.33 \cdot 10^{-5}$ mol, 26.6%) of the desired product after purification. ESI-MS: calculated: 1651.65 $[M+H]^+$, 826.33 $[M+2H]^{2+}$, found: 1651.23 $[M+H]^+$, 826.23 $[M+2H]^{2+}$; HPLC: t_R = 6.818 min.

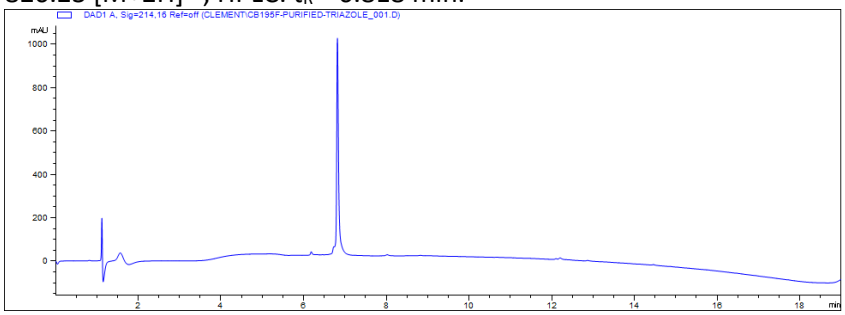

5C6 H14(3-MeH). Ac-ASSSR[CTYSHWC]S(3-MeH)-$CONH_2$, $C_{69}H_{97}N_{23}O_{22}S_2$, M_W = 1664.79 g/mol, M_{exact} = 1663.66 Da. ESI-MS: calculated: 1664.67 $[M+H]^+$, 832.84 $[M+2H]^{2+}$, found: 832.82 $[M+2H]^{2+}$; HPLC: t_R = 7.921 min.

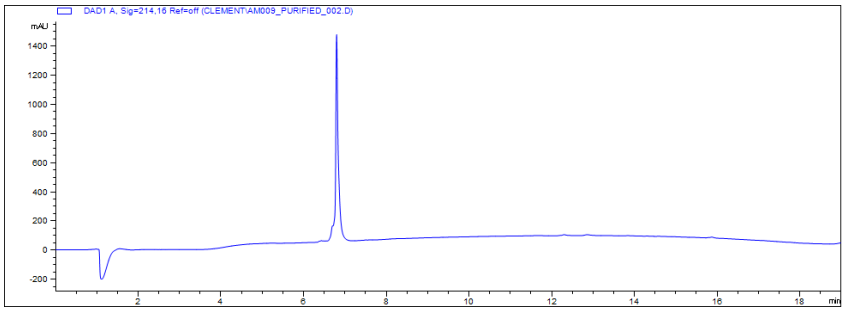

5C6 H14(1-MeH). Ac-ASSSR[CTYSHWC]S(1-MeH)-$CONH_2$, $C_{69}H_{97}N_{23}O_{22}S_2$, M_W = 1664.79 g/mol, M_{exact} = 1663.66 Da. ESI-MS: calculated: 1664.67 $[M+H]^+$, 832.84 $[M+2H]^{2+}$, found: 1664.49 $[M+H]^+$, 832.82 $[M+2H]^{2+}$; HPLC: t_R = 6.836 min.

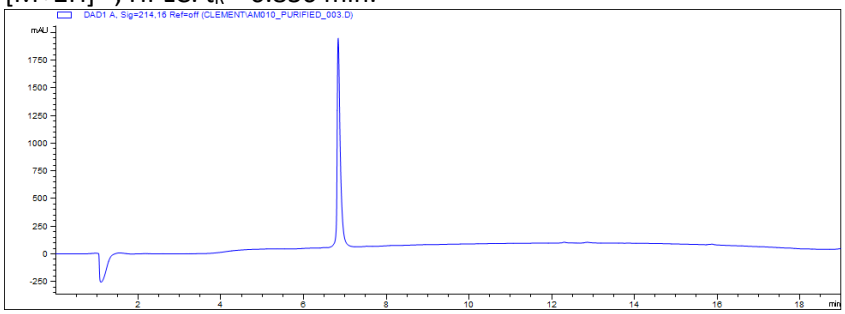

5C6 H14h. Ac-ASSSR[CTYSHWC]Sh-$CONH_2$, $C_{68}H_{95}N_{23}O_{22}S_2$, M_W = 1650.77 g/mol, M_{exact} = 1649.65 Da. ESI-MS: calculated: 1650.66 $[M+H]^+$, 825.84 $[M+2H]^{2+}$, 550.89 $[M+3H]^{3+}$, found: 1651.16 $[M+H]^+$, 825.89 $[M+2H]^{2+}$, 550.94 $[M+3H]^{3+}$; HPLC: t_R = 6.714 min.

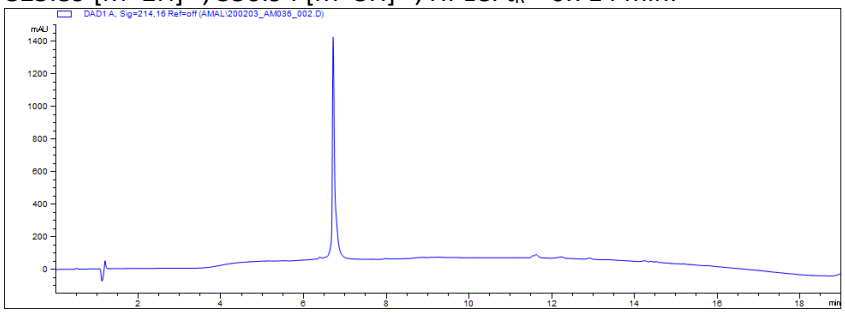

5C6 +15V. Ac-ASSSR[CTYSHWC]SHV-$CONH_2$, $C_{73}H_{104}N_{24}O_{23}S_2$, M_W = 1749.90 g/mol, M_{exact} = 1748.74 Da. ESI-MS: calculated: 1749.75 $[M+H]^+$, 875.38 $[M+2H]^{2+}$, found: 1749.51 $[M+H]^+$, 815.32 $[M+2H]^{2+}$; HPLC: t_R = 7.339 min.

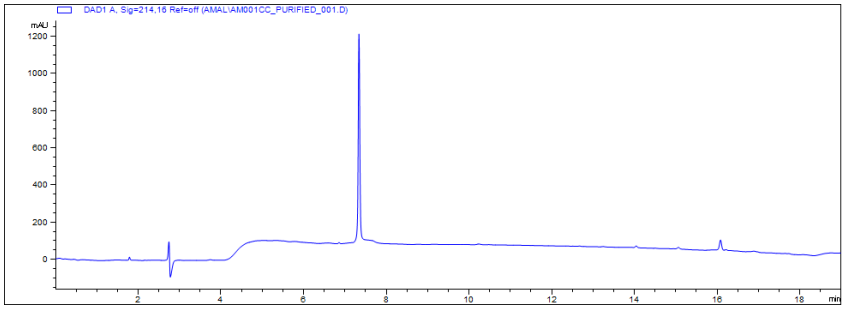

5C6 +15S. Ac-ASSSR[CTYSHWC]SHS-$CONH_2$, $C_{71}H_{100}N_{24}O_{24}S_2$, M_W = 1737.85 g/mol, M_{exact} = 1736.68 Da. ESI-MS: calculated: 1737.69 $[M+H]^+$, 868.35 $[M+2H]^{2+}$, found: 1738.30 $[M+H]^+$, 869.34 $[M+2H]^{2+}$; HPLC: t_R = 6.648 min.

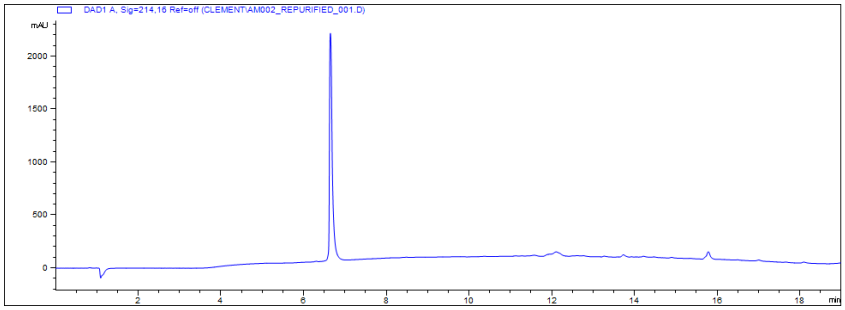

5C6 +15K. Ac-ASSSR[CTYSHWC]SHV-$CONH_2$, $C_{74}H_{174}N_{25}O_{23}S_2$, M_W = 1778.94 g/mol, M_{exact} = 1777.74 Da. ESI-MS: calculated: 1778.75 $[M+H]^+$, 889.88 $[M+2H]^{2+}$, found: 1779.15 $[M+H]^+$, 889.81 $[M+2H]^{2+}$; HPLC: t_R = 6.591 min.

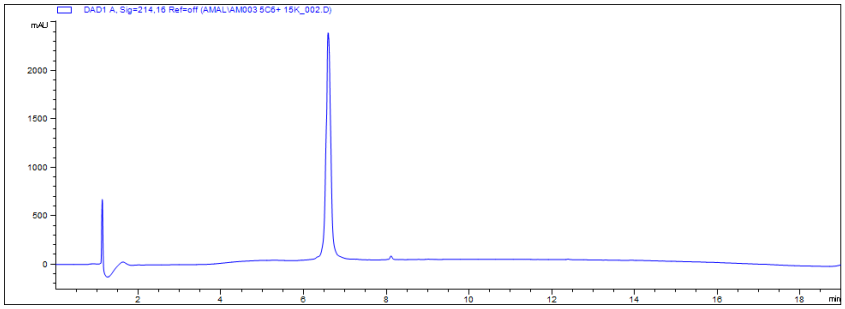

5C6 +15D. Ac-ASSSR[CTYSHWC]SHV-$CONH_2$, $C_{72}H_{100}N_{24}O_{25}S_2$, M_W = 1765.86 g/mol, M_{exact} = 1764.67 Da. ESI-MS: calculated: 1765.68 $[M+H]^+$, 883.35 $[M+2H]^{2+}$, found: 1766.23 $[M+H]^+$, 883.21 $[M+2H]^{2+}$; HPLC: t_R = 6.837 min.

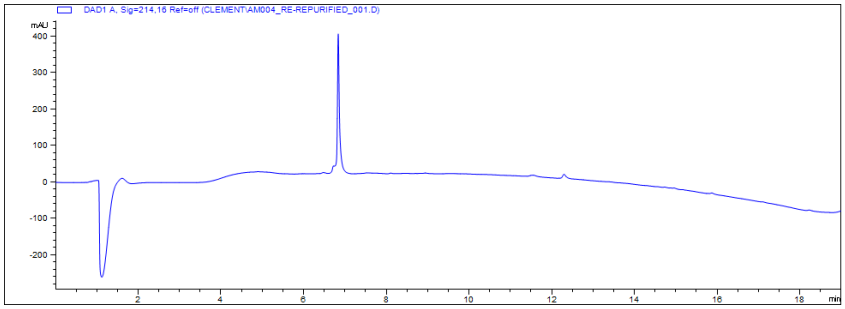

5C6 +15F. Ac-ASSSR[CTYSHWC]SHV-$CONH_2$, $C_{77}H_{104}N_{24}O_{23}S_2$, M_W = 1797.94 g/mol, M_{exact} = 1796.71 Da. ESI-MS: calculated: 1797.72 $[M+H]^+$, 899.37 $[M+2H]^{2+}$, found: 1797.36 $[M+H]^+$, 899.53 $[M+2H]^{2+}$; HPLC: t_R = 7.570 min.

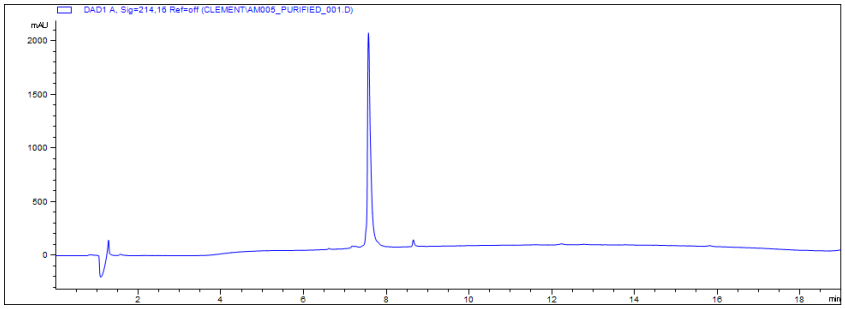

5C6 +15(pyr). Ac-ASSSR[CTYSHWC]SH(pyr)-$CONH_2$, $C_{76}H_{103}N_{25}O_{23}S_2$, M_W = 1798.93 g/mol, M_{exact} = 1797.71 Da. ESI-MS: calculated: 1798.72 $[M+H]^+$, 899.87 $[M+2H]^{2+}$, found: 1799.33 $[M+H]^+$, 899.81 $[M+2H]^{2+}$; HPLC: t_R = 6.527 min..

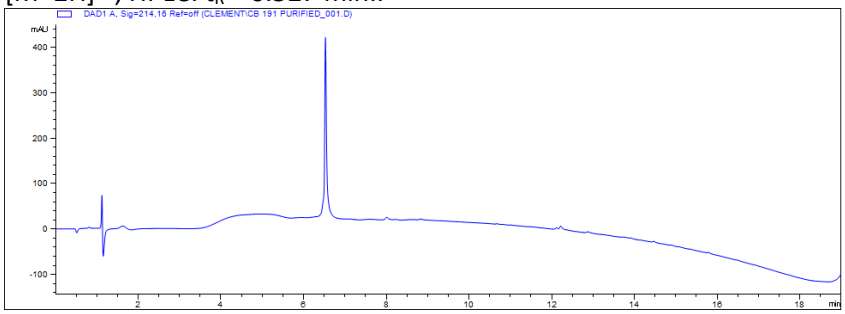

tr5C6 C6(hC). Ac-[(hC)TYSHWC]SH-$CONH_2$, $C_{51}H_{65}N_{15}O_{14}S_2$, M_W = 1176.29 g/mol, M_{exact} = 1175.43 Da. ESI-MS: calculated: 1176.43 $[M+H]^+$, 588.72 $[M+2H]^{2+}$, found: 1176.40 $[M+H]^+$, 588.75 $[M+2H]^{2+}$; HPLC: t_R = 7.254 min.

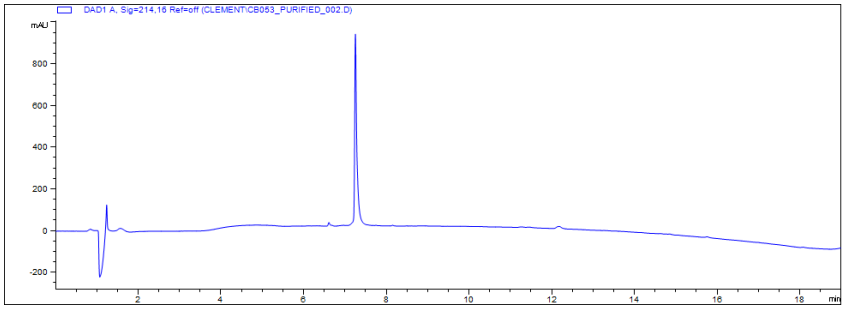

tr5C6 C6(hC) C12(hC). Ac-[(hC)TYSHW(hC)]SH-$CONH_2$, $C_{52}H_{67}N_{15}O_{14}S_2$, M_W = 1190.32 g/mol, M_{exact} = 1189.44 Da. ESI-MS: calculated: 1190.45 $[M+H]^+$, 595.73 $[M+2H]^{2+}$, found: 1190.34 $[M+H]^+$, 595.69 $[M+2H]^{2+}$; HPLC: t_R = 12.270 min.

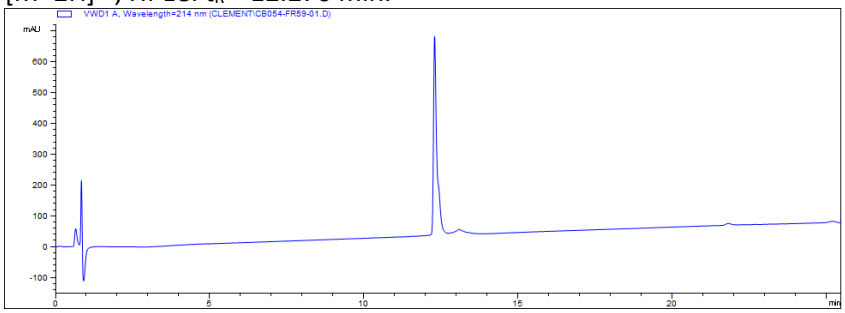

tr5C6 C6(tpa) C12(hC). Ac-[(tpa)TYSHW(hC)]SH-$CONH_2$, $C_{53}H_{69}N_{15}O_{14}S_2$, M_W = 1204.35 g/mol, M_{exact} = 1203.46 Da. ESI-MS: calculated: 602.74 $[M+2H]^{2+}$, found: 602.83 $[M+2H]^{2+}$; HPLC: t_R = 7.574 min.

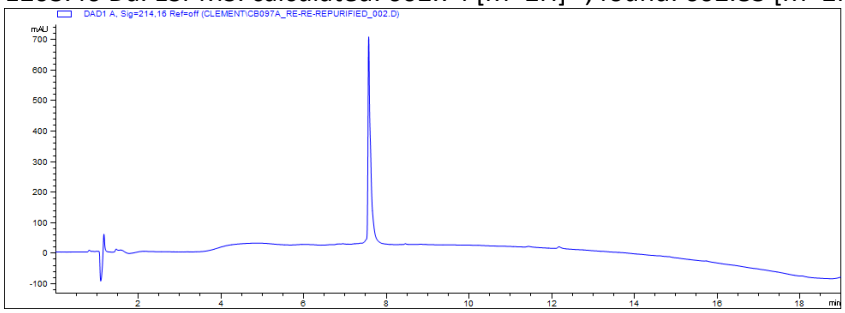

tr5C6 C6(tpa) C12(tpa). Ac-[(tpa)TYSHW(tpa)]SH-$CONH_2$, $C_{54}H_{71}N_{15}O_{14}S_2$, M_W = 1218.37 g/mol, M_{exact} = 1217.47 Da. ESI-MS: calculated: 609.72 $[M+2H]^{2+}$, found: 609.79$[M+2H]^{2+}$; HPLC: t_R = 7.896 min.

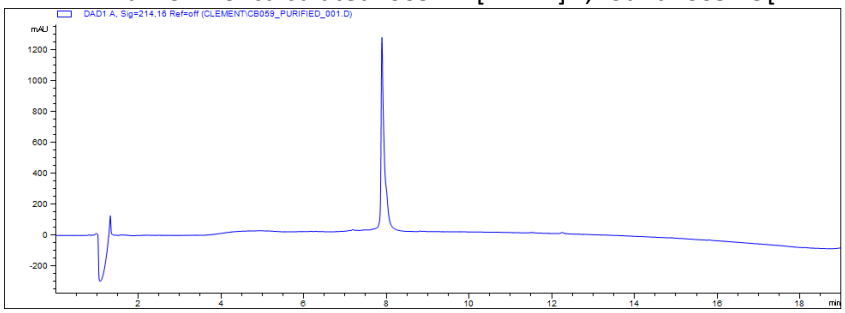

tr5C6 C6(mpa) (28). [(mpa)TYSHWC]SH-$CONH_2$, $C_{48}H_{60}N_{14}O_{13}S_2$, M_W = 1105.21 g/mol, M_{exact} = 1104.39 Da. The peptide was first assembled on a 0.1 mmol scale using the standard SPPS conditions with unprotected 3-mercaptopropionic acid (mpa) as building block, followed by the standard cleavage conditions. As substantial amounts of disulfide bridged Ac-(mpa-mpa)TYSHWCSH-$CONH_2$ (approx. 1:2 of side product:desired product) after cleavage, the peptide was treated with 4 eq. Tris(2-carboxyethyl)phosphine hydrochloride (TCEP) in 1 mL DMF for 100 min. After completion of the reaction, the solvent was removed under reduced pressure and the peptide cyclized using the standard cyclization conditions with H_2O_2 and purified to yield 8.91 mg ($8.06 \cdot 10^{-6}$ mol, yield over all steps after purification: 8.1%) of Ac-[(mpa)TYSHWC]SH-$CONH_2$.ESI-MS: calculated: 1091.38 $[M+H]^+$, 546.20 $[M+2H]^{2+}$, found: 1091.28 $[M+H]^+$, 546.18 $[M+2H]^{2+}$; HPLC: t_R = 11.719 min

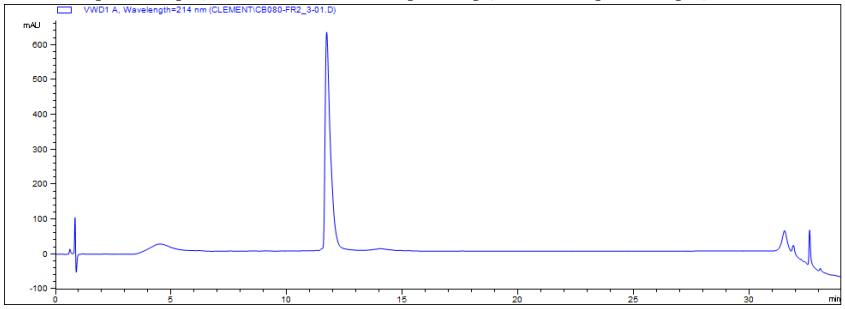

tr5C6 C6(tga). [(tga)TYSHWC]SH-$CONH_2$, $C_{47}H_{58}N_{14}O_{13}S_2$, M_W = 1091.19 g/mol, M_{exact} = 1090.37 Da. The peptide was first assembled on a 0.1 mmol scale using the standard SPPS conditions with unprotected thioglycolic acid (tga) as building block, with a double coupling at 50 °C for 10 min for tga. Preliminary work showed that there is substantial formation of disulfide-bridged Ac-(tga-tga)TYSHWCSH-$CONH_2$ after cleavage from the solid phase. Therefore, the peptide was treated on-resin with 4 eq. (0.4 mmol, 114.7 mg) TCEP in 5 mL DMF for 4 h at rt, followed by the standard cleavage, cyclization with H_2O_2 conditions and purification to yield 5.82 mg ($5.32 \cdot 10^{-6}$ mol, yield over all steps after purification: 5.3%) of Ac-[(tga)TYSHWC]SH-$CONH_2$. ESI-MS: calculated: 1091.38 $[M+H]^+$, 546.20 $[M+2H]^{2+}$, found: 1091.28 $[M+H]^+$, 546.18 $[M+2H]^{2+}$; HPLC: t_R = 7.491 min.

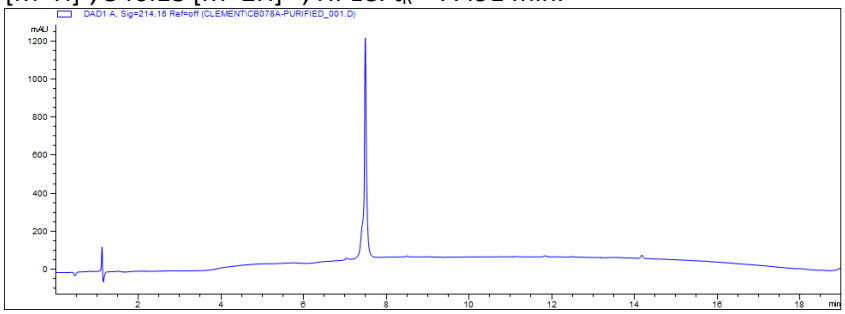

tr5C6 C6(Sec) C12(Sec) (30) Ac-[(Sec)TYSHW(Sec)]SH-$CONH_2$, $C_{50}H_{63}N_{15}O_{14}Se_2$, M_W = 1256.09 g/mol, M_{exact} = 1257.30 Da. The peptide was first assembled on a 0.05 mmol scale using the standard SPPS conditions with *N*-Fmoc-protected, side chain 4-methoxybenzyl (mob) L-selenocysteine (Sec) as building block. Fmoc-Sec(mob)-OH was coupled using 4.2 eq of it, distributed over two coupling cycles at 6 min for each position. After SPPS, cleavage from the solid phase with simultaneous side-chain deprotection and cyclization was achieved with 12 mL of a triethylsilane (TES), thioanisole, TFA cocktail (2.5:2.5:95.0, V:V:V) at 40 °C for 4 h. Additional to MS analysis, the successful cyclization was also verified by reacting a part of the product with H_2O_2 or TCEP, upon which no shift or a shift of 2 units in the MS spectrum, respectively, was achieved. After purification, 0.98 mg ($7.8 \cdot 10^{-7}$ mol, 1.6% yield) of the desired product were obtained. ESI-MS: calculated: 1258.31 $[M+H]^+$, found: 1257.99 $[M+H]^+$; HPLC: t_R = 6.362 min.

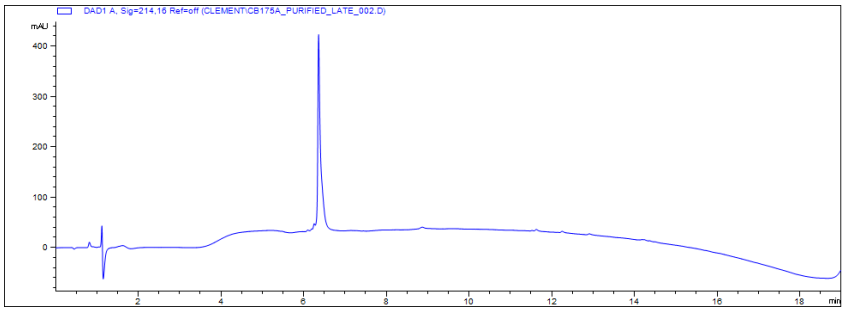

tr5C6 cyc-S (31). Ac-[CTYSHW(C-S)]SH-$CONH_2$, $C_{50}H_{63}N_{15}O_{14}S$, M_W = 1130.21 g/mol, M_{exact} = 1129.44 Da. tr5C6 (Ac-[CTYSHWC]SH-$CONH_2$) was synthesized using the standard SPPS, cleavage and disulfide formation with H_2O_2 conditions. For the desulfurization, the method described by Bernardes et al. (Bernardes et al. ACIE 2008) was used. The crude peptide (63.9 mg, $5.5 \cdot 10^{-5}$ mol) was dissolved in 11.1 mL dried and degassed MeOH, to which 3 eq. ($16.6 \cdot 10^{-5}$ mol, 30.2 µL) of hexamethylphophorous triamide (HMPT) was added. The reaction mixture was stirred at rt for 3 h under Ar and monitored by MS. The solvent was removed under reduced pressure and the crude material purified by LCMS upon which 1.36 mg ($1.2 \cdot 10^{-6}$ mol, 2.2% yield) of the desired product were obtained. ESI-MS: calculated: 1130.44 $[M+H]^+$, found: 1130.53 $[M+H]^+$; HPLC: t_R = 6.884 min.

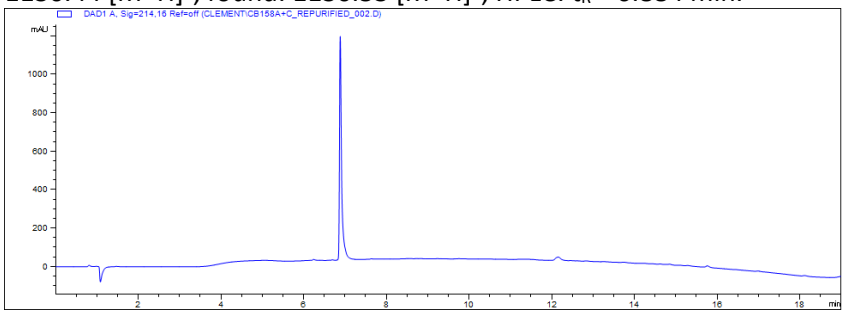

tr5C6 C6(tga) cyc-S (32). Ac-[(tga)TYSHW(C-S)]SH-$CONH_2$, $C_{47}H_{58}N_{14}O_{13}S$, M_W = 1059.13 g/mol, M_{exact} = 1058.40 Da. tr5C6 C6(tga) ([(tga)TYSHWC]SH-$CONH_2$) was synthesized as described above. For the desulfurization, the method described by Bernardes et al. (Bernardes et al. ACIE 2008) was used. The crude peptide (96.1 mg, $9.1 \cdot 10^{-5}$ mol) was dissolved in 18.2 mL dried and degassed MeOH, to which 3 eq. ($27.2 \cdot 10^{-5}$ mol, 49.5 µL) of hexamethylphophorous triamide (HMPT) was added. The reaction mixture was stirred at rt for 3 h under Ar and monitored by MS. The solvent was removed under reduced pressure and the crude material purified by LCMS upon which 0.51 mg ($4.8 \cdot 10^{-7}$ mol, 0.5% yield) of the desired product were obtained. ESI-MS: calculated: 1059.41 $[M+H]^+$, found: 1059.39 $[M+H]^+$; HPLC: t_R = 6.908 min.

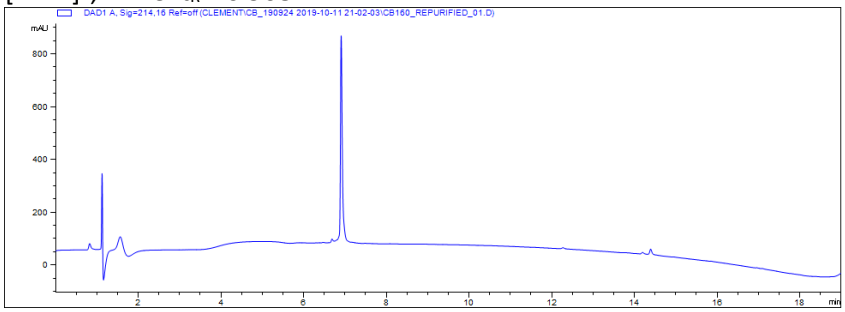

tr5C6 cyc+CH_2 (33). Ac-[CTYSHW(C+CH_2)]SH-$CONH_2$, $C_{50}H_{63}N_{15}O_{14}S_2$, M_W = 1176.29 g/mol, M_{exact} = 1175.43 Da. tr5C6 (Ac-[CTYSHWC]SH-$CONH_2$) was synthesized using the standard SPPS, cleavage and disulfide formation with H_2O_2 conditions as described above and the thioacetal was formed using the procedure reported by Kourra and Cramer (Kourra, Cramer, Chem. Sci. 2016). 30 mg ($2.6 \cdot 10^{-5}$ mol) of the crude peptide were dissolved in 5.2 mL H_2O/THF (5/1) and consequently a total of 10 eq. of NEt_3 ($25.8 \cdot 10^{-5}$ mol, 36.0 µL) and a total of 8 eq. of CH_2I_2 ($20.6 \cdot 10^{-5}$ mol, 16.6 µL) were added, distributed over two times with the second addition of reagents after 22 h reaction time. The reaction was stirred for a total of 27 h at room temperature and monitored by MS. Upon completion of the reaction, THF was removed under reduced pressure and the remaining solution lyophilized. After purification by LCMS, 5.6 mg ($0.48 \cdot 10^{-5}$ mol, 18.5% yield) of tr5C6 cyc+CH_2 were obtained. ESI-MS: calculated: 1176.44 $[M+H]^+$, found: 1176.33 $[M+H]^+$; HPLC: t_R = 7.046 min.

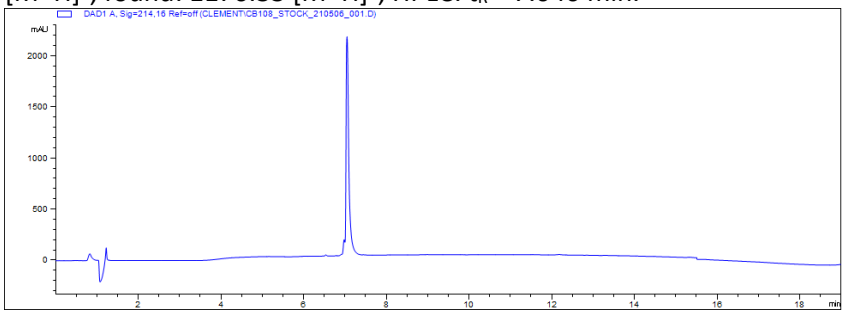

tr5C6 C6(tga) cyc+CH_2 (34). [(tga)TYSHW(C+CH_2)]SH-$CONH_2$, $C_{48}H_{60}N_{14}O_{13}S_2$, M_W = 1105.21 g/mol, M_{exact} = 1104.39 Da. tr5C6 C6(tga) ([(tga)TYSHWC]SH-$CONH_2$) was synthesized as described above, and the thioacetal was formed using the procedure reported by Kourra and Cramer (Kourra, Cramer, Chem. Sci. 2016). 55 mg ($5.1 \cdot 10^{-5}$ mol) of the crude peptide were dissolved in 10.0 mL H_2O/THF (5/1) and consequently 9 eq. of NEt_3 ($46.1 \cdot 10^{-5}$ mol, 64.2 µL) and 6 eq. of CH_2I_2 ($30.7 \cdot 10^{-5}$ mol, 24.7 µL) were added. The reaction was stirred at rt and monitored by MS. Upon completion of the reaction after 2 h, THF was removed under reduced pressure and the remaining solution lyophilized. After purification by LCMS, 9.2 mg ($0.88 \cdot 10^{-5}$ mol, 17.2% yield) of tr5C6 C6(tga) cyc+CH_2 were obtained. ESI-MS: calculated: 1105.40 $[M+H]^+$, found: 1105.35$[M+H]^+$; HPLC: t_R = 7.054 min.

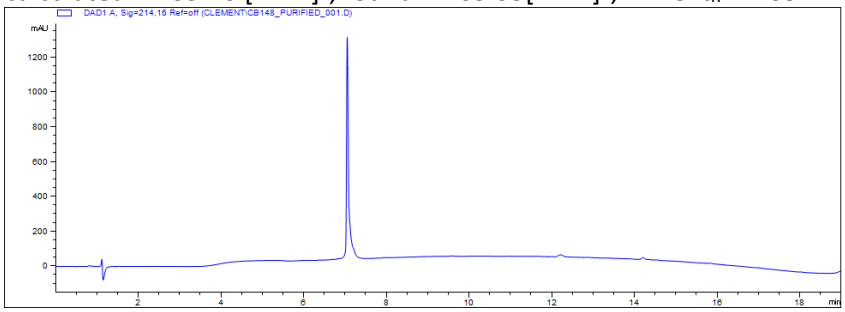

tr5C6 C6(ba) C12D (37). [(ba)TYSHWD]SH-$CONH_2$, $C_{49}H_{61}N_{15}O_{14}$, M_W = 1083.15 g/mol, M_{exact} = 1084.12 Da. The peptide was first assembled on a 0.1 mmol scale using the standard SPPS and cleavage conditions with *N*-Fmoc-protected β-alanine (ba) as building block. Following cleavage from the solid phase, the macrolactam was formed from 45 mg ($4.1 \cdot 10^{-5}$ mol) of the crude linear peptide with 2 eq. ($8.2 \cdot 10^{-5}$ mol, 38 mg) Bromotripyrrolidinophosphonium hexafluorophosphate (PyBroP) and 4 eq. ($16.3 \cdot 10^{-5}$ mol, 28.4 µL) *N*,*N*-Diisopropylethylamine (DIPEA). The linear peptide was dissolved in 41 mL dry DMF, DIPEA and then PyBroP added dropwise on ice. The reaction mixture was allowed to slowly warm up to rt and stirred until no further rection occurred, assed by MS. After 24 h, the solvent volume was reduced under reduced pressure, H_2O added to the mixture and lyophilized. The mixture was purified and yielded 3.2 mg ($0.30 \cdot 10^{-5}$ mol, yield: 7.3%) of the desired product. The absence of a free amine was verified by Kaiser test (5% ninhydrin in EtOH, 150 °C). ESI-MS: calculated: 1085.13 $[M+H]^+$, found: 1085.36 $[M+H]^+$; HPLC: t_R = 6.680 min.

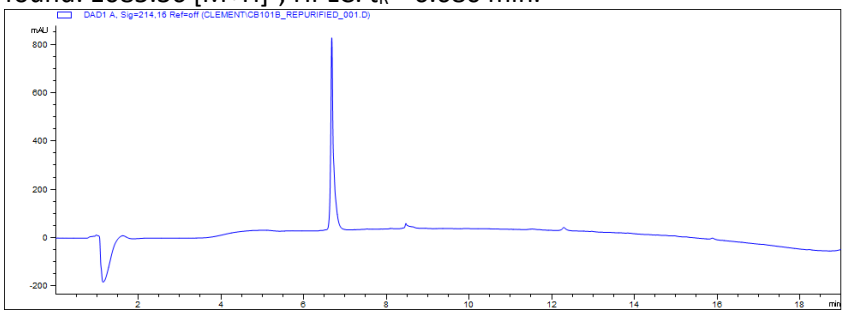

tr5C6 C6(mba) C12D (38). [(mba)TYSHWD]SH-$CONH_2$, $C_{50}H_{63}N_{15}O_{14}$, M_W = 1098.15 g/mol, M_{exact} = 1097.47 Da. The peptide was first assembled on a 0.1 mmol scale using the standard SPPS and cleavage conditions with *N*-Fmoc-protected *N*-methyl β-alanine (mba) as building block. Following cleavage from the solid phase, the macrolactam was formed from 78 mg ($7.0 \cdot 10^{-5}$ mol) of the crude linear peptide with 4 eq. ($28 \cdot 10^{-5}$ mol, 130 mg) Bromotripyrrolidinophosphonium hexafluorophosphate (PyBroP) and 8 eq. ($56 \cdot 10^{-5}$ mol, 73.8 µL) 2,4,6-trimethyl pyridine (TMP). The linear peptide was dissolved in 14 mL dry DMF, PyBroP and TMP added dropwise on ice. The reaction mixture was allowed to slowly warm up to rt and stirred until no further rection occurred, assed by MS. After 27 h, n-heptane was added to form an azeotropic mixture with DMF, the solvent was removed under reduced pressure, the crude product resuspended in H_2O and lyophilized. The mixture was purified and yielded 6.3 mg ($0.57 \cdot 10^{-5}$ mol, yield: 8.1%) of the desired product. The absence of a free amine was verified by Kaiser test (5% ninhydrin in EtOH, 150 °C). ESI-MS: calculated: 1098.48 $[M+H]^+$, found: 1098.47 $[M+H]^+$; HPLC: t_R = 6.801 min.

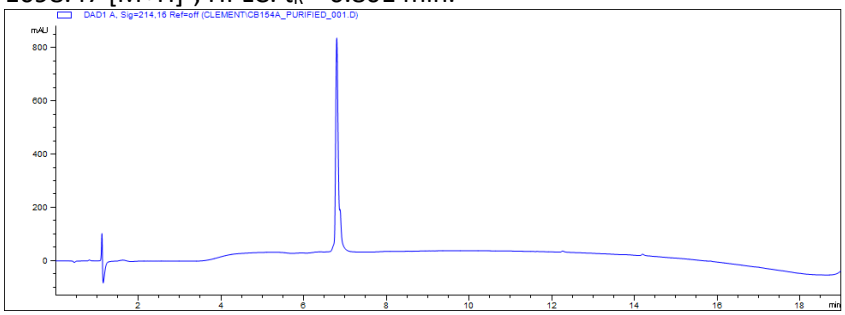

C6(aza) C12(prG) cyc1,5triA (39). Ac-[(Aza)TYSHW(prG)]SH-$CONH_2$, $C_{52}H_{64}N_{18}O_{14}$, M_W = 1165.20 g/mol, M_{exact} = 1164.48. The peptide was first assembled on a 0.1 mmol scale on a Rink Amide ProTide resin with a low loading capacity (0.19 mmol/g) using the standard SPPS conditions, with *N*-Fmoc-protected (*S*)-2-azido alanine (Aza) and Fmoc-protected (*S*)-propargyl glycine (prG) as building blocks. After SPPS, the peptidyl resin was suspended in 7 mL dry DMF and Ar bubbled through the solution for 30 min. 0.25 eq. of Cp*RuCl(COD) (Chloro(pentamethylcyclopentadienyl)(cyclooctadiene)ruthenium(II), 7.60 mg) and Ar bubbled through the solution for further 10 min. The microwave vial was sealed and reacted for 5 h at 60 °C under microwave irradiation (P_{max} = 30 W) in a Discovery microwave (CEM, Matthews, USA). Afterwards, the solution was discarded and the peptidyl resin was washed three times each with MeOH, 0.5 % sodium diethyldithiocarbamate in DMF, DMF and DCM and the resin left to dry at air overnight. Following standard cleavage conditions and purification by LCMS, 0.58 mg ($5.0 \cdot 10^{-7}$ mol, 0.5% yield overall). ESI-MS: calculated: 1165.49 $[M+H]^+$, 583.25 $[M+2H]^{2+}$, found: 1165.39 $[M+H]^+$, 583.31 $[M+2H]^{2+}$; HPLC: t_R 6.781 min. The successful cyclization was verified by the disappearance of the strong azide band at 2110 cm^{-1} in the infrared spectrum, compared to the starting material.

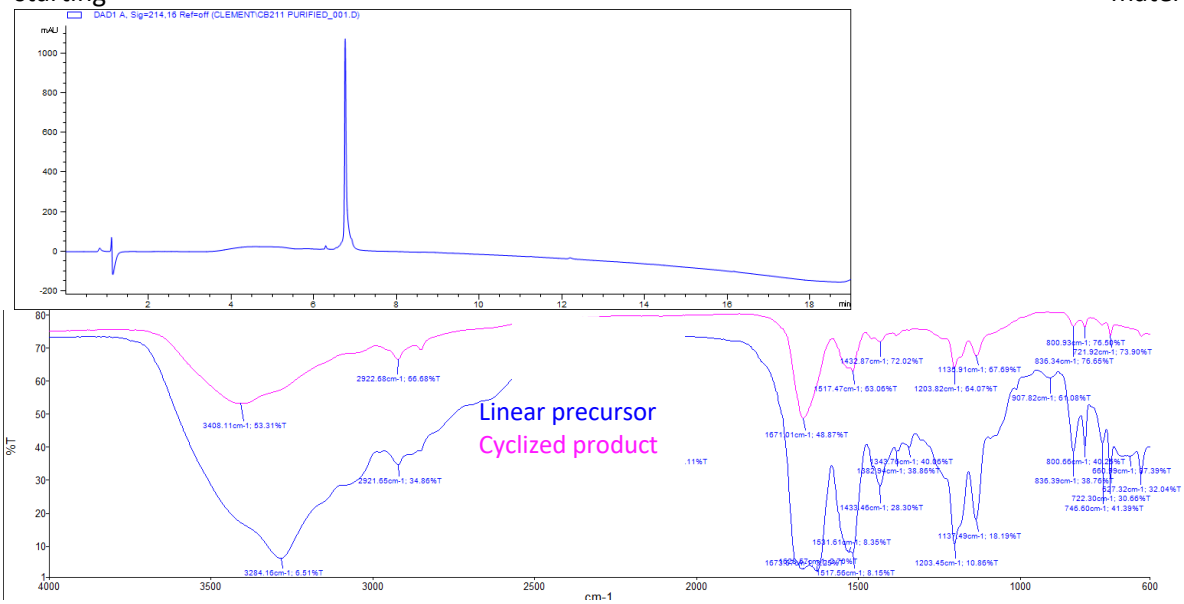

tr5C6 C6(aaa) C12(prG) cyc1,4triA (41). [(aaa)TYSHW(prG)]SH-$CONH_2$, $C_{52}H_{64}N_{18}O_{14}$, M_W = 1094.12 g/mol, M_{exact} = 1093.45. The peptide was first assembled on a 0.05 mmol scale on an MBHA Rink Amide ProTide resin with a low loading capacity (0.33 mmol/g) using the standard SPPS conditions, with 2-azido acetic acid (aaa) and Fmoc-protected (*S*)-propargyl glycine (prG) as building blocks. After SPPS, the peptidyl resin was suspended in 3.1 mL THF and 50 eq. DIPEA (435 µL) and 2 eq. CuI (19.0 mg) added. The mixture was stirred at rt for 30 h, after which the resin was washed three times with THF, H_2O, MeOH, DMF and DCM. The resin was left to dry and proceeded with the standard cleavage conditions. After purification by LCMS, 0.27 mg ($2.5 \cdot 10^{-7}$ mol, 0.25% yield overall). ESI-MS: calculated: 1094.46 $[M+H]^+$, 1116.44 $[M+Na]^+$, found: 1094.27 $[M+H]^+$, 1116.30 $[M+Na]^+$; HPLC: t_R 7.063 min. The successful cyclization was verified by the disappearance of the strong azide band at 2116 cm^{-1} in the infrared spectrum, compared to the starting material.

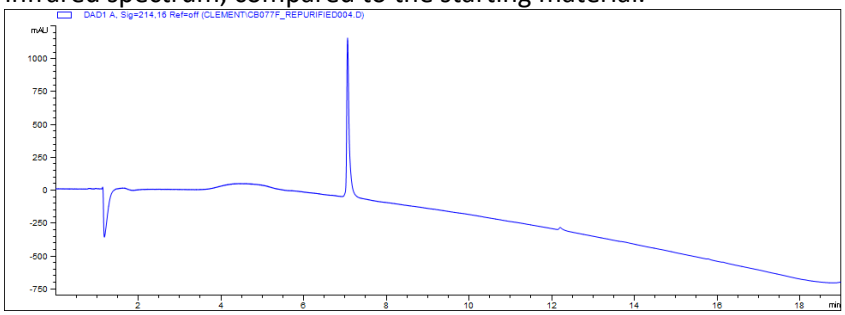

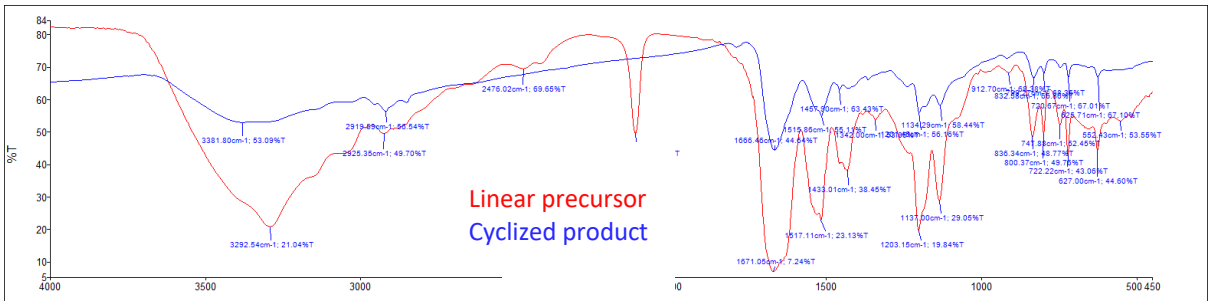

tr5C6 C6(alG) C12(alG) (45). Ac-[(alG)TYSHW(alG)]SH-$CONH_2$, $C_{52}H_{65}N_{15}O_{14}$, M_W = 1124.18 g/mol, M_{exact} = 1123.48 Da. The peptide was first assembled on a 0.05 mmol scale using the standard SPPS conditions with *N*-Fmoc-protected (*S*)-allyl-glycine (alG) as building block. Consequently, the ring-closing metathesis (RCM) was performed based on conditions reported by Robinson et al. (Robinson et al. J. Pep. Sci. 2007). The peptidyl resin was suspended in 2.38 mL DCM, degassed and 0.2 eq. (8.49 mg) second generation Grubbs catalyst M204 (CAS: 246047-72-3) as well as 125 µL of a 0.4 M LiCl solution in DMF (final concentration: 0.02 M) were added under Ar. The mixture was reacted at 100 °C for 2 h under microwave irradiation (P_{max} = 100 W) and high stirring. The resin was washed with DCM (3x), DMF (3x) and DCM (1x) and dried overnight, before proceeding with the standard cleavage conditions. After purification by LCMS, two isomers could be isolated (isomer 1 and 2, based on their order of elution during LCMS purification, expected to be the respective E- and Z-isomers. The isolated products amounted to 1.3 mg ($1.2 \cdot 10^{-6}$ mol) and 1.9 mg ($1.7 \cdot 10^{-6}$ mol), respectively, and a combined yield over all steps of 5.8%. Isomer 1: ESI-MS: calculated: 1124.49 $[M+H]^+$, found: 1124.32 $[M+H]^+$; HPLC: t_R = 7.173 min.

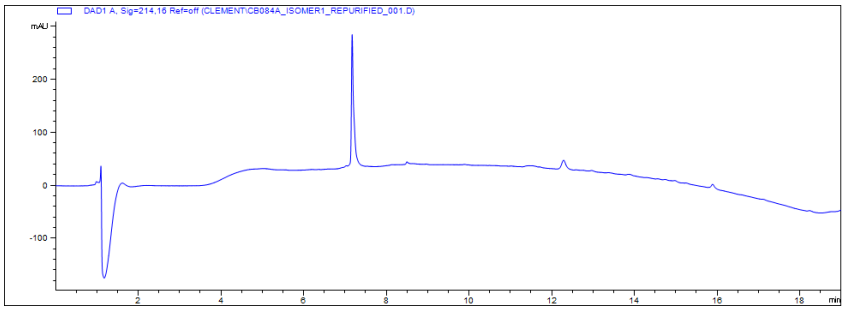

Isomer 2: calculated: 1124.49 $[M+H]^+$, found: 1125.27 $[M+H]^+$; HPLC: t_R = 7.213 min.

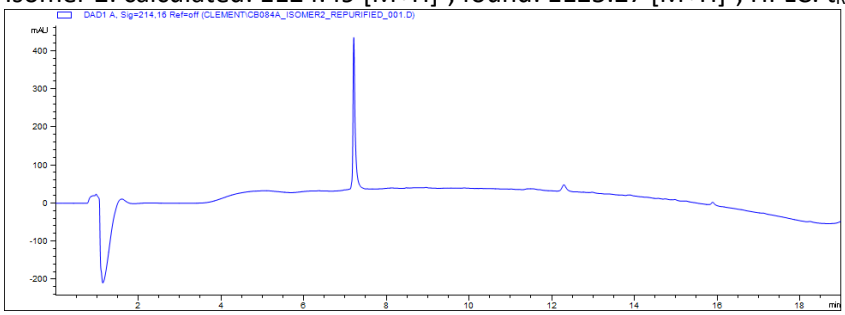

tr5C6 C6(ha) C12(alG) (46). [(ha)TYSHW(alG)]SH-$CONH_2$, $C_{51}H_{64}N_{14}O_{13}$, M_W = 1081.16 g/mol, M_{exact} = 1080.48 Da. The peptide was first assembled on a 0.05 mmol scale using the standard SPPS conditions with 5-hexenoic acid as building block. Consequently, the ring-closing metathesis (RCM) was performed based on conditions reported by Robinson et al. (Robinson et al. J. Pep. Sci. 2007). The peptidyl resin was suspended in 2.38 mL DCM, degassed and 0.2 eq. (0.01 mmol, 8.49 mg) second generation Grubbs catalyst M204 (CAS: 246047-72-3) as well as 125 µL of a 0.4 M LiCl solution in DMF (final concentration: 0.02 M) were added. The mixture was reacted at 100 °C for 2 h under microwave irradiation (P_{max} = 100 W) and high stirring. The resin was washed with DCM (3x), MeOH (3x) and DCM (1x) and dried overnight, before proceeding with the standard cleavage conditions. After purification by LCMS, two isomers could be isolated (isomer 1 and 2, based on their order of elution during LCMS purification), expected to be the respective E- and Z-isomers. The isolated products amounted to 2.0 mg ($1.8 \cdot 10^{-6}$ mol) and 0.4 mg ($3.7 \cdot 10^{-7}$ mol), respectively, and a combined yield over all steps of 4.3%. Isomer 1: ESI-MS: calculated: 1081.49 $[M+H]^+$, found: 1081.54 $[M+H]^+$; HPLC: isomer 1: t_R = 7.302 min.

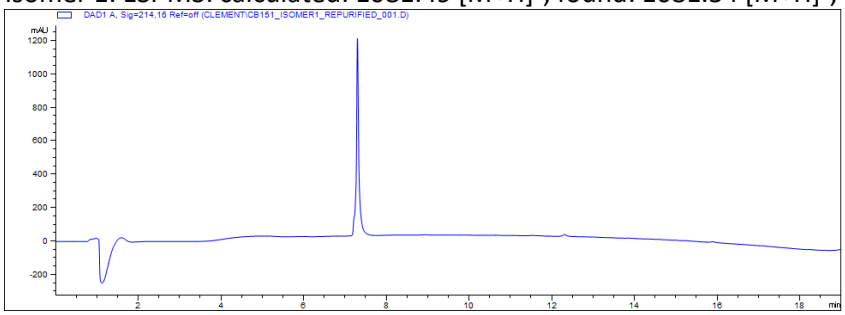

Isomer 2: ESI-MS: calculated: 1081.49 $[M+H]^+$, found: 1081.49 $[M+H]^+$; HPLC: t_R = 7.442 min.

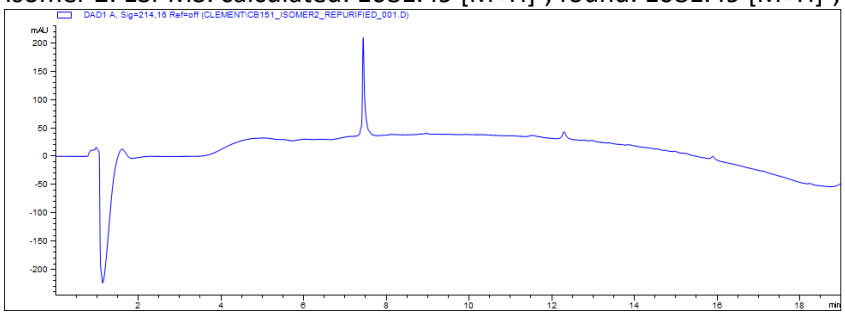

tr5C6 ΔC6 C12(asu) (47). [TYSHW(asu)]SH-$CONH_2$, $C_{50}H_{64}N_{14}O_{13}$, M_W = 1069.15 g/mol, M_{exact} = 1068.48 Da. The peptide was first assembled on a 0.05 mmol scale using the standard SPPS and cleavage conditions with Fmoc-asu(OtBu)-OH (asu: (*S*)-2-amino suberic acid) as building block. After cleavage from the solid phase, 13 mg ($1.2 \cdot 10^{-5}$ mol) of the crude linear peptide were macrolactamized with 2 eq. ($2.4 \cdot 10^{-5}$ mol, 4.36 mg) Oxyma, 2 eq. COMU ($2.4 \cdot 10^{-5}$ mol, 10.36 mg) and 4 eq. morpholine ($4.8 \cdot 10^{-5}$ mol, 4.24 µL) in 12.1 mL DMF. The reaction mixture was stirred at rt for 27 h, the solvent removed under reduced pressure and the crude product purified by LCMS, yielding 0.9 mg ($8.4 \cdot 10^{-7}$ mol, 1.7% overall yield). ESI-MS: calculated: 1069.49 $[M+H]^+$, found: 1069.64 $[M+H]^+$; HPLC: isomer 1: t_R = 7.069 min.

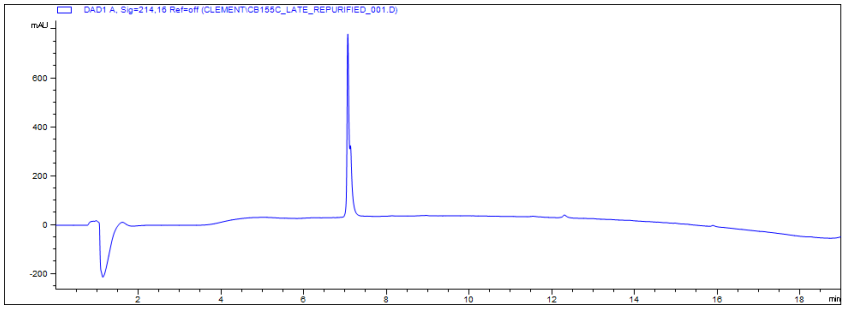

5C6 ΔT7. Ac-ASSSR[CYSHWC]SH-$CONH_2$, $C_{64}H_{88}N_{22}O_{20}S_2$, M_W = 1549.66 g/mol, M_{exact} = 1548.60 Da. ESI-MS: calculated: 1549.62 $[M+H]^+$, 775.31 $[M+2H]^{2+}$, found: 1550.70 $[M+H]^+$, 775.77 $[M+2H]^{2+}$; HPLC: t_R = 6.599 min.

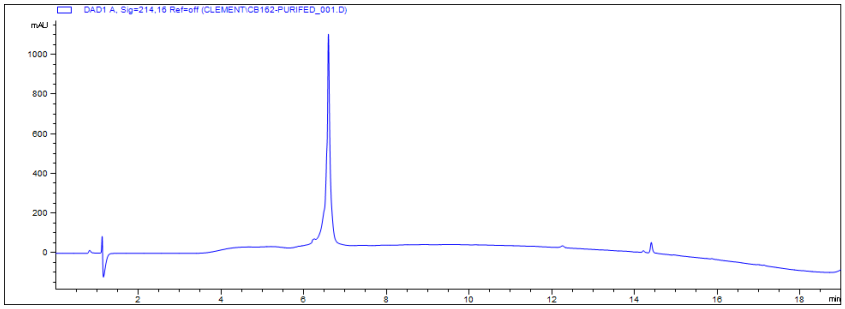

5C6 ΔS13. Ac-ASSSR[CTYSHWC]H-$CONH_2$, $C_{65}H_{90}N_{22}O_{20}S_2$, M_W = 1563.69 g/mol, M_{exact} = 1562.61 Da. ESI-MS: calculated: 1563.62 $[M+H]^+$, 782.32 $[M+2H]^{2+}$, found: 1563.34 $[M+H]^+$, 782.30 $[M+2H]^{2+}$; HPLC: t_R = 6.740 min.

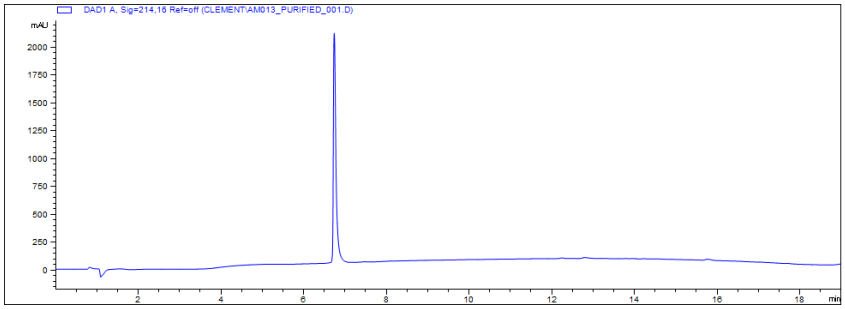

5C6 R5W S13T +15S (49). Ac-ASSSW[CTYSHWC]THS-$CONH_2$, $C_{77}H_{100}N_{22}O_{24}S_2$, M_W = 1781.90 g/mol, M_{exact} = 1780.67 Da. ESI-MS: calculated: 1781.68 $[M+H]^+$, 891.35 $[M+2H]^{2+}$, found: 1781.12 $[M+H]^+$, 891.23 $[M+2H]^{2+}$. HPLC: t_R = 8.188 min.

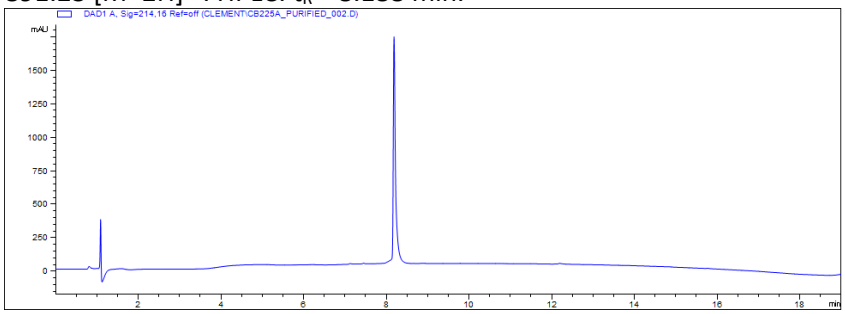

5C6 R5W S13T +15F (50). Ac-ASSSW[CTYSHWC]THF-$CONH_2$, $C_{83}H_{104}N_{22}O_{23}S_2$, M_W = 1842.00 g/mol, M_{exact} = 1840.71 Da. ESI-MS: calculated: 1841.72 $[M+H]^+$, 921.37 $[M+2H]^{2+}$, found: 1842.28 $[M+H]^+$, 921.36 $[M+2H]^{2+}$. HPLC: t_R = 9.234 min.

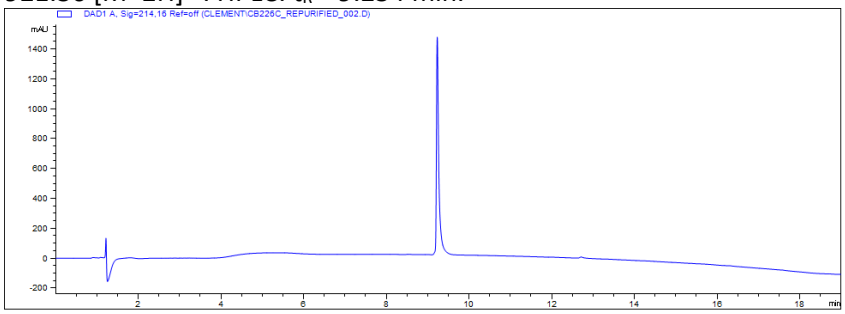

5C6 Δ1-4 R5W S13T +15F (51). Ac-W[CTYSHWC]THF-$CONH_2$, $C_{71}H_{84}N_{18}O_{16}S_2$, M_W = 1509.68 g/mol, M_{exact} = 1508.58 Da. tr5C6 +R5W S13T +15F was cyclized using the disulfide formation with DMSO method. ESI-MS: calculated: 1509.59 $[M+H]^+$, 755.30 $[M+2H]^{2+}$, found: 1510.39 $[M+H]^+$, 755.37 $[M+2H]^{2+}$; HPLC: t_R = 9.232 min.

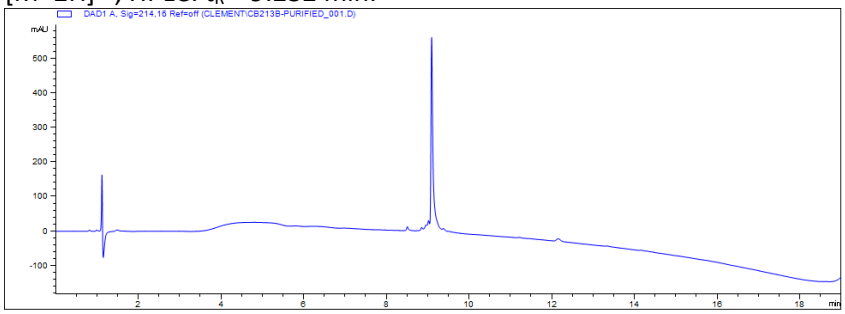

5C6 N-terminal carboxyfluorescein (CF-5C6). CF-ASSSR[CTYSHWC]SH-$CONH_2$, $C_{87}H_{103}N_{23}O_{27}S_2$, M_W = 1967.04 g/mol, M_{exact} = 1965.68 Da. ESI-MS: calculated: 983.81 $[M+2H]^{2+}$, 656.21 $[M+3H]^{3+}$, found: 983.85 $[M+2H]^{2+}$, 656.22 $[M+3H]^{3+}$; HPLC: t_R = 7.857 min.

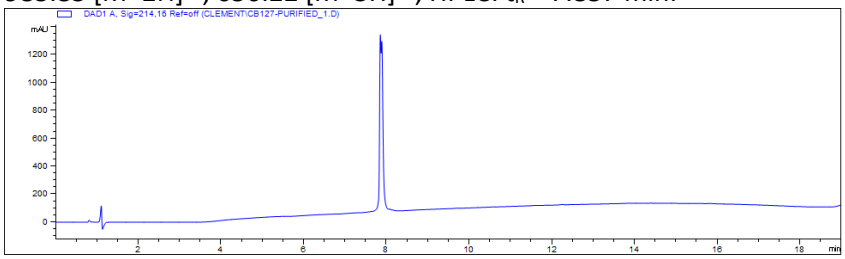

5C6 biotinylated N-term, full length, no spacer. Ac-K(biot)ASSSR[CTYSHWC]SH-$CONH_2$, $C_{84}H_{121}N_{27}O_{25}S_3$, M_W = 2005.24 g/mol, M_{exact} = 2003.82 Da. ESI-MS: calculated: 1002.92 $[M+2H]^{2+}$, 668.95 $[M+3H]^{3+}$, found: 1003.29 $[M+2H]^{2+}$, 668.87 $[M+3H]^{3+}$; HPLC: t_R = 7.019 min.

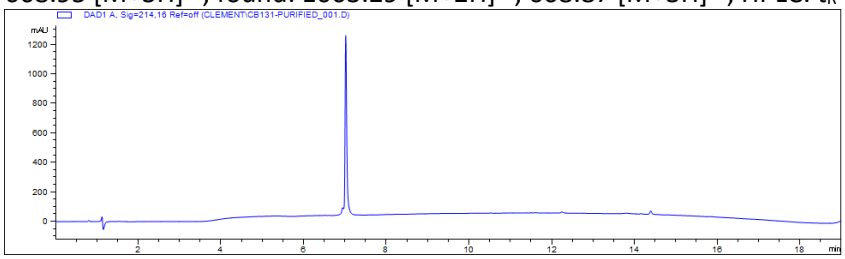

5C6 scrambled +0(PEG3)2K(biot), scrambled. Ac-K(biot)$(PEG3)_2$SSHAS[CRWSSYC]HT-$CONH_2$, $C_{100}H_{151}N_{29}O_{33}S_3$, M_W = 2383.66 g/mol, M_{exact} = 2382.02 Da. ESI-MS: calculated: 1192.02 $[M+2H]^{2+}$, 795.02 $[M+3H]^{3+}$, found: 1192.61 $[M+2H]^{2+}$, 795.38 $[M+3H]^{3+}$; HPLC: t_R = 7.220 min.

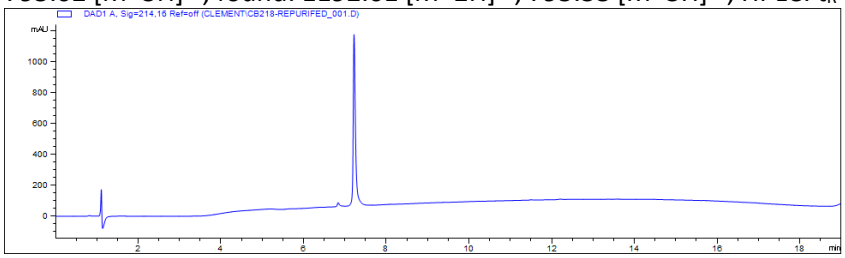

5C6 +0K(biot) R5W S13T +15F (52). Ac-K(biot)ASSSW[CTYSHWC]THF-$CONH_2$, $C_{99}H_{130}N_{26}O_{26}S_3$, M_W = 2196.47 g/mol, M_{exact} = 2194.88 Da ESI-MS: calculated: 2195.89 $[M+H]^+$, 1098.45 $[M+2H]^{2+}$, found: 2196.64 $[M+H]^+$, 1098.97 $[M+2H]^{2+}$. HPLC: t_R = 9.154 min.

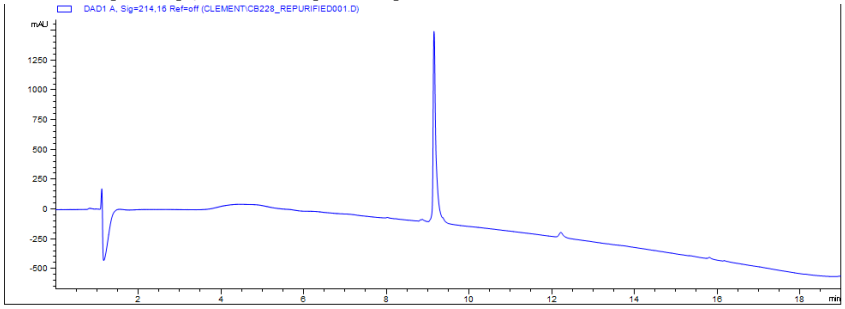

myr-5C6. myr-ASSSR[CTYSHWC]SH-$CONH_2$, $C_{80}H_{119}N_{23}O_{22}S_2$, M_W = 1819.09 g/mol, M_{exact} = 1817.83 Da. After standard SPPS synthesis, the uncapped and fully protected 5C6 was coupled twice with 6 eq. each of myristic acid, DIC and Oxyma, followed by standard cleavage and cyclization conditions, cyclization was performed in H_2O/MeOH/DMSO (8.5/1/0.5) due to low solubility instead of in a purely aqueous solution. ESI-MS: calculated: 1820.86 $[M+H]^+$, 910.94 $[M+2H]^{2+}$, 607.63 $[M+3H]^{3+}$, found: 1821.62 $[M+H]^+$, 911.02 $[M+2H]^{2+}$, 607.73 $[M+3H]^{3+}$; HPLC: t_R = 11.372 min.

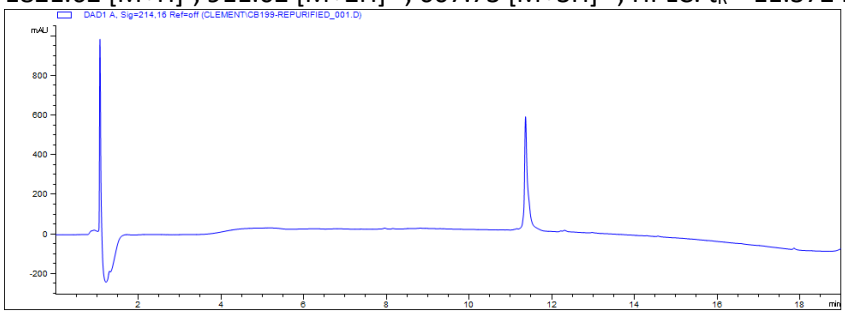

chol-5C6. chol-ASSSR[CTYSHWC]SH-$CONH_2$, $C_{94}H_{137}N_{23}O_{23}S_2$, M_W = 2021.39 g/mol, M_{exact} = 2019.97 Da. After standard SPPS synthesis, the uncapped and fully protected 5C6 was coupled with 10 eq. of cholesteryl chloroformate (1.0 mmol, 449 mg) under addition of 20 eq. of NEt_3 (2.0 mmol, 279 µL) in a total volume of 10 mL DCM. The reaction was stirred at rt for 43 h, followed by standard cleavage and cyclization conditions, cyclization was performed in H_2O/DMSO (4/1) due to low solubility instead of in a purely aqueous solution, followed by purification by LCMS. ESI-MS: calculated: 2020.98 $[M+H]^+$, 1011.46 $[M+2H]^{2+}$, found: 2021.57 $[M+H]^+$, 1011.46 $[M+2H]^{2+}$; HPLC: t_R = 15.142 min.

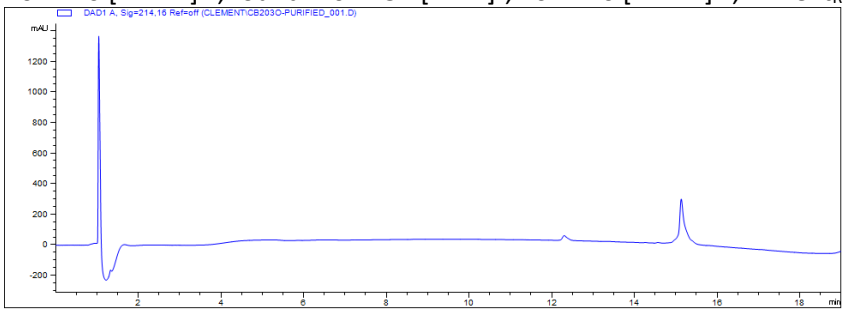

DSPE-5C6. DSPE-ASSSR[CTYSHWC]SH-$CONH_2$, $C_{111}H_{177}N_{24}O_{24}PS_2$, M_W = 2438.87 g/mol, M_{exact} = 2437.22 Da. 18.2 mg (0.011 mmol) of uncapped, fully deprotected and purified 5C6 was dissolved in 750 µL DMF (dry) and 4 eq. of DIPEA (7.9 µL) and 2 eq. of NHS-DSPE (21.4 mg), which was not fully soluble in DMF, added. The reaction mixture was stirred at rt for 24 h, diluted with 3 mL MeOH, filtered and purified by LCMS. ESI-MS: calculated: 2438.23 $[M+H]^+$, 1219.62 $[M+2H]^{2+}$, 813.42 $[M+3H]^{3+}$, found: 2349.00 $[M+H]^+$, 1220.18 $[M+2H]^{2+}$, 813.85 $[M+3H]^{3+}$; HPLC (C_8-column): t_R = 6.855 min.

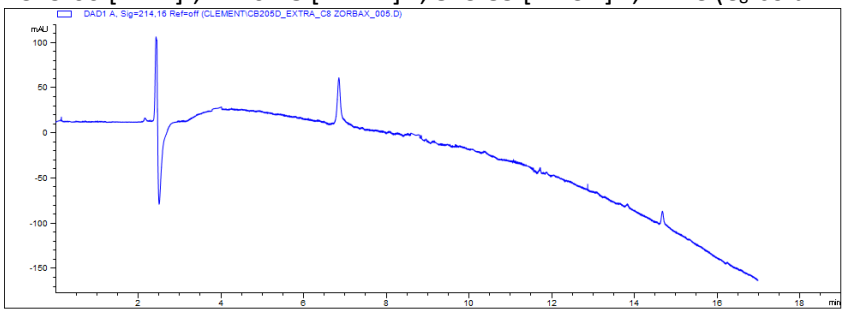

myr-5C6 lin. myr-ASSSRSTYSHWSSH-$CONH_2$, $C_{80}H_{121}N_{23}O_{24}$, M_W = 1788.99 g/mol, M_{exact} = 1787.90 Da. myr-5C6 lin was synthesized the same way as myr-5C6, but without the cyclization step. ESI-MS: calculated: 1788.91 $[M+H]^+$, 894.96 $[M+2H]^{2+}$, 596.98 $[M+3H]^{3+}$, found: 1789.49 $[M+H]^+$, 894.97 $[M+2H]^{2+}$, 596.98 $[M+3H]^{3+}$; HPLC: t_R = 11.122 min.

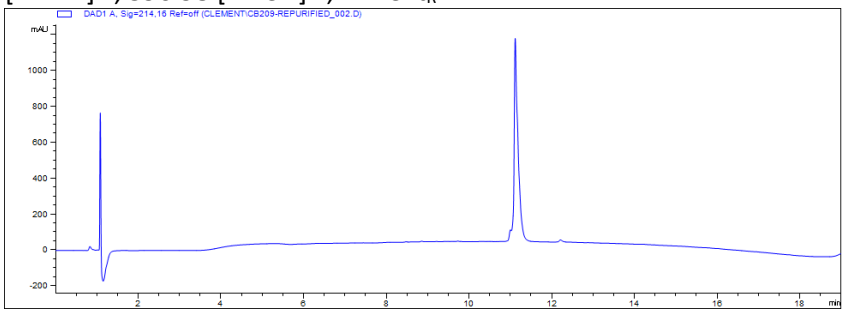

myr-5C6 +15K(CF). myr-ASSSR[CTYSHWC]SHK(CF)-$CONH_2$, $C_{107}H_{141}N_{25}O_{29}S_2$, M_W = 2305.57 g/mol, M_{exact} = 2303.98 Da. myr-5C6 +15K(CF) was synthesized the same way as myr-5C6, using Fmoc-K(CF)-OH as building block to introduce K(CF) during SPPS. ESI-MS: calculated: 1153.00 $[M+2H]^{2+}$, 769.00 $[M+3H]^{3+}$, found: 1153.31 $[M+2H]^{2+}$, 769.29 $[M+3H]^{3+}$; HPLC: t_R = 9.646 min, purity: <95%.

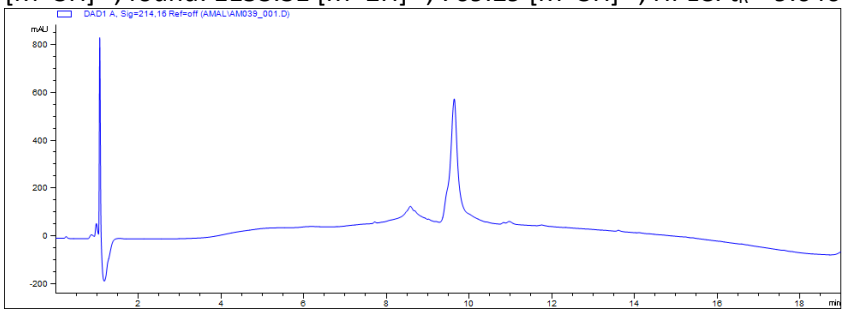

Original Article

CHAPTER 5: OPTIMIZED SYNTHESIS, POLYMER CONJUGATION AND PROOF-OF-CONCEPT STUDIES OF THE GD-IGA1 EPITOPE FOR ANTIBODY-SCAVENGING THERAPIES IN IGA NEPHROPATHY

Clément Bechtler[1,a], Ouliana Barneoud-Rousset[2,a], Lijuan Pang[2,a] Kea Martin[2], Katrin F König[3], Nick Pearson[2,b], Daniel Ricklin[1,b]

[1] Molecular Pharmacy Group, Department of Pharmaceutical Sciences, University of Basel, Basel, Switzerland
[2] Polyneuron Pharmaceuticals AG, Hochbergerstrasse 60C, Basel, Switzerland
[3] Division of Internal Medicine, University Hospital Basel, Basel, Switzerland
[a] equal contributions
[b] shared supervision

Corresponding author:
Prof. Dr. D. Ricklin
University of Basel, Department of Pharmaceutical Sciences, Klingelbergstrasse 50, CH-4056 Basel, Switzerland. E-mail: d.ricklin@unibas.ch

Contributions of Clément Bechtler:

- Design and execution of synthetic routes to glycopeptide and purification of it
- Manuscript preparation

Optimized synthesis, polymer conjugation and proof-of-concept studies of the gd-IgA1 epitope for antibody-scavenging therapies in IgA nephropathy

Clément Bechtler[1,a], Ouliana Barneoud-Rousset[2,a], Lijuan Pang[2,a] Kea Martin[2], Katrin F König[3], Pascal Hänggi[2], Nick Pearson[2,b], Daniel Ricklin[1,b]

[1] Molecular Pharmacy Group, Department of Pharmaceutical Sciences, University of Basel, Basel, Switzerland
[2] Polyneuron Pharmaceuticals AG, Hochbergerstrasse 60C, Basel, Switzerland
[3] Division of Internal Medicine, University Hospital Basel, Basel, Switzerland
[a] equal contributions
[b] shared supervision

ABSTRACT

IgA nephropathy (IgAN) is the most common glomerular autoimmune disease with severe long-term consequences for patients, with 40% of the patients eventually progressing to end-stage renal disease. Despite the severity, no causal treatment is currently available. Though IgAN is a complex disease, disease severity is linked to the autoantibodies against the gd-IgA1 epitope, a stretch in the hinge region of IgA1, which lacks *O*-glycans, that has been found in the characteristic immune complexes deposited in IgAN patients' kidneys. One elegant, causal approach would therefore be to remove the anti-gd-IgA1 autoantibodies and consequently reduce the immune complex burden on the kidneys. The administration of synthetic polymers that present autoantigens in a multivalent manner have been established as promising therapeutic strategies in other autoimmune diseases and may be applied to IgAN. We here present an improved synthetic protocol for the synthesis of the gd-IgA1 epitope, its successful coupling to a polylysine polymer and proof-of-concept experiments that the polymer-bound synthetic glycopeptide is able to capture the IgAN autoantibodies, making this approach a promising way forward for developing a targeted treatment option for IgAN patients.

INTRODUCTION

IgA nephropathy (IgAN) is a highly prevalent and severe glomerular autoimmune disease that leads to a gradual reduction of kidney function up to end-stage renal disease. Although the progression is often slow and shows large variability between patients, 40% of the patients will eventually require hemodialysis or a kidney transplant.[1–3] The pathology is complex and heterogenous, but all patients show IgA1-IgG or IgA1-IgM immune complex deposition in the kidney glomeruli.[1,4] IgA1, the more common of the two IgA subclasses, has a unique hinge region with a high number of serine, threonine and proline residues. Typically, three to six Ser and Thr within this stretch are *O*-glycosylated with *N*-acetylgalactosamine (GalNAc) β-1,3-linked galactose (Gal), with further glycosylation with sialic acids being possible. However, IgAN patients have IgA1s without full galactosation of the GalNacs, giving rise to galactose deficient IgA1 (gd-IgA1) (**Figure 1A**).[2] The gd-IgA1 are prone to aggregation and are immunogenic, raising autoimmune antibodies (mostly IgGs, but also IgA or IgGM), both aspects favoring the formation of immune complex deposits in the kidney. The presence of the gd-IgA1 immune complexes is thought to drive the disease, although IgAs without erroneous glycosylation are also found in the immune complexes. Furthermore, the complement protein C3 is colocalized with these immune complexes and complement activation can be typically observed; several complement inhibitors are therefore in clinical development as potential treatment options for IgAN.[2,3] The complexity of the disease contributes to the lack of disease-specific interventions, with current treatments being mostly limited to efforts preserving kidney function (e.g., by antihypertensive drugs) and, in specific cases, immunosuppression.[1,3] Importantly, it was demonstrated that circulating IgA and IgA immune complex levels correlate with clinical severity of the condition, thereby rendering the removal of those complexes an attractive therapeutic strategy.[2]

We present here a first proof-of-concept study, in which we were able to synthesize the gd-IgA1 epitope as a glycopeptide on a larger scale and with less equivalents of the difficult to obtain buildings blocks compared to previous reports.[5] When conjugated to a polylysine polymer, the epitope showed binding both to a commercially available antibody and to patient-derived autoantibodies, thereby demonstrating its suitability as a development candidate for treating IgAN using the previously established Antibody-Catch™ strategy.[6] This technology, in which disease-causing antibodies are sequestered by an epitope-bearing polymer, has already been successfully pursued for other conditions. The polymer complexes are then rapidly degraded by the mononuclear phagocyte system, thus reducing the antibody burden.[6]

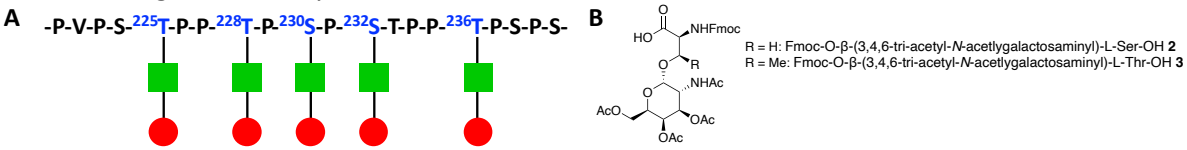

Figure 1: (**A**) Hinge region sequence of IgA1 containing the gd-IgA1 epitope. IgAN patients lack the galactose (red circles), only carrying the *N*-acetylglucosamine (green squares) glycans. (**B**) Used glycosylated building blocks in the synthesis of the gd-IgA1 epitope

RESULTS AND DISCUSSION

We aimed at synthesizing the gd-IgA1-epitope glycopeptide **1** in a linear fashion using solid-phase peptide synthesis (SPPS), introducing the glycoamino acids as acetyl-protected building blocks (*i.e.,* Fmoc-O-β-(2-acetamido-3,4,6-tri-*O*-acetyl-2-deoxy-α-D-galactopyranosyl)-L-Ser-OH **2** and Fmoc-O-β-(2-acetamido-3,4,6-tri-*O*-acetyl-2-deoxy-α-D-galactopyranosyl)-L-Thr-OH **3**, **Figure 1B**) during SPPS. This was followed by cleavage from the solid phase, concomitant with removal of the acid-labile protecting groups, and base-catalyzed deacetylation (**Scheme 1A**), all based on previously described conditions to synthesize the gd-IgA1 epitope fragment **1a** (**Figure 1A**).[5] Due to the low scale (12 nmol) used by Bolscher *et al.*[5], the synthesis required further optimization efforts for our purpose to obtain sufficient amounts of product and to lower the equivalents of the expensive glycosylated building blocks **2** and **3** used. The initial strategy consisted of coupling the C-terminal carboxylic acid directly

to a polylysine polymer. Thus, we started the synthesis on a Cl-MPA ProTide resin (0.17 mmol/g) using standard DIC/Oxyma coupling agents on a 25 µmol scale. However, neither coupling at room temperature (rt) with 1 eq. or at 50 °C with 2 eq of **2** and **3** yielded any product (**Table 1**, entries 1, 2), despite the successful use of these reactions by others for related peptides.[7,8] Increasing the eq. of **2** and **3** while also switching the coupling agents to HATU/HOBt/DIPEA and capping after each coupling step of **2** and **3** allowed us for the first time to detect product **1a**, although only at a 2% crude yield (**Table 1**, entry 3). We therefore decided to switch to an alternative polymer coupling procedure, requiring a free amino group on the glycopeptide that would allow us to use Rink Amide resins that often result in higher yields. Indeed, the crude yield for **1b** increased to 7% by switching to a Rink Amide ProTide resin (0.19 mmol/g) on a 50 µmol scale (**Table 1**, entry 4). By increasing the reaction temperature, switching from HOBt to HOAt for higher reactivity as shown for other particularly challenging couplings steps[9], and substituting DIPEA with 2,4,6-trimethylpyridine (TMP), which has been demonstrated to improve yields and reduce epimerization in the coupling during SPPS of glycosylated amino acids[10], we could substantially improve the crude yield of **1b** to 55% by only using 2 eq. of **2** and **3**. The observed degradation of the product was probably due to pH changes to work-up after the deacetylation. Controlling the pH during work-up prevented degradation (**Table 1**, entry 5). Finally, we introduced an additional Tyr at the N-terminus for improved monitoring by UV and NMR, and a Lys unit for coupling to the activated polymer backbone. Finally, we could isolate **1c** in 16% yield after LCMS purification, again by using only 2 eq. of **2** and **3** (**Table 1**, entry 6).

The production of sufficient amounts of the glycopeptide epitope allowed us to conjugate **1c** to the poly-L-lysine (400mer). In a first step, the free amine of **1c** reacted with γ-thiobutyrolactone to give glycopeptide **4** with a free thiol (**Scheme 1B**), which was subsequently coupled, as previously described[11], to 2-chloroacetyl-derivatized poly-L-lysine to yield polymer **5** (PN-251) with an epitope loading degree of 10% (determined by ^{1}H-NMR) (**Scheme 1C**).

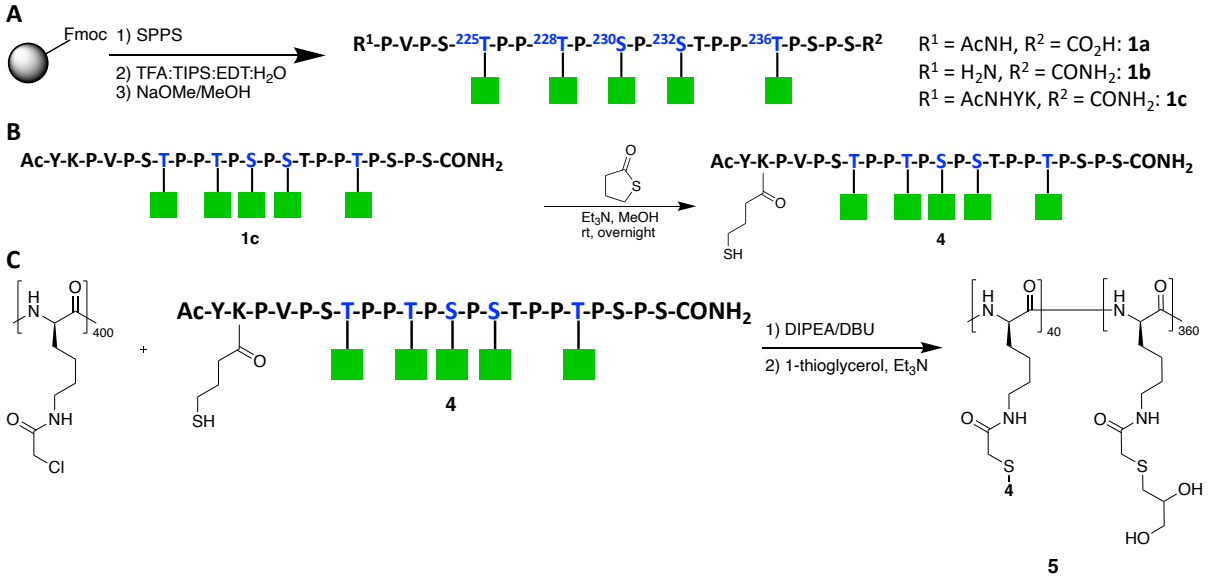

Scheme 1: (**A**) Syntheses of the glycopeptides **1a**, **1b** and **1c**, glycosylated residues highlighted in blue with their respective sequence number in the IgA1 protein sequence, green squares symbolize *N*-acetylglucosamin. TFA: trifluoroacetic acid, TIPS: triisopropylsilane, EDT: ethanedithiol. (**B**): Derivatization of the glycopeptide **1c** with γ-thiobutyrolactone to obtain thiol-containing derivative **4** for subsequent coupling to the polylysine polymer. Glycosylated residues highlighted in blue, green squares symbolize *N*-acetylglucosamine. (**C**): Conjugation of the derivatized glycopeptide **4** to chloroacetyl conjugated polylysine, yielding polymer **5** carrying the gd-IgA1 epitope.

For the functional evaluation and proof-of-concept study of the epitope-presenting polymer, we tested **5** in an ELISA with the commercially available KM55 antibody, which recognizes the gd-IgA1 epitope and has previously been used to determine gd-IgA1 levels in patients.[12] Plates were coated with KM55, incubated with **5**, and the polylysine polymer was detected with a horseradish peroxidase (HRP)-conjugated anti-polylysine antibody. KM55 was able to recognize **5** (PN-251), suggesting that

the epitope is presented on the polymer in a similar fashion as it is in vivo (**Figure 2A**). To assess whether the reactivity and specificity is maintained in the case of patient antibodies, we coated plates with **5** and incubated them with IgAN patient sera or sera from healthy donors. Anti-gd-IgA1-IgG and IgA was detected using biotinylated anti-human IgG/IgA and HRP-streptavidin. From 10 patient sera, 8 showed an increased signal compared to the healthy control, thereby confirming the reactivity, and suggesting that patient antibodies might indeed be amenable to sequestration by polymer **5** (**Figure 2B**).

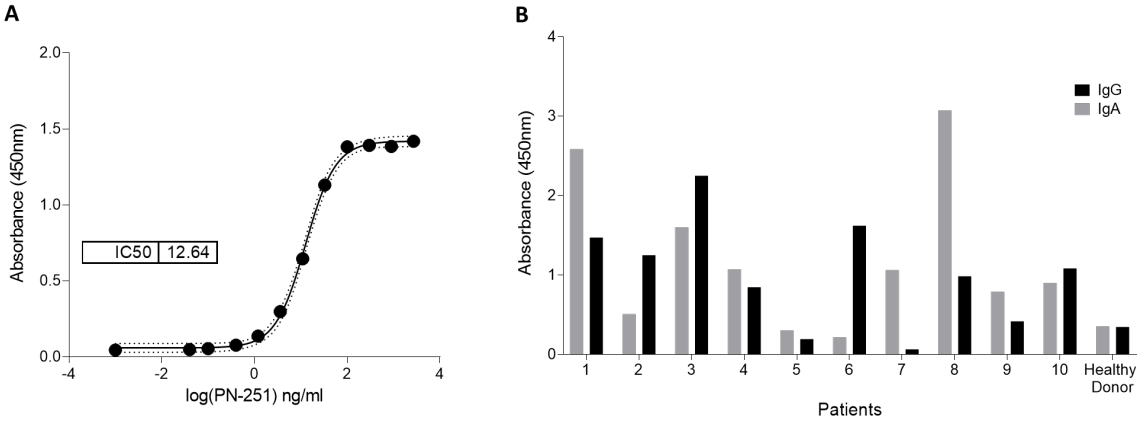

Figure 2: (**A**) Dose-response plot of detected glycopeptide polymer **5** (PN-251) using an anti-polylysine antibody, after capturing **5** (PN-251) with the anti-gd-IgA1 KM55 antibody immobilized on a microtiter well plate. (**B**) Anti-gd-IgA1 IgG and IgA bound to immobilized glycopeptide polymer **5** from IgAN patients and healthy controls at 2% serum concentration.

CONCLUSION

Herein, we presented an improved synthetic protocol for the chemical synthesis of the gd-IgA1 epitope, its successful conjugation to a polylysine polymer and demonstrated that the polymer-bound epitope was demonstrated to capture the autoimmune IgGs in patient sera. For optimizing the synthetic protocol for this challenging glycopeptide, which not only contains 5 glycosylated residues but also 10 prolines (out a total of 20 residues), the switch to the more reactive coupling reagents HATU/HOAt under addition of TMP as base proved to be critical as did higher reaction temperatures. This allowed us to isolate the gd-IgA1 epitope with a good overall yield of 16% while only using 2 eq. of the expensive glycosylated building blocks and on relatively large scale of 50 µmol. Importantly, the resulting glycopeptide could be effortlessly conjugated to a polymer using our standard protocols. Finally, the synthetic polymer was recognized by both commercial and patient-derived autoantibodies against gd-IgA1. These findings provide an important base for the future development of the approach, as it suggests that such polymers could be used, either in vivo or ex vivo, to capture immune complexes and, consequently, reduce disease burden in IgA nephropathy.

Entry number	Product	R^1	R^2	Scale (µmol)	Resin	Coupling reagents (eq.)	Total Equivalents glycoamino acids	Coupling cycles	Crude yield[§]	Overall yield
1	**1a**	AcHN	CO_2H	25	Cl-MPA ProTide LL (0.17 mmol/g)	DIC/Oxyma	2	Glycosylated amino acid: 1h at rt, double coupling, with capping Non-glycosylated: 1h at rt	-	-
2	**1a**	AcHN	CO_2H	25	Cl-MPA ProTide LL (0.17 mmol/g)	DIC/Oxyma	2	Until first glycosylated amino acid: 95 °C, 2 min; then: 50 °C, 20 min	-	-
3	**1a**	AcHN	CO_2H	Ac	Cl-MPA ProTide LL (0.17 mmol/g)	HATU/HOBt/DIPEA	3	50 °C, 20 min, capping after coupling of glycosylated amino acid	2%	-
4	**1b**	H_2N	$CONH_2$	50	Rink Amide ProTide LL (0.18 mmol/g)	HATU/HOBt/DIPEA	3	Until first glycosylated amino acid: 95 °C, 4 min, then: 50 °C, 20 min, capping	7%	-
5	**1b**	H_2N	$CONH_2$	50	Rink Amide ProTide LL (0.19 mmol/g)	HATU/HOAt/TMP	2	Glycosylated amino acids: 95 °C, 10 min, single coupling, capping Non-glycosylated amino acids: 95 °C, 4 min, double coupling	55%	-
6a	**1c**	AcHNYK	$CONH_2$	50	Rink Amide ProTide LL (0.19 mmol/g)	HATU/HOAt/TMP	2	Glycosylated amino acids: 95 °C, 10 min, single coupling, capping Non-glycosylated amino acids: 95 °C, 4 min, double coupling	46%	16%

Table 1: overview over the different reaction conditions employed in the synthesis of the gd-IgA1 epitope. 6 eq. of the coupling reagents and unglycosylated amino acid were used. When a base was used, 12 eq. were used. [§]: after cleavage from the solid phase. DIPEA: *N,N*-Diisopropylethylamine, TMP: 2,4,6-trimethylpyridine.

MATERIALS AND METHODS

Materials. Non-glycosylated amino acids were from Carbolution (St. Ingbert, Germany), solvents were from VWR (Radnor, USA) or Carl Roth (Karlsruhe, Germany), resins were from CEM (Matthews, USA) and other reagents were from Sigma-Aldrich (St. Louis, USA). The glycosylated building blocks were custom synthesized by Samuel Pharma (Shandong, China). Poly-L-lysine (400er) was from Polypeptide Therapeutic Solutions (Paterna, Spain). All reagents and solvents were used without further purification. Sera from patients with positive anti-gdIgA1 titers were obtained from the University Hospital of Basel. The use of patient sera was approved by the Ethics Committee of Northwestern and Central Switzerland (EKNZ). Informed consent was obtained from all non-anonymized participants. Healthy donor control serum was obtained from Sigma (H4522, lot SLB6544).

Synthesis and purification of 1c. SPPS was performed on a Liberty Blue Automated Peptide Synthesizer (CEM, Matthews, USA) using a microwave-assisted solid-phase peptide synthesis (SPPS) Fmoc/*t*-Bu strategy on Rink Amide ProTide LL (0.19 mmol/g) resin. The final conditions were 4 min double coupling at 95 °C for the coupling with 6 eq. of the non-glycosylated amino acids, and 10 min single coupling at 95 °C for the coupling with 2 eq. of the glycosylated amino acids **2** or **3**, followed by a capping step after coupling **2** or **3**. For coupling any of the amino acids 6 eq. each of HOAt and HATU and 12 eq. of 2,4,6-trimethylypridine were used. Capping was performed with 10% Ac_2O in DMF, Fmoc-deprotection was achieved with 10% piperazine in *N*-methylpyrrolidone (NMP)/EtOH (9/1) for 1 min at 50 °C. After cleavage from the solid phase and removal of the acid-labile side chain protecting groups with trifluoroacetic acid (TFA):triisopropylsilane (TIPS):ethanedithiol (EDT):H_2O (92.5/2.5/2.5/2.5) at room temperature (rt) for 3h and precipitation with -20 °C Et_2O, yielding 90 mg of the crude intermediate still bearing the acetyl protecting groups.

29 mg of this crude product was dissolved in dry MeOH (1 mL). A solution of NaOMe in MeOH (25%) was added dropwise until a pH of 8-9 was reached. The reaction mixture was stirred under argon for 48 h at rt. The solution with AcOH (pH 6-7) and concentrated under vacuum. The product was transferred onto a C18 cartridge (Waters, Milford, USA), and the cartridge washed with H_2O/MeOH mixtures containing 0%, 20%, 30% or 50% MeOH and **1c** eluting with 30% MeOH, yielding 17 mg if the crude product. The crude product was further purified on an Agilent 1260 Infinity II LCMS (Agilent, Santa Clara, USA) with a reverse phase C18-column (XSelect CSH Prep C_{18} 5.0 µm, 19 mm x 250 mm; Waters, Milford, USA) and a linear gradient from 95% A (H_2O + 0.1% TFA)/5% B (MeCN + 0.1% TFA) to usually 70% A/30% B over usually 25 min, yielding 8.44 mg of **1c** (2.58 µmol, 16% overall yield).

Identity was confirmed by ESI-MS on a micromassZQ (Waters, Milford, USA). Purity was determined by UV absorption at 214 nm on an Agilent 1100 HPLC (Agilent, Santa Clara, USA), using a reverse phase C18-column (Atlantis T3, 3 µM, 2.1 x 100 mm; Waters, Milford, USA). **1c** was eluted with a gradient from 95% A (H_2O + 0.1% TFA)/5% B (MeCN + 0.1% TFA) to 60% A/40% B over 20 min. Peptides were purified to at least 95%.

ESI-MS: calculated: 1092.5 $[M+3H]^{3+}$, 1638.3 $[M+4H]^{4+}$, found: 1093.2 $[M+3H]^{3+}$, 1638.8 $[M+4H]^{4+}$. HPLC: t_R = 11.499 min, purity: 98.5% (λ = 214 nm) (Supplementary Figure S1).

Synthesis of derivatized gylcopeptide 4. Triethylamine (5 µL, 35.7 µmole) and γ-thiobutyrolactone (3.1 µL, 35.7 µmole) were added to a solution of **1c** (3.92 mg, 1.19 µmole) in dry methanol (0.3 mL). The reaction mixture was stirred at rt under argon atmosphere overnight, the solvent removed under reduced pressure, the residue dissolved in H_2O (0.5 mL) and washed with EtOAc (0.5 mL, three times). The aqueous phase was lyophilized and 3.34 mg of crude **4** obtain as white solid.

Synthesis of polymer 5. The derivatized glycopeptide **5** (1.08 mg, 5.3 µmol) was dissolved in DMF (0.3 mL) and a solution of 2-chloroacetyl-derivatized polylysine[11] (3.56 mg, 1.05 µmol) in H_2O (0.03 mL) added and to which DIPEA (1.85 µL, 10.6 µmol) and 1,8-Diazabicyclo[5.4.0]undec-7-ene (DBU; 0.8 µL, 5.3 µmol) were added and the reaction mixture stirred under argon atmosphere at room temperature. After 45 min, 1-thioglycerol (1.4 µL, 15.9 µmol) and trimethylamine (2.2 µL, 15.9 µmol) were added and the mixture further stirred at rt overnight. Then, the reaction mixture was added dropwise to 2 mL of ethyl ether/ethanol (1:1, v/v) while vigorously stirring. A white precipitate was colleced and

dissolved in H_2O (2 mL). The aqueous solution was ultracentrifuged through 50kDa MWCO centrifuge filter, and then washed three times with H_2O (2 mL each). The product residue was dissolved in 1 mL H_2O and lyophilized to give the polymer **5** (2.56 mg) as white solid with an epitope loading of 10 %, calculated by ^{1}H-NMR integration of Tyr peaks (4 protons on the aromatic ring) at 6.95 and 6.65 ppm *versus* thioglycerol peaks (protons of the two -CH- groups) at 2.67-2.45 ppm.

ELISA: Dose-response on KM55-coated plate. Maxisorp 96 well microtiter plates (Nunc) were coated with 75 µl/well KM55 rat anti-human gd-IgA1 IgG (IBL 30117066, lot 1F-701) at 1 µg/ml in DPBS overnight at 4°C. Plates were washed 4 times with DPBS + 0.05% Tween 20 (PBST) and unspecific binding sites were blocked with incubation buffer (IB) for 2h at RT (IB = 0.3% non-fat dry milk (NFDM) in PBST; 100 µl/well). A 2-fold serial dilution of polymer 5 (PN-251) was prepared in IB starting from 5400 ng/mL. 50 µl/well was added to the respective wells and incubated for 2h at RT. Plates were washed 4 times and polymer 5 was detected with anti-poly-l-lysine F(ab)2-HRP (Biorad AbD27389). After 1 h incubation, plates were washed 4x and 50 µl TMB substrate (ready to use; Thermofisher, N301) was added. The colour reaction was stopped before 30 minutes with 0.16M sulfuric acid (N600, Thermofisher) and absorbance (OD) was read at 450 nm using a microtiter plate reader (Synergy H1, Biotek).

Detection of anti-gdIgA1-IgG and -IgA. Maxisorp plates were coated with 75 µl/well of polymer 5 (PN-251) at 1 µg/ml in DPBS overnight at 4°C. Plates were washed 4 times with PBST and unspecific binding sites were blocked with IB for 2h at RT (100 µl/well). Patient and healthy donor control serum was diluted 1:50 in IB. 50 µl/well was added to the respective wells and incubated for 2h at RT. Plates were washed 4 times and IgG/IgA autoantibodies bound to 5 were detected with biotinylated anti-human IgG (SAB3701268-1MG, Sigma-Aldrich) and biotinylated anti-human IgA (SAB3701227-500UG, Sigma). Detection antibodies were diluted 1:2500 in IB and 50 uL/well was added and incubated for 2h at RT. Following another wash (4x) 50 µl of 1:2000 diluted ExtrAvidin-Peroxidase (E2886-.2ML, Sigma) was added and incubated for 1h at RT Plates were washed 4x and 50 µl TMB substrate (ready to use; Thermofisher, N301) was added. The colour reaction was stopped before 30 minutes with 0.16M sulfuric acid (N600, Thermofisher) and absorbance (OD) was read at 450 nm using a microtiter plate reader.

AUTHOR CONTRUBTIONS

CB designed synthetic routes, synthesized and purified the glycopeptides. OB and KM designed, performed and analyzed ELISA experiments. LP did deacetylation of the IgA glycopeptide and semi-purification, derivatisation of glycopeptide and conjugation to polylysine polymer. KK provided sera and information from patients. KK and PH developed the study design. NP and DR conceived and supervised the studies. CB and DR wrote the initial draft of the manuscript with all authors being involved in the writing, editing and discussion of the paper.

CONFLICT OF INTEREST

DR and CB have no conflict of interest to declare. LP, KM and NP work for Polyneuron Pharmaceuticals who have commercial activity in this disease area.

REFERENCES

(1) Floege, J.; Barratt, J. IgA Nephropathy: A Perspective for 2021. *Semin. Immunopathol.* **2021**, *43* (5), 625–626. https://doi.org/10.1007/s00281-021-00890-9.

(2) Suzuki, H.; Novak, J. IgA Glycosylation and Immune Complex Formation in IgAN. *Semin. Immunopathol.* **2021**, *43* (5), 669–678. https://doi.org/10.1007/s00281-021-00883-8.

(3) Floege, J.; Rauen, T.; Tang, S. C. W. Current Treatment of IgA Nephropathy. *Semin. Immunopathol.* **2021**, *43* (5), 717–728. https://doi.org/10.1007/s00281-021-00888-3.

(4) Wyatt, R. J.; Julian, B. A. IgA Nephropathy. *N. Engl. J. Med.* **2013**, *368* (25), 2402–2414. https://doi.org/10.1056/NEJMra1206793.

(5) Bolscher, J. G. M.; Brevoord, J.; Nazmi, K.; Ju, T.; Veerman, E. C. I.; van Wijk, J. A. E.; Cummings, R. D.; Die, I. van. Solid-Phase Synthesis of a Pentavalent GalNAc-Containing Glycopeptide (Tn Antigen) Representing the Nephropathy-Associated IgA Hinge Region. *Carbohydr. Res.* **2010**, *345* (14), 1998–2003. https://doi.org/https://doi.org/10.1016/j.carres.2010.07.022.

(6) Aliu, B.; Demeestere, D.; Seydoux, E.; Boucraut, J.; Delmont, E.; Brodovitch, A.; Oberholzer, T.; Attarian, S.; Théaudin, M.; Tsouni, P.; Kuntzer, T.; Derfuss, T.; Steck, A. J.; Ernst, B.; Herrendorff, R.; Hänggi, P. Selective Inhibition of Anti-MAG IgM Autoantibody Binding to Myelin by an Antigen-Specific Glycopolymer. *J. Neurochem.* **2020**, *154* (5), 486–501. https://doi.org/10.1111/jnc.15021.

(7) Matsushita, T.; Hinou, H.; Kurogochi, M.; Shimizu, H.; Nishimura, S.-I. Rapid Microwave-Assisted Solid-Phase Glycopeptide Synthesis. *Org. Lett.* **2005**, *7* (5), 877–880. https://doi.org/10.1021/ol0474352.

(8) Ohyabu, N.; Kakiya, K.; Yokoi, Y.; Hinou, H.; Nishimura, S.-I. Convergent Solid-Phase Synthesis of Macromolecular MUC1 Models Truly Mimicking Serum Glycoprotein Biomarkers of Interstitial Lung Diseases. *J. Am. Chem. Soc.* **2016**, *138* (27), 8392–8395. https://doi.org/10.1021/jacs.6b04973.

(9) Palitzsch, B.; Gaidzik, N.; Stergiou, N.; Stahn, S.; Hartmann, S.; Gerlitzki, B.; Teusch, N.; Flemming, P.; Schmitt, E.; Kunz, H. A Synthetic Glycopeptide Vaccine for the Induction of a Monoclonal Antibody That Differentiates between Normal and Tumor Mammary Cells and Enables the Diagnosis of Human Pancreatic Cancer. *Angew. Chemie Int. Ed.* **2016**, *55* (8), 2894–2898. https://doi.org/doi:10.1002/anie.201509935.

(10) Zhang, Y.; Muthana, S. M.; Farnsworth, D.; Ludek, O.; Adams, K.; Barchi, J. J.; Gildersleeve, J. C. Enhanced Epimerization of Glycosylated Amino Acids During Solid-Phase Peptide Synthesis. *J. Am. Chem. Soc.* **2012**, *134* (14), 6316–6325. https://doi.org/10.1021/ja212188r.

(11) Thoma, G.; Patton, J. T.; Magnani, J. L.; Ernst, B.; Öhrlein, R.; Duthaler, R. O. Versatile Functionalization of Polylysine: Synthesis, Characterization, and Use of Neoglycoconjugates. *J. Am. Chem. Soc.* **1999**, *121* (25), 5919–5929. https://doi.org/10.1021/JA984183P/SUPPL_FILE/JA984183P_S.PDF.

(12) Yasutake, J.; Suzuki, Y.; Suzuki, H.; Hiura, N.; Yanagawa, H.; Makita, Y.; Kaneko, E.; Tomino, Y. Novel Lectin-Independent Approach to Detect Galactose-Deficient IgA1 in IgA Nephropathy. *Nephrol. Dial. Transplant.* **2015**, *30* (8), 1315–1321. https://doi.org/10.1093/ndt/gfv221.

SUPPLEMENTARY FIGURES

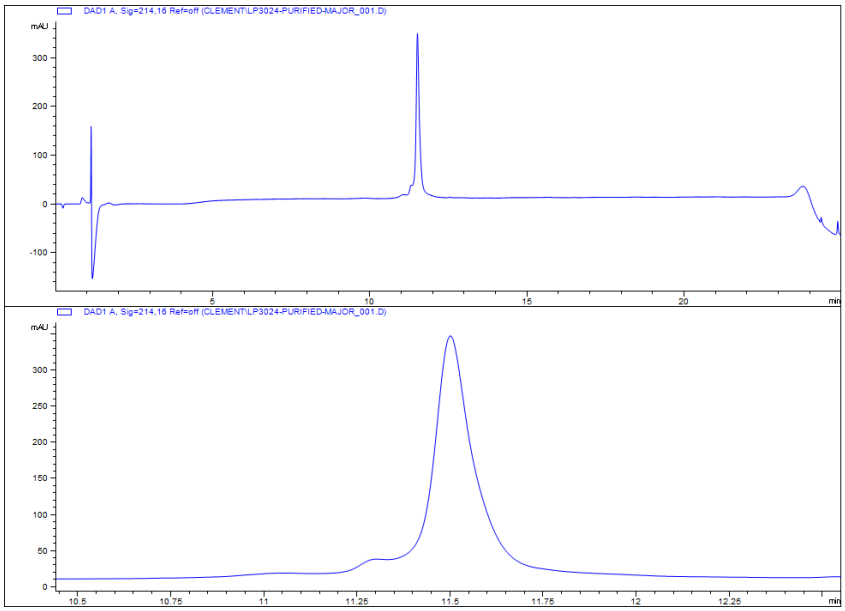

Supplementary Figure S1: Chromatogram, measured at 214 nm wavelength of the purified glycopeptide **1c**. Top: full view, bottom: focused view of signal.

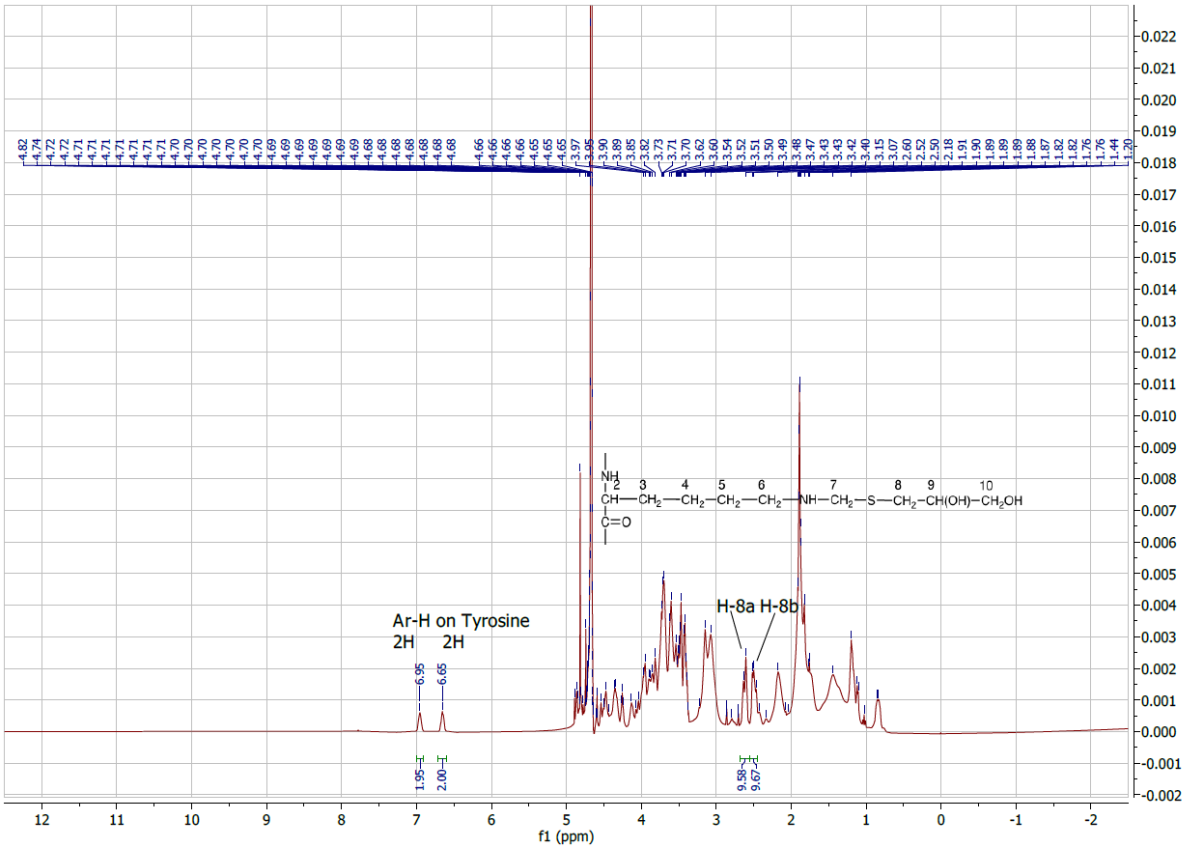

Supplementary Figure S2: ^{1}H-NMR of the glycopeptide-polylysine **5**.

Original Article

CHAPTER 6: EXPLORING THE FUNCTION OF THE FREE B SUBUNIT OF COAGULATION FACTOR XIII: INTERACTIONS WITH COMPLEMENT PROTEINS

Bojun Li[1], Clément Bechtler[2], Lorenz Jenny[1], Daniel Ricklin[2], Verena Schroeder[1]

[1] Experimental Haemostasis Group, Department for BioMedical Research DBMR, University of Bern, Bern, Switzerland
[2] Molecular Pharmacy Group, Department of Pharmaceutical Sciences, University of Basel, Basel, Switzerland

Corresponding author:
Prof. Dr. V. Schroeder
University of Bern, Department of BioMedical Research, Murtenstrasse 40, CH-3008 Basel, Switzerland. E-mail: verena.schroeder@dbmr.unibe.ch

In revision in *Research and Practice in Thrombosis and Haemostasis (RPTH)* (ISSN: 2475-0379)

Contributions of Clément Bechtler:

- Design, performance and analysis of SPR experiments
- Support in manuscript preparation

Original Article

Exploring the function of factor XIII free B-subunit: interactions with complement factors and effects on plasma clot formation and lysis

Bojun Li PhD[1], Clément Bechtler MPhil[2], Lorenz Jenny PhD[1], Daniel Ricklin PhD[2], Verena Schroeder PhD[1]

[1] Experimental Haemostasis Group, Department for BioMedical Research DBMR, University of Bern, Bern, Switzerland
[2] Molecular Pharmacy Group, Department of Pharmaceutical Sciences, University of Basel, Basel, Switzerland

Corresponding author:
Verena Schroeder, PhD, Associate Professor
Experimental Haemostasis Group
Department for BioMedical Research
University of Bern
Murtenstrasse 40
3008 Bern
Switzerland
Phone: +41 31 632 9618
E-mail: verena.schroeder@dbmr.unibe.ch

ABSTRACT
Host-defense pathways such as the complement and coagulation systems are important for protection against external threats and for tissue homeostasis, but uncontrolled activation of those pathways can lead to serious host damage, as recently observed in severe cases of COVID-19. Structural similarities and functional crosstalk between complement and coagulation is increasingly recognized, but a detailed understanding remains elusive. Within the coagulation cascade, factor XIII (FXIII) is the final protease, forming a stable blood clot by crosslinking fibrin. Its regulatory subunit FXIII-B shows high structural similarity with the complement regulators factor H (FH) and C4b-binding protein (C4BP). It has been suggested that FXIII-B also acts in analogy by binding the complement protein C3b and acting as a cofactor for the protease factor I (FI) to facilitate the degradation of C3b. In this study, we provide evidence that FXIII-B does not function as cofactor for FI nor exert other complement-regulatory effects, owing to the lack of notable interactions with complement opsonins C3b, iC3b and C4b. Although a functional interplay at another level cannot be fully excluded, our insight suggests that FXIII-B should not be added to the growing list of host defense proteins that mediate a crosstalk between complement and coagulation.

INTRODUCTION
Coagulation factor XIII (FXIII) circulates in plasma as a heterotetramer consisting of two catalytic A-subunits (FXIII-A) and two protective/inhibitory B-subunits (FXIII-B). The transglutaminase FXIII-A is synthesized by cells of bone marrow origin and is present in platelets and monocytes/macrophages in dimeric form (FXIII-A_2), also referred to as cellular factor XIII. While FXIII-B is mainly expressed in the liver and secreted by hepatocytes[1], it rapidly binds FXIII-A in plasma to create a stable complex (FXIII-A_2B_2) that circulates at an average concentration of 21.6 µg/ml[2].
FXIII-B consists of 641 amino acids, with a molecular mass of ≈80 kDa, and is assembled from ten short consensus repeat domains (SCR; also termed complement control protein, CCP, or sushi domains). Each SCR domain contains about 60 amino acids held together by a pair of internal disulfide bonds[1]. In plasma, about half of the total amount of FXIII-B circulates in complex with FXIII-A, serving as carrier and regulatory protein[3]. The B-subunit protects the A-subunit from proteolysis and thus prolongs its circulating half-life. Consequently, patients with congenital FXIII-B deficiency, which is extremely rare, show significantly decreased FXIII-A levels and moderate bleeding symptoms.[4,5] FXIII-B also mediates the interaction between the FXIII heterotetramer and fibrinogen. By facilitating the formation of a ternary complex between proenzyme (FXIII-A), substrate (fibrinogen) and activator (thrombin), FXIII-B accelerates fibrin crosslinking[6].
While plasma FXIII-A is almost exclusively present as part of the FXIII heterotetramer, only half of the total FXIII-B present in plasma is complex-bound[3]. Approximately 50% of FXIII-B exists in free form in plasma, presumably as a homodimer[3,7]. Importantly, the functional implications of this significant amount of free FXIII-B subunit remain unknown. In patients with congenital FXIII-A deficiency, the total amount of FXIII-B can decrease slightly, but the concentration of free FXIII-B remains constant[1]. This may indicate that free FXIII-B may have other functions in addition to binding and regulating the FXIII-A subunits.
The gene encoding FXIII-B is part of the regulator of complement activation (RCA) gene cluster, which also comprises 15 genes related to the complement system[8,9]. The proteins encoded by these genes share significant similarities in amino acid sequence and structural characteristics as they are all primarily composed of SCR domains. Complement factor H (FH)

and C4b-binding protein (C4BP) are the major complement regulators in the fluid phase[10]. FH serves as cofactor in the factor I (FI)-dependent inactivation of C3b to iC3b and prevents alternative pathway amplification by accelerating the decay of the C3 convertase complexes[11]. C4BP is the major soluble inhibitor of the classical and lectin pathways, with cofactor activity in the degradation of C4b and decay acceleration activity towards C3 convertases of the classical/lectin pathway[12]. Whereas FH is a single-chain protein with 20 SCR domains, the major isoform of C4BP is composed of seven identical α-chains, each containing 8 SCR domains, and a single β-chain of 3 SCR domains[13]. Intriguingly, FH is more closely related to FXIII-B than to the other complement regulators, and individual SCR domains of FXIII-B and FH share sequence homologies of 30-40%[13,14]. This could suggest a putative role of FXIII-B in the regulation of the complement system, which is even more conceivable when considering the numerous crosstalk functions between the complement and coagulation systems. A recent study employed proteomics to identify potential interaction partners for FXIII-B and reported that FXIII-B could bind to complement C1q and C3; it also found FH to be present in FXIII concentrates purified from human plasma[15]. However, another study from the same group suggested that the FXIII-B subunit has no effect on the rate of complement activation and, hence, exerts no regulatory functions in the complement system[16].
In the present study we aimed to address the open questions on potential functions of free FXIII-B and the partly conflicting results reported so far. We tested for cofactor activity of free FXIII-B in the degradation of complement C3b and C4b and used ELISA- and surface plasmon resonance (SPR)-based binding assays to investigate the interaction profile between free FXIII-B and complement components.

METHODS

Protein reagents. Recombinant FXIII-A and FXIII-B were purchased from Zedira (Darmstadt, Germany) and α2-macroglobulin and bovine serum albumin (BSA) from Sigma-Aldrich/Merck (Darmstadt, Germany). Plasma-purified C3b, C4b, FH, C4BP, and FI were purchased from Complement Technology Inc. (Tyler, Texas, USA).

Influence of free FXIII-B on the degradation of complement C3b and C4b. We tested for potential cofactor activity of FXIII-B in the FI-mediated degradation of C3b and C4b using similar protocols as described earlier[17,18]. In a final reaction volume of 30 µl, C3b (final concentration 50 µg/ml) was incubated with FI (10 µg/ml) in the presence of FH (4 µg/ml) and/or FXIII-B (10 µg/ml) for up to 20 min at 37°C. Similarly, C4b (267 µg/ml) was incubated with FI (10 µg/ml) in the presence of C4BP (4 µg/ml) and/or FXIII-B (10 µg/ml) for up to 20 min at 37°C. The reactions were stopped by adding reducing Lämmli buffer (NuPAGE™ LDS sample buffer). The samples were boiled at 70°C for 10 min and run in MES SDS running buffer on a 4-12% NuPAGE™ Novex Bis-Tris Mini Gel (Invitrogen, Thermo Fisher Scientific, Waltham MA, USA) together with a Precision Plus Protein Dual Color Standard (Bio-Rad, Hercules CA, USA). The gels were stained with Coomassie (Bio-Rad).

Binding of free FXIII-B to C3b and C4b investigated by ELISA-based binding assays. ELISA-based binding assays with FXIII-B, C3b and C4b were performed according to published protocols[17,18]. As positive controls and comparison we used purified FH and C4BP, and BSA was used as negative control. The assays were performed in both orientations. Proteins were coated onto 96-well microplates (Nunc Immuno Maxisorp, Thermo Fisher Scientific, Waltham MA, USA) over night. The plates were blocked with 1% BSA solution. The proteins to bind were added in a concentration range of 0.3-50 µg/ml and detected with polyclonal antibodies goat anti-human C3, goat anti-human C4, goat anti-human FH (all from Complement

Technology Inc., Tyler, Texas, USA), rabbit anti-FXIII-B (Calbiochem, Merck, Darmstadt, Germany), a monoclonal murine anti-human C4BP (Quidel, San Diego, CA, USA), and secondary peroxidase-labelled anti-goat IgG, anti-rabbit IgG and anti-mouse IgG (all from Sigma-Aldrich, Merck, Darmstadt, Germany).

SPR analysis of FXIII-B interactions. The interaction pattern between FXIII-B, FXIII-A, FH, C3b, C4b and α2-macroglobulin was elucidated by SPR at 20°C on a Biacore T200 instrument using a CMD200M sensor chip (Xantec, Düsseldorf, Germany). Amine coupling (NHS/EDC) for protein immobilization on separate flow cells (Fc). Fc1 served as mock-activated (EDC/NHS, then ethanolamine) reference surface. FXIII-B (6546 response units; RU) was immobilized on Fc2, C3b (8202 RU) on Fc3 and iC3b (14582 RU) on Fc4. The analytes were injected in a concentration range of 0.22 nM – 500 nM in 1:2 serial dilutions. The flow rate was 10 µL/min and the association and dissociation phases were measured for 600 s. The running buffer consisted of PBSTE (10 mM Na_2HPO_4, 140 mM NaCl, 2.7 mM KCl, 50 µM EDTA, 0.005% Tween 20, pH 7.4, 0.03% sodium azide; Xantec) if not mentioned otherwise. Other running buffer was HBST++ (10 mM HEPES, 150 mM NaCl, 1 mM $MgCl_2$, 2.5 mM $CaCl_2$, 0.005% Tween20, pH 7.4; Xantec). Regeneration was performed with 0.1 M Na_2CO_3, 30 µL/min, for 30 s and 120 s stabilization period. 0.1 M Na2CO3 by dissolving the pure salt in bidistilled H_2O without further pH adjustment. Data analysis was performed with BiaEvaluation (Cytiva) and Scrubber software (BioLogic) after reference subtraction (Fc1). For single normalization, the SPR signal was divided by the molecular weight of ligand. For double normalization, correction for ligand molecular weight and target density was calculated according to the formula: $Normalized\ binding = \frac{\frac{analyte\ binding\ [RU]}{ligand\ loading\ [RU]}}{ligand\ molecular\ weight\ [RU]}$.

RESULTS AND DISCUSSION

Free FXIII-B does not act as cofactor in the degradation of complement C3b and C4b. Complement activation fragments C3b and C4b are degraded in the fluid phase by FI in the presence of cofactors FH and C4BP, respectively. To test for potential cofactor activity of FXIII-B due to its similarities with FH and C4BP, we incubated C3b or C4b with FI in the presence of FXIII-B and/or FH or C4BP. The C3b and C4b degradation products were analyzed by SDS-PAGE. In the cofactor activity experiments shown in **Figure 1**, C3b (**Figures 1A,C**) and C4b (**Figures 1B,D**) cleavage products generated by FI in the presence of FH or C4BP could be clearly detected (indicated by arrows in **Figures 1A** and **1B**) and appeared as early as 5 min of incubation (**Figures 1C-D**). In the presence of FXIII-B, however, no C3b and C4b cleavage products were generated even after 20 min of incubation (**Figures 1A-B**). Furthermore, FXIII-B did not affect the cofactor activity of FH and C4BP: addition of FXIII-B to the digestion of C3b in presence of FH (**Figure 1C**) and to the digestion of C4b in presence of C4BP (**Figure 1D**) did not impair the digestion either, so there was no competition for binding sites between FXIII-B and FH or C4BP.

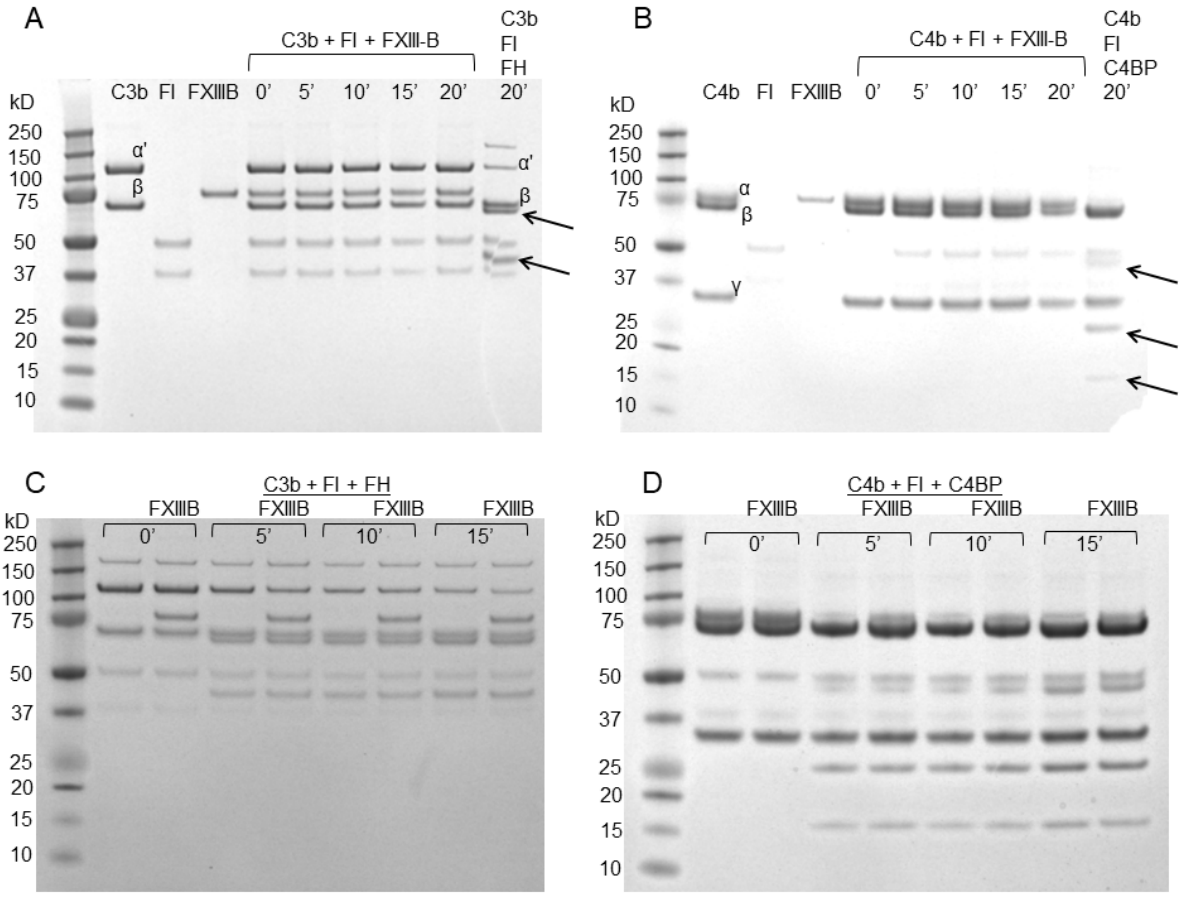

Figure 1. Cofactor activity in the degradation of complement C3b and C4b. C3b and C4b were incubated with FI in presence of cofactors FH and C4BP, respectively, and/or free FXIII-B. (**A**) The individual proteins C3b, FI and FXIII-B are shown, followed by a time-course of the incubation with FXIII-B. The last lane shows as positive control the degradation of C3b by FI in the presence of FH and the degradation products are indicated with arrows. (**B**) The individual proteins C4b, FI and FXIII-B are shown, followed by a time-course of the incubation with FXIII-B. The last lane shows as positive control the degradation of C4b by FI in the presence of C4BP and the degradation products are indicated with arrows. (**C**) C3b was incubated with FI and FH over 15 min, and in every second sample FXIII-B was added. (**D**) C4b was incubated with FI and C4BP over 15 min, and in every second sample FXIII-B was added.

Free FXIII-B does not specifically bind to complement factors to a significant extent. In a first step, we performed ELISA-based binding assays to investigate potential interactions between free FXIII-B and complement C3b and C4b. As shown in **Figures 2A** and **2B**, FXIII-B exhibited dose-dependent binding to C3b and C4b, albeit to a lesser extent compared with FH and C4BP, respectively. However, when the orientation was changed as shown in Figures **2C** and **2D**, C3b and C4b showed binding to FXIII-B to a similar extent as to the negative control BSA, suggesting nonspecific binding.

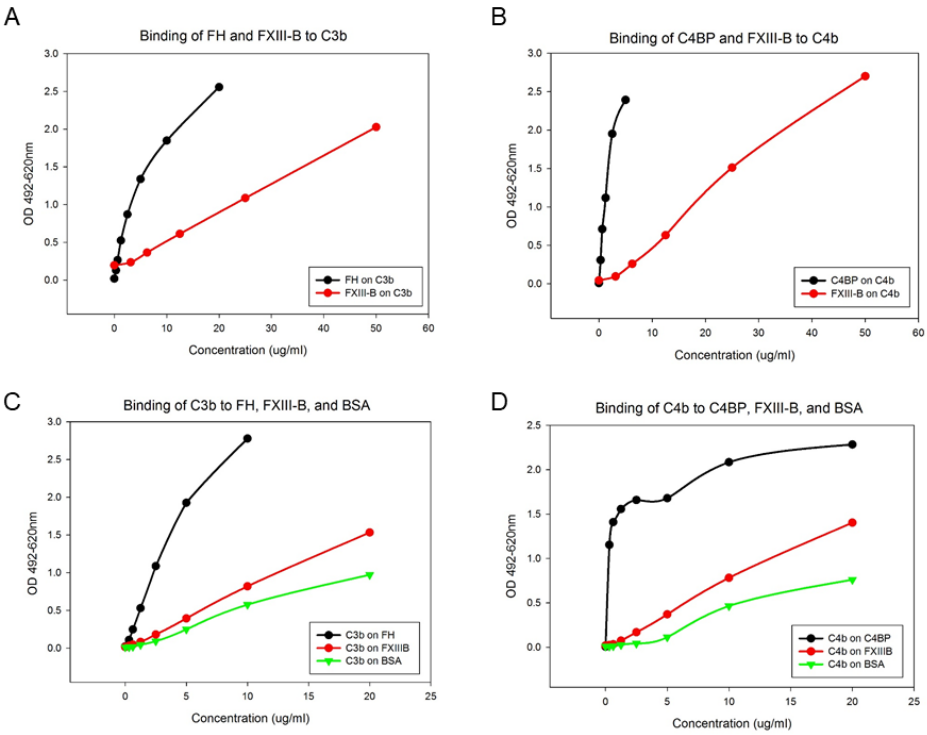

Figure 2. ELISA-based binding assays. (**A**) Dose-dependent binding of FH and free FXIII-B to C3b coated onto a microplate. (**B**) Dose-dependent binding of C4BP and free FXIII-B to C4b coated onto a microplate. (**C**) Dose-dependent binding of C3b to FH, FXIII-B and BSA coated onto a microplate. (**D**) Dose-dependent binding of C4b to C4BP, FXIII-B and BSA coated onto a microplate.

To further investigate whether there are notable, even if transient, interactions between FXIII-B and complement proteins, we employed an SPR-based direct binding assay. **Figures 3A-C** show the dose-response curves for the binding of ligands to immobilized FXIII-B. The complement components C3b, C4b and FH do not bind, with the presence of Mg^{2+} and Ca^{2+} (**Figure 3C**) buffer having no influence on the complement protein signals. As expected, only FXIII-A shows strong binding to FXIII-B in all experiments. While recombinant FXIII-A and FXIII-B proteins usually exist as dimers, some dissociation into monomers may explain the signal of FXIII-B ligand on the FXIII-B surface. Next, the orientation was reversed and the ligands were added to immobilized C3b (**Figures 3D-F**) and its degradation product iC3b. Only FH showed strong binding to C3b, as expected. Interestingly, FXIII-A showed residual binding, which is plausible as we have shown earlier that C3 is a substrate of FXIII-A and can be incorporated into a fibrin clot by FXIII-A[19]. A weak binding signal could also be observed for FXIII-B. In the presence of Ca^{2+} and Mg^{2+}, the binding signals of FXIII-A and FXIII-B to C3b increased slightly, but were still substantially lower when compared to FH. **Figure 4** shows the comparative ligand binding to FXIII-B, C3b and iC3b surfaces in the absence (**Figure 4A**) and presence of Ca^{2+} and Mg^{2+} (**Figure 4B**). The direct comparison shows strong and dose-dependent binding only between FXIII-A and FXIII-B and between FH and C3b. As expected, FH binds strongly to C3b and weakly to iC3b. C3b does not bind to immobilized FXIII-B and although some signals are observed for the binding of FXIII-B to immobilized C3b, the detection of similar signals on the FXIII-B and iC3b surfaces indicate non-specific binding. Also, in contrast to FH, no signal drop between C3b and iC3b can be observed for binding of FXIII-B, which would be expected if FXIII-B behaved similarly to FH. Taken together, the SPR analysis suggests that FXIII-B does not act as FH-type ligand for C3b.

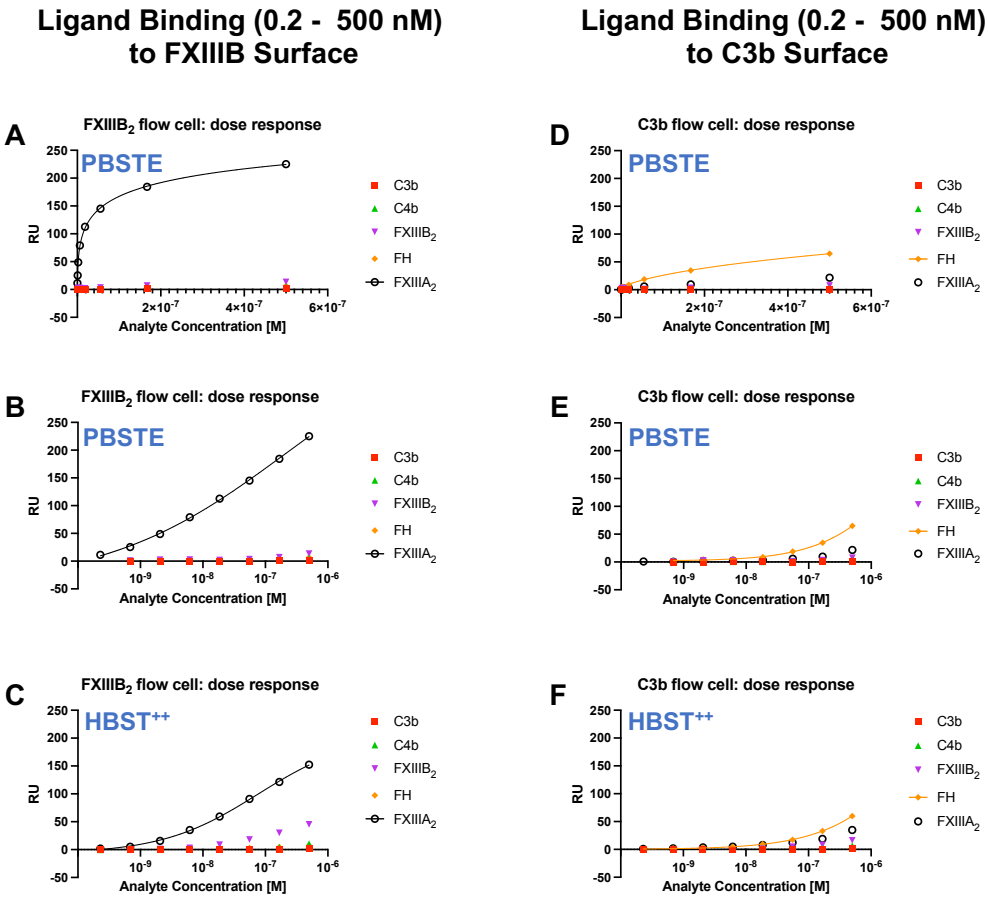

Figure 3. Dose-response curves obtained with SPR. Panels **A-C** show ligand binding to the FXIII-B surface. Panels **D-F** show ligand binding to the C3b surface. Panels **A** and **D** show normalized dose response curves in PBSTE buffer with linear concentration scale, panels **B**, **C** and **E**, **F** show logarithmic concentration scales.

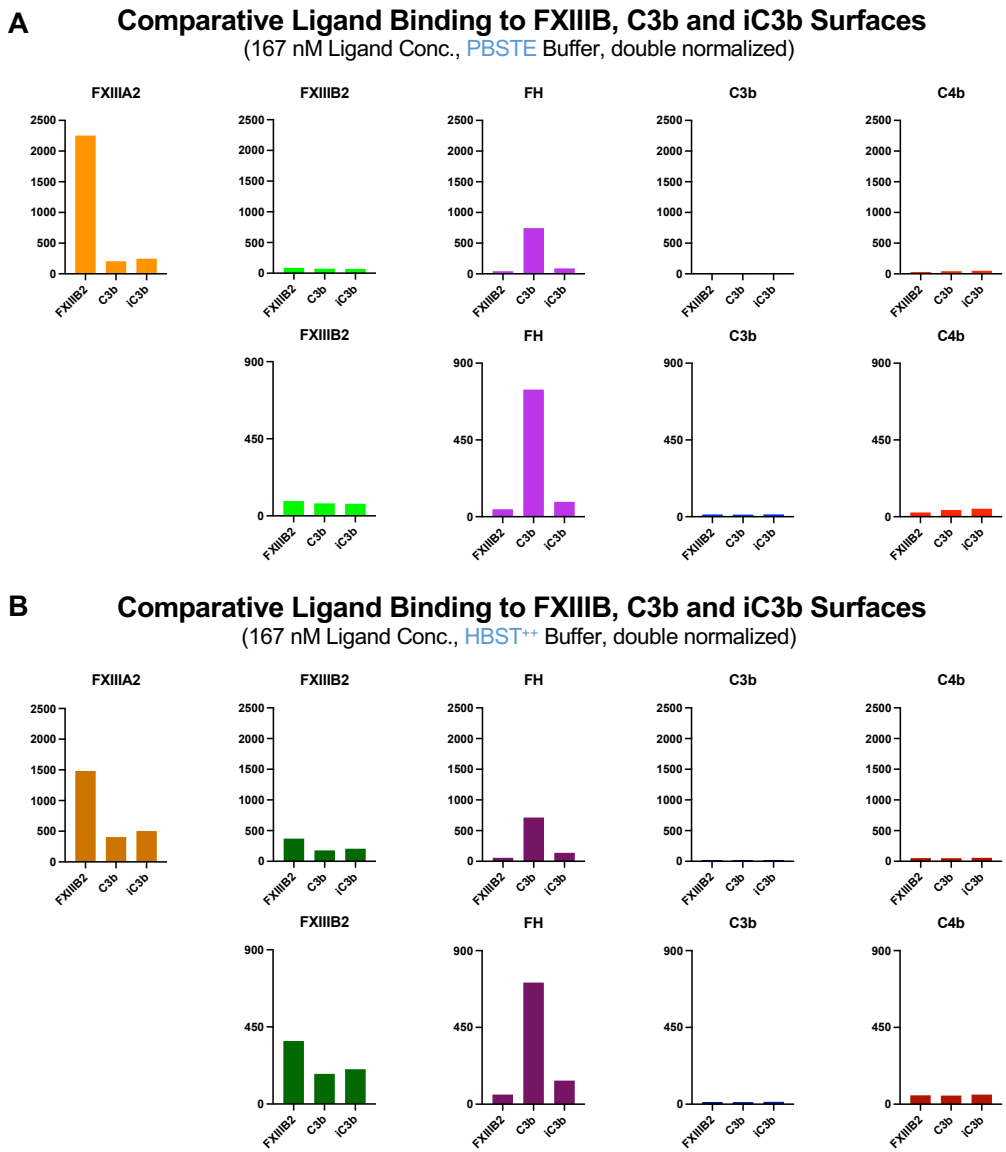

Figure 4. Comparative ligand binding to FXIII-B, C3b and iC3b surfaces obtained with SPR. Panel **A** shows the binding experiments performed in PBST-EDTA buffer, panel **B** in HBST buffer containing Ca^{2+} and Mg^{2+}. The upper rows show the scale up to 2500 RU, the rows below up to 900 RU to see smaller differences.

CONCLUSIONS

The FXIII-B subunit has a critical function as carrier protein to stabilize FXIII-A in plasma and supply it to its main substrate fibrinogen. Therefore, the body must ensure that a sufficient plasma concentration of FXIII-B, which is produced at a different site than FXIII-A, is maintained. However, the large excess of FXIII-B over FXIII-A has puzzled FXIII experts for a long time leading to the hypothesis that free FXIII-B may have other and hitherto unknown functions. Considering the structural similarity with complement regulators FH and C4BP, an interaction between free FXIII-B and components of the complement system with regulatory or other crosstalk implications had emerged as one of the functional hypotheses. In the present study we investigated whether FXIII-B may exert a functional profile similar to the cofactor activity of FH and C4BP in the degradation of C3b and C4b by FI. However, we observed no influence of FXIII-B. We also investigated the interaction of FXIII-B with C3b and C4b by ELISA- and SPR-based binding assays but could not observe notable specific binding to those complement proteins. We therefore conclude that, despite structural relation to

complement regulators, FXIII-B has no role in the regulation of the complement system that is analog to FH or C4BP.

Authorship Contributions

B. Li performed the ELISA-based binding assays, developed the approach and performed the experiments to test for binding partners of free FXIII-B. L. Jenny performed the cofactor activity experiments. C. Bechtler performed and analyzed the SPR experiments, D. Ricklin designed and analyzed the SPR experiments. V. Schroeder designed the research, analyzed the results, and co-wrote the manuscript. All authors reviewed the manuscript.

Acknowledgments

This work was supported by grants from the Swiss National Science Foundation (grant number 310030_169220 to V. Schroeder and 31003A_176104 to D. Ricklin) and OPO Foundation.

Disclosure of Conflict of Interest

The authors declare no conflicts of interest.

REFERENCES

1. Muszbek L, Bereczky Z, Bagoly Z, Komaromi I, Katona E. Factor XIII: a coagulation factor with multiple plasmatic and cellular functions. *Physiol Rev*. 2011;91:931-972.
2. Schroeder V, Kohler HP. New developments in the area of factor XIII. *J Thromb Haemost*. 2013;11:234-244.
3. Katona E, Penzes K, Csapo A, et al. Interaction of factor XIII subunits. *Blood*. 2014;123:1757-1763.
4. Rodeghiero F, Tosetto A, Di Bona E, Castaman G. Clinical pharmacokinetics of a placenta-derived factor XIII concentrate in type I and type II factor XIII deficiency. *Am J Hematol*. 1991;36:30-34.
5. Saito M, Asakura H, Yoshida T, et al. A familial factor XIII subunit B deficiency. *Br J Haematol*. 1990;74:290-294.
6. Souri M, Osaki T, Ichinose A. The non-catalytic B subunit of coagulation factor XIII accelerates fibrin cross-linking. *J Biol Chem*. 2015;290:12027-12039.
7. Souri M, Kaetsu H, Ichinose A. Sushi domains in the B subunit of factor XIII responsible for oligomer assembly. Biochemistry. 2008;47:8656-8664.
8. Rodriguez de Cordoba S, Rey-Campos J, Dykes KK, McAlpine PJ, Wong P, Rubinstein P. Coagulation factor XIII B subunit is encoded by a gene linked to the regulator of complement activation (RCA) gene cluster in man. *Immunogenetics*. 1988;28:452-454.
9. Rey-Campos J, Baeza-Sanz D, Rodriguez de Cordoba S. Physical linkage of the human genes coding for complement factor H and coagulation factor XIII B subunit. *Genomics*. 1990;7:644-646.
10. Ricklin D, Hajishengallis G, Yang K, Lambris JD. Complement: a key system for immune surveillance and immune control. *Nature Immunol*. 2010;11:785-797.
11. Ferreira VP, Pangburn MK, Cortes C. Complement control protein factor H: the good, the bad, and the inadequate. *Mol Immunol*. 2010;47:2187-2197.
12. Blom AM, Villoutreix BO, Dahlbäck B. Functions of human complement inhibitor C4b-binding protein in relation to its structure. *Arch Immunol Ther Exp*. 2004;52:83-95.
13. Krushkal J, Bat O, Gigli I. Evolutionary relationships among proteins encoded by the regulator of complement activation gene cluster. *Mol Biol Evol*. 2000;17:1718-1730.

14. Biswas A, Thomas A, Bevans CG, Ivaskevicius V, Oldenburg J. In vitro secretion deficits are common among human coagulation factor XIII subunit B missense mutants: correlations with patient phenotypes and molecular models. *Hum Mutat*. 2013;34:1490-1500.
15. Singh S, Akhter MS, Dodt J, et al. Identification of potential novel interacting partners for coagulation factor XIII B (FXIII-B) subunit, a protein associated with a rare bleeding disorder. *Int J Mol Sci*. 2019;20:2682.
16. Akhter MS, Singh S, Yadegari H, Ivaskevicius V, Oldenburg J, Biswas A. Exploring the structural similarity yet functional distinction between coagulation factor XIII-B and complement factor H sushi domains. *J Thromb Thrombolysis*. 2019;48:95-102.
17. Tortajada A, Montes T, Martinez-Barricarte R, Morgan BP, Harris CL, Rodriguez de Cordoba S. The disease-protective complement factor H allotypic variant Ile62 shows increased binding affinity for C3b and enhanced cofactor activity. *Hum Mol Genet*. 2009;18:3452-3461.
18. Happonen KE, Sjöberg AP, Mörgelin M, Heinegard D, Blom AM. Complement inhibitor C4b-binding protein interacts directly with small glycoproteins of the extracellular matrix. *J Immunol*. 2009;182:1518-1525.
19. Richardson VR, Schroeder V, Grant PJ, Standeven KF, Carter AM. Complement C3 is a substrate for activated factor XIII that is cross-linked to fibrin during clot formation. *Br J Haematol.* 2013;160:116-119.

END OF RESULTS SECTION

DISCUSSION AND OUTLOOK

Herein, we presented the development of a peptide conjugate (5C6) with the capacity to recruit the complement regulator FH to biomedical surfaces and a synthetic glycopeptide, which mimics the pathogenic gd-IgA1 epitope in IgAN, as novel potential treatment options in complement-related immune disorders. Based on our in-depth SAR studies, the affinity, activity and stability of the cyclic peptide 5C6 could be substantially improved and a preferential surface tethering position was identified. Their stability, selectivity and ability to bind murine FH render 5C6 and its derivatives attractive candidates for further development in complement-mediated diseased triggered by a local reaction to a biomaterial surface. For the gd-IgA1 glycopeptide, improved synthesis conditions could be found, enabling us to verify the concept that the immobilized epitope fragment can bind to disease-causing antibodies. This validation lay the foundation for advancing this innovative treatment strategy in a condition without causal treatment option currently available.

STRUCTURE-ACTIVITIY RELATIONSHIPS OF 5C6

The aim of this thesis was to further advance the development of the FH-binding peptide 5C6 with the intention to protect biomaterials from undesired complement attack. As 5C6 acts on material surfaces, suitable tethering positions and spacing options were explored and optimized. Moreover, a systematic SAR study was conducted to improve affinity towards FH. In this thesis, we could show that 5C6's C-terminus and cyclic nature are essential for the binding affinity towards FH, while the N-terminus only has limited contributions to the target interaction. We demonstrated that the N-terminal R5 is nevertheless involved in binding and the affinity can be further increased by replacing it with Trp. Removing residues 1-4 improves affinity, although they were found suitable as spacer during 5C6 immobilization. Within the cyclic core and exocyclic C-terminus, we could identify Y8, S9, W11 and H14 as critical residues for the interaction, as seen during a systematic replacement with alanine. Finally, by replacing S13 with Thr and expanding the peptide sequence C-terminally, in particular with Phe, we were able to further improve the affinity, resulting in a next-generation 5C6 analog (peptide **50**; Ac-ASSSW[CTYSHWC]THF-$CONH_2$) with eight-fold enhanced FH binding over the parental peptide. Besides the improved affinity, peptide **50** also showed an increased activity in our nanoparticle-like assay that was developed as part of this work, mimicking the clinical situation during nanoparticle treatment.

Based on insight gained from these comprehensive SAR studies, further optimization campaigns appear highly promising. For example, we only investigated functionally and/or stereochemically distinct substitutions of Y8; the extension to more closely related substituents, e.g. halogenated tyrosine analogs to modulate electronic properties, might yield additional benefits. A large number of modified Tyr analogs are commercially available or synthetically accessible, which may facilitate the fine-tuning of this position.[137,138] Yet, the region in 5C6 that arguably presents most room for improvement is the exocyclic C-terminus. Further expansion might allow for additional contacts, while our limited number of analogs investigated for the additional 15 position makes it plausible that screening a larger set of residues at this position, especially aromatic ones, will yield an even further improvement on the +15F addition described here. Another alternative is to perform a new round of phage- or mRNA-display screening in which the residues determined to be essential would be kept fixed, but were allowed to further extend on the C-terminus.

Of note, proteolytic cleavage of the C-terminus was identified as major route of metabolism in serum; it might therefore be interesting to investigate whether the use of D-amino acids at the C-terminus may improve stability.[97] In particular, as the exocyclic C-terminus showed to be rather flexible in the solution structure, in line with the small effect of the H14h substitution on the affinity, stereochemical inversion might not substantially diminish binding. The substitution with the respective D-amino acids can also be a propitious approach for the positions which showed no improvement so far, but without being highly sensitive towards change either (W5, T7, H10, T13 in peptide **50**). **Figure 4** summarizes the structure-activity relationship of peptide **50**.

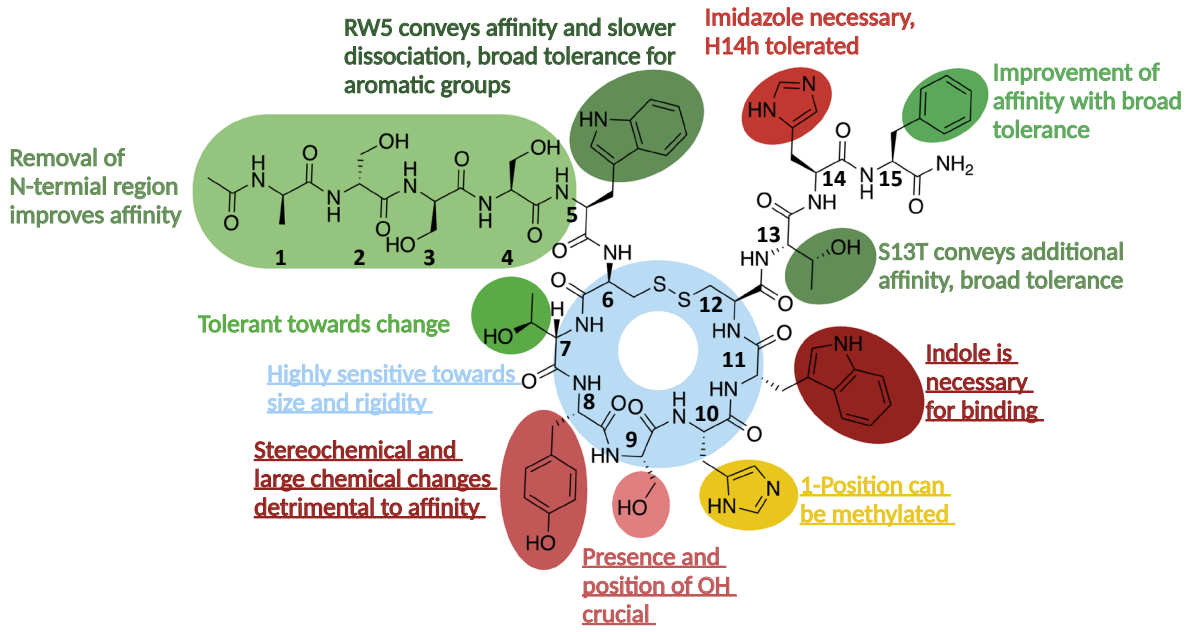

Figure 4: SAR summary of the next-generation 5C6 derivative, peptide **50**. Residue side chains highlighted in red show a high sensitivity toward change, yellow an intermediate sensitivity and green a low sensitivity. Residues whose label is underlined had a relatively fixed position in the solution structure of tr5C6.

Additional to binding affinity at equilibrium, binding kinetics also play an important role for selection of promising hit compounds and their optimization, with the role of kinetics gaining increasing recognition in the drug discovery field over the last years. Slow dissociation rates have been described as a good guide for hit optimization as it is insensitive to concentration measurement errors, thus more robust and reliable, something we can confirm from the studies presented here. Furthermore, longer target residence time also translates into improved functional activity.[126,161] Hence, combining the current improvements with other substitutions that showed slower dissociation, but slightly lower affinity (i.e. T13L, disulfide to alkene), might yield even further improved derivatives.

Solving the solution structure of tr5C6, which showed rather fixed positions for Y8, S9, H10 and W11, provided an explanation why many of the peptidomimetics with modified bridging displayed strongly reduced affinities. It appears likely that the relevant side chains of residues 8-11 are presented in a deviating way in these cycle-modified analogs, due to differences in size and geometry, leading to less favorable contacts with FH. Hence, the flexibility and size of the disulfide has thus far proven to be pivotal and, among all peptidomimetic analogs, affinity could only be improved by the thioacetal of the same size. This could prove interesting as thioacetals are reductively stable[139], but would require custom-made building blocks for retaining an N-terminal exit vector.

Another approach to achieve this would be to exploit the limited importance of T7, which could be substituted with 2-amino-5-thiopentanoic acid, allowing the formation of a thioacetal macrocycle with the same size as the native disulfide while using the amino group as an exit vector. However, as the more flexible T7G analog lost much more affinity than the T7A analog, this suggests that the current arrangement already has a well-tuned balance between flexibility and rigidity, and that introducing additional flexibility might be as harmful as additional rigidity. A screen of α-methylated amino acids, yielding conformationally more restricted analogs, might nevertheless allow additional conformational fine-tuning.[140]

An additional benefit of replacing the disulfide by another group would be the possibility to introduce a single cysteine as a handle for surface tethering, e.g. through the widely used maleimide chemistry, without the need for an orthogonal protecting group strategy or the risk of disulfide reshuffling. However, as the field of click chemistry is expanding to provide more reactions and milder conditions for established reactions, many options are now available to conjugate molecules without relying on cysteine reactivity, thereby decreasing the need of disulfide replacement for this purpose.[141–145]

Indeed, click-reactions have been shown to be superior to the cysteine-maleimide addition for conjugations as they do not show the drawbacks inherent to the cysteine-maleimide addition, e.g. regarding hydrolysis under basic conditions.[146,147]
Furthermore, as the 5C6 peptide family showed good reductive and proteolytic stability, the disulfide replacement is not expected to be critical for achieving suitable stability profiles. However, in vivo studies or ex vivo studies using whole blood will be necessary to verify the promising in vitro stability profile. For example, it could be shown for the generally more stable antibodies that in vitro models are not always able to capture all degradation processes accurately.[148] This can be due to a number of reasons, such as proteases having only a short half-life in vitro or even be missing completely under certain conditions, e.g. the proteases from the coagulation system when working with serum. The reactions might also not accurately mimic conditions under which 5C6 would be applied, such as thromboinflammatory distress, under which platelets and neutrophils secrete various mediators, including proteases.[149,150] In addition, the correlation between in vitro and in vivo hepatic stability is often poor, which suggests that similar limitations might apply to other stability aspects.[151]

STRUCTURAL ASPECTS OF THE 5C6-FH INTERACTION

The combination of SAR studies on the peptide, its structural elucidation by NMR, the determination of the minimal binding fragment of FH and advances in structural and computational methods provided us with valuable insight into structural aspects of the 5C6-FH interaction. In particular, advances in artificial intelligence allow for more accurate protein structure predictions. Very recently, a new algorithm (AlphaFold) has been described, which predicts protein structures based on the amino acid sequence with high accuracy (median backbone RMSD < 1 Å).[152] Although the applicability and accuracy to specific questions remains to be proven, the predicted structures, many already deposited in a databank[152], may provide rapid access to structural information in the absence of an experimental structure, as in the case of FH. In contrast to previous models of the full-length FH protein[23], the model predicted by AlphaFold does not show an extended structure with a compact core, but a highly folded-back and helical arrangement, overall. At the same time, the AlphaFold model matches available crystal or NMR structures of FH fragments, e.g. the extended arrangement of CCPs 1-3, followed by a bend towards CCP4 or the V-shaped arrangement of CCPs 10 and 11 (**Fig. 5A**).[21,24] This suggests that the AlphaFold model accurately reflects at least the global arrangement of proximal domains.
Based on this insight, we compared the conformation of the highly dissimilar patches between CCP10 and CCP13 of FH and the respective sequence in FHR-5 (as discussed in chapter 3) using the AlphaModel structures of FH and FHR-5. No experimental structure of FHR-5 is currently available which would allow to assess the accuracy of the AlphaFold model of FHR-5. While the overall structure of the patch in CCP10 is not affected much by the sequence differences (**Fig. 5B**, right), the patch in CCP13 changes more significantly (**Fig. 5B**, left). However, as the distance between both regions is 21 – 30 Å, it is unlikely that they both interact directly with 5C6, as the similarly affine tr5C6 has a maximum extension of about 18 Å, based on its NMR structure. This is in line with our affinity studies with FH fragments, which demonstrated that the FH10-13 fragment is not sufficient for binding to FH. However, CPPs 10 and 14 make close contact in the model. Two grooves are formed by the two domains, one being rather small and tight (**Fig. 5C**) and the other large and shallow (**Fig. 5D**), with the dissimilar patch in CCP10 forming the ridge between both grooves. With the distances in the large groove between the ridges spanning 12 – 19 Å, this would allow 5C6 to contact both of them; as a consequence, both grooves could be part of the binding site of 5C6. This putative binding site could suggest that both the ring residues and H14 indeed interact with separate domains as they are pointing towards different directions in the NMR solution structure. Given that FHR-5 has one E-to-H and one D-to-Q (although also one V-to-D) mutation compared to the FH sequence in the dissimilar patch of CCP10, this might implicate that H14 is interacting with CCP10. The presence of a positive charge of His was found critical for binding whereas the presence of an additional negative charge at the C-terminus (e.g. C-terminal carboxylic acid or additional 15D) strongly reduces binding affinity.

Mutational studies on the respective residues (i.e. E570 and D581) could confirm those hypothetical binding sites. Having established the minimal binding region as FH10-14, with a molecular weight of only 34 kDa, NMR studies of the 5C6-protein complex are more amenable to experimentally elucidate the proposed binding mode.[126] Furthermore, the next generation 5C6 analog, peptide **50**, with higher affinity and slower dissociation rates might even facilitate crystallization of the peptide-FH complex. Obtaining structural information with atomic resolution on the interaction is considered critical for rational optimization strategies in the future.

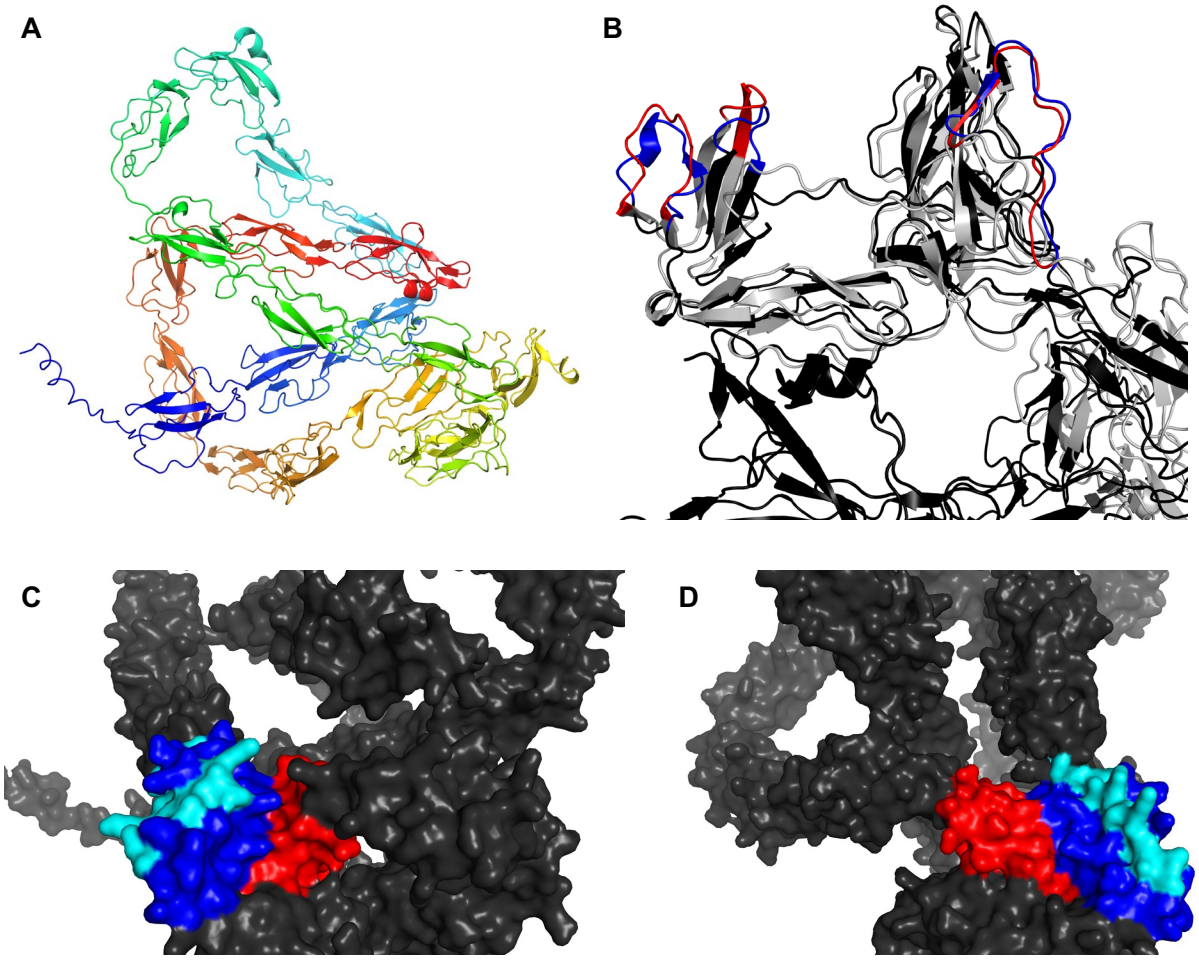

Fig. 5: Structural analysis of the AlphaFold[152] model of FH. (**A**) Full structure, rainbow-colored from N-terminus (blue) to C-terminus (red). It shows a folded-back, helical structure with characteristic bends, *e.g.* between CCPs 3 and 4 or 10 and 11. (**B**) Focused view on the dissimilar patches in CCP10 (right) and CCP13 (left) between FH (black) and FHR-5 (grey), with the patches highlighted in blue (FH) and red (FHR-5). While the overall structure in CCP10 is maintained, it differs more strongly in CCP13. (**C**) and (**D**): View of the small (**C**) and large (**D**) groove formed by CCP10 (blue), including the dissimilar patch (cyan) and CCP14 (red).

IMMOBILIZATION STRATEGIES FOR 5C6

The switch from C-terminal tethering, as derived from phage presentation, to N-terminal immobilization strategies profoundly increased the FH recruitment ability and complement-inhibitory activity in the nanoparticle-like assay. However, this enhancement did not readily translate into improved activity in hemolytic or liposomolytic assays when using lipid-conjugates of 5C6. Although the insertion of a conjugate into erythrocytes was successful, no FH recruitment could be observed. While this is in contrast to the previously reported anti-hemolytic activity of 5C6 conjugates, it needs to be noted that previous studies employed 5C6 constructs with large PEG spacers between peptide and lipid[95]. Additionally, as in the nanoparticle-like assay, the surface tether (biotin) is conjugated to the ε-amino group of Lys, this provides already some additional spacing which is lacking when the lipids are coupled directly to the N-terminus of 5C6. Our preliminary results here using the crude

product of a PEG2000-spaced lipid conjugate of 5C6 suggests that, for Doxil® protection, conjugates with longer spacing might be needed. As Doxil® itself contains PEG2000, it seems probable that similarly sized spacing is required so that 5C6 would be accessible for FH. Also, the glycocalyx of cells is up to 5 µm thick and might shield 5C6 without the use of extended spacing[153] ,with the excocyclic N-terminus having an expected length of 1 – 3 nm, depending on its conformation. 5C6 might thus also need additional spacing to protrude out of the glycocalyx to enable efficient FH recruitment from serum. Nevertheless, as we had previously shown that high molecular weight PEG can itself protect from immune attack, further experiments are required to exclude artefacts from residual unconjugated PEG-lipid.[95] If longer spacing units are indeed required, alternative polymers with low immunogenicity, such as polysarcosine, could also be employed.[154] Additionally, as polysarcosine is more rigid than PEG, it might also prove beneficial regarding the entropic contribution to binding. Another approach to enhance the recruitment capability might be to exploit a different tether and spacer architecture. By using dendrimers, multiple 5C6 peptides could be coupled to one core unit carrying one surface tether and might increase the surface coverage of 5C6. As FH recognizes many ligands found on self-surfaces (e.g. sialic acid, heparin[20]), this could be exploited by coupling sialic acid, for example, to 5C6 and obtain a dual binder to FH. The binding sites (CCPs 7 and 19-20 for sialic acid[20], CCPs 10-14 for 5C6) are distant from each other and therefore require optimization for appropriate spacing, but if successful might prove to strongly enhance affinity as demonstrated by multivalent ligands in other areas, e.g. carbohydrate-protein interactions and as well exploited here in the IgAN project.[162] Finally, future studies conducted with peptide **50** might also improve outcomes based on stronger FH binding and consequently enhance recruitment.

TRANSLATIONAL FUTURE OF 5C6

If 5C6 conjugates prove efficacious in our liposomal lysis assay, a quick progression to in vivo studies is considered important to understand whether the in vitro results also apply to full organisms. Pigs are the preferred animal model for CARPA studies as they show a similar sensitivity and symptoms as humans.[155–158] Dogs show a similar sensitivity, but a different set of responses, whereas rodents show a much weaker sensitivity.[157,158] Nevertheless, rodents show the most important symptoms of CARPA, such as changes in blood pressure and respiratory distress, and can be used as a valid model system.[159] Additionally, the activation of complement in murine serum by pegylated liposomal drug formulations was demonstrated in vitro, thereby providing a mechanistic link.[160] Therefore, mice confer a suitable model for initial studies, especially when considering the species specificity profile of 5C6. If next-generation analogs of 5C6 are found to bind porcine or rat FH, this would largely extend the number of available model systems. Furthermore, structural insight into the binding mode of 5C6 with murine FH could also allow the rational development of 5C6 derivatives for different species, simplifying translational development. Furthermore, as we have previously shown that combing 5C6 with other host-defense regulators yields superior biomaterial protection, this approach could also be applied to future studies.[95] This could both be horizontal (i.e. hitting different pathways) as we have done previously[95], as well as vertical (i.e. hitting different targets within the same pathway), an approach widely used in antimicrobial drug development.[163] For acute applications, e.g. during liposome infusion, 5C6 might be combined with systemically applied complement inhibitors such as the C3-inhibtor pegcetacoplan or other inhibitors currently in development, e.g. inhibiting the AP proteases FB and FD or the LP protease MASP-2.[61, 70] This would allow for potent complement inhibition during this acute indication during which severe reactions can occur and therefore, short-term, but strong inhibition might be suitable. Another intriguing approach would be to combine 5C6 with a recently described antibody enhancing FH's activity.[164] As its epitope was determined to be located on CCP18[164], no interference between the antibody and 5C6 would be expected.

Many future optimization and application paths exist for 5C6. We hope to have contributed to this important endeavor by our work described in this thesis and to have brought 5C6 one step closer to the bedside.

REFERENCES

(1) Ricklin, D.; Hajishengallis, G.; Yang, K.; Lambris, J. D. Complement: A Key System for Immune Surveillance and Homeostasis. *Nat. Immunol.* **2010**, *11* (9), 785–797. https://doi.org/10.1038/ni.1923.

(2) Orsini, F.; De Blasio, D.; Zangari, R.; Zanier, E. R.; De Simoni, M. G. Versatility of the Complement System in Neuroinflammation, Neurodegeneration and Brain Homeostasis. *Front. Cell. Neurosci.* **2014**, *8* (November), 380. https://doi.org/10.3389/fncel.2014.00380.

(3) Kaufmann, S. H. E. Immunology's Foundation: The 100-Year Anniversary of the Nobel Prize to Paul Ehrlich and Elie Metchnikoff. *Nat. Immunol.* **2008**, *9* (7), 705–712. https://doi.org/10.1038/ni0708-705.

(4) Ricklin, D.; Lambris, J. D. Preformed Mediators of Defense-Gatekeepers Enter the Spotlight. *Immunol Rev* **2016**, *274* (1), 5–8. https://doi.org/10.1111/imr.12497.

(5) Ricklin, D.; Reis, E. S.; Lambris, J. D. Complement in Disease: A Defence System Turning Offensive. *Nat. Rev. Nephrol.* **2016**, *12* (7), 383–401. https://doi.org/10.1038/nrneph.2016.70.

(6) Pouw, R. B.; Ricklin, D. Tipping the Balance: Intricate Roles of the Complement System in Disease and Therapy. *Semin. Immunopathol.* **2021**, 1–15. https://doi.org/10.1007/s00281-021-00892-7.

(7) Kouser, L.; Madhukaran, S. P.; Shastri, A.; Saraon, A.; Ferluga, J.; Al-Mozaini, M.; Kishore, U. Emerging and Novel Functions of Complement Protein C1q. *Front. Immunol.* **2015**, *6* (JUN), 317. https://doi.org/10.3389/fimmu.2015.00317.

(8) Wallis, R.; Mitchell, D. A.; Schmid, R.; Schwaeble, W. J.; Keeble, A. H. Paths Reunited: Initiation of the Classical and Lectin Pathways of Complement Activation. *Immunobiology* **2010**, *215* (1), 1–11. https://doi.org/10.1016/j.imbio.2009.08.006.

(9) Bohlson, S. S.; Garred, P.; Kemper, C.; Tenner, A. J. Complement Nomenclature-Deconvoluted. *Front. Immunol.* **2019**, *10* (JUN), 1308. https://doi.org/10.3389/FIMMU.2019.01308/BIBTEX.

(10) Merle, N. S.; Church, S. E.; Fremeaux-Bacchi, V.; Roumenina, L. T. Complement System Part I - Molecular Mechanisms of Activation and Regulation. *Front. Immunol.* **2015**, *6* (JUN), 262. https://doi.org/10.3389/fimmu.2015.00262.

(11) Nauser, C. L.; Farrar, C. A.; Sacks, S. H. Complement Recognition Pathways in Renal Transplantation. *J. Am. Soc. Nephrol.* **2017**, *28* (9), 2571–2578. https://doi.org/10.1681/asn.2017010079.

(12) Engberg, A. E.; Sandholm, K.; Bexborn, F.; Persson, J.; Nilsson, B.; Lindahl, G.; Ekdahl, K. N. Inhibition of Complement Activation on a Model Biomaterial Surface by Streptococcal M Protein-Derived Peptides. *Biomaterials* **2009**, *30* (13), 2653–2659. https://doi.org/10.1016/j.biomaterials.2009.01.001.

(13) Reis, E. S.; Mastellos, D. C.; Hajishengallis, G.; Lambris, J. D. New Insights into the Immune Functions of Complement. *Nat. Rev. Immunol.* **2019**, *19* (8), 503–516. https://doi.org/10.1038/s41577-019-0168-x.

(14) Ghannam, A.; Fauquert, J. L.; Thomas, C.; Kemper, C.; Drouet, C. Human Complement C3 Deficiency: Th1 Induction Requires T Cell-Derived Complement C3a and CD46 Activation. *Mol. Immunol.* **2014**, *58* (1), 98–107. https://doi.org/10.1016/j.molimm.2013.11.010.

(15) Dunkelberger, J. R.; Song, W. C. Complement and Its Role in Innate and Adaptive Immune Responses. *Cell Res.* **2010**, *20* (1), 34–50. https://doi.org/10.1038/cr.2009.139.

(16) Foley, J. H. Examining Coagulation-Complement Crosstalk: Complement Activation and Thrombosis. *Thromb. Res.* **2016**, *141*, S50–S54. https://doi.org/10.1016/S0049-3848(16)30365-6.

(17) Oikonomopoulou, K.; Ricklin, D.; Ward, P. A.; Lambris, J. D. Interactions between Coagulation and Complement - Their Role in Inflammation. *Semin. Immunopathol.* **2012**, *34* (1), 151–165. https://doi.org/10.1007/s00281-011-0280-x.

(18) Schmidt, C. Q.; Lambris, J. D.; Ricklin, D. Protection of Host Cells by Complement Regulators. *Immunol. Rev.* **2016**, *274* (1), 152–171. https://doi.org/10.1111/imr.12475.
(19) Long, A. T.; Kenne, E.; Jung, R.; Fuchs, T. A.; Renné, T. Contact System Revisited: An Interface between Inflammation, Coagulation, and Innate Immunity. *J. Thromb. Haemost.* **2016**, *14* (3), 427–437. https://doi.org/10.1111/JTH.13235.
(20) Sánchez-Corral, P.; Pouw, R. B.; López-Trascasa, M.; Józsi, M. Self-Damage Caused by Dysregulation of the Complement Alternative Pathway: Relevance of the Factor H Protein Family. *Front. Immunol.* **2018**, *9* (1607). https://doi.org/10.3389/fimmu.2018.01607.
(21) Wu, J.; Wu, Y. Q.; Ricklin, D.; Janssen, B. J. C.; Lambris, J. D.; Gros, P. Structure of Complement Fragment C3b-Factor H and Implications for Host Protection by Complement Regulators. *Nat. Immunol.* **2009**, *10* (7), 728–733. https://doi.org/10.1038/ni.1755.
(22) Schmidt, C. Q.; Bai, H.; Lin, Z.; Risitano, A. M.; Barlow, P. N.; Ricklin, D.; Lambris, J. D. Rational Engineering of a Minimized Immune Inhibitor with Unique Triple-Targeting Properties. *J. Immunol.* **2013**, *190* (11), 5712–5721. https://doi.org/10.4049/jimmunol.1203548.
(23) Okemefuna, A. I.; Nan, R.; Gor, J.; Perkins, S. J. Electrostatic Interactions Contribute to the Folded-Back Conformation of Wild Type Human Factor H. *J. Mol. Biol.* **2009**, *391* (1), 98–118. https://doi.org/https://doi.org/10.1016/j.jmb.2009.06.010.
(24) Makou, E.; Mertens, H. D. T.; Maclejewski, M.; Soares, D. C.; Matis, I.; Schmidt, C. Q.; Herbert, A. P.; Svergun, D. I.; Barlow, P. N. Solution Structure of CCP Modules 10–12 Illuminates Functional Architecture of the Complement Regulator, Factor H. *J. Mol. Biol.* **2012**, *424* (5), 295–312. https://doi.org/10.1016/J.JMB.2012.09.013.
(25) Brangulis, K.; Petrovskis, I.; Kazaks, A.; Bogans, J.; Otikovs, M.; Jaudzems, K.; Ranka, R.; Tars, K. Structural Characterization of CspZ, a Complement Regulator Factor H and FHL-1 Binding Protein from Borrelia Burgdorferi. *FEBS J.* **2014**, *281* (11), 2613–2622. https://doi.org/10.1111/FEBS.12808.
(26) Mannes, M.; Dopler, A.; Huber-Lang, M.; Schmidt, C. Q. Tuning the Functionality by Splicing: Factor H and Its Alternative Splice Variant FHL-1 Share a Gene but Not All Functions. *Front. Immunol.* **2020**, *11*, 2667. https://doi.org/10.3389/FIMMU.2020.596415/BIBTEX.
(27) Pouw, R. B.; Vredevoogd, D. W.; Kuijpers, T. W.; Wouters, D. Of Mice and Men: The Factor H Protein Family and Complement Regulation. *Mol. Immunol.* **2015**, *67* (1), 12–20. https://doi.org/https://doi.org/10.1016/j.molimm.2015.03.011.
(28) Muszbek, L.; Bereczky, Z.; Bagoly, Z.; Komáromi, I.; Katona, É. Factor XIII: A Coagulation Factor with Multiple Plasmatic and Cellular Functions. *Physiol. Rev.* **2011**, *91* (3), 931–972. https://doi.org/10.1152/PHYSREV.00016.2010/ASSET/IMAGES/LARGE/Z9J0031125840010.JPEG.
(29) Schroeder, V.; Kohler, H. P. Factor XIII: Structure and Function. *Semin. Thromb. Hemost.* **2016**, *42* (4), 422–428. https://doi.org/10.1055/S-0036-1571341/ID/JR02290-33.
(30) Singh, S.; Akhter, M. S.; Dodt, J.; Volkers, P.; Reuter, A.; Reinhart, C.; Krettler, C.; Oldenburg, J.; Biswas, A. Identification of Potential Novel Interacting Partners for Coagulation Factor XIII B (FXIII-B) Subunit, a Protein Associated with a Rare Bleeding Disorder. *Int. J. Mol. Sci. 2019, Vol. 20, Page 2682* **2019**, *20* (11), 2682. https://doi.org/10.3390/IJMS20112682.
(31) Akhter, M. S.; Singh, S.; Yadegari, H.; Ivaskevicius, V.; Oldenburg, J.; Biswas, A. Exploring the Structural Similarity yet Functional Distinction between Coagulation Factor XIII-B and Complement Factor H Sushi Domains. *J. Thromb. Thrombolysis* **2019**, *48* (1), 95–102. https://doi.org/10.1007/S11239-019-01841-W/FIGURES/3.
(32) Skendros, P.; Mitsios, A.; Chrysanthopoulou, A.; Mastellos, D. C.; Metallidis, S.; Rafailidis, P.; Ntinopoulou, M.; Sertaridou, E.; Tsironidou, V.; Tsigalou, C.; Tektonidou, M.; Konstantinidis, T.; Papagoras, C.; Mitroulis, I.; Germanidis, G.; Lambris, J. D.; Ritis, K. Complement and Tissue Factor–Enriched Neutrophil Extracellular Traps Are Key Drivers in COVID-19 Immunothrombosis. *J. Clin. Invest.* **2020**, *130* (11), 6151–6157. https://doi.org/10.1172/JCI141374.

(33) Cugno, M.; Meroni, P. L.; Gualtierotti, R.; Griffini, S.; Grovetti, E.; Torri, A.; Lonati, P.; Grossi, C.; Borghi, M. O.; Novembrino, C.; Boscolo, M.; Uceda Renteria, S. C.; Valenti, L.; Lamorte, G.; Manunta, M.; Prati, D.; Pesenti, A.; Blasi, F.; Costantino, G.; Gori, A.; Bandera, A.; Tedesco, F.; Peyvandi, F. Complement Activation and Endothelial Perturbation Parallel COVID-19 Severity and Activity. *J. Autoimmun.* **2021**, *116*, 102560. https://doi.org/10.1016/J.JAUT.2020.102560.

(34) Li, Q.; Chen, Z. An Update: The Emerging Evidence of Complement Involvement in COVID-19. *Med. Microbiol. Immunol.* **2021**, *210* (2–3), 101–109. https://doi.org/10.1007/S00430-021-00704-7/TABLES/3.

(35) Pfister, F.; Vonbrunn, E.; Ries, T.; Jäck, H. M.; Überla, K.; Lochnit, G.; Sheriff, A.; Herrmann, M.; Büttner-Herold, M.; Amann, K.; Daniel, C. Complement Activation in Kidneys of Patients With COVID-19. *Front. Immunol.* **2021**, *11*, 3833. https://doi.org/10.3389/FIMMU.2020.594849/BIBTEX.

(36) Risitano, A. M. Paroxysmal Nocturnal Hemoglobinuria and Other Complement-Mediated Hematological Disorders. *Immunobiology* **2012**, *217* (11), 1080–1087. https://doi.org/10.1016/J.IMBIO.2012.07.014.

(37) Suzuki, H.; Novak, J. IgA Glycosylation and Immune Complex Formation in IgAN. *Semin. Immunopathol.* **2021**, *43* (5), 669–678. https://doi.org/10.1007/s00281-021-00883-8.

(38) Medjeral-Thomas, N. R.; Cook, H. T.; Pickering, M. C. Complement Activation in IgA Nephropathy. *Semin. Immunopathol.* **2021**, *43* (5), 679–690. https://doi.org/10.1007/s00281-021-00882-9.

(39) Eltzschig, H. K.; Eckle, T. Ischemia and Reperfusion-from Mechanism to Translation. *Nat. Med.* **2011**, *17* (11), 1391–1401. https://doi.org/10.1038/nm.2507.

(40) Nieuwenhuijs-Moeke, G. J.; Pischke, S. E.; Berger, S. P.; Sanders, J. S. F.; Pol, R. A.; Struys, M. M. R. F.; Ploeg, R. J.; Leuvenink, H. G. D. Ischemia and Reperfusion Injury in Kidney Transplantation: Relevant Mechanisms in Injury and Repair. *J. Clin. Med.* **2020**, *9* (1), 253. https://doi.org/10.3390/jcm9010253.

(41) Grafals, M.; Thurman, J. M. The Role of Complement in Organ Transplantation. *Front. Immunol.* **2019**, *10*, 2380. https://doi.org/10.3389/fimmu.2019.02380.

(42) Gorbet, M. B.; Sefton, M. V. Biomaterial-Associated Thrombosis: Roles of Coagulation Factors, Complement, Platelets and Leukocytes. *Biomaterials* **2004**, *25* (26), 5681–5703. https://doi.org/10.1016/j.biomaterials.2004.01.023.

(43) Ekdahl, K. N.; Soveri, I.; Hilborn, J.; Fellström, B.; Nilsson, B. Cardiovascular Disease in Haemodialysis: Role of the Intravascular Innate Immune System. *Nat. Rev. Nephrol.* **2017**, *13* (5), 285–296. https://doi.org/10.1038/nrneph.2017.17.

(44) Moghimi, S. M.; Simberg, D.; Papini, E.; Farhangrazi, Z. S. Complement Activation by Drug Carriers and Particulate Pharmaceuticals: Principles, Challenges and Opportunities. *Adv. Drug Deliv. Rev.* **2020**, *157*, 83–95. https://doi.org/10.1016/j.addr.2020.04.012.

(45) Szebeni, J.; Fontana, J. L.; Wassef, N. M.; Mongan, P. D.; Morse, D. S.; Dobbins, D. E.; Stahl, G. L.; Bünger, R.; Alving, C. R. Hemodynamic Changes Induced by Liposomes and Liposome-Encapsulated Hemoglobin in Pigs. *Circulation* **1999**, *99* (17), 2302–2309. https://doi.org/10.1161/01.CIR.99.17.2302.

(46) Szebeni, J. Complement Activation-Related Pseudoallergy: A Stress Reaction in Blood Triggered by Nanomedicines and Biologicals. *Mol. Immunol.* **2014**, *61* (2), 163–173. https://doi.org/10.1016/j.molimm.2014.06.038.

(47) Fülöp, T.; Mészáros, T.; Kozma, G.; Szebeni, J.; Józsi, M. Infusion Reactions Associated with the Medical Application of Monoclonal Antibodies: The Role of Complement Activation and Possibility of Inhibition by Factor H. *Antibodies* **2018**, *7* (1), 14. https://doi.org/10.3390/antib7010014.

(48) Vu, V. P.; Gifford, G. B.; Chen, F.; Benasutti, H.; Wang, G.; Groman, E. V.; Scheinman, R.; Saba, L.; Moghimi, S. M.; Simberg, D. Immunoglobulin Deposition on Biomolecule Corona Determines Complement Opsonization Efficiency of Preclinical and Clinical Nanoparticles.

Nat. Nanotechnol. **2019**, *14* (3), 260–268. https://doi.org/10.1038/s41565-018-0344-3.
(49) Szebeni, J.; Bedőcs, P.; Rozsnyay, Z.; Weiszhár, Z.; Urbanics, R.; Rosivall, L.; Cohen, R.; Garbuzenko, O.; Báthori, G.; Tóth, M.; Bünger, R.; Barenholz, Y. Liposome-Induced Complement Activation and Related Cardiopulmonary Distress in Pigs: Factors Promoting Reactogenicity of Doxil and AmBisome. *Nanomedicine Nanotechnology, Biol. Med.* **2012**, *8* (2), 176–184. https://doi.org/10.1016/J.NANO.2011.06.003.
(50) Stone, N. R. H.; Bicanic, T.; Salim, R.; Hope, W. Liposomal Amphotericin B (AmBisome®): A Review of the Pharmacokinetics, Pharmacodynamics, Clinical Experience and Future Directions. *Drugs* **2016**, *76* (4), 485–500. https://doi.org/10.1007/s40265-016-0538-7.
(51) Gabizon, A.; Szebeni, J. Complement Activation: A Potential Threat on the Safety of Poly(Ethylene Glycol)-Coated Nanomedicines. *ACS Nano* **2020**, *14* (7), 7682–7688. https://doi.org/10.1021/acsnano.0c03648.
(52) Chen, E.; Chen, B. M.; Su, Y. C.; Chang, Y. C.; Cheng, T. L.; Barenholz, Y.; Roffler, S. R. Premature Drug Release from Polyethylene Glycol (PEG)-Coated Liposomal Doxorubicin via Formation of the Membrane Attack Complex. *ACS Nano* **2020**, *14* (7), 7808–7822. https://doi.org/10.1021/acsnano.9b07218.
(53) Mohamed, M.; Abu Lila, A. S.; Shimizu, T.; Alaaeldin, E.; Hussein, A.; Sarhan, H. A.; Szebeni, J.; Ishida, T. PEGylated Liposomes: Immunological Responses. *Sci. Technol. Adv. Mater.* **2019**, *20* (1), 710–724. https://doi.org/10.1080/14686996.2019.1627174.
(54) Wibroe, P. P.; Ahmadvand, D.; Oghabian, M. A.; Yaghmur, A.; Moghimi, S. M. An Integrated Assessment of Morphology, Size, and Complement Activation of the PEGylated Liposomal Doxorubicin Products Doxil®, Caelyx®, DOXOrubicin, and SinaDoxosome. *J. Control. Release* **2016**, *221*, 1–8. https://doi.org/10.1016/j.jconrel.2015.11.021.
(55) Neun, B. W.; Barenholz, Y.; Szebeni, J.; Dobrovolskaia, M. A. Understanding the Role of Anti-PEG Antibodies in the Complement Activation by Doxil in Vitro. *Molecules* **2018**, *23* (7), 1700. https://doi.org/10.3390/molecules23071700.
(56) Klein, R. J.; Zeiss, C.; Chew, E. Y.; Tsai, J. Y.; Sackler, R. S.; Haynes, C.; Henning, A. K.; SanGiovanni, J. P.; Mane, S. M.; Mayne, S. T.; Bracken, M. B.; Ferris, F. L.; Ott, J.; Barnstable, C.; Hoh, J. Complement Factor H Polymorphism in Age-Related Macular Degeneration. *Science (80-.).* **2005**, *308* (5720), 385–389. https://doi.org/10.1126/science.1109557.
(57) Edwards, A. O.; Ritter, R.; Abel, K. J.; Manning, A.; Panhuysen, C.; Farrer, L. A. Complement Factor H Polymorphism and Age-Related Macular Degeneration. *Science (80-.).* **2005**, *308* (5720), 421–424. https://doi.org/10.1126/science.1110189.
(58) Haines, J. L.; Hauser, M. A.; Schmidt, S.; Scott, W. K.; Olson, L. M.; Gallins, P.; Spencer, K. L.; Shu, Y. K.; Noureddine, M.; Gilbert, J. R.; Schnetz-Boutaud, N.; Agarwal, A.; Postel, E. A.; Pericak-Vance, M. A. Complement Factor H Variant Increases the Risk of Age-Related Macular Degeneration. *Science (80-.).* **2005**, *308* (5720), 419–421. https://doi.org/10.1126/science.1110359.
(59) Heesterbeek, T. J.; Lorés-Motta, L.; Hoyng, C. B.; Lechanteur, Y. T. E.; den Hollander, A. I. Risk Factors for Progression of Age-related Macular Degeneration. *Ophthalmic Physiol. Opt.* **2020**, *40* (2), 140–170. https://doi.org/10.1111/opo.12675.
(60) Ambati, J.; Atkinson, J. P.; Gelfand, B. D. Immunology of Age-Related Macular Degeneration. *Nat. Rev. Immunol.* **2013**, *13* (6), 438–451. https://doi.org/10.1038/nri3459.
(61) Mastellos, D. C.; Ricklin, D.; Lambris, J. D. Clinical Promise of Next-Generation Complement Therapeutics. *Nat. Rev. Drug Discov.* **2019**. https://doi.org/10.1038/s41573-019-0031-6.
(62) Rother, R. P.; Rollins, S. A.; Mojcik, C. F.; Brodsky, R. A.; Bell, L. Discovery and Development of the Complement Inhibitor Eculizumab for the Treatment of Paroxysmal Nocturnal Hemoglobinuria. *Nat. Biotechnol.* **2007**, *25* (11), 1256–1264. https://doi.org/10.1038/nbt1344.
(63) Morgan, B. P.; Harris, C. L. Complement, a Target for Therapy in Inflammatory and Degenerative Diseases. *Nat. Rev. Drug Discov.* **2015**, *14* (12), 857–877.

https://doi.org/10.1038/nrd4657.
(64) Ricklin, D.; Mastellos, D. C.; Reis, E. S.; Lambris, J. D. The Renaissance of Complement Therapeutics. *Nat. Rev. Nephrol.* **2018**, *14* (1), 26–47. https://doi.org/10.1038/nrneph.2017.156.
(65) Heier, J. S.; Pieramici, D.; Chakravarthy, U.; Patel, S. S.; Gupta, S.; Lotery, A.; Lad, E. M.; Silverman, D.; Henry, E. C.; Anderesi, M.; Tschosik, E. A.; Gray, S.; Ferrara, D.; Guymer, R. Visual Function Decline Resulting from Geographic Atrophy: Results from the Chroma and Spectri Phase 3 Trials. *Ophthalmol. Retin.* **2020**, *4* (7), 673–688. https://doi.org/10.1016/j.oret.2020.01.019.
(66) Gupta, A.; Kafetzis, K. N.; Tagalakis, A. D.; Yu-Wai-Man, C. RNA Therapeutics in Ophthalmology - Translation to Clinical Trials. *Exp. Eye Res.* **2021**, *205*, 108482. https://doi.org/10.1016/j.exer.2021.108482.
(67) Mainolfi, N.; Ehara, T.; Karki, R. G.; Anderson, K.; Mac Sweeney, A.; Liao, S. M.; Argikar, U. A.; Jendza, K.; Zhang, C.; Powers, J.; Klosowski, D. W.; Crowley, M.; Kawanami, T.; Ding, J.; April, M.; Forster, C.; Serrano-Wu, M.; Capparelli, M.; Ramqaj, R.; Solovay, C.; Cumin, F.; Smith, T. M.; Ferrara, L.; Lee, W.; Long, D.; Prentiss, M.; De Erkenez, A.; Yang, L.; Liu, F.; Sellner, H.; Sirockin, F.; Valeur, E.; Erbel, P.; Ostermeier, D.; Ramage, P.; Gerhartz, B.; Schubart, A.; Flohr, S.; Gradoux, N.; Feifel, R.; Vogg, B.; Wiesmann, C.; Maibaum, J.; Eder, J.; Sedrani, R.; Harrison, R. A.; Mogi, M.; Jaffee, B. D.; Adams, C. M. Discovery of 4-((2 S,4 S)-4-Ethoxy-1-((5-Methoxy-7-Methyl-1 H-Indol-4-Yl)Methyl)Piperidin-2-Yl)Benzoic Acid (LNP023), a Factor B Inhibitor Specifically Designed to Be Applicable to Treating a Diverse Array of Complement Mediated Diseases. *J. Med. Chem.* **2020**, *63* (11), 5697–5722. https://doi.org/10.1021/acs.jmedchem.9b01870.
(68) Mastellos, D. C.; Yancopoulou, D.; Kokkinos, P.; Huber-Lang, M.; Hajishengallis, G.; Biglarnia, A. R.; Lupu, F.; Nilsson, B.; Risitano, A. M.; Ricklin, D.; Lambris, J. D. Compstatin: A C3-Targeted Complement Inhibitor Reaching Its Prime for Bedside Intervention. *Eur. J. Clin. Invest.* **2015**, *45* (4), 423–440. https://doi.org/10.1111/eci.12419.
(69) Hoy, S. M. Pegcetacoplan: First Approval. *Drugs* **2021**, *81* (12), 1423–1430. https://doi.org/10.1007/s40265-021-01560-8.
(70) Mastellos, D. C.; Ricklin, D.; Sfyroera, G.; Sahu, A. From Discovery to Approval: A Brief History of the Compstatin Family of Complement C3 Inhibitors. *Clin. Immunol.* **2021**, in press. https://doi.org/10.1016/j.clim.2021.108785.
(71) Mészáros, T.; Csincsi, Á. I.; Uzonyi, B.; Hebecker, M.; Fülöp, T. G.; Erdei, A.; Szebeni, J.; Józsi, M. Factor H Inhibits Complement Activation Induced by Liposomal and Micellar Drugs and the Therapeutic Antibody Rituximab in Vitro. *Nanomedicine Nanotechnology, Biol. Med.* **2016**, *12* (4), 1023–1031. https://doi.org/10.1016/j.nano.2015.11.019.
(72) Yang, Y.; Denton, H.; Davies, O. R.; Smith-Jackson, K.; Kerr, H.; Herbert, A. P.; Barlow, P. N.; Pickering, M. C.; Marchbank, K. J. An Engineered Complement Factor H Construct for Treatment of C3 Glomerulopathy. *J. Am. Soc. Nephrol.* **2018**, *29* (6), 1649–1661. https://doi.org/10.1681/ASN.2017091006.
(73) de Boer, E. C. W.; van Mourik, A. G.; Jongerius, I. Therapeutic Lessons to Be Learned From the Role of Complement Regulators as Double-Edged Sword in Health and Disease. *Front. Immunol.* **2020**, *11* (December), 1–21. https://doi.org/10.3389/fimmu.2020.578069.
(74) Castellano, G.; Melchiorre, R.; Loverre, A.; Ditonno, P.; Montinaro, V.; Rossini, M.; Divella, C.; Battaglia, M.; Lucarelli, G.; Annunziata, G.; Palazzo, S.; Selvaggi, F. P.; Staffieri, F.; Crovace, A.; Daha, M. R.; Mannesse, M.; Van Wetering, S.; Schena, F. P.; Grandaliano, G. Therapeutic Targeting of Classical and Lectin Pathways of Complement Protects from Ischemia-Reperfusion-Induced Renal Damage. *Am. J. Pathol.* **2010**, *176* (4), 1648–1659. https://doi.org/10.2353/ajpath.2010.090276.
(75) Kassimatis, T.; Greenlaw, R.; Hunter, J. P.; Douiri, A.; Flach, C.; Rebollo-Mesa, I.; Nichols, L. L.; Qasem, A.; Danzi, G.; Olsburgh, J.; Drage, M.; Friend, P. J.; Neri, F.; Karegli, J.; Horsfield, C.;

Smith, R. A.; Sacks, S. H. Ex Vivo Delivery of Mirococept: A Dose-finding Study in Pig Kidney after Showing a Low Dose Is Insufficient to Reduce Delayed Graft Function in Human Kidney. *Am. J. Transplant.* **2020**, *21* (3), 1012–1026. https://doi.org/10.1111/ajt.16265.

(76) Takasumi, M.; Omori, T.; Machida, T.; Ishida, Y.; Hayashi, M.; Suzuki, T.; Homma, Y.; Endo, Y.; Takahashi, M.; Ohira, H.; Fujita, T.; Sekine, H. A Novel Complement Inhibitor SMAP-FH Targeting Both the Lectin and Alternative Complement Pathways. *FASEB J.* **2020**, *34* (5), 6598–6612. https://doi.org/10.1096/fj.201902475R.

(77) Huang, Z.; He, Y.; Li, Q.-J.; Wen, H.; Zhang, X.-Y.; Tu, R.-H.; Zhong, G.-Q. Postconditioning Attenuates Myocardial Ischemia-reperfusion Injury by Inhibiting Complement Activation and Upregulation of MiR-499. *Exp. Ther. Med.* **2021**, *22* (1), 1–9. https://doi.org/10.3892/etm.2021.10116.

(78) Ruiz-Molina, N.; Parsons, J.; Müller, M.; Hoernstein, S. N. W.; Bohlender, L. L.; Pumple, S.; Zipfel, P. F.; Häffner, K.; Reski, R.; Decker, E. L. A Synthetic Protein as Efficient Multitarget Regulator against Complement Over-Activation. *bioRxiv* **2021**, 2021.04.27.441647. https://doi.org/10.1101/2021.04.27.441647.

(79) Bongoni, A. K.; Vikstrom, I. B.; McRae, J. L.; Salvaris, E. J.; Fisicaro, N.; Pearse, M. J.; Wymann, S.; Rowe, T.; Morelli, A. B.; Hardy, M. P.; Cowan, P. J. A Potent Truncated Form of Human Soluble CR1 Is Protective in a Mouse Model of Renal Ischemia–Reperfusion Injury. *Sci. Reports 2021 111* **2021**, *11* (1), 1–12. https://doi.org/10.1038/s41598-021-01423-y.

(80) Lazar, H. L.; Bokesch, P. M.; van Lenta, F.; Fitzgerald, C.; Emmet, C.; Marsh, H. C.; Ryan, U. Soluble Human Complement Receptor 1 Limits Ischemic Damage in Cardiac Surgery Patients at High Risk Requiring Cardiopulmonary Bypass. *Circulation* **2004**, *110* (11_suppl_1), II-274-II–279. https://doi.org/10.1161/01.CIR.0000138315.99788.eb.

(81) Biglarnia, A. R.; Nilsson, B.; Nilsson, T.; Von Zur-Mühlen, B.; Wagner, M.; Berne, C.; Wanders, A.; Magnusson, A.; Tufveson, G. Prompt Reversal of a Severe Complement Activation by Eculizumab in a Patient Undergoing Intentional ABO-Incompatible Pancreas and Kidney Transplantation. *Transpl. Int.* **2011**, *24* (8). https://doi.org/10.1111/j.1432-2277.2011.01290.x.

(82) Kassimatis, T.; Qasem, A.; Douiri, A.; Ryan, E. G.; Rebollo-Mesa, I.; Nichols, L. L.; Greenlaw, R.; Olsburgh, J.; Smith, R. A.; Sacks, S. H.; Drage, M. A Double-Blind Randomised Controlled Investigation into the Efficacy of Mirococept (APT070) for Preventing Ischaemia Reperfusion Injury in the Kidney Allograft (EMPIRIKAL): Study Protocol for a Randomised Controlled Trial. *Trials* **2017**, *18* (1), 255. https://doi.org/10.1186/s13063-017-1972-x.

(83) Berger, M.; Lefaucheur, C.; Jordan, S. C. Update on C1 Esterase Inhibitor in Human Solid Organ Transplantation. *Transplantation* **2019**, *103* (9), 1763–1775. https://doi.org/10.1097/TP.0000000000002717.

(84) Stegall, M. D.; Diwan, T.; Raghavaiah, S.; Cornell, L. D.; Burns, J.; Dean, P. G.; Cosio, F. G.; Gandhi, M. J.; Kremers, W.; Gloor, J. M. Terminal Complement Inhibition Decreases Antibody-Mediated Rejection in Sensitized Renal Transplant Recipients. *Am. J. Transplant.* **2011**, *11* (11), 2405–2413. https://doi.org/10.1111/j.1600-6143.2011.03757.x.

(85) Cornell, L. D.; Schinstock, C. A.; Gandhi, M. J.; Kremers, W. K.; Stegall, M. D. Positive Crossmatch Kidney Transplant Recipients Treated With Eculizumab: Outcomes Beyond 1 Year. *Am. J. Transplant.* **2015**, *15* (5), 1293–1302. https://doi.org/10.1111/ajt.13168.

(86) Christensen, K.; Larsson, R.; Emanuelsson, H.; Elgue, G.; Larsson, A. Heparin Coating of the Stent Graft - Effects on Platelets, Coagulation and Complement Activation. *Biomaterials* **2001**, *22* (4), 349–355. https://doi.org/10.1016/S0142-9612(00)00190-3.

(87) Fridkis-Hareli, M.; Storek, M.; Mazsaroff, I.; Risitano, A. M.; Lundberg, A. S.; Horvath, C. J.; Holers, M. V. Design and Development of TT30, a Novel C3d-Targeted C3/C5 Convertase Inhibitor for Treatment of Human Complement Alternative Pathway-Mediated Diseases. *Blood* **2011**, *118* (17), 4705–4713. https://doi.org/10.1182/blood-2011-06-359646.

(88) Naito, N.; Ukita, R.; Wilbs, J.; Wu, K.; Lin, X.; Carleton, N. M.; Roberts, K.; Jiang, S.; Heinis, C.;

Cook, K. E. Combination of Polycarboxybetaine Coating and Factor XII Inhibitor Reduces Clot Formation While Preserving Normal Tissue Coagulation during Extracorporeal Life Support. *Biomaterials* **2021**, *272*, 120778. https://doi.org/10.1016/j.biomaterials.2021.120778.

(89) Andersson, J.; Larsson, R.; Richter, R.; Ekdahl, K. N.; Nilsson, B. Binding of a Model Regulator of Complement Activation (RCA) to a Biomaterial Surface: Surface-Bound Factor H Inhibits Complement Activation. *Biomaterials* **2001**, *22* (17), 2435–2443. https://doi.org/10.1016/S0142-9612(00)00431-2.

(90) Andersson, J.; Bexborn, F.; Klinth, J.; Nilsson, B.; Ekdahl, K. N. Surface-Attached PEO in the Form of Activated Pluronic with Immobilized Factor H Reduces Both Coagulation and Complement Activation in a Whole-Blood Model. *J. Biomed. Mater. Res. Part A* **2006**, *76A* (1), 25–34. https://doi.org/10.1002/jbm.a.30377.

(91) Lambris, J. D.; Ricklin, D.; Geisbrecht, B. V. Complement Evasion by Human Pathogens. *Nat. Rev. Microbiol.* **2008**, *6*, 132. https://doi.org/10.1038/nrmicro1824https://www.nature.com/articles/nrmicro1824#supplementary-information.

(92) Macleod, O. J. S.; Bart, J. M.; MacGregor, P.; Peacock, L.; Savill, N. J.; Hester, S.; Ravel, S.; Sunter, J. D.; Trevor, C.; Rust, S.; Vaughan, T. J.; Minter, R.; Mohammed, S.; Gibson, W.; Taylor, M. C.; Higgins, M. K.; Carrington, M. A Receptor for the Complement Regulator Factor H Increases Transmission of Trypanosomes to Tsetse Flies. *Nat. Commun.* **2020**, *11* (1), 1–12. https://doi.org/10.1038/s41467-020-15125-y.

(93) Moore, S. R.; Menon, S. S.; Cortes, C.; Ferreira, V. P. Hijacking Factor H for Complement Immune Evasion. *Front. Immunol.* **2021**, *12*, 1. https://doi.org/10.3389/fimmu.2021.602277.

(94) Wu, Y.-Q. Q.; Qu, H.; Sfyroera, G.; Tzekou, A.; Kay, B. K.; Nilsson, B.; Nilsson Ekdahl, K.; Ricklin, D.; Lambris, J. D. Protection of Nonself Surfaces from Complement Attack by Factor H-Binding Peptides: Implications for Therapeutic Medicine. *J. Immunol.* **2011**, *186* (7), 4269–4277. https://doi.org/10.4049/jimmunol.1003802.

(95) Nilsson, P. H.; Ekdahl, K. N.; Magnusson, P. U.; Qu, H.; Iwata, H.; Ricklin, D.; Hong, J.; Lambris, J. D.; Nilsson, B.; Teramura, Y. Autoregulation of Thromboinflammation on Biomaterial Surfaces by a Multicomponent Therapeutic Coating. *Biomaterials* **2013**, *34* (4), 985–994. https://doi.org/10.1016/j.biomaterials.2012.10.040.

(96) Lau, J. L.; Dunn, M. K. Therapeutic Peptides: Historical Perspectives, Current Development Trends, and Future Directions. *Bioorganic Med. Chem.* **2018**, *26* (10), 2700–2707. https://doi.org/10.1016/j.bmc.2017.06.052.

(97) Muttenthaler, M.; King, G. F.; Adams, D. J.; Alewood, P. F. Trends in Peptide Drug Discovery. *Nat. Rev. Drug Discov.* **2021**, *20* (4), 309–325. https://doi.org/10.1038/s41573-020-00135-8.

(98) Schwardt, O.; Lamers, C.; Bechtler, C.; Ricklin, D. Therapeutic Peptides as Emerging Options to Restore Misguided Host Defence and Homeostasis: From Teaching to Concept to Clinic. *Chim. Int. J. Chem.* **2021**, *75* (6), 495–499. https://doi.org/10.2533/CHIMIA.2021.495.

(99) Henninot, A.; Collins, J. C.; Nuss, J. M. The Current State of Peptide Drug Discovery: Back to the Future? *J. Med. Chem.* **2017**. https://doi.org/10.1021/acs.jmedchem.7b00318.

(100) Lipinski, C. A.; Lombardo, F.; Dominy, B. W.; Feeney, P. J. Experimental and Computational Approaches to Estimate Solubility and Permeability in Drug Discovery and Development Settings. *Adv. Drug Deliv. Rev.* **1997**, *23* (1–3), 3–25. https://doi.org/10.1016/S0169-409X(96)00423-1.

(101) Lipinski, C. A.; Lombardo, F.; Dominy, B. W.; Feeney, P. J. Experimental and Computational Approaches to Estimate Solubility and Permeability in Drug Discovery and Development Settings. *Adv. Drug Deliv. Rev.* **2012**, *64* (SUPPL.), 4–17. https://doi.org/10.1016/j.addr.2012.09.019.

(102) Lipinski, C. A. Rule of Five in 2015 and beyond: Target and Ligand Structural Limitations, Ligand Chemistry Structure and Drug Discovery Project Decisions. *Adv. Drug Deliv. Rev.* **2016**, *101*, 34–41. https://doi.org/10.1016/j.addr.2016.04.029.

(103) Scannell, J. W.; Blanckley, A.; Boldon, H.; Warrington, B. Diagnosing the Decline in Pharmaceutical R&D Efficiency. *Nat. Rev. Drug Discov.* **2012**, *11* (3), 191–200. https://doi.org/10.1038/nrd3681.
(104) Scott, D. E.; Bayly, A. R.; Abell, C.; Skidmore, J. Small Molecules, Big Targets: Drug Discovery Faces the Protein-Protein Interaction Challenge. *Nat. Rev. Drug Discov.* **2016**, *15* (8), 533–550. https://doi.org/10.1038/nrd.2016.29.
(105) Davies, T. G.; Wixted, W. E.; Coyle, J. E.; Griffiths-Jones, C.; Hearn, K.; McMenamin, R.; Norton, D.; Rich, S. J.; Richardson, C.; Saxty, G.; Willems, H. M. G.; Woolford, A. J. A.; Cottom, J. E.; Kou, J. P.; Yonchuk, J. G.; Feldser, H. G.; Sanchez, Y.; Foley, J. P.; Bolognese, B. J.; Logan, G.; Podolin, P. L.; Yan, H.; Callahan, J. F.; Heightman, T. D.; Kerns, J. K. Monoacidic Inhibitors of the Kelch-like ECH-Associated Protein 1: Nuclear Factor Erythroid 2-Related Factor 2 (KEAP1:NRF2) Protein-Protein Interaction with High Cell Potency Identified by Fragment-Based Discovery. *J. Med. Chem.* **2016**. https://doi.org/10.1021/acs.jmedchem.6b00228.
(106) Norton, D.; Bonnette, W. G.; Callahan, J. F.; Carr, M. G.; Griffiths-Jones, C. M.; Heightman, T. D.; Kerns, J. K.; Nie, H.; Rich, S. J.; Richardson, C.; Rumsey, W.; Sanchez, Y.; Verdonk, M. L.; Willems, H. M. G.; Wixted, W. E.; Wolfe, L.; Woolford, A. J.-A.; Wu, Z.; Davies, T. G. Fragment-Guided Discovery of Pyrazole Carboxylic Acid Inhibitors of the Kelch-like ECH-Associated Protein 1: Nuclear Factor Erythroid 2 Related Factor 2 (KEAP1:NRF2) Protein−Protein Interaction. *J. Med. Chem.* **2021**, *21*, acs.jmedchem.1c01351. https://doi.org/10.1021/acs.jmedchem.1c01351.
(107) Valeur, E.; Guéret, S. M.; Adihou, H.; Gopalakrishnan, R.; Lemurell, M.; Waldmann, H.; Grossmann, T. N.; Plowright, A. T. New Modalities for Challenging Targets in Drug Discovery. *Angew. Chemie - Int. Ed.* **2017**, *56* (35), 10294–10323. https://doi.org/10.1002/anie.201611914.
(108) Aliu, B.; Demeestere, D.; Seydoux, E.; Boucraut, J.; Delmont, E.; Brodovitch, A.; Oberholzer, T.; Attarian, S.; Théaudin, M.; Tsouni, P.; Kuntzer, T.; Derfuss, T.; Steck, A. J.; Ernst, B.; Herrendorff, R.; Hänggi, P. Selective Inhibition of Anti-MAG IgM Autoantibody Binding to Myelin by an Antigen-Specific Glycopolymer. *J. Neurochem.* **2020**, *154* (5), 486–501. https://doi.org/10.1111/jnc.15021.
(109) Pratt, M. R.; Bertozzi, C. R. Synthetic Glycopeptides and Glycoproteins as Tools for Biology. *Chem. Soc. Rev.* **2005**, *34* (1), 58–68. https://doi.org/10.1039/b400593g.
(110) Palitzsch, B.; Gaidzik, N.; Stergiou, N.; Stahn, S.; Hartmann, S.; Gerlitzki, B.; Teusch, N.; Flemming, P.; Schmitt, E.; Kunz, H. A Synthetic Glycopeptide Vaccine for the Induction of a Monoclonal Antibody That Differentiates between Normal and Tumor Mammary Cells and Enables the Diagnosis of Human Pancreatic Cancer. *Angew. Chemie Int. Ed.* **2016**, *55* (8), 2894–2898. https://doi.org/doi:10.1002/anie.201509935.
(111) Reily, C.; Stewart, T. J.; Renfrow, M. B.; Novak, J. Glycosylation in Health and Disease. *Nat. Rev. Nephrol.* **2019**, *15* (6), 346–366. https://doi.org/10.1038/s41581-019-0129-4.
(112) Lovering, F.; Bikker, J.; Humblet, C. Escape from Flatland: Increasing Saturation as an Approach to Improving Clinical Success. *J. Med. Chem.* **2009**, *52* (21), 6752–6756. https://doi.org/10.1021/jm901241e.
(113) Marsault, E.; Peterson, M. L. Macrocycles Are Great Cycles: Applications, Opportunities, and Challenges of Synthetic Macrocycles in Drug Discovery. *J. Med. Chem.* **2011**, *54* (7), 1961–2004. https://doi.org/10.1021/JM1012374.
(114) Hill, T. A.; Shepherd, N. E.; Diness, F.; Fairlie, D. P. Constraining Cyclic Peptides To Mimic Protein Structure Motifs. *Angew. Chemie Int. Ed.* **2014**, *53* (48), 13020–13041. https://doi.org/10.1002/anie.201401058.
(115) Milroy, L. G.; Grossmann, T. N.; Hennig, S.; Brunsveld, L.; Ottmann, C. Modulators of Protein-Protein Interactions. *Chem. Rev.* **2014**, *114* (9), 4695–4748. https://doi.org/10.1021/cr400698c.
(116) Cromm, P. M.; Spiegel, J.; Grossmann, T. N. Hydrocarbon Stapled Peptides as Modulators of

Biological Function. *ACS Chem. Biol.* **2015**, *10* (6), 1362–1375. https://doi.org/10.1021/cb501020r.
(117) Guéret, S. M.; Thavam, S.; Carbajo, R. J.; Potowski, M.; Larsson, N.; Dahl, G.; Dellsén, A.; Grossmann, T. N.; Plowright, A. T.; Valeur, E.; Lemurell, M.; Waldmann, H. Macrocyclic Modalities Combining Peptide Epitopes and Natural Product Fragments. *J. Am. Chem. Soc.* **2020**, *142* (10), 4904–4915. https://doi.org/10.1021/jacs.0c00269.
(118) White, C. J.; Yudin, A. K. Contemporary Strategies for Peptide Macrocyclization. *Nat Chem* **2011**, *3* (7), 509–524.
(119) Bechtler, C.; Lamers, C. Macrocyclization Strategies for Cyclic Peptides and Peptidomimetics. *RSC Med. Chem.* **2021**, *12* (8), 1325–1351. https://doi.org/10.1039/d1md00083g.
(120) Copolovici, D. M.; Langel, K.; Eriste, E.; Langel, Ü. Cell-Penetrating Peptides: Design, Synthesis, and Applications. *ACS Nano* **2014**, *8* (3), 1972–1994. https://doi.org/10.1021/nn4057269.
(121) Dougherty, P. G.; Sahni, A.; Pei, D. Understanding Cell Penetration of Cyclic Peptides. *Chem. Rev.* **2019**, *119* (17), 10241–10287. https://doi.org/10.1021/acs.chemrev.9b00008.
(122) Fletcher, J. M.; Hughes, R. A. Modified Low Molecular Weight Cyclic Peptides as Mimetics of BDNF with Improved Potency, Proteolytic Stability and Transmembrane Passage in Vitro. *Bioorg. Med. Chem.* **2009**, *17* (7), 2695–2702. https://doi.org/10.1016/J.BMC.2009.02.053.
(123) Etayash, H.; Pletzer, D.; Kumar, P.; Straus, S. K.; Hancock, R. E. W. Cyclic Derivative of Host-Defense Peptide IDR-1018 Improves Proteolytic Stability, Suppresses Inflammation, and Enhances in Vivo Activity. *J. Med. Chem.* **2020**, *63* (17), 9228–9236. https://doi.org/10.1021/ACS.JMEDCHEM.0C00303/SUPPL_FILE/JM0C00303_SI_002.CSV.
(124) Pelay-Gimeno, M.; Glas, A.; Koch, O.; Grossmann, T. N. Structure-Based Design of Inhibitors of Protein-Protein Interactions: Mimicking Peptide Binding Epitopes. *Angew. Chemie - Int. Ed.* **2015**, *54* (31), 8896–8927. https://doi.org/10.1002/anie.201412070.
(125) Pellecchia, M.; Bertini, I.; Cowburn, D.; Dalvit, C.; Giralt, E.; Jahnke, W.; James, T. L.; Homans, S. W.; Kessler, H.; Luchinat, C.; Meyer, B.; Oschkinat, H.; Peng, J.; Schwalbe, H.; Siegal, G. Perspectives on NMR in Drug Discovery: A Technique Comes of Age. *Nat. Rev. Drug Discov.* **2008**, *7* (9), 738–745. https://doi.org/10.1038/nrd2606.
(126) Renaud, J.-P.; Chung, C.; Danielson, U. H.; Egner, U.; Hennig, M.; Hubbard, R. E.; Nar, H. Biophysics in Drug Discovery: Impact, Challenges and Opportunities. *Nat. Rev. Drug Discov.* **2016**, *15*, 679. https://doi.org/10.1038/nrd.2016.123.
(127) Merrifield, R. B. Solid Phase Peptide Synthesis. I. The Synthesis of a Tetrapeptide. *J. Am. Chem. Soc.* **1963**, *85* (14), 2149–2154. https://doi.org/10.1021/ja00897a025.
(128) Behrendt, R.; White, P.; Offer, J. Advances in Fmoc Solid-Phase Peptide Synthesis. *J. Pept. Sci.* **2016**, *22* (1), 4–27. https://doi.org/10.1002/psc.2836.
(129) Kim, Y.-W.; Grossmann, T. N.; Verdine, G. L. Synthesis of All-Hydrocarbon Stapled α-Helical Peptides by Ring-Closing Olefin Metathesis. *Nat. Protoc.* **2011**, *6* (6), 761–771. https://doi.org/10.1038/nprot.2011.324.
(130) Sengupta, S.; Mehta, G. Macrocyclization: Via C-H Functionalization: A New Paradigm in Macrocycle Synthesis. *Org. Biomol. Chem.* **2020**, *18* (10), 1851–1876. https://doi.org/10.1039/c9ob02765c.
(131) Rivera, D. G.; Ojeda-Carralero, G. M.; Reguera, L.; Van Der Eycken, E. V. Peptide Macrocyclization by Transition Metal Catalysis. *Chem. Soc. Rev* **2020**, *49*, 2039. https://doi.org/10.1039/c9cs00366e.
(132) Raynal, L.; Rose, N. C.; Donald, J. R.; Spicer, C. Photochemical Methods for Peptide Macrocylization. *Chem. – A Eur. J.* **2020**, chem.202003779. https://doi.org/10.1002/chem.202003779.
(133) Goodnow, R. A.; Dumelin, C. E.; Keefe, A. D. DNA-Encoded Chemistry: Enabling the Deeper Sampling of Chemical Space. *Nat. Rev. Drug Discov.* **2017**, *16* (2), 131–147. https://doi.org/10.1038/nrd.2016.213.
(134) Newton, M. S.; Cabezas-Perusse, Y.; Tong, C. L.; Seelig, B. In Vitro Selection of Peptides and

Proteins-Advantages of MRNA Display. *ACS Synth. Biol.* **2020**, *9* (2), 181–190. https://doi.org/10.1021/acssynbio.9b00419.
(135) Sohrabi, C.; Foster, A.; Tavassoli, A. Methods for Generating and Screening Libraries of Genetically Encoded Cyclic Peptides in Drug Discovery. *Nat. Rev. Chem.* **2020**, *4* (2), 90–101. https://doi.org/10.1038/s41570-019-0159-2.
(136) Stress, C. J.; Sauter, B.; Schneider, L. A.; Sharpe, T.; Gillingham, D. A DNA-Encoded Chemical Library Incorporating Elements of Natural Macrocycles. *Angew. Chemie Int. Ed.* **2019**, *58* (28), 9570–9574. https://doi.org/10.1002/anie.201902513.
(137) Salwiczek, M.; Nyakatura, E. K.; Gerling, U. I. M.; Ye, S.; Koksch, B. Fluorinated Amino Acids: Compatibility with Native Protein Structures and Effects on Protein–Protein Interactions. *Chem. Soc. Rev.* **2012**, *41* (6), 2135–2171. https://doi.org/10.1039/c1cs15241f.
(138) Blaskovich, M. A. T. Unusual Amino Acids in Medicinal Chemistry. *Journal of Medicinal Chemistry*. American Chemical Society December 22, 2016, pp 10807–10836. https://doi.org/10.1021/acs.jmedchem.6b00319.
(139) Kourra, C. M. B. K.; Cramer, N. Converting Disulfide Bridges in Native Peptides to Stable Methylene Thioacetals. *Chem. Sci.* **2016**, *7* (12), 7007–7012. https://doi.org/10.1039/C6SC02285E.
(140) Balducci, D.; Lazzari, I.; Monari, M.; Piccinelli, F.; Porzi, G. (S)-α-Methyl,α-Amino Acids: A New Stereocontrolled Synthesis. *Amino Acids* **2010**, *38* (3), 829–837. https://doi.org/10.1007/s00726-009-0289-9.
(141) McKay, C. S.; Finn, M. G. Click Chemistry in Complex Mixtures: Bioorthogonal Bioconjugation. *Chem. Biol.* **2014**, *21* (9), 1075–1101. https://doi.org/10.1016/j.chembiol.2014.09.002.
(142) Pickens, C. J.; Johnson, S. N.; Pressnall, M. M.; Leon, M. A.; Berkland, C. J. Practical Considerations, Challenges, and Limitations of Bioconjugation via Azide-Alkyne Cycloaddition. *Bioconjugate Chemistry*. American Chemical Society March 21, 2018, pp 686–701. https://doi.org/10.1021/acs.bioconjchem.7b00633.
(143) Kim, E.; Koo, H. Biomedical Applications of Copper-Free Click Chemistry: In Vitro, in Vivo, and Ex Vivo. *Chem. Sci.* **2019**, *10* (34), 7835–7851. https://doi.org/10.1039/c9sc03368h.
(144) Barrow, A. S.; Smedley, C. J.; Zheng, Q.; Li, S.; Dong, J.; Moses, J. E. The Growing Applications of SuFEx Click Chemistry. *Chem. Soc. Rev.* **2019**, *48* (17), 4731–4758. https://doi.org/10.1039/c8cs00960k.
(145) Fairbanks, B. D.; Macdougall, L. J.; Mavila, S.; Sinha, J.; Kirkpatrick, B. E.; Anseth, K. S.; Bowman, C. N. Photoclick Chemistry: A Bright Idea. *Chemical Reviews*. American Chemical Society June 23, 2021, pp 6915–6990. https://doi.org/10.1021/acs.chemrev.0c01212.
(146) van Moorsel, M. V. A.; Urbanus, R. T.; Verhoef, S.; Koekman, C. A.; Vink, M.; Vermonden, T.; Maas, C.; Pasterkamp, G.; Schiffelers, R. M. A Head-to-Head Comparison of Conjugation Methods for VHHs: Random Maleimide-Thiol Coupling versus Controlled Click Chemistry. *Int. J. Pharm. X* **2019**, *1*, 100020. https://doi.org/10.1016/J.IJPX.2019.100020.
(147) Marques, A. C.; Costa, P. J.; Velho, S.; Amaral, M. H. Functionalizing Nanoparticles with Cancer-Targeting Antibodies: A Comparison of Strategies. *J. Control. Release* **2020**, *320*, 180–200. https://doi.org/10.1016/J.JCONREL.2020.01.035.
(148) Yang, N.; Tang, Q.; Hu, P.; Lewis, M. J. Use of in Vitro Systems to Model in Vivo Degradation of Therapeutic Monoclonal Antibodies. *Anal. Chem.* **2018**, *90* (13), 7896–7902. https://doi.org/10.1021/acs.analchem.8b00183.
(149) Golebiewska, E. M.; Poole, A. W. Platelet Secretion: From Haemostasis to Wound Healing and Beyond. *Blood Rev.* **2015**, *29* (3), 153–162. https://doi.org/10.1016/J.BLRE.2014.10.003.
(150) Rosales, C. Neutrophil: A Cell with Many Roles in Inflammation or Several Cell Types? *Front. Physiol.* **2018**, *9* (FEB), 113. https://doi.org/10.3389/FPHYS.2018.00113/BIBTEX.
(151) Schrezenmeier, E.; Zollmann, F. S.; Seidel, K.; Böhm, C.; Schmerbach, K.; Kroh, M.; Kirsch, S.; Klare, S.; Bernhard, S.; Kappert, K.; Goldin-Lang, P.; Skuballa, W.; Unger, T.; Funke-Kaiser, H. Moderate Correlations of in Vitro versus in Vivo Pharmacokinetics Questioning the Need of

Early Microsomal Stability Testing. *Pharmacology* **2012**, *90* (5–6), 307–315. https://doi.org/10.1159/000343241.

(152) Jumper, J.; Evans, R.; Pritzel, A.; Green, T.; Figurnov, M.; Ronneberger, O.; Tunyasuvunakool, K.; Bates, R.; Žídek, A.; Potapenko, A.; Bridgland, A.; Meyer, C.; Kohl, S. A. A.; Ballard, A. J.; Cowie, A.; Romera-Paredes, B.; Nikolov, S.; Jain, R.; Adler, J.; Back, T.; Petersen, S.; Reiman, D.; Clancy, E.; Zielinski, M.; Steinegger, M.; Pacholska, M.; Berghammer, T.; Bodenstein, S.; Silver, D.; Vinyals, O.; Senior, A. W.; Kavukcuoglu, K.; Kohli, P.; Hassabis, D. Highly Accurate Protein Structure Prediction with AlphaFold. *Nature* **2021**, *596* (7873), 583–589. https://doi.org/10.1038/s41586-021-03819-2.

(153) Tarbell, J. M.; Cancel, L. M. The Glycocalyx and Its Significance in Human Medicine. *J. Intern. Med.* **2016**, *280* (1), 97–113. https://doi.org/10.1111/joim.12465.

(154) Hu, Y.; Hou, Y.; Wang, H.; Lu, H. Polysarcosine as an Alternative to PEG for Therapeutic Protein Conjugation. *Bioconjug. Chem.* **2018**, *29* (7), 2232–2238. https://doi.org/10.1021/acs.bioconjchem.8b00237.

(155) Szebeni, J.; Alving, C. R.; Rosivall, L.; Bünger, R.; Baranyi, L.; Bedöcs, P.; Tóth, M.; Barenholz, Y. Animal Models of Complement-Mediated Hypersensitivity Reactions to Liposomes and Other Lipid-Based Nanoparticles. *http://dx.doi.org/10.1080/08982100701375118* **2008**, *17* (2), 107–117. https://doi.org/10.1080/08982100701375118.

(156) Urbanics, R.; Bedocs, P.; Szebeni, J. Lessons Learned from the Porcine CARPA Model: Constant and Variable Responses to Different Nanomedicines and Administration Protocols. *Eur. J. Nanomedicine* **2015**, *7* (3), 219–231. https://doi.org/10.1515/EJNM-2015-0011/PDF.

(157) Zamboni, W. C.; Szebeni, J.; Kozlov, S. V.; Lucas, A. T.; Piscitelli, J. A.; Dobrovolskaia, M. A. Animal Models for Analysis of Immunological Responses to Nanomaterials: Challenges and Considerations. *Adv. Drug Deliv. Rev.* **2018**, *136–137*, 82–96. https://doi.org/10.1016/J.ADDR.2018.09.012.

(158) Bedőcs, P.; Szebeni, J. The Critical Choice of Animal Models in Nanomedicine Safety Assessment: A Lesson Learned From Hemoglobin-Based Oxygen Carriers. *Front. Immunol.* **2020**, *11*, 2524. https://doi.org/10.3389/FIMMU.2020.584966/BIBTEX.

(159) Dézsi, L.; Rosivall, L.; Hamar, P.; Szebeni, J.; Szénási, G. Rodent Models of Complement Activation-Related Pseudoallergy: Inducers, Symptoms, Inhibitors and Reaction Mechanisms. *Eur. J. Nanomedicine* **2015**, *7* (1), 15–25. https://doi.org/10.1515/EJNM-2015-0002/PDF.

(160) Banda, N. K.; Mehta, G.; Chao, Y.; Wang, G.; Inturi, S.; Fossati-Jimack, L.; Botto, M.; Wu, L. P.; Moghimi, S. M.; Simberg, D. Mechanisms of Complement Activation by Dextran-Coated Superparamagnetic Iron Oxide (SPIO) Nanoworms in Mouse versus Human Serum. *Part. Fibre Toxicol.* **2014**, *11* (1), 1–10. https://doi.org/10.1186/S12989-014-0064-2/FIGURES/4.

(161) Copeland, R. A. The Drug-Target Residence Time Model: A 10-Year Retrospective. *Nat. Rev. Drug Discov.* **2016**, *15* (2), 87–95. https://doi.org/10.1038/nrd.2015.18.

(162) Fasting, C.; Schalley, C. A.; Weber, M.; Seitz, O.; Hecht, S.; Koksch, B.; Dernedde, J.; Graf, C.; Knapp, E. W.; Haag, R. Multivalency as a Chemical Organization and Action Principle. *Angew. Chemie Int. Ed.* **2012**, *51* (42), 10472–10498. https://doi.org/10.1002/ANIE.201201114.

(163) Lewis, K. The Science of Antibiotic Discovery. *Cell*. Cell Press April 2, 2020, pp 29–45. https://doi.org/10.1016/j.cell.2020.02.056.

(164) Pouw, R. B.; Brouwer, M. C.; de Gast, M.; van Beek, A. E.; van den Heuvel, L. P.; Schmidt, C. Q.; van der Ende, A.; Sánchez-Corral, P.; Kuijpers, T. W.; Wouters, D. Potentiation of Complement Regulator Factor H Protects Human Endothelial Cells from Complement Attack in AHUS Sera. *Blood Adv.* **2019**, *3* (4), 621–632. https://doi.org/10.1182/bloodadvances.2018025692.